Handbook on the Physics and Chemistry of Rare Earths, volume 25

Elsevier, 1998

Edited by: Karl A. Gschneidner, Jr. and LeRoy Eyring
ISBN: 978-0-444-82871-2

Handbook on the Physics and Chemistry of Rare Earths
Vol. 25
edited by K.A. Gschneidner, Jr. and L. Eyring

PREFACE

Karl A. GSCHNEIDNER, Jr., and LeRoy EYRING

These elements perplex us in our rearches [sic], *baffle us in our speculations, and haunt us in our very dreams. They stretch like an unknown sea before us – mocking, mystifying, and murmuring strange revelations and possibilities.*

Sir William Crookes (February 16, 1887)

This is the 25th Volume of the HANDBOOK since the first appeared in 1978. The aim of the first four volumes was to combine and integrate the physics and chemistry of the rare earths. It became clear that it was necessary to continue these publications to facilitate the contribution these elements make to the new "high-tech" revolution as-well-as to societal needs to assure energy sufficiency for the future and to relieve pollution problems in the present. This serial publication has enjoyed the full collaboration and respect between the authors, editors and publishers which should continue to serve the scientific community into the future.

In that first issue 20 years ago the same expression of awe, from Sir William Crookes, that introduces this volume was used. It might seem that after 20 years and 164 reviews this wonder would no longer express the unfinished business of the study of these enigmatic elements. This, however, is not the reality. As must be true of any study of great scientific depth, full understanding is an unreachable goal.

To be sure, even 20 years ago many of the most profound questions in Sir William Crookes' mind had been answered: the correct number and identification of all of the rare earths, their most obvious physical and chemical properties, and a number of important applications for science and industry had been found. These elements have played key roles in the development of theories of electronic structure, magnetic properties and spectroscopy which are central to the development of physics and chemistry. They have also enriched the fields of the earth sciences, biological sciences, and medicine by providing insights and parallel testing systems for theory and application. Nevertheless, the extraordinary properties which give these materials their important place in the science and technology of today continue to perplex if not mystify us. It is certain that in the next breakthrough to a higher level of human understanding of nature, the rare earth elements and their compounds will play an important part in its elaboration.

The reviews contained in this Volume continue this quest. In chapter 165, Professor Hiroshi Nagai of Osaka University reveals the effects of the addition of the rare earths on steels. These elements were introduced to the enterprise of steel-making in the 1920's to effect deoxidization and desulfurization. Today, with the reductions in their cost, it is possible to extend their usefulness to provide steels with desired characteristics. The description of why and how additions of the rare earths effect micro- and nano-structures in steels which provide these beneficial modifications is explored.

Dr. Roger Marchand from the CNRS in the University of Rennes reviews ternary and higher order nitride materials in chapter 166. The synthesis of ternary compounds is reviewed and the products are categorized by their composition and the nature of the chemical bonding they exhibit. The structures of the compounds are discussed where possible. The consequences of the chemical properties for the physical properties are considered wherever studies have been made.

The spectral intensities of f–f transitions in lanthanide compounds are discussed at length in chapter 167. Professor Christine Görller-Walrand and Dr. Koen Binnemans, from the Catholic University at Leuven, have presented an exhaustive consideration of the unique appearance of intraconfigurational electronic transitions in f-type materials, particularly the lanthanides. This didactic presentation follows one, by the same authors, on the crystal-field splitting that provides information on the symmetry of the R site presented as chapter 155 of Volume 23.

Finally, Professors Gabriella Bombieri of the University of Milan and Gino Paolucci of the University of Venice review the prodigious literature on the organometallic π complexes of the f-elements. In this work they consider the main classes of complexes of both the lanthanide and actinide organometallics. Synthesis and structure are prominent in their presentation.

CONTENTS

CONTENTS OF VOLUMES 1–24

VOLUME 4: Non-metallic compounds – II

1979, 1st repr. 1984; ISBN 0-444-85216-6

VOLUME 5

1982, 1st repr. 1984; ISBN 0-444-86375-3

VOLUME 6

1984; ISBN 0-444-86592-6

VOLUME 7

1984; ISBN 0-444-86851-8

VOLUME 8

1986; ISBN 0-444-86971-9

VOLUME 9

1987; ISBN 0-444-87045-8

VOLUME 10: High energy spectroscopy

1988; ISBN 0-444-87063-6

VOLUME 11: Two-hundred-year impact of rare earths on science

1988; ISBN 0-444-87080-6

VOLUME 12

1989; ISBN 0-444-87105-5

VOLUME 13

1990; ISBN 0-444-88547-1

VOLUME 14

1991; ISBN 0-444-88743-1

VOLUME 15

1991; ISBN 0-444-88966-3

MASTER INDEX, Vols. 1–15
1993; ISBN 0-444-89965-0

VOLUME 16
1993; ISBN 0-444-89782-8

VOLUME 17: Lanthanides/Actinides: Physics – I
1993; ISBN 0-444-81502-3

VOLUME 18: Lanthanides/Actinides: Chemistry
1994; ISBN 0-444-81724-7

VOLUME 19: Lanthanides/Actinides: Physics – II

1994; ISBN 0-444-82015-9

VOLUME 20

1995; ISBN 0-444-82014-0

VOLUME 21

1995; ISBN 0-444-82178-3

VOLUME 22

1996; ISBN 0-444-82288-7

VOLUME 23

1996; ISBN 0-444-82507-X

VOLUME 24

1997; ISBN 0-444-82607-6

Handbook on the Physics and Chemistry of Rare Earths
Vol. 25
edited by K.A. Gschneidner, Jr. and L. Eyring

Chapter 165

RARE EARTHS IN STEELS

H. NAGAI
Osaka University, Department of Materials Science and Engineering, Osaka, Japan

Contents

List of symbols and abbreviations

a_0	lattice parameter of the nucleated solid
Δa_0	difference between the lattice parameters of the substrate and the nucleated solid
b.p.	boiling point
C/W	cast and wrought
C	appropriate elastic coefficient
D	diffusion coefficient of solute atom
EDX	energy dispersive X-ray analysis
EPMA	electron probe microanalysis
ΔG_A	activation energy for nucleation
G	Young's modulus
h	Planck's constant
h_X	Henrian activity of element X
HAZ	heat-affected zone
HIP	hot isostatic pressing
H_S	latent heat of solidification
IM	ingot metallurgy
k	Boltzmann's constant
K_{ISCC}	stress intensity threshold for stress corrosion cracking

l_c	effective radius of solute atmosphere	TEM	transmission electron microscope
MA	mechanical alloying	$_VT_E$	ductile–brittle impact transition temperature
N	point at which nucleation starts	T_0	equilibrium solidification temperature
N_S	number of molten iron atoms contacting the unit area of the catalyst	ΔT	supercooling temperature
		V_c	moving velocity of dislocations with the solute atom atmosphere
ODS	oxide dispersion strengthening		
P/M	powder metallurgy	δ	planar disregistry, $\Delta a_0/a_0$
PPB	prior particle boundary	η	size factor
R	atomic radius of matrix	σ_{LC}	interfacial energy for catalyst–liquid interface
S_0	surface area of the catalyst per unit area of molten iron	σ_{SC}	interfacial energy for catalyst–crystal interface
SSC	sulfide shape control		
S_V	entropy of fusion per volume	σ_{SL}	interfacial energy for liquid–crystal interface

1. Introduction

Since the early 1920s, rare earths have been used as additives for deoxidation and desulfurization in steelmaking, because they are the strongest deoxidizers as well as desulfurizers that can be added to and retained in steel. Later, a great amount of research revealed that rare earths show an excellent improvement of the physical, chemical and mechanical properties of steels, but costs preclude this function in most instances.

As is well-known, however, rare earths are not really rare. The modern processing methods have led to the production of fairly large quantities of pure rare earths and their alloys, and their price is lower than ever. This fact coupled with the interesting finding of the rare earths' excellent effects on steels, cast irons, and other alloys have excited interest in the exploitation of rare earths in engineering metallurgy.

As a survey by this author shows, literature sources concerning the effects of rare earth additions on the properties of steels have markedly decreased recently compared to those in the 1960s and 1970s. However, rare earths are still widely used in steelmaking, and the understanding of the role of rare earths in steels as well as the technology to treat rare earths in steelmaking have greatly improved in recent years.

In this review, the author aims to clarify the fundamental aspects of why and how rare earth additions show such excellent improvements on physical, chemical and mechanical properties of steels, for example, cleanliness, toughness, grain refinement, directionality of mechanical properties, weldability, hydrogen damage, aqueous corrosion and high temperature corrosion of steels, etc.

The reader should also be directed to the reviews which have been written by Hirshhorn (1968), Prochovnick (1958), Kippenhan and Gschneidner (1970) and Gschneidner and Kippenhan (1971). Furthermore, although the effects of rare earths on aqueous corrosion and high temperature corrosion are excellent, this chapter will not contain the faintest allusion to these topics. The reader should refer to the reviews by Hinton (1995) in Chapter 140 and Ryan (1995) in Chapter 141 of this Handbook series.

Table 1
Physical properties of the more common rare earth elements and, for comparison, those of pure calcium, magnesium, aluminum, silicon and iron

Element	Melting point (°C)	Boiling point (°C)	Density (g/cm^3)	References
Fe	1536	2859	7.87	Grayson (1985), Bingel and Scott (1973)
Ce	798	3433	6.66	Beaudry and Gschneidner (1978)
La	918	3464	6.15	Beaudry and Gschneidner (1978)
Y	1522	3338	4.47	Beaudry and Gschneidner (1978)
Nd	1021	3074	7.00	Beaudry and Gschneidner (1978)
Pr	931	3520	6.77	Beaudry and Gschneidner (1978)
Ca	839	1484	1.55	Grayson (1985)
Mg	650	1110	1.74	Grayson (1985)
Al	660	2494	2.70	Grayson (1985)
Si	1410	2355	2.33	Grayson (1985)

1.1. *Physical properties of rare earths*

Table 1 shows some of the physical properties of the more common rare earth elements and, for comparison, those of reactive metals and iron (Beaudry and Gschneidner 1978, Grayson 1985, Bingel and Scott 1973). Figure 1 shows the temperature dependence of the vapor pressure of these elements (Barin 1989). The melting points and vapor pressures of rare earths differ from those of iron to such an extent that problems of dissolution

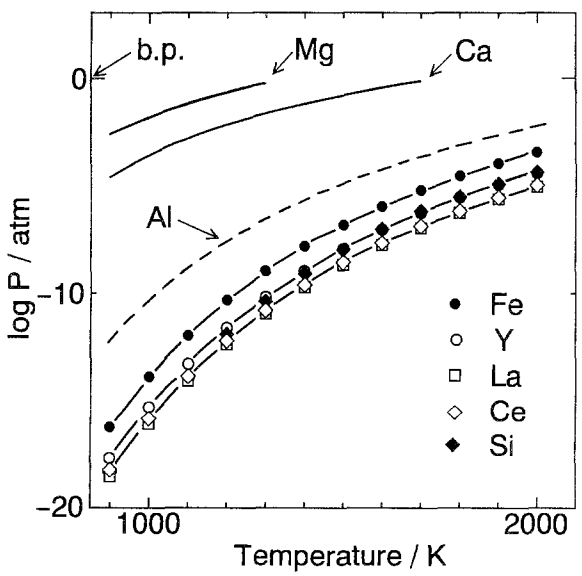

Fig. 1. Temperature dependence of vapor pressures of the more common rare earths, some reactive metals and iron.

or vaporization during addition to molten steel are not likely to occur. The lower vapor pressure of the rare earths at steelmaking temperatures is, in fact, the major advantage they have over alternative elements such as calcium and magnesium (Hilty 1967).

When the quantity of rare earths added is in excess of that required to react completely with the oxygen and sulfur in steels, however, the residual rare earth metals segregate to the as-cast grain boundaries where they tend to form an eutectic. Excessive amounts of rare earths such as this are not only needlessly expensive, but in high concentrations can cause serious hot-shortness problems during hot rolling, because the melting points of eutectics are low, and generally below the primary rolling temperature (Luyckx and Jackman 1973).

2. Thermodynamic fundamentals

It is well-known that rare earths are reactive and readily combine with oxygen, sulfur and nitrogen forming oxides, sulfides, oxysulfides and nitrides. They do not readily form carbides in iron and steels (Gschneidner and Kippenhan 1971). This is the basis for their use in ferrous process metallurgy for deoxidation and desulfurizing steels and cast iron. The standard free energies of formation of the more common rare earth compounds of interest are compared in fig. 2 (Gschneidner and Kippenhan 1971, Gschneidner et al. 1973, Barin 1989).

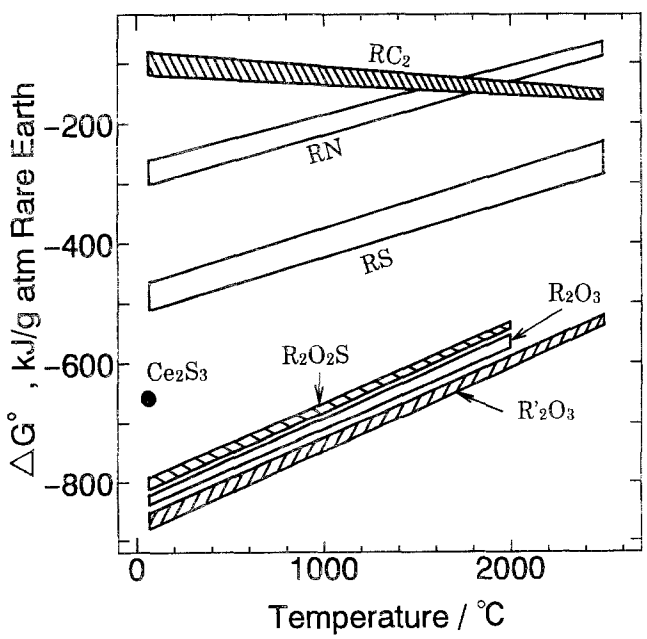

Fig. 2. Standard free energies of formation of the more common rare earth compounds. The symbol R represents the light lanthanide metals, while R′ represents yttrium and the heavy lanthanide metals.

As can be seen in this figure, the values of a compound series are drawn as a broad band, because they lie close to one another. However, in order to clarify the effect of individual rare earths on the steelmaking processes and properties of steels, it is necessary to know the values of individual rare earth compounds.

Gschneidner (1990) reported that the variation in the heat of formation in a compound series (i.e. RM_x) correlated well with the lanthanide contraction in the compound series relative to the contraction in the pure metals. Of the 20 compound series examined, he found no exception. Gschneidner (1969) proposed that this correlation can be used to predict unknown values with considerable success if at least one heat of formation value is known in the RM_x series of compounds. As an example, Gschneidner et al. (1973) used the reasonably well established free energy and heat of formation of Ce_2O_2S, the experimental observation of Eick (1958) and the relative volume ratios to predict the remaining lanthanide and yttrium oxysulfide values. Eick found that reaction of CS_2 gas with the light sesquioxides (R = La through Eu) yields the corresponding oxysulfides, but not for the heavy sesquioxides Gd through Lu. Thus, Gschneidner et al. (1973) estimated the limiting $\Delta G^0_{f,1100K}$ values from this reaction, and the shape of the ΔG^0_f vs. atomic number curve from the shape of the relative volume ratio curve. The reliability of these values was verified experimentally fourteen years later by Akila et al. (1987), whose data show excellent agreement with the values measured by Kumar and Kay (1985) for La_2O_2S and those by Fukatsu et al. (1985) for Nd_2O_2S and Gd_2O_2S. The values estimated by Gschneidner et al. (1973) are plotted in fig. 3, along with the measured values by Akila et al. (1987). The average error for these 11 phases by Akila et al. was ±12 kJ/mole or 0.8%. The estimated values were thought to be accurate to ±60 kJ/mole or ~5%. Considering these error limits, the agreement between the experimental and the

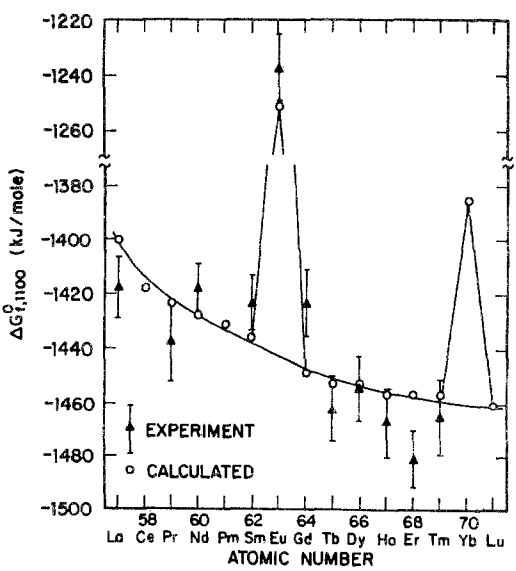

Fig. 3. Free energy of formation at 1100 K for the R_2O_2S phases. The experimental values are taken from Akila et al. (1987), and the calculated values from Gschneidner et al. (1973).

Table 2
Standard free energies of formation of some rare earth (Wilson et al. 1974) and reactive metal (Chipman and Elliott 1963, Gokcen and Chipman 1952) compounds in steelmaking: $\Delta G^0 = -X + YT$ cal/g.f.w.

Reaction[a]	X	Y	Activity product	K' (1900 K)
$[Ce]_{1W/O} + 2[O]_{1W/O} = CeO_2(s)$	204 000	59.8	$h_{Ce}h_O^2$	4.0×10^{-11}
$2[Ce]_{1W/O} + 3[O]_{1W/O} = Ce_2O_3(s)$	341 810	86.0	$h_{Ce}^2h_O^3$	3.0×10^{-21}
$2[La]_{1W/O} + 3[O]_{1W/O} = La_2O_3(s)$	344 865	80.5	$h_{La}^2h_O^3$	8.4×10^{-23}
$[Ce]_{1W/O} + [S]_{1W/O} = CeS(s)$	100 980	27.9	$h_{Ce}h_S$	3.0×10^{-6}
$3[Ce]_{1W/O} + 4[S]_{1W/O} = Ce_3S_4(s)$	357 180	105.1[b]	$h_{Ce}^3h_S^4$	7.6×10^{-19}[b]
$2[Ce]_{1W/O} + 3[S]_{1W/O} = Ce_2S_3(s)$	256 660[b]	78.0[b]	$h_{Ce}^2h_S^3$	3.3×10^{-13}[b]
$[La]_{1W/O} + [S]_{1W/O} = LaS(s)$	91 750	25.5	$h_{La}h_S$	1.0×10^{-5}
$2[Ce]_{1W/O} + 2[O]_{1W/O} + [S]_{1W/O} = Ce_2O_2S(s)$	323 300	79.2	$h_{Ce}^2h_O^2h_S$	1.3×10^{-20}
$2[La]_{1W/O} + 2[O]_{1W/O} + [S]_{1W/O} = La_2O_2S(s)$	320 340[b]	71.9[b]	$h_{La}^2h_O^2h_S$	7.3×10^{-22}[b]
$[Si]_{1W/O} + 2[O]_{1W/O} = SiO_2(s)$	146 500	56.3	$h_{Si}h_O^2$	2.8×10^{-5}
$2[Al]_{1W/O} + 3[O]_{1W/O} = Al_2O_3(s)$	292 870	93.7	$h_{Al}^2h_O^3$	6.2×10^{-14}

[a] [ ] Represents a component in solution in steel and the subscript 1W/O standard state.
[b] Estimated.

estimated values is excellent. Thus, unknown thermochemical values can be estimated with considerable accuracy.

Based on the comparison of the free energy values (fig. 2), one would expect that, with the addition of rare earths in steelmaking, the first compounds that would form would be oxides, followed by the oxysulfides, R_xS_y compounds, monosulfides, nitrides, and finally the rare earth carbides. However, this situation would change depending on the concentration of these elements dissolved in steels. Stated another way, it is rather complex and depends on the "deoxidation and desulfurization constants" or "solubility products", regarding what kind of compound would form when rare earths are added to steels.

In order to make more detailed predictions about the reactions of rare earths with elements in steel and steelmaking, for example, oxygen, sulfur, nitrogen and carbon, it is necessary to know the standard free energies of formation of the rare earth compounds as well as the free energies of solution of these non-metallic elements and the rare earths in iron. The free energies of solution for oxygen, sulfur and carbon are well-known (Schenck and Pfaff 1961, Ejima et al. 1975, Ban-ya and Matoba 1962). The free energies of solution of the rare earths in iron (R = [R]) can be calculated from the relevant phase diagrams (Gschneidner 1961) and it is therefore possible to calculate the standard free energies of formation of the rare earth compounds using rare earths, oxygen, and sulfur dissolved in steel as reactants instead of the pure liquids, solids and gases at a pressure of one atmosphere.

The standard free energies of formation of compounds for some rare earths and reactive metals in steelmaking are given in table 2. The reciprocals, K', of the equilibrium

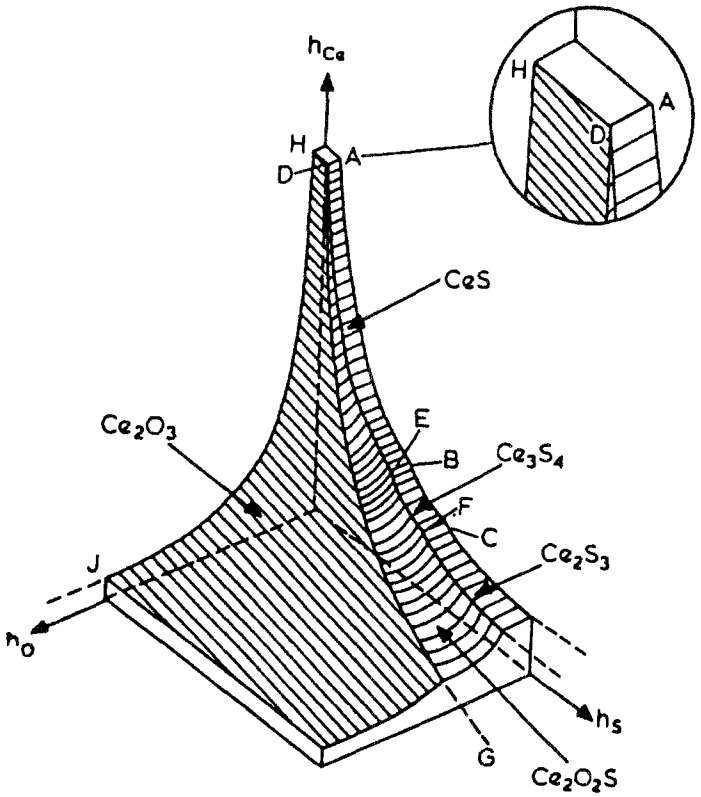

Fig. 4. Inclusion precipitation diagram for the Fe–Ce–O–S system.

constants K calculated for these reactions are also included in this table. The K' are "deoxidation and desulfurization constants" in terms of Henrian activities.

Using these K' values calculated for cerium oxides, sulfides, and oxysulfides, Wilson et al. (1974, 1976) have constructed an inclusion precipitation diagram for the Fe–Ce–O–S system (fig. 4), where h_{Ce}, h_O and h_S represent the Henrian activities of cerium, oxygen and sulfur, respectively. This composite precipitation diagram gives a clear, qualitative picture of the conditions of phase formations and transformations.

As an illustration of the usefulness of this diagram, assume a situation in a heat of steel where the cerium content and the sulfur content are high but the oxygen content is low. This composition occurs above the Ce_2O_2S surface and therefore precipitation of this compound would occur. The precipitation of Ce_2O_2S would proceed with the concentrations of cerium, sulfur, and oxygen diminishing until the amount of cerium, sulfur, and oxygen would be represented by a point on the Ce_2O_2S surface. If this point on the Ce_2O_2S surface is below the level of the Ce_xS_y surface, then a certain amount of cerium and sulfur will remain in solution in the steel. However, if after the precipitation of Ce_2O_2S is completed, the cerium and sulfur contents are above either the Ce_2S_3, the

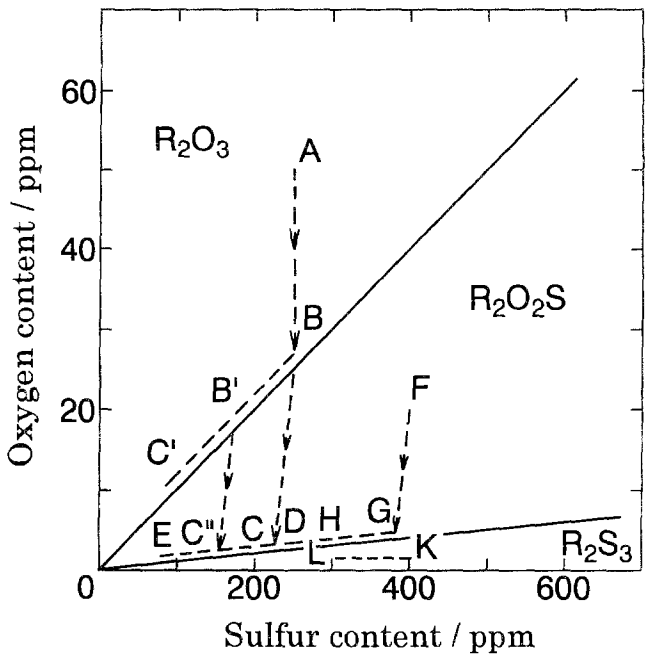

Fig. 5. Possible reaction paths for sequential and coupled deoxidation–desulfurization reactions superimposed on fields of stability for oxide, oxysulfide, and sulfide at 1600°C.

Ce_3S_4, or the CeS surface, then a Ce_xS_y phase of some form would precipitate until the composition reaches a point on the line DEF of the precipitation diagram.

Computations based on the transformation of Ce_2O_3 to Ce_2O_2S indicate that Ce_2O_3 and Ce_2O_2S will co-precipitate at the ratio $h_S/h_O = \sim 4.3$. This ratio indicates that the sulfur content of the steel, to which rare earths are added, may have to be as much as five times higher than the oxygen content to prevent the precipitation of Ce_2O_3. As an example, if we assume a sulfur content of 0.020%, it may be necessary to have more than 0.0047% oxygen or 47 ppm in order to precipitate Ce_2O_3.

Lu and McLean (1974a,b) have also determined the thermodynamic relationships for the simultaneous deoxidation and desulfurization reactions which occur when rare earth elements are added to molten steel and have expressed their results graphically. Figure 5 shows several possible reaction paths for sequential and coupled deoxidation–desulfurization reactions superimposed on fields of stability for oxide, oxysulfide, and sulfide at 1600°C. The actual path followed after rare earth addition depends on the initial oxygen O_i and sulfur S_i contents. For example, if $S_i < 10\,O_i$, the reaction starts in the oxide field. Thus, when $O_i = 50$ ppm and $S_i = 250$ ppm (point A in fig. 5), the first phase to precipitate out is R_2O_3.

As R_2O_3 precipitates, the oxygen content decreases with no change in the sulfur content until point B is reached, corresponding to 25 ppm oxygen. At this point, oxysulfide will begin to precipitate, and provided that all the oxide has separated from the melt, the

melt composition will move across the oxysulfide field in the direction BC. The slope of BC is determined by the oxygen/sulfur stoichiometric ratio for the precipitation of oxysulfide. At point C, the oxygen and sulfur contents are 2.27 and 227 ppm, respectively. The melt composition then moves along the equilibrium line CE with the precipitation of both oxysulfide and sulfide. The final sulfur level attained is determined by the initial conditions of the melt and the size of the rare earth addition. Under these circumstances, one would expect to observe inclusions consisting of an oxysulfide core surrounded by rare earth sulfides.

If, when the melt composition reaches point B, all of the precipitated oxide has not yet separated from the melt, a reaction will occur between the melt and the oxide to form oxysulfide, and the melt composition will move along the transient-state line toward C′ until all the oxide has been consumed, or, as is more likely in practice, has been coated with a layer of oxysulfide which will isolate the oxide from further reaction with the melt. At this stage, when oxide is no longer in contact with the melt, the melt composition will move away from the transient-state line BC′ toward the final equilibrium line CE on a path parallel to BC (i.e. B′C″ in fig. 5).

If S_i is >10 O_i but <100 O_i, the initial melt composition is located within the oxysulfide field, for example, at F. On the addition of rare earths, oxysulfide will precipitate and the melt composition will move from F towards G. When the oxygen content has been reduced to G, both sulfide and oxysulfide will separate until the final required sulfur level is reached.

Comparing the results reported by Wilson et al. (1974) and Lu and McLean (1974a,b), the oxygen and sulfur contents in steels at which precipitates change from oxide to oxysulfide and from oxysulfide to sulfide are markedly different. This is due to the difference in the standard free energy values of formation of these compounds used for calculation. As seen in table 3, these values are markedly different depending on the researchers.

For example, Ejima et al. (1975) studied the Ce–S equilibrium in liquid iron with a low oxygen content at 1550–1650°C using an alumina crucible lined with CeS to prevent oxygen contamination from the crucible and obtained the standard free energy of formation of CeS. They also derived the standard free energy of solution for Ce(l) = [Ce], as $\Delta G^0 = -4900 - 16.0\,T$. They interpreted the disagreement with the data previously reported (table 3) as follows: (1) dependence of $K' = [\%Ce]\,[\%S]$ on [%Ce] and [%S] has not been taken into account in most of the other studies. That is, extrapolation of other researchers' data to [%Ce] + 4.37[%S] = 0 gives almost the same value. (2) The standard free energy of solution for R(l) = [R] estimated from the Fe–R phase diagram might be erroneous for calculation of the standard free energy of formation of the compounds listed in table 3. (3) The oxygen content of molten iron in other studies might have been high. Because the oxygen content strongly affects the R–S equilibrium in liquid iron, deoxidation prior to rare earth addition and prevention of oxygen contamination from the crucible and atmosphere should be carefully carried out.

Table 3
Summary of values evaluated for the solubility product of rare earths and impurity elements in liquid iron at 1600°C

Reaction[a]	Solubility product	Remarks	Reference
$CeS(s)=[Ce]+[S]$	1.5×10^{-3}	CeS and MgO, in Ar	Langenberg and Chipman (1958)
	1.0×10^{-3}	MgO, in vacuum	Singleton (1959)
	2.5×10^{-4}	MgO, in vacuum	Kusagawa and Ohtani (1965)
	1.0×10^{-3}	MgO, in Ar	Schinderova and Buzek (1965)
	1.9×10^{-4}	CaO, in vacuum	Fischer and Bertram (1973)
	2.5×10^{-5}	CaO coated with CeS, Ar	Ejima et al. (1975)
	2.0×10^{-3}	Estimated	Narita et al. (1964)
	3.0×10^{-6}	Estimated	Wilson et al. (1974)
$Ce_2S_3(s)=2[Ce]+3[S]$	8.0×10^{-6}	Estimated	Narita et al. (1964)
	3.3×10^{-13}	Estimated	Wilson et al. (1974)
$LaS(s)=[La]+[S]$	1.5×10^{-4}	Estimated	Fischer and Bertram (1973)
	1.0×10^{-5}	CaO, in vacuum	Wilson et al. (1974)
$La_2S_3(s)=2[La]+3[S]$	4.0×10^{-5}	Estimated	Narita et al. (1964)
$Ce_2O_3(s)=2[\underline{Ce}]+3[O]$	4.0×10^{-15}	CaO, in Ar	Ishikawa et al. (1973)
	1.8×10^{-9}	CaO, in vacuum	Fischer and Bertram (1973)
	1.0×10^{-20}	Estimated	Kinne et al. (1963)
	3.0×10^{-21}	Estimated	Wilson et al. (1974)
$CeO_2(s)=[Ce]+2[O]$	1.0×10^{-12}	Estimated	Kinne et al. (1963)
	1.1×10^{-10}	Al_2O_3, in Ar	Schinderova and Buzek (1965)
	4.0×10^{-11}	Estimated	Wilson et al. (1974)
$La_2O_3(s)=2[La]+3[O]$	6.0×10^{-10}	CaO, in vacuum	Fischer and Bertram (1973)
	4.0×10^{-21}	Estimated	Narita et al. (1964)
	8.4×10^{-23}	Estimated	Wilson et al. (1974)
$Ce_2O_2S(s)=2[Ce]+2[O]+[S]$	1.3×10^{-20}	Estimated	Wilson et al. (1974)
$LaN_2(s)=[La]+2[N]$	1.0×10^{-5}	CaO, in vacuum	Fischer and Bertram (1973)
$CO(g)=[C]+[O]$	2.4×10^{-3}	CaO, in CO–CO_2 gas	Ban-ya and Matoba (1962)
$Al_2O_3(s)=2[Al]+3[O]$	2.0×10^{-14}	MgO, in Ar	Chipman and Elliott (1963)
$SiO_2(s)=[Si]+2[O]$	1.6×10^{-5}	CaO, in Ar	Gokcen and Chipman (1952)

[a] [ ] Represents a component in solution in steel.

2.1. *Practical examples of rare earth effects on steelmaking*

Leary et al. (1968) showed the practical effectiveness of rare earths as deoxidizers, comparing the oxygen contents in the steels deoxidized with rare earths and other elements (carbon, aluminum, silicon) commonly used in steelmaking. The results are shown in fig. 6. Leary's results show that rare earths can reduce oxygen levels in steel to values below those obtained with other deoxidizers or with vacuum carbon treatment ($<0.30\%$ carbon). These findings have been verified by a number of laboratory and plant

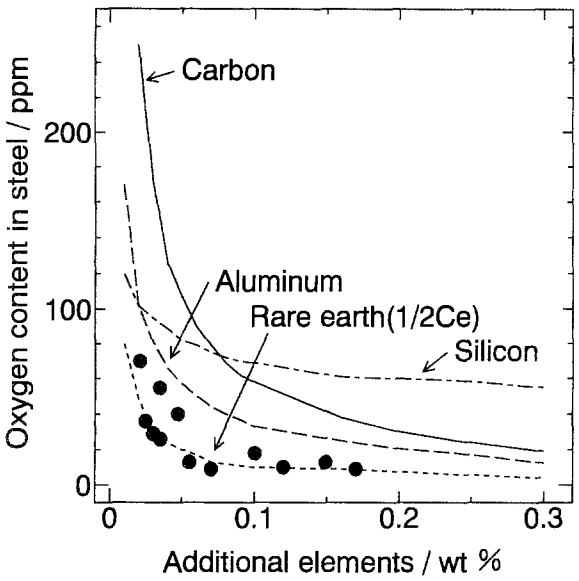

Fig. 6. Oxygen contents in the steels deoxidized with rare earths and other elements (carbon, aluminum, silicon) commonly used in steelmaking.

trials. Problems encountered with rare earth additions, inconsistent recovery and poor cleanliness, have hampered a broader use of these elements (Lillieqvist and Mickelson 1952, Rusel 1954, Sims 1959). Rare earths form extremely stable oxides and this is one of the reasons for their poor recovery under steelmaking conditions. For optimum recovery, therefore, it is essential that rare earths are normally added to steel after an appropriate aluminum or silicon addition is made to lower the oxygen and to improve the recovery of the rare earths.

Because rare earths are strong deoxidizers, refractories used for steelmaking or melting should be carefully selected. The standard free energy of formation of silica is small compared to the standard free energy of the formation of R_2O_3. Therefore, refractories with $>30\%$ SiO_2 serve as a constant source of oxygen in the presence of any significant rare earth residual with the result that the full potential of rare earths as deoxidizers can not be achieved. If a more stable refractory such as magnesia is used, the oxygen content associated with a 0.10% addition of rare earths can be achieved to approximately 4 ppm, close to the limit of accuracy for oxygen determination by vacuum fusion.

As described above, it is obvious from the free energy data that oxides and oxysulfides would be formed first when rare earths are added to molten iron, and sulfur removal is effective only when the oxygen content and its activity are low. Use of a heavy basic slag and 0.2% mischmetal (residual Ce in steel 0.002–0.015%) reduced the sulfur content in one case from 0.012% to $<0.001\%$ in plain carbon steels and $\ll 0.003\%$ in 12–13% Cr stainless steels (Grevillius et al. 1971). A 0.5% mischmetal addition resulted in 94% sulfur removal in another case (Bernard 1967). Similar results have been obtained by Dahl et al. (1973).

The rare earth addition also eliminates the harmful effects of impurities such as lead, tin, arsenic, etc., which concentrate at the grain boundary and decrease the hot workability of steel. According to the phase diagrams (Gschneidner 1961, Gschneidner and Verkade 1974), some of the rare earth compounds with these impurity elements have melting points which are several times higher than the melting point of either the pure rare earths or these impurity elements. In addition, the melting points of some of these compounds are higher than the ordinary steel rolling temperatures. Therefore, from the phase diagrams of some of the rare earths and these impurity elements, it is possible to predict that rare earths should be able to obviate the deleterious effect of some of these elements on the mechanical properties of steel. In practice, Breyer (1973) showed the detrimental effect of lead on the ductility of 4130 steel at elevated temperatures and demonstrated that rare earth addition (0.5 w/o) markedly increases the hot ductility (reduction of area) in the temperature range from 250 to 450°C.

3. Shape control of inclusions

The role of non-metallic inclusions as nucleating sites for void formation in the ductile fracture of steels and their consequent deleterious effect on ductility and toughness is well established. For this reason, considerable effort has been made in the production of "clean" steels for many applications.

There is a well-known relationship between the volume fraction of second-phase particles (inclusions) and the ductility as measured by the strain at the fracture (or percentage reduction of area) in a tensile test. As a typical example, fig. 7 shows the effect of volume fraction and shape of a second phase on the ductility and Charpy shelf energy. It is clear that the ductility is adversely affected by an increasing volume fraction of

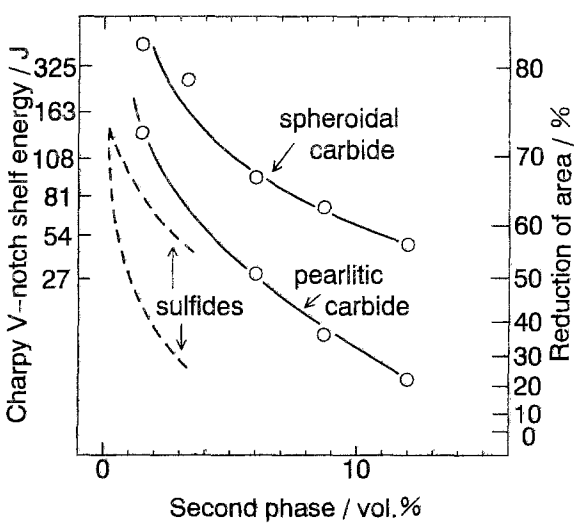

Fig. 7. Effect of volume fraction and shape of second phase on the ductility and Charpy shelf energy.

inclusions. In addition, the shape of the inclusions of either carbides or sulfides markedly affects the ductility (Waudby 1978). It should be pointed out that the deleterious effect of sulfide inclusions is more pronounced than that of carbides, especially that of sulfides on the transverse direction.

As will be described later, however, extensive research has recently been done to positively utilize these non-metallic inclusions to improve the properties of steels. That is, utilization of inclusions as nucleation sites for grain refinement during casting, welding and phase transformations, and as dispersoids for ODS alloys are anticipated.

3.1. *Directionality of mechanical properties*

Directionality of mechanical properties such as toughness and formability is typical of hot-rolled steels processed on modern, hot strip mills. Various researchers (Little and Henderson 1971, Matsuoka and Ohmori 1972) reported that this difference is caused primarily by the presence of elongated manganese sulfide inclusions during hot rolling which are oriented parallel to the plane of fracture in the transverse specimens. Directionality can be reduced by retaining the original globular shape of the precipitated sulfides. Control of the sulfide shape contributed to a marked improvement in toughness and formability of steel in the direction transverse to the rolling direction. This is of considerable interest especially in the automobile industry and other applications.

The shape of manganese sulfide inclusions can be partially altered by cross rolling. This method is being used on plate mills for producing high quality steel. Even when this technique is used, the sulfide shape control is incomplete because the inclusions still retain a biaxial ellipsoidal shape. Furthermore, cross rolling on modern continuous hot strip mills is currently impractical.

The shape of sulfide inclusions can be altered from elongated to globular by chemical means. This is accomplished by adding an element which forms a high melting point sulfide, more stable than manganese sulfide and not as readily deformable at hot rolling temperatures.

Luyckx et al. (1970) reported that the major factor affecting the plasticity of manganese-based sulfides is the oxygen content of the steel; the higher the oxygen, the lower the plasticity. However, it is not possible to take advantage of this effect without losing the benefit of the controlled oxide morphology. They also found that, at low oxygen levels, the plasticity of the sulfide is also affected to some extent by the manganese-to-sulfur ratio of the steel. The smaller this ratio, the lower will be the plasticity. Thus, inclusions which are less susceptible to deformation can be obtained by decreasing the manganese and/or increasing the sulfur. However, manganese provides significant solution strengthening, and low sulfur levels are required to ensure that the size and number of inclusions are not excessive.

From the data of Elliott and Gleiser (1960), it appears that additions of Ti, Zr, Mg, Ca, and rare earths form stable high melting point sulfides. It is possible that each of these elements could be used to form sulfide inclusions which would not elongate during hot rolling. Before introducing these additives to a specific alloy system, however, other

factors must be considered. In general, the following criteria are important: interactions of the additions with oxygen, nitrogen, and carbon (Elliott and Gleiser 1960, Faircloth et al. 1968), also their solubility in molten steel, vapor pressure, availability, and cost.

The high affinity of Ti and Zr for nitrogen and their tendency to form coarse nitride particles preclude the use of these elements in hot-rolled steels strengthened by finely dispersed nitride precipitates (Lichy et al. 1965, Bucher et al. 1969). Ti and Zr will combine with carbon in the solid state to form lath-shaped crystals of their carbides, which can cause embrittlement (Arrowsmith 1968). Ti and Zr are available at moderate cost, but their reactivity with O, S, C, and N makes accurate control of the final properties of steels with these elements somewhat difficult. It is also interesting to note that steels treated with rare earths show consistently higher ductility than Zr-treated steels (Wilson and Klems 1974).

Thermodynamic data indicate that Mg forms a high melting point, stable sulfide and has little tendency for nitride or carbide formation. Because of its low boiling point, however, addition of Mg to molten steel is hazardous and extremely difficult. The sulfide of Ca is more stable than that of Mg, and the tendency for nitride or carbide formation is quite weak. The boiling point is higher than that of Mg, although the solubility in molten steel at atmospheric pressure is low. Ca is readily available at moderate cost, and exploratory work with this element has been regarded as justified. Even with very large additions of Ca alloys (CaSi), however, metallographic examination revealed that only 60% of the sulfides were converted to a globular shape. The ineffectiveness of Ca is attributed to its high vapor pressure and low solubility in this steel. Because the same degree of sulfide shape control was achieved with much smaller additions of rare earths, efforts were centered on the effect of rare earth additions.

3.2. *Rare earth effects on directionality*

Rare earths form extremely stable sulfides and oxysulfides, as described above. Free energies of formation of the nitrides suggest that Al and rare earths have an almost similar behavior. No problems related to nitride formation have been encountered in the past with Al at levels of typical killed steels, therefore, no difficulty was anticipated with rare earths. This assumption has been substantiated by several investigators. In view of the low free energy of formation of rare earth carbides, it is unlikely that carbide formation would be a problem.

The melting points and densities of these compounds for the major rare earth elements are high as shown in table 4 (Bingel and Scott 1973). The best known element of this series is cerium, and the melting point of its sulfide, CeS, is about 2450°C. Owing to their high density, however, removal by floatation will be not easy in some cases.

As a typical example, fig. 8 illustrates the effect of rare earth addition on toughness: the impact curves are plotted for both longitudinal and transverse Charpy V-notch specimens (Luyckx et al. 1970). In longitudinal specimens, the impact energy at 100% shear, commonly called the shelf energy, is in excess of 5.5 kg m (40 ft lb); in transverse specimens, it is 2 kg m (15 ft lb), which is doubled to 4 kg m at the Ce/S ratio of 1.5–2.0.

Table 4
Physical properties of rare earth compounds and other common compounds occurring in steel[a]

Compound	Melting point	Density (g/cm^3)	Compound	Melting point	Density (g/cm^3)
Y_2O_3	2440	4.8	LaS	~1971	5.8
CeO_2	~2599	7.3	La_2S_3	~2099	5.0
Ce_2O_3	~1691	6.867	NdS	~2138	6.2
La_2O_3	~2249	6.580	Nd_2S_3	~2199	5.4
Nd_2O_3	~2271	7.308	Pr_2S_3	1795	6.6
Pr_2O_3	~2199	7.067	MnS	1530	4.0
Al_2O_3	~2030	4.0	Ce_2O_2S	1949	6.0
CaO	~2600	3.4	La_2O_2S	1993	5.8
CeS	~2099	5.9	Nd_2O_2S	1988	6.3
Ce_2S_3	~2149	5.2	Pr_2O_2S		6.2

[a] Gschneidner (1961), Bingel and Scott (1973).

With Ce/S ratios greater than 2, the transverse shelf energy appears to decrease slightly, although no explanation for this effect has been given.

On the other hand, it is reported that high transverse impact values can be achieved when the R/S ratio is greater than 4 (Waudby 1978). Ackert and Crozier (1973) have shown that the improvement in the Charpy V-notch shelf energy at −18°C occurs at an R/S ratio of 5 to 6 which is much higher than those described above. Ballance and Mintus (1972) have also shown that a marked improvement in the bend performance of steels is obtained at R/S ratios higher than 4. The difference in R/S ratios reported by various

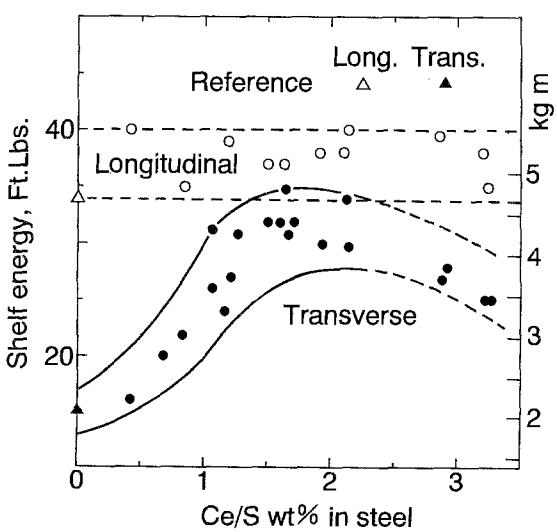

Fig. 8. Effect of rare earth addition on Charpy V-notch toughness in longitudinal and transverse directions.

researchers, where high ductility and toughness are achieved, is supposed to be due to the difference in the original oxygen contents of steels, which results in the formation of different types of inclusions.

3.3. *Grain refinement by rare earths*

Recently, extensive studies have been done on the utilization of rare earth metals and Ca in the ingot-making and continuous casting processes, with the objective of high-grade steel production. Rare earths and Ca control not only the inclusion shape (Luyckx et al. 1970), but also the solidification structure itself (Sakuraya et al. 1976, Chistyakov et al. 1966). It is well known that the addition of rare earths results in the grain refinement of steels.

Formation of the rare earth compounds facilitates heterogeneous nucleation during solidification which leads to grain refinement. The inclusions are made finer and nearly spherical, and the rare earth additions make them disperse uniformly within the grains, unlike the film-like appearance of MnS along the grain boundary (Kepka et al. 1973, Rowntree et al. 1973). These changes in the microstructure lead to improvement in mechanical properties.

Some characteristics of rare-earth-added steels compared with ordinary steels are as follows:

(1) primary dendrite arm spacing is narrower,
(2) primary dendrite arm length is shorter,
(3) the growth direction of dendrite arms is less oriented,
(4) the microsegregation of C, S, P, Si and Mn is less.

It is concluded that new primary dendrite arms are generated due to the heterogeneous nucleation by rare earth additions in the region of comparatively small supercooling near the liquid–solid interface.

Several researchers have revealed a marked effect of rare earths on improving the thicknesswise ductility of steels resistant to lamellar tear, reducing the anisotropy of steels, and preventing hydrogen-induced cracking, etc. Basically, all these seem to be attributable to the following four principal functions achieved by rare earths and Ca addition to the molten steels:

(1) formation of nucleation catalysts having high nucleation potency,
(2) improvement of solidification structure,
(3) formation of non-metallic inclusions with low plastic deformability at hot working temperatures,
(4) enhancement of molten steel cleanliness.

Many studies have disclosed interesting facts about (3) and (4), as described above, whereas few reports have been reported on (1) and (2).

3.4. *Heterogeneous nucleation potencies of rare earths for δ-iron*

The heterogeneous nucleation potency of inclusion catalyzers is dependent upon the difference in interfacial energy between the inclusion and δ-iron. This interfacial energy

can be theoretically explained by the disregistry between crystals. The contribution of lattice disregistry to heterogeneous nucleation behavior has been emphasized by Turnbull and Vonnegut (1952) who theorized that the effectiveness of a substrate in promoting heterogeneous nucleation depends on the crystallographic disregistry between the substrate and the nucleated solid. The "planar disregistry" can be written as $\delta=(\Delta a_0/a_0)$, where Δa_0 is the difference between the lattice parameters of the substrate and the nucleated solid for a low-index plane, and a_0 is the lattice parameter for the nucleated phase. The degree of supercooling of a liquid was postulated to be a parabolic function of the disregistry factor;

$$\Delta T = \frac{c}{\Delta S_V}\delta^2,$$

where ΔS_V is the entropy of fusion per volume, and c is the appropriate elastic coefficient.

The frequency I of heterogeneous nucleation is represented by the following equation (Turnbull and Vonnegut 1952):

$$I = N_S S_0 \frac{\kappa T}{h}\exp\left[-\frac{\Delta G_A}{\kappa T}\right]\exp\left[\frac{-16\pi f(\theta)\sigma_{SL}^3 T_0^2}{3\kappa\Delta T^2 H_S^2 T}\right],$$

$$f(\theta) = (2+\cos\theta)\frac{(1-\cos\theta)^2}{4}, \qquad \cos\theta = \frac{(\sigma_{LC}-\sigma_{SC})}{\sigma_{SL}},$$

where N_S is the number of molten iron atoms contacting the unit area of the catalyst; S_0, the surface area of the catalyst per unit area of molten iron; κ, Boltzmann's constant; h, Planck's constant; ΔG_A, the activation energy for nucleation; σ_{LC}, σ_{SC} and σ_{SL}, the values of σ for the catalyst–liquid, catalyst–crystal and liquid–crystal interfaces; T_0, the equilibrium solidification temperature; H_S, the latent heat of solidification; and ΔT, the supercooling temperature.

This equation shows that decreasing the supercooling temperature (ΔT) gives rise to an increase in the heterogeneous nucleation frequency; that is, more crystalline nuclei form per unit time and consequently result in grain refinement.

Estimating the ability of rare earths and Ca to improve the solidification structure is very important for their effective utilization. To estimate the heterogeneous nucleation potencies of various oxides and sulfides suspended in molten steel, Ohashi et al. (1976) and Nuri et al. (1982) experimentally determined the corresponding supercooling temperatures of liquid iron. In their experiments, because the concentration products of the added elements and S (%) or O (%) in the molten steel were greater than their thermodynamic solubility products (shown in table 2), their oxides, sulfides and/or oxysulfides had already precipitated in the molten steel. As an example, fig. 9 shows the time–temperature curves of various supercooling experiments for iron with and without Si, Al and rare earth metal (Ohashi et al. 1976). In this figure, nucleation starts at point N. It is clear from this figure that the supercooling temperature ΔT is

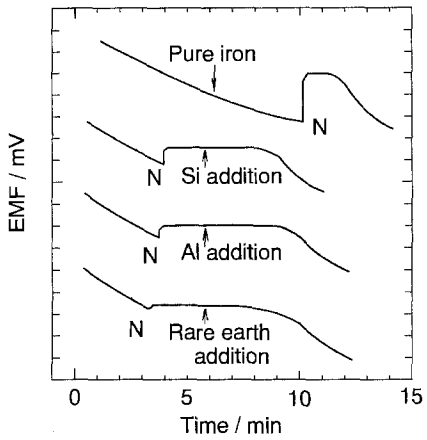

Fig. 9. Time–temperature curves of various supercooling experiments for iron with and without Si, Al and rare earth metals. N denotes the points at which nucleation starts.

decreased by the addition of Si, Al and rare earths in this order. As seen in this figure, rare-earth-added steel, in spite of lower supercooling, requires less arrest time during which solidification proceeds than rare-earth-free steel. This suggests that, at the same supercooling, rare-earth-added steel produces more crystalline nuclei than rare-earth-free steel.

As a typical example, fig. 10 shows the crystallographic relationships at the interface between the (100) of CaS, CeS and the (100) of δ-Fe (Nuri et al. 1982). The crystallographic disregistry between them is small, that is 3.0% for CaS and 1.6% for CeS. Figure 11 shows the relationship between the calculated disregistry δ and the critical

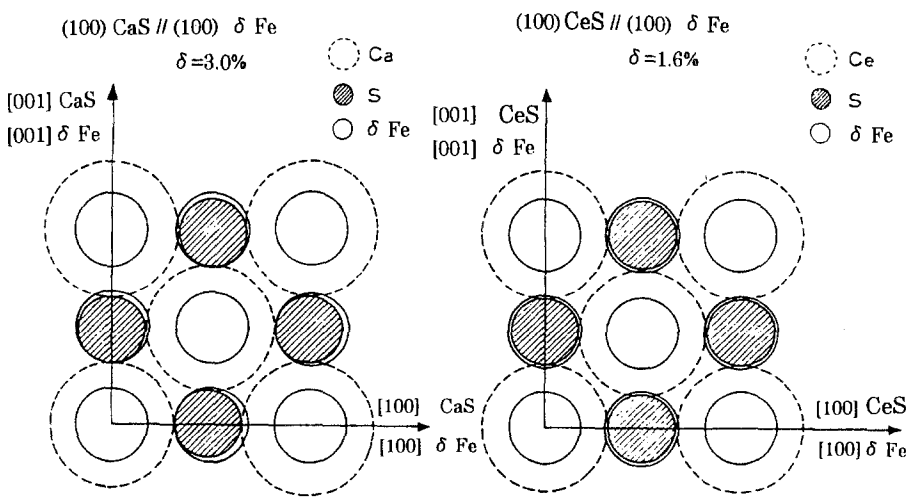

Fig. 10. Crystallographic relationships at the interface between the (100) plane of CaS, CeS and the (100) plane of δ-Fe.

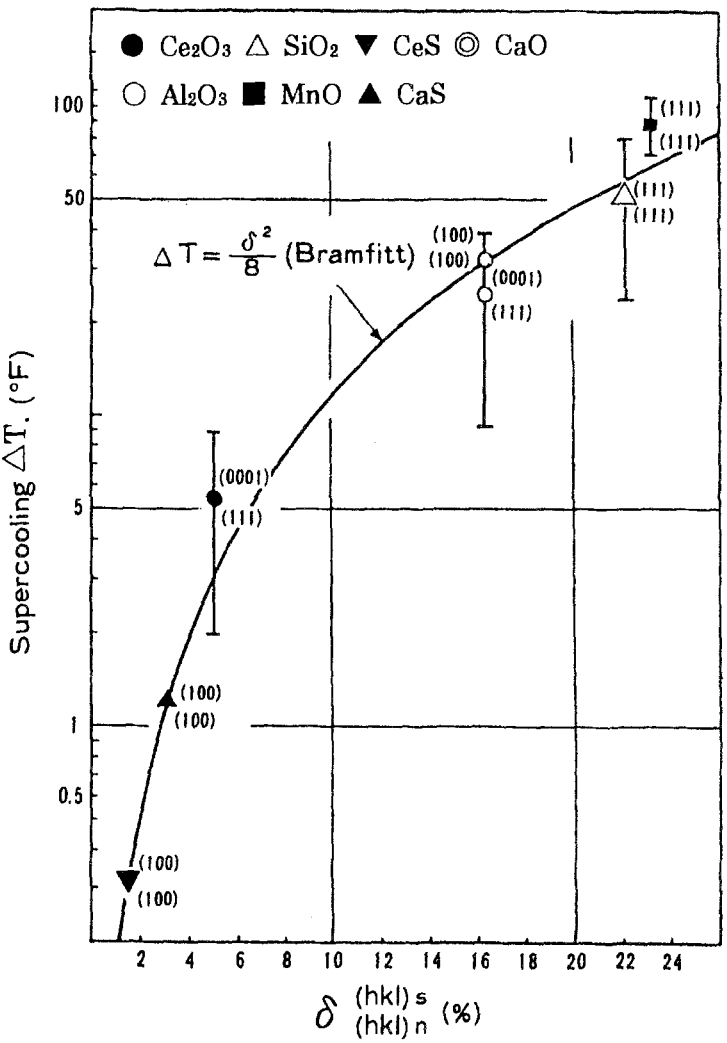

Fig. 11. Relation between the calculated disregistry δ and critical supercooling temperature for various compounds.

supercooling temperature which decreases in the order of MnO, SiO_2, CaO, Al_2O_3, Ce_2O_3, CaS and CeS. The potential of the heterogeneous nucleation increases in this order and this relationship fits well the parabolic trend reported by Bramfitt (1970). Bramfitt (1970) and Reynolds and Tottle (1951) suggested that, when the disregistry is less than about 12%, the nucleating agent is potent; when the disregistry is above 12%, the potency is poor. This means that rare earths, especially rare earth sulfides, show extremely good potential for the grain size refinement of δ-iron.

3.5. *Effect of rare earths on grain refinement during γ/α transformation of steels*

It is now widely accepted that the decomposition of austenite generally begins with the nucleation and growth of coarse ferrite grains at the prior austenite grain boundaries during γ/α transformation of steels, which cause a remarkable decrease in the ductility of steels. If inclusions of appropriate character are present to provide intergranular nucleation sites or prevent the formation of ferrite at prior austenite grain boundaries, nucleation and growth of intergranular ferrite occurs, which significantly improves the ductility of steels (Abson 1989).

Sawai et al. (1996) and Wakoh et al. (1992) proposed a concept to obtain a fine ferrite grain structure utilizing MnS as the nucleant. That is, the combination of two types of oxides: one in which a uniform distribution and very fine particles can easily be obtained, and another on which MnS easily precipitates. Ueshima et al. (1989) found that the number of oxide inclusions formed in the steels is larger in Hf-, Ce-, Y- and Zr-treated steels than those in Al- and Ti-treated steels, but the difference in the size of the inclusions is not large (fig. 12a,b), when these elements are added to molten iron in the same concentration. They interpreted the differences in these results due to the difference in the floatation rates U (fig. 13) of these oxides in molten iron by the following Stokes equation. That is, it is concluded that many of the oxide particles with a larger density

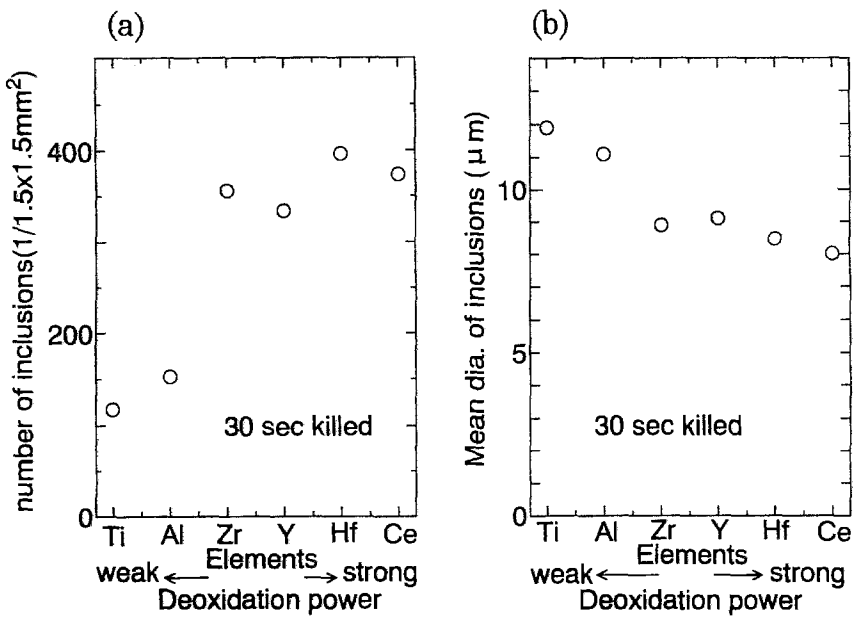

Fig. 12. (a) Number and (b) mean diameter of oxide inclusions formed in iron, for which various deoxidation elements were added in the melt at 1570°C, held for 30 s, and then furnace-cooled.

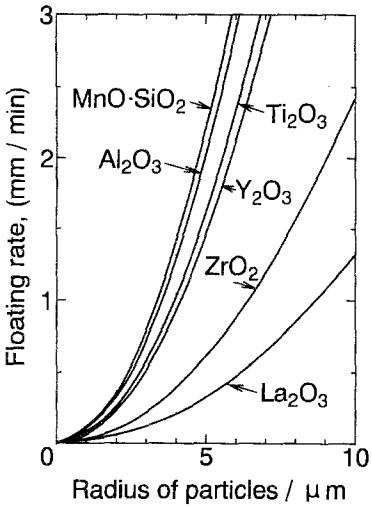

Fig. 13. Calculated floatation rate of various oxide particles in molten iron.

are suspended in the molten iron, while the oxide particles with a smaller density float away, and the number of oxide particles decreases.

$$U = 2g(\rho_{Fe} - \rho_{OX})\frac{r^2}{9\eta},$$

where g is the gravitational acceleration (980 cm/s^2); ρ_{Fe} and ρ_{OX}, the densities of molten iron (7.0 g/cm^2) and oxide; r, the radius of the particles; and η, the viscosity of molten iron (0.048 poise).

Funakoshi et al. (1977) found that simultaneous addition of rare earth with boron accelerates the formation of fine ferrite grains inside prior austenite grains, resulting in a remarkable improvement in toughness. The effects of rare earth and boron additions on the ductile–brittle transition temperature are shown in fig. 14. Although the effect of a single addition of rare earth or boron is small, the simultaneous addition of both elements markedly decreased the transition temperature. They observed spherical inclusions of R_2O_2S and BN in the center of ferrite grains, and the number of fine ferrite grains increased remarkably with increasing BN content. They concluded that fine rare earth inclusions uniformly dispersed in the steel act as precipitation sites for BN, on which ferrite grains nucleate and grow.

It has been reported that fine oxide, sulfide, oxysulfide, boride and nitride particles uniformly distributed in the steels act as effective nuclei for intergranular ferrite (Funakoshi et al. 1977, Nakanishi et al. 1983, Ito and Nakanishi 1975, Mori et al. 1981, Honma et al. 1986, Ohno et al. 1987, Ricks et al. 1982). Although the mechanism by which the more effective nucleants facilitate the nucleation of intergranular ferrite is not certain, Abson (1989) noted that in order to obtain fine ferrite grains, the crystallographic matching (disregistry), wettability between nucleants and ferrite phase, and size of inclusions must be important.

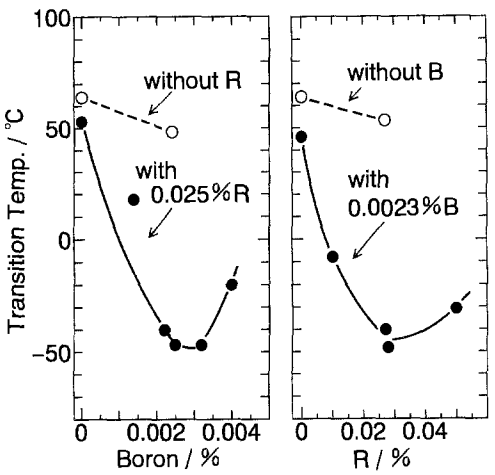

Fig. 14. Effect of simultaneous addition of rare earth with boron on the ductile–brittle transition temperature of Fe–0.12C–0.25Si–1.50Mn–0.006N steel.

3.6. *Dendritic structure*

Nuri et al. (1982) reported on the characteristics of rare-earth-added steels, especially the solidification microstructure (including the spacing, length and inclination of dendrite arms) and microsegregation with some consideration of the relevant mechanisms. Microstructural observations revealed that in the rare-earth-added steel fine-grained dendrites at the surface develop extensively, with the adjoining columnar dendrites growing less than those in rare-earth-free steel. This difference in the solidification structure has an effect on the secondary structure after solidification.

These characteristics of the dendritic structure in rare-earth-added steel will have an indirect effect on the pattern of occurrence of the inverted V segregate (Nuri et al. 1976, Suzuki and Miyamoto 1977, Iwata et al. 1976), the formation of a loose structure in the ingot, the macrosolidification structure, including the ratio of equiaxed crystals, and the central segregation in the continuously cast slab. They will also greatly affect the heat-treatment conditions and mechanical properties of the rolled products.

Figure 15 shows the primary and secondary dendrite arm spacings in the specimens. Both primary and secondary arm spacings increase with an increase in the distance from the chilled surface. The secondary arm spacing differs little between the two steels, whereas the primary arm spacing, compared at the same location, is smaller in rare-earth-added steel than in rare-earth-free steel. This distinct tendency was observed in both ingots and continuously cast slabs.

The closely packed arm spacing is hardly influenced by the flow of the unsolidified liquid metal. As a consequence, this is thought to be responsible for the reduced inverted V segregation in the ingot (Iwata et al. 1976).

The effect of rare earth addition on the dendritic structure is not limited to the primary arm spacing but extends to the primary arm length. Figure 16 shows the distribution of the primary arm length in a continuously cast slab at different superheating temperatures. As seen in fig. 16, the primary arm length is much shorter in rare-earth-added steel than

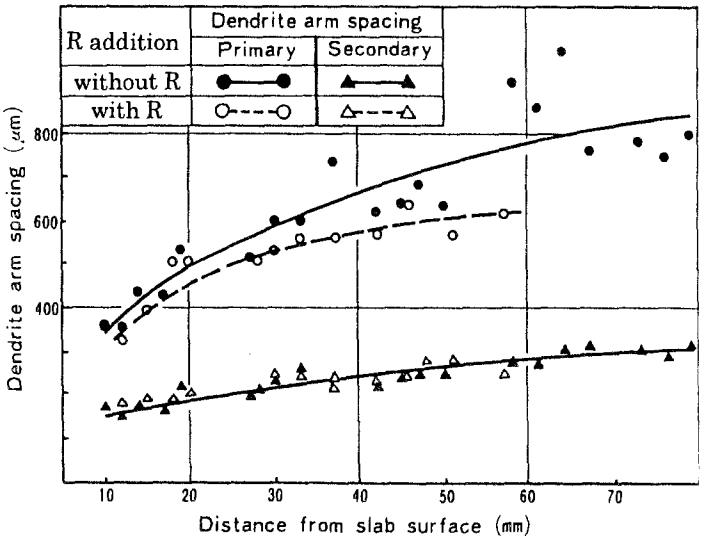

Fig. 15. Primary and secondary dendrite arm spacings in the specimens.

in rare-earth-free steel. The effect of the rare earth addition increases with a decrease in the superheating temperature. Accordingly, the number of arms in a given area is much greater in rare-earth-added steel. As a consequence, rare-earth-added steel has a highly compact solidification structure.

The above-described characteristics of the dendrite structure of rare-earth-added steel, of course, has an effect on the macrosolidification structure. Rare-earth-added steel, having a small arm spacing and length, has a fine-grained macrostructure.

EPMA analyses on C, P, S, Si and Mn for the axes and branches of dendrites in rare-earth-added and rare-earth-free steels revealed that carbon exhibits the most pronounced difference between the two steels. The difference between the maximum and minimum

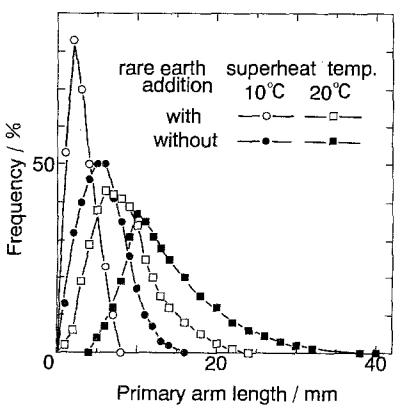

Fig. 16. Effect of rare earth addition on the distribution of the primary arm length at different superheating temperatures.

values for carbon is smaller in rare-earth-added steel, leveling off in many areas. The addition of rare earths also moderates the segregation of P, S, Si and Mn. Thus, rare-earth-added steel is shown to have an effect on reducing the microsegregation, and this phenomenon supported the aforementioned characteristics of the dendritic solidification structure.

Based on the above-described facts and experimental results, it is estimated that, in rare-earth-added steel, new primary arms occur due to the heterogeneous nucleation by rare earth additions, in the relatively small supercooling zones near the solid–liquid phase, while dendrites are solidifying.

3.7. *Effect of rare earths on surface tension and contact angle*

A knowledge of the surface tension of molten iron and contact angle between molten iron and various oxides and sulfides is essential to an understanding of metallurgical processes. In steelmaking and casting operations, the surface tension and the contact angle are dominating factors for phenomena such as nucleation and growth of non-metallic inclusions, and slag/metal as well as metal/refractory interactions. Unfortunately, although experimental and theoretical investigations of the nature and behavior of surfaces and interfaces between molten iron and compounds are unsatisfactory, a few researchers reported that rare earth additions decrease the surface tension of molten iron. Pirogov et al. (1971) reported that the surface tension of molten steel decreases from 1870 to 1404 J/m^2 with 0.133% Ce and 0.049% B at 1600°C. Surface tension also decreases with increasing sulfur content: 0.03% S reduces it to 1460 J/m^2 (Puzyrev et al. 1970). Etelis et al. (1974) have studied the effect of 0.05–0.5% Y, 0.1–0.5% La, and 0.1–0.3% Ce on the surface tensions of steels not only as a function of rare earth content but also as a function of time after addition and reported similar findings. The rare earth additions improve the fluidity of steels (Rostovtsev and Obrazov 1968). This is probably due to the reduction in the number of inclusions in the molten iron (Raman 1976). Contact angles between molten iron and substrates of various rare earth oxides are reported to be in the region from 100° to 110° at 1550°C by Chernov (1983). Mrdjenovich et al. (1970) reported that the contact angle between molten iron and Y_2O_3 significantly decreases with increasing Y content in the molten iron.

3.8. *Effects of rare earths on cast irons*

Rare earths are added to cast irons mainly to modify their microstructure and to improve their ductility and toughness (Morrogh 1949, 1958, Millis et al. 1949). The amount of rare earths added, the time and location of addition and the holding time after addition are important factors that determine the extent of modification or demodification. Rare earths modify the shape of graphite grains in cast irons and make them spherical. The rare earths also refine the grain size of graphite, eutectics and dendrites (Selcuk and Kirkwood 1973, Jackson 1973, Hong 1971, Basutkar and Loper 1971). The topic of nodulation of graphite by rare earths addition is extremely important in the technology of cast irons and

has attracted considerable attention (Church 1973, Miska 1972, Morrogh 1952). When optimum quantities are added, several benefits resulted.

(1) Wear resistance is improved by a factor of 2 to 3 due to its modified microstructure and the lubricable nature of graphite (Ivanov 1972).
(2) Ingot molds made from treated cast irons have 50–70% higher strength than regular cast irons with lamellar graphite (Dubinin and Abakumov 1972).
(3) The brittleness is considerably reduced and the bending strength is nearly doubled, and the impact strength is nearly tripled (Hartley and Henderson 1973).
(4) The machinability is improved (Sharan et al. 1969).
(5) The corrosion resistance in acidic and alkaline solutions is improved (Morozof and Goranskii 1973).
(6) The damping capacity is improved.
(7) Microporosity and pinholes are eliminated in the castings because of degassing.

Several mechanisms have been advanced to explain the growth of graphite nuclei into spheres. Rare earths and several other elements are surface active on graphite and are absorbed selectively during the nucleation process. This increases the surface tension of the graphite and facilitates spheroidal growth. The increase in interfacial energy due to adsorption of rare earths is definitely a factor aiding nodularization. Szpunar (1969), Akhmatov et al. (1972) and Sidorenko (1971) proposed that the surface tension becomes uniform along the different facets of the graphite crystals, which causes uniform growth in all directions.

Although the mechanism for the change in morphology of graphite by rare earth additions has been investigated and discussed in detail by several authors (Morrogh and Williams 1974, Hunter and Chadwick 1972, Lux 1970, Double and Hellawell 1969, Buhr 1971, Oldfield and Kangilaski 1971), further detailed research is required in order to define the correct mechanism.

4. Hydrogen embrittlement cracking

The deleterious effects resulting from hydrogen in ferrous materials have been known since 1926, when it was reported that ductility losses in steels were attributed to the presence of hydrogen in the materials (Fast 1965, Cotterill 1961). Considerable experimental evidence exists indicating that hydrogen can degrade the properties of a wide variety of materials, ranging from high strength steels to soft iron (Bernstein and Thompson 1974). Recently, the magnitude of the hydrogen problem has come to be appreciated primarily because of the increasing demands for strength and toughness required of modern materials exposed to hydrogen environments.

A particularly important observation is the fact that hydrogen can be introduced in a component at any time during its fabrication (casting, welding, surface treatment, heat treatment, etc.) or when used in various applications such as pipelines, containers, gas wells, nuclear reactors, and ships (Folkhard et al. 1972, Glikman and Orlov 1968, Kudryavtsev et al. 1972, Smialowski 1962, Sheinker and Wood 1971).

The most recent type of hydrogen embrittlement to be investigated results from the direct exposure of a metal surface to a gaseous hydrogen environment (Hofmann and Rauls 1961). This form of hydrogen embrittlement has been regarded with increasing concern because of the predicted future widespread use of hydrogen as a fuel (Smialowski 1962). Absorption of hydrogen gas in metals is potentially a serious problem for electric current generating fuel cells and propulsion systems which utilize the hydrogen oxygen reaction as a source of energy or for systems being considered for the storage of high pressure gaseous hydrogen fuel (Schwartz and Ward 1968, Moeckel 1969).

Although an appreciable understanding of the effects of hydrogen on steels has been achieved, and some progress has been made in mitigating the embrittlement problem, the fact still remains that design engineers must incorporate considerable safety factors to insure the prevention of catastrophic failure in structural steel components.

A number of methods of inhibiting hydrogen embrittlement in high strength steels have been under study. These techniques include changes in microstructure (Cain and Troiano 1965, McCoy 1974, Bernstein and Thompson 1976), changes in alloy composition (Lagneborg 1969, Beck et al. 1971), baking (Johnson et al. 1958, Sims 1959, Troiano 1959), surface prestressing (Bates 1970, Carter 1972), plating, cathodic protection (McEowan and Elsea 1965), non-metallic coating (Speller 1951, Brewer 1974), selective changes in surface composition by heat treatment, and modification of the embrittling environment (Baker and Singleterry 1972, Zecher 1976).

In general, however, these techniques cannot always be applied, because a number of serious limitations exist. For example, for microstructural and base alloy composition modifications, overall mechanical properties, fabricability and economic considerations control the applicability of such methods to the extent that little flexibility exists for wide variations without other accompanying problems. Numerous methods have been studied to prevent hydrogen entry into a high strength steel component by the formation of a barrier between the steel and the service environment. Cathodic protection of steels can be limited by the absorption of hydrogen generated at the cathodic surfaces if high local current densities are applied (Uhlig 1963, McEowan and Elsea 1965). Metallic platings have been developed for the protection of steels, but there has been an accompanying embrittling action resulting from the plating process itself (Williams et al. 1960, Beck and Jankowsky 1960).

Because limitations exist with all of these techniques, research is being conducted to improve the current methods and to develop new ones to inhibit hydrogen embrittlement in high strength steels. One new method is the use of rare earth additions in these alloys.

4.1. *Effect of rare earths on hydrogen-induced delayed failure*

Several studies indicate that rare earth additions to steels offer potential to minimize hydrogen embrittlement without degrading the baseline properties of the alloys themselves. The important consideration here is the mechanism by which rare earths minimize embrittlement. In one instance, improvement was attributed to the absorption of hydrogen to form stable, non-embrittling hydrides. In another instance, improvement was attributed

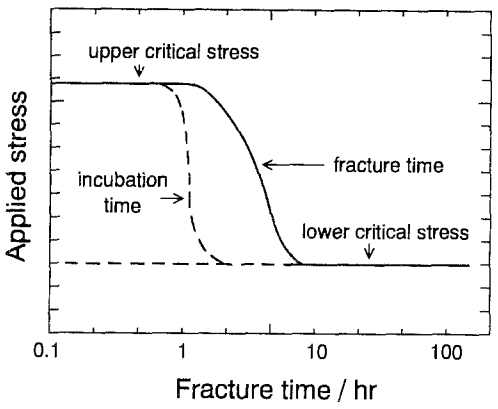

Fig. 17. Schematic illustration of delayed failure behavior.

to a change in sulfide morphology. An additional important consideration is the amount of rare earth additions required to inhibit hydrogen embrittlement. It is well established that embrittlement results from hydrogen contents as low as 10 ppm (Vennett and Ansell 1969). Enough rare earth must be in the alloy system to provide improvement in resistance to hydrogen embrittlement without causing a significant alteration in the mechanical properties of the base alloy itself. Fabricability and workability of alloy systems containing these rare earths are also important factors in determining their potential use.

Ce additions at the 0.2 w/o level in 4340 type steels have resulted in lower susceptibility to the blister or flake formation type of hydrogen embrittlement by forming stable hydrides below 1010°C (Kortovich 1977). Kortovich (1977) investigated the hydrogen embrittlement cracking resistance of vacuum-induction-melted AISI 4340 steel containing Ce or La in the 0.03–0.17 w/o range. As a basis for studying the hydrogen embrittlement resistance of rare-earth-modified steel, delayed failure tests were conducted on specimens cathodically charged in sulfuric acid and plated with cadmium. Delayed failure tests, which employ a series of varying static loads, represent the most sensitive method for studying hydrogen embrittlement. The essential characteristics of classical delayed failure are summarized schematically in fig. 17 (Troiano 1960). The most significant characteristic of delayed failure behavior is the fact that there is a minimum critical value of stress (the lower critical stress) below which failure does not occur. Studies performed on hydrogen-induced delayed failure of sharply notched high strength steel specimens indicate that an incubation time precedes crack initiation. Once a critical amount of hydrogen has reached the area in front of the crack tip, cracking proceeds discontinuously until a critical length is attained and rapid failure occurs (Johnson et al. 1958, Steigerwald et al. 1959).

The delayed failure curves for precracked specimens of hydrogenated and Cd plated (a) AISI 4340 steel without rare earths, (b) with 0.03% Ce, (c) with 0.09 and 0.17 w/o Ce, (d) with 0.08 and 0.16 w/o La are shown in fig. 18a–d. The Ce and La additions showed a dramatic improvement in the delayed failure of 4340 steel both in fracture times and lower critical stress intensity. The lower critical stress intensity represents a three-fold

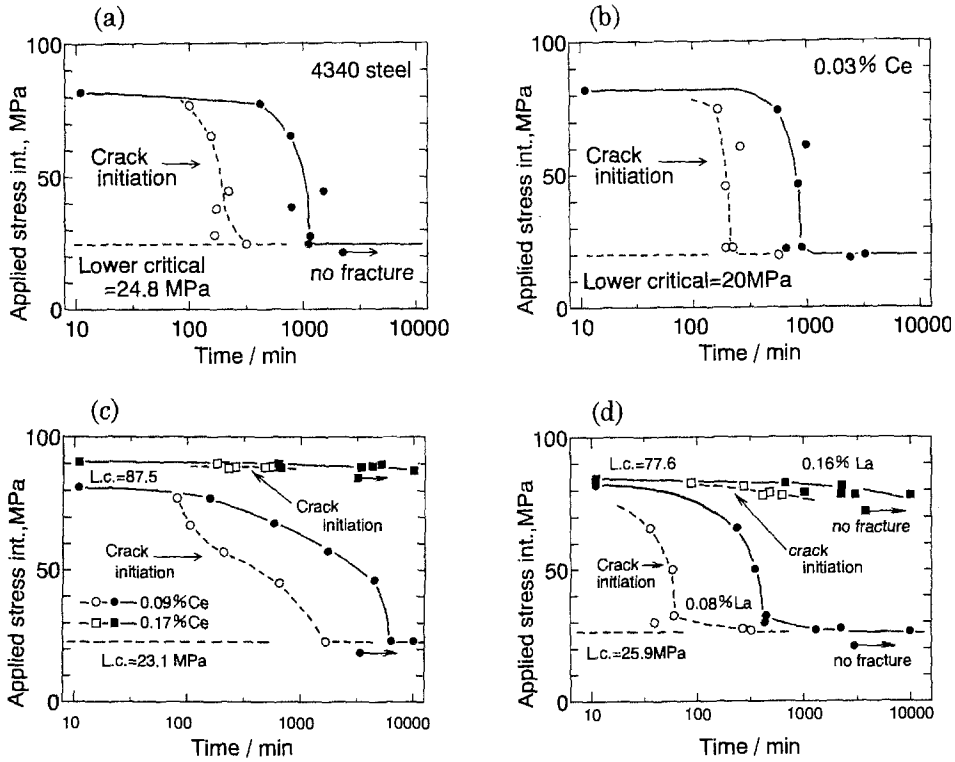

Fig. 18. Effect of rare earth additions on the delayed failure behavior of hydrogenated 4340 steel: (a) without rare earth, (b) with 0.03% Ce, (c) with 0.09 and 0.17% Ce, (d) with 0.08 and 0.16% La.

improvement over the non-rare-earth baseline material. Crack initiation times were also much higher in materials with a higher Ce or La content. More important, however, was the shape of the delayed failure curve itself. The standard type curve exhibited by the baseline in fig. 18a was characterized by a rather sudden decrease from the upper critical to the lower critical stress intensity over a fairly constant range of failure times. The significance of this behavior lies in the fact that design engineers must insure that service conditions do not exceed the lower critical stress intensity. If this value is exceeded, delayed failure from hydrogen embrittlement can be expected. For the high Ce and La content materials, however, the difference between the upper and lower critical values was substantially smaller than for the baseline, and the decrease was much more gradual. These results suggest a significant improvement in resistance to hydrogen embrittlement compared to the baseline 4340. In particular, the high Ce and La content materials can be used to a substantially higher percentage of its upper critical stress intensity without danger of delayed failure from hydrogen embrittlement. This is particularly significant for high strength steel components such as landing gears, cables and so on. Their production includes such operations as acid pickling cleaning and electroplating which can introduce hydrogen into the component.

Crack growth kinetics measured with the use of compliance gages which recorded crack opening displacements during each of the delayed failure tests revealed that the crack growth rate in the baseline 4340 and low rare earth steels was an order of magnitude faster than that exhibited by the high rare earth steels. As a first approximation, these results indicate that the safe operating life for high rare earth steel components would be considerably greater than for the baseline or low rare earth steels. This crack growth behavior can be explained on the basis of hydrogen diffusing to the crack tip, resulting in discontinuous crack growth. In the baseline material and the low rare earth steel, the transport of hydrogen was not seriously affected and thus crack propagation was not retarded.

The delayed failure results clearly indicated that a substantial improvement could be obtained in the hydrogen embrittlement resistance of 4340 steel through additions of Ce and La. This improvement was manifested by longer times to crack initiation (incubation time), longer failure times and higher values of lower critical stress intensity. Maximum improvement, however, was obtained only at the high rare earth levels (e.g. 0.16–0.17 w/o). The microstructures for these rare-earth-modified steels exhibited almost continuous grain boundary inclusion formation along prior austenite boundaries. In the high rare earth content material, the continuous grain boundary inclusions acted to entrap hydrogen, inhibiting its transport to the crack tip. Crack propagation was subsequently retarded. These observations suggest a possible mechanism to rationalize the enhanced resistance to hydrogen embrittlement exhibited by rare-earth-modified steel.

Room temperature tensile results for both uncharged and hydrogen charged material were comparative and indicated little difference between the elements. A maximum occurred in the ultimate and 0.2% yield strengths at approximately 0.1 w/o for both rare earth additions. This strengthening behavior was attributed to the deoxidizing and desulfurizing action of the rare earths.

The results shown above suggest that the ability of rare earth elements to getter or otherwise entrap hydrogen was responsible for the improved resistance to hydrogen embrittlement. That maximum improvement was obtained only at the higher rare earth levels can be rationalized by the fact that the larger amounts of Ce and La were required to effectively delay the critical value of hydrogen concentration from being reached at the crack tip. At lower rare earth levels, it was apparent that the critical hydrogen concentration was achieved in spite of the fact that certain amounts were probably entrapped en route to the crack tip.

Delayed failure test showed that, at higher rare earth levels, the threshold stress intensity (i.e., the stress intensity level below which failure did not occur) increased by a factor of about four, and the crack growth rate decreased by about an order of magnitude compared with 4340 steel without rare earth additions. This improvement was attributed to the ability of the rare earth elements to interact with hydrogen, thereby reducing the supply of hydrogen available for embrittlement and impeding the diffusion of hydrogen to the crack tip where it would accumulate and cause crack growth by local embrittlement.

The room temperature elongation, reduction of area and Charpy impact energy all, however, decreased with the addition of both Ce and La. The ductility and impact losses

in these steels were attributed to the formation of massive and continuous grain boundary inclusions which offered ideal paths for crack propagation.

4.2. *Stress corrosion cracking*

Hydrogen embrittlement has also been observed in steel structural components exposed to aqueous environments (Sheinker and Wood 1971). Termed stress corrosion cracking, this natural process can result in the failure of a component from the combined action of stress and chemical attack. It is now fairly well established that stress corrosion cracking of steels in aqueous solutions is governed, at least to some extent, by a series of electrochemical reactions at the surface which permit the entry of hydrogen into the metal (Parkins 1964).

Sheinker (1978) extended the concept of rare earth additions to high strength steels to stress corrosion cracking behavior, because this type of failure in high strength steels is believed to be a form of hydrogen embrittlement. The resistance to stress corrosion cracking for 4340 steels containing 0, 0.20 and 0.30 w/o Ce in 3.5% sodium chloride solution at room temperature was evaluated. The Ce addition had a much smaller effect on the stress corrosion cracking resistance than the Ce and La additions had on the hydrogen embrittlement cracking resistance described above. The stress corrosion cracking threshold (K_{ISCC}) was about the same for all three steels. The higher Ce (0.30%) material, however, had longer failure times and lower average crack growth rates than the lower Ce (0.20%) material. It was found that the failure times for non-Ce steel would be shorter and the average crack rates higher than those for the lower Ce steel. The difference between the effects of the rare earth additions on stress corrosion cracking and hydrogen embrittlement cracking was attributed to the difference in the source of hydrogen in the two cracking phenomena, which affects the amounts of hydrogen available for embrittlement and the processes of hydrogen transport to the tip of the crack.

4.3. *Hydrogen permeability in steels*

Sheinker (1978) conducted permeability measurements to determine whether hydrogen transport through the steel was affected by the presence of the rare earth additions, which increased the resistance to hydrogen embrittlement as well as stress corrosion cracking.

Hydrogen permeability measurements were made on 4340 steels containing 0% and 0.21% Ce. The permeability of hydrogen through membranes of these materials was determined using a cell developed by Devanathan and Stachurski (1962) containing a charging solution of 1N sulfuric acid with 20 ppm arsenic added to promote hydrogen entry. The steady state hydrogen permeation flux was measured galvanostatically (Chatterjee et al. 1978).

The half-time to reach the steady state hydrogen permeation flux, which corresponds to the apparent hydrogen diffusivity in the metal, was four times longer in the Ce-bearing steel than in the non-Ce steel in the 480 K temper condition and 2.5 times longer in the Ce-bearing steel than in the non-Ce steel tempered at 670 K. These results indicate that

the apparent hydrogen diffusivity is lower in the steel containing Ce at both tempering temperatures. However, because hydrogen permeation transients are affected by hydrogen trapping and surface reactions (Chatterjee et al. 1978, Oriani 1970), it cannot be deduced whether the Ce reduced the true (lattice) hydrogen diffusivity. Ce compounds in the steel could be potent traps for hydrogen because the rare earth elements are known to combine readily with hydrogen (Gschneidner 1961). In addition, because most of the Ce in the steel was present as oxide inclusions and solid–solid interfaces are believed to be important sites for hydrogen trapping (Oriani 1970), the inclusion–matrix interface may be a potent hydrogen trap in Ce-bearing 4340 steel. Although the surfaces of the Ce-bearing and non-Ce steel membranes were identically prepared, the electrochemical reactions at the surface of the former could be affected by the presence of Ce. Thus, hydrogen trapping and changes in surface chemistry may have been responsible for reducing the apparent hydrogen diffusivity of 4340 steel when Ce was added to this alloy.

Their results also show that the steady state hydrogen permeation flux was three to four times lower in the Ce-bearing steel than in the non-Ce steel at both tempering temperatures. Because permeability is the product of solubility and diffusivity, the effect of Ce on the steady state permeation flux could be due to its effect on either or both the hydrogen solubility and the hydrogen diffusivity in the steel. The separate effects of Ce on the solubility and the diffusivity of hydrogen in steels are not presently known, but in view of the strong affinity of the rare earth elements for hydrogen, the solubility would be expected to be increased and the diffusivity decreased by the addition of Ce to steels. Thus, the reduced hydrogen permeability in the Ce-bearing 4340 steel is probably associated with a lower hydrogen diffusivity. Hydrogen permeability has been reported to decrease slightly and hydrogen diffusivity to remain constant for a similar high strength steel when the tempering temperature was increased from 480 to 670 K (Radhakrishnan and Schreir 1967). In general, it can be concluded that the presence of Ce retarded the permeability of hydrogen through 4340 steel at both tempering temperatures. This would reduce the rate of flow of hydrogen from the bulk of the metal to the tip of the crack. Therefore, the presence of Ce would be expected to decrease the rate of hydrogen-induced crack growth and increase the delayed failure time in a high strength steel.

4.4. *Rare-earth-modified powder metallurgy steel*

As described above, it has been demonstrated that the resistance of AISI 4340 steel wrought plate to hydrogen embrittlement could be substantially improved by La and Ce additions of approximately 0.2 w/o (Kortovich 1977). The main limitation, however, in these rare-earth-modified high strength steels was the degradation of mechanical properties due to the presence of larger rare earth oxide inclusions in the microstructure. Additions of 0.16/0.17 w/o of La or Ce were desired for resistance to hydrogen embrittlement, but such high levels were undesirable due to reduced Charpy impact strength. Clearly, these studies showed that a homogeneous distribution of the rare earths and a fine size of the dispersoids are desired to optimize the improvement in resistance to hydrogen embrittlement without degradation of mechanical properties.

The powder metallurgy approach offers a means of obtaining a more uniform distribution of the rare earth elements in the steel and minimizing the formation of large rare earth oxide inclusions. In order to minimize the problems associated with a non-uniform distribution of rare earth compounds so that the benefit of rare earths could be optimized, Sheinker and Ferguson (1982) produced rare-earth-metal-treated 4340 steel bars from hydrogen-gas-atomized powder and from attrited powder by both HIP and hot extrusion. A master alloy (75%Ce–25%Ni) was added prior to atomization or during attrition. Oxygen levels of both the atomized powders and the attrited powders were higher than the desired maximum limit of 300 ppm.

The steel powders were consolidated by hot extrusion and by hot isostatic pressing (HIP), and the tensile properties and toughnesses were determined. These properties were compared with C/W properties for both 4340 baseline and rare-earth-treated 4340 steels.

The mechanical properties of the HIP consolidated powders were unacceptable, with ductility and toughness being extremely poor because of fracture along prior particle boundaries (PPB). The high oxygen levels and the low amount of deformation involved in HIP are the root of this property problem because PPB cracking provides easy crack paths.

Extruded bars for both atomized and attrited 4340 + rare earth powders have significantly superior properties in comparison to HIPed bars. Extrusion, which involves metal flow and particle deformation, effectively breaks up PPB films to enhance metallurgical bonding between particles. The result is a ductility and toughness improvement for both atomized and attrited powders. Strength levels higher than those of C/M plates are achieved, but the ductility, although improved, still falls below that of C/W values.

Extruded bars show a beneficial effect of metal flow during particle deformation. Ductility and toughness are improved as inclusions and embrittling films are broken up and strung out so that metallurgical bonding between powder particles is enhanced.

It has been demonstrated that rare-earth-treated steel can be produced by P/M techniques, but that the final oxygen level of the powder should be lowered, because rare earths are extremely reactive with oxygen, and the P/M process permits a high surface area/volume ratio to exist during processing.

5. Effect of rare earth addition on creep behavior

In the previous section, it was demonstrated that rare earth additions show excellent improving effects on the toughness, bend formability, and ductility of steels mainly by sulfide shape control and by elimination of impurities, such as S, P and hydrogen (Eyring 1964, Anderson and Spreadborough 1967). However, there is no obvious evidence that the tensile properties of steels, such as yield strength, ultimate tensile strength, and elongation and reduction of area, are significantly improved by rare earth additions. The small variation in these properties is considered to be attributed to minor processing and chemistry variations and not to rare earth additions. However, it has been reported by

several researchers that effects of rare earths addition on the tensile properties become significant at elevated temperatures, especially on creep strength.

5.1. *Cast and wrought material*

Toyoda and Endo (1995) investigated the effect of simultaneous addition of carbon (50–300 ppm) and La (0.04–0.15 mass%) on the high temperature creep characteristics of a Fe–20Cr–5Al ferritic stainless steel at 1173 K. Figure 19 shows the effect of carbon and La additions on the creep curve of this alloy. Figure 19a shows that creep life of steel without La is not prolonged significantly when the carbon concentration exceeds 150 ppm. For steel with 0.1 wt% La, however, creep life increases with an increase in carbon up to 300 ppm. For steel with 150 ppm carbon, creep life increases with increasing La content (fig. 19b). Because no precipitations, such as carbides, were found by TEM and EDX, the observed increase in creep life is considered to be due to solution strengthening. Solution strengthening at elevated temperature is mainly dependent on the elastic interaction between dislocations and solute atoms. The maximum moving velocity V_c of dislocations with the solute atmosphere is given by the equation (Cottrell 1953)

$$V_c = \frac{4D}{l_e},$$

where D is the diffusion coefficient of solute atoms and l_e the effective radius of the solute atmosphere, given by

$$l_e = \frac{4G\eta R^3}{\kappa T},$$

where G is the Young's modulus, η the size factor, R the atomic radius of the matrix and κT has its usual meaning.

They interpreted the marked effect of the simultaneous addition of carbon and La on the creep life due to the I–S (interstitial–substitutional) interaction, which forms clusters by chemical affinity around dislocations (Monma and Suto 1966). That is, carbon and La (which has a large atomic radius) form clusters with a large apparent size of the solute atmosphere around dislocations, which markedly decrease the moving velocity of dislocations by anchoring them to the atmosphere. Dislocations can move, however, by a process in which the solute atoms migrate with dislocations, and this will be controlled by the diffusion rate of the solute. The diffusion rate of La atoms is considered to be small, especially when they form clusters by the I–S interaction. Further detailed research is required on this diffusion controlled mechanism.

5.2. *Powder metallurgy material*

Oxide dispersion strengthened (ODS) alloys, which are mechanically alloyed (MA) with yttria, possess excellent mechanical properties in comparison with conventional ingot

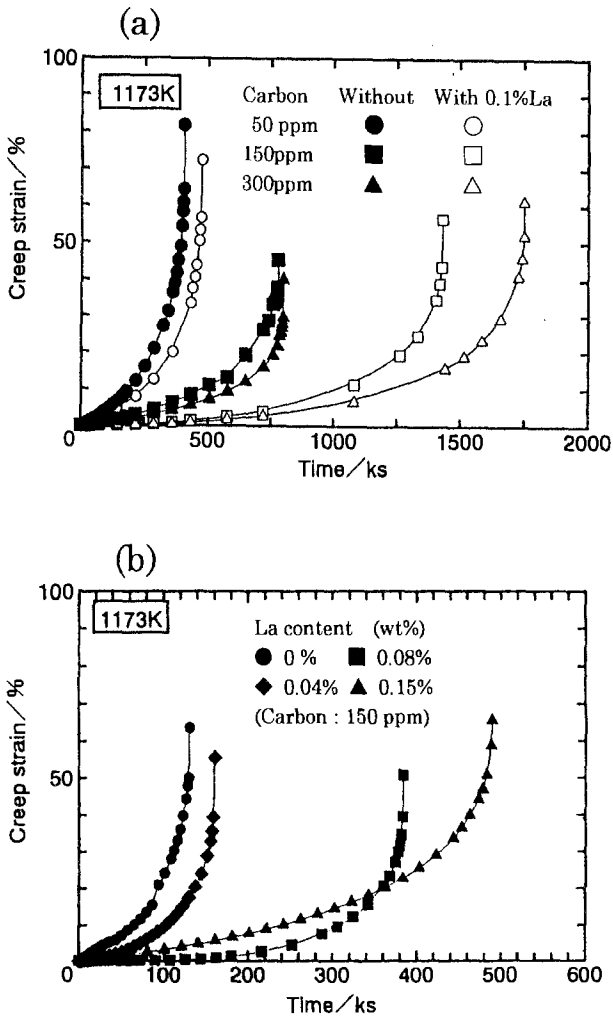

Fig. 19. Effect of simultaneous addition of rare earth with carbon on the creep behavior of Fe–20Cr–5Al ferritic stainless steel at 1173 K: (a) effect of carbon addition with and without 0.1 wt% La; (b) effect of La addition with 150 ppm carbon.

metallurgy (IM) materials at elevated temperatures even higher than 1000°C (Benjamin 1970, 1976, Curwick 1981, Hack 1984). However, recently there has been an increasing demand for powder metallurgy (PM) materials, because of lower production cost, for high temperature applications where such high strength as that of ODS alloys is not necessarily required.

There is no extensive literature dealing with mechanical properties above 800°C of the fully dense powder metallurgy (PM) materials without MA. In the PM TP304 steel consolidated by hot extrusion, Isomoto and Nagai (1995a,b) revealed that PM materials

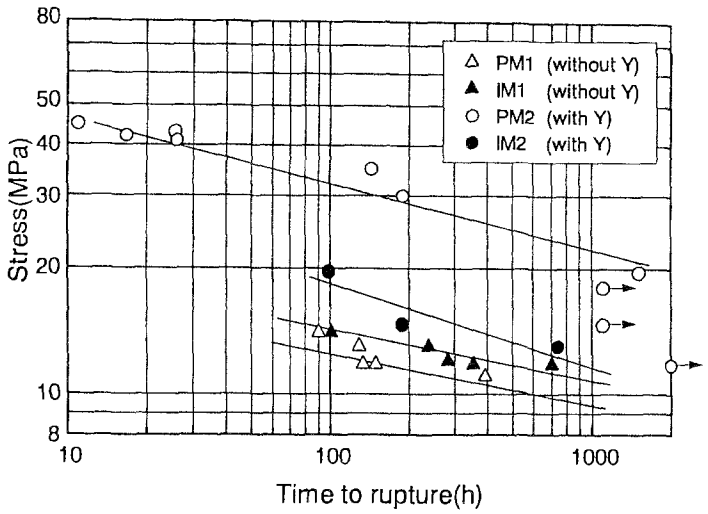

Fig. 20. Effect of yttrium addition on creep rupture lives of powder metallurgy (PM) and ingot metallurgy (IM) 304 stainless steels at 950°C.

showed shorter creep rupture life than IM materials and their creep rupture strengths decrease with increasing oxide inclusions originating mainly from oxidation of the powder. It was also shown that the kinds of oxide inclusions observed in the consolidated materials were strongly dependent on the contents of strong oxide-forming elements such as Al, Si and Mn in the melt before atomization. The mechanical behavior at elevated temperatures was affected by those kinds of oxides to a greater extent in PM materials than in IM materials (Isomoto and Nagai 1996). Isomoto et al. (1997) recently investigated the effect of yttrium addition on high temperature tensile properties and creep rupture strengths using TP304 steel fully dense materials consolidated by hot extrusion, compared to those of IM materials.

The results of creep rupture tests at 950°C under various stress levels are shown in fig. 20. It is seen that PM materials with yttrium have markedly excellent creep rupture lives compared with those of IM materials with and without yttrium and PM materials without yttrium, although the tensile strengths of PM material with yttrium are almost equivalent to those of IM material with yttrium above 800°C. It is considered that this improvement is attributed to the finer and more uniform dispersion of yttria in the PM materials than in the IM materials with yttrium.

6. Effect of rare earth additions on weldments

In recent years, there has been an increasing need for high strength steels for use in highly stressed structures, including many critical applications in aerospace and industry. Because welding is the major fabricating process employed in the construction of various

steel structures, it is imperative that a thorough understanding of the weldability of steels is developed. Performance and safety requirements in these applications dictate that weldments must be sound and of good quality. The higher strength steels, however, are generally more sensitive to both minor weldment flaws and the hydrogen embrittlement phenomenon than lower strength materials. For this reason, the fabricator of quenched and tempered steels must pay more attention to the control of welding procedures and eliminate even the smallest of defects, such as microcracks.

Most welding procedures involve the application of an intense local source of heat to the material being welded. This results in:

(1) the introduction of a rapidly cooled casting into the joint,
(2) rapid heating and cooling of the surrounding base metal,
(3) plastic straining of the material surrounding the joint during both heating and cooling, and of the weld metal during cooling,
(4) the presence of residual stresses in the joint after welding is completed.

These general effects of welding may lead to practical problems which manifest themselves either during welding, immediately following welding, or in service. The problems are:

(1) burning and hot tearing in the heat-affected zone (HAZ),
(2) hydrogen-induced HAZ cracking,
(3) HAZ cracking during heat treatment,
(4) brittle fracture,
(5) knife line attack.

It has been reported that many of these problems are significantly improved by the additions of rare earths. Although some of the mechanisms by which rare earths suppress these problems have not been fully understood, the role of rare earths in avoiding such problems is briefly reviewed in this chapter.

6.1. *Burning and hot tearing in the HAZ*

If structural steels are maintained at temperatures approaching the solidus, their fractural ductility can be permanently impaired due to the onset of a problem known as "burning". The metallurgical aspects of this problem are as follows. At high temperatures, sulfide inclusions existing in the steel may spread as eutectic films around the grain boundaries. When the steel is cooled, the liquid films solidify as sulfide films at the grain boundaries, and the fracture toughness of the steel is reduced. In this condition, the steel is said to be "burned" and its former properties cannot be recovered by heat treatment. The presence of liquid films in the grain boundaries at high temperatures introduces the risk that microcracks may be opened up under the influence of the thermal strains accompanying welding, to produce what is known as "hot tearing" or "hot cracking". This problem has been known for many years (Brammar 1963, Boniszewski and Baker 1964). Electron microprobe studies indicated a marked change in composition and morphology of the sulfide inclusions in the HAZ compared to that in the plate material. It is postulated

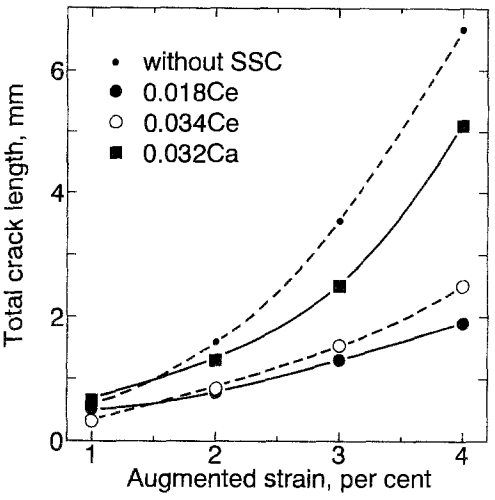

Fig. 21. Effect of Ce and Ca additions on the variation in total crack length. The symbol SSC represents sulfide shape control elements such as rare earths and Ca.

that these areas of liquation are the nuclei of microfissures which subsequently propagate because of welding strains and/or strains due to service.

The ability of residual rare earth elements in structural steels to minimize hot tearing in the HAZ has been demonstrated in studies by Emmanuel and Seng (1963), Meitzner and Stout (1966), Ratz et al. (1973), Wilson (1971).

Figure 21 shows the variation in total crack length at different Ce and Ca levels. Small amounts of Ce and Ca are beneficial for hot cracking resistance. Moreover, the resistance to cracking obtained with Ce was greater than that attained by a similar amount of Ca. The optimum amount appears to be about 0.018% Ce.

Microprobe analysis of the steels with rare earths indicate that the manganese sulfides which would otherwise fuse on heating to form film-type or work-elongated inclusions are absent and that the inclusions contained in the steel may be either rare earth oxides or rare earth sulfides, both of which are globular in nature.

It is suggested that, with rare earth elements present in the plate material, either one or both of the following mechanisms might occur to reduce microcracking and subsequent microcracking near welds:

(1) The formation of stable high melting point sulfides which float up into the slag of the heat and reduce its sulfur content.

(2) The preferential formation of globular high melting point rare earth sulfides rather than sulfur compounds of other metals (e.g., manganese) which could melt and redistribute in the fusion lines of the weld.

Thermodynamic data and melting point data of rare earth sulfides support the theory that rare earth sulfide inclusions will form and not liquate or redistribute in the HAZ near welds.

6.2. *Hydrogen-induced HAZ cracking*

Instances of cracking in the past have indicated that small amounts (less than 10 ppm) of hydrogen might be sufficient to cause cracking and that even the residual hydrogen content of the base plate and/or electrode might be troublesome in welds made under otherwise dry or hydrogen-free conditions. It was reported (Cottrell 1944) that a martensitic structure, hydrogen, residual stresses and a temperature near ambient were necessary conditions for cracking to occur.

Meitzner and Stout (1966) determined the critical hydrogen contents of the electrode necessary to cause hydrogen-induced delayed failures in highly restrained weldments of various steels. Critical levels were found to vary from 3.3 to 6.8 ppm, depending upon the materials and restraint involved. They also reported that rare earth additions show a beneficial effect in preventing hydrogen-induced delayed cracking of these steels but did not put forth a mechanism describing the nature of the role of rare earths.

It has often been suggested in the literature that small microcracks in the HAZ could serve as initiation points for delayed, hydrogen-associated cracking (Flanigan and Kaufman 1951, Flanigan and Saperstein 1956, Winterton 1957). Such proposals generally stem from the hydrogen embrittlement theories which postulate the migration of hydrogen to internal defects in the material, such as microcracks.

Because rare earths trap the hydrogen and retard the hydrogen migration, as described in sections 4.1 and 4.3, delayed hydrogen-associated cracking of weldments is considered to be suppressed by the same mechanisms. The residual hydrogen content of high-strength steel welding electrodes must be carefully controlled during processing.

6.3. *Reheat cracking*

During high temperature service or stress relief heat treatment following welding, deep cracks of an intergranular nature could be produced in the HAZ of welds in thick sectioned components. This problem is known as "reheat cracking of weldments" (Fairchild 1957, Younger and Baker 1960, 1961, Younger et al. 1963, Truman and Kirkby 1960). Welded specimens without heat treatment did not exhibit this phenomenon.

The problem of heat-treatment cracking following welding became generally recognized following the introduction of austenitic steel into electrical power plants and so on (Asbury 1960, Curran and Rankin 1957), because of its attractive high temperature strength and oxidation resistance and because its welding behavior had been very satisfactory.

Baker (1968) showed by metallographic investigation that the microstructure in the vicinity of the cracks consisted of austenitic grains containing a dense precipitate of fine niobium carbide particles, which nucleated on dislocations following aging. It was concluded that the fine precipitate stiffened the austenitic grains, allowing the creep deformation which occurred during stress relief to be concentrated at the grain boundaries. This could lead to intergranular cracking in the thicker sections. It is now clear that a

similar problem may occur in ferritic materials during stress relief following welding (Murray 1967) when these contain certain carbide-forming elements.

Fujii et al. (1981) found with an Auger spectrometer a remarkable enrichment of sulfur rather than phosphorus on the intergranular facets in the welded specimens which showed susceptibility to intergranular fracture at about 600°C. It should be emphasized that no enrichment of S and P occurred on the facet and grain boundaries of the specimens reheated under no stress. They concluded that the reduction of the dissolved sulfur content corresponded to the decrease in the susceptibility to intergranular fracture, and therefore the addition of rare earth metals to form stable sulfides is quite effective in suppressing the reheat cracking. Furthermore, they reported that the addition of 0.001–0.002% B accelerated the reheat cracking, but Ce addition suppressed the deleterious effect of B.

Nakao et al. (1986) also reported beneficial effects of rare earth metal additions on reheat cracking susceptibility of 1Cr–0.5Mo and HT80 weldments. Figure 22 shows the effect of rare earth addition on reduction of area and area fraction of intergranular fracture for HT80 and 1Cr–0.5Mo steels in hot tensile tests at 600°C. The hot ductility at 600°C of these steels was improved from approximately 10 to 80% with an increase in rare earth metal content. Moreover, any reheat cracking did not occur in 1Cr–0.5Mo steel weldment after adding 0.02–0.13 wt% rare earth metal. Both steels containing more than 0.1 wt% rare earth metal, however, were susceptible to liquation cracking due to the formation of $CeFe_2$ which has a low melting point. Therefore, the reasonable range of rare earth metal content for preventing reheat cracking was from approximately 0.02 to 0.05–wt% in these steels. They concluded that the reason why rare earth metal improved reheat cracking susceptibilities of these steels was the reduction of grain boundary segregation of impurity elements such as P, S, etc., due to the scavenging effect of the rare earth metal.

6.4. *Brittle fracture*

Increasing the chromium level of iron–chromium alloys increases resistance to oxidation, chloride corrosion and stress corrosion cracking (Rocha and Lennartz 1955, King and Uhlig 1959, Steigerwald 1966). However, the application of high chromium ferritic stainless steels has been severely limited by their poor weldability (Demo 1974, Sawhill and Bond 1976, Pollard 1972). Welding of ferritic stainless steels is reported to cause severe embrittlement (Demo 1974), and the ductility and toughness of ferritic stainless steels are reported to be improved by lowering the carbon and nitrogen. The tolerance for both is 0.03–0.06 wt% depending on the composition of the steels (Binder and Spendelow 1951, Gregory and Knoth 1970).

The increases in nitrogen and oxygen in the weld metal cause the precipitation of fine intergranular chromium nitrides and spherical oxide inclusions of more than 1 μm diameter, which induce the embrittlement of the weld metal. Carbides and nitrides can precipitate upon cooling (Hochmann 1951, Baerlecken 1961, von Bungardt et al. 1958, Plumtree and Gullberg 1976, Grubb and Wright 1979). The preferred locations for

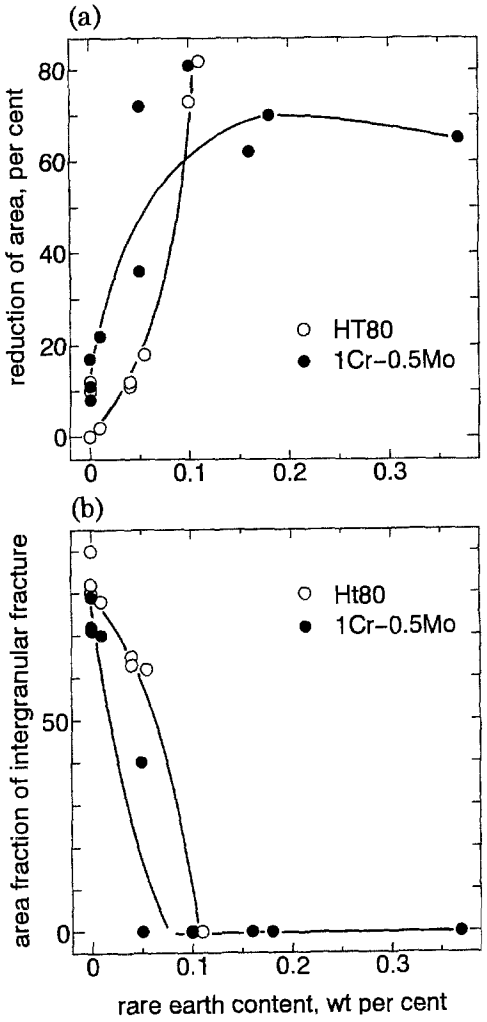

Fig. 22. Effect of rare earth content on reduction of (a) area and (b) area fraction of intergranular fracture region on hot tensile test at 600°C.

precipitates are high energy sites such as grain boundaries where they may be expected to have a strong influence on the ductility of the material.

Nakao et al. (1981) and Nakao and Nishimoto (1984) investigated the effect of rare earth additions on the weld toughness using Charpy V-notch specimens of high purity 19Cr–2Mo and 30Cr–2Mo steels welded in argon shielding gas with various amounts of nitrogen, oxygen and air. They reported that contamination by air, oxygen and/or nitrogen in the shielding gas drastically deteriorates the toughness of the weld metal due to the pick-up of nitrogen and oxygen and that the weld toughness is significantly improved by rare earth addition. As a typical example, fig. 23 shows the transition curves of Charpy absorbed energy for 19Cr–2Mo steel welded in argon and Ar+0.5% air shielding gas.

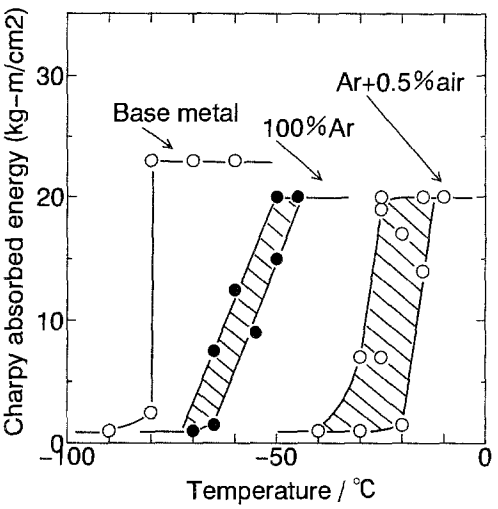

Fig. 23. Effect of welding atmosphere on transition curves of Charpy absorbed energy of 19Cr–2Mo steel.

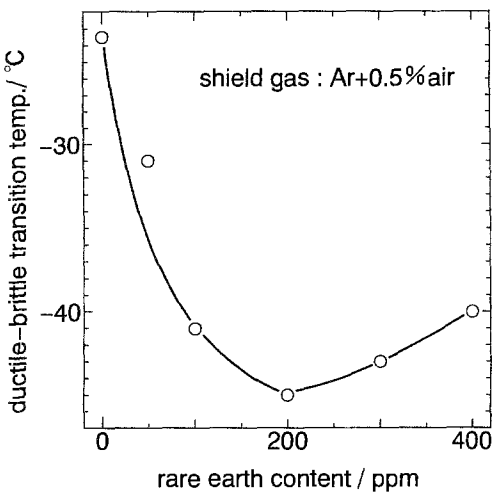

Fig. 24. Effect of rare earth content on the ductile–brittle transition temperature of 19Cr–2Mo steel welded in Ar + 0.5% air.

It is clear from this figure that the ductile–brittle impact transition temperatures ($_{V}T_{E}$) increase with increasing air content in the argon shielding gas. Figure 24 shows the effect of rare earth addition on the ductile–brittle impact transition temperature for 19Cr–2Mo steels welded in Ar + 0.5% air. $_{V}T_{E}$ decreases with increasing rare earth content, and the effective rare earth content ranges from 100 to 400 ppm when the amount of air in the shielding gas is less than 1%. They concluded that the absorption rate of nitrogen and oxygen in the rare-earth-bearing weld metal seems to decrease due to the formation of the rare earth oxide film or the rare-earth-absorbed layer on the surface of the molten pool (Belton 1972). Consequently, the amounts of nitrogen and oxygen picked-up in the weld metal decrease, which results in improving the weld toughness.

The low ductility of these ferritic weld steels has also been attributed to their large grain size, because grain refinement can be produced only by working and recrystallization due to the absence of a phase transformation. As described above, the addition of rare earths is very effective on grain refinement (see section 3.3); therefore, some of the improvement in weld ductility may be attributed to their grain refinement effect.

6.5. *Knife line attack*

The susceptibility of austenitic stainless steels to intergranular corrosion is well-known. The hypothesis most widely accepted to explain sensitization of stainless steel is the chromium impoverishment theory (Bain et al. 1933). This theory postulates the formation of cubic chromium carbide, $Cr_{23}C_6$, when the material is heated between 427 and 760°C for a sufficient length of time. Under normal conditions, the formation of the chromium carbide occurs along grain boundaries. Thus, the chromium content of the material adjacent to the grain boundary is supposedly lowered so that this area no longer contains sufficient chromium. Hence, the chromium-depleted area is susceptible to attack by certain corrosive media, and intergranular corrosion occurs.

One of the preferred methods for preventing sensitization in stainless steels consists of the addition of an element that has a greater tendency than chromium to combine with carbon. This method is commonly known as "stabilization" (Houdremont and Schafmeister 1933). The two elements most commonly used are niobium and titanium. Tantalum also possesses carbide-forming properties similar to those of niobium.

Even in these stabilized steels, however, serious intergranular corrosion occurs in the narrow region immediately adjacent to the weld metal and sometimes gives rise to failures of the welded joints. This peculiar and somewhat unsuspected type of corrosion is designated as "knife line attack". In the stabilized steels, granular TiC and Nb(C,N) are formed in the matrix. If the welded joints are subsequently heat-treated at sensitizing temperature (~650°C), a ditch caused by knife line attack is observed in the HAZ adjacent to the weld metal. Microstructural observation shows that $Cr_{23}C_6$ precipitates so as to enclose the grain boundaries in the HAZ where TiC or Nb(C,N) has dissolved during welding, depleted zones of Cr are formed along the grain boundaries and the corrosion resistance in this region deteriorates. If the welded joints are exposed to corrosive circumstances, the intercrystalline corrosion locally occurs in the HAZ adjacent to the weld metal and consequently, a sharp ditch is formed there. Welded specimens without reheat treatment did not exhibit this phenomenon (Scheil 1950, Helzworth et al. 1951).

It is reported that addition of rare earths to SUS304, SUS321 and SUS347 was effective in reducing the precipitation of $M_{23}C_6$ during sensitizing heat treatment and in improving intercrystalline corrosion resistance (Ikawa et al. 1977). Figure 25 shows the knife line attack sensitivities of rare-earth-bearing SUS321 (a) and SUS 347 (b), sensitized at 650°C for 50 h. As shown in this figure, knife line attack sensitivities in both steels considerably decreased due to addition of 0.1–0.15% rare earth metals. An excess of rare earths, however, is rather ineffective in improving the knife line attack sensitivity. From the microstructural observation, they concluded that the improvement in knife line attack

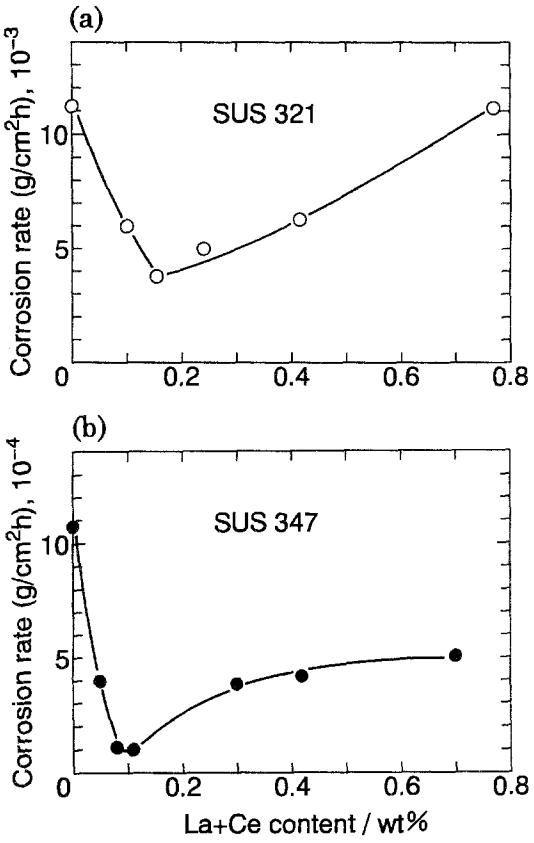

Fig. 25. Effect of rare earth addition on the knife line attack sensitivity of (a) SUS321 and (b) SUS347.

sensitivities by addition of rare earths is due to the decrease in $M_{23}C_6$ precipitated at γ grain boundaries, caused by the accelerated precipitation of MC type carbides in the matrix. However, they did not explain the reason why the rare earth additions suppress the precipitation of $M_{23}C_6$ carbide and accelerate the formation of the MC carbide.

6.6. *Arc weldability*

Steels with sulfide shape control (SSC) elements, such as rare earth metals, have greatly improved ductility and impact strength properties in the transverse direction, and reduced susceptibility to hydrogen-induced cracking and lamellar tearing of the weldments, as described above (see sections 3.2 and 6.2, respectively) (Hasegawa et al. 1965, Seriu and Koshino 1980, Savage et al. 1978). Because welding is the major fabricating process employed in the construction of many structures and parts, it is imperative that understanding of the role of SSC elements in the weldability of steels be developed.

Ratz et al. (1973) investigated the weldability of line pipe and high strength low alloy steels treated with Ca, rare earth metals and Te. In order to determine the effects of additions of the aforementioned SSC elements on the following behavior:

(1) arcing behavior (arc voltage, arc length and so on),

(2) fusion zone geometry (volume, depth and width of the weld crater, etc.).

It is reported that the addition of rare earths and Ca decreased the average depth and pool volume of the weld crater (Matsuyama and Akahide 1979). Compared to steel without SSC elements, additions of either Ca or Ce decreased arc voltage and increased arc length. The extent of the changes appeared to be somewhat greater with Ce than Ca. However, a steel with 0.034% Ce showed results comparable to that of a steel with 0.018% Ce. This indicates that larger additions did not exacerbate this tendency.

Ratz et al. (1973) explained that these effects could be attributed primarily to the lower values of the work function and ionization potential of these elements and their oxides. Examination of the ionization potential values of the alloying elements present in the steels shows that the ionization potentials of Ca and the rare earths are much lower than those of the other elements in the steel.

The arc length is also an important factor because the heat lost through radiation from the plasma is considerable. With longer arc lengths, there is less heat transfer to the material. Therefore, the addition of Ca and Ce causes a decrease in fusion zone dimensions and a reduction in arc voltage.

Others have observed the formation of oversized drops on the electrode tip when welding steels containing Ca or Ce (Matsuyama and Akahide 1979, Ludwig 1968, Chase 1971, Sasaki et al. 1976). At high Ce contents there was some deterioration in bead appearance; however this change in appearance could not be considered detrimental. The data in the literature (Agusa et al. 1981) suggest that Ca or rare earth additions to steels should not present any significant adverse welding problems, when welding steel relatively low in Ca or rare earths (0.06%).

These general effects of welding may lead to practical problems which manifest themselves either during welding, immediately following welding, or in service, through the development of either cracks or of mechanical properties inferior to those of the base metal, or both. In considering the welding behavior or "weldability" of different materials, it should be recognized that, although welding problems may manifest themselves in the same general way (i.e., as cracks or inferior properties), they may arise for a number of different reasons. For example, some problems, such as burning and hot tearing in steels, may occur at elevated temperatures during welding; others, such as hydrogen-induced cold cracking, may occur at low temperatures following welding; others, such as heat-treatment cracking, may occur during stress relief or in service following welding. Welding behavior or weldability then depends upon the susceptibility of the base metal to a number of specific potential welding problems, each of which may be influenced by different metallurgical factors. There are thus no grounds for expecting that weldability can be defined as though it were a unique material property, and it is very unlikely that any single test can provide adequate means of assessment.

7. Summary

In this review, practical examples of improvements in the properties of steels achieved by rare earth additions, and the fundamentals to understand the cause of these improvements have been discussed.

In spite of the progress so far in understanding the influence of rare earth additions on the physical, chemical and mechanical properties of steels, it is apparent that many questions remain unanswered.

For example, although many reports revealed that the rare earth additions change the shape, size and composition of non-metallic inclusions formed in the steels and that they play a very important role in improving the various properties of steels, research is still not adequate. Thermodynamic data are still too scattered to accurately predict these characteristics of non-metallic inclusions and the conditions under which the shape, size and composition of inclusions are controlled. Data for the effects of rare earths on the surface and interfacial properties; surface tension, contact angle, etc., of steels, are also unsatisfactory. Precise solubilities of rare earths in molten and solid iron and steels are still not available. Studies are also required on the nucleation process of the non-metallic inclusions themselves in the steels. Knowledge of all of these is essential to understand the metallurgical process and the various properties of steels.

References

Abson, D.J., 1989, Weld. World **27**(3/4), 11.

Ackert, R.J., and P.A. Crozier, 1973, Paper presented at the 12th Annual Conf. of Metallurgists, Canadian Inst. Min. Metall. (Quebec City, August).

Agusa, K., N. Nishiyama and J. Tuboi, 1981, Met. Constr. **13**, 570.

Akhmatov, Yu.S., K.P. Bunin and Yu.N. Taran, 1972, Smachivaemost. Poverkh, Svoistva Rasplavov Tverd. Tel., p. 250; Chem. Abstr. 34154z (August).

Akila, R., K.T. Jacob and A.K. Shuukla, 1987, Metall. Trans. B **18**, 163.

Anderson, E., and J. Spreadborough, 1967, Rev. Met. **64**, 177.

Arrowsmith, J.M., 1968, BISRA Rep. SNW(C)/E. 7/21, August.

Asbury, F.E., 1960, Br. Weld. J. **7**, 667.

Baerlecken, E., 1961, Stahl Eisen **81**, 768.

Bain, E.C., R.H. Aborn and J.J. Rutherford, 1933, Nature and prevention of intergranular corrosion of austenic steels, Trans. Am. Soc. Steel Treat. **21**, 481.

Baker, H.R., and C.R. Singleterry, 1972, Corrosion **28**, 340, 384.

Baker, R.G., 1968, Weld. J. **47**, 323S.

Ballance, J.B., and R.E. Mintus, 1972, Paper presented at the AIME Conf. of Mechanical Working and Steel Processing, Chicago.

Ban-ya, S., and S. Matoba, 1962, Tetsu To Hagane **48**, 925.

Barin, I., 1989, Thermochemical Data of Pure Substances, ed I. Barin (VCH Verlagsgesell. mbH, Weinheim).

Basutkar, P.K., and C.R. Loper Jr, 1971, Trans. Am. Foundrymen's Soc. **79**, 176.

Bates, J.F., 1970, Mater. Prot. **9**, 27.

Beaudry, B.J., and K.A. Gschneidner Jr, 1978, in: Handbook on the Physics and Chemistry of Rare Earths, Vol. 1, ed K.A. Gschneidner Jr and L. Eyring (North-Holland, Amsterdam) ch 2.

Beck, W., and E.J. Jankowsky, 1960, Proc. Am. Electroplaters' Soc. **47**, 152.

Beck, W., P.K. Subramanyan and F.S. Williams, 1971, Nav. Air Devel. Center Rep. NADC-MA-7140, Dec. **23**, 195.

Belton, G.R., 1972, Metall. Trans. **3A**, 1465.

Benjamin, J.S., 1970, Metall. Trans. **1**, 2943.

Benjamin, J.S., 1976, Sci. Am. **234**, 40.
Bernard, P.G., 1967, Rept. Inv. No. 6907 (U.S. Bureau of Mines).
Bernstein, I.M., and A.W. Thompson, 1974, Hydrogen in Metals (American Society of Metals, Metals Park, OH).
Bernstein, I.M., and A.W. Thompson, 1976, Int. Metall. Rev., Dec., p. 269.
Binder, W.O., and H.R. Spendelow, 1951, Trans. Am. Soc. Met. **43**, 759.
Bingel, C.J., and L.V. Scott, 1973, AIME Electric Furnace Conf. **31**, 171.
Boniszewski, T., and R.G. Baker, 1964, J. Iron. Steel. Inst. London **202**, 921.
Bramfitt, B.L., 1970, Metall. Trans. **1**, 1987.
Brammar, I.S., 1963, J. Iron Steel Inst. London **201**, 752.
Brewer, G.E.F., 1974, Met. Finish., Aug., p. 49.
Breyer, N.N., 1973, AIME Electric Furnace Conf. **31**, 162.
Bucher, J.H., G.C. Duderstadt and K. Piene, 1969, J. Iron Steel Inst. London **207**, 225.
Buhr, R.K., 1971, Trans. Am. Foundrymen's Soc. **79**, 247.
Cain, W.M., and A.R. Troiano, 1965, Pet. Eng., May, p. 78.
Carter, C.S., 1972, Metall. Trans. **3**, 584.
Chase, T.F., 1971, Weld. J. **50**, 467.
Chatterjee, S.S., B.G. Ateya and H.W. Pickering, 1978, Metall. Trans. A **9A**, 389.
Chernov, B.G., 1983, Iz. Vuz. Chem. Metall. **6**, 4.
Chipman, J., and J.F. Elliott, 1963, Electr. Furn. Steelmak. **11**, 133.
Chistyakov, S.L., E.D. Mokhir and S.K. Filatov, 1966, Stal' **2**, 1041.
Church, N.L., 1973, Trans. Am. Foundrymen's Soc. **81**, 301.
Cotterill, P., 1961, The hydrogen embrittlement of metals, Prog. Mater. Sci. **9**, 205.
Cottrell, A.H., 1944, Trans. Inst. Weld. London **7**, 54.
Cottrell, A.H., 1953, Dislocations and Plastic Flow in Crystals, Clarendon Press, Oxford.
Curran, R.M., and A.W. Rankin, 1957, Trans. ASME **79**, 1398.
Curwick, L.R., 1981, in: Frontiers of High Temperature Materials, ed. J.B. Benjamin (International Nickel Company, Inc.) p. 3.
Dahl, W., T.E. Gammal and L.L. Aachen, 1973, Arch. Eisenhuettenwes. **44**, 843.
Demo, J.J., 1974, Metall. Trans. **5A**, 2253.
Devanathan, M.A.V., and Z.O.J. Stachurski, 1962, Proc. R. Soc. London Ser. A **270**, 90.
Double, D.D., and A. Hellawell, 1969, Acta. Met. **17**, 1071.
Dubinin, N.P., and Yu.F. Abakumov, 1972, Chem. Abstr. 130331p.
Eick, H.A., 1958, J. Am. Chem. Soc. **80**, 43.
Ejima, A., K. Suzuki, N. Harada and K. Sanbongi, 1975, Tetsu To Hagane **61**, 2784.
Elliott, J.F., and M. Gleiser, 1960, Thermochemistry for Steelmaking, Vol. 1 (Addison-Wesley, Reading, MA) p. 258.
Emmanuel, G.N., and J.L. Seng, 1963, Nobs-84169, Final Summary, Report No.564, Jan. 11.
Etelis, L.S., M.I. Gladkov, E.N. Kurteev, D.Z. Ryabova and G.F. Slasyuk, 1974, Liteinoe Proizvod. **10**, 40.
Eyring, L., 1964, Progress in the Science and Technology of the Rare Earths, 2 volumes (Pergamon Press/Macmillan, New York).
Fairchild, F.P., 1957, Trans. ASME **79**, 1371.
Faircloth, R.L., R.H. Flowers and F.C.W. Pummery, 1968, J. Inorg. Nucl. Chem. **30**, 499.
Fast, J.D., 1965, Interaction of Metals and Gases (Academic Press, New York).
Fischer, W.A., and H. Bertram, 1973, Arch. Eisenhuettenwes. **44**, 87.
Flanigan, A.E., and M. Kaufman, 1951, Weld. J. **30**, 193S.
Flanigan, A.E., and Z.P. Saperstein, 1956, Weld. J. **35**, 541S.
Folkhard, E., H. Schabereiter, G. Rabensteiner and H. Tettenbacher, 1972, L'Hydrogene dans les Métaux, p. 501.
Fujii, T., K. Yamamoto and M. Ueno, 1981, Tetsu To Hagane **67**, 1523.
Fukatsu, N., N. Shidawara and Z. Kozuka, 1985, J. Electrochem. Soc. **132**, 2258.
Funakoshi, T., T. Tanaka, S. Ueda, M. Ishikawa, N. Koshizuka and K. Kobayashi, 1977, Tetsu To Hagane **63**, 303.
Glikman, L.A., and V.A. Orlov, 1968, Soc. Mat. Sci. **4**, 106.
Gokcen, N.A., and J. Chipman, 1952, J. Met. **4**, 171.
Grayson, M., ed., 1985, Kirk-Othmer, Concise Encyclopedia of Chemical Technology, (Wiley-Interscience, New York).
Gregory, E., and R. Knoth, 1970, Met. Prog. **97**, 114.
Grevillius, N.F., L.E. Carlsson and L. Hellner, 1971, Neue Huette **16**, 72.
Grubb, J.F., and R.N. Wright, 1979, Metall. Trans. **10A**, 1247.

Gschneidner Jr, K.A., 1961, Rare Earth Alloys (Van Nostrand, Princeton, NY).
Gschneidner Jr, K.A., 1969, J. Less-Common Met. **17**, 1.
Gschneidner Jr, K.A., 1990, Met. Mater. Proc. **1**, 241.
Gschneidner Jr, K.A., and N. Kippenhan, 1971, Thermochemistry of rare earth carbides, nitrides and sulfides for steelmaking, Report IS-RIC-5 (Rare Earth Information Center, Iowa State University, Ames, IA).
Gschneidner Jr, K.A., and M.F. Verkade, 1974, Selected cerium phase diagrams, Report IS-RIC-7 (Rare Earth Information Center, Iowa State University, Ames, IA).
Gschneidner Jr, K.A., N. Kippenhan and O.D. McMasters, 1973, Thermochemistry of rare earths, Report IS-RIC-6 (Rare Earth Information Center, Iowa State University, Ames, IA).
Hack, G.A.J., 1984, Powder Metall. **27**, 73.
Hartley, S.B., and M. Henderson, 1973, Ger. Pat. 2 234 324.
Hasegawa, M., M. Sano and I. Tanabe, 1965, Tetsu To Hagane **51**, 1162.
Helzworth, M.L., F.H. Beck and M.G. Fontana, 1951, Corrosion **7**, 441.
Hilty, D.C., ed., 1967, Electric Furnace Steelmaking, Vol. 2, (AIME, New York) p. 43.
Hinton, B.W., 1995, in: Handbook on the Physics and Chemistry of Rare Earths, Vol. 21, eds K.A. Gschneidner Jr and L. Eyring (Elsevier, Amsterdam) ch. 140.
Hirshhorn, I.S., 1968, Use of mishmetal in steels, Ronson Report.
Hochmann, J., 1951, Rev. Metall. **48**, 734.
Hofmann, W., and W. Rauls, 1961, Arch. Eisenhuettenswes. **32**, 169.
Hong, J.H., 1971, Kumsok Hakhoe Chi, 9, 149; Chem. Abstr. 78206f (Sept. 1972).
Honma, H., S. Ohkita, M. Wakabayashi and S. Matsuda, 1986, Tetsu To Hagane 72, s625.
Houdremont, E., and P. Schafmeister, 1933, Arch. Eisenhuettenwes. **7**, 187.
Hunter, M.H., and G.A. Chadwick, 1972, J. Iron Steel Inst. **210**, 117.
Ikawa, H., Y. Nakao and K. Nishimoto, 1977, Trans. Jpn. Weld. Soc. **8**, 9.
Ishikawa, R., H. Inoue and K. Sanbongi, 1973, Dressing and metallurgy (Tohoku University); Bull. Res. Inst. Mineral **29**, 193.
Isomoto, T., and H. Nagai, 1995a, J. Jpn. Powder Powder Met. **42**, 616.
Isomoto, T., and H. Nagai, 1995b, J. Jpn. Powder Powder Met. **42**, 1350.
Isomoto, T., and H. Nagai, 1996, J. Jpn. Powder Powder Met. **43**, 1147.
Isomoto, T., T. Kida and H. Nagai, 1997, Scr. Metall. **36**, 305.
Ito, Y., and M. Nakanishi, 1975, J. Jpn. Weld. Soc. **44**, 815.
Ivanov, D.P., 1972, Liteinoe Proizvod. **8**, 24.
Iwata, Y., H. Tada, T. Niimi, M. Miura and H. Nagata, 1976, Tetsu To Hagane 62, A37, 1419.
Jackson, R.S., 1973, J. Iron Steel Inst. **211**, 375.
Johnson, H.H., J.G. Morlet and A.R. Troiano, 1958, Trans. AIME **212**, 528.
Kepka, M., Z. Kletecka and K. Stransky, 1973, Neue Huette **18**, 200.
King, P.F., and H.H. Uhlig, 1959, J. Phys. Chem. **63**, 2026.
Kinne, G., A.F. Vishkarev and V.I. Yavoiskii, 1963, Izv. Vyssh. Uchebn. Zaved. Cher. Metall. **5**, 65.
Kippenhan, N., and K.A. Gschneidner Jr, 1970, Rare earth metals in steels, March, Report No. IS-RIC-4 (Rare Earth Information Center, Iowa State University, Ames, IA).
Kortovich, C.S., 1977, TRW Tech. Report ER-7814-2.
Kudryavtsev, V.N., K.S. Pedan, N.K. Baraboshkina and A.T. Vagramyan, 1972, L'Hydrogene dans les Métaux, p. 253.
Kumar, R.V., and D.A.R. Kay, 1985, Metall. Trans. B **16**, 287.
Kusagawa, T., and T. Ohtani, 1965, Tetsu To Hagane **51**, 1987.
Lagneborg, R., 1969, J.I.R.S.I. **207**, 363.
Langenberg, F.C., and J. Chipman, 1958, Trans. Met. Soc. AIME **212**, 290.
Leary, R.J., R.T. Coulehan, H.A. Tucker and W.G. Wilson, 1968, R.I. 7091, March (U.S. Department of Interior, Bureau of Mines) p. 28.
Lichy, E.J., G.C. Duderstadt and N.L. Swamways, 1965, J. Met. **17**, 769.
Lillieqvist, G.A., and C.G. Mickelson, 1952, J. Met. **4**, 1024.
Little, J.H., and W.J.M. Henderson, 1971, Proc. Conf. Iron Steel Inst. (London), p. 182.
Lu, W.K., and A. McLean, 1974a, Ironmaking Steelmaking **1**, 228.
Lu, W.K., and A. McLean, 1974b, Met. Mater., Oct., p. 452.
Ludwig, H.C., 1968, Weld. J. **47**, 234.
Lux, B., 1970, Giessereiforschung **22**, 161.

Luyckx, L., and J.R. Jackman, 1973, AIME Electr. Furn. Conf. **31**, 175.

Luyckx, L., J.R. Bell, A. McLean and M. Korchysky, 1970, Metall. Trans. **1**, 3341.

Matsuoka, T., and Y. Ohmori, 1972, Jpn. Patent 7109537; Chem. Abstr. 27487v.

Matsuyama, J., and K. Akahide, 1979, Report UTR 79024 (Kawasaki Steel Corporation).

McCoy, R.A., 1974, in: Hydrogen in Metals, eds I.M. Bernstein and A.W. Thompson (ASM) p. 169.

McEowan, L.J., and A.R. Elsea, 1965, Corrosion **21**, 28.

Meitzner, C.F., and R.D. Stout, 1966, Weld. J. **45**, 393S.

Millis, M.D., A.P. Gagnenebin and N.B. Pilling, 1949, U.S. Patent 2485760 (Oct.)

Miska, K.H., 1972, Mater. Eng. **76**, 58.

Moeckel, W.E., 1969, Propulsion systems for manned exploration of the solar system, NASA Techn. Memo. X-1864 (NASA, Washington, D.C.).

Monma, K., and H. Suto, 1966, J. Jpn. Inst. Met. **30**, 558.

Mori, N., H. Honma, M. Wakabayashi and S. Okita, 1981, J. Jpn. Weld. Soc. **50**, 174.

Morozof, I.F., and G.E. Goranskii, 1973, Chem. Abstr., 117496.

Morrogh, H., 1949, U.S. Patent 2488511 (Nov.)

Morrogh, H., 1952, Trans. Am. Foundrymen's Soc. **60**, 439.

Morrogh, H., 1958, U.S. Patent 2841488 (Jul.)

Morrogh, H., and W.J. Williams, 1974, J. Iron Steel Inst. **155**, 321.

Mrdjenovich, R., S.M. Kaufman, T.J. Whalen and C.L. Corey, 1970, Metall. Trans. **1**, 2175.

Murray, J.D., 1967, Br. Weld. J. **14**, 447.

Nakanishi, M., Y. Komizo, I. Seta, M. Nakamura and Y. Saitoh, 1983, Sumitomo Met. Industry Rep. **35**, 133.

Nakao, Y., and K. Nishimoto, 1984, Q. J. Jpn. Weld. Soc. **2**, 325.

Nakao, Y., K. Nishimoto and M. Terashima, 1981, J. Jpn. Weld. Soc. **50**, 508.

Nakao, Y., K. Shinozaki and K. Kuriyama, 1986, Q. J. Jpn. Weld. Soc. **4**, 741.

Narita, K., A. Miyamoto and E. Takahashi, 1964, Tetsu To Hagane **50**, 2011.

Nuri, Y., O. Kitamura and T. Hiromoto, 1976, Tetsu To Hagane 62, S462.

Nuri, Y., T. Ohashi, T. Hiromoto and O. Kitamura, 1982, Trans. Iron Steel Inst. Jpn. **22**, 399.

Ohashi, T., T. Hiromoto, H. Fujii, Y. Nuri and K. Asano, 1976, Tetsu To Hagane **62**, 614.

Ohno, Y., Y. Okamura, S. Matsuda, K. Yamamoto and T. Mukai, 1987, Tetsu To Hagane **73**, 1010.

Oldfield, W., and M. Kangilaski, 1971, Trans. Am. Foundrymen's Soc. **79**, 455.

Oriani, R.A., 1970, Acta Met. **18**, 147.

Parkins, R.N., 1964, Met. Rev. **9**, 201.

Pirogov, N.A., S.A. Bliznyukov and Yu.V. Kryakovskii, 1971, Fiz. Khim. Poverkh. Yavlenii Vys. Temp. **106**; Chem. Abstr. (Jan. 1973), 6971r.

Plumtree, A., and R. Gullberg, 1976, Metall. Trans. **7A**, 1451.

Pollard, B., 1972, Weld. J. **51**, 223S.

Prochovnick, A., 1958, Metallurgical applications of the rare earths, Davison Chemical Co. Report.

Puzyrev, A.V., D.Ya. Povolotskii, A.I. Strogamov and M.A. Ryss, 1970, Izv. Vyssh. Uchebn. Zaved. Chem. Metall. **13**, 14.

Radhakrishnan, T.P., and L.L. Schreir, 1967, Electrochem. Acta **12**, 889.

Raman, A., 1976, Z. Metallkd. **67**, 780.

Ratz, G.A., W.H. Baek, J. Mathew and E.F. Nippoes, 1973, in: Conf. on Effects of Residual, Impurity and Microalloying Elements on Weldability and Weld Properties (London, Nov.) p. 356.

Reynolds, J.A., and C.R. Tottle, 1951, J. Inst. Met. **80**, 1328.

Ricks, R.A., P.R. Howell and G.S. Barrite, 1982, J. Mater. Sci. **17**, 732.

Rocha, H., and G. Lennartz, 1955, Arch. Eisenhuettenwes. **26**, 117.

Rostovtsev, L.I., and O.S.N. Obrazov, 1968, Liteinykh Spiavov, Tr. Soveshch. Teor. Liteinykh Protessov, 14th, p. 250; in: Chem. Abstr. May, 1971, 90036w.

Rowntree, G., R.T. Weiner and B. Mickelthwaite, 1973, J. Iron Steel Inst. **211**, 83.

Rusel, J.V., 1954, J. Met. **6**, 438.

Ryan, N.E., 1995, in: Handbook on the Physics and Chemistry of Rare Earths, Vol. 21, eds K.A. Gschneidner Jr and L. Eyring (Elsevier, Amsterdam) ch. 141.

Sakuraya, T., T. Emi, Y. Habu, A. Ejima and K. Sanbongi, 1976, Tetsu To Hagane **62**, 1653.

Sasaki, H., K. Akahide and J. Tsuboi, 1976, Trans. Jpn. Weld. Soc. 7, 18.

Savage, W.F., E.F. Nippes and F.J. Zanner, 1978, Weld. J. **57**, 201S.

Sawai, T., M. Wakoh and S. Mizoguchi, 1996, Tetsu To Hagane **82**, 687.

Sawhill Jr, J.M., and A.P. Bond, 1976, Weld. J. **55**, 33S.
Scheil, M.A., 1950, Met. Prog. **32**, 699.
Schenck, H., and W. Pfaff, 1961, Arch. Eisenhuettenwes. **32**, 741.
Schinderova, V., and Z. Buzek, 1965, Sb. Ved. Prac. Vys. Sk. Banske Ostrave **11**, 3.
Schwartz, J.H., and J.J. Ward, 1968, Direct energy conversion, NASA SP-5057 (NASA, Washington, D.C.).
Selcuk, E., and D.H. Kirkwood, 1973, J. Iron Steel Inst. **211**, 134.
Seriu, N., and T. Koshino, 1980, Nippon Steel Co., 61st Annual Meeting, p. 13.
Sharan, R., J.L. Gaindhar and R. Narayan, 1969, Trans. Indian Inst. Met. **22**, 57.
Sheinker, A.A., 1978, TRW Tech. Report No. ER-7814-3, prepared for ONR Contract No. N00014-74-C-0365.
Sheinker, A.A., and B.L. Ferguson, 1982, Met. Hydrogen Syst. p. 309.
Sheinker, A.A., and J.D. Wood, 1971, in: Stress Corrosion Cracking of Metals, ASTM STP 518, Oct. 16, ch. 2.
Sidorenko, R.A., 1971, Poluch. Svoitsva Primen Chuguno Sharovid Grafitom, 37; Chem. Abstr. 22118c.
Sims, C.E., 1959, Trans. AIME **215**, 367.
Singleton, R.H., 1959, Trans. Met. Soc. AIME **215**, 675.
Smialowski, M., 1962, Hydrogen in Steel (Addison-Wesley, Reading, MA).
Speller, F.N., 1951, Corrosion, Causes and Prevention, 3rd Ed. (McGraw-Hill, NY) p. 320.
Steigerwald, E.A.F., W. Schaller and A.R. Troiano, 1959, Trans. AIME **215**, 1048.
Steigerwald, R.F., 1966, Corrosion **22**, 107.
Suzuki, K., and T. Miyamoto, 1977, Tetsu To Hagane **63**, 45.
Szpunar, E., 1969, Pr. Inst. Mech. Precyz **17**, 17; Chem. Abstr., Oct., 79732d.
Toyoda, T., and T. Endo, 1995, Tetsu To Hagane **81**, 83.
Troiano, A.R., 1959, Corrosion **15**, 207.
Troiano, A.R., 1960, Trans. ASM **52**, 54.
Truman, R.J., and H.W. Kirkby, 1960, J. Iron Steel Inst. **196**, 180.
Turnbull, D., and B. Vonnegut, 1952, Ind. Eng. Chem. **44**, 1292.
Ueshima, Y., H. Yuyama, S. Mizoguchi and H. Kajioka, 1989, Tetsu To Hagane **75**, 501.
Uhlig, H.H., 1963, Corrosion and Corrosion Control (Wiley, New York) p. 182.
Vennett, R.M., and G.S. Ansell, 1969, ASM Trans. **62**(Dec.).
von Bungardt, K., E. Kunze and E. Horn, 1958, Arch. Eisenhuettenwes. **29**, 193.
Wakoh, M., T. Sawai and S. Mizoguchi, 1992, Tetsu To Hagane **78**, 1697.
Waudby, P.E., 1978, Int. Met. Rev. **2**, 74.
Williams, F.S., W. Beck and E.J. Jankowsky, 1960, Proc. ASTM **60**, 1192.
Wilson, W.G., 1971, Weld. J. **50**, 42.
Wilson, W.G., and G.J. Klems, 1974, Ind. Heat, p. 12.
Wilson, W.G., D.A.R. Kay and A. Vahed, 1974, J. Met., p. 14.
Wilson, W.G., D.A.R. Kay and A. Vahed, 1976, Metall. Trans. **7B**, 375.
Winterton, K., 1957, Weld. J. **36**, 449S.
Younger, R.N., and R.G. Baker, 1960, J. Iron Steel Inst. **196**, 188.
Younger, R.N., and R.G. Baker, 1961, Br. Weld. J. **8**, 579.
Younger, R.N., D.M. Haddrill and R.G. Baker, 1963, J. Iron. Steel. Inst. **201**, 693.
Zecher, D.C., 1976, Mater. Perform., p. 33.

Handbook on the Physics and Chemistry of Rare Earths
Vol. 25
edited by K.A. Gschneidner, Jr. and L. Eyring

Chapter 166

TERNARY AND HIGHER ORDER NITRIDE MATERIALS

Roger MARCHAND
Laboratoire des Verres et Céramiques, UMR 6512 CNRS, Université de Rennes I, Campus de Beaulieu, 35042 Rennes Cedex (France)

Contents

1. Introduction. General considerations

Nitrogen combines with numerous elements of the Periodic Table less electronegative than itself, to give rise to nitrides; rare-earth metals (R) do not disobey this assertion: the stable RN binary solids formed are characterized, in particular, by high melting points, around 2500°C.

While Pauling's electronegativity of nitrogen is 3.0, the electronegativity values of rare-earth elements range from 1.1 to 1.5. The large difference explains the great affinity of the rare-earth elements for nitrogen and the predominant ionic character – more than 50% – of the R–N bond.

The binary rare-earth nitrides were covered in Volume 4 of this Handbook series (Hulliger 1979) in a chapter devoted to rare-earth pnictides. The present chapter essentially aims at reviewing ternary and higher order rare-earth nitride materials.

Such multinary nitride materials result from association to rare-earth metal and nitrogen of other elements which can belong, generally speaking, either to the cationic or anionic subnetwork.

Considering R–M–N ternary nitrides, where M is a cationic element, different categories of compounds are found depending on M, more precisely on the nature of the M–N chemical bond. It is well-known that nitrogen, which is located in the Periodic Table between carbon and oxygen, gives rise to two main classes of binary nitrides having similarities either with carbides or with oxides. Transition metal nitrides thus are closely related to transition metal carbides, and they are essentially metallic in character since they can be generally described as insertion compounds of nitrogen in the metal network. Iono-covalent nitrides, with more or less significant ionic or covalent character, form the second class of compounds, close to oxides, which includes the rare-earth nitrides.

The same situation is met in R–M–N ternary nitrides in which the nature of the M element determines the dominating type of bond involved in the material. This is illustrated by the fact that with lithium (or barium) as a cationic element, the R–M–N corresponding nitride is essentially ionic in character, whereas with silicon, more covalent nitrido-silicates are formed. In addition, metallic nitrided alloys exist, with nitrogen located as an interstitial element in octahedral voids of the metal atom lattice. The presence of insertion nitrogen (as well as carbon) in such compounds is sometimes necessary for their existence, and can strongly modify the physical properties.

Concerning quaternary R–M–O–N oxynitrides, nitrogen and oxygen play a similar role in the anionic network so that these compounds can be considered from a crystallographical point of view as pseudo-oxides. This can be summarized by the following equation which expresses equivalence between the R^{3+}/N^{3-} and, for example, Ca^{2+}/O^{2-} couples:

$$R^{3+} + N^{3-} = Ca^{2+} + O^{2-}.$$

However, with respect to divalent oxygen, presence in oxynitrides of trivalent nitrogen, which in addition forms more covalent bonds, results in interesting applications as new

materials, in particular in the field of ceramics and glasses, as illustrated by the R–Si–Al–O–N (R–sialon) systems.

Nitride halides and nitride sulfides constitute another family of rare-earth-containing compounds. The variety concerns the richness of the different formulations as well as the nature itself of the compounds. Except in the case of nitride fluorides which have a clear salt behavior, nitrogen atoms generally do not play the same role as Cl^- or S^{2-} anions; in some cases it is even difficult to know whether the borderline between a valence compound and a cluster compound has not been crossed.

Finally, we would like to note that considerable progress has been made recently in the study of nitrides, in general, and that is especially true in the case of rare-earth multinary nitride-type compounds. Many of the papers have appeared in recent years, often describing novel types of materials. The best illustration is provided by the R–T–N (T = transition metal) intermetallic nitrides in which several new families have been discovered since 1990. The challenge has given rise to a lot of papers which continue to appear simultaneously, motivated by the potential offered by these phases for development as permanent-magnet materials.

2. Binary nitrides

Some outstanding findings concerning the preparation and properties of rare-earth binary nitrides, which have been published since Hulliger's review in 1979, are noted below.

2.1. *Preparation of binary nitrides*

As described by Hulliger (1979) in Volume 4 of the Handbook, all the rare-earth metals combine with nitrogen to form RN mononitrides corresponding, only formally in the case of CeN, to the trivalent oxidation state of R. These nitrides possess the fcc rock-salt-type structure (cubic, $Fm\bar{3}m$). Whatever conventional method of synthesis, nitrogenolysis or ammonolysis of the metal or metal hydride or metal amalgam that was used, two kinds of difficulties were being encountered for many years. First, the easy oxygen contamination due to the sensitivity of the starting products to oxygen and humidity, and of the prepared nitrides to hydrolysis; and second, the nitrided materials were often slightly nitrogen deficient (RN_{1-x}) or contained occluded unreacted metal.

Kaldis et al. (1982) succeeded in preparing pure and stoichiometric rare-earth nitrides by direct heating of the metals in nitrogen at high temperature (~2000°C). They used very well-controlled atmosphere conditions (in particular a residual oxygen concentration lower than 3 ppm), and pure sublimed metals (99.99% purity) which were transformed into metal turnings, then nitrided several times with intermediate grindings. Chemical analysis of nitrogen content by a micro Kjeldhal method (Kaldis and Zürcher 1976) proved the prepared nitrides to be stoichiometric (±0.5%). The last step was the preparation of large single crystals (several mm edge length) which were grown by keeping the polycrystalline material at high temperature in a temperature gradient.

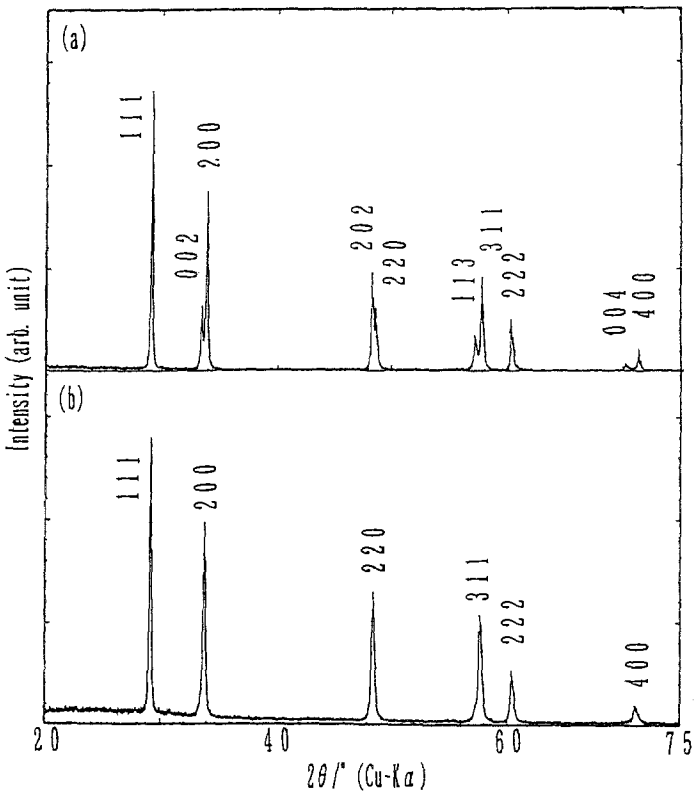

Fig. 1. X-ray diffraction powder patterns of (a) tetragonal and (b) cubic lanthanum nitride (Kikkawa et al. 1997).

Different stoichiometries have been reported in the literature concerning scandium nitride (Dismukes et al. 1970, Aivazov and Rezchikova 1977, Aivazov et al. 1977, Bogdanov et al. 1981). Lengauer (1988) prepared ScN_{1-x} bulk samples by direct nitridation of Sc metal: in the 1380–1770 K temperature range, ScN_{1-x} had a homogeneity range $ScN_{0.87}$–$ScN_{1.00}$. For example, chemical analysis of nitrogen and oxygen in a sample prepared at 25 kPa nitrogen pressure and 1770 K yielded experimental composition $ScN_{0.98\pm0.005}O_{0.02\pm0.01}$.

Let us note that, very recently, a tetragonal form of LaN, prepared by nitriding La metal in N_2 after heating at 1223 K in vacuo, was reported by Kikkawa et al. (1997). Figure 1 shows the tetragonal distortion ($a = 0.5284$ nm, $c = 0.5357$ nm, $c/a = 1.014$) in comparison with cubic LaN ($a = 0.5303$ nm, Vendl et al. 1977). This tetragonal lanthanum nitride, of experimental composition $LaN_{0.926}O_{0.062}$, transforms into normal cubic form by high isostatic pressure (HIP) annealing in a nitrogen atmosphere.

LaDuca and Wolczanski (1992) developed a low-temperature method for the preparation of rare-earth metal nitrides involving the ammonolysis of molten molecular

Table 1
Characteristics of rare-earth binary nitrides produced from $[(Me_3Si)_2N]_3R$ precursors[a]

LnN	Color at 210°C	Color after annealing	Crystallite size (Å)
YN	brick-red	blue-violet	250
LaN	orange	gray	>275
PrN	purple	purple-black	275
NdN	green	dark-green	>275
SmN	purple	dark-purple	>275
EuN	orange	brown	>275
TbN	orange-red	black	200
ErN	orange	purple-black	200
YbN	orange	orange-brown	275

[a] After LaDuca and Wolczanski (1992).

precursors. The precursors were three-coordinate amido complexes, $[(Me_3Si)_2N]_3R$ (R = Y, La, Pr, Nd, Sm, Eu, Tb, Er, Yb), which were obtained from the chlorides:

$$RCl_3 + 3LiN(SiMe_3)_2 \xrightarrow[-3LiCl]{THF} [(Me_3Si)_2N]_3R.$$

The synthesis is summarized in the following scheme:

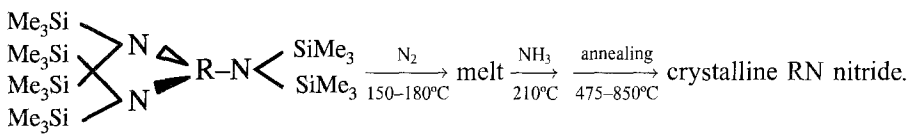

Ammonolysis and subsequent annealing yielded colored nitride phases, in contrast to the black powders often obtained by conventional processes, as shown in table 1. These melt-prepared rare-earth nitrides are nitrogen deficient RN_{1-x} nitrides, without occluded metal, but no data exist concerning different physical properties.

This molten molecular precursor technique could henceforth be extended to ternary systems. Preparation of $R_{1-y}R'_yN_{1-x}$ solid solutions has already been performed.

Fitzmaurice et al. (1993, 1994), using Li_3N, and Hector and Parkin (1995), using Mg_3N_2 and Ca_3N_2, have described a method to produce metal nitrides in metathetical reactions, with lithium, magnesium, and calcium nitrides as nitrogen sources. Li_3N, Mg_3N_2 and Ca_3N_2 react with anhydrous rare-earth chlorides RCl_3 (and also with other transition metal chlorides) at 400–900°C with formation of corresponding nitrides accompanied with lithium, magnesium or calcium chloride.

Heating a mixture of lanthanide chloride RCl_3 (R = Nd, Sm, Gd, Tb, Er) and either Mg_3N_2 or Ca_3N_2 to 900°C rapidly forms the corresponding nitride, as in the case of gadolinium:

$$GdCl_3 + \tfrac{1}{2}Mg_3N_2 \rightarrow GdN + \tfrac{3}{2}MgCl_2 \qquad \Delta H_r^0 = +41\ \text{kJ mol}^{-1},$$
$$GdCl_3 + \tfrac{1}{2}Ca_3N_2 \rightarrow GdN + \tfrac{3}{2}CaCl_2 \qquad \Delta H_r^0 = -202\ \text{kJ mol}^{-1}.$$

According to the reaction energetics, a general trend is observed of reactions with Ca_3N_2 occurring more readily than those with Mg_3N_2. Lowering the temperature or reducing the reaction time enables intermediates R_2NCl_3 (R = Sm, Gd, Tb, Er) and Ca_2NCl to be observed. The formation of these nitride chlorides in the reaction pathway is interpreted as characteristic of ionic metathesis, i.e. of a reaction proceeding by the exchange of ions.

In the case of lithium nitride, YCl_3 and $LaCl_3$ were the first rare-earth chlorides investigated (Fitzmaurice et al. 1993). The highly exothermic reactions, once initiated at 400°C, were extremely rapid, leading to crystalline YN and LaN nitrides which were isolated from LiCl after tetrahydrofuran trituration. The same type of rapid exothermic solid-state metathesis reaction was then applied to produce all the RN rare-earth nitrides (R = Y, La, Pr, Nd, Sm, Eu, Gd, Tb, Dy, Ho, Er, Yb) as well as mixed lanthanide nitrides (RR′)N (RR′ = PrNd, DyHo, TbDy) (Fitzmaurice et al. 1994). Note that the reaction requires initiation via a conventional or microwave oven but is self-sustaining. The prepared nitrides have a stoichiometry LnN_{1-x} ($x = 0.1$–0.2).

A similar solid-state metathesis (SSM) reaction, whereby lanthanum oxide was combined with calcium nitride as a nitriding agent, leading to lanthanum nitride and calcium oxide, had been previously described by Marchand and Lemarchand (1981):

$$\tfrac{1}{2}La_2O_3 + \tfrac{1}{2}Ca_3N_2 \xrightarrow{900\text{–}1000^\circ C} LaN + \tfrac{3}{2}CaO.$$

Such a reaction can probably be written for all rare earths. The same idea was successfully exploited by these authors to prepare a ternary lanthanum chromium nitride, identified by Broll and Jeitschko (1995) as $La_3Cr_{10-x}N_{11}$, from a mixture of lanthanum and chromium binary oxides according to

$$3La_2O_3 + (10-x)Cr_2O_3 + (13-x)Ca_3N_2 \rightarrow 2La_3Cr_{10-x}N_{11} + (39-x)CaO + (2-x)N_2\uparrow.$$

Thus, it seems to be possible to involve calcium nitride as a nitrogen source in different types of SSM reactions where ternary rare-earth nitrides would be synthesized either from appropriate mixtures of binary compounds such as oxides or chlorides, or, in some favorable cases, directly from single-phase ternary oxide (or chloride) compositions.

Continuing with this idea, rare-earth binary nitrides themselves could be considered, like calcium nitride, as interesting nitriding agents to produce transition metal nitrides for example from oxides (Barker and Gareh 1994, Gareh 1996). By way of illustration, the following equations compare from a thermodynamic point of view the preparation of vanadium nitride, VN, from V_2O_3 at 1100 K using either YN or Ca_3N_2:

$$YN + \tfrac{1}{2}V_2O_3 \rightarrow VN + \tfrac{1}{2}Y_2O_3 \qquad \Delta H_r^0 = -259\ \text{kJ mol}^{-1},$$

$$\tfrac{1}{2}Ca_3N_2 + \tfrac{1}{2}V_2O_3 \rightarrow VN + \tfrac{3}{2}CaO \qquad \Delta H_r^0 = -332\ \text{kJ mol}^{-1}.$$

2.2. *Properties of binary nitrides*

The physical properties of the rare-earth pnictides have been reviewed by Hulliger (1979). For a long time, rather contradictory results were reported, due mainly in the case of

the binary nitrides, to the synthesis of imperfect materials. In particular, the deviation from the ideal one to one stoichiometry has a direct influence on the properties, and measurements of the intrinsic magnetic, electronic and conductivity properties were thus difficult to achieve without synthesis of stoichiometric samples. Experimental procedures to prepare chemically well-defined single crystals of RN nitrides have been described by Kaldis et al. (1982).

Schlegel (1979) and Wachter and Kaldis (1980) prepared single crystals of stoichiometric gadolinium nitride and showed that GdN, contrary to the ferromagnetic semiconductor EuO, is a metamagnet with a T_N of 40 K, and that the carrier concentration at 300 K is 6% per Gd ion.

Travaglini et al. (1986) obtained pure scandium nitride ScN with such perfect stoichiometry and stability that the single crystals could be boiled for hours in a mixture of HNO_3 and H_2SO_4 before being dissolved. ScN exhibits metallic behavior, having a carrier concentration of about 10^{20} cm^{-3} at room temperature. A band-structure calculation was performed by Monnier et al. (1985).

Large single crystals of YbN – between 3 and 5 mm edge length – were prepared by Degiorgi et al. (1990). These crystals had, with $a = 4.781$ Å, the smallest lattice constant ever measured, which is associated with a nearly (weakly hybridized) pure $4f^{13}$ ground state without any population of a (larger) $4f^{14}$ state (as previously concluded by Greber et al. 1987 from photoemission measurements). It was shown from a series of physical measurements that YbN is a self-compensated semimetal with a carrier concentration of about 10^{20} cm^{-3}, the occupied $4f^{13}$ state is about 6 eV below E_F, the empty $4f^{14}$ state is about 0.2 eV above E_F, and the effective mass of the carriers is about $2.2\,m_e$. Therefore, YbN is not a heavy fermion but probably a Kondo system.

2.3. *Solid solutions of the NaCl-type*

The rare-earth NaCl-type RN mononitrides are mutually miscible as shown by several studies involving in particular the high-melting phase GdN (2600°C). However, while monophasic products were obtained by arc-melting in the LaN–GdN, GdN–EuN, GdN–YbN and GdN–CeN pseudo-binary systems (Gambino and Cuomo 1966), only partial miscibility was observed at 1000°C in the systems LaN–GdN and PrN–GdN (Magyar 1968). Vendl (1979) studied the miscibility between LaN, CeN, NdN and GdN and showed it was complete in all cases in the range 1300–1800°C (N_2 pressure of 30 bar), with the cubic lattice parameters obeying Vegard's law.

In the context of using uranium and actinide nitride materials as nuclear fuels, Holleck et al. (1968, 1969) reported total miscibility of the rare-earth nitrides with UN, as well as Ettmayer et al. (1979) who noted that the lattice parameters of the RN–UN solid solutions (R = La, Ce, Pr, Nd, Sm, Gd, Dy, Er) generally showed negative deviations from the additivity rule. It can be noted here that in the system U_2N_3–LaN, a ternary nitride material $La_2U_2N_5$ was observed and characterized by Waldhart and Ettmayer (1979), with the metal atoms, in the tetragonal unit cell, located in the same positions as in the CsCl-type structure. ThN is also completely miscible with LaN, CeN, PrN, NdN, SmN, GdN,

DyN, ErN and YN (Holleck and Smailos 1980, Ettmayer et al. 1980b). Contrary to the other systems, no linearity of the unit cell parameter was observed in the (Th, Ce)N mixed phases, due to the variation of the Ce^{III}–Ce^{IV} ratio as the Ce concentration varied in the solid solution alloy. In the same way, uranium and thorium monocarbides form mixed crystals with several RN nitrides (R = La, Ce, Pr, Nd, Sm, Gd, Dy, Er) (Ettmayer et al. 1980a,c), except for the system UC–LaN. A miscibility gap was also observed, at 1800°C, in the system ThC–ErN.

NaCl-type RO_xN_{1-x} phases have been reviewed by Hulliger (1979). We will report here the RN miscibility with the divalent europium oxide the study of which was of particular interest due to the ferromagnetic semiconducting behavior of EuO (Curie temperature $T_c = 69.5$ K, activation energy $\Delta E = 1.1$ eV). Chevalier et al. (1973, 1976) and Etourneau et al. (1980) prepared and studied NaCl-type oxynitride solid solutions in the systems EuO–RN with R = Nd, Eu and Gd. The homogeneity ranges of these $Eu_{1-x}R_xO_{1-x}N_x$ oxynitrides in the oxygen-rich part of each system are $0 \leqslant x \leqslant 0.26$ (R = Nd, at $T = 1250$°C), $0 \leqslant x \leqslant 0.30$ (R = Eu, at $T = 1300$°C) and $0 \leqslant x \leqslant 0.26$ (R = Gd, at $T = 1850$°C). The oxynitrides $Eu_{1-x}Nd_xO_{1-x}N_x$ exhibit a ferrimagnetic behavior and a semiconductor–metal transition for $x \approx 0.22$ which was related to the presence of Eu^{3+} ions for high values of x (Chevalier et al. 1980). In the semiconducting range ($x < 0.22$), the Curie temperature T_c increases and the activation energy ΔE decreases with increasing x. Such a semiconductor–metal transition occurs also at low temperatures for $EuO_{1-\delta}$ and $EuO_{1-x-\delta}N_x$ (Penney et al. 1972, Chevalier et al. 1978). The oxynitrides $Eu^{2+}_{1-x}R^{3+}_xO_{1-x}N_x$ (R = Eu, Gd) are ferromagnetic semiconducting compounds with T_c values higher than T_c of EuO, and ΔE decreases when x increases. It is also noted that a complete miscibility between EuO and NdN was observed at $T = 1650$°C.

Chevalier et al. (1977) studied also the magnetic and electrical transport properties of NdO_xN_{1-x} phases which differ from those of the europium-containing phases since they are ferromagnetic and metallic. Conductivity increases with increasing oxide content and resistivities vary from $10^{-3}\ \Omega$ cm for $x = 0.09$ to $10^{-4}\ \Omega$ cm for $x = 0.22$.

Several pseudo-binary and pseudo-ternary rare-earth oxynitrides were also prepared between 1500 and 1800°C by Liu et al. (1993) in the systems LaN–CeO_2 and CeN–CeO_2, LaN–R_2O_3 and CeN–R_2O_3 (R = La, Y), and YN–R_2O_3 (R = La, Lu, Y, Sc). Surprisingly, the LaO_xN_{1-x} and CeO_xN_{1-x} fired samples possess a doubled cubic lattice parameter. The LaO_xN_{1-x} compositions corresponding to $x = 0.31$ (dark blue) and $x = 0.45$ (deep red) are weakly paramagnetic and metallic. The resistivities which are 4.8×10^{-3} and $5.9 \times 10^{-5}\ \Omega$ cm, respectively, at room temperature, linearly decrease as the temperature is lowered.

We note here the existence in the Ce–O–N system of a cerium(IV) oxynitride with the defined composition Ce_2N_2O (Barker and Alexander 1974) which has the trigonal ($P\bar{3}m1$) La_2O_3-type structure (cf. section 3.1.1).

Recently, Clarke and DiSalvo (1997) prepared defect rock-salt nitrides $La_{1-x}Ca_xN_{1-x/3}$ ($0 < x < 0.7$) by reacting together the binary nitrides LaN and Ca_3N_2 at 1200–1300°C.

3. Ternary and higher (oxy)nitrides

3.1. *Cerium compounds*

Among cerium-containing nitride-type compounds, ternary nitrides in which Ce is tetravalent are formed with electropositive metals such as lithium or barium. These hygroscopic compounds are essentially ionic in character. In addition, oxynitrides containing cerium and barium are also known. However, surprisingly, no ionic ternary nitride (or quaternary oxynitride) involving other R elements has been described.

3.1.1. *Li_2CeN_2 and Ce_2N_2O*

Li_2CeN_2 is the only known rare-earth lithium ternary nitride. First reported by Halot and Flahaut (1971), this red-orange, very moisture-sensitive Ce^{IV} nitride was prepared by heating, at 600–700°C under nitrogen atmosphere, an equimolecular mixture of the binary nitrides Li_3N and CeN. Li_2CeN_2 is isostructural with the two ternary lithium nitrides of group IV transition metals Li_2ZrN_2 and Li_2HfN_2 (Palisaar and Juza 1971, Barker and Alexander 1974, Niewa and Jacobs 1995) (fig. 2). The anti-La_2O_3 trigonal ($P\bar{3}m1$) structure contains hexagonal close-packed nitrogen atoms with cerium in octahedral coordination forming filled layers of edge-sharing octahedra $^2_\infty[CeN_{6/3}]$, as in the CdI_2 structure type. Lithium atoms, which occupy all edge-sharing tetrahedral holes, form alternate layers.

The anti-type structure is illustrated by another Ce^{IV} nitride-type compound, the green cerium oxynitride Ce_2N_2O, analogous to La_2O_3, which was obtained by Barker and Alexander (1974) on heating a 3:1 mixture of cerium mononitride and cerium dioxide

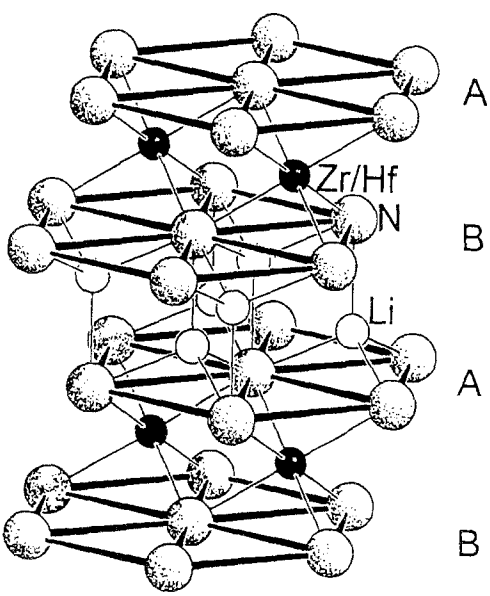

Fig. 2. Structure of Li_2CeN_2 which is isostructural with $Li_2Zr(Hf)N_2$. The solid, open and shaded spheres represent Ce or Zr(Hf), Li and N, respectively (after Niewa and Jacobs 1995).

at 1100°C under nitrogen. Th_2N_2O and $Th_2N_2(NH)$ are isostructural thorium compounds (Benz and Zachariasen 1966, Juza and Gerke 1968), just as the cerium oxysulfide Ce_2O_2S but where Ce is formally trivalent.

3.1.2. *$BaCeN_2$*

Besides Li_2CeN_2, Ce(IV) is associated with an electropositive element and nitrogen in $BaCeN_2$. This ternary nitride was prepared by Seeger and Strähle (1994), either from the reaction of Ba_3N_2 with CeN in the stoichiometric ratio 1:3 at 850°C under N_2 atmosphere, or directly from elements. This moisture sensitive product crystallizes hexagonally ($P6_3/mmc$) with the anti-TiP structure, like β-$RbScO_2$ or some other ternary oxides of lanthanides ($CsRO_2$), but the zirconium compound $BaZrN_2$ is structurally different (Seeger et al. 1994).

The stacking sequence along [001] can be described as AβAγBαBγ with an AABB arrangement of nitrogen atoms. The Ce atoms occupy octahedral holes γ while the Ba atoms in α and β are in trigonal prismatic coordination. N atoms are thus octahedrally surrounded by 3 Ce + 3 Ba. $MnTa_3N_4$ (Schönberg 1954), Li_3TaN_4 (Brokamp and Jacobs 1992) and $Li_3NbN_{4-\varepsilon}$ (Tessier et al. 1997) have the same structure but with a partially disordered metal arrangement due to the 3:1 proportion. Let us note that $ScTaN_{1-x}$ and $ScNbN_{1-x}$ which have also an anti-TiP type structure are nitrided alloys and they have been described as a nitrogen insertion between metal atom layers (Lengauer and Ettmayer 1988, Lengauer 1989).

The distances Ce–N = 242.4 pm in $BaCeN_2$ are shorter than in the Li_2CeN_2 structure (253 pm) which contains also edge-sharing CeN_6 octahedra. They correspond to the sum of covalent radii while the Ba–N distances are essentially ionic in character: $BaCeN_2$ could thus be considered as a barium nitrido-cerate, formulated $Ba^{2+}[CeN_2]^{2-}$.

The hypothesis of a second modification of $BaCeN_2$ crystallizing with the α-$NaFeO_2$ structure has been envisaged by Seeger and Strähle (1994).

3.1.3. *$BaCeR(O,N)_4$ oxynitrides*

Heating $BaCeO_3$ perovskite with RN nitride (R = La, Ce) at 800°C leads to the formation of reddish-colored hygroscopic $BaCeR(O,N)_4$ oxynitride powders, with cerium ions in a mixed-valence state (Liu and Eick 1990). These phases have the same orthorhombic (Pnma) $CaFe_2O_4$-type structure (Wyckoff 1965) as the purely oxygenated compound $BaCe_2O_4$ in which cerium is trivalent. The lanthanide ions are octahedrally surrounded while barium has eight close (O + N) neighbors.

3.2. *Ternary and higher nitrides formed with non-metal elements*

The non-metals considered are boron and silicon. The corresponding binary nitrides, BN, either in the graphite-like or diamond-like form, and Si_3N_4 are well-known as high-performance materials owing to excellent thermal, electrical, mechanical and chemical properties. Their low reactivity explains that ternary nitrides with lanthanides are only

formed at elevated temperatures. Whereas the ternary silicon nitrides are unambiguously nitrido-silicates with SiN_4 tetrahedra, the structure of which presents similarities to framework silicate structures, there are several types of ternary boron nitrides depending on whether they can be compared to borates or to borides.

It can be noted here, and this remark has some general character in this study of multinary rare-earth nitride-type compounds, that the tendency toward compound formation diminishes with increasing atomic number of the rare-earth elements.

Ternary rare-earth phosphorus nitrides are not known so far, probably because of the great difference of thermal stability between R–N and P–N bonds.

3.2.1. *Ternary and quaternary silicon nitrides*

Ternary rare-earth silicon nitrides have been obtained only with the early lanthanides and with yttrium. Until recently, $LaSi_3N_5$ (Inoue et al. 1980, Holcombe and Kovach 1981, Inoue 1985) and $Sm_3Si_6N_{11}$ (Gaudé et al. 1983) were the only described compounds. They were prepared by reacting the corresponding binary nitrides at high temperature. Single crystals of $LaSi_3N_5$ were isolated from a Si_3N_4/La_2O_3 mixture heated at 2000°C under 50 bar N_2. On the other hand, Thompson (1986) indicated the existence of three yttrium silicon nitrides, YSi_3N_5 (hexagonal), $Y_2Si_3N_6$ (structure unknown) and $Y_6Si_3N_{10}$ (orthorhombic, pseudo-hexagonal) as a result of firing YN–Si_3N_4 compositions in nitrogen at 1750°C.

Woike and Jeitschko (1995) have shown that the tetragonal (P4bm) $R_3Si_6N_{11}$ (R = La, Ce, Pr, Nd, Sm) and the orthorhombic ($P2_12_12_1$) RSi_3N_5 (R = La, Ce, Pr, Nd) isotypic nitrides could be prepared by reaction of the binary lanthanide silicides RSi_2 and the two-phase alloys "RSi_3" with nitrogen at 1500°C. From the plot of the different cell volumes, it was concluded that cerium is trivalent in both series of compounds. $Ce_3Si_6N_{11}$ was obtained at the same time from cerium metal and silicon diimide $Si(NH)_2$ (Schlieper and Schnick 1995), as well as $Pr_3Si_6N_{11}$ (Schlieper and Schnick 1996). Both structure types consist of corner-sharing SiN_4 tetrahedra, thus forming covalent three-dimensional anionic networks in which nitrogen atoms determine voids occupied by the trivalent lanthanide ions (fig. 3). So, it is clear that such nitrido-silicates cannot be structurally compared to lanthanide silicon carbides (or silicide carbides) where the silicon atoms must be considered as anionic.

All the ternary lanthanide silicon nitrides exhibit an excellent thermal and chemical stability which predestines them for use as high-temperature materials.

Let us add that phase equilibria in three ternary systems R–Si–N (R = Sc, Ce, Ho) have been investigated at 1000°C by Weitzer et al. (1991) from appropriate arc-melted R–Si compositions mixed with Si_3N_4. No new ternary phase was found. The authors mention only a $Ho_5Si_3N_{1-x}$ phase which is a nitrided $D8_8$–Ho_5Si_3 silicide, of CrB-type structure, with a slightly larger c hexagonal parameter.

Two isotypic quaternary nitrido-silicates, $SrYbSi_4N_7$ and $BaYbSi_4N_7$, have been recently synthesized by Huppertz and Schnick (1996, 1997) by reaction of silicon diimide with metallic strontium/barium and ytterbium at 1650°C. Their hexagonal structure

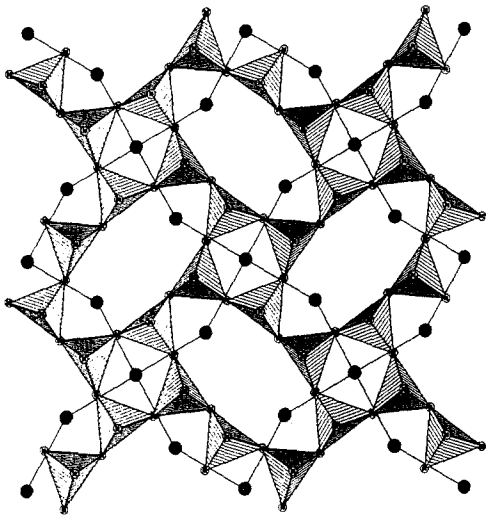

Fig. 3. Layers of condensed four- and eight-membered rings of corner-sharing SiN_4 tetrahedra in $Ce_3Si_6N_{11}$ as viewed along the [001] direction. The solid circles are Ce^{3+}, and the shortest Ce–Ce distances (372 pm) are line-drawn (Schlieper and Schnick 1995).

($P6_3mc$) is also built up from a three-dimensional network of corner-sharing SiN_4 tetrahedra in which, for the first time, N atoms connecting four Si atoms have been found.

3.2.2. *Ternary boron nitrides*

Boron behaves in rare-earth ternary nitrides as a particular element in the sense that it is able to form both BN_3 units similar to BO_3 units found in borates, and B–B pairs as in borides. Quaternary boro-nitrides analogous to boro-carbides will be discussed in section 3.4.3.4.

Many ternary metal–boron–nitrogen systems have been systematically investigated, just as M–Si–N systems, in order to provide basic information on the thermodynamic phase equilibria and compatibility in these systems. Concerning rare-earth metals, no ternary compound exists with the late lanthanides Tb to Lu and with Sc and Y. Klesnar and Rogl (1990) have established the corresponding thermodynamic phase equilibria at 1400°C and 1 bar of argon (in the absence of external nitrogen pressure), which are characterized by a stable three-phase equilibrium $RN + RB_4 + BN$ (for scandium $ScN + ScB_2 + BN$). Accordingly, there is no compatibility between boron nitride and the rare-earth metal.

Klesnar and Rogl (1992) have also studied phase relations and phase stabilities at $T = 1400$°C in the ternary systems R–B–N where R is Nd, Sm or Gd: in this case ternary compounds are found to be stable. Three different stoichiometries were observed with these early lanthanides: RBN_2, $R_3B_2N_4$ and $R_{15}B_8(N,O)_{25}$. In addition, Kikkawa et al. (1997) have recently reported the preparation under high pressure of another orthorhombic "La–B–N" phase. All these ternary lanthanide boron(oxy)nitrides are rather unstable under moist conditions.

3.2.2.1. *$PrBN_2$-type.* The existence of ternary compounds associating nitrogen, boron and a lanthanide was first mentioned by Gaudé (1983) with the RBN_2 nitrides (R = Nd, Sm),

prepared as gray and moisture-sensitive powders at $T \approx 1550$°C from RN–BN mixtures. In a more recent study, Rogl and Klesnar (1992) determined the crystal structure of the isostructural $PrBN_2$ compound from single crystals obtained by direct sintering of mixtures of BN and praseodymium metal under nitrogen at 1800°C. The gadolinium compound, which is only observed at temperatures above 1400°C, has also the same type of structure. The corresponding rhombohedral crystal structure (R3c) appears as a combination of planar B_3N_3 hexagons which are stacked to form infinite columns along the [001] direction of the hexagonal unit cell, as in hexagonal BN, and of irregular bipyramidal [Pr_5B] units centered by other nitrogen atoms, as in the $Ce_3B_2N_4$-type. Each boron atom is thus bonded to three N atoms to form a BN_3 triangle. Such a nitrogen triangular coordination of boron has also been found in the $Ce_{15}B_8N_{25}$-type.

3.2.2.2. *$Ce_3B_2N_4$-type.* The $R_3B_2N_4$ nitrides are the metal-rich lanthanide boron nitrides. They were synthesized with all the large lanthanides R = La, Ce, Pr, Nd (and mischmetal) as isotypic compounds (Rogl et al. 1990). The orthorhombic (Immm) crystal structure was determined for the cerium compound from X-ray and neutron powder diffraction data. As shown in fig. 4, boron atoms are in triangular prismatic coordination [Ce_6B], forming covalently bonded B–B pairs. In a tetrakaidecahedral surrounding [Ce_6B]BN_2, each boron atom forms single bonds with two adjacent N atoms. Nitrogen atoms thus are in rectangular pyramidal metal coordination [Ce_5N] with one additional boron atom completing a distorted octahedron [Ce_5BN]. It can be noted that the formation of such a distorted octahedron [Ce_5B](N) is a typical structural feature of different lanthanide (or actinide) boron carbides. The structure of $Ce_3B_2N_4$ reveals a close resemblance to those of the ternary borides $CeCr_2B_6$ (written as $(CeCr_2)B_2B_4$) (Kuzma and Svarichevskaya 1973) and W_2CoB_2 (written as $(W_2Co)B_2\square_4$) (Rieger et al. 1966).

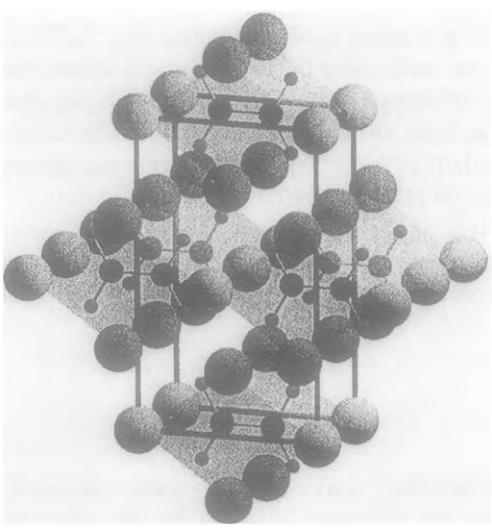

Fig. 4. Crystal structure of $Ce_3B_2N_4$ in a three-dimensional view (Rogl et al. 1990).

3.2.2.3. *$Ce_{15}B_8N_{25}$-type.* The rhombohedral ($R\bar{3}c$) crystal structure of the mixed-valence cerium nitride $Ce_{15}B_8N_{25}$, which was determined from single crystal data by Gaudé et al. (1985), can be described as a three-dimensional arrangement of NCe_6 metal octahedra linked together by trigonal planar (BN_3) units. These planar BN_3 units, similar to the (BO_3) entities in orthoborates – $[BN_3]^{6-}$ anions are isoelectronic with $[BO_3]^{3-}$ anions – give to the structure its main originality. Isotypic lanthanum and praseodymium compounds are also known (Klesnar et al. 1989). In comparison, remember that the ternary alkali metal boron nitrides M^IBN_2 (M^I = Li, Na) and also Mg_3BN_3 are characterized by linear, symmetrical $(NBN)^{3-}$ ions.

A partial oxygen/nitrogen substitution, with formation of $R_{15}B_8N_{25-x}O_x$ oxynitrides, was evidenced in the case of R = La and Ce (L'Haridon and Gaudé 1985, Klesnar et al. 1989). In particular, in the $La_{15}B_8N_{19}O_6$ ($La^{3+}_{15}B^{3+}_8N^{3-}_{19}O^{2-}_6$) composition, O atoms were shown to statistically replace N atoms, but within the BN_3 units rather than within the La_6N octahedra (L'Haridon and Gaudé 1985).

3.3. *Chromium ternary nitrides*

Broll and Jeitschko (1995) have reported the existence of the ternary nitrides Ce_2CrN_3 and $R_3Cr_{10-x}N_{11}$ (R = La, Ce, Pr) which are prepared by direct reaction of the corresponding binary nitrides RN and CrN at 900°C (Ce_2CrN_3) or 1160°C ($R_3Cr_{10-x}N_{11}$). Existence of a La–Cr–N lanthanum compound had been reported some time ago with the approximate composition $La_6Cr_{21}N_{23}$, superconducting below 2.7 K, which could be also obtained by the reaction of calcium nitride with a mixture of the oxides La_2O_3 and Cr_2O_3 (Marchand and Lemarchand 1981). The crystal structures of Ce_2CrN_3 and $La_3Cr_{9.24}N_{11}$ have been determined using single crystals obtained from a Li_3N flux.

The orthorhombic (Immm) Ce_2CrN_3 nitride is isostructural with U_2CrN_3 and Th_2CrN_3 (Benz and Zachariasen 1970) and the structure may be considered either as a "filled" U_2IrC_2 type structure (Bowman et al. 1971) or as a defect K_2NiF_4 structure (fig. 5). While the predominantly tetravalent cerium atoms are surrounded by seven nitrogen atoms, the chromium atoms are in a distorted square-planar nitrogen coordination. The CrN_4 squares are linked via corner-sharing nitrogen atoms, thus forming infinite, straight –N–CrN_2–N–CrN_2– chains, corresponding to the formula $(Ce^{4+})_2(CrN_3)^{8-}$. An isotypic manganese compound Ce_2MnN_3 has been recently prepared (DiSalvo 1997).

In the face-centered cubic ($Fm\bar{3}m$) structure of the Pauli paramagnetic $La_3Cr_{9.24}N_{11}$ nitride, the lanthanum atoms are coordinated by nine nitrogen atoms while the chromium and most nitrogen atoms form a three-dimensionally infinite polyanionic network of corner- and edge-sharing CrN_4 tetrahedra.

3.4. *Interstitial nitrides. Nitrided alloys*

3.4.1. *Scandium ternary nitrides*

The two scandium ternary nitride phases $ScTaN_{1-x}$ and $ScNbN_{1-x}$ were commonly prepared by nitridation of Sc–Ta (Lengauer and Ettmayer 1988) or Sc–Nb alloys in

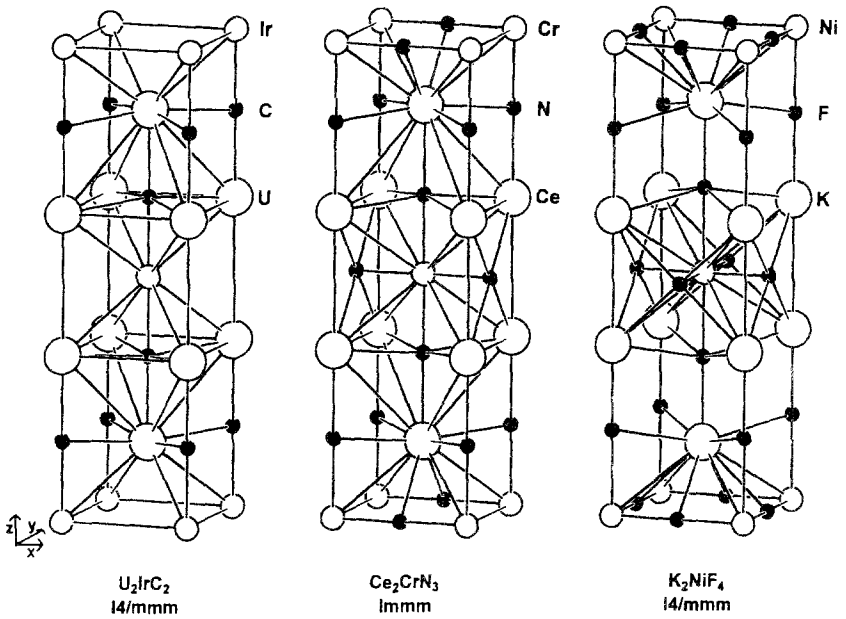

Fig. 5. The crystal structure of Ce_2CrN_3 and its relation to the structures of U_2IrC_2 and K_2NiF_4 (Broll and Jeitschko 1995).

a nitrogen atmosphere at temperatures up to 1770 K (Lengauer 1989). In the case of tantalum, an impure product could also be obtained from a mixture of ScN and ε-TaN binary nitrides.

The hexagonal structure ($P6_3/mmc$) consists of a nearly close packed metal atom arrangement with a stacking sequence ABAC, ABAC, etc., along the *c*-axis, where A represents the layers of scandium atoms and B and C the layers of tantalum (or niobium) atoms (fig. 6). The nitrogen atoms are located in the interstitial octahedral sites N – 3Sc + 3Ta(Nb), with a random occupancy of 50%.

$ScTaN_{1-x}$ and $ScNbN_{1-x}$ have an anti-TiP structure (Wyckoff 1963) with an ordered arrangement of scandium and tantalum atoms at the phosphorus sites and nitrogen at the titanium sites. They are isostructural with the ternary barium and cerium nitride $BaCeN_2$ (Ba ↔ Ta or Nb, Ce ↔ Sc) (Seeger and Strähle 1994), in which all the nitrogen positions are occupied. However, whereas $BaCeN_2$ is a iono-covalent compound, $ScTaN_{1-x}$ and $ScNbN_{1-x}$ contain a combination of metallic bonds between transition metal and nitrogen and ionic bonds between lanthanide-like IIIB metal and nitrogen.

Besides these golden yellow hexagonal ternary nitrides, gray-blue cubic phases δ-(Ta,Sc)N and δ-(Nb,Sc)N have also been observed in the systems Sc–Ta(Nb)–N. They correspond to a partial solubility of ScN in the fcc high-temperature phases δ-TaN and δ-NbN (Lengauer 1989).

ScN also exhibits a limited solubility in TiN and VN (Aivazov and Rezchikova 1977).

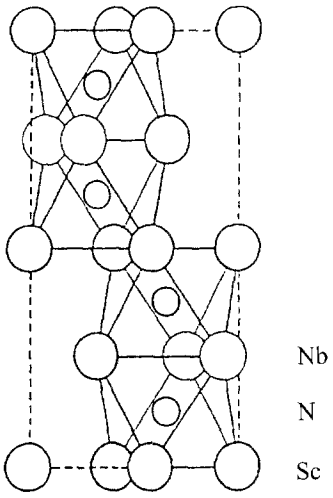

Fig. 6. Crystal structure of ScNbN (Lengauer 1989).

3.4.2. *Antiperovskites R_3MN_x*

R_3MN_x ternary compounds exist, belonging to the T_3MX of perovskite-type structure family of metallic carbides, nitrides and borides, where T is a transition metal; M, a metal; and X = C, N or B. Haschke et al. (1967) reported Nd_3AlN and the probable existence of such a composition in the systems Nd–(Ga, In, Tl, Sn, Pb)–N. Schuster (1985) described the cubic ternary phases R_3AlN_x, which exist for R = La, Ce, Pr, Nd, Sm and can be considered either as antiperovskites or as phases of ordered Cu_3Au-type with an almost complete filling of the R_6 octahedral voids by nitrogen. It has to be noted, as shown by Buschow and van Vucht (1967), that no R_3Al binary phase is known for R = Al, Nd and Sm in the absence of nitrogen.

3.4.3. *Ternary and higher intermetallic nitrides*

Rare-earth intermetallics are able to absorb nitrogen, as first observed by Soga et al. (1979) for $LaNi_5$ and by Higano et al. (1987) for R_2M_{17} compounds (R = Pr, Nd, Sm, Dy; M = Fe, Co), The discovery in 1990 (Coey and Sun 1990, Y.-C. Yang et al. 1990), that introducing nitrogen into the two families of iron alloys $R_2(Fe,M)_{17}$ and $R(Fe,M)_{12}$ (M = metal) remarkably improved their intrinsic magnetic properties over those of the parent compounds, motivated an important effort of research in this field, because these new nitride compounds show great potential as permanent-magnet materials. Permanent-magnet applications require large values of magnetization, uniaxial anisotropy, high Curie temperature T_c, and coercivity at or above room temperature. Even more recently, a third family of ferromagnetic rare-earth intermetallic phases $R_3(Fe,M)_{29}$ and corresponding nitrides was discovered with also interesting magnetic properties. As a result, a considerable number of papers have appeared during the past few years and still at the present time, giving evidence of interest devoted to the search for new compositions whose magnetic properties might surpass those of $Nd_{12}Fe_{14}B$ which is

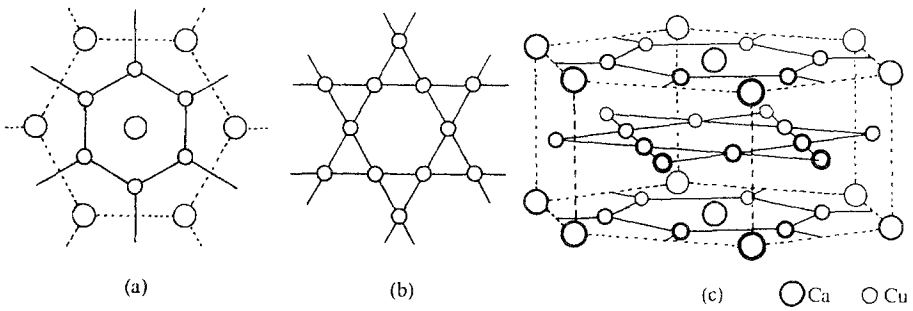

Fig. 7. (a,b) The two types of alternate layers in (c) the crystal structure of $CaCu_5$ (Wells 1975).

limited in application by its comparatively low Curie temperature (585 K) (Croat et al. 1984, Sagawa et al. 1984).

The stoichiometries and structures of these three families of compounds, denoted as 2:17, 1:12 and 3:29 compounds, are derived from a RT_5 composition having the hexagonal $CaCu_5$-type structure. The structure of $CaCu_5$ is built from alternate layers of the types shown in fig. 7a,b (Wells 1975) so that each Ca atom is surrounded by six Cu atoms in one plane and by two more sets of six in adjacent planes, making a total coordination number of 18. The ordered replacement in a RT_5 composition of rare-earth R atoms by two small transition metal atoms forming T–T dumbbells can lead to R_2T_{17}, RT_{12} and R_3T_{29} compositions. This process can be described by

$$RT_5 \rightarrow R_{1-x}(2T)_xT_5 \rightarrow RT_z.$$

The 2:17 structure corresponds to $x = 1/3$, the 1:12 structure to $x = 1/2$ and the 3:29 structure to $x = 2/5$. As indicated by Cadogan et al. (1994b), such structural relationships had been previously considered by Stadelmaier (1984), thus predicting the occurrence of novel structures.

Insertion of nitrogen (and also of carbon or hydrogen) into rare-earth intermetallics, which is usually called "gas-phase interstitial modification" (GIM) process (Zhong et al. 1990), generally consists of heat treatment of the alloys in ammonia or nitrogen (or/and in methane or hydrogen). The resulting compounds are thus not only nitrides, but also carbonitrides, carbides and hydrides. Plasma reactions with plasma glow discharges of the mixed gases N_2–H_2 or CH_4–N_2–H_2 are also used for nitriding or carbonitriding the alloy powders. A general survey of the three above mentioned main families of intermetallic nitrides will be given below.

3.4.3.1. *2:17 nitrides (of the Th_2Zn_{17}- or Th_2Ni_{17}-type structure).* The R_2Fe_{17} rare-earth intermetallic compounds (R = Ce–Lu, Y) which are the most iron-rich of all binary R–Fe alloys, are known to crystallize in the rhombohedral ($R\bar{3}m$) Th_2Zn_{17}-type structure for R lighter than Gd, and in the hexagonal ($P6_3/mmc$) Th_2Ni_{17}-type structure for R heavier than Dy and for R = Y. Both structure types exist for R = Gd, Tb, Dy. The slight differences

between them are related to the stacking sequence of hexagonal planes along the *c*-axis (Khan 1973).

Coey and Sun (1990) showed that Sm_2Fe_{17} and Y_2Fe_{17}, by heating in ammonia or nitrogen, absorb nitrogen without structural change, except that the lattice expands by 6 to 7% by volume. Interstitial $R_2Fe_{17}N_{3-\delta}$ ternary nitrides are formed, with nitrogen in octahedral coordination surrounded by 2 R and 4 Fe atoms (Coey et al. 1991, Stalick et al. 1991, Ibberson et al. 1991, Melamud et al. 1994). Similar results were observed for the whole $R_2Fe_{17}Ny$ series (H. Sun et al. 1990, Huang et al. 1991). This introduction of interstitial nitrogen into the R_2Fe_{17} structure results in dramatically improved magnetic properties. Whereas the R_2Fe_{17} parent alloys have a low Curie temperature and a planar magnetocrystalline anisotropy, the samarium nitride compound $Sm_2Fe_{17}N_y$, in particular, has a strong uniaxial anisotropy, large saturation induction and a high Curie temperature – 740 K (H.-S. Li and Coey 1991); the attributes required of a high energy product permanent-magnet material (Wallace and Huang 1992). Many other studies on improving the magnetic properties of R_2Fe_{17} compounds have been performed, in particular by substituting for Fe with several elements such as Al (X.-W. Li et al. 1993) Ga, Si and Co (W.-Z. Li et al. 1994).

The off-stoichiometric compositions $Sm_2Fe_{14-x}Co_xSi_2N_y$ ($x=0$ and $x=4$) have been also recently reported by Hadjipanayis et al. (1995) who observed a large anisotropy field at low temperature (1.5 K) for $Sm_2Fe_{14}Si_2N_{2.6}$ ($H_a=227$ kOe) and $Sm_2Fe_{10}Co_4Si_2N_{2.3}$ ($H_a=276$ kOe).

3.4.3.2. *1:12 nitrides (of the $ThMn_{12}$-type structure).* Like Sm_2Fe_{17} which absorbs nitrogen to give $Sm_2Fe_{17}N_{3-\delta}$, interstitial nitrogen enters the structure of intermetallic $Nd(Fe,Ti)_{12}$ to form the ternary nitride $Nd(Fe,Ti)_{12}N_{1-\delta}$. This nitride, with also uniaxial anisotropy and high Curie temperature, is the most representative term of a family of compounds formulated $Nd(Fe,M)_{12}Ny$ (M = Ti, V, Mo, W, Si, Cr, etc.), which might also be candidates for permanent-magnet applications (Y.-C. Yang et al. 1990, 1991a–c, 1992, Schultz et al. 1991, Buschow 1991, H.-S. Li and Cadogan 1992, Wei and Hadjipanayis 1992, Endoh et al. 1992, H. Sun et al. 1993, Q. Pan et al. 1994, Kalogirou et al. 1994, Qi et al. 1994). For example, as compared to the starting materials $RTiFe_{11}$, the nitride compounds $RTiFe_{11}N_x$ have been shown to increase the Curie temperature by about 150–170 K and by 17% in the Fe moment.

Both the parent and nitride compounds crystallize in the tetragonal $ThMn_{12}$ structure ($Z=2$), with space group I_4/mmm. Nitrogen is located in the 2b interstitial site and is surrounded, as in the 2:17 compounds, by 2R + 4Fe atoms (S.-M. Pan et al. 1994a,b).

Compared to the case of 2:17 nitrides, more problems are encountered in developing high-performance magnets based on 1:12 nitrides because of the difficulty in stabilizing the Fe-rich tetragonal phase with a light lanthanide. As indicated in the above general formula, it can be stabilized only by replacing iron with a small amount of a third metal M element. However, according to Y.-C. Yang et al. (1994) and J. Yang et al. (1995) the 1:12 nitrides, which have a more favorable ratio of transition metal to lanthanide, would

be also commercially interesting due to much cheaper neodymium than samarium in the 2:17 nitrides.

3.4.3.3. *3:29 nitrides (of the $Nd_3(Fe,Ti)_{29}$-type structure).* A novel ternary intermetallic phase has been recently discovered (Collocot et al. 1992), with a composition finally identified as $Nd_3(Fe,Ti)_{29}$. It is the first member of another family of rare-earth iron intermetallic compounds, and corresponding nitrides $R_3(Fe,T)_{29}Ny$ (R = Ce, Pr, Nd, Sm, Gd, Y; T = Ti, V, Cr, Mn, Mo, Al) (H.-S. Li et al. 1994b, F.-M. Yang et al. 1994a,b, Ivanova et al. 1990, Shcherbakova et al. 1992, Collocot et al. 1992, Ryan et al. 1994, Hadjipanayis et al. 1995, Kalogirou et al. 1995a,b). The symmetry of these 3:29 phases is monoclinic (Cadogan et al. 1994a) with space group $P2_1/c$ (Fuerst et al. 1994, H.-S. Li et al. 1994a), however a description of the structure in the A2/m space group has been preferred by Kalogirou et al. (1995b) and was recently confirmed by Yelon and Hu (1996). The $Nd_3(Fe,Ti)_{29}$ crystal structure, determined by X-ray (H.-S. Li et al. 1994a) and neutron diffraction (Hu and Yelon 1994) is intermediate between the 1:12- and 2:17-type structures. As already indicated, all the 1:12, 2:17 and 3:29 structures are formed from a hexagonal RT_5 (1:5) structure ($CaCu_5$-type) by the replacement of R atoms by T–T dumbbells. The 3:29 structure thus corresponds to a 2/5 replacement of R atoms and is formed by the alternate stacking of 2:17 and 1:12 segments in the ratio 1:1 (Cadogan et al. 1994b, H.-S. Li et al. 1995). The possibility of such a structural arrangement, previously predicted by Stadelmaier (1984), is illustrated by the relation

$$R_2M_{17}N_3 + RM_{12}N_1 \rightarrow R_3M_{29}N_4.$$

This gives $R_3(Fe,T)_{29}N_4$ as the maximum nitrogen enrichment (Ryan et al. 1994, Kalogirou et al. 1995a). Two 4e interstitial sites ($Z = 2$) are available to N atoms in the structure.

The $R_3(Fe_{1-x}Ti_x)_{29}Ny$ nitride series has excellent intrinsic magnetic properties so that they might be alternative hard nitride magnets besides $Sm_2Fe_{17}N_{3-\delta}$ (H.-S. Li and Coey 1991). The samarium compound seems to have the best potential for use in permanent magnets (F.-M. Yang et al. 1994a, Hu et al. 1994, Hadjipanayis et al. 1995, Suzuki et al. 1995). F.-M. Yang et al. (1994a) have reported a 7.1% volume increase relative to the parent phase, and for the $Sm_3(Fe_{0.933}Ti_{0.067})_{29}$ and corresponding nitride compositions, Hadjipanayis et al. (1995) have observed upon nitridation an increase in the Curie temperature from 486 to 750 K and in the room-temperature saturation magnetization from 119 to 145 emu g^{-1}, and the change of the easy magnetization direction (EMD) from planar to uniaxial (see also H.-S. Li et al. 1995). The anisotropy field for the nitride is 12 T at room temperature, and 25 T at 4.2 K.

3.4.3.4. *Quaternary boro-nitrides.* The well-known magnetic properties of $R_2T_{14}B$ ternary borides (T = transition metal) are typified by the neodymium iron compound $Nd_{12}Fe_{14}B$, discovered in 1983. Several studies aimed at introducing interstitial nitrogen in the composition of such permanent-magnet materials in order to improve their characteristics, in particular the Curie temperature.

Cava et al. (1994) have discovered superconductivity in a new quaternary intermetallic system, associating lanthanum, nickel, boron and nitrogen. $La_3Ni_2B_2N_3$ has a superconducting transition temperature of 12–13 K, while in the same system LaNiBN is a metallic but non-superconducting phase (above 4.2 K). The two-dimensional crystal structure of tetragonal $La_3Ni_2B_2N_3$ (Zandbergen et al. 1994), related to that of $LuNi_2B_2C$ superconducting boro-carbide (Siegrist et al. 1994), consists here of three rock-salt-type LaN layers (instead of one LuC layer in $LuNi_2B_2C$) alternating with single tetrahedral Ni_2B_2 layers, yielding the stoichiometry $La_3Ni_2B_2N_3$. LaNiBN, isostructural with LuNiBC, has a related structure, with two LaN layers stacked with Ni_2B_2 layers. Such results are promising for further research in this field.

4. Quaternary and higher oxynitrides

In the rare-earth-containing quaternary oxynitrides, the rare-earth element R is associated to another element M in the cationic network. Such R–M–O–N compounds, regarded as intermediate between pure oxides and nitrides, can be easily compared with R–M–O ternary oxides, because nitrogen and oxygen, generally speaking, play the same role in the anionic network. A quaternary R–M–O–N oxynitride may thus be considered a ternary oxide in which part of divalent oxygen has been replaced by trivalent nitrogen, while the trivalent R elements have been replaced by divalent or univalent cations in order to maintain electroneutrality, as illustrated by the following equations:

$$R^{3+} + N^{3-} = Ca^{2+} + O^{2-}, \qquad R^{3+} + 2N^{3-} = Na^{+} + 2O^{2-}.$$

This is the cross-substitution principle, which allows the same stoichiometry to be kept, and possibly also the same structure type, if other parameters, such as a compatible size of the substituting cations, have been taken into account. This parallel drawn with oxides, the corresponding structures of which are well-known, has led to a comprehensive structural study of nitride-type compounds (see for example Marchand et al. 1991a).

As for the corresponding iono-covalent ternary oxides, the structure of the quaternary R–M–O–N and higher oxynitrides will be advantageously described from the coordination polyhedra of M atoms, the tetrahedra for example in silicates, the larger R atoms being located within the holes formed by the different arrangements of these structural units. Such a description is particularly well adapted to the case of tetrahedra and octahedra. Three types of environment for M atoms can be pointed out in the rare-earth-containing oxynitrides, namely tetrahedral, octahedral and "cubic".

4.1. *Tetrahedral environment*

4.1.1. *Scheelite-type structure*

If calcium in scheelite $CaWO_4$ is replaced by a lanthanide atom R = Nd, Sm, Gd or Dy, taking into consideration the cross-substitution

$$R^{III+} + N^{III-} = Ca^{II+} + O^{II-},$$

this leads to the oxynitride series with the formulation RWO_3N which has the same structure as the calcium tungstate (Antoine et al. 1987). The tetragonal ($I4_1/a$) structure is made up of $[WO_3N]$ isolated tetrahedra which are linked to each other by R cations, the coordination number of which is equal to 8. These nitrido-tungstates are prepared, as brown non-hygroscopic powders, by heating the corresponding tungstates $R_2W_2O_9$ at 700–750°C in flowing ammonia. Their insulating behavior is consistent with tungsten W^{VI+} which is thus stabilized in a tetrahedral nitrogen environment. Yet, the reducing character of the NH_3 atmosphere was a priori unfavorable to keep this high oxidation state, as was the fact that no corresponding nitride (i.e. WN_2) exists in the W–N binary system, where only WN and W_2N are known.

4.1.2. *Silicate and alumino-silicate structures*

This subsection covers R–Si–O–N and R–Si–Al–O–N oxynitrides where $Si(O,N)_4$ and $(Si,Al)(O,N)_4$ tetrahedra are the structural units.

The different crystalline and glassy phases of the R–Si–O–N and R–Si–Al–O–N systems have given rise to many studies, because they form during sintering of silicon nitride and related nitrogen ceramics called "Sialons", the acronym of the four elements Si, Al, O, N. This important class of ceramic materials has much attracted interest for high-temperature engineering applications owing to their excellent properties, firstly the mechanical ones. The sintering is achieved by means of oxide additives such as rare-earth oxides, mainly Y_2O_3, with formation of phases mentioned above, the composition of which is located in the quinary R–Si–Al–O–N system.

The R–Si–Al–O–N system is represented by the so-called Jänecke's triangular prism (Jänecke 1907) in which all edges are equal. Figure 8 outlines this representation in the case of yttrium. It is based on a Si_3N_4–Al_4N_4–Al_4O_6–Si_3O_6 square in which concentrations are expressed in equivalent units, with yttrium also in equivalent units, along a third dimension. This forms two additional squares Si_3N_4–Y_4N_4–Y_4O_6–Si_3O_6 and Al_4N_4–Y_4N_4–Y_4O_6–Al_4O_6. The front triangular face of the prism thus represents oxides and the rear face nitrides. So, any point of the prism is a combination of 12 +ve and 12 −ve valencies, the compounds being regarded in ionic terms, regardless of the real character of the interatomic bonding (Gauckler et al. 1975, Jack 1976, Gauckler and Petzow 1977).

4.1.2.1. *Apatites.* Apatites constitute a large family of compounds, the most representative member of which is fluorapatite $Ca_{10}(PO_4)_6F_2$, corresponding to various cationic and anionic substitutions with, in addition, possibility of vacancies in both subnetworks. Although their formulation is comparable to that of fluorapatite, the rare-earth silicon oxynitrides $R_{10}Si_6O_{24}N_2$ (R = La, Ce, Nd, Sm, Gd, Y) and $R_{10-x}R'_xSi_6O_{24}N_2$ (Gaudé et al. 1975a, Hamon et al. 1975, Wills et al. 1976a, Mitomo et al. 1978, Guha 1980a) and the chromium Cr^{III}-substituted compounds $R_8Cr_2Si_6O_{24}N_2$ (R = La–Dy) (Hamon et al. 1975) are somewhat different because the two nitrogen atoms are not located in the same position as the two fluorine atoms in the hexagonal structure. Whereas F atoms occupy the trigonal

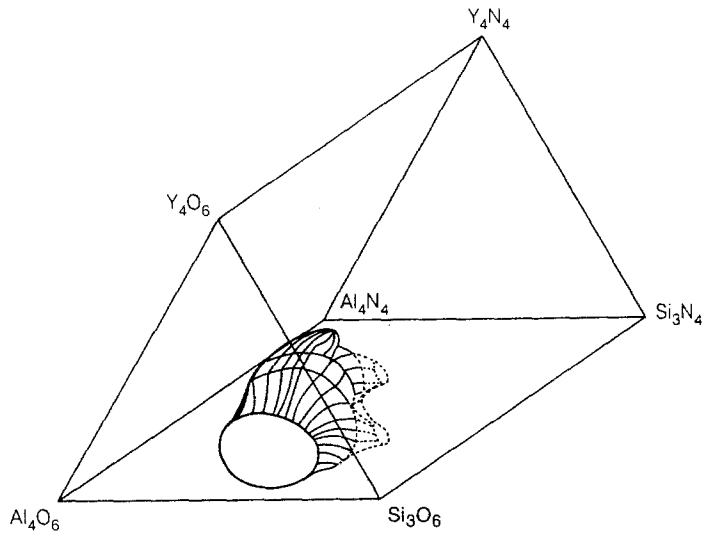

Fig. 8. Outline representation of the Y–Si–Al–O–N system. Glass-forming region within the yttrium–sialon triangular prism on cooling from 1700°C (Drew et al. 1981).

site 2a, the so-called "tunnel" position, N atoms are part of the silicon environment, thus forming mixed $[SiO_{4-x}N_x]$ individual tetrahedra (Gaudé et al. 1975b, 1977, Maunaye et al. 1976, Morgan 1979a). As shown by Morgan (1979a), such an occupancy agrees well with Pauling's second crystal rule (PSCR), which is essentially a local charge/bond strength balancing rule (McKie and McKie 1974):

$$V_{\text{anion}} \cong \sum_{1}^{N} \frac{V_{\text{cation}}}{C_{\text{cation}}},$$

where V is the valence and C the coordination of the N cations.

Figure 9 shows the $Sm_{10}(Si_6O_{22}N_2)O_2$ structure (space group $P6_3$). The nitrogen apatites are thought to exist over a range of compositions extending to silicate phases with defect apatite structure $R_{9.33}(SiO_4)_6O_2$ and $R_8\square_2(SiO_4)_6\square_2$ ($\square$ = vacancy).

Presence of nitrogen in the silicon tetrahedral environment means that there is the possibility to introduce more than two nitrogen atoms per unit cell (Lang et al. 1975): this was demonstrated by the preparation of $R_8M^{IV}_2Si_6N_4O_{22}$ (M^{IV} = Ti or Ge) nitrogen apatites, the maximum enrichment reported so far being in a vanadium V^V-containing composition, i.e. $Sm_{8.65}V_{1.35}Si_6N_{4.7}N_{21.3}$ (Guyader et al. 1975, 1978).

4.1.2.2. *Melilites.* Whereas apatites contain isolated tetrahedral units, melilites, which are natural alumino-silicates having the general formula $(Ca,Na)_2(Mg,Al)(Si,Al)_2O_7$, belong to the sorosilicate family. This family is characterized by $[Si_2O_7]$ disilicate groupings formed by two tetrahedra sharing one corner. Typical examples of melilites are given by akermanite $Ca_2Mg[Si_2O_7]$ and gehlenite $Ca_2Al[SiAlO_7]$. In the tetragonal

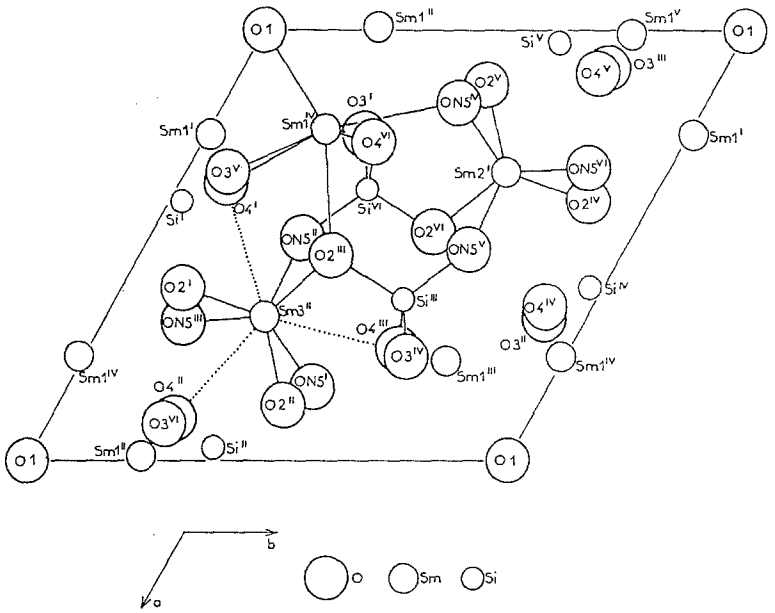

Fig. 9. Projection of the hexagonal apatite structure of $Sm_{10}Si_6N_2O_{24}$ along the *c*-axis (Gaudé et al. 1975b).

($P42_1m$) structure, the coordination number of calcium is 8 whereas magnesium (or aluminum) occupies a tetrahedral site. Introduction of rare-earth atoms into the calcium site (R^{3+} instead of Ca^{2+}) coupled with N/O substitution leads to several possibilities to form isostructural rare-earth-containing melilite-type oxynitrides (N-melilites), and a maximum nitrogen enrichment was obtained in the $R_2Si_3O_3N_4$ series (R = La–Yb, Y) by simultaneous replacement of Ca by R and Mg by Si in akermanite (Rae et al. 1975, Marchand et al. 1976, Wills et al. 1976b). These N-melilites were prepared by heating pressed pellets of $1R_2O_3$–$1Si_3N_4$ stoichiometric mixtures at 1500°C in nitrogen atmosphere. As silicon atoms occupy now all the tetrahedral (Si + Mg) sites, their structure may be described, considering the arrangement of silicon tetrahedra, as a sheet structure formed by an infinite linkage of $Si(O,N)_4$ tetrahedra lying in the plane perpendicular to the [001] direction, stacked one on top of the other and held together by layers of larger R^{3+} ions sandwiched between them (Jack 1976, Horiuchi and Mitomo 1979) (fig. 10). According to a preliminary neutron diffraction study of the $Y_2Si_3O_3N_4$ phase, Roult et al. (1984) concluded that the $[Si_2O_3N_4]$ grouping was arranged as two $[SiO_2N_2]$ tetrahedra with the third Si in a pure nitrogen $[SiN_4]$ environment. However, more recent ^{29}Si MAS-NMR results (Dupree et al. 1988) favor another nitrogen distribution, i.e. a structure with all silicon atoms in $[SiO_2N_2]$ tetrahedra, according to the presence of a single peak at –56.7 ppm.

In rare-earth–Si–Al–O–N systems, the $R_2Si_3O_3N_4$ melilites are the highest nitrogen-containing compounds, apart from α-sialons, and they are characterized by a high melting point: ~1900°C for $Y_2Si_3O_3N_4$ (Jack 1986).

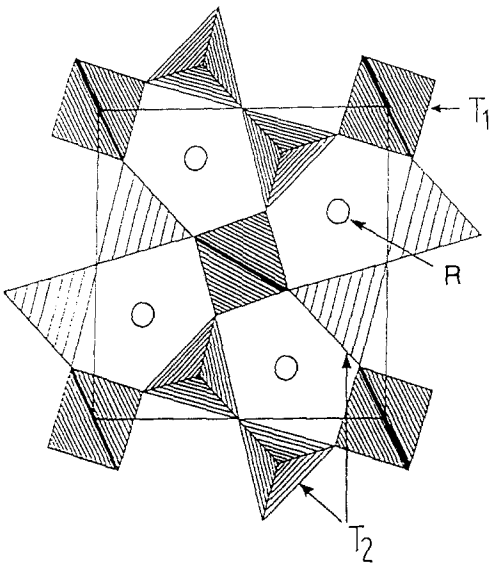

Fig. 10. Projection onto the (001) plane of the $R_2Si_3O_3N_4$ melilite structure in which both T_1 and T_2 tetrahedra are occupied by silicon atoms (after Lejus et al. 1994).

N-melilites, e.g. $Y_2Si_3O_3N_4$, form a continuous series of solid solutions with other members of the melilite series of silicates, e.g. akermanite and gehlenite (Jack 1976, Thompson 1989), and, recently, a significant solubility of Al in $R_2Si_3O_3N_4$ was observed, in particular for R = Sm by Cheng and Thompson (1994a) and for R = Y by Chee et al. (1994), resulting in the formation of a melilite solid solution $R_2Si_{3-x}Al_xO_{3+x}N_{4-x}$ ($0 \leqslant x \leqslant 1$), with Al atoms in the Mg sites of the akermanite structure.

This substitution of Al–O for Si–N bonds results in an improved oxidation resistance of the material, compared to the original N-melilite phases (Chee et al. 1994). Such a kind of composition appears as an intermediate phase during sintering of α-sialon ceramics and also forms in SiAlON materials as a grain boundary phase with good refractory properties (Cheng and Thompson 1994a,b).

4.1.2.3. *Cuspidines.* The structure of the mineral cuspidine $Ca_4Si_2O_7F_2$ (monoclinic, $P2_1/c$) is made up of $[Si_2O_7]$ groupings (Saburi et al. 1977). This structure is also that of rare-earth aluminates $R_4Al_2O_9$ (Brandle and Steinfink 1969). Starting from such $R_4M^{III}_2O_9$ oxide compositions, the cross-substitution

$$Si^{IV+} + N^{III-} = M^{III+} + O^{II-}$$

leads to the oxynitride compositions $R_4Si_2O_7N_2$ which were characterized as nitrogen cuspidines for R = Nd–Yb and Y (Marchand et al. 1976, Wills et al. 1976a,b, Mah et al. 1979, Morgan 1979b, Guha 1980b). They were prepared by solid-state firing of stoichiometric mixtures of R_2O_3, SiO_2 and Si_3N_4 powders at high temperatures (1550–1700°C). Large single crystals of $La_4Si_2O_7N_2$ were obtained by Ii et al. (1980) by the floating zone method. It was of interest to know whether the nitrogen atoms bond

to silicon or whether they replace fluorine atoms. Morgan (1986) developed crystal chemistry arguments using Pauling's second crystal rule (PSCR) for nitrogen bonding to silicon. On the other hand, neutron diffraction showed that oxygen and nitrogen atoms are crystallographically ordered with the only presence of $[SiO_3N]$ tetrahedra, which means that the bridging atom in the $Si_2O_5N_2$ disilicate groupings is an oxygen atom: $O_2NSi–O–SiO_2N$ (Roult et al. 1984, Marchand et al. 1985). This result is in agreement with the ^{29}Si MAS-NMR spectrum which shows a single resonance at –74.4 ppm (Dupree et al. 1988). Note finally that intermediate cuspidine members between $R_4Si_2O_7N_2$ and $R_4Al_2O_9$ compositions such as pseudo-tetragonal Y_4SiAlO_8N are also known (Thompson 1986).

4.1.2.4. *Pyroxene-type.* The yttrium compound $MgYSi_2O_5N$, which can be regarded as being derived from diopside $[CaMg(SiO_3)_2]_n$ with replacement of Ca by Y and of one O by N is the only known example so far of nitrided silicate with chain structure of pyroxene-type (Patel and Thompson 1988).

4.1.2.5. *Wollastonites.* The structure of α-$CaSiO_3$ or pseudo-wollastonite, one of the $CaSiO_3$ polymorphs, is characterized by polytypism. In the predominant polytype, the structure is formed by four layers, one of which is composed of $[Si_3O_9]$ rings of three tetrahedra (Yamanaka and Mori 1981). The structure thus consists of alternate layers of 3-membered rings and close-packed metal cations stacked perpendicular to the *c*-axis. Isostructural $RSiO_2N$ oxynitrides (R = La, Ce, Y) result from the rare-earth/calcium–oxygen/nitrogen substitution, with $[SiO_2N_2]$ tetrahedra forming $[Si_3O_6N_6]$ rings (Morgan and Caroll 1977, Morgan et al. 1977, Roult et al. 1984). Each tetrahedron is connected via nitrogen to the other two tetrahedra (Morgan et al. 1977) and the corresponding ^{29}Si NMR resonance peak, studied in the case of $YSiO_2N$, is situated at –65.3 ppm (Dupree et al. 1988). Similar structures have also been observed along solid solutions between $RSiO_2N$ and $RAlO_3$. In the nitrogen wollastonites, the number of layers is determined by the nature of the R cation and by the Si/Al ratio: $YSiO_2N$ has a 4-layer structure, $CeSiO_2N$ a 6-layer structure and Y_2SiAlO_5N a 2-layer structure (Korgul and Thompson 1989).

4.1.2.6. *α-Sialons.* The general composition for α-sialon is $M_xSi_{12-(m+n)}Al_{m+n}O_nN_{16-n}$ – or more simply $M_x(Si,Al)_{12}(O,N)_{16}$ – with $x \leqslant 2$, where M is a modifying cation such as Li^+, Mg^{2+}, Ca^{2+} or R^{3+} (Hampshire et al. 1978, Park et al. 1980; review article: Cao and Metselaar 1991); or a multication (Ekström et al. 1991, Hwang et al. 1995). As the name indicates, the structure of α-sialons is derived from α-Si_3N_4 (trigonal, P31c) (Marchand et al. 1969). In α-Si_3N_4, the lower half of the hexagonal unit cell is the same as in β-Si_3N_4 (hexagonal, $P6_3/m$), and the upper part is related to the lower half by a *c*-glide plane. In this way, a large interstitial site is formed (two per unit cell) – instead of the large channel observed in the β-Si_3N_4 structure – in which M cations can be introduced, without structural change. They insure the charge balance after partial replacement of Si by Al and N by O. In the case of rare-earth metal ions R_x, x is equal to $m/3$ (if v is the valency of the metal M, electroneutrality requires $x = m/v$) and the upper limiting composition of

a purely nitrided R α-sialon is $R_2Si_6Al_6N_{16}$. The value $x=2$ has not been achieved, and x decreases as the size of the modifying R^{3+} cation becomes larger, from ytterbium to neodymium (Huang et al. 1986a,b).

Y–Si–Al–O–N has been studied the most extensively of the α-sialon systems (Huang et al. 1983, Stutz et al. 1986, Slasor and Thompson 1987). In this case $0.33 \leqslant x \leqslant 1$ (Y) and $0.5 \leqslant n < 1.5$ (O). A $Y_{0.5}Si_{9.75}Al_{2.25}O_{0.75}N_{15.25}$ ($m=1.5$, $n=0.75$) yttrium α-sialon composition, for example, was prepared by hot-pressing a powder mixture of Y_2O_3, Si_3N_4 and AlN at 1750–1900°C. A structure refinement of this Y-sialon composition from X-ray powder profile data showed that the structure is built up of $[(Si,Al)(N,O)_4]$ tetrahedra, each Y atom being surrounded by seven (N,O) neighbors in the interstitial sites (Izumi et al. 1982, 1984, Stutz et al. 1986). Cao et al. (1993) showed from neutron diffraction results that Al and Si atoms are ordered.

Cao and Metselaar (1991) have described the properties of α-sialons. These ceramics offer good high-temperature mechanical properties, in particular excellent hardness and thermal shock resistance. Two-phase yttrium α–β-sialon composite materials (β-sialons: $Si_{6-x}Al_xO_xN_{8-x}$ with $0 \leqslant x \leqslant 4.2$) are also of great interest (Cao et al. 1992, Van den Heuvel et al. 1996). The β-phase forms elongated grains in an isomorphic α-matrix, and because of the analogy to whisker-toughened materials, they are called self-reinforced Si_3N_4 (Metselaar 1994). Such materials show high fracture toughness, $K_{Ic} > 8\,MPa\,m^{1/2}$, and high flexture strengths, > 1000 MPa (Pyzik and Beaman 1993).

The parameters affecting pressureless sintering of α-sialons with rare-earth modifying cations have been specified by O'Reilly et al. (1993). Hwang and Chen (1994) have studied the reaction hot-pressing mechanism of yttrium α- and α–β-sialons and, recently, Menon and Chen (1995a,b) have reported the densification behavior during the reaction hot-pressing of different α-Si_3N_4, Al_2O_3, AlN and M oxide powder mixtures (M = Li, Mg, Ca, Y, Nd, Sm, Gd, Dy, Er and Yb), forming α-sialon ceramics.

4.1.2.7. *U-phases.* The so-called "U-phase" occurs in rare-earth sialon ceramics as a crystalline grain-boundary phase (Spacie et al. 1988). Its composition corresponds to $R_3Al_{3+x}Si_{3-x}O_{12+x}N_{2-x}$ with R = La, Ce, Nd, Sm, Dy and Y, and $0 \leqslant x \leqslant 1$. The structure of the neodymium phase, determined first from X-ray powder data (Käll et al. 1991b), then from $Nd_3Al_{3.5}Si_{2.5}O_{12.5}N_{1.5}$ single crystals obtained by heating mixtures of Si_3N_4, SiO_2, Al_2O_3 and Nd_2O_3 at 1550 K under nitrogen (Käll et al. 1991a), is of the trigonal (P321) $La_3Ga_5GeO_{14}$ structure type (Kaminskii et al. 1983). It exhibits layers of corner-sharing $(Si,Al)(O,N)_4$ tetrahedra interconnected with $Al(O,N)_6$ octahedra. The larger Nd atoms are located between the tetrahedral layers and coordinate to eight (O,N) atoms forming a distorted cubic antiprism, as in the melilite structure (Belokoneva and Belov 1981). A partially ordered distribution of Al and Si atoms was deduced from the M–(O,N) bond distance values.

4.1.2.8. *β-K_2SO_4-type oxynitrides.* From a crystallographical point of view, silicate minerals of the olivine group, sometimes called "hexagonal spinels", and compounds crystallizing with the β-K_2SO_4 type structure can easily be confused due to similarities

in crystal symmetry and unit cell dimensions (orthorhombic, Pnma). The $REu^{II}SiO_3N$ oxynitrides (R = La, Nd, Sm) (Marchand 1976b) are isotypic with the high-temperature modification of $Eu_2^{II}SiO_4$ which is stabilized at room temperature, probably by the presence of $(Eu^{3+} + N^{3-})$ traces (Marchand et al. 1978). Their structure is of β-K_2SO_4 type, with isolated $[SiO_3N]$ tetrahedra held together by the two kinds of crystallographically independent lanthanide ions. The method used to prepare these divalent europium compounds is quite original. The oxidation–reduction reaction:

$$3Eu^{3+} + N^{3-} \rightarrow 3Eu^{2+} + \tfrac{1}{2}N_2^{\uparrow},$$

which was carried out "in situ" enables the use of Eu_2O_3 rather than EuO. So, an excess of Si_3N_4 is introduced in the reaction mixture in order to obtain the following reaction:

$$3Eu_2O_3 + 3R_2O_3 + 2Si_3N_4 \xrightarrow{1350°C} 6REuSiO_3N + N_2^{\uparrow}.$$

With respect to $REuSiO_3N$ compositions, a second substitution N/O leading to isostructural $R_2Si_2O_2N_2$ oxynitrides, with isolated $[SiO_2N_2]$ tetrahedra, has not been reported so far.

4.1.2.9. *Oxynitride glasses and glass ceramics.* Oxynitride glasses, included those containing rare-earth elements as modifier cations, were first observed in the 1970s when an intensive effort of research was made on the sintering of Si_3N_4-based ceramics, either silicon nitride itself or sialon ceramics (Jack 1976).

It was found that addition of a metal oxide, such as MgO or Y_2O_3, induces a liquid-phase densification process which results in the formation of a grain-boundary oxynitride glass. The mechanical properties of the nitrogen ceramics at elevated temperatures depend markedly on the amount and characteristics of these intergranular glassy phases which need to be eliminated by crystallization. In particular, they can deteriorate the high-temperature strength, and the creep and oxidation resistance of the ceramic.

Later, it was realized that oxynitride glasses, which revealed themselves to be more resistant to high temperatures than the corresponding non-nitrided glasses, were of interest in their own right. Various systems, in particular the Y–Si–Al–O–N quinary system, were extensively investigated with the preparation and study of properties of a wide variety of bulk glass compositions.

The R–Si–Al–O–N rare-earth oxynitride glasses have been generally prepared by melting, then quenching, mixed powder batches of R_2O_3, SiO_2, Al_2O_3 and AlN. Si_3N_4 was also used as nitrogen source. High temperatures up to 1700°C are necessary for melting and homogenization which require also a very low oxygen partial pressure to avoid oxidizing the glass. Nitrogen overpressures have been used in some cases (Makishima et al. 1980, 1983, Mittl et al. 1985). Note that the choice of non-reactive crucible materials is somewhat limited: molybdenum and boron nitride are the most used materials.

Above all, the characteristics of the glasses are closely related to the amount of nitrogen incorporated. First of all is the extent of the vitreous domains which, at the

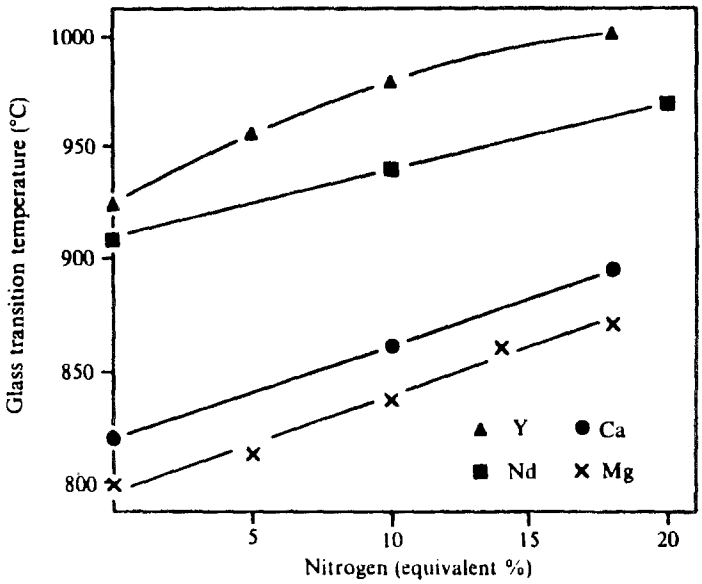

Fig. 11. Variation of T_g with nitrogen content for M-sialon glasses with the same cation composition M:Si:Al=28:56:16 (Hampshire et al. 1985).

same temperature, is smaller in the oxynitride systems than in the corresponding oxide systems, for example in the Y_2O_3–SiO_2–AlN cut as compared to the Y_2O_3–SiO_2–Al_2O_3 cut.

For oxynitride glasses of the same cation composition but of varying O/N ratios, a wide range of glass properties, e.g. density, glass transition temperature T_g, viscosity, microhardness, Young's elastic modulus, fracture toughness, refractive index, chemical durability, all increase or improve with increasing nitrogen content, while the linear thermal expansion coefficient decreases. As an illustration, figs. 11 and 12 present the variation of glass transition temperature for different M-sialon glasses (M=Y, Nd, Ca, Mg), and the change in viscosity at two different temperatures for yttrium sialon glasses with the same cation ratios. All the observed changes point out that the replacement of O by N strengthens the glass structure. This is evidence for the structural role played by nitrogen which substitutes for oxygen in the aluminosilicate glass network to produce a more tightly bonded and highly cross-linked structure. The general improvement of the glass properties has been mainly attributed to the nitrogen coordinating to three Si (Al) atoms as compared with only two for oxygen.

Among the rare-earth oxynitride glass systems, yttrium sialon glasses have been the most extensively investigated, certainly because of the interest in Y_2O_3 as a sintering aid for sialon ceramics. After the first reports of Mulfinger et al. (1973) and Jack (1976, 1978), extensive compositional studies have been carried out on the entire five component Y–Si–Al–O–N system by Loehman (1979, 1980) and Drew et al. (1981, 1983). Shillito et al. (1978), Milberg and Miller (1978), Messier (1982), Messier and Broz (1982) and

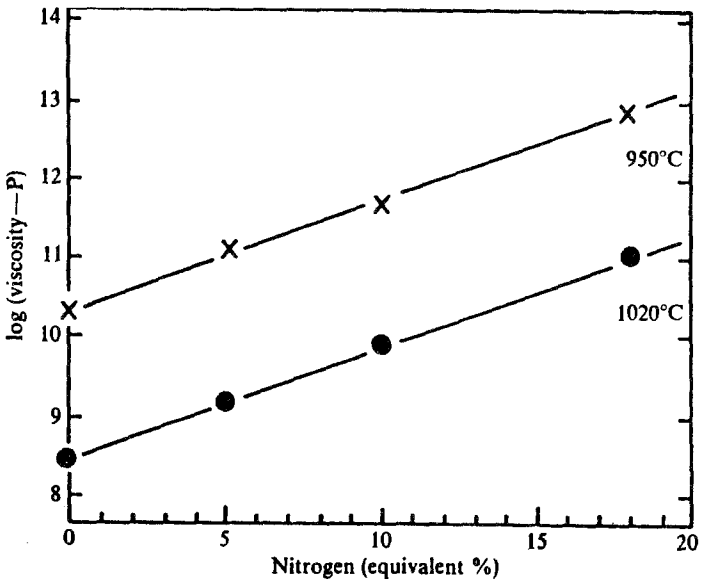

Fig. 12. Effect of nitrogen on viscosity of Y-sialon glasses (Y:Si:Al=28:56:16) at 950 and 1020°C (Hampshire et al. 1985).

Loehman (1982) have also prepared yttrium sialon glasses which appear to be highly refractory glasses and require high processing temperatures (up to 1700°C).

Y–Si–Al–O–N glasses have been studied or reviewed in many other papers dealing with oxynitride glasses (Loehman 1983, 1985, Messier 1985, 1987, Hampshire et al. 1985, Lang 1986, Sakka 1986, 1995, Rouxel et al. 1992, 1994, Murakami and Yamamoto 1994, E.Y. Sun et al. 1996).

Figure 8 gives a general view of the glass-forming region in the quinary Y–Si–Al–O–N system at 1700°C (Drew et al. 1981). $Y_9Si_{20}Al_9O_{53}N_9$ and $Y_{15}Si_{15}Al_{10}O_{45}N_{15}$ are two examples of glassy compositions containing 9 and 15 at.% nitrogen, respectively.

Concerning the properties of such glasses, Shillito et al. (1978) showed that the microhardness of a series of Y–Si–Al–O–N glasses increased by up to 30% as the nitrogen content increased from 0 to 4.4 wt.%. It continues to increase with higher nitrogen contents, as shown by Messier and Broz (1982), who also measured high values of the elastic moduli, up to 186 GPa, by an ultrasonic technique.

Hampshire et al. (1984) reported on the N content dependence of T_g, viscosity and microhardness for homogeneous series of glass compositions. Their results corroborated the general conclusions concerning the structural role of nitrogen in the glass network. Loehman (1985) showed that nitrogen increased the chemical durability by measuring sample weight losses in Soxhlet apparatus. The electrical behavior of Y–Si–Al–O–N glasses was mainly studied by Leedecke and Loehman (1980), Leedecke (1980) and Kenmuir et al. (1983). All the glasses exhibited high resistivities, and dielectric constants increased with increasing N content. As reported by Messier and DeGuire (1984), the

Table 2
Glass formation in the Nd_2O_3-SiO_2-AlN and Nd_2O_3-SiO_2-Al_2O_3 systems at 1350°C

Limits	Nd–Si–Al–O–N system			Nd–Si–Al–O system		
	Nd_2O_3 (%)	SiO_2 (%)	AlN (%)	Nd_2O_3 (%)	SiO_2 (%)	AlN (%)
Lower limit	10	50	30	12	42	13
Upper limit	15	60	40	24	68	39

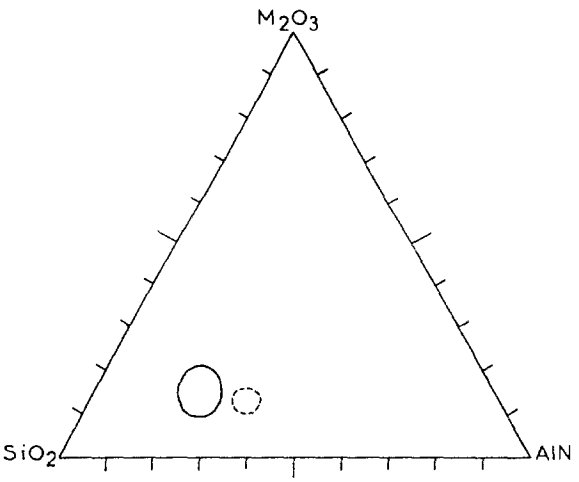

Fig. 13. Comparison of the glass-forming region at 1400°C in the Gd_2O_3–SiO_2–AlN (solid edge) and Nd_2O_3–SiO_2–AlN (dashed edge) systems (Rocherullé et al. 1989).

Y–Si–Al–O–N glasses, as many other oxynitride glasses, have often a grey color and poor optical quality.

Sakka (1995) has reported neutron diffraction results on yttrium sialon glasses which give a more precise idea of the oxynitride glass structure. They indicate that not all N atoms are bonded to three Si atoms but some are bonded to two or one Si (Jin et al. 1994). Kruppa et al. (1991), using ^{15}N MAS-NMR, also identified previously twofold and threefold coordinated nitrogen. On the other hand, ^{27}Al MAS-NMR results indicate that N atoms have a much stronger tendency to form bonds with Si than with Al. These results confirm the experiments of Aujla et al. (1986), who had used ^{29}Si NMR, and are in agreement with IR (Loehman 1983) and Raman (Rouxel et al. 1990) studies. Very recently, in a study of Y–Ba–Si–O–N glasses by neutron diffraction, Jin et al. (1996) have also found 3- and 2-coordinated nitrogen atoms, with a decrease in the 3-/2- ratio as the N content increases.

Neodymium glass compositions were first studied by Lang et al. (1980, 1982), mainly in the Nd_2O_3–SiO_2–AlN cut of the quinary system. At 1350°C, up to 7 wt.% nitrogen could be introduced into the glass network. The limits of glass formation determined in the oxynitride and oxide pseudo-ternary systems are indicated in table 2 (Lang et al. 1980, Marchand et al. 1985).

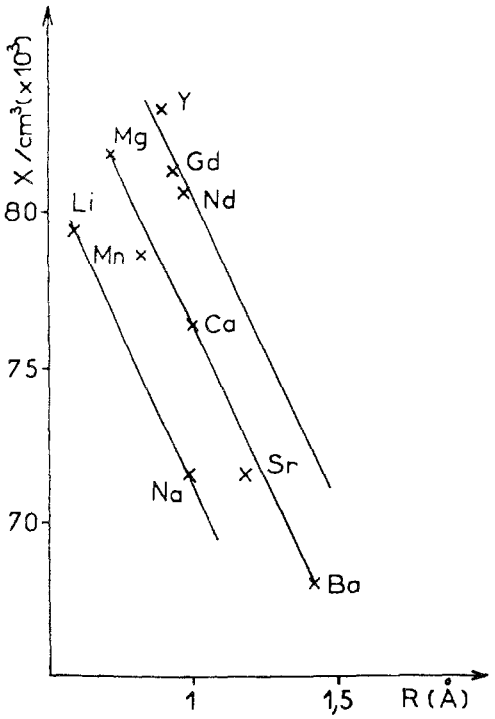

Fig. 14. Variation of the anion density X versus modifier cation radius M^{n+} in different M–Si–Al–O–N oxynitride glasses (Rocherullé et al. 1989).

Figure 13 compares the R_2O_3–SiO_2–AlN vitreous domains at 1400°C for R = Nd and Gd (Rocherullé et al. 1989). Verdier et al. (1982) and Pastuszak and Verdier (1983) made a comparative study between Nd glasses and other oxynitride (Mg, Ca, Ba, Mn) glasses. Figure 14 gives the anion density X as a function of the modifier cation radius (Rocherullé et al. 1989): the higher value of X, the higher compactness of the glass structure. For Nd, $X = 80.6 \times 10^3$ g anion cm^{-3}, which is not as high as the value for Y. As shown in fig. 14, a group of parallel lines is obtained according to the formal charge of the modifier cation. As in the yttrium glasses, the replacement of oxygen by nitrogen in the neodymium glasses results in a more strongly bonded glass network (Drew et al. 1981, 1983, Hampshire et al. 1985).

Korgul and Thompson (1989) showed that $RSiO_2N$ wollastonite (see section 4.1.2.5) compositions in the Nd–Si–O–N and Ce–Si–O–N systems could be melted and cooled to form glasses with a high (20 at.%) nitrogen content. They are interesting materials, both as glasses and as precursors for the preparation of glass ceramics.

Besides yttrium and neodymium, several studies were also carried out with other R elements, for example in the R–Si–O–N systems by Ohashi et al. (1995). Makishima et al. (1980, 1983) prepared a La–Si–O–N oxynitride glass containing 18 at.% N at 1650–1700°C under high N_2 pressure (3 MPa). The glass was transparent and very hard, with a Vickers hardness of 12.0 GPa.

The glass formation at 1450°C in the quinary La–Si–Al–O–N and senary Mg–La–Si–Al–O–N systems was studied by Avignon-Poquillon et al. (1992). In the same way, Tredway and Loehman (1985) had studied the atom-for-atom substitution of Sc^{3+} for Mg^{2+} in the Mg–Si–O–N and Mg–Si–Al–O–N systems. Good quality glasses containing up to 7 mol.% Sc_2O_3 (15 wt.%) were obtained. R–Si–Al–O–N nitrogen glasses were also reported for R = Sm, Gd, Yb, Y (Lang et al. 1980). The glass-forming region in the gadolinium sialon pseudo-ternary system Gd_2O_3–SiO_2–AlN was determined at 1400°C by Rocherullé (1986) and Rocherullé et al. (1989), and compared to the glass-forming composition in the oxide system Gd_2O_3–SiO_2–Al_2O_3. As in other R–Si–Al–O–N systems, the oxynitrided region is smaller than the purely oxygenated one. When compared, however, with results obtained in the corresponding neodymium systems, these regions are larger. The Gd_2O_3 content can reach 30 mol.% in the oxide system which is equivalent to a Gd content of about 10^{22} atoms cm^{-3}. These gadolinium-containing glasses, in addition to good mechanical and chemical properties, may be used as neutron-absorbent glasses, because of the high nuclear cross-section of gadolinium (46,000 barns).

Recently, Murakami and Yamamoto (1994) determined the glass transition and softening temperatures, and the oxidation resistance of various R–Si–Al–O–N glasses (R = La, Nd, Sm, Gd, Dy, Er, Yb and Y). Ytterbium glasses, having the smallest R^{3+} ionic radius, have the best oxidation resistance. Sebaï et al. (1995) determined the oxidation behavior of Y and Nd oxynitride glasses. The thermal expansion coefficients and glass transition temperatures of Y–Mg–Si–Al–O–N glasses were measured by Peterson and Tien (1995) using dilatometry, and compared to values calculated on the basis of composition. Their devitrification was studied by Rocherullé et al. (1997) using DTA: nitrogen does not change the crystallization mechanism which is controlled by a diffusion process.

Ramesh et al. (1997) have measured the effect of the R cationic substitution on density, glass transition temperature, viscosity and hardness in a homogeneous series $R_{12.3}Si_{18.5}Al_7O_{54.7}N_{7.5}$ (R = Ce, Nd, Sm, Eu, Dy, Ho, Er). All these characteristics increase from Ce to Er, with the exception of Eu, which has been shown to be in the Eu^{2+} state in this glass.

Numerous oxynitride glass compositions were investigated by Chyung and Wusirika (1978) and Wusirika and Chyung (1980) for their crystallization behavior. They found that the oxynitride glasses were self-nucleating and able to produce, after heating at appropriate temperatures, fine-grained glass ceramics. The crystallization of Y–Si–Al–O–N glasses which are quite stable to devitrification, was examined by several authors (Loehman 1980, Leedecke 1980, Drew et al. 1981, Messier 1982) and more particularly by Thomas et al. (1982) and Leng-Ward and Lewis (1985, 1989) by means of electron microscopy, differential thermal analysis, X-ray diffraction and EDAX analysis. They concluded that the nature of the oxide and oxynitride phases that will crystallize depends not only on the initial glass composition but also on the processing temperature and time.

Rouxel et al. (1989), who determined the viscosity against temperature through creep tests, have followed the crystallization of an Y–Si–Al–O–N glass by ultrasonic

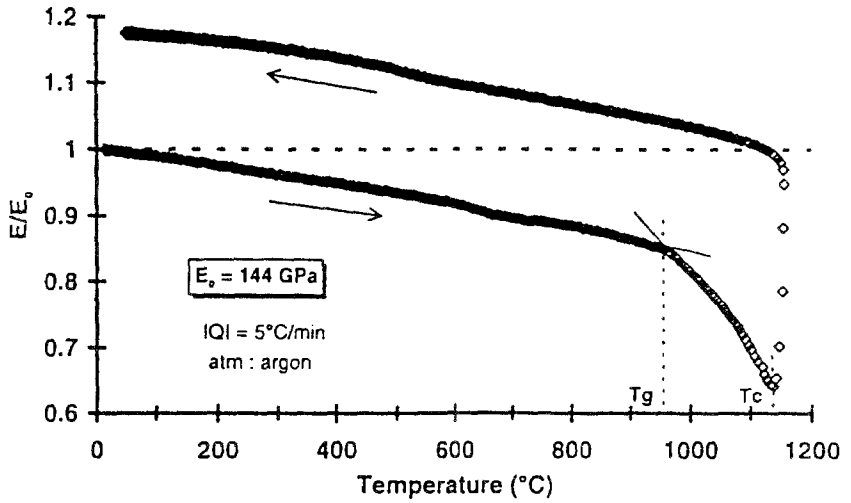

Fig. 15. Changes in Young's modulus with temperature for an $Y_{40}Si_{56}Al_4O_{83}N_{17}$ glass composition (Lemercier et al. 1997).

measurements of Young's modulus variation. The changes in Young's modulus with temperature are illustrated in fig. 15 (Lemercier et al. 1997).

In the Nd–Si–Al–O–N glass-forming region, Fernie et al. (1989) isolated, as a crystallization product, a single phase of the $Nd_3Si_3Al_3O_{12}N_2$ composition which is stable up to temperatures of 1400–1450°C.

Rare-earth sialon glasses may also have practical applications, for example as fibers for reinforcement, joining agent for ceramics, protective coatings, nuclear waste materials or as seen before, as neutron-absorbent glasses.

4.2. *Octahedral environment*

4.2.1. *Perovskite-type structure*

If one considers ABO_3 oxide perovskites, the different possibilities for the A–B couple with respect to the valence conditions are listed in table 3.

Formation of rare-earth-containing oxynitride perovskites $ABO_{3-x}N_x$ must, after introduction of R atoms in site A, comply with the relation $a+b=6+x$, in which a and b are the respective "charges" of A- and B-type atoms. It can be seen that the sum $(a+b)$, which can range in a continuous way between 6 and 9, allows various possibilities of substitution. These are discussed in the following paragraphs.

$RTiO_2N$ (R = La, Nd), $RTaON_2$ (R = La–Dy) and $LaNbON_2$ oxynitrides (Marchand et al. 1991b) were prepared at 950°C by reaction between ammonia and the corresponding ternary oxides, and were characterized as orthorhombic perovskites of the $GdFeO_3$-type (Muller and Roy 1974). The slight deformation, which induces the loss of cubic

Table 3
Various ABO_3 perovskite compositions

A–B couple	Example of A element in site 12	Example of B element in site 6	Formula
3–3	La	Al	$LaAlO_3$
2–4	Ba	Ti	$BaTiO_3$
1–5	Li	Nb	$LiNbO_3$
0–6	□	Re	$\square ReO_3$

symmetry of the "ideal" perovskite structure, gives an (8+4) coordination for A atoms, instead of 12.

$LaTiO_2N$ and $NdTiO_2N$ (Ti^{IV+}) brown powders have almost the same unit cell as the analogous black $RTiO_3$ compounds which formally correspond to Ti^{III+}, but they have an insulating character whereas $LaTiO_3$ is metallic at $T > 100\,K$ and $NdTiO_3$ is a semiconductor at room temperature (Maclean et al. 1981, Greedan 1985). This reminds one of the existence of only metallic TiN and Ti_2N in the Ti–N binary system.

The oxynitrides $RTiO_2N$, $RTaON_2$ and $LaNbON_2$, which have insulating properties, have been considered, as well as other oxynitride perovskites such as $BaTaO_2N$ and $BaNbO_2N$ (Marchand et al. 1986), as possible substitutes for $BaTiO_3$-based dielectric materials in high dielectric constant ceramic capacitors (Marchand and Laurent 1984). In addition to these bulk oxynitrides, Cohen and Riess (1994) have prepared oxynitride/thin films – 0.5 to 2.5 μm thick – by reactive sputtering under Ar + N_2 atmosphere, in particular amorphous $LaNb(O_yN_2)_x$ films ($x = 8/(2y+6)$ and $0.24 \leqslant y \leqslant 0.32$ from a multiphase LaN + NbN target. The $LaNb(O_{0.24}N_2)_{1.24}$ composition had an electrical resistivity at room temperature of $1.5 \times 10^2\,\Omega$ cm. The high-gloss colored tantalum compounds, especially $GdTaON_2$ and $PrTaON_2$, could be used as pigments in paints and plastics (Cerdec AG Keramische Farben 1994).

In the nitrogen-containing perovskite family, one could hope to observe a maximum nitrogen enrichment, i.e. an ABN_3 composition, using for example La^{III+}–W^{VI+} as an A–B couple. However, nitridation of $La_2W_2O_9$ in flowing ammonia (in the 700–900°C temperature range) led to the perovskite-type oxynitrides $LaWO_yN_{3-y}$ ($y \approx 0.6$) (Bacher et al. 1988) in which W is in a reduced mixed-valence state, as in the oxygen tungsten bronzes Na_xWO_3 of similar structure (Magneli and Blomberg 1951). A time-of-flight neutron diffraction study indicated a tetragonal symmetry ($I\bar{4}$, $a \approx a_0\sqrt{2}$; $c \approx 2c_0$, fig. 16) with disordered O and N atoms. The RWO_yN_{3-y} perovskites (R = La, Nd) show a n-type semiconducting behavior (Antoine et al. 1988).

Mixed-valence oxynitride perovskites were also obtained with vanadium. Regarding the La–V system, the homogeneity range extends from $LaV^{III+}O_3$ to $LaVO_{2.1}N_{0.9}$ where vanadium has the V^{III+}–V^{IV+} mixed valence. Those $LaVO_{3-x}N_x$ oxynitrides behave as p-type semiconductors throughout the whole composition range (Antoine et al. 1989).

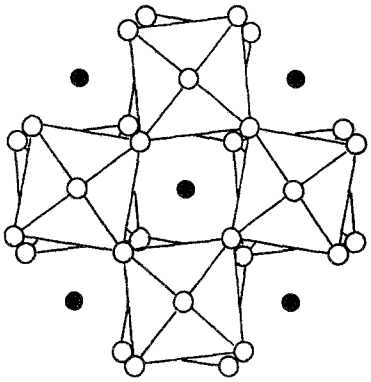

Fig. 16. Projection onto the (001) plane of the tetragonal structure of $LaWO_{0.6}N_{2.4}$ showing that the $W(N,O)_6$ octahedra are rotated by $\pm 8°$ along the *c*-axis. The open circles are (N,O) and the solid circles are La. The tungsten atoms are not represented (Antoine et al. 1988).

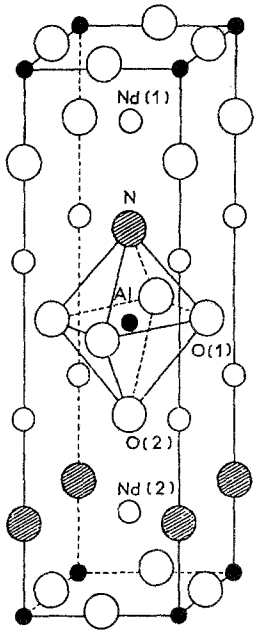

Fig. 17. Perspective view of the tetragonal unit cell (space group I4mm) of Nd_2AlO_3N. O(1) atoms are at bridge sites, O(2) and N are at apical sites (Marchand et al. 1982).

4.2.2. *K_2NiF_4-type structure*

The well-known K_2NiF_4-type structure is closely related to the perovskite structure and the AB_2X_4 tetragonal compounds belonging to this family are often called "bidimensional perovskites" (Muller and Roy 1974). Yellow, air stable R_2AlO_3N oxynitride powders with that structure (R = La, Ce, Pr, Nd, Sm, Eu) (Marchand 1976a, Huang et al. 1990) were prepared from pressed mixtures of $R_2O_3 + AlN$ sintered at 1350°C in sealed nickel tubes. Their formulation is deduced from that of isostructural $RM^{II}AlO_4$ aluminates (M^{II} = Ca, Sr, Eu) by the cross-substitution

$$R^{III+} + N^{III-} = M^{II+} + O^{II-}.$$

A comprehensive determination of the Nd_2AlO_3N structure by neutron diffraction showed that oxygen and nitrogen, which have quite different Fermi lengths ($b(O) = 0.58 \times 10^{-12}$ cm; $b(N) = 0.94 \times 10^{-12}$ cm), are ordered in the structural arrangement. The $[AlO_5N]$ octahedra share only the four oxygen corners of the octahedron median plane and the nitrogen atoms occupy one of the free corners. Octahedra thus form layers which are linked to each other by the neodymium atoms and, as shown in fig. 17, there are two independent Nd atoms, having a coordination of 9, instead of 12 in the perovskite structure (Marchand et al. 1982).

Let us note that another series of oxynitrides, $M^{II}_2TaO_3N$ (M^{II} = Ca, Sr, Ba), exists with the K_2NiF_4-type structure (Pors et al. 1991, Assabaa-Boultif et al. 1994).

4.2.3. *Magnetoplumbite-type structure*

This type of structure is reported here because it can be considered as a "spinel-type" structure.

Lanthanide and aluminum oxynitrides having a composition close to $RAl_{12}O_{18}N$ (R = La–Gd) (Wang et al. 1988, W.Y. Sun and Yen 1989, W.Y. Sun et al. 1991a,b), have a hexagonal structure ($P6_1/mmc$) which is similar to that of magnetoplumbite $PbFe_{12}O_{19}$. It is made up of spinel blocks which are separated by mirror planes containing the lanthanide atoms. It is assumed, when compared to defect lanthanide hexaaluminates $RAl_{11}\square O_{18}$ (R = La–Sm) (Roth and Hasko 1958, Warshaw 1961) that nitrogen has a role in the stabilization of the magnetoplumbite structure, probably because of the presence of Al_3O_3N units in the spinel blocks (Wang 1989). Wang et al. (1990) have reported the oxidation behavior of these magnetoplumbite oxynitrides. Note that magnetoplumbite and β-alumina structures are quite similar.

4.3. *"Cubic" environment*

Oxynitrides with fluorite or pyrochlore structure have been chosen to be classified under this heading. Yet, the "cubic" environment of the M coordinating element (and also of R) is in fact defect and distorted when compared to the true cubic environment.

4.3.1. *Fluorite-type structure*

In the $R_{2.67}W_{1.33}(O,N,\square)_8$ cubic oxynitride phases (R = Nd–Yb, Y), which were prepared as brown powders by reaction at 800°C between ammonia and tungstates R_2WO_6 (Marchand et al. 1993), the oxygen and nitrogen atoms occupy the corners of cubes, while rare earth and tungsten atoms are at the center, thus forming a face-centered cubic arrangement, as calcium in CaF_2. The observed cation/anion stoichiometry, which is always close to $A_4X_{6.6}$ whatever the R element, is about halfway between that of fluorite (A_4X_8) and that of Mn_2O_3 bixbyite (A_4X_6). As shown in fig. 18, in Mn_2O_3, only six out of the eight corners of the anionic cubes are occupied and the vacancies are regularly distributed, either according to the diagonal of a face or according to the main diagonal of the cube.

Concerning the defect fluorites $R_{2.67}W_{1.33}(O,N,\square)_8$, fig. 18 shows that while maintaining the cationic arrangement with R and W atoms in the same 4a crystallographic position of the $Fm\bar{3}m$ space group, a displacement of certain anions from their ideal position, added to the presence of vacancies, would allow the high coordination environment to be kept for the large rare-earth atoms, and to obtain a convenient tetrahedral coordination for tungsten which has the VI+ oxidation state in these oxynitrides. It would be interesting to carry out a neutron diffraction study.

4.3.2. *Pyrochlore-type structure*

Cubic oxynitrides $R_2Ta_2O_5N_2$ (R = Nd–Yb, Y), which were prepared by heating the corresponding $RTaO_4$ tantalates in ammonia at 900–950°C (Pors et al. 1993), have

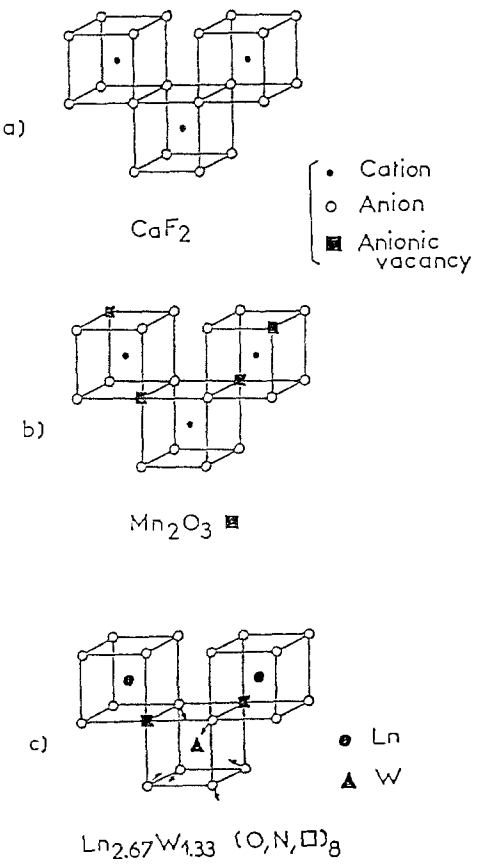

Fig. 18. Structural filiation between: (a) fluorite CaF_2, (b) bixbyite Mn_2O_3 and (c) $R_{2.67}W_{1.33}(O,N,\square)_8$ oxynitrides (Marchand et al. 1993).

enriched the family of pyrochlores $A_2B_2X_7$ which already accepts a lot of substitutions in the different cationic and anionic sites of the structure, not to mention the possibility of vacancies at the A and X sites. From a crystallographical point of view, the general formula may be written as $A_2B_2X_6X'$, the variable value of the coordinate x of anions X being responsible for the more or less distorted environment of cations A(6X + 2X′) and B(6X). In the studied $R_2Ta_2O_5N_2$ oxynitrides, this distortion is expected to be maximum for the largest lanthanides, the trigonal antiprism around tantalum atoms thus becoming an octahedron, whereas R elements having a smaller ionic radius would tend towards a defect fluorite structure. Note that the $A_2B_2O_5N_2$ stoichiometry implies a partial disorder for at least one of the two anionic positions. A neutron diffraction study could answer the question.

Dolgikh and Lavut (1991) have reported pyrochlore-type phases with a composition close to $R_2Ti_2O_{5.5}N$ (R = Sm, Dy, Y) after nitridation at 1000°C of the oxide pyrochlores $Ln_2Ti_2O_7$.

4.4. *Y–Zr–O–N system*

The possibility to stabilize the high-temperature polymorphs of zirconia, tetragonal or cubic, at ambient temperature by doping monoclinic ZrO_2 is well-known. As a consequence of cationic substitutions for Zr^{4+} by Mg^{2+}, Ca^{2+}, Y^{3+}, or of anionic substitution N^{3-}/O^{2-}, anion vacancies are created, as required by charge neutrality. These anion vacancies are responsible for the ionic conductivity properties of zirconia ceramics and the vacancy distribution is an important factor for the anionic mobility which determines the ionic conductivity.

In the system Y–Zr–O–N, tetragonal and cubic phases are observed with randomly distributed vacancies. There is no essential structural difference between the cation-related and the anion-related vacancies and their effects on the stabilization of zirconia are additive. A total of 6% of vacancies can be tolerated in the anion sublattice of the fluorite structure (Cheng and Thompson 1991, 1993, Lerch et al. 1996).

5. Nitride halides and nitride sulfides

5.1. *Ternary and higher nitride halides*

5.1.1. *Nitride fluorides*

Nitride fluoride compounds correspond to the idea, expressed by Andersson (1967), to substitute in an anionic oxide network the couple $(N^{3-} + F^-)$ for two O^{2-} in order to make pseudo-oxides. Lanthanide nitride fluorides are known for R = La, Ce, Pr and Gd (Tanguy et al. 1971, 1972, Pezat et al. 1976, Vogt et al. 1989), but with a N/F ratio different from unity. They are cubic solid solutions of general formula RN_xF_{3-3x} ($0.33 \leqslant x \leqslant \sim 0.5$) except for R = Gd where x is strictly equal to 0.33 corresponding to Gd_3NF_6. They were prepared either by reaction between nitride RN and fluoride RF_3, or by heating the fluoride in flowing ammonia. Attempts to obtain Eu or Tm compounds, the latter being representative of a lanthanide with a small ionic radius, were unsuccessful. Also, to date no one has been able to obtain a Ce^{IV} nitride fluoride CeNF, like ThNF or UNF, and similar to ceria CeO_2. A neutron diffraction investigation of CeN_xF_{3-3x}, which is very sensitive to air, and of PrN_xF_{3-3x} with $x \approx 0.33$ (Vogt et al. 1989) confirmed an anion-excess-fluorite-related structure and revealed that the tetrahedral holes within the fluorite structure are occupied by nitrogen and fluorine, and that additional interstitials are fluorine atoms occupying the position 32f: x,x,x ($x = 0.41$) in the $Fm\bar{3}m$ space group.

5.1.2. *Nitride chlorides, bromides and iodides*

Rare-earth nitride chlorides have been reported essentially for the early lanthanides and for yttrium with the three main stoichiometries R_2NCl_3 (R = La, Ce, Pr, Nd, Gd, Y), R_3NCl_6 (R = La, Ce, Gd) and RNCl where R = Ce, however a great richness of structural arrangements has already been found.

Whereas CeNF was not obtained as a cerium^{IV} nitride fluoride, CeNCl was shown by Ehrlich et al. (1994) to crystallize with the layered tetragonal (P4/nmm) BiOCl-type structure, like ThNCl (Juza and Sievers 1968).

All the crystal structures of the nitride chlorides have as a common feature that they contain N^{3-}-centered R_4^{3+} tetrahedra, the electroneutrality of the compound being assured by the chlorine ligands. This dominating structural feature, underlined recently by Schleid (1996), is common to (oxy)nitride bromides and iodides and also to nitride sulfides and nitride sulfide chlorides.

Gd_3NCl_6 (Simon and Koehler 1986) contains isolated pairs of Gd_4N tetrahedra that share a common edge. A similar cerium compound, formulated $Ce_6Cl_{12}N_2$ (Ehrlich et al. 1994), also contains these $[R_6N_2]^{12+}$ edge-sharing units formed by two cerium tetrahedra centered by nitrogen, but the arrangement of chlorine ligand atoms about the tetrahedra is different. La_3NCl_6 also exists in the same series (Meyer, Lissner and Schleid, unpublished results).

In orthorhombic (Pbcn) α-Gd_2NCl_3, which was the first reported nitride chloride (Schwanitz-Schüller and Simon 1985), all the nitrogen-containing gadolinium tetrahedra are connected via shared opposite edges to form one-dimensional infinite chains $^1_\infty[R_{4/2}N]^{3+}$, as well as in the isostructural compounds α-Y_2NCl_3 (Meyer et al. 1989) and Nd_2NCl_3 (Uhrlandt and Meyer 1995). The corresponding nitride chlorides with La, Ce and Pr contain also these anti-SiS_2 analogous chains but their symmetry (orthorhombic, Ibam) is somewhat different (Meyer and Uhrlandt 1993, Uhrlandt and Meyer 1995).

Meyer et al. (1989) described a β-form for Gd_2NCl_3 and Y_2NCl_3 in which the pairs of R_4N tetrahedra, thus forming $[R_2NR_2NR_2]$ units, are connected by sharing all four terminal vertices to generate double infinite chains according to $^1_\infty[(R_1)_{4/4}(R_2)_{2/2}N]^{3+}$. Save for the presence of nitrogen, β-Y_2Cl_3N is isostructural with the binary yttrium sesquichloride Y_2Cl_3.

All the R_3NCl_6 or R_2NCl_3 nitride chlorides are formally R(III) compounds, therefore with empty R d bands and negligible metal–metal bonding. On the other hand, they present strong R–N interactions. However, as noted by Meyer et al. (1989), the borderline between a cluster and a valence compound is not so obvious, in particular in the case of the β-phases. β-Y_2Cl_3N: which is not colorless as α-Y_2Cl_3N but black; which looks like Y_2Cl_3 in color and in its fibrous nature; and which requires a small amount of metal in its synthesis, contrary to the α-form; could be somewhat deficient in nitrogen, i.e. $Y_2Cl_3N_{1-x}$. Thus, a normal phase transition between α- and β-Y_2NCl_3 does not seem likely.

The borderline between cluster and valence compounds is clearly crossed with the scandium nitride chlorides which are unambiguously cluster compounds. Scandium shows here its difference in behavior, with compounds such as Sc_4Cl_6N, $Sc_7Cl_{12}N$ (Hwu and Corbett 1986) or Sc_5Cl_8N (Hwu et al. 1987), where nitrogen is an interstitial element.

The nitride chlorides were generally obtained from non-stoichiometric proportions of RCl_3, R metal and NaN_3, but nitrides RN were also used as a source of nitrogen. Meyer et al. (1989) have noted the need for metal in the synthesis of β-Gd_2NCl_3 and β-Y_2NCl_3 and suggested a small nitrogen deficiency.

Mattausch et al. (1996) have recently reported the nitride iodide $Ce_{15}N_7I_{24}$ that they obtained as red and transparent needles by reaction at 1050 K of a mixture $8CeI_3 + 7CeN$ in sealed Ta tube. The structure contains two crystallographically different types of nitrogen atoms: not only N atoms tetrahedrally coordinated by Ce atoms, but also N atoms in a triangular environment of Ce atoms. The Ce_4N tetrahedra are condensed via opposite edges to form chains. This air and moisture sensitive compound $Ce_{15}N_7I_{24}$ is paramagnetic ($\mu_{eff} = 2.55\,\mu_B$).

Mattausch et al. (1996) have mentioned the preparation of other new ternary nitride halides containing cerium and/or bromine with the formula Ce_3Cl_6N, Ce_3Br_6N, Ce_2Br_3N and Gd_2Br_3N.

The orthorhombic (Fddd) structure of the compound $Cs_xNa_{1-x}La_9I_{16}N_4$ (Lulei and Corbett 1996) contains two kinds of lanthanum atoms: La atoms forming infinite zigzag $^1_\infty[La_{4/2}N]$ chains of edge-sharing La_4 tetrahedra centered by nitrogen atoms (as in α-Gd_2NCl_3), and "isolated" La atoms that interconnect the chains via common iodine atoms. The alkali-metal atoms are statistically distributed within channels in the structure. Isostructural compositions $ALa_9I_{16}N_4$ (A = Na, Rb or Cs) have also been prepared.

Finally, $CsPr_9NbBr_5N_6$ (Lulei and Corbett 1997) is a recently reported quinary nitride bromide in which a partial substitution of niobium for praseodymium has been achieved, resulting in mixed $Pr_3Nb(N)$ tetrahedra.

5.2. *Ternary nitride sulfides*

Lissner and Schleid (1993a,b, 1994b) have prepared the lanthanide nitride sulfides R_2NS_3 (R = La, Ce, Pr, Nd, Sm) and $Sm_4N_2S_3$ from mixtures of metal R, sulfur, and NaN_3 as a nitrogen source (an also $SmCl_3$ in the case of $Sm_4N_2S_3$), in the presence of NaCl as a flux at 850°C in evacuated sealed silica tubes. In addition, Gd_2NS_3, Tb_2NS_3 and Dy_2NS_3 compositions have also been recently reported by Meyer et al. (1997). These nitride sulfides are not water sensitive. In all these compounds, nitrogen atoms are tetrahedrally surrounded by the lanthanide atoms. In the orthorhombic (Pnma) R_2NS_3 nitride sulfides (R = La–Nd), these $[(N^{3-})(R^{3+})_4]$ tetrahedra are connected via two corners forming linear chains $^1_\infty[N(R_1)_{1/1}(R_2)_{1/1}(R_3)_{2/2}]$ or $^1_\infty[NR_4]^{6+}$. In the monoclinic (C2/m) $Sm_4N_2S_3$ compound they share two cis-oriented edges to form chains $^1_\infty[N(Sm_1)_{3/3}(Sm_2)_{1/1}]^{3+}$ or $^1_\infty[NR_4]^{3+}$. The lanthanide atoms are sixfold or sevenfold coordinated by nitrogen and sulfur, the role of the S^{2-} anions in the structural arrangement being to assume the charge neutrality and the three-dimensional interconnection.

5.3. *Quaternary nitride sulfide chlorides*

Several compositions with the early lanthanides are known: $R_4NS_3Cl_3$ (R = La, Ce, Pr, Nd, Gd) (Lissner and Schleid 1994a, Schleid and Meyer 1996), $R_6N_3S_4Cl$ (R = La, Ce, Pr, Nd) (Lissner et al. 1996), $Pr_5N_3S_2Cl_2$ (Lissner and Schleid 1997) and $R_{10}NS_{13}Cl$ (Meyer and Schleid, unpublished results).

The $R_4NS_3Cl_3$ compounds, like the lanthanide nitride sulfides, are not sensitive to hydrolysis. They were obtained from appropriate molar ratios of R metal, sulfur and NaN_3, in the presence of NaCl. Their symmetry is hexagonal ($P6_3mc$) and they are isostructural with oxychloride Ba_4OCl_6 (Frit et al. 1970) or oxide sulfide chlorides $R_4OS_4Cl_2$ (R = La–Nd) (Schleid 1991, Schleid and Lissner 1994).

The structure is built up from isolated $^0_\infty[NR_4]^{9+}$ tetrahedra which are interconnected via S^{2-} and Cl^- anions which assume the charge neutrality.

The chlorine-poor isotypic series of nitride sulfide chlorides $R_6N_3S_4Cl$ (R = La–Nd) were prepared by Lissner et al. (1996) from appropriate molar ratios of metal R, sulfur, NaN_3 and RCl_3 chloride at 850°C. Their orthorhombic (Pnma) crystal structure, determined from single crystal data of the lanthanum compound, exhibits two different chains of connected $[NR_4]$ tetrahedra, which are held together by the X-ray diffraction indistinguishable anions S^{2-} and Cl^-.

In addition, two new compositions $Pr_5N_3S_2Cl_2$ and $R_{10}NS_{13}Cl$ (R = La–Pr), which were only briefly mentioned by Uhrlandt and Meyer (1995) and also recently by Schleid (1996), will be discussed in full detail by Schleid and coworkers. Both contain $[R_4N]$ tetrahedra, however, whereas in the first one the $[Pr_4N]$ tetrahedra are connected to form chains, isolated tetrahedral units can be found in the second ones. These $R_{10}NS_{13}Cl$ nitride sulfide chlorides can be structurally compared to the oxysulfide $Pr_{10}OS_{14}$ (Schleid and Lissner 1991) and to the new quaternary nitride sulfide $NaPr_{10}NS_{14}$ (Schleid 1996).

5.4. *Quaternary and higher oxynitride bromides*

Quaternary and higher oxynitride bromides are illustrated by the praseodymium(III) compounds $Na_2Pr_4Br_9NO$ (monoclinic, $P2_1/m$) and $Pr_8Br_3N_3O$ (monoclinic, C2/c), which are structurally and electronically similar to each other (Lulei et al. 1995), and also related to the nitride chlorides α-R_2NCl_3 (R = Gd, Y, La–Nd) reported earlier. Both structures can be described as being built up of infinite zigzag chains of trans-edge-sharing N- and O-centered Pr_4 tetrahedra. These chains $^1_\infty[Pr_{4/2}(O,N)]$ are interconnected by Br atoms. It may be noticed that the mixed N and O interstitials, which play the same role in the structure, are necessary to fulfill Pr(III) valence requirements. Thus, both compounds appear to be normal Pr^{III} valence compounds. However, $Na_2Pr_4Br_9NO$ is isotypic (but not isoelectronic) with $Na_2Pr_4Cl_9O_2$ (Mattfeld and Meyer 1994). This shows that these "interstitially stabilized" Pr(III) compounds have structures which lie on the border between salts and clusters.

5.5. *Quaternary carbide nitride halides*

Mattausch et al. (1994, 1995) have recently reported several stoichiometries for this new class of compounds: R_4X_6CN (R = Gd, X = Br; R = La, Gd, X = I), $R_7I_{12}C_2N$ (R = Y, Ho) and $Y_6I_9C_2N$. All of these compounds are air and moisture sensitive. Gd_4I_6CN exists with two modifications.

The tetragonal ($P4_2/mnm$) α-Gd_4I_6CN structure, which is also that of La_4I_6CN and Gd_4Br_6CN, contains R_6 octahedra centered by C_2^{6-} anionic groups and double tetrahedra centered by N atoms (N^{3-}). The units are alternately connected via common edges to form linear chains $[R_2R_{4/2}C_2]$ $[R_{2/2}R_{2/2}N]_2$. In the hexagonal (P6) β-Gd_4I_6CN, which is obtained at 1300 K from the α form, the chains are more densely packed.

The same units, C_2-centered octahedra and N-centered double tetrahedra are found in the two isotypic triclinic ($P\bar{1}$) compounds $Y_7I_{12}C_2N$ and $Ho_7I_{12}CN$. They exhibit a semiconducting behavior.

Lastly, the structure of $Y_6I_9C_2N$ is composed of chains of pairs of Y-octahedra and Y-tetrahedra, respectively. The octahedra are centered by C_2 groups, the tetrahedra by N atoms.

6. Conclusion

Several authors have noticed for a long time that relatively little was known about nitrides compared to oxides. Indeed, they only form a small class of compounds which are much more difficult to prepare and to study than oxides, essentially because of a lower stability. This can be a thermal instability, with nitrogen loss, resulting from the higher bond energy of the N_2 molecule (941 kJ mol^{-1}) compared to O_2 (499 kJ mol^{-1}), or it could be a chemical instability due to their sensitivity to oxygen and moisture. The rare-earth binary nitrides are a typical illustration of the difficulties which can be encountered.

However, the nitride chemistry appears now as a new challenge for solid-state chemists because the presence of nitrogen is expected to cause specific properties in structure and bonding relations, and this fact is particularly verified by the ternary and higher order rare-earth nitride-type compounds. Considerable progress has been made in their study during the past few years. A great variety of new compositions has been prepared and structures elucidated. Their properties are interesting both from a fundamental view point and for applications as materials because the presence of other elements than R and N in multinary rare-earth nitride materials generally results in a stabilizing effect which permits their practical use.

References

Aivazov, M.I., and T.V. Rezchikova, 1977, Russ. J. Inorg. Chem. **22**, 250.

Aivazov, M.I., T.V. Rezchikova and S.V. Gurov, 1977, Izv. Akad. Nauk SSSR, Neorg. Mater. **13**, 1235.

Andersson, S., 1967, Ark. Kemi **26**, 521.

Antoine, P., R. Marchand and Y. Laurent, 1987, Rev. Int. Hautes Tempér. Réfract. **24**, 43.

Antoine, P., R. Marchand, Y. Laurent, C. Michel and B. Raveau, 1988, Mater. Res. Bull. **23**, 953.

Antoine, P., R. Assabaa, P. L'Haridon, R. Marchand, Y. Laurent, C. Michel and B. Raveau, 1989, Mater. Sci. Eng. **B5**, 43.

Assabaa-Boultif, R., R. Marchand, Y. Laurent and J.-J. Videau, 1994, Mater. Res. Bull. **29**, 667.

Aujla, R.S., G. Leng-Ward, M.H. Lewis, E.F.W. Seymour, G.A. Styles and G.W. West, 1986, Philos. Mag. B **54**, 251.

Avignon-Poquillon, L., B. Viot, P. Verdier, Y. Laurent,

E. Menessier and C. Drouet, 1992, Silic. Ind. **9–10**, 131.

Bacher, P., P. Antoine, R. Marchand, P. L'Haridon, Y. Laurent and G. Roult, 1988, J. Solid State Chem. **77**, 67.

Barker, M.G., and I.C. Alexander, 1974, J. Chem. Soc. Dalton Trans. 2166.

Barker, M.G., and J.E. Gareh, 1994, J. Chem. Soc. Chem. Commun. 2745.

Belokoneva, E.L., and N.V. Belov, 1981, Sov. Phys. Dokl. **26**, 931.

Benz, R., and W.H. Zachariasen, 1966, Acta Crystallogr. **21**, 838.

Benz, R., and W.H. Zachariasen, 1970, J. Nucl. Mater. **37**, 109.

Bogdanov, V.S., V.S. Neshpor, Y.D. Kondrasher, A.B. Goncharuk and A.N. Pityulin, 1981, Poroshk. Metall. Kiev **5**, 79.

Bowman, A.L., G.P. Arnold, N.H. Krikorian and W.H. Zachariasen, 1971, Acta Crystallogr. B **27**, 1067.

Brandle, C.D., and H. Steinfink, 1969, Inorg. Chem. **8**, 1320.

Brokamp, Th., and H. Jacobs, 1992, J. Alloys & Compounds **183**, 325.

Broll, S., and W. Jeitschko, 1995, Z. Naturforsch. B **50**, 905.

Buschow, K.H.J., 1991, J. Magn. Magn. Mater. **100**, 79.

Buschow, K.H.J., and J.H.N. van Vucht, 1967, Philips Res. Rep. **22**, 233.

Cadogan, J.M., H.-S. Li, R.L. Davis, A. Margarian, J.B. Dunlop and P.B. Gwan, 1994a, J. Appl. Phys. **75**, 7114.

Cadogan, J.M., H.-S. Li, A. Margarian, J.B. Dunlop, D.H. Ryan, S.J. Collocot and R.L. Davis, 1994b, J. Appl. Phys. **76**, 6138.

Cao, G.Z., and R. Metselaar, 1991, Chem. Mater. **3**, 242.

Cao, G.Z., R. Metselaar and G. Ziegler, 1992, Mater. Forum **16**, 299.

Cao, G.Z., R. Metselaar and W.G. Haije, 1993, J. Mater. Sci. Lett. **12**, 459.

Cava, R.J., H.W. Zandbergen, B. Batlogg, H. Eisaki, H. Takagi, J.J. Krajewski, W.F. Peck Jr, E.M. Gyorgy and S. Uchida, 1994, Nature **372**, 245.

Cerdec AG Keramische Farben, 1994, German Patent 4317421.

Chee, K.S., Y.-B. Cheng, M.E. Smith and T.J. Bastow, 1994, Int. Ceram. Monogr. **1**, 1031.

Cheng, Y.-B., and D.P. Thompson, 1991, J. Am. Ceram. Soc. **74**, 1135.

Cheng, Y.-B., and D.P. Thompson, 1993, J. Am. Ceram. Soc. **76**, 683.

Cheng, Y.-B., and D.P. Thompson, 1994a, J. Am. Ceram. Soc. **77**, 143.

Cheng, Y.-B., and D.P. Thompson, 1994b, J. Eur. Ceram. Soc. **14**, 343.

Chevalier, B., J. Etourneau, B. Tanguy, J. Portier and P. Hagenmuller, 1973, C. R. Acad. Sci. Paris Ser. C **277**, 1029.

Chevalier, B., J. Etourneau and P. Hagenmuller, 1976, C. R. Acad. Sci. Paris Ser. C **282**, 375.

Chevalier, B., J. Etourneau and P. Hagenmuller, 1977, Mater. Res. Bull. **12**, 473.

Chevalier, B., J. Etourneau, J. Portier, P. Hagenmuller, R. Georges and J.B. Goodenough, 1978, J. Phys. Chem. Solids **39**, 539.

Chevalier, B., J. Etourneau and P. Hagenmuller, 1980, Rare Earth Mod. Sci. Technol. **2**, 403.

Chyung, C.K., and R.R. Wusirika, 1978, U.S. Patent 4070198.

Clarke, S.J., and F.J. DiSalvo, 1997, J. Solid State Chem. **129**, 144.

Coey, J.M.D., and H. Sun, 1990, J. Magn. Magn. Mater. **87**, L251.

Coey, J.M.D., J.F. Lawler, H. Sun and J.E.M. Allan, 1991, J. Appl. Phys. **69**, 3007.

Cohen, Y., and I. Riess, 1994, Mat. Sci. Eng. **B25**, 197.

Collocot, S.J., R.K. Day, J.B. Dunlop and R.L. Davis, 1992, in: Proc. 7th Int. Symp. on Magnetic Anisotropy and Coercivity in R–T alloys, pp. 437–444.

Croat, J.J., J.F. Herbst, R.W. Lee and F.E. Pinkerton, 1984, J. Appl. Phys. **55**, 2078.

Degiorgi, L., W. Bacsa and P. Wachter, 1990, Phys. Rev. B **42**, 530.

DiSalvo, F.J., 1997, personal communication.

Dismukes, J.P., W.M. Yim, J.J. Tietjen and R.E. Novak, 1970, RCA Rev. **31**, 680.

Dolgikh, V.A., and E.A. Lavut, 1991, Zh. Neorg. Khim. **36**, 2470; Russ. J. Inorg. Chem. **36**, 1389.

Drew, R.A.L., S. Hampshire and K.H. Jack, 1981, in: Special Ceramics, Vol. 7, eds D. Taylor and P. Popper, Proc. Br. Ceram. Soc. **31**, pp. 119–132.

Drew, R.A.L., S. Hampshire and K.H. Jack, 1983, in: Progress in Nitrogen Ceramics (Nijhoff, Boston) p. 323.

Dupree, R., M.H. Lewis and M.E. Smith, 1988, J. Am. Chem. Soc. **110**, 1083.

Ehrlich, G.M., M.E. Badding, N.E. Brese, S.S. Trail and F.J. DiSalvo, 1994, J. Alloys & Compounds **206**, 95.

Ekström, T., K. Jansson, P.-O. Olsson and J. Persson, 1991, J. Eur. Ceram. Soc. **8**, 3.

Endoh, M., K. Nakamura and H. Mikami, 1992, IEEE Trans. Magn. **28**, 2560.

Etourneau, J., B. Chevalier, P. Hagenmuller and R. Georges, 1980, J. Phys. **41**, C5-193.

Ettmayer, P., J. Waldhart and A. Vendl, 1979, Monatsh. Chem. **110**, 1109.

Ettmayer, P., J. Waldhart, A. Vendl and G. Banik, 1980a, J. Nucl. Mater. **91**, 293.

Ettmayer, P., J. Waldhart, A. Vendl and G. Banik, 1980b, Monatsh. Chem. **111**, 945.

Ettmayer, P., J. Waldhart, A. Vendl and G. Banik, 1980c, Monatsh. Chem. **111**, 1185.

Fernie, J.A., M.H. Lewis and G. Leng-Ward, 1989, Mater. Lett. **9**, 29.

Fitzmaurice, J.C., A.L. Hector and I.P. Parkin, 1993, J. Chem. Soc. Dalton Trans. 2435.

Fitzmaurice, J.C., A.L. Hector, A.T. Rowley and I.P. Parkin, 1994, Polyhedron **13**, 235.

Frit, B., B. Holmberg and J. Galy, 1970, Acta Crystallogr. B **26**, 16.

Fuerst, C.D., F.E. Pinkerton and J.F. Herbst, 1994, J. Magn. Magn. Mater. **129**, L115.

Gambino, R.J., and J.J. Cuomo, 1966, J. Electrochem. Soc. **113**, 401.

Gareh, J.E., 1996, personal communication.

Gauckler, L.J., and G. Petzow, 1977, in: Nitrogen Ceramics, ed. F.L. Riley (Noordhoff, Leiden) p 183.

Gauckler, L.J., H.L. Lukas and G.J. Petzow, 1975, J. Am. Ceram. Soc. **58**, 346.

Gaudé, J., 1983, C. R. Acad. Sci. Paris Ser. II **297**, 717.

Gaudé, J., J. Guyader and J. Lang, 1975a, C. R. Acad. Sci. Paris Ser. C **280**, 883.

Gaudé, J., P. L'Haridon, C. Hamon, R. Marchand and Y. Laurent, 1975b, Bull. Soc. Fr. Minéral. Cristallogr. **98**, 214.

Gaudé, J., R. Marchand, Y. Laurent and J. Lang, 1977, in: Nitrogen Ceramics, ed. F.R. Riley (Noordhoff, Leiden) pp. 137–139.

Gaudé, J., J. Lang and D. Louër, 1983, Rev. Chim. Minér. **20**, 523.

Gaudé, J., P. L'Haridon, J. Guyader and J. Lang, 1985, J. Solid State Chem. **59**, 143.

Greber, T., L. Degiorgi, R. Monnier, L. Schlapbach, F. Hulliger and E. Kaldis, 1987, J. Phys. (Paris) Colloq. **48**, C9-943.

Greedan, J.E., 1985, J. Less-Common Met. **111**, 335.

Guha, J.P., 1980a, J. Mater. Sci. **15**, 521.

Guha, J.P., 1980b, J. Mater. Sci. **15**, 263.

Guyader, J., R. Marchand, J. Gaudé and J. Lang, 1975, C.R. Acad. Sci. Paris Ser. C **281**, 307.

Guyader, J., F.F. Grekov, R. Marchand and J. Lang, 1978, Rev. Chim. Miner. **15**, 431.

Hadjipanayis, G.C., Y.H. Zheng, A.S. Murthy, W. Gong and F.M. Yang, 1995, J. Alloys & Compounds **222**, 49.

Halot, D., and J. Flahaut, 1971, C. R. Acad. Sci. Paris Ser. C **272**, 469.

Hamon, C., R. Marchand, M. Maunaye, J. Gaudé and J. Guyader, 1975, Rev. Chim. Miner. **12**, 259.

Hampshire, S., H.K. Park, D.P. Thompson and K.H. Jack, 1978, Nature **274**, 880.

Hampshire, S., R.A.L. Drew and K.H. Jack, 1984, J. Am. Ceram. Soc. **67**, C46.

Hampshire, S., R.A.L. Drew and K.H. Jack, 1985, Phys. Chem. Glasses **26**, 182.

Haschke, H., H. Nowotny and F. Benesovsky, 1967, Monatsh. Chem. **98**, 2157.

Hector, A.L., and I.P. Parkin, 1995, Chem. Mater. **7**, 1728.

Higano, S., K. Yamagata, K. Tokoro, M. Fukuda and K. Kamino, 1987, IEEE Trans. Magn. **23**, 3098.

Holcombe, C.E., and L. Kovach, 1981, Am. Ceram. Soc. Bull. **60**, 546.

Holleck, H., and E. Smailos, 1980, J. Nucl. Mater. **91**, 237.

Holleck, H., E. Smailos and F. Thümmler, 1968, J. Nucl. Mater. **28**, 105.

Holleck, H., E. Smailos and F. Thümmler, 1969, J. Nucl. Mater. **32**, 281.

Horiuchi, S., and M. Mitomo, 1979, J. Mater. Sci. **14**, 2543.

Hu, B.-P., G.-C. Liu, Y.-Z. Wang, B. Nasunjilegal, R.-W. Zhao, F.-M. Yang, H.-S. Li and J.M. Cadogan, 1994, J. Phys. Condens. Matter. **6**, L197.

Hu, Z., and W.B. Yelon, 1994, J. Appl. Phys. **76**, 6147.

Huang, M.Q., Y. Zheng, K. Miller, J.M. Elbicki, S.G. Sankar, W.E. Wallace and R. Obermyer, 1991, J. Magn. Magn. Mater. **102**, 91.

Huang, Z.K., P. Greil and G. Petzow, 1983, J. Am. Ceram. Soc. **66**, C96.

Huang, Z.-K., T.-Y. Tien and D.S. Yan, 1986a, J. Am. Ceram. Soc. **69**, C241.

Huang, Z.-K., D.S. Yan and T.-Y. Tien, 1986b, Inorg. Mater. **1**, 55.

Huang, Z.K., D.S. Yan, T.-S. Yen and T.-Y. Tien, 1990, J. Solid State Chem. **85**, 51.

Hulliger, F., 1979, in: Handbook on the Physics and Chemistry of Rare Earths, Vol. 4, eds K.A. Gschneidner Jr and L. Eyring (North-Holland, Amsterdam) pp. 153–236.

Huppertz, H., and W. Schnick, 1996, Angew. Chem. **108**, 17.

Huppertz, H., and W. Schnick, 1997, Z. Anorg. Allg. Chem. **623**, 212.

Hwang, C.J., D.W. Susnitzky and D.R. Beaman, 1995, J. Am. Ceram. Soc. **78**, 588.

Hwang, S.L., and I-W. Chen, 1994, J. Am. Ceram. Soc. **77**, 165.

Hwu, S.-J., and J.D. Corbett, 1986, J. Solid State Chem. **64**, 331.

Hwu, S.-J., D.S. Dudis and J.D. Corbett, 1987, Inorg. Chem. **26**, 469.

Ibberson, R.M., O. Moze, T.H. Jacobs and K.H.J. Buschow, 1991, J. Phys. Condens. Matter. **3**, 1219.

Ii, N., M. Mitomo and Z. Inoue, 1980, J. Mater. Sci. **15**, 1691.

Inoue, Z., 1985, J. Mater. Sci. Lett. **4**, 656.

Inoue, Z., M. Mitomo and N. Ii, 1980, J. Mater. Sci. **15**, 2915.

Ivanova, G.V., Y.V. Shcherbakova, Y.V. Belozerov, A.S. Yermolenko and Y.I. Teytel, 1990, Phys. Met. Metall. **70**, 63.

Izumi, F., M. Mitomo and J. Suzuki, 1982, J. Mater. Sci. Lett. **1**, 533.

Izumi, F., M. Mitomo and Y. Bando, 1984, J. Mater. Sci. **19**, 3115.

Jack, K.H., 1976, J. Mater. Sci. **11**, 1135.

Jack, K.H., 1978, in: Nitrogen Ceramics, ed. F.L. Riley (Noordhoff, Reading, MA) pp. 257–262.

Jack, K.H., 1986, Silicon nitride, sialons and related ceramics, in: Ceramics and Civilization, Vol. 3, High-Technology Ceramics (American Ceramic Society, Columbus, OH) pp. 259–288.

Jänecke, E., 1907, Z. Anorg. Chem. **53**, 319.

Jin, J.S., T. Yoko, F. Miyaji, S. Sakka, T. Fukunaga and M. Misawa, 1994, Philos. Mag. B **70**, 191.

Jin, J.S., H. Kozuka, T. Yoko and T. Fukunaga, 1996, Phys. Status Solidi B **193**, 295.

Juza, R., and H. Gerke, 1968, Z. Anorg. Allg. Chem. **363**, 245.

Juza, R., and R. Sievers, 1968, Z. Anorg. Allg. Chem. **363**, 258.

Kaldis, E., and Ch. Zürcher, 1976, in: Proc. 12th Rare Earth Research Conference, ed C.E. Lundin (Denver Research Institute, Denver) p. 915.

Kaldis, E., B. Steinmann, B. Fritzler, E. Jilek and A. Wizard, 1982, in: Modern Science and Technology, Vol. 3, The Rare Earths, eds J. McCarthy et al. (Plenum, New York) p. 224.

Käll, P.-O., J. Grins and M. Nygren, 1991a, Acta Crystallogr. C **47**, 2015.

Käll, P.-O., J. Grins, P.-O. Olsson, K. Liddell, P. Korgul and D.P. Thompson, 1991b, J. Mater. Chem. **1**, 239.

Kalogirou, O., V. Psycharis, L. Saettas and D.N. Niarchos, 1994, J. Appl. Phys. **76**, 6722.

Kalogirou, O., V. Psycharis, M. Gjoka and D.N. Niarchos, 1995a, J. Magn. Magn. Mater. **147**, L7.

Kalogirou, O., V. Psycharis, L. Saettas and D.N. Niarchos, 1995b, J. Magn. Magn. Mater. **146**, 335.

Kaminskii, A.A., B.V. Mill, E.L. Belokoneva and G.G. Khodzhabagya, 1983, Izv. Akad. Nauk SSSR, Neorg. Mater. **19**, 1762.

Kenmuir, S.V.J., J.S. Thorp and B.L.J. Kulesza, 1983, J. Mater. Sci. **18**, 1725.

Khan, Y., 1973, Acta Crystallogr. B **29**, 2502.

Kikkawa, S., T. Ohmura, M. Takahashi, F. Kanamaru and O. Ohtaka, 1997, J. Eur. Ceram. Soc. **17**, 1831.

Klesnar, H., and P. Rogl, 1990, High Temp. High Pressures **22**, 453.

Klesnar, H., and P. Rogl, 1992, J. Am. Ceram. Soc. **75**, 2825.

Klesnar, H., P. Rogl, J. Bauer and J. Debuigne, 1989, Proc. 12th Int. Plansee Seminar, Reutte, vol. II, eds H. Bildstein and H. Ortner (Tyrolia Verlag, Innsbrück) pp. 609–616.

Korgul, P., and D.P. Thompson, 1989, in: Complex Microstructures, eds R. Stevens and D. Taylor (Proc. Br. Ceram. Soc. **42**) pp. 69–80.

Kruppa, D., R. Dupree and M.H. Lewis, 1991, Mater. Lett. **11**, 195.

Kuzma, Yu.B., and S.I. Svarichevskaya, 1973, Sov. Phys. Crystallogr. **17**, 830. In English.

LaDuca, R.L., and P.T. Wolczanski, 1992, Inorg. Chem. **31**, 1311.

Lang, J., 1986, Bull. Soc. Sci. Bretagne **58**, 99.

Lang, J., R. Marchand, C. Hamon, P. L'Haridon and J. Guyader, 1975, Bull. Soc. Fr. Mineral. Cristallogr. **98**, 284.

Lang, J., P. Verdier, R. Pastuszak and R. Marchand, 1980, Ann. Chim. France **5**, 663.

Lang, J., R. Marchand, P. Verdier and R. Pastuszak, 1982, Mat. Sci. Monographs **10**, 506.

Leedecke, C.J., 1980, J. Am. Ceram. Soc. **63**, 479.
Leedecke, C.J., and R.E. Loehman, 1980, J. Am. Ceram. Soc. **63**, 190.
Lejus, A.M., A. Kahn-Harari, J.M. Benitez and B. Viana, 1994, Mater. Res. Bull. **29**, 725.
Lemercier, H., M. Sebaï, T. Rouxel, P. Goursat, S. Hampshire and J.-L. Besson, 1997, J. Eur. Ceram. Soc. **17**, 1949.
Leng-Ward, G., and M.H. Lewis, 1985, Mater. Sci. Eng. **71**, 101.
Leng-Ward, G., and M.H. Lewis, 1989, in: Glass and Glass Ceramics, ed M.H. Lewis (Chapman & Hall) pp. 106–155.
Lengauer, W., 1988, J. Solid State Chem. **76**, 412.
Lengauer, W., 1989, J. Solid State Chem. **82**, 186.
Lengauer, W., and P. Ettmayer, 1988, J. Less-Common Met. **141**, 157.
Lerch, M., J. Wrba and J. Lerch, 1996, in: Proc. Int. Symp. on Nitrides, St. Malo, France.
L'Haridon, P., and J. Gaudé, 1985, Abstracts of the 9th European Crystallogr. Meeting, Torino, Italy.
Li, H.-S., and J.M. Cadogan, 1992, J. Magn. Magn. Mater. **109**, L153.
Li, H.-S., and J.M.D. Coey, 1991, in: Handbook of Magnetic Materials, Vol. 6, ed. K.H.J. Buschow (Elsevier, Amsterdam) ch. 1, p. 1.
Li, H.-S., J.M. Cadogan, R.L. Davis, A. Margarian and J.B. Dunlop, 1994a, Solid State Commun. **90**, 487.
Li, H.-S., Suharyana, J.M. Cadogan, G.J. Bowden, J.-M. Xu, S.X. Dou and H.K. Liu, 1994b, J. Appl. Phys. **75**, 7120.
Li, H.-S., J.M. Cadogan, B.-P. Hu, F.-M. Yang, B. Nasunjilegal, A. Margarian and J.B. Dunlop, 1995, J. Magn. Magn. Mater. **140**, 1037.
Li, W.-Z., N. Tang, J.-L. Wang, F. Yang, Y.W. Zeng, J.J. Zhu and F.R. de Boer, 1994, J. Appl. Phys. **76**, 6743.
Li, X.-W., N. Tang, Z.-H. Lu, T.-Y. Zhao, W.-G. Li, R.-W. Zhao and F.-M. Yang, 1993, J. Appl. Phys. **73**, 5890.
Lissner, F., and Th. Schleid, 1993a, Z. Anorg. Allg. Chem. **619**, 1771.
Lissner, F., and Th. Schleid, 1993b, Z. Kristallogr. Suppl. **7**, 123.
Lissner, F., and Th. Schleid, 1994a, Z. Anorg. Allg. Chem. **620**, 1998,
Lissner, F., and Th. Schleid, 1994b, Z. Anorg. Allg. Chem. **620**, 2003.
Lissner, F., and Th. Schleid, 1997, Z. Anorg. Allg. Chem. **623**, 1747.
Lissner, F., M. Meyer and Th. Schleid, 1996, Z. Anorg. Allg. Chem. **622**, 275.
Liu, G., and H.A. Eick, 1990, J. Solid State Chem. **89**, 366.
Liu, G., X. Chen and H.A. Eick, 1993, J. Solid State Chem. **103**, 208.
Loehman, R.E., 1979, J. Am. Ceram. Soc. **62**, 491.
Loehman, R.E., 1980, J. Non-Cryst. Solids **42**, 433.
Loehman, R.E., 1982, Ceram. Eng. Sci. Proc. **3**, 35.
Loehman, R.E., 1983, J. Non-Cryst. Solids **56**, 123.
Loehman, R.E., 1985, Treatise Mater. Sci. Technol. **26**, 119.
Lulei, M., and J.D. Corbett, 1996, Eur. J. Solid State Inorg. Chem. **33**, 241.
Lulei, M., and J.D. Corbett, 1997, Angew. Chem., in press.
Lulei, M., S.J. Steinwand and J.D. Corbett, 1995, Inorg. Chem. **34**, 2671.
Maclean, D.A., K. Seto and J.E. Greedan, 1981, J. Solid State Chem. **40**, 241.
Magneli, A., and B. Blomberg, 1951, Acta Chem. Scand. **5**, 372.
Magyar, B., 1968, J. Inorg. Chem. **7**, 1457.
Mah, T.-I., K.S. Mazdiyasni and R. Ruh, 1979, J. Am. Chem. Soc. **62**, 12.
Makishima, A., M. Mitomo, H. Tanaka, N. Ii and M. Tsutsumi, 1980, Yogyo Kyokai Shi **88**, 701.
Makishima, A., M. Mitomo, N. Ii and M. Tsutsumi, 1983, J. Am. Ceram. Soc. **66**, C55.
Marchand, R., 1976a, C. R. Acad. Sci. Paris Ser. C **282**, 329.
Marchand, R., 1976b, C. R. Acad. Sci. Paris Ser. C **283**, 281.
Marchand, R., and Y. Laurent, 1984, French Patent 84-17274.
Marchand, R., and V. Lemarchand, 1981, J. Less-Common Met. **80**, 157.
Marchand, R., Y. Laurent, J. Lang and M.Th. Le Bihan, 1969, Acta Crystallogr. B **25**, 2157.
Marchand, R., S.A.A. Jayaweera, P. Verdier and J. Lang, 1976, C. R. Acad. Sci. Paris Ser. C **283**, 675.
Marchand, R., P. L'Haridon and Y. Laurent, 1978, J. Solid State Chem. **24**, 71.
Marchand, R., R. Pastuszak, Y. Laurent and G. Roult, 1982, Rev. Chim. Miner. **19**, 684.
Marchand, R., G. Roult, P. Verdier and Y. Laurent, 1985, Ann. Chim. Fr. **10**, 317.
Marchand, R., F. Pors, Y. Laurent, O. Regreny, J. Lostec and J.M. Haussonne, 1986, J. Phys. **47**, C1-901.

Marchand, R., Y. Laurent, J. Guyader, P. L'Haridon and P. Verdier, 1991a, J. Eur. Ceram. Soc. **8**, 197.

Marchand, R., F. Pors and Y. Laurent, 1991b, Ann. Chim. Fr. **16**, 553.

Marchand, R., P. Antoine and Y. Laurent, 1993, J. Solid State Chem. **107**, 34.

Mattausch, Hj., H. Borrmann, R. Eger, R.K. Kremer and A. Simon, 1994, Z. Anorg. Allg. Chem. **620**, 1889.

Mattausch, Hj., H. Borrmann, R. Eger, R.K. Kremer and A. Simon, 1995, Z. Naturforsch. B **50**, 931.

Mattausch, Hj., R.K. Kremer and A. Simon, 1996, Z. Anorg. Allg. Chem. **622**, 649.

Mattfeld, H., and G. Meyer, 1994, Z. Anorg. Allg. Chem. **620**, 85.

Maunaye, M., C. Hamon, P. L'Haridon and Y. Laurent, 1976, Bull. Soc. Fr. Mineral. Cristallogr. **99**, 203.

McKie, D., and C. McKie, 1974, in: Crystalline Solids, ed. Nelson, pp. 324–326.

Melamud, M., L.H. Bennett and R.E. Watson, 1994, J. Appl. Phys. **76**, 6044.

Menon, M., and I-W. Chen, 1995a, J. Am. Ceram. Soc. **78**, 545.

Menon, M., and I-W. Chen, 1995b, J. Am. Ceram. Soc. **78**, 553.

Messier, D.R., 1982, Ceram. Eng. Sci. Proc. **3**, 565.

Messier, D.R., 1985, Rev. Chim. Miner. **22**, 518.

Messier, D.R., 1987, Int. J. High Technol. Ceram. **3**, 33.

Messier, D.R., and A. Broz, 1982, J. Am. Ceram. Soc. **65**, C123.

Messier, D.R., and E.J. DeGuire, 1984, J. Am. Ceram. Soc. **67**, 602.

Metselaar, R., 1994, Pure Appl. Chem. **66**, 1815.

Meyer, G., and S. Uhrlandt, 1993, Angew. Chem. **105**, 1379; Angew. Chem. Int. Ed. Engl. **32**, 1318.

Meyer, H.-J., N.L. Jones and J.D. Corbett, 1989, Inorg. Chem. **28**, 2635.

Meyer, M., F. Lissner and Th. Schleid, 1997, Z. Naturforsch., to be published.

Milberg, M.E., and W.M. Miller, 1978, J. Am. Ceram. Soc. **61**, 1979.

Mitomo, M., N. Kuramoto and H. Suzuki, 1978, J. Mater. Sci. **13**, 2523.

Mittl, J.C., R.L. Tallmann, P.V. Kelley Jr and J.G. Jolley, 1985, J. Non-Cryst. Solids **71**, 287.

Monnier, R., J. Rhyner, T.M. Rice and D.D. Koelling, 1985, Phys. Rev. B **31**, 5554.

Morgan, P.E.D., 1979a, J. Mater. Sci. **14**, 2778.

Morgan, P.E.D., 1979b, J. Am. Ceram. Soc. **62**, 636.

Morgan, P.E.D., 1986, J. Mater. Sci. Lett. **5**, 372.

Morgan, P.E.D., and P.J. Caroll, 1977, J. Mater. Sci. **12**, 2343.

Morgan, P.E.D., P.J. Caroll and F.F. Lange, 1977, Mater. Res. Bull. **12**, 251.

Mulfinger, H.O., A. Dietzel and J.M. Fernandez-Navarro, 1973, Glastech. Ber. **45**, 389.

Muller, O., and R. Roy, 1974, in: The Major Ternary Structural Families (Springer, Berlin).

Murakami, Y., and H. Yamamoto, 1994, J. Ceram. Soc. Jpn. **102**, 234.

Niewa, R., and H. Jacobs, 1995, Z. Kristallogr. **210**, 513.

Ohashi, M., K. Nakamura, K. Hirao, S. Kanzaki and S. Hampshire, 1995, J. Am. Ceram. Soc. **78**, 71.

O'Reilly, K.P.J., M. Redington, S. Hampshire and M. Liegh, 1993, in: Silicon Nitride Ceramics Scientific and Technological Advances, eds I-W. Chen, P.F. Becher, M. Mitomo, G. Petzow and T.S. Yen (Mater. Res. Soc., Pittsburg, PA) pp. 393–398.

Palisaar, A.P., and R. Juza, 1971, Z. Anorg. Allg. Chem. **384**, 1.

Pan, Q., Z.-X. Liu and Y.-C. Yang, 1994, J. Appl. Phys. **76**, 6728.

Pan, S.-M., H. Chen, D.-K. Liu, Z.-X. Xu, R.-Z. Ma, J.-L. Yang, B.-S. Zhang, D.-Y. Xue and Q. Ni, 1994a, J. Appl. Phys. **76**, 6749.

Pan, S.-M., H. Chen, Z.-X. Xu, R.-Z. Ma, J.-L. Yang, B.-S. Zhang, D.-Y. Xue and Q. Ni, 1994b, J. Appl. Phys. **76**, 6720.

Park, H.K., D.P. Thompson and K.H. Jack, 1980, Sci. Ceram. **10**, 251.

Pastuszak, R., and P. Verdier, 1983, J. Non-Cryst. Solids **56**, 141.

Patel, J.K., and D.P. Thompson, 1988, Br. Ceram. Trans. J. **87**, 70.

Penney, T., M.W. Shafer and J.B. Torrance, 1972, Phys. Rev. **B5**, 3669.

Peterson, I.M., and T.-Y. Tien, 1995, J. Am. Ceram. Soc. **78**, 1977.

Pezat, M., B. Tanguy, M. Vlasse, J. Portier and P. Hagenmuller, 1976, J. Solid State Chem. **18**, 381.

Pors, F., R. Marchand and Y. Laurent, 1991, Ann. Chim. Fr. **16**, 547.

Pors, F., R. Marchand and Y. Laurent, 1993, J. Solid State Chem. **107**, 39.

Pyzik, A.J., and D.R. Beaman, 1993, J. Am. Ceram. Soc. **76**, 2737.

Qi, Q.-N., B.-P. Hu and J.M.D. Coey, 1994, J. Appl. Phys. **75**, 6235.

Rae, A.W.J.M., D.P. Thompson, N.J. Pipkin and K.H. Jack, 1975, Spec. Ceram. **6**, 347.

Ramesh, R., E. Nestor, M.J. Pomeroy and S. Hampshire, 1997, J. Eur. Ceram. Soc. **17**, 1933.

Rieger, W., H. Nowotny and F. Benesovsky, 1966, Monatsh. Chem. **97**, 378.

Rocherullé, J., 1986, Thesis (University of Rennes).

Rocherullé, J., P. Verdier and Y. Laurent, 1989, Mater. Sci. Eng. B **2**, 265.

Rocherullé, J., M. Matecki, P. Verdier and Y. Laurent, 1997, J. Non-Cryst. Solids **211**, 222.

Rogl, P., and H. Klesnar, 1992, J. Solid State Chem. **98**, 99.

Rogl, P., H. Klesnar and P. Fischer, 1990, J. Am. Ceram. Soc. **73**, 2634.

Roth, S.H., and S. Hasko, 1958, J. Am. Ceram. Soc. **41**, 146.

Roult, G., P. Bacher, C. Liébaut, R. Marchand, P. Goursat and Y. Laurent, 1984, Acta Crystallogr. A **40** (Suppl.), C226.

Rouxel, T., J.L. Besson, C. Gault, P. Goursat, M. Leigh and S. Hampshire, 1989, J. Mater. Sci. Lett. **8**, 1158.

Rouxel, T., J.L. Besson, E. Rzepka and P. Goursat, 1990, J. Non-Cryst. Solids **122**, 298.

Rouxel, T., M. Huger and J.L. Besson, 1992, J. Mater. Sci. **27**, 279.

Rouxel, T., J.L. Besson, D. Fargeot and S. Hampshire, 1994, J. Non-Cryst. Solids **175**, 44.

Ryan, D.H., J.M. Cadogan, A. Margarian and J.B. Dunlop, 1994, J. Appl. Phys. **76**, 6150.

Saburi, S., A. Kawahara, C. Henmi, I. Kusachi and K. Kihara, 1977, Mineral. J. **8**, 286.

Sagawa, M., S. Fujimura, N. Togawa, H. Yamamoto and Y. Matsuura, 1984, J. Appl. Phys. **55**, 2083.

Sakka, S., 1986, Ann. Rev. Mater. Sci. **16**, 29.

Sakka, S., 1995, J. Non-Cryst. Solids **181**, 215.

Schlegel, A., 1979, PhD. Thesis (ETH Zürich).

Schleid, Th., 1991, Eur. J. Solid State Inorg. Chem. **28**, 737.

Schleid, Th., 1996, Eur. J. Solid State Inorg. Chem. **33**, 227.

Schleid, Th., and F. Lissner, 1991, J. Less. Common Met. **175**, 309.

Schleid, Th., and F. Lissner, 1994, Z. Naturforsch. B **49**, 340.

Schleid, Th., and M. Meyer, 1996, Z. Kristallogr. **211**, 187.

Schlieper, T., and W. Schnick, 1995, Z. Anorg. Allg. Chem. **621**, 1535.

Schlieper, T., and W. Schnick, 1996, Z. Kristallogr. **211**, 254.

Schönberg, N., 1954, Acta Chem. Scand. A **8**, 213.

Schultz, L., K. Schnitzke, J. Wecker and C. Kuhrt, 1991, J. Appl. Phys. **70**, 6339.

Schuster, J.C., 1985, J. Less-Common Met. **105**, 327.

Schwanitz-Schüller, U., and A. Simon, 1985, Z. Naturforsch. B **40**, 705.

Sebaï, M., J. Sjöberg, P. Goursat, E. Nestor, B. Flynn, R. Ramesh and S. Hampshire, 1995, J. Eur. Ceram. Soc. **15**, 1015.

Seeger, O., and J. Strähle, 1994, Z. Naturforsch. B **49**, 1169.

Seeger, O., M. Hofmann, J. Strähle, J.P. Laval and B. Frit, 1994, Z. Anorg. Allg. Chem. **620**, 2008.

Shcherbakova, Y.V., G.V. Ivanova, A.S. Yermolenko, Y.V. Belozerov and V.S. Gaviko, 1992, J. Alloys & Compounds **182**, 199.

Shillito, K.R., R.R. Wills and R.B. Bennett, 1978, J. Am. Ceram. Soc. **61**, 537.

Siegrist, T., H.W. Zandbergen, R.J. Cava, J.J. Krajewski and W.F. Peck Jr, 1994, Nature **367**, 254.

Simon, A., and T. Koehler, 1986, J. Less-Common Met. **116**, 279.

Slasor, S., and D.P. Thompson, 1987, J. Mater. Sci. Lett. **6**, 315.

Soga, I., M. Sato, T. Sano and S. Ikeda, 1979, J. Less-Common Met. **68**, 59.

Spacie, C.J., K. Liddell and D.P. Thompson, 1988, J. Mater. Sci. Lett. **7**, 95.

Stadelmaier, H.H., 1984, Z. Metallkd. **75**, 227.

Stalick, J.K., J.A. Gotass, S.F. Cheng, J. Cullen and A.E. Clark, 1991, Mater. Lett. **12**, 93.

Stutz, D., P. Greil and G. Petzow, 1986, J. Mater. Sci. Lett. **5**, 335.

Sun, E.Y., P.F. Becher, S.-L. Hwang, S.B. Waters, G.M. Pharr and T.Y. Tsui, 1996, J. Non-Cryst. Solids **208**, 162.

Sun, H., J.M.D. Coey, Y. Otani and D.P.F. Herly, 1990, J. Phys. Cond. Matter. **2**, 6465.

Sun, H., M. Akayama, K. Tatami and H. Fujii, 1993, Physica B **183**, 33.

Sun, W.Y., and T.S. Yen, 1989, Mater. Lett. **8**, 145.

Sun, W.Y., T.S. Yen and T.-Y. Tien, 1991a, J. Solid State Chem. **95**, 424.

Sun, W.Y., D. Yan and T. Yen, 1991b, Sci. China Ser. A **34**, 105.

Suzuki, S., S. Suzuki and M. Kawasaki, 1995, Intermag'95, IEEE Trans. Mag. **31**, 3695.

Tanguy, B., M. Pezat, J. Portier and P. Hagenmuller, 1971, Mater. Res. Bull. **6**, 57.

Tanguy, B., M. Pezat, J. Portier and P. Hagenmuller, 1972, C. R. Acad. Sci. Paris Ser. C **274**, 1344.

Tessier, F., R. Marchand and Y. Laurent, 1997, J. Eur. Ceram. Soc. **17**, 1825.

Thomas, G., C. Ahn and J. Weiss, 1982, J. Am. Ceram. Soc. **65**, C185.

Thompson, D.P., 1986, Mater. Sci. Res. **20**, 79.

Thompson, D.P., 1989, Mater. Sci. Forum **47**, 21.

Travaglini, G., F. Marabelli, R. Monnier, E. Kaldis and P. Wachter, 1986, Phys. Rev. **B34**, 3876.

Tredway, W.K., and R.E. Loehman, 1985, J. Am. Ceram. Soc. **68**, C131.

Uhrlandt, S., and G. Meyer, 1995, J. Alloys & Compounds **225**, 171.

Van den Heuvel, F.E.W., H.T. Hintzen and R. Metselaar, 1996, Key Eng. Mater. **113**, 33.

Vendl, A., 1979, J. Nucl. Mater. **79**, 246.

Vendl, A., P. Ettmayer and W. Prohaska, 1977, High Temp. High Pressures **9**, 313.

Verdier, P., R. Pastuszak and Y. Laurent, 1982, Verres Refract. **36**, 547.

Vogt, T., E. Schweda, J.P. Laval and B. Frit, 1989, J. Solid State Chem. **83**, 324.

Wachter, P., and E. Kaldis, 1980, Solid State Commun. **34**, 241.

Waldhart, J., and P. Ettmayer, 1979, Monatsh. Chem. **110**, 21.

Wallace, W.E., and M.Q. Huang, 1992, IEEE Trans. Magn. **28**, 2312.

Wang, X.H., 1989, Thesis (Paris).

Wang, X.H., A.M. Lejus, D. Vivien and R. Collongues, 1988, Mater. Res. Bull. **23**, 43.

Wang, X.H., A.M. Lejus and D. Vivien, 1990, J. Am. Ceram. Soc. **73**, 770.

Warshaw, I., 1961, Diss. Abstr. **22**, 279.

Wei, G., and G.C. Hadjipanayis, 1992, IEEE Trans. Magn. Magn. **28**, 2563.

Weitzer, F., J.C. Schuster, J. Bauer and B. Jounel, 1991, J. Mater. Sci. **26**, 2076.

Wells, A.F., 1975, in: Structural Inorganic Chemistry, 4th Ed. (Clarendon Press, Oxford) p. 1036.

Wills, R.R., S. Holmquist, J.M. Wimmer and J.A. Cunningham, 1976a, J. Mater. Sci. 11, 1305.

Wills, R.R., R.W. Stewart, J.A. Cunningham and J.M. Wimmer, 1976b, J. Mater. Sci. **11**, 749.

Woike, M., and W. Jeitschko, 1995, Inorg. Chem. **34**, 5105.

Wusirika, R.R., and C.K. Chyung, 1980, J. Non-Cryst. Solids **38**, 39.

Wyckoff, R.W.G., 1963, Crystal Structures, Vol. 1, 2nd Ed. (Interscience Publishers) p. 146.

Wyckoff, R.W.G., 1965, Crystal Structures, Vol. 3, 2nd Ed. (Interscience Publishers) pp. 87–90.

Yamanaka, T., and H. Mori, 1981, Acta Crystallogr. B **37**, 1010.

Yang, F.-M., B. Nasunjilegal, H.-Y. Pan, J.-L. Wang, R.-W. Zhao, B.-P. Hu, Y.-Z. Wang, H.-S. Li and J.M. Cadogan, 1994a, J. Magn. Magn. Mater. **135**, 298.

Yang, F.-M., B. Nasunjilegal, J.-L. Wang, H.-Y. Pan, W.-D. Qing, R.-W. Zhao, B.-P. Hu, Y.-Z. Wang, G.-C. Liu, H.-S. Li and J.M. Cadogan, 1994b, J. Appl. Phys. **76**, 1971.

Yang, J., S. Dong, W. Mao, P. Xuan, Z. Liu, Y. Sun, Y. Yang and S. Ge, 1995, J. Appl. Phys. **78**, 1140.

Yang, Y.-C., X.-D. Zhang, S.-L. Ge, L.S. Kong, Q. Pan, Y.T. Hou, S. Huang and L. Yang, 1990, in: Proc. 6th Int. Symp. on Magnetic Anisotropy and Coercivity, Pittsburgh, ed. S.G. Sankar (Rare-Earth Transition Metal Alloys) p. 190.

Yang, Y.-C., X.-D. Zhang, S.-L. Ge, Q. Pan, L.-S. Kong, S.-L. Ge, H. Li, J.-L. Yang, P.-S. Zhang, Y.-F. Ding and C.-T. Ye, 1991a, J. Appl. Phys. **70**, 6001.

Yang, Y.-C., X.-D. Zhang, L.-S. Kong, Q. Pan and S.-L. Ge, 1991b, Appl. Phys. Lett. **58**, 2042.

Yang, Y.-C., X.-D. Zhang, L.-S. Kong, Q. Pan and S.-L. Ge, 1991c, Solid State Commun. **78**, 317.

Yang, Y.-C., Q. Pan, X.-D. Zhang, J. Yang, M.-H. Zhang and S.-L. Ge, 1992, Appl. Phys. Lett. **61**, 2723.

Yang, Y.-C., Q. Pan, B.-P. Cheng, X.-D. Zhang, Z.-X. Liu, Y.-X. Sun and S.-L. Ge, 1994, J. Appl. Phys. **76**, 6725.

Yelon, W.B., and Z. Hu, 1996, J. Appl. Phys. **79**, 1330.

Zandbergen, H.W., J. Jansen, R.J. Cava, J.J. Krajewski and W.F. Peck Jr, 1994, Nature **372**, 759.

Zhong, X.-P., R.J. Radwanski, F.R. de Boer, T.H. Jacobs and K.H.J. Buschow, 1990, J. Magn. Magn. Mater. **86**, 333.

Handbook on the Physics and Chemistry of Rare Earths
Vol. 25
edited by K.A. Gschneidner, Jr. and L. Eyring

Chapter 167

SPECTRAL INTENSITIES OF f–f TRANSITIONS

Christiane GÖRLLER-WALRAND and Koen BINNEMANS
K.U. Leuven, Department of Chemistry, Coordination Chemistry Division, Celestijnenlaan 200F, 3001 Heverlee, Belgium

Contents

List of symbols and abbreviations

A	absorbance
$A(\Psi J, \Psi' J')$	probability for spontaneous emission (Einstein coefficient)
A_{kq}	crystal-field coefficient
A^λ_{tp}	intensity parameter
A^λ_{tc*v*}	intensity parameter for vibronic transitions
A_{JKM}	intensity parameter
B^k_q	crystal field coefficient (or parameter)
$B_{\lambda kq}$	intensity parameter
c	speed of light
C	concentration
CDA	chelidamate
CDO	chelidonate
Cp	cyclopentadiene
d	optical pathlength
D	dipole strength (randomly-oriented system)
D'	dipole strength (oriented system)
D_{exp}	experimental dipole strength
D^0_{exp}	experimental dipole strength for ED transition, corrected for the MD contribution
D	Debye
DBM	1,3-diphenyl-1,3-propanedione
DC	dynamic coupling
dim.	dimension
DPA	dipicolinate (2,6-pyridinedicarboxylate)
DTPA	diethylenetriaminepentaacetate
e	elementary charge
$\boldsymbol{E}$	electric field
E	energy
E_{CT}	charge-transfer energy
ED	(induced) electric dipole transition
EDTA	ethylenediaminetetraacetate
exp	experimental

f	oscillator strength
g	Landé factor
g_A	degeneracy of the initial state
g_e	electron g-factor
g_i	degeneracy of level i
h	Planck's constant
$\hbar$	$h/2\pi$
$\boldsymbol{H}$	magnetic field
HEDTA	N-(2-hydroxyethyl)ethylene-diaminetriacetate
IDA	iminodiacetate
J	total angular momentum (quantum number)
k	Boltzmann constant
l	liter
L	length (dimension)
L	orbital angular momentum (quantum number)
M	mass (dimension)
M	magnetic quantum number
m_e	electron mass
$\hat{\boldsymbol{m}}_\rho$	electric dipole operator
MAL	malate
MCD	magnetic circular dichroism
MD	magnetic dipole transition
MIDA	(methylimino)acetate
n	principal quantum number
n	refractive index
N	number of f electrons
N_A	Avogadro's number
NTA	nicotinic acid
$\hat{\boldsymbol{O}}$	dipole operator
OCTPA	one-color two-photon absorption
ODA	oxydiacetate
OPA	one-photon absorption
o-phen	1,10-phenanthroline
P	oscillator strength (randomly-oriented system)
P'	oscillator strength (oriented system)
P_{CT}	charge-transfer oscillator strength
picNO	picolinic acid-N-oxide
RMS	root mean square deviation error
S	spin angular momentum (quantum number)
S_{ed}	line strength of induced electric dipole transition
S_{md}	line strength of magnetic dipole transition
SC	static coupling
T	time (dimension)
T_λ	intensity parameter (Judd's notation)
TBP	tributylphosphate
TCTPA	two-photon two-color absorption
Terpy	2,2:6′,2″″-terpyridine
THD	2,2,6,6-tetramethyl-3,5-heptanedione
TNA	nitrilotriacetate
TPA	two-photon absorption
$U^{(\lambda)}$	squared reduced matrix element
V	crystal-field Hamiltonian
V_u	volume of the crystallographic unit cell
$X_A(T)$	fractional thermal population
α, π, σ	polarization directions
β_R	branching ratio
χ	correction factor for medium effects
χ_{ED}	correction factor for medium effects of an induced electric dipole transition
χ_{MD}	correction factor for medium effects of a magnetic dipole transition
δ	fractional doping concentration
δ_{ij}	Kronecker delta
ε	molar absorptivity
ε_0	dielectric constant
λ_p	wavelength of peak emission
η	quantum efficiency
$\hat{\boldsymbol{\mu}}_\rho$	magnetic dipole operator
ρ	polarization number
σ	uncertainty on the experimental dipole strength
$\sigma(\Psi J, \Psi' J')$	peak stimulated emission cross-section
τ	additional quantum number to discriminate between levels with same S and L quantum number
τ_{meas}	measured lifetime
τ_R	radiative lifetime
ν	frequency
$\overline{\nu}$	wavenumber

v	seniority number	Ψ_f	wavefunction of the final state
$\Delta\lambda_{eff}$	effective linewidth	ψ	short notation for the quantum numbers S, L and τ
Ω_λ	intensity parameter		
$\Xi(k,\lambda)$	radial integral	$\Im_\lambda$	intensity parameter (Carnall's notation)
Ψ	wavefunction		
Ψ_i	wavefunction of the initial state		

1. Introduction

The trivalent lanthanide ions have unique spectroscopic properties. Since the 4f shell is efficiently shielded by the closed 5s and 5p shells, the ligand environment has only a weak influence on the electronic cloud of the lanthanide ion. Although weak, this perturbation is responsible for the spectral fine structure. The absorption spectra of lanthanide ions doped into single crystals show groups of many fine lines, resembling an atomic spectrum. In solutions and glasses, the line transitions within one group have been broadened to one band. However, the linewidth of this band is still much smaller than in absorption spectra of transition metal ions. The peak position of the spectral lines reveals the electronic structure (of a part) of the $4f^N$ configuration. The crystal-field splitting gives information about the symmetry of the rare-earth site and about the shape of the coordination polyhedron. This has been discussed in detail by us in a previous chapter of this Handbook (Görller-Walrand and Binnemans 1996). The intensities of spectral transitions reflect also the interaction between the lanthanide ion and its environment.

The intensities of intraconfigurational f–f transitions are the subject of this chapter. First, the transition mechanisms for lanthanide ions are presented, namely the magnetic dipole transition, the induced electric dipole transition and the electric quadrupole transition (sect. 2). Then, we discuss how experimental intensities can be determined from the spectra. The definitions of the terms used in intensity studies are given (sect. 3). Special attention is paid to the expression of the dipole strength and the oscillator strength in oriented and in randomly-oriented systems. Correction factors for lanthanide ions in a dielectric medium are introduced. Although only a few magnetic dipole transitions exist for the trivalent lanthanide ions, magnetic dipole transitions are of interest, because their intensities are in a first approximation independent of the ligand environment and can thus be used as intensity standards. Moreover, the intensity of a magnetic dipole transition can be calculated exactly, provided that suitable wavefunctions are available. These wavefunctions can be obtained from diagonalization of the energy matrix (sect. 4).

Induced electric dipole transitions occur much more frequently than magnetic dipole transitions and therefore the largest part of this review is devoted to the former. However, induced electric dipole transitions have the disadvantage that the knowledge of wavefunctions is not sufficient for the calculation of electric dipole intensities and a parametrization is necessary. Judd and Ofelt developed independently the theoretical background for the calculation of the induced electric dipole matrix element. Their work is known under the common name *Judd–Ofelt theory* (sections 5 and 7). The papers of Judd

(1962) and Ofelt (1962) are the most often cited publications in the field of lanthanide spectroscopy. However, for non-physicists it is very hard to understand the mathematical formulae in those papers. Therefore, we will unravel the theoretical model given by Judd. A more profound derivation of the basic formulas is given than in the original paper of Judd. Special attention is paid to the approximations in the theory and to the derivation of the expression of the dipole strength for rare-earth ions in solution. Dimensions and units are given for the different intensity quantities and parameters. In this way, we hope to offer to the reader a clear presentation of the ideas behind the fundamental intensity formulas. Although the largest part of the intensity studies have been limited to transitions between J-manifolds (in solutions, glasses or even in single crystals), parametrization of the intensities of transitions between crystal-field levels (in single crystals) is also possible (sect. 6). However, such a parametrization in terms of $B_{\lambda kq}$ or A^{λ}_{tp} parameters is much more difficult than the parametrization of transitions between J-manifolds. It is shown how the theoretical work can be cast into a form that allows a practicable parametrization of intensities between J-manifolds (sect. 7). The parametrization in terms of Ω_λ parameters is discussed and we will give a convenient method for the determination of these parameters. One of the advantages of the Ω_λ parameters is that they can be used not only for the intensity of absorption spectra, but also for the intensity of luminescence spectra. In general, the parameters are determined semi-empirically from the intensities of the spectra. However, some authors have tried to calculate these parameters from first principles. An overview of their work is given.

The intensities of the majority of the f–f transitions vary only within a factor of 2–3 from host matrix to host matrix, but some transitions are much more host dependent. These transitions are called *hypersensitive transitions*. These induced electric dipole transitions obey the selection rules for electric quadrupole transitions and are therefore sometimes called *pseudo-quadrupole transitions*. In sect. 8, we will discuss hypersensitivity in detail. The dependence of the Ω_λ intensity parameters on the host matrix is the subject of sect. 9. Two-photon spectra (sect. 10) and vibronic transitions (sect. 11) are discussed briefly. On the other hand, chiroptical methods will not be considered. Since the color of the lanthanide ions is related to the spectral intensities of f–f transitions, we want to give attention to the phenomenon of color (sect. 12). Finally, the intensities of actinide ions are reviewed (sect. 13).

2. Transition mechanisms for lanthanide ions

2.1. *Interaction between light and matter*

In order to describe the interaction between light and matter, it is convenient to consider light as a wave phenomenon. A light beam is composed of electric and magnetic fields, situated perpendicular to each other and to the propagating direction, and oscillating sinusoidally both in space and time. In other words, light is electromagnetic radiation. A quantum system bathed in these oscillating electric and magnetic fields will sense both

the variations in space and time. Because the wavelength of UV, visible and IR light is much larger than the spatial extension of an atom, an ion or a small molecule, the spatial variation of the fields over this atom, ion or molecule can be neglected. Therefore, from the point of view of an atom, an ion or a molecule, light consists of spatially uniform electric and magnetic fields, oscillating in time. Light can interact in different ways with matter. First of all, high frequency electromagnetic waves can ionize atoms, ions or molecules (= photo-ionization). In the case of molecules, light can produce dissociation of bonds and other kinds of photochemical reactions. When atoms, ions or molecules are illuminated with electromagnetic radiation, they will receive energy from the light beam. In the absence of light, each electron will circulate within the atom, ion or molecule because of the presence of the electric and magnetic fields of all other constituents of the system. When the radiation arrives, the electrons will be pushed to and fro by the oscillating electric fields (and to a lesser extent by the magnetic fields) in the light beam. Therefore, the kinetic and potential energy of the system will be higher than in the absence of light. The quantum system may dispose of this excess of energy either by reradiating it (= radiative relaxation) or by turning it into other forms such as heat (= non-radiative relaxation).

If the frequency of the light, ν, is close to one of the natural frequencies of the atomic, ionic or molecular system, ν_0, the interaction is termed *resonant.* In this case, there is a maximal energy transfer from the radiation field to the system. If the frequencies ν and ν_0 do not match, the interaction is *non-resonant.* The molecules obtain an induced dipole moment. The amount of energy excess received by an atom, ion or molecule when it interacts non-resonantly with an electromagnetic wave is ordinarily quite small, and it is disposed of with great efficiency by reradiation. The direction of reradiation by an individual atomic system needs not to be the same as the direction of the incident beam. For this reason, non-resonant interactions are frequently called *light scattering.* If a large number of scatterers are present (a condition which is fulfilled in dense media like solutions, glasses and crystals), there will be interference (constructive and destructive) between the rays reradiated by any pair of them. If the scattering medium is perfectly homogeneous, the only scattered waves that will survive are those which are propagated in the same direction as that of the incident beam. This scattering process (dominant in many real systems in spite of small inhomogeneities) is called *transmission.* The degree of response of the electrons to the non-resonant electromagnetic wave is the *polarizability.* Polarizability can be defined as the ratio of the induced moment to the applied electric field strength. If the intensity of the light beam is not too strong, there is a linear relation between the induced dipole moment and the applied field. However in the case of very strong intensities (e.g. in a laser beam), non-linear optical effects will be observed.

Resonant interactions are ordinarily much stronger than non-resonant ones. Each characteristic frequency is actually a band of frequencies of width $\Delta\nu$ more or less symmetrically distributed around the same center ν_0. The resonant transfer of energy from a radiation field to matter is called *absorption.* The absorption process creates also an induced dipole moment, but a larger one than in the case of polarization. The transfer of energy from matter to the radiation field is termed *emission* (or *luminescence*). We

prefer to use the term luminescence instead of fluorescence, because the former term is more general. Normally, fluorescence is used for spin-allowed transitions in organic systems (Blasse and Grabmaier 1994).

2.2. *Intraconfigurational f–f transitions*

Absorption and luminescence spectroscopy are important techniques in the study of lanthanide systems, because they allow to determine the natural frequencies of a lanthanide ion. So one is able to settle the energy level scheme of a lanthanide ion. The absorption spectra of lanthanide-doped single crystals and lanthanide salts show groups of narrow lines. In solutions and in glasses, the lines within a group are broadened to one absorption band. These lines and bands have to be ascribed to electronic transitions inside the 4f shell. Each small line within a group corresponds to a transition between two crystal-field levels. Each group (or band), corresponds to transitions between two $^{2S+1}L_J$ free ion levels (or J-manifolds). They are not accompanied by a change in configuration (i.e. intraconfigurational transitions). The principal argument for this interpretation is that the lines are sharp and weak, while the wavelengths of the groups of lines are very similar for the different lanthanide systems. The sharpness and the wavelength independence of the peaks are not compatible with transitions to excited configurations (e.g., $4f^{N-1}5d^1$), because such transitions are more influenced by the surrounding ions. The $4f \leftarrow 4f$ transitions are sharp because the 4f electrons are very effectively shielded by the filled 5s and 5p shells, which have a higher energy than the 4f shell. The intensity of the transitions is weak. Three mechanisms must be considered for the interpretation of the observed transitions (Broer et al. 1945): (1) magnetic dipole transitions, (2) induced electric dipole transitions and (3) electric quadrupole transitions.

2.2.1. *Magnetic dipole transitions*

A *magnetic dipole transition* is caused by interaction of the spectroscopic active ion (i.e. the lanthanide ion) with the magnetic field component of the light through a magnetic dipole. If during a transition charge is displaced over a curved path, it will possess magnetic transition dipole intensity. In a region as small as the extent of an ion, the curvature of the displacement will be only weakly apparent. Since the intensity is proportional to the square of the transition dipole moment (see sect. 3), the intensity of the magnetic dipole transition is weak. Magnetic dipole radiation can also be considered as a rotational displacement of charge. Because the sense of a rotation is not reversed under inversion through a point (or inversion center), a magnetic dipole transition has even parity. Therefore, a magnetic dipole operator possesses even transformation properties under inversion and allows transitions between states of equal parity (i.e. intra-configurational transitions).

2.2.2. *Induced electric dipole transitions*

The majority of the observed optical transitions in lanthanide ions are *induced electric dipole transitions.* An electric dipole transition is the consequence of the interaction of

the spectroscopicly active ion (the lanthanide ion) with the electric field vector through an electric dipole. The creation of an electric dipole supposes a linear movement of charge. Such a transition has odd parity. The electric dipole operator has therefore odd transformation properties under inversion with respect to an inversion center. Intra-configurational electric dipole transitions are forbidden by the Laporte selection rule. Non-centrosymmetrical interactions allow the mixing of electronic states of opposite parity. The observed transitions are much weaker than the ordinary electric dipole transitions. They are often called induced electric dipole transitions. The induced electric dipole transitions are described by the Judd–Ofelt theory (see sect. 5).

2.2.3. *Electric quadrupole transitions*

The *electric quadrupole transition* arises from a displacement of charge that has a quadrupolar nature. An electric quadrupole consists of four point charges with overall zero charge and zero dipole moment. It may be pictured as two dipoles arranged so that their dipole moments cancel. An electric quadrupole has even parity. Electric quadrupole transitions are much weaker than magnetic dipole and induced electric dipole transitions. At this moment no experimental evidence exists for the occurrence of quadrupole transitions in lanthanide spectra, although some authors have claimed the existence of such transitions (e.g. Chrysochoos and Evers 1973). However, the so-called hypersensitive transitions (see sect. 8) are considered as pseudo-quadrupole transitions, because these transitions obey the selection rules of quadrupole transitions.

2.3. *Determination of the induced electric dipole or magnetic dipole character of a transition*

Experimentally, induced electric dipole transitions can be distinguished from magnetic dipole transitions by the selection rules (see Görller-Walrand and Binnemans 1996). In the case of lanthanide ions doped into single crystals, *polarized absorption spectroscopy* is very helpful. The oriented sample is irradiated with polarized light. For uniaxial crystals, three different polarized spectra can be recorded, depending on the vibration direction of the electric field vector $\boldsymbol{E}$ and the magnetic field vector $\boldsymbol{H}$ with respect to the crystallographic c-axis:

α spectrum: $\boldsymbol{E} \perp \boldsymbol{c}$, $\boldsymbol{H} \perp \boldsymbol{c}$,
σ spectrum: $\boldsymbol{E} \perp \boldsymbol{c}$, $\boldsymbol{H} \parallel \boldsymbol{c}$,
π spectrum: $\boldsymbol{E} \parallel \boldsymbol{c}$, $\boldsymbol{H} \perp \boldsymbol{c}$.

The Greek letters are abbreviations for the German words "*axial*" (α), "*senkrecht*" (= perpendicular, σ) and "*parallel*" (π). In an α spectrum or axial spectrum, the light propagates along the c-axis, which has the same direction as the optic axis. Both $\boldsymbol{E}$ and $\boldsymbol{H}$ are perpendicular to $\boldsymbol{c}$. An α spectrum is recorded with unpolarized light. In σ and π spectra, the light propagates perpendicular to the c-axis. These spectra are therefore also called orthoaxial spectra. In a σ spectrum, the electric field vector $\boldsymbol{E}$ is perpendicular to the c-axis, which requires that $\boldsymbol{H}$ be parallel to the c-axis. In a π spectrum, the electric field vector is parallel to the c-axis and the magnetic field vector is perpendicular to it.

For orthorhombic, monoclinic and triclinic crystal fields, the labels α, σ and π cannot be used. Here the nomenclature is to say that an ED transition is allowed in x, y or z polarization and an MD transition is allowed in R_x, R_y or R_z polarization.

An effective method for the prediction of the magnetic dipole character of a transition is intensity calculation. The intensity of a magnetic dipole transition can be calculated if appropriate wavefunctions are available (see sect. 4). Wavefunctions are obtained from a set a free-ion (and crystal-field) parameters. The parameter sets are derived from the energetic positions of the transitions. If a zero or nearly zero intensity is calculated for the magnetic dipole contribution of a particular transition observed in the spectrum, we can conclude that this transition has mainly an induced electric dipole character.

3. Definition of terms employed in intensity theory

3.1. *Introductory remarks on dimensions and units*

The intensity theory will be explained with emphasis on the relationships between theoretical quantities and experimental results. It may look confusing that the molar absorptivities obtained from optical absorption spectra are expressed in terms of $\mathrm{mol}^{-1}\,\mathrm{l\,cm}^{-1}$, whereas the phenomenological intensity parameters Ω_λ are expressed in cm^2. Therefore, we will emphasize the dimensions of the different quantities and, if appropriate, units will be mentioned. For the dimensions of the quantities, only length (L), mass (M) and time (T) are used; with dimensionless quantities we use a slash (/). In order to simplify certain formulae, the dimension of a charge ($\mathrm{M}^{1/2}\,\mathrm{L}^{3/2}/\mathrm{T}$) is not always written explicitly, but e will be given instead. The same is true for the dimension of an energy ($\mathrm{M\,L}^2/\mathrm{T}^2$), which will be reported in the dimension formulae as *energy*:

$$e^2/\mathrm{L} = \mathrm{ML}^2/\mathrm{T}^2 = \textit{energy}.$$

We use the same units for both induced electric dipole and magnetic dipoles (esu cm), because the induced electric and magnetic dipole transitions are found together in the spectra of lanthanide ions. We are conscious of the fact that we do not use the SI system but the CGS system. In spectroscopy, SI units are not easy to handle and their use often obscures simple relations between different quantities.

3.2. *Molar absorptivity*

The intensities of transitions of organic compounds and transition metal complexes are frequently reported in terms of the *molar absorptivity* ε at the maximum of the absorption

band (ε_{max}). The ε values can be calculated from the absorbance A by use of Lambert–Beer's law:

$$A = \varepsilon \cdot C \cdot d \qquad \text{[dim: /]}, \qquad (1)$$

where ε is the molar absorptivity[1] [dim: L^2, units: $mol^{-1}\,l\,cm^{-1}$], C is the concentration [dim: L^{-3}, units: $mol\,l^{-1}$], and d is the optical pathlength [dim: L, units: cm].

Although the ε_{max} values can be given also for lanthanide compounds, this practice is not very accurate, especially not for lanthanide ions in a crystalline host matrix, since the ratio of the spectral bandwidth to the natural bandwidth is often larger than 0.1, even with the smallest slit width of the spectrophotometer. When the spectral bandwidth is one-tenth of the natural bandwidth of the peak, deviation from the true peak height is less than 0.5%. A larger spectral bandwidth will increase this error. A smaller spectral bandwidth will increase the noise without significantly improving the quality of the data. If the absorption band is not completely resolved, the observed bandwidth is wider than the natural bandwidth and the absorption maximum is lower (ε_{max} is reduced). This is the reason why, upon the availability of high resolution recording spectrophotometers, researchers found higher ε_{max} values for the same lanthanide systems than their predecessors with low-resolution equipment. The maximum molar absorptivity of an absorption band can be used for the spectrophotometric determination of trivalent lanthanide ions, because in this case calibration curves have to be constructed. The fact that an absorption band is not totally resolved is not a problem in this case, as long as the same slit width is used for recording the spectra of both the standards and the samples. A procedure for the spectrophotometric dosage of lanthanide ions has been given by Banks and Klingman (1956) and by Stewart and Kato (1958).

It is not always possible to know the exact doping concentration of lanthanide ions diluted in a host crystal or in a glass. Often, the nominal concentration of the components is taken, i.e. the concentration of the starting composition of the batch. However, the true concentration may deviate from this value, because of losses of volatile compounds and because of inhomogeneities in the matrix. The concentration C of lanthanide ions doped into a host single crystal is given by

$$C = \frac{10^{27}}{V_u \times N_A} \times Z \times \delta \qquad \text{[dim: } L^{-3}\text{, units: } mol\,l^{-1}\text{]}, \qquad (2)$$

where V_u is the volume of the crystallographic unit cell [dim: L^3, units: $Å^3$], N_A is Avogadro's number [dim: /], Z is the number of formula units per unit cell [dim: /], and δ is the doping fraction (e.g. $\delta = 0.05$ for a doping concentration of 5%) [dim: /].

As opposed to doped matrices, for undiluted lanthanide salts the concentration can be so high that the linear relationship between absorbance and concentration no longer holds (violation of Beer's Law). If the two crystal faces through which the light beam

[1] In older textbooks, the term *molar extinction coefficient* is used instead of molar absorptivity.

travels are not parallel or if the crystal faces are not flat, there will be a variation in the optical pathlength. The determination of the pathlength of tiny crystals is also a factor of uncertainty. Reflection losses may result from defects and inclusions inside the crystal. The reflection losses will not cause major problems, because these result in a gradual increase of the baseline towards the ultraviolet. The peaks of the lanthanide ions are simply superposed on this broad band absorption. In the case of single crystals and glasses, often no reference sample is placed in the reference beam. For solutions, the reference sample is the solvent. The reader can find further information about apparent deviations from the law of Lambert–Beer in textbooks on analytical chemistry.

The area under an absorption peak is a better measure of the intensity than the molar absorptivity at the peak maximum, because the area is the same for both the resolved and the unresolved band. The area can be determined by integrating the peak, which is equivalent to the calculation of the integral

$$\int \varepsilon(\bar{\nu})\, \mathrm{d}\bar{\nu} \qquad \text{[dim: L]}, \qquad (3)$$

where $\bar{\nu}$ is the wavenumber [dim: L^{-1}, units: cm^{-1}].

The integrated molar absorptivity can be seen as the sum of the $\varepsilon(\bar{\nu})$ values over the whole absorption band. Instead of the molar absorptivity, the dipole strength D or the oscillator strength P are reported. One has to be cautious of the fact that the sample can be an oriented crystal or a medium in which the molecules are randomly oriented (solution, glass, powder). Throughout the text, we will emphasize this orientational problem. We use the symbols D' and P' for oriented systems, and D and P for randomly-oriented systems.

3.3. *Dipole strength (D') and oscillator strength (P') of a single spectral line in an oriented system*

A single spectral line in an oriented system is equivalent to the case of a single crystal studied with polarized light. Here, the molar absorptivity $\varepsilon(\bar{\nu})$ at a wavenumber $\bar{\nu}$ is related to the dipole strength by:

$$\varepsilon(\bar{\nu}) = \frac{8\pi^3}{hc}\,\frac{N_A}{2303} f(\bar{\nu})\, \bar{\nu} D' \qquad \text{[dim: } L^2\text{]}, \qquad (4)$$

where

$N_A = 6.02214 \times 10^{23}$ (Avogadro's number) [dim: /],

$h = 6.62554 \times 10^{-27}$ erg s (Planck's constant) [dim: $M L^2 T^{-1}$],

$c = 2.997925 \times 10^{10}$ cm s^{-1} (speed of light) [dim: $L T^{-1}$],

$\bar{\nu}$: wavenumber [dim: L^{-1}],

$f(\bar{\nu})$: line shape function [dim: L],

D': dipole strength [dim: $M L^5 T^{-2}$ or $e^2 L^2$].

The line shape function must fulfil the following conditions:

$$\text{(a)} \quad \int f(\bar{\nu})\,\bar{\nu}^n\,\mathrm{d}\bar{\nu} = \bar{\nu}_0^n \qquad [\text{dim: } \mathrm{L}^{-n}] \tag{5}$$

$$\text{and} \quad \int f(\bar{\nu})\,\mathrm{d}\bar{\nu} = 1 \qquad [\text{dim: /}], \tag{6}$$

$$\text{(b)} \quad \int \frac{\partial f(\bar{\nu})}{\partial \bar{\nu}}\,\mathrm{d}\bar{\nu} = 0 \qquad [\text{dim: L}], \tag{7}$$

$$\text{(c)} \quad \int \frac{\partial f(\bar{\nu})}{\partial \bar{\nu}}\,\bar{\nu}\,\mathrm{d}\bar{\nu} = 1 \qquad [\text{dim: /}]. \tag{8}$$

The dipole strength D' is defined as the absolute square of the matrix element in the dipole operator $\hat{\boldsymbol{O}}_\rho^{(1)}$ (MD or ED operator) between the wavefunction Ψ_i of the initial state and the wave function of Ψ_f of the final state:

$$\begin{aligned} D' &= \left|\left\langle \Psi_\mathrm{i} \left| \hat{\boldsymbol{O}}_\rho^{(1)} \right| \Psi_\mathrm{f} \right\rangle\right|^2 = \left\langle \Psi_\mathrm{i} \left| \hat{\boldsymbol{O}}_\rho^{(1)} \right| \Psi_\mathrm{f} \right\rangle^* \left\langle \Psi_\mathrm{i} \left| \hat{\boldsymbol{O}}_\rho^{(1)} \right| \Psi_\mathrm{f} \right\rangle \\ &= \left| \hat{\boldsymbol{O}}_{\rho,\,\mathrm{f\text{-}i}}^{(1)} \right|^2 \qquad [\text{dim: M L}^5\,\mathrm{T}^{-2} \text{ or } \mathrm{e}^2\,\mathrm{L}^2, \text{ units: esu}^2\,\mathrm{cm}^2], \end{aligned} \tag{9}$$

where $\hat{\boldsymbol{O}}_\rho^{(1)}$ corresponds to a single component of the transition electric or magnetic dipole in the molecular axis system (ρ can be x, y, z or $+1, -1, 0$). The term $\left\langle \Psi_\mathrm{i} \left| \hat{\boldsymbol{O}}_\rho^{(1)} \right| \Psi_\mathrm{f} \right\rangle^*$ is the complex conjugate of $\left\langle \Psi_\mathrm{i} \left| \hat{\boldsymbol{O}}_\rho^{(1)} \right| \Psi_\mathrm{f} \right\rangle$. For instance, the dipole strength of an induced electric dipole transition of an oriented molecule with its x-axis parallel to the electric field vector is given by:

$$D' = \left|\left\langle \Psi_\mathrm{i} \left| \hat{\boldsymbol{m}}_x^{(1)} \right| \Psi_\mathrm{f} \right\rangle\right|^2 \qquad [\text{dim: } \mathrm{e}^2\,\mathrm{L}^2], \tag{10}$$

where $\hat{\boldsymbol{m}}_x^{(1)}$ is the electric dipole operator.

The integrated molar absorptivity is

$$\int \varepsilon(\bar{\nu})\,\mathrm{d}\bar{\nu} = \frac{8\pi^3}{hc}\,\frac{N_\mathrm{A}}{2303}\,D' \int f(\bar{\nu})\,\bar{\nu}\,\mathrm{d}\bar{\nu} \qquad [\text{dim: L}], \tag{11}$$

or, by using eq. (5),

$$\int \varepsilon(\bar{\nu})\,\mathrm{d}\bar{\nu} = \frac{8\pi^3}{hc}\,\frac{N_\mathrm{A}}{2303}\,\bar{\nu}_0 D' \qquad [\text{dim: L}], \tag{12}$$

with $\bar{\nu}_0$ the wavenumber of the absorption maximum (in cm^{-1}). Filling in the constants in eq. (12) results in

$$\int \varepsilon(\bar{\nu})\,\mathrm{d}\bar{\nu} = \frac{8 \times (3.14159)^3 \times (6.02214 \times 10^{23})}{(6.62554 \times 10^{-27}\mathrm{erg\,s}) \times (2.997925 \times 10^{10}\mathrm{cm\,s^{-1}}) \times 2303}\,\bar{\nu}_0 D', \tag{13}$$

or

$$\int \varepsilon(\bar{\nu})\,\mathrm{d}\bar{\nu} = 3 \times 108.9 \times 10^{36}\,\bar{\nu}_0 D' \qquad \text{[dim: L; D' in esu}^2\,\text{cm}^2\text{]}. \tag{14}$$

In eq. (14), the dipole strength D' is expressed in esu^2 cm^2. Often, D' is expressed in Debye^2 (D^2). The conversion is straightforward, since 1 Debye = 10^{-18} esu cm:

$$\int \varepsilon(\bar{\nu})\,\mathrm{d}\bar{\nu} = 3 \times 108.9 \bar{\nu}_0 D' \qquad \text{[dim: L; D' in Debye}^2\ (\text{D}^2)\text{]}. \tag{15}$$

It is also possible to report D' in cm^2, by multiplying the right-hand side of eq. (14) by e^2:

$$\int \varepsilon(\bar{\nu})\,\mathrm{d}\bar{\nu} = 3 \times 108.9 \times 10^{36}\bar{\nu}_0\, e^2 D' = 0.75 \times 10^{20}\bar{\nu}_0 D' \qquad \text{[dim: L; D' in cm}^2\text{]}. \tag{16}$$

In eq. (12) it is assumed that the absorption band is symmetric (i.e., the band can be described by a Gaussian or Lorentzian line shape function). It is however more general to determine the integral $\int[\varepsilon(\bar{\nu})/\bar{\nu}]\,\mathrm{d}\bar{\nu}$:

$$\int \frac{\varepsilon(\bar{\nu})}{\bar{\nu}}\,\mathrm{d}\bar{\nu} = \frac{8\pi^3}{hc}\,\frac{N_\mathrm{A}}{2303} D' \int f(\bar{\nu})\,\mathrm{d}\bar{\nu} \qquad \text{[dim: L}^2\text{]} \tag{17}$$

or

$$\int \frac{\varepsilon(\bar{\nu})}{\bar{\nu}}\,\mathrm{d}\bar{\nu} = 3 \times 108.9 \times 10^{36} D' \tag{18}$$

[dim: L^2, units: mol^{-1} l cm^{-1}; D' in esu^2 cm^2].

The dipole strength D' is related to the oscillator strength P' by

$$P' = \frac{8\pi^2 m_\mathrm{e} c}{he^2}\,\bar{\nu}_0 D' = \frac{8\pi^2 m_\mathrm{e} c}{he^2}\,\bar{\nu}_0 \left|\hat{\boldsymbol{O}}^{(1)}_{\rho,\,\mathrm{f\text{–}i}}\right|^2 \qquad \text{[dim: /]}, \tag{19}$$

where

$e = 4.803 \times 10^{-10}$ esu (elementary charge),

$m_\mathrm{e} = 9.10904 \times 10^{-28}$ g (electron mass),

$h = 6.6261 \times 10^{-27}$ erg s (Planck's constant),

$c = 2.997925 \times 10^{10}$ cm s^{-1} (speed of light),

$\bar{\nu}_0$ = wavenumber at the absorption maximum (in cm^{-1}).

Upon filling in the constants, eq. (19) results in

$$\begin{aligned} P' &= \frac{8 \times (3.14159)^2 \times (9.10904 \times 10^{-18}\text{g}) \times (2.997925 \times 10^{10}\text{cm s}^{-1})}{(6.6261 \times 10^{-27}\text{erg s})(4.803 \times 10^{-10}\text{esu})}\,\bar{\nu}_0 D' \\ &= 4.702 \times 10^{-7} \times 3 \times 10^{36} \times \bar{\nu}_0 \times D' \end{aligned} \tag{20}$$

$$P' = 1.41 \times 10^{30} \times \bar{\nu}_0 \times D', \tag{21}$$

and

$$D' = \frac{(7.089 \times 10^{-31} \times P')}{\bar{\nu}_0} \qquad [D' \text{ in esu}^2\,\text{cm}^2]. \tag{22}$$

Equations (21) and (22) can be used to convert the dipole strength D' to the oscillator strength P' and vice versa (in oriented systems).

Since

$$\bar{\nu}_0 D' = \frac{2303hc}{8\pi^3 N_A} \int \varepsilon(\bar{\nu})\, d\bar{\nu} \qquad [\text{dim: } e^2\,L], \tag{23}$$

eq. (19) can be rewritten as

$$\begin{aligned} P' &= \frac{8\pi^2 m_e c}{he^2} \frac{2303hc}{8\pi^3 N_A} \int \varepsilon(\bar{\nu})\, d\bar{\nu} \\ &= \frac{2303\, m_e c^2}{N_A \pi\, e^2} \int \varepsilon(\bar{\nu})\, d\bar{\nu} \\ &= \frac{2303 \times (9.10904 \times 10^{-28}\,\text{g}) \times (2.997925 \times 10^{10}\,\text{cm s}^{-1})^2}{(6.02214 \times 10^{23}) \times 3.14159 \times (4.803 \times 10^{-10}\,\text{esu})^2} \int \varepsilon(\bar{\nu})\, d\bar{\nu}, \end{aligned} \tag{24}$$

or

$$P' = 4.32 \times 10^{-9} \int \varepsilon(\bar{\nu})\, d\bar{\nu} \qquad [\text{dim: /}]. \tag{25}$$

Equation (25) relates the oscillator strength P' to the integrated molar absorptivity $\int \varepsilon(\bar{\nu})\, d\bar{\nu}$.

As defined here, the dipole strength D' (eq. 9) and the oscillator strength P' (eq. 19) are theoretical quantities. In sect. 3.6 we will introduce the experimental dipole strength D'_{exp} and oscillator strength P'_{exp}, which can be compared directly with the calculated values.

3.4. *Dipole strength (D) and oscillator strength (P) of a transition in a randomly-oriented system*

Randomly-oriented systems are ions in solutions, glasses or powders. These systems are studied by unpolarized light. In this case, the molar absorptivity $\varepsilon(\bar{\nu})$ at a wavenumber $\bar{\nu}$ is related to the dipole strength D by

$$\varepsilon(\bar{\nu}) = \frac{8\pi^3}{hc} f(\bar{\nu})\, \bar{\nu}\, \frac{N_A}{2303} \frac{1}{3} D \qquad [\text{dim: } L^2], \tag{26}$$

where

$$D = \left|\langle \Psi_i \left|\hat{\boldsymbol{O}}\right| \Psi_f \rangle\right|^2 = \langle \Psi_i \left|\hat{\boldsymbol{O}}\right| \Psi_f \rangle^* \langle \Psi_i \left|\hat{\boldsymbol{O}}\right| \Psi_f \rangle = \left|\hat{\boldsymbol{O}}_{f-i}\right|^2 \quad [\text{dim: } M\,L^5\,T^{-2}], \tag{27}$$

with

$$|\hat{\boldsymbol{O}}_{\text{f–i}}|^2 = |\hat{\boldsymbol{O}}_{x,\text{f–i}}|^2 + |\hat{\boldsymbol{O}}_{y,\text{f–i}}|^2 + |\hat{\boldsymbol{O}}_{z,\text{f–i}}|^2 \tag{28}$$

or

$$|\hat{\boldsymbol{O}}_{\text{f–i}}|^2 = |\hat{\boldsymbol{O}}_{+1,\text{f–i}}|^2 + |\hat{\boldsymbol{O}}_{-1,\text{f–i}}|^2 + |\hat{\boldsymbol{O}}_{0,\text{f–i}}|^2. \tag{29}$$

We notice the introduction of a factor 1/3 in eq. (26) and the fact that $|\hat{\boldsymbol{O}}_{\text{f–i}}|^2$ is now a sum over the three orientations x, y and z.

The other symbols in eq. (26) are the same as in eq. (4). The integrated molar absorptivity is

$$\int \varepsilon(\bar{\nu})\, \mathrm{d}\bar{\nu} = \frac{8\pi^3}{hc}\,\frac{N_\mathrm{A}}{2303}\,\frac{1}{3}D\int f(\bar{\nu})\,\bar{\nu}\,\mathrm{d}\bar{\nu}, \tag{30}$$

$$\int \varepsilon(\bar{\nu})\, \mathrm{d}\bar{\nu} = \frac{8\pi^3}{hc}\,\frac{N_\mathrm{A}}{2303}\,\bar{\nu}_0\frac{1}{3}D, \tag{31}$$

or, after filling in the constants,

$$\int \varepsilon(\bar{\nu})\, \mathrm{d}\bar{\nu} = 108.9 \times 10^{36}\,\bar{\nu}_0 D \qquad [D \text{ in esu}^2\,\text{cm}^2]. \tag{32}$$

In eq. (32), the dipole strength D is expressed in $\text{esu}^2\,\text{cm}^2$. Often, D is expressed in Debye^2 (D^2). The conversion is straightforward, since 1 Debye $= 10^{-18}$ esu cm:

$$\int \varepsilon(\bar{\nu})\, \mathrm{d}\bar{\nu} = 108.9\bar{\nu}_0 D \qquad [\text{dim: L; } D \text{ in Debye}^2\ (\text{D}^2)]. \tag{33}$$

It is also possible to report D in cm^2, by multiplying the right-hand side of eq. (32) by e^2:

$$\int \varepsilon(\bar{\nu})\, \mathrm{d}\bar{\nu} = 108.9 \times 10^{36}\bar{\nu}_0\, e^2 D = 0.25 \times 10^{20}\bar{\nu}_0 D \qquad [\text{dim: L; } D \text{ in cm}^2]. \tag{34}$$

In terms of the integral $\int[\varepsilon(\bar{\nu})/\bar{\nu}]\,\mathrm{d}\bar{\nu}$, we find:

$$\int \frac{\varepsilon(\bar{\nu})}{\bar{\nu}}\,\mathrm{d}\bar{\nu} = \frac{8\pi^3}{hc}\,\frac{N_\mathrm{A}}{2303}\,\frac{1}{3}D\int f(\bar{\nu})\,\mathrm{d}\bar{\nu}, \tag{35}$$

or

$$\int \frac{\varepsilon(\bar{\nu})}{\bar{\nu}}\,\mathrm{d}\bar{\nu} = 108.9 \times 10^{36} D \qquad [D \text{ in esu}^2\,\text{cm}^2]. \tag{36}$$

The dipole strength D is related to the oscillator strength P by

$$P = \frac{8\pi^2 m_e c \bar{\nu}_0}{he^2} \frac{1}{3} D = \frac{8\pi^2 m_e c \bar{\nu}_0}{he^2} \frac{1}{3} \left| \hat{\boldsymbol{O}}_{f-i} \right|^2 \qquad \text{[dim: /]}, \tag{37}$$

where

$e = 4.803 \times 10^{-10}$ esu (elementary charge),
$m_e = 9.10904 \times 10^{-28}$ g (electron mass),
$h = 6.6261 \times 10^{-27}$ erg s (Planck's constant),
$c = 2.997925 \times 10^{10}$ cm s^{-1} (speed of light),
$\bar{\nu}_0$ = wavenumber at the absorption maximum (in cm^{-1}).

Filling in the constants yields

$$P = 4.702 \times 10^{-7} \times 10^{36} \times \bar{\nu}_0 \times D = 4.702 \times 10^{29} \times \bar{\nu}_0 \times D \tag{38}$$

and

$$D = \frac{(2.127 \times 10^{-30} \times P)}{\bar{\nu}_0}. \tag{39}$$

Equations (38) and (39) can be used to convert the dipole strength D to the oscillator strength P and vice versa (in randomly-oriented systems).

Since

$$\tfrac{1}{3} \bar{\nu}_0 D = \frac{2303hc}{8\pi^3 N_A} \int \varepsilon(\bar{\nu})\, d\bar{\nu}, \tag{40}$$

we find

$$P = \frac{2303\, m c^2}{N_A \pi\, e^2} \int \varepsilon(\bar{\nu})\, d\bar{\nu} = 4.32 \times 10^{-9} \int \varepsilon(\bar{\nu})\, d\bar{\nu}. \tag{41}$$

The result is the same as what we found for a single line in an oriented system (eq. 25), and the expression has been used by several authors, e.g. Carnall et al. (1968a). The concept of the oscillator strength was introduced by Ladenburg (1921). Sometimes, the notation f is used instead of P. The oscillator strength is a measure of the strength of a transition and it is the ratio of the actual intensity to the intensity radiated by one electron oscillating harmonically in three dimensions (Atkins 1983). For a harmonic oscillator in three dimensions, $P = 1$. This is essentially the value found for transitions, such as the D-lines of sodium, in which we can expect that only one electron contributes to the transition. For weaker transitions, we may say that less than one electron is participating in the transition, but it is more realistic to say that the transition involves compensating changes in the distribution of the other electrons. It is nevertheless convenient to consider

the problem as if it involves a fractional part of an oscillator. For allowed electric dipole transitions, P lies theoretically in the neighborhood of unity, although often smaller values are found. If the transition is forbidden by the selection rules, $P \ll 1$. A perturbation can break the selection rules. A general review dealing with the measuring methods of oscillator strengths has been given by Huber and Sandeman (1986). According to the *Kuhn–Thomas sum rule,* the sum of the oscillator strengths in a system with N electrons is equal to N (Atkins 1983). For trivalent lanthanide ions, the oscillator strength P of allowed magnetic dipole (MD) and forbidden (induced) electric dipole (ED) transitions is on the order of 10^{-6}. The ε_{max} values in lanthanide spectra are seldom larger than $10\,mol^{-1}\,l\,cm^{-1}$ and are more frequently close to $1\,mol^{-1}\,l\,cm^{-1}$. Exceptions are the hypersensitive transitions (see sect. 8). The strongest 4f–4f transition known is the hypersensitive transition $^5G_{5/2} \leftarrow {}^4I_{9/2}$ of NdI_3 vapor, which has $\varepsilon_{max} = 345\,l\,mol^{-1}\,cm^{-1}$ and $P = 5.35 \times 10^{-4}$ (Gruen and DeKock 1966).

One has to be cautious when comparing the intensities of transitions in different spectral regions. For instance, if an absorption band A in the infrared region has a smaller oscillator strength than an absorption band B in the ultraviolet region, it is possible that the dipole strength of A is larger than the dipole strength of B, because of the factor $1/\bar{\nu}_0$ in the conversion from P to D. Or, in other words, transitions in the infrared region tend to have a larger oscillator strength than transitions in the ultraviolet spectral region, although their dipole strength is the same. Since the oscillator strength is directly proportional to the integrated absorption band $\int \varepsilon(\bar{\nu})\,d\bar{\nu}$, the oscillator strength is convenient for comparing experimental intensities. However, the dipole strength has the advantage that its definition is simpler (absolute square of the matrix element) and is therefore preferred for theoretical calculations of intensities of transitions between crystal-field levels. Moreover, the dipole strength is wavelength independent (and of course also wavenumber independent), because of the integral $\int [\varepsilon(\bar{\nu})/\bar{\nu}]\,d\bar{\nu}$.

As defined here, the dipole strength D (eq. 27) and the oscillator strength P (eq. 37) are theoretical quantities. In sect. 3.6 we will introduce the experimental dipole strength D_{exp} and oscillator strength P_{exp}, which can be compared directly with the calculated values.

3.5. *Effect of the dielectric medium*

The dipole strength of an induced electric dipole transition is proportional to the square of the matrix element in the dipole operator and therefore also to the square of the electric field at the lanthanide site. However, in intensity studies, the lanthanide ions are not in a vacuum, but embedded in a dielectric medium. The lanthanide ion in a dielectric medium not only feels the radiation field of the incident light, but also the field from the dipoles in the medium outside a spherical surface. The total field consisting of the electric field E of the incident light (electric field in the vacuum), plus the electric field of the dipoles is called the *effective field* E_{eff}, i.e. the field effective in inducing the electric dipole transition. The square of the matrix element in the electric dipole operator has to be multiplied by a factor $(E_{eff}/E)^2$. In a first approximation, $(E_{eff}/E)^2 = (n^2+2)^2/9$. The factor $(n^2+2)^2/9$ is the *Lorentz local field correction* and accounts for dipole–dipole corrections.

For the absorption process, the transition probability has to be divided by the energy (or photon) flux. The photon flux of a light beam does not alter when it enters from the vacuum into the dielectric medium. The flux in the vacuum is $(c/4\pi)E_0^2$, and that in the dielectric medium is $(v/4\pi)n^2E_0^2$, where c is the speed of light in the vacuum, v is the speed of light in the medium, and $v = c/n$. Therefore, an additional factor $1/n$ has to be included in the expression of the correction factor χ_{ED} for induced electric dipole transitions, so that we find the expression $(n^2+2)^2/9n$ for χ_{ED}. For emission, the transition probability is not divided by an energy density, but instead by an energy flux, i.e. by n^2. Moreover, the emission probability is proportional to the density of photon states, i.e. to the cube of the photon momentum. The correction factor has to be multiplied by n^3, giving the expression $n(n^2+2)^2/9$. For magnetic dipole transitions, the transition is induced by the magnetic field component of the incident light and no *Lorentz local field correction* has to be considered. The medium is characterized by the magnetic permeability μ. For a dielectric medium, $\mu \approx 1$, which results in the correction factors $\chi_{MD} = n$ for absorption and $\chi_{MD} = n^3$ for emission (Dexter 1958, Fowler and Dexter 1962).

In summary, the correction factors for an absorption spectrum are :

$$\chi_{ED} = \frac{(n^2+2)^2}{9n}, \qquad \chi_{MD} = n \qquad \text{(absorption)}, \tag{42,43}$$

where n is the refractive index of the medium. The correction factors for emission spectra are different:

$$\chi_{ED} = \frac{n(n^2+2)^2}{9}, \qquad \chi_{MD} = n^3 \qquad \text{(emission)}. \tag{44,45}$$

The correction factors are valid for lanthanide ions in an *isotropic* dielectric medium. It is assumed that (1) the centers are not in resonance with the host medium, i.e. the transitions occur at an energy for which the medium is transparent, and that (2) the lanthanide ions are so far apart that interactions among them can be neglected. Each lanthanide ion can be treated as an isolated center in a medium characterized by a real refractive index. For n, we can take the value of the refractive index n_D for the sample illuminated by the sodium D line (589.3 nm). Some authors take the wavelength dependence of λ (= dispersion) into account. The dispersion is described by the dispersion formula of Cauchy:

$$n(\lambda) = A + \frac{B}{\lambda^2} + \cdots, \tag{46}$$

where A and B are positive constants. These constants can be determined by measuring the refractive index at at least two wavelengths. Higher-order corrections are usually omitted. Alternative expressions for the dispersion formula can be found in the literature. By considering the dispersion, the correction factors χ_{ED} and χ_{MD} are different for each transition.

For isotropic media such as solutions and glasses, only one refractive index n has to be considered. However, if the lanthanide ion is doped into an anisotropic single crystal, two

main refractive indices n_o and n_e are present for uniaxial crystals and three main refractive indices n_x, n_y and n_z for biaxial crystals. As long as the birefringence is not too large, it is a good approximation to use a mean value of the main refractive indices for n. If polarized absorption spectra are recorded for a uniaxial crystal with a large birefringence, n_o has to be taken to calculate the correction factor for the axial α spectrum. For the orthoaxial σ spectrum, n_o has to be used for the calculation of χ_{ED} and n_e for the calculation of χ_{MD}. Finally for the orthoaxial π spectrum, n_o is used for the calculation of χ_{MD} and n_e for the calculation of χ_{ED}. For biaxial crystals the situation is even more complicated, and that case will not be discussed here.

3.6. *Experimental dipole strength and oscillator strength*

In order to compare the calculated dipole strength (or oscillator strength) with the experimental values, it is not only necessary to introduce a correction factor for the dielectric medium (see sect. 3.5), but the degeneracy of the initial levels has also to be taken into account. For single crystals, the degeneracy of the initial state is g_A, where $g_A = 1$ for a non-degenerate level and $g_A = 2$ for a doubly-degenerate level. For non-cubic crystals, no crystal-field level degeneracy higher than 2 is found. For randomly-oriented systems, a weighing factor $2J + 1$ is introduced in the expression for the dipole strength. This weighing factor is the degeneracy of the ground state $^{2S+1}L_J$ and is added because the matrix elements are summed over all the M components of the ground state. It is assumed that all the crystal-field levels of the ground state are equally populated.

The dipole strength and oscillator strength corrected for medium effects and degeneracy are:

$$D'_{exp} = \frac{\chi}{g_A} D', \tag{47}$$

$$P'_{exp} = \frac{\chi}{g_A} P', \tag{48}$$

$$D_{exp} = \frac{1}{2J+1} \chi D, \tag{49}$$

$$P_{exp} = \frac{1}{2J+1} \chi P, \tag{50}$$

where χ can be both χ_{MD} and χ_{ED}. Equations (47)–(50) allow to make the connection between experiment and theory. The quantities D', P', D and P are determined by evaluation of matrix elements (eqs. 9, 19, 27, 37). Using the correction factors, they can

be compared with the experimental quantities determined from the absorption spectrum by

$$D'_{\text{exp}} = \frac{1}{3 \times 108.9 \times 10^{36}} \int \frac{\varepsilon(\bar{\nu})}{\bar{\nu}} \, \mathrm{d}\bar{\nu},$$
$$P'_{\text{exp}} = 4.32 \times 10^{-9} \int \varepsilon(\bar{\nu}) \, \mathrm{d}\bar{\nu}, \qquad \text{(oriented system)}, \tag{52}$$

$$D_{\text{exp}} = \frac{1}{108.9 \times 10^{36}} \int \frac{\varepsilon(\bar{\nu})}{\bar{\nu}} \, \mathrm{d}\bar{\nu},$$
$$P_{\text{exp}} = 4.32 \times 10^{-9} \int \varepsilon(\bar{\nu}) \, \mathrm{d}\bar{\nu}, \qquad \text{(randomly-oriented system)}. \tag{54}$$

3.7. *Mixed ED–MD transitions*

In general, a transition is not a pure induced electric dipole or a magnetic dipole transition, but contains both ED and MD contributions. The ED and MD dipole strengths have to be calculated separately. The experimental dipole strength can be compared with the total calculated dipole strength for an oriented system by the expression

$$D'_{\text{exp}} = \frac{1}{g_{\text{A}}} \left(\chi_{\text{MD}} D'_{\text{MD}} + \chi_{\text{ED}} D'_{\text{ED}} \right) \qquad \text{(oriented system)}, \tag{55}$$

where D'_{MD} and D'_{ED} are the calculated MD and ED contributions of the transition, respectively. For randomly-oriented systems, we have

$$D_{\text{exp}} = \frac{1}{2J+1} \left(\chi_{\text{MD}} D_{\text{MD}} + \chi_{\text{ED}} D_{\text{ED}} \right) \qquad \text{(randomly-oriented system)}. \tag{56}$$

3.8. *Fractional thermal population*

At 0 K, only the lowest energy level is populated. An increase in temperature will additionally populate levels at higher energy. The fractional thermal population $X_{\text{A}}(T)$ of the initial level A (= level from which the absorption or luminescence process starts) at temperature T can be calculated by using the formula for the Boltzmann distribution:

$$X_{\text{A}}(T) = \frac{g_{\text{A}} \exp(-\Delta E_{\text{A}}/kT)}{\sum_i g_i \exp(-\Delta E_i/kT)}, \tag{57}$$

where g_i is the degeneracy of level i, g_{A} is the degeneracy of the initial level A, ΔE_i is the energy difference between level i and the ground state (in cm^{-1}), $k = 0.695 \, \text{cm}^{-1} \, \text{K}^{-1}$ (Boltzmann's constant), and T is the temperature (in K).

The summation in the denominator of eq. (57) is a partition function. In principle, the summation runs over all energy levels of the $4f^N$ configuration. In practice, the summation can be truncated at 2000 cm^{-1} or at an even lower energy, since contributions of higher energy levels to the sum are very small. Level A can be both a crystal-field level or a $^{2S+1}L_J$ free-ion level. In the latter case the degeneracy g_A is equal to $2J+1$ (see also sect. 3.6).

The experimental dipole strength D'_{exp} or D_{exp} can be corrected for the fractional thermal population as follows:

$$D'_{exp} = \frac{1}{3 \times 108.9 \times 10^{36} \times X_A(T)} \int \frac{\varepsilon(\bar{\nu})}{\bar{\nu}} \, d\bar{\nu} \qquad \text{(oriented system)}, \tag{58}$$

$$D_{exp} = \frac{1}{108.9 \times 10^{36} \times X_A(T)} \int \frac{\varepsilon(\bar{\nu})}{\bar{\nu}} \, d\bar{\nu} \qquad \text{(randomly-oriented system)}. \tag{59}$$

For lanthanide ions in solutions and glasses, no crystal-field fine structure is observed, and transitions between $^{2S+1}L_J$ spin-orbit levels are considered. For the majority of the lanthanide ions, the energy between the $^{2S+1}L_J$ ground state and the second-lowest $^{2S+1}L_J$ state is so large (>2000 cm^{-1}) that even at room temperature the thermal population of the first excited $^{2S+1}L_J$ level can be neglected in comparison with the population of the ground state. The factor $X_A(T)$ is then equal to unity and can be omitted. Only for Eu^{3+} ($^7F_1$ at ~350 cm^{-1} and $^7F_2$ at ~1000 cm^{-1} above the ground state $^7F_0$), and to a lesser extent for Sm^{3+} ($^6H_{7/2}$ at ~1100 cm^{-1} above the ground state $^6H_{5/2}$), must the $X_A(T)$ factor be considered.

4. Magnetic dipole (MD) transitions

4.1. *Magnetic dipole matrix element for a single spectral line in an oriented system*

The calculated magnetic dipole strength for a transition between a state with wavefunction $\langle l^N \tau SLJM|$ and a state with wavefunction $|l^N \tau' S'L'J'M'\rangle$ can be found by evaluating the matrix element in the dipole operator $\hat{\boldsymbol{O}}_{MD}$. This operator is also denoted as $\hat{\boldsymbol{\mu}}_p^{(1)}$. Pay attention to the fact that several authors use this notation for the electric dipole operator. The magnetic dipole matrix element is given by

$$\langle l^N \tau SLJM | \hat{\boldsymbol{\mu}}_p^{(1)} | l^N \tau' S'L'J'M' \rangle = \left\langle l^N \tau SLJM \left| -\frac{e\hbar}{2m_e c} \left(\hat{\boldsymbol{L}} + 2\hat{\boldsymbol{S}}\right)_p^{(1)} \right| l^N \tau' S'L'J'M' \right\rangle$$

[dim: $M^{1/2} L^{5/2} T^{-1}$ or eL, units: esu cm], (60)

where $\hat{\boldsymbol{L}}$ is the total orbital angular momentum operator, $\hat{\boldsymbol{S}}$ is the total spin angular momentum operator, $\hbar = h/2\pi$, and $e\hbar/(2m_e c) = 9.273 \times 10^{-21}$ esu cm. However, note that instead of $\hat{\boldsymbol{L}} + 2\hat{\boldsymbol{S}}$, one should strictly write $\hat{\boldsymbol{L}} + g_e\hat{\boldsymbol{S}}$, where g_e is the electron g-factor (Atkins 1988) and its numerical value is 2.00223. This approximation has little effect on the calculated magnetic dipole strengths. The magnetic dipole operator $\hat{\boldsymbol{\mu}}_p^{(1)}$ is a tensor

of rank 1 with components ρ. The components ρ are called polarization numbers. For a magnetic dipole transition in the σ-polarization $\rho = 0$, for α and π polarization $\rho = \pm 1$:

$$\sigma \quad (\rho = 0): \qquad \hat{\boldsymbol{\mu}}_0^{(1)} = \hat{\boldsymbol{\mu}}_z^{(1)} = -\frac{e\hbar}{2m_e c}\left(\hat{\boldsymbol{L}}_z + 2\hat{\boldsymbol{S}}_z\right)_0^{(1)}, \tag{61}$$

$$\alpha, \pi \quad (\rho = \pm 1): \qquad \hat{\boldsymbol{\mu}}_{\pm 1}^{(1)} = \mp\frac{1}{\sqrt{2}}\left(\hat{\boldsymbol{\mu}}_x^{(1)} \pm i\hat{\boldsymbol{\mu}}_y^{(1)}\right) = -\frac{e\hbar}{2m_e c}\left(\hat{\boldsymbol{L}} + 2\hat{\boldsymbol{S}}\right)_{\pm 1}^{(1)}. \tag{62}$$

The magnetic dipole operator $\hat{\boldsymbol{\mu}}_\rho^{(1)}$ has the intrinsic $C_{\infty h}$ symmetry. The calculation of the magnetic dipole matrix elements has been discussed by Shortley (1940) and by Pasternak (1940). The wavefunctions used for the calculation of the magnetic dipole strength are pure $4f^N$ eigenfunctions of the even components (k = even) of the crystal-field Hamiltonian. The wavefunctions are obtained using the same parameter set (both free ion and crystal-field parameters) required for the energy level calculation. It is assumed that the incident light does not interact with the ligand charge distributions. The matrix element in eq. (60) is calculated by application of the Wigner–Eckart theorem (Weissbluth 1978) to remove the ρ dependence,

$$\begin{aligned}&\left\langle l^N \tau SLJM \left| \left(\hat{\boldsymbol{L}} + 2\hat{\boldsymbol{S}}\right)_\rho^{(1)} \right| l^N \tau' S'L'J'M' \right\rangle \\ &\quad = (-1)^{J-M} \begin{pmatrix} J & 1 & J' \\ -M & \rho & M' \end{pmatrix} \left\langle l^N \tau SLJ \left\| \left(\hat{\boldsymbol{L}} + 2\hat{\boldsymbol{S}}\right)^{(1)} \right\| l^N \tau' S'L'J' \right\rangle.\end{aligned} \tag{63}$$

Here, $\begin{pmatrix} J & 1 & J' \\ -M & \rho & M' \end{pmatrix}$ is a 3-j symbol and its value is tabulated in the work of Rotenberg et al. (1959). The reduced matrix element

$$\left\langle l^N \tau SLJ \left\| \left(\hat{\boldsymbol{L}} + 2\hat{\boldsymbol{S}}\right)^{(1)} \right\| l^N \tau' S'L'J' \right\rangle$$

can be worked out by splitting the terms in $\hat{\boldsymbol{L}}$ and $\hat{\boldsymbol{S}}$ and by an additional application of the Wigner–Eckart theorem (Weissbluth 1978). For the matrix element in $\hat{\boldsymbol{L}}$ one finds

$$\begin{aligned}&\left\langle l^N \tau SLJ \left\| \hat{\boldsymbol{L}} \right\| l^N \tau' S'L'J' \right\rangle \\ &\quad = \delta_{\tau\tau'}\,\delta_{SS'}\,\delta_{LL'}\,(-1)^{S+L+J+1} \begin{Bmatrix} L & J & S \\ J' & L & 1 \end{Bmatrix} \left[(2L+1)(2J+1)\left(2J'+1\right)L(L+1)\right]^{1/2},\end{aligned} \tag{64}$$

where the Kronecker delta $\delta_{if} = 0$ if $i \neq f$ and $\delta_{if} = 1$ if $i = f$.

For the matrix element in $\hat{\boldsymbol{S}}$, the result is analogous:

$$\begin{aligned}&\left\langle l^N \tau SLJ \left\| \hat{\boldsymbol{S}} \right\| l^N \tau' S'L'J' \right\rangle \\ &\quad = \delta_{\tau\tau'}\,\delta_{SS'}\,\delta_{LL'}\,(-1)^{S+L+J+1} \begin{Bmatrix} S & J & L \\ J' & S & 1 \end{Bmatrix} \left[(2S+1)(2J+1)\left(2J'+1\right)S(S+1)\right]^{1/2}.\end{aligned} \tag{65}$$

4.2. *Selection rules for magnetic dipole transitions*

From eqs. (63)–(65), the selection rules for magnetic dipole transitions can be derived to be

(1) $\Delta\tau = 0$,
(2) $\Delta S = 0$,
(3) $\Delta L = 0$,
(4) $\Delta J = 0, \pm 1$, but $0 \leftrightarrow 0$ is forbidden,
(5) $-M + \rho + M' = 0$, where $\rho = 0, \pm 1$,
$M' - M = 0$ (σ polarization), $M' - M = \pm 1$ (α or π polarization).

The selection rules on ΔS and ΔL are not very strict and are only valid in the Russell–Saunders coupling scheme. In the Russell–Saunders coupling scheme, magnetic dipole transitions will be limited to the J-levels within a single term ^{2S+1}L (i.e. the ground term for transitions observed in the absorption spectrum). Most of these transitions occur at low transition energies (several hundred cm^{-1}) and are thus outside the spectroscopic range for absorption and luminescence measurements. These selection rules can be relaxed in the intermediate coupling scheme, where only J remains a good quantum number. The selection rule on J is more rigid and can only be broken down by J-mixing, which is a weak effect due to the crystal-field perturbation. Because the magnetic dipole operator $\hat{\boldsymbol{\mu}}_\rho^{(1)}$ has even parity, magnetic dipole transitions are allowed within one configuration (e.g. intra-configurational 4f–4f transitions).

With the knowledge of the selection rule $\Delta J = 0, \pm 1$, three different cases can be distinguished for the magnetic dipole matrix elements:

$$(1)\ J = J',$$
$$\left\langle l^N \tau SLJ \left\| (\hat{\boldsymbol{L}} + 2\hat{\boldsymbol{S}})^{(1)} \right\| l^N \tau SLJ \right\rangle = g\,[J(J+1)(2J+1)]^{1/2}, \tag{66}$$

where g is the Landé factor, given by

$$g = 1 + \frac{J(J+1) - L(L+1) + S(S+1)}{2J(J+1)}. \tag{67}$$

The Landé factor describes the effective magnetic momentum of an atom or electron, in which the orbital angular momentum L and the spin angular momentum S are combined to give a total angular momentum J.

$$(2)\ J' = J - 1,$$
$$\left\langle l^N \tau SLJ \left\| (\hat{\boldsymbol{L}} + 2\hat{\boldsymbol{S}})^{(1)} \right\| l^N \tau SLJ - 1 \right\rangle = \left[\frac{1}{4J}(S+L+J+1)(S+L+J-1)(J+S-L)(J+L-S)\right]^{1/2}, \tag{68}$$

$$(3)\ J' = J + 1,$$
$$\left\langle l^N \tau SLJ \left\| (\hat{\boldsymbol{L}} + 2\hat{\boldsymbol{S}})^{(1)} \right\| l^N \tau SLJ + 1 \right\rangle = \left[\frac{1}{4(J+1)}(S+L+J+2)(S+J+1-L)(L+J+1-S)(S+L-J)\right]^{1/2}. \tag{69}$$

These equations are valid in the Russell–Saunders coupling scheme, for terms which are described by only one quantum number τ. In general, a $^{2S+1}L_J$ Russell–Saunders term is a linear combination of $^{2S+1}L_J(\tau)$ terms, where the summation runs over the quantum number τ. In the intermediate coupling scheme, for each wavefunction the proper linear combination of the $^{2S+1}L_J$ Russell–Saunders terms with the same J value has to be made before evaluating the matrix elements. The matrix element of a magnetic dipole transition in the intermediate coupling scheme or after J-mixing can therefore be written as

$$\left\langle \Psi_i \left| \hat{\boldsymbol{\mu}}_\rho^{(1)} \right| \Psi_f \right\rangle = \sum_{JJ'} \sum_{MM'} a_{JM} a_{J'M'} \sum_{\tau S L} \sum_{\tau' S' L'} h_{\tau S L} h'_{\tau' S' L'} \left\langle l^N \tau S L J M \left| \hat{\boldsymbol{\mu}}_\rho^{(1)} \right| l^N \tau' S' L' J' M' \right\rangle, \tag{70}$$

where $h_{\tau SL}$ and $h'_{\tau' S' L'}$ are the coefficients for the wavefunction in the Russell–Saunders coupling scheme, and a_{JM} and $a_{J'M'}$ are the coefficients for the wavefunction in the intermediate coupling scheme or after J-mixing.

Special note: After evaluation of the magnetic dipole matrix element and taking the absolute square, the calculated magnetic dipole strength is found, expressed in (Bohr magneton)^2 or β^2. The matrix element can also be expressed in esu^2 cm^2, by applying the conversion

$$1\beta = 9.273 \times 10^{-21} \text{ esu cm.} \tag{71}$$

This transformation is important for mixed ED–MD transitions, where both ED and MD contributions have to be summed (see eqs. 55 and 56).

The expression for the matrix element in eq. (60) is only valid for one spectral line in an oriented system, studied by polarized light. The magnetic dipole strength of a randomly-oriented system is given by

$$D_{MD} = \left| \hat{\boldsymbol{\mu}}_{+1,\,f\text{–}i}^{(1)} \right|^2 + \left| \hat{\boldsymbol{\mu}}_{-1,\,f\text{–}i}^{(1)} \right|^2 + \left| \hat{\boldsymbol{\mu}}_{0,\,f\text{–}i}^{(1)} \right|^2, \tag{72}$$

and the oscillator strength for a randomly-oriented system is given by

$$P_{MD} = \frac{8\pi^2 m_e c \bar{\nu}_0}{he^2} \frac{1}{3} \left(\left| \hat{\boldsymbol{\mu}}_{+1,\,f\text{–}i}^{(1)} \right|^2 + \left| \hat{\boldsymbol{\mu}}_{-1,\,f\text{–}i}^{(1)} \right|^2 + \left| \hat{\boldsymbol{\mu}}_{0,\,f\text{–}i}^{(1)} \right|^2 \right). \tag{73}$$

Sometimes, the symbol S_{md} (line strength) is used instead of D_{MD}. In practice, the magnetic dipole strength D_{MD} for a randomly-oriented system can be obtained by the formula

$$D_{MD} = \frac{e^2 \hbar^2}{4 m_e^2 c^2} \left| \left\langle l^N \tau S L J \left\| \left(\hat{\boldsymbol{L}} + 2\hat{\boldsymbol{S}} \right)^{(1)} \right\| l^N \tau' S' L' J' \right\rangle \right|^2 \qquad \text{[units: esu}^2 \text{ cm}^2\text{]}, \tag{74}$$

where the matrix elements in Russell–Saunders coupling scheme are calculated according to eqs. (66)–(69). For the intermediate coupling scheme, eq. (70) has to be considered. As

Table 1
Principal magnetic dipole transitions in the absorption spectra of the trivalent lanthanide ions[a]

Ion	Transition	Energy (cm^{-1})[b]	Oscillator strength (10^{-8})[c]	Dipole strength (10^{-6} Debye^2)
Pr^{3+}	$^3H_5 \leftarrow {}^3H_4$	2300	9.76	90
Nd^{3+}	$^4I_{11/2} \leftarrow {}^4I_{9/2}$	2000	14.11	15
Pm^{3+}	$^5I_5 \leftarrow {}^5I_4$	1600	16.36	217
Sm^{3+}	$^6H_{7/2} \leftarrow {}^6H_{5/2}$	1100	17.51	339
	$^4G_{5/2} \leftarrow {}^6H_{5/2}$	17900	1.76	2.1
Eu^{3+}	$^5D_0 \leftarrow {}^7F_1$	16900	7.47[d,e]	9.4[d,e]
	$^5D_1 \leftarrow {}^7F_0$	19000	1.62[d]	1.8[d]
	$^5F_1 \leftarrow {}^7F_1$	33400	2.16[d]	1.4[d]
Gd^{3+}	$^6P_{7/2} \leftarrow {}^8S_{7/2}$	32200	4.13	2.7
	$^6P_{5/2} \leftarrow {}^8S_{7/2}$	32800	2.33	1.5
Tb^{3+}	$^7F_5 \leftarrow {}^7F_6$	2100	12.11	123
	$^7G_6 \leftarrow {}^7F_6$	26400	5.03	4.1
	$^5G_5 \leftarrow {}^7F_6$	27800	6.66	4.9
Dy^{3+}	$^6H_{13/2} \leftarrow {}^6H_{15/2}$	3500	22.68	138
	$^4I_{15/2} \leftarrow {}^6H_{15/2}$	22300	5.95	5.7
Ho^{3+}	$^5I_7 \leftarrow {}^5I_8$	5100	29.47	123
	$^3K_8 \leftarrow {}^5I_8$	21300	6.39	6.4
Er^{3+}	$^4I_{13/2} \leftarrow {}^4I_{15/2}$	6600	30.82	99
	$^2K_{15/2} \leftarrow {}^4I_{15/2}$	27800	3.69	2.8
Tm^{3+}	$^3H_5 \leftarrow {}^3H_6$	8400	27.25	69
Yb^{3+}	$^2F_{7/2} \leftarrow {}^2F_{5/2}$	10400	17.76	36

[a] Adapted from Carnall (1979).
[b] An approximated value of the energy in cm^{-1} is given (rounded to the nearest hundred).
[c] The values are those for transitions in aqueous $HClO_4$ solution.
[d] The population of the $^7F_0$ (ca. 65%) and $^7F_1$ (ca. 35%) levels at room temperature is taken into account.
[e] Values from Görller-Walrand et al. (1991).

described in sect. 3.6, D_{MD} and P_{MD} have to be multiplied by $\chi_{MD}/(2J+1)$ to compare them with the experimental values. In table 1, the principal magnetic dipole (MD) transitions in the absorption spectra of trivalent lanthanide ions and their intensities are summarized (after Carnall 1979). The values are valid for randomly-oriented systems. Magnetic dipole transitions are weak. Their intensity is in general a factor of magnitude weaker than electric dipole transitions. Several transitions show a mixed dipole character, which means that they gain intensity by both the MD and the ED mechanisms.

4.3. *Sum rule*

The intensity of an MD transition is relatively independent of the surroundings of the lanthanide. So, the kind of ligands or the symmetry of the coordination polyhedron around

the lanthanide ion do not influence the MD intensity largely. It has been shown by Görller-Walrand et al. (1991) that in the intermediate coupling scheme, the total magnetic dipole strength of all the crystal-field transitions (over all the polarizations) between two $^{2S+1}L_J$ manifolds is symmetry independent. This sum rule is not valid in the case of J-mixing, but since the J-mixing effect is small for most systems, deviations from the ideal sum rule are expected to be small also. Mean theoretical sum values of 18×10^{-7} D^2, 94×10^{-7} D^2 and 9×10^{-7} D^2 have been found for the respective magnetic dipole transitions $^5D_1 \leftarrow {}^7F_0$, $^5D_0 \leftarrow {}^7F_1$ and $^5D_2 \leftarrow {}^7F_1$ of Eu^{3+}. The detailed theoretical derivation of this sum rule is not given here, but can be found in the article by Görller-Walrand et al. (1991). The influence of J-mixing is especially reflected by the intensity ratio between two crystal-field transitions within one J-manifold (Porcher and Caro 1980).

5. Judd–Ofelt theory for induced electric dipole (ED) transitions

5.1. *Preliminary remarks*

Judd (1962) and independently Ofelt (1962) worked out the theoretical background for the calculation of the induced electric dipole matrix element. The basic idea of Judd and Ofelt is that the intensity of the forbidden f–f electric dipole transitions can arise from the admixture into the $4f^N$ configuration of configurations of opposite parity (e.g., $4f^{N-1}n'd^1$ and $4f^{N-1}n'g^1$). As already mentioned in the introduction, we will unravel here in detail the theoretical model developed by Judd. Special attention will be given to the dimensions, units and selection rules. Our symbolism is close to Judd's. The difference is that we represent the crystal-field coefficient by A_{kq} (instead of Judd's A_{tp}), the light polarization by ρ (instead of Judd's q), and the additional quantum number by τ (Judd's γ).

Judd considered the odd part of the crystal-field potential as the perturbation for mixing states of different parity into the f^N configuration. He cast his intensity formula in a form which allows an easy parametrization and he gave expressions for the intensity of rare-earth ions in solution. Therefore, all practical applications of the Judd–Ofelt theory to rare-earth ions in solutions and glasses are based on Judd's paper, although Judd and Ofelt are mostly cited simultaneously. It is interesting to note that Judd considered solution spectra, rather than single-crystal spectra, because of the lack of intensity data of rare-earth ions in crystalline matrices at that time.

5.2. *Induced electric dipole matrix element for a single spectral line in an oriented system*

First, we consider a single spectral line in an oriented system, i.e., a crystal-field transition in an oriented single crystal. The calculated induced electric dipole strength for a transition between a state with wavefunction $\langle l^N \tau SLJM|$ and a state with wavefunction $|l^N \tau' S'L'J'M'\rangle$ can be found by evaluating the matrix element in the dipole operator $\hat{\boldsymbol{O}}_{\mathrm{ED}}$. This operator is also denoted as $\hat{\boldsymbol{m}}_{\rho}^{(1)}$. Pay attention to the fact that several authors

use this notation for the magnetic dipole operator. The induced dipole matrix element is given by

$$\begin{aligned}\left\langle l^N \tau SLJM \left| \hat{\boldsymbol{m}}_\rho^{(1)} \right| l^N \tau' S'L'J'M' \right\rangle &= \left\langle l^N \tau SLJM \left| -e\hat{\boldsymbol{D}}_\rho^{(1)} \right| l^N \tau' S'L'J'M' \right\rangle \\ &= \left\langle l^N \tau SLJM \left| -e\sum_j \hat{\boldsymbol{r}}_\rho^{(1)}(r_j, \theta_j, \varphi_j) \right| l^N \tau' S'L'J'M' \right\rangle \\ &= \left\langle l^N \tau SLJM \left| -e\sum_j r_j \hat{\boldsymbol{C}}_\rho^{(1)}(\theta_j, \varphi_j) \right| l^N \tau' S'L'J'M' \right\rangle \\ &\quad [\text{dim: } \mathrm{M}^{1/2}\,\mathrm{L}^{5/2}\,\mathrm{T}^{-1} \text{ or } e\mathrm{L}],\end{aligned} \tag{75}$$

where

$\hat{\boldsymbol{m}}_\rho^{(1)}$, electric dipole operator [dim: eL],

$\hat{\boldsymbol{D}}_\rho^{(1)}$, transition operator [dim: L],

$\hat{\boldsymbol{r}}_\rho^{(1)}(r_j, \theta_j, \varphi_j)$, position vector of electron j [dim: L],

$\hat{\boldsymbol{C}}_\rho^{(1)}(\theta_j, \varphi_j)$, irreducible tensor operator of rank 1 containing the angular coordinates of electron j [dim: /].

The irreducible tensor operator $\hat{\boldsymbol{C}}_\rho^{(1)}(\theta_j, \varphi_j)$ can be related to the spherical harmonics $Y_\rho^{(1)}(\theta_j, \varphi_j)$:

$$\hat{\boldsymbol{C}}_\rho^{(1)}(\theta_j, \varphi_j) = \sqrt{\frac{3\pi}{4}}\, Y_\rho^{(1)}(\theta_j, \varphi_j). \tag{76}$$

The electric dipole operator $\hat{\boldsymbol{m}}_\rho^{(1)}$ is a tensor of rank 1 with components ρ. These components ρ are called polarization numbers. For electric dipole transitions in π polarization $\rho = 0$, for α and σ polarization $\rho = \pm 1$:

$$\pi \quad (\rho = 0): \qquad \hat{\boldsymbol{m}}_0^{(1)} = \hat{\boldsymbol{m}}_z^{(1)} = -e\hat{\boldsymbol{D}}_0^{(1)}, \tag{77}$$

$$\alpha, \sigma \quad (\rho = \pm 1): \qquad \hat{\boldsymbol{m}}_{\pm 1}^{(1)} = \mp\frac{1}{\sqrt{2}}\left(\hat{\boldsymbol{m}}_x^{(1)} \pm \mathrm{i}\hat{\boldsymbol{m}}_y^{(1)}\right) = -e\hat{\boldsymbol{D}}_{\pm 1}^{(1)}. \tag{78}$$

The electric dipole operator has odd parity for an inversion symmetry operation. The parity label *ungerade* can be attached to it. The operator $\hat{\boldsymbol{m}}_\rho^{(1)}$ has an intrinsic $C_{\infty v}$ symmetry.

5.3. *Description of the states* Ψ_i *and* Ψ_f

In order to evaluate the matrix element $\left\langle \Psi_i \left| \hat{\boldsymbol{m}}_p^{(1)} \right| \Psi_f \right\rangle$, a detailed description of the initial state Ψ_i and the final state Ψ_f is needed. Due to the small crystal-field strength, the total angular momentum J is assumed to remain a good quantum number. No J-mixing is considered. S is the same in both Ψ_i and Ψ_f, because the dipole operator cannot influence the spin part of the wave function. In other words, $S = S'$ or $\delta_{SS'} = 0$. Corresponding to the component Ψ_i of the ground level of the configuration l^N, there exists to the first approximation a linear combination

$$\langle A| \equiv \sum_M \langle l^N \psi J M|\ a_M \qquad \text{[Judd 1962, eq. (2)]}, \tag{79}$$

where A is a crystal-field level, ψ stands for the additional quantum numbers that are necessary to define a level uniquely [e.g., in the Russell–Saunders coupling scheme L (total angular momentum), S (total spin angular momentum) and the quantum number τ, where the latter is used to distinguish between levels with equal L, S and J], M is the quantum number of the projection J_z of J, and a_M is a coefficient arising from crystal-field mixing.

By analogy, a linear combination can be written for the final level:

$$|A'\rangle \equiv \sum_{M'} a'_{M'} \left| l^N \psi' J' M' \right\rangle \qquad \text{[Judd 1962, eq. (3)]}. \tag{80}$$

It is assumed that the coefficients a_M and $a'_{M'}$ do not vary in time. The states $\langle A|$ and $|A'\rangle$ are constructed from the same configuration l^N (e.g. $4f^N$ or $5f^N$). According to the Laporte selection rule, electric dipole transitions are allowed between two states of opposite parity. These transitions result in a change of the dipole moment of the ion. Strictly speaking, only transitions which belong to states of configurations of opposite parity will be observed. In a first approximation, no intra-configurational 4f–4f transitions can occur by an electric dipole mechanism, because the matrix element $\left\langle A \left| \hat{\boldsymbol{m}}_p^{(1)} \right| A' \right\rangle$ is equal to zero. Nevertheless, most observed transitions in the absorption and luminescence spectra of trivalent lanthanide ions are electric dipole transitions (see sect. 2). Van Vleck (1937) and Broer et al. (1945) stated that a non-zero electric dipole matrix element can result from an admixing into $\langle A|$ and $|A'\rangle$ of states built from configurations of opposite parity to the l^N electronic states ($4f^N$ for the lanthanide ions). These perturbing configurations have a higher energy than the $4f^N$ configuration and are mostly of the type $4f^{N-1}n'l'$, e.g. $4f^{N-1}n'd^1$, $4f^{N-1}n'g^1$. There are also contributions from hole-type configurations, e.g. $4d^9 4f^{N+1}$. To distinguish such configurations, the argument l' is augmented with the principal quantum number n'. The symbol n is reserved for the analogous quantum number for the electrons of the ground configuration l^N. Because of this admixing, these transitions are called *forced electric dipole transitions* or *induced electric dipole transitions*. It is more difficult to evaluate the electric dipole

matrix elements than the magnetic dipole matrix elements, because for a calculation of the electric dipole elements, not only the energies and wavefunctions of the $4f^N$ configuration have to be known, but also the energies and wavefunctions of the perturbing configurations.

5.4. *Crystal-field Hamiltonian*

According to Judd–Ofelt theory (Judd 1962, Ofelt 1962), the mixing of electronic states of opposite parity into the $4f^N$ electronic configuration of non-centrosymmetric lanthanide systems is induced by the odd-parity terms (k = odd) of the crystal-field Hamiltonian. The crystal field is generated by point charges situated at the atomic positions of the perturbing ligands. The centrosymmetric lanthanide systems cannot gain intensity by this mechanism, because the odd part of the crystal-field Hamiltonian vanishes if an inversion center is present. The crystal-field parametrization has been described in detail by Görller-Walrand and Binnemans (1996). We choose here an expansion of the crystal-field Hamiltonian in terms of A_{kq} coefficients, instead of the B_q^k coefficients. [It will become clear below that this notation has some advantages, namely the separation of the angular and radial parts in the crystal-field coefficients]. The A_{kq} coefficients can however be related to the angular part of the B_q^k coefficients. Note that the A_{kq} are coefficients and not crystal-field parameters (see Görller-Walrand and Binnemans 1996).

The crystal-field Hamiltonian is

$$V = \sum_{k,q} A_{kq} \hat{\boldsymbol{D}}_q^{(k)} = \sum_{k,q} A_{kq} \sum_j r_j^k \hat{\boldsymbol{C}}_q^{(k)} (\theta_j, \varphi_j), \tag{81}$$

where

V, crystal-field Hamiltonian [dim: ML^2T^{-2} or *energy*],

$\hat{\boldsymbol{D}}_q^{(k)}$, tensor of rank k with components q [dim: L^k],

A_{kq}, crystal-field coefficient [dim: $ML^{2-k}T^{-2}$ or *energy* L^{-k}],

r_j^k, position of electron j (to the kth power) [dim: L^k],

$\hat{\boldsymbol{C}}_q^{(k)} (\theta_j, \varphi_j)$, irreducible tensor operator of rank k containing the angular coordinates of electron j [dim: /].

Note that the dimension of the crystal-field coefficient A_{kq} is *energy* L^{-k}, whereas the dimension of the crystal-field parameter B_q^k is ML^2T^{-2}, or *energy* (Görller-Walrand and Binnemans 1996). The B_q^k include the radial integral r^k. The Hamiltonian for the crystal-field perturbation is written here as a potential, because this is commonly done in the literature.

5.5. *First-order perturbation*

The crystal field is considered as a first-order perturbation which mixes states of an excited configuration $|l^{N-1}(n'l')\psi''J''M''\rangle$ with a parity opposite to l^N in the states $\langle A|$ and $|A'\rangle$. The states $\langle A|$ and $|A'\rangle$ become $\langle B|$ and $|B'\rangle$ respectively:

$$\langle B| = \sum_M \langle l^N \psi JM|\, a_M + \sum_K \langle l^{N-1}(n'l')\psi''J''M''|\, b\,(n'l'\psi''J''M''), \tag{82}$$

$$|B'\rangle = \sum_{M'} a'_{M'}\, |l^N \psi' J'M'\rangle + \sum_K b'\,(n'l'\psi''J''M'')\, |l^{N-1}(n'l')\psi''J''M''\rangle, \tag{83}$$

where

$$b\,(n'l'\psi''J''M'') = \frac{\sum_M a_M \langle l^N \psi JM|\hat{\boldsymbol{V}}_{\text{odd}}|\, l^{N-1}(n'l')\psi''J''M''\rangle}{E(\psi J) - E(n'l'\psi''J'')}, \tag{84}$$

$$b'\,(n'l'\psi''J''M'') = \frac{\sum_{M'} a'_{M'} \langle l^{N-1}(n'l')\psi''J''M''|\hat{\boldsymbol{V}}_{\text{odd}}|\, l^N \psi' J'M'\rangle}{E(\psi' J') - E(n'l'\psi''J'')}. \tag{85}$$

The operator $\hat{\boldsymbol{V}}_{\text{odd}}$ is the odd part of the crystal-field Hamiltonian (k = odd). The summation over K runs over all ψ'', J'', M'', n', and over those values of l' for which $l^{N-1}(n'l')$ is an excited configuration with parity opposite to $4f^N$. The $\langle A|$ and $|A'\rangle$ functions, together with the a_M and $a'_{M'}$ coefficients, are thus incorporated in the $\langle B|$ and $|B'\rangle$ functions. All the approximations for the calculations of the matrix element are applied to the latter functions.

5.6. *Matrix elements in the transition operator*

From now on, we will work on a matrix element which has the dimension of a length, L. The units of the matrix element are cm, or cm^2 if squared. With the knowledge of the wavefunctions the electric dipole matrix element can be worked out:

$$\begin{aligned}
&\langle B|\hat{\boldsymbol{D}}^{(1)}_\rho|\, B'\rangle \\
&= \sum_M \sum_{M'} \langle l^N \psi JM|\, a_M \hat{\boldsymbol{D}}^{(1)}_\rho a'_{M'}|\, l^N \psi' J'M'\rangle && \text{[dim: L]} \\
&\quad + \sum_K \sum_M \sum_{M'} \langle l^N \psi JM|\, a_M \hat{\boldsymbol{D}}^{(1)}_\rho b'\,(n'l'\psi''J''M'')|\, l^{N-1}(n'l')\psi''J''M''\rangle && \text{[dim: L]} \\
&\quad + \sum_K \sum_M \sum_{M'} \langle l^{N-1}(n'l')\psi''J''M''|\, b\,(n'l'\psi''J''M'')\, \hat{\boldsymbol{D}}^{(1)}_\rho a'_{M'}|\, l^N \psi' J'M'\rangle && \text{[dim: L]} \\
&\quad + \sum_K \sum_{K'} \langle l^{N-1}(n'l')\psi''J''M''|\, b\,(n'l'\psi''J''M'')\, \hat{\boldsymbol{D}}^{(1)}_\rho \\
&\qquad\qquad \times b'\,(n'l'\psi''J''M'')|\, l^{N-1}(n'l')\psi''J''M''\rangle, && \text{[dim: L],}
\end{aligned} \tag{86}$$

or

$$
\begin{aligned}
&\langle B \,|\hat{\boldsymbol{D}}_p^{(1)}|\, B'\rangle \\
&\quad = \sum_M \sum_{M'} a_M a'_{M'} \langle l^N \psi J M \,|\hat{\boldsymbol{D}}_p^{(1)}|\, l^N \psi' J' M'\rangle \\
&\qquad + \sum_K \sum_M \sum_{M'} a_M a'_{M'} \langle l^N \psi J M \,|\hat{\boldsymbol{D}}_p^{(1)}|\, l^{N-1}(n'l')\psi'' J'' M''\rangle \\
&\qquad\qquad \times \sum_{k,q} A_{kq} \frac{\langle l^{N-1}(n'l')\psi'' J'' M'' \,|\hat{\boldsymbol{D}}_q^{(k)}|\, l^N \psi' J' M'\rangle}{E(\psi' J') - E(n'l'\psi'' J'')} \qquad (87) \\
&\qquad + \sum_K \sum_M \sum_{M'} a_M a'_{M'} \sum_{k,q} A_{kq} \frac{\langle l^N \psi J M \,|\hat{\boldsymbol{D}}_q^{(k)}|\, l^{N-1}(n'l')\psi'' J'' M''\rangle}{E(\psi J) - E(n'l'\psi'' J'')} \\
&\qquad\qquad \times \langle l^{N-1}(n'l')\psi'' J'' M'' \,|\hat{\boldsymbol{D}}_p^{(1)}|\, l^N \psi' J' M'\rangle \\
&\qquad + \textit{second-order term} \qquad\qquad [\text{dim: L}].
\end{aligned}
$$

Be aware that this matrix element has the dimension of a length, L, because the dimension of $\hat{\boldsymbol{D}}_p^{(1)}$ is L, the dimension of $\hat{\boldsymbol{D}}_p^{(k)}$ is L^k, the dimension of A_{kq} is *energy* L^{-k}, and the terms in the denominator are energies.

The first term in eq. (87) cancels, because $\langle l^N \psi J M|$ and $|l^N \psi' J' M'\rangle$ have the same parity. The second-order term also cancels. Thus, eq. (87) can be rewritten as

$$
\begin{aligned}
&\langle B \,|\hat{\boldsymbol{D}}_p^{(1)}|\, B'\rangle \\
&= \sum_K \sum_M \sum_{M'} \sum_{k,q} a_M a'_{M'} A_{kq} \frac{\langle l^N \psi J M \,|\hat{\boldsymbol{D}}_p^{(1)}|\, l^N \psi' J' M'\rangle \langle l^{N-1}(n'l')\psi'' J'' M'' \,|\hat{\boldsymbol{D}}_p^{(k)}|\, l^N \psi' J' M'\rangle}{(E(\psi' J') - E(n'l'\psi'' J''))} \\
&\quad + \sum_K \sum_M \sum_{M'} \sum_{k,q} a_M a'_{M'} A_{kq} \frac{\langle l^N \psi J M \,|\hat{\boldsymbol{D}}_q^{(k)}|\, l^{N-1}(n'l')\psi'' J'' M''\rangle \langle l^{N-1}(n'l')\psi'' J'' M'' \,|\hat{\boldsymbol{D}}_q^{(1)}|\, l^N \psi' J' M'\rangle}{(E(\psi J) - E(n'l'\psi'' J''))}
\end{aligned}
$$

[Judd 1962, eq. (6)]. (88)

The summation runs over nine terms: M, M', k, q, and the quantum numbers implied by the symbol K: ψ'', J'', M'', and l' and n', where $l^{N-1}(n'l')$ is a configuration with a parity opposite to l^N.

5.7. *Approximations*

The calculation of the electric dipole matrix element in eq. (88) is not easy, because of the ninefold summation: M, M', k, q, ψ'', J'', M'', n' and l' for which $l^{N-1}(n'l')$ is a configuration with a parity opposite to l^N. A detailed analysis of the expression and a knowledge of the tensor algebra developed by Racah (1942, 1943, 1949), reveals that simplifications are possible. The main suggestion made by Judd and Ofelt is that

the presence of the structure $|l^{N-1}(n'l')\psi''J''M''\rangle\langle l^{N-1}(n'l')\psi''J''M''|$ in eq. (88) makes it possible to apply the *closure procedure* (Griffith 1960) in some way. The number of summations absorbed into the closure procedure depends on how far the energy of the mixing configurations can be assumed invariant with respect to n', l', ψ'' and J'' and M''. The closure procedure allows to replace $\hat{\boldsymbol{D}}_p^{(1)}$ and $\hat{\boldsymbol{D}}_q^{(k)}$ by a single operator acting between states of l^N. The advantage is that neither the wavefunctions of the excited configurations, nor their energy values have to be known. The wavefunctions $|l^{N-1}(n'l')\psi''J''M''\rangle$ vanish in the expression for the electric dipole matrix element and the individual energies of the excited configurations will be replaced by the global energy of the configurations. The *closure procedure* is introduced in successive steps. The dependence of $E(n'l'\psi''J'')$ on the quantum numbers n', l', ψ'', J'' and M'' is checked. In other words, it is considered to which extent the perturbing configuration can be considered degenerate.

5.7.1. *First approximation: J'' and M'' are degenerate*

No crystal-field splitting of the perturbing configuration $|l^{N-1}(n'l')\psi''J''M''\rangle$ is considered. Therefore, the M'' functions are degenerate. Furthermore, the splittings of the ${}^{2S+1}L_{J''}$ multiplets within one ${}^{2S+1}L$ term of the perturbing configuration are negligible compared to the energy difference between the perturbing configuration $|l^{N-1}(n'l')\psi''J''M''\rangle$ and the ground configuration $|l^N\psi JM\rangle$. The spin–orbit coupling is neglected in the excited configuration, and the energy of the excited configuration $E(n'l'\psi''J'')$ is independent of J''. The sums over J'' and M'' can be worked out in several steps for a single Russell–Saunders term.

Step 1: The Wigner–Eckart theorem (Weissbluth 1978) can be applied to the term

$$\sum_{J''M''} \langle l^N\psi JM|\hat{\boldsymbol{D}}_p^{(1)}|l^{N-1}(n'l')\psi''J''M''\rangle\langle l^{N-1}(n'l')\psi''J''M''|\hat{\boldsymbol{D}}_q^{(k)}|l^N\psi'J'M'\rangle$$
$$= \sum_{J''M''} \langle l^N\tau SLJM|\hat{\boldsymbol{D}}_p^{(1)}|l^{N-1}(n'l')\tau''SL''J''M''\rangle\langle l^{N-1}(n'l')\tau''SL''J''M''|\hat{\boldsymbol{D}}_q^{(k)}|l^N\tau'SL'J'M'\rangle \quad (89)$$
$$[\text{dim: } L^{k+1}].$$

It should be remembered that the crystal-field Hamiltonian does not work on the spin part of the formula:

$$S = S' = S''. \quad (90)$$

The first part of eq. (89) becomes

$$\langle l^N\tau SLJM|\hat{\boldsymbol{D}}_p^{(1)}|l^{N-1}(n'l')\tau''SL''J''M''\rangle$$
$$= (-1)^{J-M}\begin{pmatrix} J & 1 & J'' \\ -M & p & M'' \end{pmatrix}\langle l^N\tau SLJ\|\hat{\boldsymbol{D}}^{(1)}\|l^{N-1}(n'l')\tau''SL''J''\rangle, \quad (91)$$

and the second part becomes

$$\begin{aligned}&\left\langle l^{N-1}(n'l')\tau''SL''J''M''\left|\hat{\boldsymbol{D}}_q^{(k)}\right|l^N\tau'SL'J'M'\right\rangle\\&\quad=(-1)^{J''-M''}\begin{pmatrix}J'' & k & J'\\ -M'' & q & M'\end{pmatrix}\left\langle l^{N-1}(n'l')\tau''SL''J''\left\|\hat{\boldsymbol{D}}^{(k)}\right\|l^N\tau'SL'J'\right\rangle.\end{aligned}\tag{92}$$

Step 2: The reduced matrix element of a tensor operator $\hat{\boldsymbol{T}}^{(k)}$ working only on one part in the coupled scheme $(\gamma j_1 j_2 J)$ is given by eq. (3-37) of Judd (1963):

$$\begin{aligned}&\left\langle\gamma' j_1' j_2' J'\left\|\hat{\boldsymbol{T}}^{(k)}\right\|\gamma j_1 j_2 J\right\rangle\\&\quad=\delta\left(j_1,j_1'\right)(-1)^{j_1+j_2+J'+k}\sqrt{(2J+1)(2J'+1)}\begin{Bmatrix}j_2' & J' & j_1\\ J & j_2 & k\end{Bmatrix}\left\langle\gamma' j_2'\left\|\hat{\boldsymbol{T}}^{(k)}\right\|\gamma j_2\right\rangle.\end{aligned}\tag{93}$$

First, with

$$\gamma'=l^N\tau,\quad \gamma=l^{N-1}(n'l')\tau'',\quad j_1'=S,\quad j_1=S,$$
$$j_2'=L,\quad j_2=L'',\quad J'=J,\quad J=J'',\quad k=1,$$

and $\hat{\boldsymbol{D}}^{(1)}$ working only on L, we obtain

$$\begin{aligned}&\left\langle l^N\tau SLJ\left\|\hat{\boldsymbol{D}}^{(1)}\right\|l^{N-1}(n'l')\tau''SL''J''\right\rangle\\&\quad=(-1)^{S+L''+J+1}\sqrt{(2J+1)(2J''+1)}\begin{Bmatrix}L & J & S\\ J'' & L'' & 1\end{Bmatrix}\left\langle l^N\tau SL\left\|\hat{\boldsymbol{D}}^{(1)}\right\|l^{N-1}(n'l')\tau''SL''\right\rangle.\end{aligned}\tag{94}$$

Secondly, with

$$\gamma'=l^{N-1}(n'l')\tau'',\quad \gamma=l^N\tau',\quad j_1'=S,\quad j_1=S,$$
$$j_2'=L'',\quad j_2=L',\quad J'=J'',\quad J=J',\quad k=k,$$

and $\hat{\boldsymbol{D}}^{(k)}$ working only on L, we obtain

$$\begin{aligned}&\left\langle l^{N-1}\left(n'l'\right)\tau''SL''J''\left\|\hat{\boldsymbol{D}}^{(k)}\right\|l^N\tau'SL'J'\right\rangle\\&=(-1)^{S+L'+J''+k}\sqrt{(2J''+1)(2J'+1)}\begin{Bmatrix}L'' & J'' & S\\ J' & L' & k\end{Bmatrix}\left\langle l^{N-1}(n'l')\tau''SL''\left\|\hat{\boldsymbol{D}}^{(k)}\right\|l^N\tau'SL'\right\rangle.\end{aligned}\tag{95}$$

So we find:

$$\begin{aligned}&\sum_{J'',M''}\left\langle l^N\psi JM\left|\hat{\boldsymbol{D}}_\rho^{(1)}\right|l^{N-1}(n'l')\psi''J''M''\right\rangle\left\langle l^{N-1}(n'l')\psi''J''M''\left|\hat{\boldsymbol{D}}_q^{(k)}\right|l^N\psi'J'M'\right\rangle\\&\quad=\sum_{J'',M''}(-1)^{J-M}\begin{pmatrix}J & 1 & J''\\ -M & \rho & M''\end{pmatrix}(-1)^{S+L''+J+1}\left[(2J+1)\left(2J''+1\right)\right]^{1/2}\\&\qquad\times\begin{Bmatrix}L & J & S\\ J'' & L'' & 1\end{Bmatrix}\left\langle l^N\tau SL\left\|\hat{\boldsymbol{D}}^{(1)}\right\|l^{N-1}(n'l')\tau''SL''\right\rangle\\&\qquad\times(-1)^{J''-M''}\begin{pmatrix}J'' & k & J'\\ -M'' & q & M'\end{pmatrix}(-1)^{S+L'+J''+k}\left[\left(2J''+1\right)\left(2J'+1\right)\right]^{1/2}\\&\qquad\times\begin{Bmatrix}L'' & J'' & S\\ J' & L' & k\end{Bmatrix}\left\langle l^{N-1}(n'l')\tau''SL''\left\|\hat{\boldsymbol{D}}^{(k)}\right\|l^N\tau' SL'\right\rangle.\end{aligned}\tag{96}$$

Notice that from the properties for the 3-j symbols in eq. (96), the following relations can be derived:

$$M'' = M - \rho, \tag{97}$$

$$M'' = q + M', \tag{98}$$

$$M = \rho + q + M'. \tag{99}$$

Step 3: We consider the sum over M'' of the 3-j symbols in eq. (96):

$$\sum_{M''} \begin{pmatrix} J & 1 & J'' \\ -M & \rho & M'' \end{pmatrix} \begin{pmatrix} k & J' & J'' \\ q & M' & -M'' \end{pmatrix}. \tag{100}$$

The components of the second 3-j symbol have changed place by two permutations of the columns. Based on the sum rule for 3-j symbols:

$$\sum_{m_3} \begin{pmatrix} j_1 & j_2 & j_3 \\ m_1 & m_2 & m_3 \end{pmatrix} \begin{pmatrix} l_1 & l_2 & j_3 \\ n_1 & n_2 & -m_3 \end{pmatrix}$$
$$= \sum_{l_3, n_3} (-1)^{j_3+l_3+m_1+n_1} (2l_3+1) \begin{Bmatrix} j_1 & j_2 & j_3 \\ l_1 & l_2 & l_3 \end{Bmatrix} \begin{pmatrix} l_1 & j_2 & l_3 \\ n_1 & m_2 & n_3 \end{pmatrix} \begin{pmatrix} j_1 & l_2 & l_3 \\ m_1 & n_2 & -n_3 \end{pmatrix}, \tag{101}$$

with $j_1 = J$, $l_1 = k$, $m_1 = -M$, $n_1 = q$, $j_2 = 1$, $l_2 = J'$, $m_2 = \rho$, $n_2 = M'$, $j_3 = J''$, $l_3 = \lambda$, $m_3 = M''$, $n_3 = -q - \rho$, the sum over M'' becomes

$$\sum_{M''} \begin{pmatrix} J & 1 & J'' \\ -M & \rho & M'' \end{pmatrix} \begin{pmatrix} k & J' & J'' \\ q & M' & -M'' \end{pmatrix}$$
$$= \sum_{\lambda, -q-\rho} (-1)^{J''+\lambda-M+q} (2\lambda+1) \begin{Bmatrix} J & 1 & J'' \\ k & J' & \lambda \end{Bmatrix} \begin{pmatrix} k & 1 & \lambda \\ q & \rho & -q-\rho \end{pmatrix} \begin{pmatrix} J & J' & \lambda \\ -M & M' & \rho+q \end{pmatrix}. \tag{102}$$

Note: A factor λ is introduced in eq. (102), which is even because of the properties of the 3-j symbols and because $M' - M = -\rho - q$ (eq. 99).

We can rewrite eq. (96) as:

$$\sum_{J''} \sum_{\lambda, -\rho-q} (-1)^{J''+\lambda-M+q} (2\lambda+1) \begin{Bmatrix} J & 1 & J'' \\ k & J' & \lambda \end{Bmatrix} \begin{pmatrix} k & 1 & \lambda \\ q & \rho & -q-\rho \end{pmatrix} \begin{pmatrix} J & J' & \lambda \\ -M & M' & q+\rho \end{pmatrix}$$
$$\times (-1)^{J-M+S+L''+J+1+J''-M''+S+L'+J''+k} \left[(2J+1)(2J'+1)\right]^{1/2} (2J''+1)$$
$$\times \begin{Bmatrix} L & J & S \\ J'' & L'' & 1 \end{Bmatrix} \begin{Bmatrix} L'' & J'' & S \\ J' & L' & k \end{Bmatrix}$$
$$\langle l^N \tau SL \| \hat{\boldsymbol{D}}^{(1)} \| l^{N-1}(n'l')\tau'' SL'' \rangle \langle l^{N-1}(n'l')\tau'' SL'' \| \hat{\boldsymbol{D}}^{(k)} \| l^N \tau' SL' \rangle. \tag{103}$$

Step 4: The sum over J'' of the product of the 6-j symbols

$$\begin{Bmatrix} J & 1 & J'' \\ k & J' & \lambda \end{Bmatrix} \begin{Bmatrix} L & J & S \\ J'' & L'' & 1 \end{Bmatrix} \begin{Bmatrix} L'' & J'' & S \\ J' & L' & k \end{Bmatrix}$$

can be simplified utilizing the Biedenharn–Elliot sum rule (Biedenharn 1953, Elliot 1953, Judd 1963, Edmonds 1974):

$$\sum_x (2x+1)(-1)^{x+p+q+r+a+b+c+d+e+f} \begin{Bmatrix} a & b & x \\ c & d & p \end{Bmatrix} \begin{Bmatrix} c & d & x \\ e & f & q \end{Bmatrix} \begin{Bmatrix} e & f & x \\ b & a & r \end{Bmatrix} = \begin{Bmatrix} p & q & r \\ e & a & d \end{Bmatrix} \begin{Bmatrix} p & q & r \\ f & b & c \end{Bmatrix}. \tag{104}$$

With $p=L$, $q=\lambda$, $r=L'$, $a=L''$, $b=S$, $c=J$ and $d=1$, $e=k$, $f=J'$, $x=J''$, the sum over J'' results in

$$\sum_{J''} (2J''+1)(-1)^{J''+L+\lambda+L'+L''+S+J+1+k+J'} \begin{Bmatrix} J & 1 & J'' \\ k & J' & \lambda \end{Bmatrix} \begin{Bmatrix} L & J & S \\ J'' & L'' & 1 \end{Bmatrix} \begin{Bmatrix} L'' & J'' & S \\ J' & L' & k \end{Bmatrix} = \begin{Bmatrix} L & \lambda & L' \\ k & L'' & 1 \end{Bmatrix} \begin{Bmatrix} L & \lambda & L' \\ J' & S & J \end{Bmatrix}. \tag{105}$$

From the sums over M'' and over J'', the right-hand side of eq. (96) becomes

$$\begin{aligned} &\sum_{\lambda,-\rho-q} (-1)^{J''+\lambda-M+q} (2\lambda+1) \begin{pmatrix} k & 1 & \lambda \\ q & \rho & -q-\rho \end{pmatrix} \begin{pmatrix} J & J' & \lambda \\ -M & M' & q+\rho \end{pmatrix} \\ &\times (-1)^{J-M+S+L''+J+1+J''-M''+S+L'+J''+k} \left[(2J+1)(2J'+1)\right]^{1/2} (-1)^{-J''-L-\lambda-L'-L''-S-J-1-k-J'} \\ &\times \begin{Bmatrix} L & \lambda & L' \\ k & L'' & 1 \end{Bmatrix} \begin{Bmatrix} L & \lambda & L' \\ J' & S & J \end{Bmatrix} \\ &\times \left\langle l^N \tau SL \left\| \hat{\boldsymbol{D}}^{(1)} \right\| l^{N-1}(n'l')\tau'' SL'' \right\rangle \left\langle l^{N-1}(n'l')\tau'' SL'' \left\| \hat{\boldsymbol{D}}^{(k)} \right\| l^N \tau' SL' \right\rangle, \end{aligned} \tag{106}$$

or

$$\begin{aligned} &\sum_{\lambda,-\rho-q} (-1)^{J-2M+2J''-M'+S-L-J'} (2\lambda+1) \begin{pmatrix} k & 1 & \lambda \\ q & \rho & -q-\rho \end{pmatrix} \begin{pmatrix} J & J' & \lambda \\ -M & M' & q+\rho \end{pmatrix} \\ &\times \begin{Bmatrix} L & \lambda & L' \\ k & L'' & 1 \end{Bmatrix} \begin{Bmatrix} L & \lambda & L' \\ J' & S & J \end{Bmatrix} \left[(2J+1)(2J'+1)\right]^{1/2} \\ &\times \left\langle l^N \tau SL \left\| \hat{\boldsymbol{D}}^{(1)} \right\| l^{N-1}(n'l')\tau'' SL'' \right\rangle \left\langle l^{N-1}(n'l')\tau'' SL'' \left\| \hat{\boldsymbol{D}}^{(k)} \right\| l^N \tau' SL' \right\rangle. \end{aligned} \tag{107}$$

From the properties of the second 3-j symbol of eq. (107), one has $(M'-M)=-(\rho+q)$. The terms J'' and M can be either integer or half-integer, but if J'' is an integer (half-integer), M has to be an integer (half-integer) as well. Therefore, $M+J''$ is an integer and $2M+2J''$ is even, which results in $(-1)^{2M+2J''}=1$.

Step 5: The operators $\hat{\boldsymbol{D}}^{(1)}$ and $\hat{\boldsymbol{D}}^{(k)}$ are combined into the operator $\hat{\boldsymbol{T}}^{(\lambda)}$ acting on the states of one configuration (nl). The operator $\hat{\boldsymbol{T}}^{(\lambda)}$ is also called *transition operator*. The amplitude of the tensor $\hat{\boldsymbol{T}}^{(\lambda)}$ is determined by

$$\left\langle L \left\| \hat{\boldsymbol{T}}^{(\lambda)} \right\| L' \right\rangle = \left\langle L \left\| \hat{\boldsymbol{D}}^{(1)} \right\| L'' \right\rangle \left\langle L'' \left\| \hat{\boldsymbol{D}}^{(k)} \right\| L' \right\rangle \qquad \text{[Judd 1962, eq. (8)]}. \tag{108}$$

Equation (107) transforms into

$$\begin{aligned} &\sum_{\lambda,-\rho-q} (-1)^{J-M+\rho+q+S-L-J'} (2\lambda+1) \\ &\quad \times \begin{pmatrix} k & 1 & \lambda \\ q & \rho & -q-\rho \end{pmatrix} \begin{pmatrix} J & J' & \lambda \\ -M & M' & q+\rho \end{pmatrix} \begin{Bmatrix} L & \lambda & L' \\ k & L'' & 1 \end{Bmatrix} \begin{Bmatrix} L & \lambda & L' \\ J' & S & J \end{Bmatrix} \\ &\quad \times \left[(2J+1)(2J'+1)\right]^{1/2} \left\langle l^N \tau SL \left\| \hat{\boldsymbol{T}}^{(\lambda)} \right\| l^N \tau' SL' \right\rangle. \end{aligned} \tag{109}$$

Since

$$\begin{aligned} &\left\langle l^N \tau SLJM \left\| \hat{\boldsymbol{T}}^{(\lambda)}_{q+\rho} \right\| l^N \tau' S'L'J'M' \right\rangle \\ &\quad = (-1)^{J-M} \begin{pmatrix} J & \lambda & J' \\ -M & q+\rho & M' \end{pmatrix} \delta(S,S') (-1)^{S+L'+J+\lambda} \left[(2J+1)(2J'+1)\right]^{1/2} \\ &\qquad \times \begin{Bmatrix} L & J & S \\ J' & L' & \lambda \end{Bmatrix} \left\langle l^N \tau SL \left\| T^{(\lambda)} \right\| l^N \tau' SL' \right\rangle, \end{aligned} \tag{110}$$

and based on the permutation properties of the 3-j and the 6-j symbols, eq. (109) may be rewritten as

$$\begin{aligned} &\sum_{\lambda,-\rho-q} (-1)^{\rho+q-L'-L-J'-J-\lambda} (2\lambda+1) \begin{pmatrix} k & 1 & \lambda \\ q & \rho & -q-\rho \end{pmatrix} \begin{Bmatrix} L & \lambda & L' \\ k & L'' & 1 \end{Bmatrix} \\ &\quad \times (-1)^{J+J'+\lambda} \left\langle l^N \tau SLM \left\| \hat{\boldsymbol{T}}^{(\lambda)}_{q+\rho} \right\| l^N \tau' SL'M' \right\rangle. \end{aligned} \tag{111}$$

After rearrangement and since $(-1)^{q+\rho-L'-L} = (-1)^{q+\rho+L'+L}$ (L and L' are integers):

$$\sum_{\lambda,-q-\rho} (-1)^{q+\rho-L'+L} (2\lambda+1) \begin{pmatrix} k & 1 & \lambda \\ q & \rho & -q-\rho \end{pmatrix} \begin{Bmatrix} L & \lambda & L' \\ k & L'' & 1 \end{Bmatrix} \left\langle l^N \tau SLM \left\| \hat{\boldsymbol{T}}^{(\lambda)}_{q+\rho} \right\| l^N \tau' SL'M' \right\rangle. \tag{112}$$

Finally, by an even permutation of the first 3-j symbol, a compact expression for the summation over J'' is obtained:

$$\begin{aligned} &\sum_{J'',M''} \left\langle l^N \psi JM \left| \hat{\boldsymbol{D}}^{(1)}_{\rho} \right| l^{N-1}(n'l')\psi''J''M'' \right\rangle \left\langle l^{N-1}(n'l')\psi''J''M'' \left| \hat{\boldsymbol{D}}^{(k)}_{q} \right| l^N \psi' J'M' \right\rangle \\ &\quad = \sum_{\lambda} (-1)^{q+\rho+L+L'} (2\lambda+1) \begin{pmatrix} 1 & \lambda & k \\ \rho & -q-\rho & q \end{pmatrix} \begin{Bmatrix} 1 & \lambda & k \\ L' & L'' & L \end{Bmatrix} \left\langle l^N \psi JM \left| \hat{\boldsymbol{T}}^{(\lambda)}_{q+\rho} \right| l^N \psi' J'M' \right\rangle \\ &\qquad \text{[Judd 1962, eq. (7)]}. \end{aligned} \tag{113}$$

5.7.2. *Second approximation: ψ'' and J'' are degenerate*

In the second approximation, each perturbing configuration $l^{N-1}(n'l')$ is considered as being totally degenerate. It is supposed that $E(n'l'\psi''J'')$ is invariant with respect to

ψ'' as well as to J''. The term $E(n'l'\psi''J'')$ is set equal to the mean energy of the configuration. This assumption is only moderately fulfilled and therefore constitutes a weak link in the theory. For instance, the $4f^7 5d^1$ configuration of Tb^{3+} is smeared out over a broad energy range. Dieke (1968) has shown that the mean energetic position of the $4f^{N-1}5d$ configuration of all the trivalent lanthanide ions is above $50\,000\,cm^{-1}$. Absorption spectra of lanthanide complexes are generally restricted to the energy region beneath $40\,000\,cm^{-1}$. The second approximation is applied because it leads to a considerable simplification of the mathematical expression for the electric dipole matrix element.

Starting from eq. (113), one can sum over ψ'' (assuming the configuration as degenerate). The sum over all possible values τ'', L'' and S of the excited configuration is equivalent to summing (1) over all possible values of $\bar{\tau}$, $\bar{L}$ and $\bar{S}$ of the parent term l^{N-1} and (2) over all values L'' and S that are part of the coupling of the l^{N-1} configuration with an $(n'l')$ electron (Racah 1943):

$$\begin{aligned}
&\sum_{\psi''} \left\langle l^N \tau SL \left\| \hat{\boldsymbol{D}}^{(1)} \right\| l^{N-1}(n'l')\tau''SL'' \right\rangle \\
&\quad = \sum_{\substack{\bar{\tau}\bar{S}\bar{L} \\ L''}} \left\langle l^N \tau SL \left\| \hat{\boldsymbol{D}}^{(1)} \right\| l^{N-1}(\bar{\tau}\bar{S}\bar{L})l'SL'' \right\rangle \\
&\quad = \sum_{\substack{\bar{\tau}\bar{S}\bar{L} \\ L''}} \sqrt{n} \left\langle l^N \tau SL \left\{ \left| l^{N-1}\left(\bar{\tau}\bar{S}\bar{L}\right) l SL \right\rangle \left\langle \bar{S}\bar{L}l_i SL \left\| r_i \hat{\boldsymbol{C}}_i^{(1)}(\theta_i, \varphi_i) \right\| \bar{S}\bar{L}l_i' SL'' \right\rangle \right.\right.
\end{aligned} \tag{114}$$

By analogy,

$$\begin{aligned}
&\sum_{\psi''} \left\langle l^{N-1}(n'l')\tau''SL'' \left\| \hat{\boldsymbol{D}}^{(k)} \right\| l^N \tau' SL' \right\rangle \\
&\quad = \sum_{\substack{\bar{\tau}\bar{S}\bar{L} \\ L''}} \left\langle l^{N-1}(\bar{\tau}\bar{S}\bar{L})l'SL'' \left\| \hat{\boldsymbol{D}}^{(k)} \right\| l^N \tau' SL' \right\rangle, \\
&\quad = \sum_{\substack{\bar{\tau}\bar{S}\bar{L} \\ L''}} \sqrt{n} \left\langle l^{N-1}\left(\bar{\tau}\bar{S}\bar{L}\right) l SL' \right\} l^N \tau' SL' \left\rangle \left\langle \bar{S}\bar{L}l_i' SL'' \left\| r_i^k \hat{\boldsymbol{C}}_i^{(k)}(\theta_i, \varphi_i) \right\| \bar{S}\bar{L}l_i SL' \right\rangle .
\end{aligned} \tag{115}$$

The factors $\left\langle l^N \tau SL \left\{ \left| l^{N-1}\left(\bar{\tau}\bar{S}\bar{L}\right) l SL \right\rangle \right.\right.$ and $\left\langle l^{N-1}\left(\bar{\tau}\bar{S}\bar{L}\right) l SL' \right\} l^N \tau SL' \right\rangle$ are the *coefficients of fractional parentage*. These coefficients were introduced by Racah (1943) to facilitate the computation of matrix elements for complicated configurations. Every state $\Psi(\tau SL)$ of the l^N configuration is expanded as a linear combination of product functions $\overline{\Phi}$ of the states $\overline{\Psi}\left(\bar{\tau}\bar{S}\bar{L}\right)$ of the l^{N-1} configuration and of the states of the Nth electron:

$$\Psi\left(l^N \tau SL\right) = \sum_{\bar{\tau}\bar{S}\bar{L}} \left\langle l^{N-1}\bar{\tau}\bar{S}\bar{L} \right\} l^N \tau SL \left\rangle \overline{\Phi}\left(l^{N-1}\left(\bar{\tau}\bar{S}\bar{L}\right); l\right). \right. \tag{116}$$

The brace in the *coefficient of fractional parentage* always points to the configuration with the greatest number of electrons. The summation runs over all possible states $\overline{\Psi}\left(\bar{\tau}\bar{S}\bar{L}\right)$

of the l^{N-1} configuration. These states are the so-called *parents* of the state $\Psi(\tau SL)$ of the l^N configuration. Detailed information on the coefficients of fractional parentage has been given by Judd (1963), and coefficients for all states of the f^N configurations with $N \leqslant 7$ have been tabulated by Nielson and Koster (1964). With each state of the configuration l^N a state of the l^{4l+2-N} configuration is associated. The two states have the same quantum numbers. In order to obtain the coefficients of a configuration l^N with $N > 7$, we can use the equation which relates the coefficients of fractional parentage of the configurations l^N and l^{4l+2-N} (Racah 1943):

$$\begin{aligned}&\left(l^{4l+2-N}\tau SL\right\}\left\}l^{4l+2-N}\bar{\tau}\bar{S}\bar{L}\right)\\&\quad=(-1)^{S+\bar{S}+L+\bar{L}-l-s+1/2(\upsilon+\bar{\upsilon}+1)}\left[\frac{(N+1)(2S+1)(2L+1)}{(4l+2-N)(2\bar{S}+1)(2\bar{L}+1)}\right]^{1/2}\left(l^{N+1}\bar{\tau}\bar{S}\bar{L}\right\}\left\}l^N\tau SL\right),\end{aligned} \tag{117}$$

where υ is the *seniority number*. This extra quantum number has been introduced by Racah for the construction of states from the *shell*-concept. The *seniority number* for a particular state has the value N of the l^N configuration in which this state occurs for the first time. For instance, the ^{7}F state of Tb^{3+} ($4f^8$) occurs for the first time in the $4f^6$ configuration and thus $\upsilon = 6$.

Using the formula

$$\begin{aligned}&\left\langle\gamma' j_1' j_2' J'\left\|\hat{\boldsymbol{T}}^{(k)}\right\|\gamma j_1 j_2 J\right\rangle\\&\quad=\delta\left(j_1, j_1'\right)(-1)^{j_1+j_2+J'+k}\sqrt{(2J+1)(2J'+1)}\begin{Bmatrix} j_2' & J' & j_1\\ J & j_2 & k\end{Bmatrix}\left\langle\gamma' j_2'\left\|\hat{\boldsymbol{T}}^{(k)}\right\|\gamma j_2\right\rangle,\end{aligned} \tag{118}$$

with

$$\gamma' = l^N\tau', \quad \gamma = l^N\tau, \qquad j_1' = \bar{L}, \quad j_1 = \bar{L}, \qquad j_2' = l, \quad j_2 = l',$$
$$J' = L, \quad J = L'', \qquad k = 1,$$

we find for eq. (114)

$$\begin{aligned}&\left\langle\bar{S}\bar{L}l_i SL\left\|r_i\hat{\boldsymbol{C}}_i^{(1)}\right\|\bar{S}\bar{L}l_i' SL''\right\rangle\\&=\langle nl\,|r_i|\,n'l'\rangle\left\langle\bar{S}\bar{L}l_i SL\left\|\hat{\boldsymbol{C}}_i^{(1)}\right\|\bar{S}\bar{L}l_i' SL''\right\rangle,\\&\quad=\langle nl\,|r_i|\,n'l'\rangle(-1)^{\bar{L}+l'+L+1}\left[(2L+1)(2L''+1)\right]^{1/2}\begin{Bmatrix} L & 1 & L''\\ l' & \bar{L} & l\end{Bmatrix}\left\langle l\left\|\hat{\boldsymbol{C}}_i^{(1)}\right\|l'\right\rangle,\end{aligned} \tag{119}$$

and with

$$\gamma' = l^N\tau', \quad \gamma = l^N\tau, \qquad j_1' = \bar{L}, \quad j_1 = \bar{L}, \qquad j_2' = l, \quad j_2 = l,$$
$$J' = L'', \quad J = L', \qquad k = k,$$

we find for eq. (115)

$$\begin{aligned}
&\left\langle \overline{S}\,\overline{L} l_i' S L'' \left\| r_i^k \hat{\boldsymbol{C}}_i^{(k)} \right\| \overline{S}\,\overline{L} l_i S L' \right\rangle \\
&\quad = \left\langle nl \left| r_i^k \right| n'l' \right\rangle \left\langle \overline{S}\,\overline{L} l_i' S L'' \left\| \hat{\boldsymbol{C}}_i^{(k)} \right\| \overline{S}\,\overline{L} l_i S L' \right\rangle, \qquad (120) \\
&= \left\langle nl \left| r_i^k \right| n'l' \right\rangle (-1)^{\overline{L}+l+L''+k} \left[(2L'+1)(2L''+1) \right]^{1/2} \begin{Bmatrix} L'' & k & L' \\ l & \overline{L} & l' \end{Bmatrix} \left\langle l' \left\| \hat{\boldsymbol{C}}_i^{(k)} \right\| l \right\rangle.
\end{aligned}$$

From the Biedenharn–Elliot sum rule and the properties of the 6-j symbols, eq. (113) becomes

$$\begin{aligned}
&\sum_{J'',M'',\psi''} \left\langle l^N \psi J M \left| \hat{\boldsymbol{D}}_\rho^{(1)} \right| l^{N-1}(n'l')\psi'' J'' M'' \right\rangle \left\langle l^{N-1}(n'l')\psi'' J'' M'' \left| \hat{\boldsymbol{D}}_q^{(k)} \right| l^N \psi' J' M' \right\rangle \\
&= \sum_{\bar{\tau},\bar{S},\bar{L}} \sum_{\lambda} (-1)^{\rho+q+L-S-M+\bar{L}+l-L'} (2\lambda+1) \left[(2J+1)(2J'+1)(2L+1)(2L'+1) \right]^{1/2} \\
&\quad \times \begin{pmatrix} k & 1 & \lambda \\ q & \rho & -q-\rho \end{pmatrix} \begin{pmatrix} J & \lambda & J' \\ -M & q+\rho & M' \end{pmatrix} \begin{Bmatrix} \lambda & L' & L \\ S & J & J' \end{Bmatrix} \begin{Bmatrix} \lambda & l & l \\ \overline{L} & L & L' \end{Bmatrix} \begin{Bmatrix} \lambda & l & l \\ l' & 1 & k \end{Bmatrix} \\
&\quad \times \left\langle nl \left| \hat{r} \right| n'l' \right\rangle \left\langle n'l' \left| \hat{\boldsymbol{r}}^k \right| nl \right\rangle \left\langle l \left\| \hat{\boldsymbol{C}}^{(1)} \right\| l' \right\rangle \left\langle l' \left\| \hat{\boldsymbol{C}}^{(k)} \right\| l \right\rangle \\
&\quad \times n \left\langle l^{N-1} \left(\bar{\tau}\,\overline{S}\,\overline{L} \right) l S L \right| \Big\} l^N \tau S L \Big\rangle \left\langle l^{N-1} \left(\bar{\tau}\,\overline{S}\,\overline{L} \right) l L' S \right| \Big\} l^N \tau' L' S \Big\rangle.
\end{aligned} \qquad (121)$$

From the Wigner–Eckart theorem and eq. (118), using eq. (21.2-9) of Weissbluth (1978) one finds

$$\begin{aligned}
&\left\langle l^N \psi J M \left| \hat{\boldsymbol{U}}_{q+\rho}^{(\lambda)} \right| l^N \psi' J' M' \right\rangle \\
&\quad = (-1)^{J-M+L'+S+J+\lambda} \delta(S,S') \left[(2J+1)(2J'+1) \right]^{1/2} \begin{pmatrix} J & \lambda & J' \\ -M & q+\rho & M' \end{pmatrix} \begin{pmatrix} J & \lambda & J' \\ L' & S & L \end{pmatrix} \\
&\quad \times n \sum_{\bar{\tau},\bar{S},\bar{L}} \left\langle l^{N-1} \left(\bar{\tau}\,\overline{S}\,\overline{L} \right) l S L \right| \Big\} l^N \tau S L \Big\rangle \left\langle l^{N-1} \left(\bar{\tau}\,\overline{S}\,\overline{L} \right) l L' S \right| \Big\} l^N \tau' L' S \Big\rangle \qquad (122) \\
&\quad \times (-1)^{\overline{L}+l+L+\lambda} \left[(2L+1)(2L'+1) \right]^{1/2} \begin{Bmatrix} L & \lambda & L' \\ l & \overline{L} & l \end{Bmatrix}.
\end{aligned}$$

Finally, from eq. (121) and eq. (122):

$$\begin{aligned}
&\sum_{J'',M'',\psi''} \left\langle l^N \psi J M \left| \hat{\boldsymbol{D}}_\rho^{(1)} \right| l^{N-1}(n'l')\psi'' J'' M'' \right\rangle \left\langle l^{N-1}(n'l')\psi'' J'' M'' \left| \hat{\boldsymbol{D}}_q^{(k)} \right| l^N \psi' J' M' \right\rangle \\
&\quad = \sum_{\lambda} (-1)^{q+\rho} (2\lambda+1) \begin{pmatrix} 1 & \lambda & k \\ \rho & -q-\rho & q \end{pmatrix} \begin{Bmatrix} 1 & \lambda & k \\ l & l' & l \end{Bmatrix} \qquad (123) \\
&\quad \times \left\langle nl \left| \hat{r} \right| n'l' \right\rangle \left\langle nl \left| \hat{\boldsymbol{r}}^k \right| n'l' \right\rangle \left\langle l \left\| \hat{\boldsymbol{C}}^{(1)} \right\| l' \right\rangle \left\langle l' \left\| \hat{\boldsymbol{C}}^{(k)} \right\| l \right\rangle \left\langle l^N \psi J M \left| \hat{\boldsymbol{U}}_{q+\rho}^{(\lambda)} \right| l^N \psi' J' M' \right\rangle \\
&\quad \text{[dim: } \mathrm{L}^{k+1}, \quad \text{Judd 1962, eq. (9)]}.
\end{aligned}$$

The sum over $-q-\rho$ has been omitted, because of the condition $-M+q+\rho+M'=0$ from the 3-j symbol in eq. (123). The radial integrals are defined as

$$\left\langle nl \left| \hat{r} \right| n'l' \right\rangle = \int_0^\infty R(nl) r\, R(n'l') r^2 \mathrm{d}r \qquad \text{[dim: L]}, \qquad (124)$$

$$\langle nl\,|\hat{\boldsymbol{r}}^k|\,n'l'\rangle = \int_0^\infty R(nl)r^k\,R(n'l')r^2\mathrm{d}r \qquad [\dim:\ \mathrm{L}^k], \tag{125}$$

where $R(nl)$ is a radial function with dimension $\mathrm{L}^{-3/2}$.

The unitary operator $\hat{\boldsymbol{U}}^{(\lambda)}$ is the sum over all the electrons of the single-electron tensor operators $\hat{\boldsymbol{u}}^{(\lambda)}$ for which $\langle nl\,|\hat{\boldsymbol{u}}^{(\lambda)}|\,n'l'\rangle = \delta_{nn'}\delta_{ll'}$.

The reduced matrix elements in eq. (123) can be calculated exactly:

$$\langle l\,\|\hat{\boldsymbol{C}}^{(1)}\|\,l'\rangle = (-1)^{l'}\left[(2l+1)(2l'+1)\right]^{1/2}\begin{pmatrix} l & 1 & l' \\ 0 & 0 & 0\end{pmatrix}, \tag{126}$$

$$\langle l'\,\|\hat{\boldsymbol{C}}^{(k)}\|\,l\rangle = (-1)^{l}\left[(2l+1)(2l'+1)\right]^{1/2}\begin{pmatrix} l' & k & l \\ 0 & 0 & 0\end{pmatrix}. \tag{127}$$

5.7.3. *Third approximation: n', l', ψ'' and J'' are degenerate*

If $E(n'l'\psi''J'')$ is assumed invariant with respect to n' as well as to ψ'' and J'', and if the full description of the ground configuration (i.e. also taking the closed shell into account) contains no electrons with azimuthal quantum number l', then the fact that the radial functions $R(n'l')$ for all n' form a complete set allows us to write (*closure procedure*)

$$\sum_{n'}\langle nl\,|\hat{\boldsymbol{r}}|\,n'l'\rangle\,\langle nl\,|\hat{\boldsymbol{r}}^k|\,n'l'\rangle = \langle nl\,|\hat{\boldsymbol{r}}^{k+1}|\,nl\rangle \qquad [\dim:\ \mathrm{L}^{k+1}]. \tag{128}$$

It is no longer necessary to calculate radial integrals between different configurations, because it is assumed that these configurations are degenerate. Since the 3d and 4d shells of the lanthanide ions are filled, the third approximation cannot be applied to the configuration $4f^{N-1}5d^1$ ($l' = 2$). The approximation can be applied to $4f^{N-1}5g^1$ ($l' = 4$), since no g orbitals are occupied in the ground configuration. The influence of g orbitals on the intensity was considered as dominant by several authors (Judd 1962, Axe 1963, Krupke 1966). Jankowski and Smentek-Mielczarek (1981) have demonstrated that contributions from g orbitals are very significant for the description of electron correlation effects of induced electric dipole transitions (see also sect. 7.5). Becker et al. (1985) have shown that linear combinations of the s and p orbitals on the neighboring ligands can transform like components of a g-electron wave function under the symmetry operations of the point group corresponding to the site symmetry of the lanthanide ion. Burdick et al. (1989) have pointed out the importance of g orbitals on the basis of Raman experiments.

5.7.4. *Fourth approximation: $l^{N-1}(n'l')$ far above l^N*

Until now, only one term of the right-hand side of eq. (88) has been worked out. The second term can be calculated analogously. Because of the relation

$$\begin{pmatrix} 1 & \lambda & k \\ \rho & -q-\rho & q\end{pmatrix} = (-1)^{1+\lambda+k}\begin{pmatrix} k & \lambda & 1 \\ q & -q-\rho & \rho\end{pmatrix}, \tag{129}$$

both terms will cancel to a large extent if $1+\lambda+k$ is odd. Since only the odd terms in the expansion of the crystal-field potential are responsible for the mixing which induces

electric dipole intensity, k is odd. The terms will thus vanish to a large extent if λ is odd. Total cancelling is observed if the energy denominators $[E(\psi J) - E(n'l'\psi''J'')]$ and $[E(\psi'J') - E(n'l'\psi''J'')]$, which are supposed to be independent of ψ'' and J'', could be assumed equal (eq. 12 of Judd 1962). This is equivalent to the assumption that the perturbing configurations lie far above the states involved in the optical transitions within the 4f shell. The energy denominators are replaced by the single energy difference $\Delta(n'l')$. This approximation is called the *average energy denominator method* (Bebb and Gold 1966, Malta et al. 1991) and is acceptable for the majority of the lanthanide ions. Consider for instance Eu^{3+}. The highest levels of the $4f^6$ configuration which have been observed in the absorption spectra are at ~40 000 cm^{-1} [$E(\psi J) = 0\ cm^{-1}$ and $E(\psi'J') = 40\,000\ cm^{-1}$). According to Dieke (1968), the mean energy $E(n'l'\psi''J'')$ of the perturbing configuration is at ~125 000 cm^{-1}, so that

$$\frac{|E(\psi J) - E(n'l'\psi''J'')| + |E(\psi'J') - E(n'l'\psi''J'')|}{|E(\psi J) - E(n'l'\psi''J'')| + |E(\psi'J') - E(n'l'\psi''J'')|} = \frac{210\,000}{40\,000} = 5.25. \tag{130}$$

For Pr^{3+}, $E(\psi J)$ is at ~60 000 cm^{-1}, whereas $E(\psi'J')$ is at most ~25 000 cm^{-1}. The ratio is now only 3.8. If the ratio is small, a non-negligible contribution will come from terms with λ = odd (see also sect. 6.2.5).

5.8. *Judd's final expression for the matrix in the transition operator*

The four approximations in the Judd–Ofelt theory can be summarized as:

(1) $E(n'l'\psi''J'')$ is invariant with respect to J'' and M'';
(2) $E(n'l'\psi''J'')$ is invariant with respect to ψ'' and J'';
(3) $E(n'l'\psi''J'')$ is invariant with respect to n', l', ψ'' and J'';
(4) $l^{N-1}(n'l')$ lies far above l^N.

By taking these four approximations into account, eq. (88),

$$\begin{aligned}
&\langle B | \hat{\boldsymbol{D}}_p^{(1)} | B' \rangle \\
&= \sum_K \sum_M \sum_{M'} \sum_{k,q} a_M a'_{M'} A_{kq} \frac{\langle l^N \psi J M | \hat{\boldsymbol{D}}_p^{(1)} | l^N \psi' J' M' \rangle \langle l^{N-1}(n'l')\psi'' J'' M'' | \hat{\boldsymbol{D}}_p^{(k)} | l^N \psi' J' M' \rangle}{(E(\psi'J') - E(n'l'\psi''J''))} \\
&\quad + \sum_K \sum_M \sum_{M'} \sum_{k,q} a_M a'_{M'} A_{kq} \frac{\langle l^N \psi J M | \hat{\boldsymbol{D}}_q^{(k)} | l^{N-1}(n'l')\psi'' J'' M'' \rangle \langle l^{N-1}(n'l')\psi'' J'' M'' | \hat{\boldsymbol{D}}_q^{(1)} | l^N \psi' J' M' \rangle}{(E(\psi J) - E(n'l'\psi''J''))}
\end{aligned}$$

[Judd 1962, eq. (6)],

with

$$\langle B| = \sum_M \langle l^N \psi J M | a_M + \sum_K \langle l^{N-1}(n'l')\psi'' J'' M'' | b(n'l'\psi''J''M''), \tag{131}$$

and

$$|B'\rangle = \sum_{M'} a'_{M'} |l^N \psi' J' M'\rangle + \sum_K b'(n'l'\psi''J''M'') |l^{N-1}\psi''J''M''\rangle, \tag{132}$$

can be written as

$$\left\langle B \left| \hat{\boldsymbol{D}}_{\rho}^{(1)} \right| B' \right\rangle = \sum_{k,q} \sum_{\lambda=\text{even}} (2\lambda+1)(-1)^{q+\rho} A_{kq} \begin{pmatrix} 1 & \lambda & k \\ \rho & -q-\rho & q \end{pmatrix} \left\langle A \left| \hat{\boldsymbol{U}}_{q+\rho}^{(\lambda)} \right| A' \right\rangle \Xi(k,\lambda),$$

[dim: L; Judd 1962, eq. (13)], (133)

where A_{kq} is a crystal-field coefficient with dimension *energy* L^{-k}, and

$$\Xi(k,\lambda) = 2\sum_{n'l'} (2l+1)(2l'+1)(-1)^{l+l'} \begin{Bmatrix} 1 & \lambda & k \\ l & l' & l \end{Bmatrix} \begin{pmatrix} l & 1 & l' \\ 0 & 0 & 0 \end{pmatrix} \begin{pmatrix} l' & k & l \\ 0 & 0 & 0 \end{pmatrix} \times \frac{\langle nl \,|\hat{\boldsymbol{r}}|\, n'l' \rangle \langle nl \,|\hat{\boldsymbol{r}}^k|\, n'l' \rangle}{\Delta(n'l')},$$

[dim: L^{k+1} $(energy)^{-1}$; Judd 1962, eq. (14)]. (134)

The summation in eq. (134) runs over all values of n' and l' consistent with $l^{N-1}(n'l')$ being an excited configuration. The matrix element $\left\langle A \left| \hat{\boldsymbol{U}}_{q+\rho}^{(\lambda)} \right| A' \right\rangle$ can be calculated by standard tensor operator techniques (Weissbluth 1978), remembering (eqs. 79 and 80)

$$\langle A| \equiv \sum_{M} \langle l^N \psi J M|\, a_M, \tag{135}$$

$$|A'\rangle \equiv \sum_{M'} a'_{M'} \left| l^N \psi' J' M' \right\rangle. \tag{136}$$

5.9. *Calculation of the reduced matrix elements*

The matrix element in eq. (133) can be expressed as a sum over reduced matrix elements involving Russell–Saunders coupled states:

$$\left\langle A \left| \hat{\boldsymbol{U}}_{q+\rho}^{(\lambda)} \right| A' \right\rangle = \sum_{M,M'} a_M a'_{M'} \left\langle l^N \psi J M \left| \hat{\boldsymbol{U}}_{q+\rho}^{(\lambda)} \right| l^N \psi' J' M' \right\rangle. \tag{137}$$

Application of the Wigner–Eckart theorem results in

$$\sum_{M,M'} a_M a'_{M'} \left\langle l^N \psi J M \left| \hat{\boldsymbol{U}}_{q+\rho}^{(\lambda)} \right| l^N \psi' J' M' \right\rangle = \sum_{M,M'} a_M a'_{M'} (-1)^{J-M} \begin{pmatrix} J & \lambda & J' \\ -M & q+\rho & M' \end{pmatrix} \left\langle l^N \psi J \left\| U^{(\lambda)} \right\| l^N \psi' J' \right\rangle. \tag{138}$$

It is possible to carry out expansions of the type

$$\left\langle l^N \psi J \right| = \sum_{\tau,S,L} h(\tau S L) \left\langle l^N \tau S L J \right|, \tag{139}$$

where $h(\tau SL)$ are the expansion coefficients of the states coupled in a Russell–Saunders coupling scheme. The right-hand side of eq. (138) can be rewritten as

$$\sum_{M,M'} a_M a'_{M'} \sum_{\tau,S,L} \sum_{\tau',S',L'} h(\tau SL) h'(\tau' S' L') (-1)^{J-M} \begin{pmatrix} J & \lambda & J' \\ -M & q+\rho & M' \end{pmatrix} \langle l^N \psi J \| U^{(\lambda)} \| l^N \psi' J' \rangle . \quad (140)$$

$U^{(\lambda)}$ is working only on L. On the basis of the following property for the reduced matrix element of a tensor $\hat{\boldsymbol{T}}^{(k)}$ which only works on part 2 in the coupled scheme (not on the spin functions) (Edmonds 1974):

$$\begin{aligned} \langle \gamma' j'_1 j'_2 J' \| \hat{\boldsymbol{T}}^{(k)} \| \gamma j_1 j_2 J \rangle &= \delta(j'_1, j_1) (-1)^{j_1+j_2+J'+k} \left[(2J+1)(2J'+1)\right]^{1/2} \\ &\times \begin{Bmatrix} j'_2 & J' & j_1 \\ J & j_2 & k \end{Bmatrix} \langle \gamma' j'_2 \| \hat{\boldsymbol{T}}^{(k)} \| \gamma j_2 \rangle , \end{aligned} \quad (141)$$

with

$$\gamma' = l^N \tau, \quad \gamma = l^N \tau, \quad j'_1 = S, j_1 = S', \quad j'_2 = L, j_2 = L', \quad J' = J, J = J', \quad k = \lambda,$$

and since $\begin{Bmatrix} L & J & S \\ J' & L' & \lambda \end{Bmatrix} = \begin{Bmatrix} L & \lambda & L' \\ J' & S & J \end{Bmatrix}$, one obtains for the reduced matrix element

$$\begin{aligned} \left\langle l^N \tau SLJ \left\| U^{(\lambda)} \right\| l^N \tau' SL' J' \right\rangle &= (-1)^{S+L'+J+\lambda} \left[(2J+1)(2J'+1)\right]^{1/2} \\ &\times \begin{Bmatrix} L & \lambda & L' \\ J' & S & J \end{Bmatrix} \left\langle l^N \tau SL \left\| U^{(\lambda)} \right\| l^N \tau' SL' \right\rangle . \end{aligned} \quad (142)$$

The doubly reduced matrix elements $\langle l^N \tau SL \| U^{(\lambda)} \| l^N \tau' SL' \rangle$ have been tabulated by Nielson and Koster (1964).

5.10. *Matrix element of the electric dipole operator of a single line in an oriented system*

Finally, the induced electric dipole matrix element between two states B and B' of the f^N configuration can be written as

$$\begin{aligned} &\langle B | \hat{\boldsymbol{m}}_\rho^{(1)} | B' \rangle \\ &= \langle B | -e\hat{\boldsymbol{D}}_\rho^{(1)} | B' \rangle \\ &= -e \sum_M \sum_{M'} a_M a'_{M'} \sum_{\tau,S,L} \sum_{\tau',S',L'} h(\tau SL) h'(\tau' S' L') \\ &\quad \times \sum_{k,q} \sum_{\lambda=\text{even}} A_{kq} \Xi(k,\lambda) (-1)^{(q+\rho)+(J-M)+(S+L'+J+\lambda)} \\ &\qquad \times \begin{pmatrix} 1 & \lambda & k \\ \rho & -q-\rho & q \end{pmatrix} \begin{pmatrix} J & \lambda & J' \\ -M & q+\rho & M' \end{pmatrix} \begin{Bmatrix} L & \lambda & L' \\ J' & S & J \end{Bmatrix} \\ &\qquad \times (2\lambda+1) \left[(2J+1)(2J'+1)\right]^{1/2} \left\langle l^N \tau SL \left\| \hat{\boldsymbol{U}}^{(\lambda)} \right\| l^N \tau' SL' \right\rangle \qquad [\text{dim: } e\text{L}], \end{aligned} \quad (143)$$

where (see eq. 134)

$$\Xi(k,\lambda) = 2\sum_{n'l'}(2l+1)(2l'+1)(-1)^{l+l'}\begin{Bmatrix}1 & \lambda & k\\ l & l' & l\end{Bmatrix}\begin{pmatrix}l & 1 & l'\\ 0 & 0 & 0\end{pmatrix}\begin{pmatrix}l' & k & l\\ 0 & 0 & 0\end{pmatrix} \times \frac{\langle nl\,|\hat{\mathbf{r}}|\,n'l'\rangle\langle nl\,|\hat{\mathbf{r}}^k|\,n'l'\rangle}{\Delta(n'l')},$$

[dim: $L^{k+1}\,(energy)^{-1}$]. (144)

5.11. *Dipole strength of an induced electric dipole transition (single line and oriented system)*

The dipole strength D' of a single spectral line in an oriented molecule is obtained by taking the absolute square of the matrix element in eq. (143):

$$D' = \left|\left\langle B\left|\hat{\boldsymbol{m}}_\rho^{(1)}\right|B'\right\rangle\right|^2 = \left\langle B\left|\hat{\boldsymbol{m}}_\rho^{(1)}\right|B'\right\rangle^*\left\langle B\left|\hat{\boldsymbol{m}}_\rho^{(1)}\right|B'\right\rangle \quad [\text{dim: } e^2\,\mathrm{L}^2, \text{ units: esu}^2\,\mathrm{cm}^2]. \tag{145}$$

The experimental dipole strength D'_{exp} can be related to D' by (see also sect. 3.6)

$$D'_{\mathrm{exp}} = \frac{\chi}{g_A}D', \tag{146}$$

where χ is defined in sect. 3.5.

5.12. *Oscillator strength of an induced electric dipole transition (single line and oriented system)*

The calculated oscillator strength P_{ED} of a single spectral line in an oriented system is given by

$$P' = \frac{8\pi^2 m_e c}{he^2}\bar{\nu}_0 D' \qquad [\text{dim: /; Judd 1962, eq. (1)}], \tag{147}$$

or

$$P' = 4.702\times10^{-7}\times3\times10^{36}\times\bar{\nu}_0\times D' \qquad [D' \text{ in esu}^2\,\mathrm{cm}^2]. \tag{148}$$

Note that Judd (1962) used the frequency ν_0 (in s^{-1}) instead of the wavenumber $\bar{\nu}_0$ (in cm^{-1}). Moreover, he did not include e^2 in his definition of D'. Therefore, we find in eq. (147) a factor c in the numerator and a factor e^2 in the denominator.

The experimental oscillator strength P'_{exp} can be related to P' by

$$P'_{\mathrm{exp}} = \frac{\chi}{g_A}P', \tag{149}$$

where χ is defined in sect. 3.5.

5.13. *Selection rules for induced electric dipole transitions*

From eq. (143) selection rules for induced electric dipole transitions can be derived:

(1) λ = even. This follows directly from the fourth approximation.

(2) k = odd. Mixing of a configuration of opposite parity into the $4f^N$ configuration is only possible by odd terms in the crystal-field potential of the point group in question. The odd terms are non-zero if the lanthanide ion is not at a center of symmetry.

(3) $\lambda = 0, 2, 4, 6$. According to the triangle condition for the triad indicated in bold face, $\begin{Bmatrix} 1 & \boldsymbol{\lambda} & \boldsymbol{k} \\ \boldsymbol{3} & l' & \boldsymbol{3} \end{Bmatrix}$, one has $0 \leqslant \lambda \leqslant 6$. The selection rule follows directly from the fact that λ is even (selection rule 1).

(4) $k = 1, 3, 5, 7$. According to the triangle condition for the triad indicated in bold face, $\begin{Bmatrix} \boldsymbol{1} & \boldsymbol{l} & \boldsymbol{k} \\ 3 & l' & 3 \end{Bmatrix}$, one has $|\lambda - 1| \leq k \leq |\lambda + 1|$. Since k is odd and λ is even, it follows that $k = |\lambda \pm 1|$.

(5) $\Delta l = \pm 1$. From the 6-j symbol $\begin{Bmatrix} \boldsymbol{1} & \lambda & k \\ 3 & \boldsymbol{l'} & \boldsymbol{3} \end{Bmatrix}$ or the 3-j symbol $\begin{pmatrix} \boldsymbol{3} & \boldsymbol{1} & \boldsymbol{l'} \\ 0 & 0 & 0 \end{pmatrix}$ in eq. (143), one has $2 \leq l' \leq 4$. Moreover, l' has to be different from l, so that the parity of the configuration $l^{N-1}(n'l')$ is opposite to the parity of the configuration l^N. The perturbing configurations are thus of the type $4f^{N-1}n'd^1$ and $4f^{N-1}n'g^1$. There is an additional constraint on l' if $k = 7$: $\begin{Bmatrix} 1 & \lambda & \boldsymbol{7} \\ \boldsymbol{3} & \boldsymbol{l'} & 3 \end{Bmatrix}$. In this case, $l' = 4$ and the perturbing configuration has to be $4f^{N-1}n'g^1$.

(6) $\Delta S = 0$. Neither the crystal-field Hamiltonian, nor the electric dipole operator acts on the spin part of the wavefunction.

(7) $|\Delta J| \leq \lambda \leq J + J'$. This follows directly from the indicated condition $\begin{Bmatrix} L & \boldsymbol{\lambda} & \boldsymbol{L'} \\ \boldsymbol{J'} & S & \boldsymbol{J} \end{Bmatrix}$. Moreover, if either J or J' is equal to zero, the selection rule simplifies to $|\Delta J| = 2, 4, 6$ (with $J = 0 \rightarrow J' = 0$ forbidden). Since λ is even, transitions with ΔJ = odd are forbidden in principle. An example is the $^5D_3 \leftarrow {}^7F_0$ transition for Eu^{3+}. The $^5D_1 \leftarrow {}^7F_0$ transition is observed for Eu^{3+}, because it is a magnetic dipole transition. In general, $|\Delta J| \leq 6$.

(8) $|\Delta L| \leq \lambda \leq L + L'$. This can be found from the condition $\begin{Bmatrix} \boldsymbol{L} & \boldsymbol{\lambda} & \boldsymbol{L'} \\ J' & S & J \end{Bmatrix}$. Since λ is smaller than or equal to 6, the selection rule can be rewritten as $|\Delta L| \leq 6$.

(9) $\Delta M = M' - M = -(q + \rho)$. The selection rule on M is derived from the 3-j symbol $\begin{pmatrix} J & \lambda & J' \\ \boldsymbol{-M} & \boldsymbol{q+\rho} & \boldsymbol{M'} \end{pmatrix}$ in eq. (143). For π-polarized spectra ($\rho = 0$), $\Delta M = -q$, while for α- and σ-polarized spectra ($\rho = \pm 1$) one has $\Delta M = -q \pm 1$.

Just as for magnetic dipole transitions, the selection rules are only valid in strict conditions and can be relaxed under certain circumstances. The selection rules on ΔL and ΔS are only applicable in the Russell–Saunders coupling scheme. These selection rules are relaxed in the intermediate coupling scheme, because in this scheme L and S are not good quantum numbers. Since J remains a good quantum number in the intermediate coupling scheme, the selection rule on ΔJ is harder to break down; it can be relaxed

Table 2
Selection rules for magnetic dipole and induced electric dipole transitions

Magnetic dipole transitions (MD)	*Induced electric dipole transitions (ED)*
$\Delta\tau = \Delta S = \Delta L = 0$;	$\Delta l = \pm 1$; $\Delta\tau = 0$; $\Delta S = 0$; $\lvert\Delta L\rvert \leq 6$;
$\Delta J = 0, \pm 1$, but $0 \leftrightarrow 0$ is forbidden;	$\lvert\Delta J\rvert \leq 6$, $\lvert\Delta J\rvert = 2, 4, 6$ if $J = 0$ or $J' = 0$;
$M' - M = -\rho$, where $\rho = \pm 1$.	$M' - M = -(q + \rho)$.

only by J-mixing, which is a weak effect. The selection rule on ΔM depends on the point group symmetry of the rare-earth site. The selection rules for both magnetic dipole and electric dipole transitions are summarized in table 2.

A well-known example of the breakdown of the selection rules of the Judd–Ofelt theory is the occurrence of the $^5D_0 \leftarrow {}^7F_0$ and $^5D_0 \rightarrow {}^7F_0$ transitions in some Eu^{3+} compounds. For instance, Blasse and coworkers found that the $^5D_0 \rightarrow {}^7F_0$ transition in Sr_2TiO_4:Eu^{3+} is 1.65 times more intense than the magnetic dipole transition $^5D_0 \rightarrow {}^7F_1$ (Nieuwpoort and Blasse 1966, Blasse and Bril 1966). The $^5D_0 \leftrightarrow {}^7F_0$ transitions are forbidden by the selection rule on ΔJ ($0 \leftrightarrow 0$ is forbidden). Several mechanisms have been proposed to account for the occurrence of the $^5D_0 \rightarrow {}^7F_0$ transition. The problem was also discussed by Peacock (1975). The breakdown of the *closure approximation* in the Judd–Ofelt theory can be an explanation for this exceptional behavior (Tanaka et al. 1994). Blasse and Bril (1966) noticed that the $^5D_0 \rightarrow {}^7F_0$ transition has only a high intensity if the crystal-field potential of the symmetry of the Eu^{3+} site contains A_{1q} terms, i.e., if the site symmetry is C_{nv}, C_n and C_s. Blasse and Bril (1966) suggest the introduction of an additional parameter Ω_0. However, Wybourne (1967) has shown that the (second-order) matrix element $U^{(0)}$ is zero, so that no intensity can come from this mechanism. Wybourne proposed a mechanism in which the spin-selection rule is relaxed by scalar third-order contributions involving spin–orbit interactions acting within the higher-lying perturbing states. The model was further developed by Downer and coworkers (Downer et al. 1988, Burdick et al. 1989, Burdick and Downer 1991). The $^5D_0 \rightarrow {}^7F_0$ transition can be caused by a linear term ($k = 1$) in the crystal-field potential. Another mechanism is J-mixing. Here, mixing of the $4f^6$ states into $^7F_0$ and $^5D_0$ is due to the even part of the crystal-field potential. In this way, the $^5D_0 \rightarrow {}^7F_0$ transition can borrow intensity from the $^5D_0 \rightarrow {}^7F_J$ ($J = 2, 4, 6$) and from the $^5D_J \leftarrow {}^7F_0$ ($J = 2, 4$) transitions (Wybourne 1967, Porcher and Caro 1980, Malta 1981, Nishimura and Kushida 1988, 1991, Nishimura et al. 1991, Tanaka et al. 1994). Tanaka et al. (1994) have investigated the $^5D_0 \rightarrow {}^7F_0$ transition in Eu^{3+}-doped sodium silicate and germanate glasses, in Eu^{3+}-doped polyvinyl alcohol film, and in Y_2O_2S:Eu^{3+} crystalline powder. They have shown that the transition in the Eu^{3+}-doped glasses is caused by the admixture of the $M = 0$ component of the $^7F_2$ manifold into the $^7F_0$ ground state through the second-order term ($k = 2$) of the crystal-field potential (J-mixing). In Eu^{3+}-doped polyvinyl alcohol film and in Y_2O_2S:Eu^{3+} the breakdown of the *closure approximation* in the Judd–Ofelt theory or the mechanisms proposed by Wybourne and by Downer and coworkers are considered to be the dominant mechanisms.

6. Intensity parametrization of transitions between crystal-field levels

6.1. *Static-coupling model for line transitions*

The matrix element in eq. (143) is valid for transitions between two crystal-field levels. Because of the radial integrals, the calculation of the matrix element is very tedious and can in fact only be done if some approximations are made. Axe (1963) treated the quantities $A_{kq}\Xi(k,\lambda)$ in eq. (143) as adjustable parameters. In this expression, λ is equal to 2, 4 or 6, and k is restricted to values of $\lambda\pm1$. The values of q are determined by crystal-field symmetry constraints and lie between 0 and $\pm k$. This parametrization scheme was used by Axe for the intensity analysis of the fluorescence spectrum of $Eu(C_2H_5SO_4)_3\cdot 9H_2O$. Porcher and Caro (1978) introduced the notation $B_{\lambda kq}$ for the intensity parameters:

$$B_{\lambda kq} = A_{kq}\Xi(k,\lambda) \qquad \text{[dim: L]}. \tag{150}$$

All the quantities of eq. (143) not included in the $B_{\lambda kq}$ parameters are taken together in a coefficient $a_{\lambda kq}$. When the coefficients $a_{\lambda kq}$ of the intensity parameters $B_{\lambda kq}$ have been calculated and when the experimental dipole strength has been corrected for the magnetic dipole contribution, the $B_{\lambda kq}$ parameters can be determined by a fitting procedure. For a crystal-field transition ($\beta \leftarrow \alpha$) a quadratic equation is constructed:

$$\frac{1}{\chi_{ED}}\left[D_{exp} - \chi_{MD}D_{MD}\right] = \left[\sum_{\lambda,k,q} a^{\rho\alpha\beta}_{\lambda kq}B_{\lambda kq}\right]^2 \tag{151}$$

or

$$D^0_{exp} = \left[\sum_{\lambda,k,q} a^{\rho\alpha\beta}_{\lambda kq}B_{\lambda kq}\right]^2, \tag{152}$$

where D^0_{exp} is the experimental dipole strength corrected for the magnetic dipole contribution, and ρ is the polarization number. In π-polarization $\rho=0$, and in σ-polarization $\rho=\pm1$. The symbols α and β stand for the ground state and the excited state, respectively. In general, one has to write down such an equation for each of the M transitions for which a value of the experimental dipole strength is available and $M \geqslant N$ (N is the number of intensity parameters). The parameters are determined by finding the minimum of a function which consists of the sum of the M non-linear quadratic functions in N variables. The equations to be solved are of the form

$$\sum_M \left[\sum_{\rho,\alpha,\beta}\left[\sum_{\lambda kq} a^{\rho\alpha\beta}_{\lambda kq}B_{\lambda kq}\right]^2 - D^0_{exp}\right] = 0. \tag{153}$$

The optimized phenomenological intensity parameters depend to a large extent on the starting values chosen for those parameters, because the minimalization procedure stops

Table 3
$B_{\lambda kq}$ intensity parameters for $KY_3F_{10}:Eu^{3+}$ (C_{4v} symmetry)[a]

Parameter	Value (10^{-12} cm)	Parameter	Value (10^{-12} cm)
B_{210}	−18.5	B_{670}	3.2
B_{230}	109	B_{454}	71
B_{430}	−14.5	B_{654}	58
B_{450}	29.5	B_{674}	19
B_{650}	23		

[a] From Porcher and Caro (1978).

Table 4
$B_{\lambda kq}$ intensity parameters for $LiYF_4:R^{3+}$ (D_{2d} symmetry)

Parameter	Value (10^{-12} cm)		Parameter	Value (10^{-12} cm)	
	$LiYF_4:Nd^{3+}$ [a]	$LiYF_4:Eu^{3+}$ [b]		$LiYF_4:Nd^{3+}$ [a]	$LiYF_4:Eu^{3+}$ [b]
B_{232}	156i	−123i	B_{652}	−200i	11i
B_{432}	−37i	111i	B_{672}	325i	111i
B_{452}	−57i	−191i	B_{676}	−71i	18i

[a] From Görller-Walrand et al. (1989). [b] From Fluyt et al. (1995).

at the first local minimum. Different starting sets can be used, but it is advisable to retain those which have the same signs as those predicted by theoretical models. Since the equations are quadratic, the sign of all the intensity parameters may be changed without changing the calculated values of the dipole strengths. Only the relative signs are important.

Intensity parametrizations of spectral transitions between crystal-field levels in lanthanide-doped single crystals have been reported for $LaAlO_3:Pr^{3+}$ (Delsart and Pelletier-Allard 1971), $LaCl_3:Pr^{3+}$ (Dirckx 1995), $LaF_3:Pr^{3+}$ (Dirckx 1995), $Pr_2Mg_3(NO_3)_{12}\cdot 24H_2O$ (Hens and Görller-Walrand 1995), $Nd_2Mg_3(NO_3)_{12}\cdot 24H_2O$ (Görller-Walrand et al. 1993), $LiYF_4:Nd^{3+}$ (Görller-Walrand et al. 1989), $KY_3F_{10}:Eu^{3+}$ (Porcher and Caro 1978), $LiYF_4:Eu^{3+}$ (Görller-Walrand et al. 1986, Fluyt et al. 1995), $Na_5Eu(MoO_4)_4$ (Hölsä et al. 1990), $Na_5Eu(WO_4)_4$ (Hölsä et al. 1990), $Eu(C_2H_5SO_4)_3\cdot 9H_2O$ (Axe 1963, Ohaka and Kato 1983), $YPO_4:Ho^{3+}$ (Becker 1971), $CaF_2:Er^{3+}$ (Freeth et al. 1982, Reid 1981), $Tm(C_2H_5SO_4)_3\cdot 9H_2O$ (Krupke and Gruber 1965), and $LiTmF_4$ (Christensen 1979). A selection of the parameter sets is presented in tables 3–5.

The parametrization scheme by Judd and Ofelt for J-multiplet transition intensities in terms of Ω_λ parameters (sect. 7.3) is completely general. It is only limited to the assumption of one-electron, one-photon interaction. The parametrization scheme is independent of the nature of the metal–ligand interactions. In this way, the Judd–Ofelt theory can also be used for the parametrization of vibronic interactions (see sect. 11). The

Table 5
$B_{\lambda kq}$ intensity parameters for $R_2Mg_3(NO_3)_{12}\cdot 24H_2O$ (C_{3v} symmetry)

Parameter	Value (10^{-12} cm)			Parameter	Value (10^{-12} cm)		
	R=Pr[a]	R=Nd[b]	R=Eu[a]		R=Pr[a]	R=Nd[b]	R=Eu[a]
B_{210}	1.48	14.61	43.99	B_{453}	9.57	1.42	(1.42)
B_{230}	−27.43	−1.83	−11.59	B_{650}	−8.53	0.34	(0.34)
B_{233}	−12.01	8.06	12.52	B_{653}	−1.71	−2.91	(−2.91)
B_{430}	−0.44	−9.60	(−9.60)	B_{670}	8.78	−8.18	(−8.18)
B_{433}	−22.38	3.02	(3.02)	B_{673}	−9.74	−14.98	(−14.98)
B_{450}	21.09	1.35	(1.35)	B_{676}	−9.26	3.29	(3.29)

[a] From Hens (1996). [b] From Görller-Walrand et al. (1992).

parametrization scheme of Axe for describing the intensities of crystal-field transitions in terms of $B_{\lambda kq}$ is not so general in its applicability. In addition to the one-electron, one-photon assumption, the parametrization scheme requires that the *superposition approximation* is valid, which means that all metal–ligand pairwise interactions have to be cylindrically symmetric (e.g. have $C_{\infty v}$ local symmetry) and independent (Newman and Balasubramanian 1975). It is also assumed that no phonon is involved in the transition (Reid and Richardson 1984a). The superposition approximation poses problems for lanthanide systems with polyatomic ligands with highly anisotropic charge distributions. If these conditions (cylindrical symmetry and independence) are not satisfied, additional parameters are required to describe the spectral intensities adequately.

6.2. *Reid–Richardson intensity model*

A first parametrization scheme with inclusion of extra parameters for taking the invalidity of the superposition approximation into account (see sect. 6.1) was developed by Newman and Balasubramanian (1975). They introduced a more general set of intensity parameters denoted as A_{JKM}. The parameters $J=K\pm 1$ have counterparts in the $B_{\lambda kq}$ parametrization scheme of Axe, whereas the $J=K$ parameters are extra parameters. The A_{JKM} parametrization scheme is equally general as the Ω_λ parameters (see sect. 7.3) in the sense that only the one-electron, one-photon approximation has to be fulfilled.

Reid and Richardson (1983a–c, 1984a,b) developed a parametrization scheme which is essentially identical to the scheme of Newman and Balasubramanian and which thus only requires the one-electron, one-photon approximation. They have pointed out that the intensity parameters can be interpreted and calculated in terms of two intensity mechanisms, namely the static-coupling (SC) mechanism and the dynamic-coupling (DC) mechanism. Both in the static and in the dynamic coupling model, the interactions are purely electrostatic and thus an overlap between the charge distributions of the ligand and the central metal ion is neglected. In the static coupling model, the electronic configuration of the lanthanide ion is perturbed by the ligands. The ligands produce

a static potential of odd parity around the lanthanide ion, so that 4f states of mixed parity are formed. Transitions between these states can be induced directly by the electric dipole component of the incident light. The ligands can be polarized isotropically by the lanthanide ion. The basic assumption of the static coupling model is however that the ligands are not influenced by the radiation field of the incident light. The intermediate perturbing wavefunctions are fully localized on the lanthanide ion. The Judd–Ofelt theory is an example of a static coupling model (see sect. 6.1). In this theory, the ligands are approximated by point charges.

In the *dynamic-coupling (DC) model*, the change of the distribution of the ligand charges under influence of the radiation field of light is taken into account. The electric dipole component of the light induces transient dipoles on the ligands, which in turn induce 4f–4f transitions in the lanthanide ion. Two possibilities can be considered: (1) *isotropic polarizability* and (2) *anisotropic polarizability.* In the case of isotropic polarizability, the ligands are isotropic (e.g. halogenide ions) and the ligand–ligand interaction is cylindrically symmetric ($C_{\infty v}$) and independent. In the case of anisotropic polarizability, the ligands are anisotropic (e.g. BO_3^{3-}, NO_3^-, ODA, ...) and it is no longer possible to consider the lanthanide–ligand interactions as cylindrically symmetric. In the dynamic-coupling model, the perturbing wavefunctions are localized on the ligands.

In order to facilitate the *ab initio* calculation of the intensity parameters in terms of the static and the dynamic coupling mechanism, Reid and Richardson defined their intensity parameters A_{tp}^{λ} in such a way that an easy differentiation between the two contributions of the two intensity mechanisms is possible. The $t=\lambda$ parameters reflect the lanthanide–ligand pairwise interactions which are not cylindrically symmetric. Their magnitudes and signs depend upon the shapes and orientations of the ligand polarizability ellipsoids. These extra parameters are symmetry-allowed in all point groups, except $C_{\infty v}$. The total number of parameters in each of the 21 non-centrosymmetric crystallographic point-groups and $C_{\infty v}$ is reported in table 6. From this table it is clear that the $t=\lambda$ parameters are the only parameters allowed in the O group and the only parameters with $\lambda=2$ in the D_4 and D_6 point groups (Reid and Richardson 1983a).

The *static-coupling (SC) scheme* gives rise to A_{tp}^{λ} parameters with $\lambda=2,4$ or 6 and with $t=\lambda\pm1$. The SC mechanism is the only mechanism which can contribute to the $t=\lambda-1$ parameters. For isotropic ligands in the dynamic-coupling (DC) mechanism, only A_{tp}^{λ} parameters with $t=\lambda+1$ are non-vanishing. Given that the ligands have negative charges, the A_{tp}^{λ}[SC] and A_{tp}^{λ}[DC, isotropic] parameters have opposite signs. This has also been proved in detail by Chertanov et al. (1994). The sign relationship can be used to determine which of the two mechanisms is dominant in the case of isotropic ligands. The experimental signs of the A_{tp}^{λ} parameters have to be compared with the A_{tp}^{λ} parameters calculated for each of the two intensity mechanisms. It should be noted that the relative signs have to be compared, since the absolute signs cannot be obtained from intensity data (see also sect. 9.1). A comparison of calculated and experimental signs of intensity parameters for several lanthanide complexes with isotropic ligands has been published by Reid et al. (1983). The dynamic coupling mechanism for anisotropic ligands

Table 6
Number of A_{tp}^{λ} intensity parameters for non-centrosymmetric point groups[a,b]

Point group	Number of intensity parameters			Point group	Number of intensity parameters		
	$t=\lambda\pm1$	$t=\lambda$	Total		$t=\lambda\pm1$	$t=\lambda$	Total
C_1	54	27	81	C_{3h}	10	4	14
C_2	24	15	39	D_2	9	9	18
C_3	18	9	27	D_3	6	6	12
C_4	12	7	19	D_4	3	5	8
C_6	8	5	13	D_6	1	4	5
C_s	30	12	42	D_{2d}	6	4	10
C_{2v}	15	6	21	D_{3h}	5	2	7
C_{3v}	12	3	15	S_4	12	8	20
C_{4v}	9	2	11	T	3	3	6
C_{6v}	7	1	8	T_d	3	1	4
$C_{\infty v}$	6	0	6	O	0	2	2

[a] After Reid and Richardson (1983b).
[b] Only the number of A_{tp}^{λ} parameters is reported for which no differentiation between the A_{tp}^{λ} and A_{t-p}^{λ} is possible.

is responsible for the additional parameters with $t=\lambda$. The signs and the magnitudes of these parameters depend on the shapes and the orientations of the ligand polarizability ellipsoids. Anisotropic ligand polarization contributions to the f–f transitions were discussed by Stewart (1983) and by Reid and Richardson (1983a). Berry and Richardson (1986) have calculated the dynamic ligand-polarization contributions to the f–f electric dipole strengths and rotatory strengths of the $^5D_2 \leftarrow {}^7F_0$ and $^5D_0 \rightarrow {}^7F_2$ transition in EuODA. An electric dipole transition induced via the static coupling mechanism can either be constructive or destructive in producing electric dipole intensity, depending on the sign of the parameters. The Ω_λ parameters cannot be used to decide which mechanism dominates, because the Ω_λ parameters are essentially sums of squares of the A_{tp}^{λ} parameters and they do not contain the necessary phase information for making the differentiation between the different mechanisms on the basis of the sign. Since the A_{tp}^{λ} parametrization scheme is general, it can absorb several contributions, such as second-order crystal-field effects, covalency and ligand polarizability. However, the A_{tp}^{λ} parameters are not able to account for third-order effects, i.e. effects involving the spin–orbit interaction or the Coulombic interaction within the excited configuration. Therefore, Burdick et al. (1995) took the excited configuration $4f^{N-1}5d^1$ of the lanthanide ion into account for intensity calculations of Nd^{3+} in YAG. Chertanov et al. (1994) have performed intensity calculations on Nd_2O_2S in terms of contributions from the SC and DC(isotropic) mechanisms. The agreement between the experimental and calculated total oscillator strengths for transitions between the ground state and $^{2S+1}L_J$ manifolds is good, but the relative intensities of the crystal-field transitions are not well reproduced. Better agreement for the relative intensities of the strongest transitions is found when

the dynamic coupling mechanism is favoured by increasing the ionic polarizabilities. No covalency contributions were considered. The authors refer to Garcia and Faucher (1992), who showed by direct calculation that the ligand part of the rare-earth wavefunctions (and thus the covalency) has a negligible effect on the total oscillator strengths.

Strictly speaking, it is only in the static coupling scheme that the A^{λ}_{tp} parameters can be related to the $B_{\lambda kq}$ parameters of the Judd–Ofelt–Axe parametrization scheme. Some authors use the notation $B_{\lambda kq}$ also for $\lambda = k$ parameters (Görller-Walrand et al. 1994a,b):

$$A^{\lambda}_{tp} = -A_{kq}\,\Xi(k,\lambda)\,\frac{2\lambda+1}{(2k+1)^{1/2}} = -B_{\lambda kq}\,\frac{2\lambda+1}{(2k+1)^{1/2}}, \tag{154}$$

or

$$B_{\lambda kq} = -A^{\lambda}_{tp}\,\frac{(2t+1)^{1/2}}{2\lambda+1}, \tag{155}$$

with $k \equiv t$ and $q \equiv p$.

Intensity parameters have been reported for $LiYF_4:Pr^{3+}$ (Reid and Richardson 1984e), $Na_3[Nd(ODA)_3]\cdot 2NaClO_4\cdot 6H_2O$ (May et al. 1989, Fluyt et al. 1996), $Y_3Al_5O_{12}:Nd^{3+}$ (Burdick et al. 1994), $[Nd(H_2O)_9](CF_3SO_3)_3$ (Quagliano et al. 1995), $Na_3[Sm(ODA)_3]\cdot 2NaClO_4\cdot 6H_2O$ (Carter et al. 1986, May et al. 1987), $Na_3[Eu(ODA)_3]\cdot 2NaClO_4\cdot 6H_2O$ (Berry et al. 1988, Görller-Walrand et al. 1994a), $GdAl_3(BO_3)_4:Eu^{3+}$ (Görller-Walrand et al. 1994b), and $Na_3[Ho(ODA)_3]\cdot 2NaClO_4\cdot 6H_2O$ (Moran et al. 1989, Moran and Richardson 1990). The A^{λ}_{tp} intensity parameter sets for the $Na_3[R(ODA)_3]\cdot 2NaClO_4\cdot 6H_2O$ systems (D_3 symmetry) are presented in table 7.

Based on the superposition model of Newman for crystal-field parameters (Newman 1971, 1978), Reid and Richardson (1983b) developed a superposition model for intensity parameters. By the superposition model, intensity parameters for lanthanide ions in different host matrices (with different geometries) can be compared. Moreover, the number of intensity parameters is reduced to six. It is assumed that the lanthanide–ligand interactions are cylindrically symmetric and independent. The intrinsic intensity parameters are denoted by $\bar{A}^{\lambda}_{t}$. The superposition model for intensity studies was discussed also by Newman and Ng (1989). The method was applied to $LaAlO_3:Pr^{3+}$ (Reid and Richardson 1983c), to $[Nd(H_2O)_9](CF_3SO_3)_3$ (Quagliano et al. 1995), and to several Eu^{3+} compounds (Reid 1987, Chan and Reid 1989). Reid et al. (1988) used many-body perturbation theory for the calculation of the intrinsic parameters of Pr^{3+} in $LaCl_3$. Contributions from excitations of 4f electrons into unoccupied orbitals and excitations to unoccupied 4f orbitals from the core orbitals on Pr^{3+} and Cl^- ions were considered. A simplified parametrization scheme based on the idea of the angular overlap model (AOM) was introduced by Gajek (1993). Intensity calculations for crystal-field transitions of Eu^{3+} in KY_3F_{10}, $LiYF_4$ and LaOCl have been reported by Malta et al. (1991). The odd-rank crystal-field parameters have been evaluated by an overlap model and the energy differences between the $4f^6$ configuration and the perturbing configurations by

Table 7
A^{λ}_{tp} intensity parameters for $Na_3[R(ODA)_3]\cdot 2NaClO_4\cdot 6H_2O$ (RODA) systems[a]

Parameter	Value (10^{-12} cm)						
	NdODA[b]	NdODA[c]	SmODA[d]	EuODA[e]	EuODA[f]	HoODA[g]	HoODA[h]
A^2_{20}	242i	−351i	310i	97i	−243i	287i	284i
A^2_{33}	−33i	−55i	−91i	−211i	−57i	−115i	−133i
A^4_{33}	29i	−39i	−30i	79i	−82i	105i	95i
A^4_{40}	63i	−86i	143i	106i	−54i	13i	24i
A^4_{43}	−7i	30i	−35i	−0.9i	−12i	6i	14i
A^4_{53}	−245i	−245i	−397i	−298i	−318i	−300i	−296i
A^6_{53}	361i	512i	753i	583i	517i	348i	356i
A^6_{60}	−18i	32i	189i	40i	−40i	54i	56i
A^6_{63}	−16i	10i	144i	34i	−18i	64i	52i
A^6_{66}	6i	−57i	27i	29i	−29i	−56i	−45i
A^6_{73}	−96i	−239i	−42i	−115i	−101i	−49i	−45i
A^6_{76}	−152i	199i	−162i	−167i	148i	−117i	−125i

[a] The symmetry of the lanthanide site in $Na_3[R(ODA)_3]\cdot 2NaClO_4\cdot 6H_2O$ is D_3.
[b] May et al. (1989).
[c] Fluyt et al. (1996).
[d] May et al. (1987).
[e] Berry et al. (1988).
[f] Görller-Walrand et al. (1994a).
[g] Moran et al. (1989).
[h] Moran and Richardson (1990).

the *average energy denominator method.* Dynamic coupling was also taken into account. Brown et al. (1988a–c) published a comprehensive study of the *angular overlap model* (renamed as the *cellular ligand field model*) as applied to d–d transitions, but this formalism can be extended easily to f–f transitions.

In any sample, optical activity can be induced by placing the sample in a magnetic field. The differential absorption of left and right circularly polarized light of a sample in a longitudinal magnetic field can be measured. In a longitudinal magnetic field, the magnetic field lines are parallel to the light beam. This technique is called magnetic circular dichroism or MCD, and is based on the Zeeman effect. The principles of MCD spectroscopy have been described by P.J. Stephens (1970,1976) and by Piepho and Schatz (1983). The use of MCD in analytical chemistry was discussed by Hollebone (1993). Application of the MCD theory to lanthanide ions was discussed by Görller-Walrand and co-workers (Görller-Walrand and Godemont 1977, Görller-Walrand 1985, Görller-Walrand and Fluyt-Adriaens 1985). The major advantage of MCD over Zeeman spectroscopy is the fact that MCD spectra can be recorded also in cases where the bandwidth is larger than the Zeeman splitting. A disadvantage is that no transverse Zeeman spectra can be measured by the MCD method. Simulation of MCD spectra provides a check of the reliability of intensity parameters and wave functions. The extracted parameter set depends largely on the chosen starting values. Different parameter sets may give the same figure of merit for the calculated dipole strengths. It is very difficult to select the most adequate set of intensity parameters. Simulation of the MCD

spectrum can help. Calculation of the MCD signals does not require more parameters than the crystal-field and intensity parameters extracted from the absorption spectrum. If these parameters are adequate, they should allow a good simulation of the MCD spectrum. In the past, the MCD spectrum was often described by the Faraday parameters or MCD parameters A_1, B_0 and C_0 (Stephens formalism) (P.J. Stephens 1976, Piepho and Schatz 1983). In the Stephens formalism several approximations are made, and these are not always valid for lanthanide systems, especially not for single crystals. For instance, one assumption is that the Zeeman splitting is small compared to the crystal-field splitting within a multiplet. This is not true for small crystal-field splittings and a strong magnetic field. The Zeeman effect cannot be considered as a small perturbation compared to the crystal-field effect. Not only the free-ion and the crystal-field Hamiltonian have to be included in the total Hamiltonian, but also the Zeeman Hamiltonian. After diagonalization, the Zeeman levels are directly found, instead of the crystal-field levels. The MCD of a transition is calculated as the difference in intensity between the absorption of left circularly polarized light to the Zeeman levels of a $^{2S+1}L_J$ term and the absorption of right circularly polarized light. The MCD of a transition has to be reported as a difference in absorbance. A positive sign indicates that left circularly polarized light is absorbed more effectively than right circularly polarized light. A negative sign indicates the opposite. In the case of overlapping bands, the bandwidth of the curves used for the simulation will affect to a large extent the overall appearance of the MCD signal. For single crystals, a Lorentzian shape function often gives the best results for the graphical simulation. A simulation of the MCD spectrum of NdODA was presented by Fluyt et al. (1997).

Theoretical schemes similar to the Judd–Ofelt theory for the interpretation of magneto-optic spectra of transitions between J-manifolds were developed by Livshits (1972), by Pink (1975), and by Klochkov and coworkers (Valiev et al. 1990, Klochkov et al. 1991). Klochkov et al. (1991) applied this parametrization scheme to the MCD spectra of f–f transitions in $Er(PO_3)_3$ glass.

7. Intensity parametrization of transitions between J-multiplets

7.1. *Judd's parametrization scheme*

7.1.1. *Solutions of rare-earth ions*

For rare-earth ions in solutions and glasses, the crystal-field fine structure is not resolved because of inhomogenous line broadening. Each broad absorption band corresponds to a transition between the ground level $^{2S+1}L_J$ and the excited level $^{2S'+1}L'_{J'}$. The measured oscillator strength of the various component lines is therefore the sum of the oscillator strengths of the various component lines, suitable weighed to allow for the differential probability of occupation of the components of the ground level. However, the observed splittings of the ground levels of rare-earth ions in crystals seldom exceed 250 cm^{-1}. For a level where the ratio of the probabilities of occupation of the highest to the lowest

component is as high as 0.3 at room temperature, not too great an error is introduced if it is assumed that all the components of the ground level are equally likely to be occupied.

Judd's expression for the matrix element of an induced electric dipole transition (see eq. 143),

$$\left\langle B \left| \hat{\boldsymbol{D}}_\rho^{(1)} \right| B' \right\rangle = \sum_{k,q} \sum_{\lambda \text{ even}} (2\lambda+1)(-1)^{q+\rho} A_{kq} \begin{pmatrix} 1 & \lambda & k \\ \rho & -q-\rho & q \end{pmatrix} \left\langle A \left| \hat{\boldsymbol{U}}_{q+\rho}^{(\lambda)} \right| A' \right\rangle \Xi(k,\lambda), \tag{156}$$

is only valid for a single line transition, e.g. for a transition between two crystal-field levels. For solutions, we have to consider the random orientation of the molecules and the random orientation of the light polarization tensor. We will also sum over all the polarizations $(-1, 0, +1)$ and all the components $\langle A|$ and $|A'\rangle$ of the final and initial level. Therefore, we have to work out the summation

$$\sum_{M, M', \text{all } \rho} \left| \left\langle B \left| \hat{\boldsymbol{D}}_\rho^{(1)} \right| B' \right\rangle \right|^2. \tag{157}$$

Starting from eq. (156), we have

$$\begin{aligned} &\left| \left\langle B \left| \hat{\boldsymbol{D}}_\rho^{(1)} \right| B' \right\rangle \right|^2 \\ &= \left| \left\langle l^N \psi J M \left| \hat{\boldsymbol{D}}_\rho^{(1)} \right| l^N \psi' J' M' \right\rangle \right|^2 \\ &= \sum_{\substack{k_1, k_2, q_1, q_2, \\ \lambda_1, \lambda_2 \text{ even}}} A_{k_1 q_1} \left(A_{k_2 q_2}\right)^* (-1)^{q_1+\rho+q_2+\rho} (2\lambda_1+1)(2\lambda_2+1)\, \Xi(\lambda_1, k_1)\, \Xi(\lambda_2, k_2) \\ &\quad \times \begin{pmatrix} 1 & \lambda_1 & k_1 \\ \rho & q_1-\rho & q_1 \end{pmatrix} \begin{pmatrix} 1 & \lambda_2 & k_2 \\ \rho & q_2-\rho & q_2 \end{pmatrix} \left\langle A \left| U_{q_1+\rho}^{\lambda_1} \right| A' \right\rangle \left\langle A \left| U_{q_2+\rho}^{\lambda_2} \right| A' \right\rangle, \end{aligned} \tag{158}$$

with

$$\langle A| \equiv \sum_M \langle l^N \psi J M|\, a_M, \tag{159}$$

and

$$|A'\rangle \equiv \sum_{M'} a'_{M'} \left| l^N \psi' J' M' \right\rangle. \tag{160}$$

$$\begin{aligned} &\left\langle A \left| U_{q_1+\rho}^{\lambda_1} \right| A' \right\rangle \left\langle A \left| U_{q_2+\rho}^{\lambda_2} \right| A' \right\rangle \\ &= \sum_M \sum_K \sum_{M'} \sum_{K'} a_M a_K a_{M'} a_{K'} (-1)^{J-M} (-1)^{J-K} \\ &\quad \times \begin{pmatrix} J & \lambda_1 & J' \\ -M & \rho+q_1 & M' \end{pmatrix} \begin{pmatrix} J & \lambda_2 & J' \\ -K & \rho+q_2 & K' \end{pmatrix} \\ &\quad \times \left\langle J \left\| U^{\lambda_1} \right\| J' \right\rangle \left\langle J \left\| U^{\lambda_2} \right\| J' \right\rangle. \end{aligned} \tag{161}$$

The orthogonality conditions for the M components are

$$\sum_{M,K,M',K'} a_M a_K a_{M'} a_{K'} = \delta_{MK}\delta_{M'K'}, \tag{162}$$

so that

$$\begin{aligned}&\left\langle A \left| U^{\lambda_1}_{q_1+\rho} \right| A' \right\rangle \left\langle A \left| U^{\lambda_2}_{q_2+\rho} \right| A' \right\rangle \\ &\quad = \begin{pmatrix} J & \lambda_1 & J' \\ -M & q_1+\rho & M' \end{pmatrix} \begin{pmatrix} J & \lambda_2 & J' \\ -M & q_2+\rho & M' \end{pmatrix} \left\langle J \left\| U^{\lambda_1} \right\| J' \right\rangle \left\langle J \left\| U^{\lambda_2} \right\| J' \right\rangle .\end{aligned} \tag{163}$$

Equation (158) can be rewritten as

$$\begin{aligned}&\left| \left\langle B \left| \hat{\boldsymbol{D}}^{(1)}_{\rho} \right| B' \right\rangle \right|^2 \\ &\quad = \left| \left\langle l^N \psi J M \left| \hat{\boldsymbol{D}}^{(1)}_{\rho} \right| l^N \psi' J' M' \right\rangle \right|^2 \\ &\quad = \sum_{\substack{k_1,k_2,q_1,q_2,\\ \lambda_1,\lambda_2 \text{ even}}} A_{k_1 q_1} A^*_{k_2 q_2} (-1)^{q_1+\rho+q_2+\rho} (2\lambda_1+1)(2\lambda_2+1)\, \Xi(\lambda_1,k_1)\, \Xi(\lambda_2,k_2) \\ &\qquad \times \begin{pmatrix} 1 & \lambda_1 & k_1 \\ \rho & -q_1-\rho & q_1 \end{pmatrix} \begin{pmatrix} 1 & \lambda_2 & k_2 \\ \rho & -q_2+\rho & q_2 \end{pmatrix} \\ &\qquad \times \begin{pmatrix} J & \lambda_1 & J' \\ -M & q_1+\rho & M' \end{pmatrix} \begin{pmatrix} J & \lambda_2 & J' \\ -M & q_2+\rho & M' \end{pmatrix} \\ &\qquad \times \left\langle J \left\| U^{\lambda_1} \right\| J' \right\rangle \left\langle J \left\| U^{\lambda_2} \right\| J' \right\rangle .\end{aligned} \tag{164}$$

7.1.2. *Effect of random orientation on the crystal-field operator*

Recall that the crystal-field Hamiltonian is given by

$$V = \sum_{k,q} A_{kq} \hat{\boldsymbol{D}}^{(k)}_q \qquad [\text{dim: } \textit{energy}], \tag{165}$$

with

$$\hat{\boldsymbol{D}}^{(k)}_q = \sum_j r^{(k)}_j \hat{\boldsymbol{C}}^{(k)}_q (\theta_j, \varphi_j) \qquad [\text{dim: } \mathrm{L}^k]. \tag{166}$$

The orientational dependence of the crystal-field Hamiltonian V is obtained by considering the properties under rotation of the tensor $\hat{\boldsymbol{C}}^{(k)}_q$ and therefore also the tensor $\hat{\boldsymbol{D}}^{(k)}_q$. Since the $\hat{\boldsymbol{D}}^{(k)}_q$ terms are the components of an irreducible tensor operator of rank k, they satisfy the same commutation rule with respect to the angular momentum J as the

spherical harmonics $Y_q^{(k)}$, and consequently, they have the same properties with respect to a rotation. The result of rotation $R(\alpha,\beta,\gamma)$ of the $\hat{\boldsymbol{D}}_q^{(k)}$ through the Euler angle (α,β,γ) is some linear combination of the complete set

$$R(\alpha,\beta,\gamma)\hat{\boldsymbol{D}}_q^{(k)} = \sum_{q'} d_{q'q}^{(k)}(\alpha,\beta,\gamma)\,\hat{\boldsymbol{D}}_q^{(k)}, \tag{167}$$

where $d_{q'q}^{(k)}(\alpha,\beta,\gamma)$ are the elements of the rotation representation matrix and themselves components of a rank-k tensor.

If the crystal-field Hamiltonian is initially specified for some reference orientation $(0,0,0)$ as

$$V(0,0,0) = \sum_{k,q} A_{kq}\hat{\boldsymbol{D}}_q^{(k)}, \tag{168}$$

then for a specific, but completely arbitrary orientation (α,β,γ), one can write

$$V(\alpha,\beta,\gamma) = \sum_{k,q,q'} d_{q'q}^{(k)}(\alpha,\beta,\gamma)A_{kq}\hat{\boldsymbol{D}}_q^{(k)}. \tag{169}$$

The matrix element between two states characterized by $\langle B|$ and $|B'\rangle$ is now given by

$$\langle B|\hat{\boldsymbol{D}}_\rho^{(1)}|B'\rangle = \sum_{\substack{k,q,\\ \lambda\ \text{even}}} (2\lambda+1)A_{kq}\sum_{q'} d_{q'q}^{(k)}(\alpha,\beta,\gamma)(-1)^{q'-\rho}\begin{pmatrix}1 & \lambda & k\\ \rho & -q'-\rho & q'\end{pmatrix}\Xi(\lambda,k)\langle A|U_{q'+\rho}^{(\lambda)}|A'\rangle. \tag{170}$$

After expanding the matrix element of the unit tensor and the modulus squared, we obtain

$$\begin{aligned}
&\left|\langle B|\hat{\boldsymbol{D}}_\rho^{(1)}|B'\rangle\right|^2\\
&\quad = \left|\langle l^N\psi JM|\hat{\boldsymbol{D}}_\rho^{(1)}|l^N\psi' J'M'\rangle\right|^2\\
&\quad = (-1)^\rho \sum_{\substack{k_1,k_2,q_1,q_2,\\ \lambda_1,\lambda_2\ \text{even}}} (2\lambda_1+1)(2\lambda_2+1)A_{k_1q_1}A_{k_2q_2}^*\Xi(\lambda_1,k_1)\Xi(\lambda_2,k_2)\\
&\qquad \times \sum_{q_1',q_2'} d_{q_1'q_1}^{(k_1)}(\alpha,\beta,\gamma)\,d_{q_2'q_2}^{(k_2)*}(\alpha,\beta,\gamma)(-1)^{q_1'+q_2'}\begin{pmatrix}1 & \lambda_1 & k_1\\ \rho & -q_1'-\rho & q_1'\end{pmatrix}\begin{pmatrix}1 & \lambda_2 & k_2\\ -\rho & -q_2'+\rho & q_2'\end{pmatrix}\\
&\qquad \times (-1)^{J-M}(-1)^{J'-M'}\begin{pmatrix}J & \lambda_1 & J'\\ -M & q_1'+\rho & M'\end{pmatrix}\begin{pmatrix}J' & \lambda_2 & J\\ -M' & q_2'-\rho & M\end{pmatrix}\\
&\qquad \times \left\langle A\left\|U^{(\lambda_1)}\right\|A'\right\rangle\left\langle A\left\|U^{(\lambda_2)}\right\|A'\right\rangle,
\end{aligned} \tag{171}$$

where the sum over the primed and unprimed quantities runs over all allowed values.

Using the general properties of the $d_{qq}^{(k)}$ under complex conjugation,

$$d_{q'q}^{(k)*}(\alpha,\beta,\gamma) = (-1)^{q'-q}\, d_{-q'-q}^{(k)}(\alpha,\beta,\gamma), \tag{172}$$

and assuming the potential to be real, that is

$$A_{kq}^{*} = (-1)^{q} A_{k,-q}, \tag{173}$$

we obtain

$$\begin{aligned}
&\left|\left\langle B \left| \hat{\boldsymbol{D}}_{\rho}^{(1)} \right| B' \right\rangle\right|^2 \\
&= \left|\left\langle l^N \psi J M \left| \hat{\boldsymbol{D}}_{\rho}^{(1)} \right| l^N \psi' J' M' \right\rangle\right|^2 \\
&= (-1)^{\rho} \sum_{\substack{k_1,k_2,q_1,q_2,\\ \lambda_1,\lambda_2 \text{ even}}} A_{k_1 q_1} (-1)^{q_2} A_{k_2,-q_2} (2\lambda_1+1)(2\lambda_2+1)\, \Xi(\lambda_1,k_1)\, \Xi(\lambda_2,k_2) \\
&\quad \times \sum_{q_1',q_2'} d_{q_1' q_1}^{(k_1)}(\alpha,\beta,\gamma)(-1)^{q_2'-q_2}\, d_{-q_2'-q_2}^{(k_2)}(\alpha,\beta,\gamma)(-1)^{q_1'+q_2'} \begin{pmatrix} 1 & \lambda_1 & k_1 \\ \rho & -q_1'-\rho & q_1' \end{pmatrix} \begin{pmatrix} 1 & \lambda_2 & k_2 \\ -\rho & -q_2'+\rho & q_2' \end{pmatrix} \\
&\qquad \times (-1)^{J-M} (-1)^{J'-M'} \begin{pmatrix} J & \lambda_1 & J' \\ -M & q_1'+\rho & M' \end{pmatrix} \begin{pmatrix} J' & \lambda_2 & J \\ -M' & q_2'-\rho & M \end{pmatrix} \\
&\quad \times \left\langle A \left\| U^{(\lambda_1)} \right\| A' \right\rangle \left\langle A \left\| U^{(\lambda_2)} \right\| A' \right\rangle,
\end{aligned} \tag{174}$$

For a large number of ions with random orientation of V relative to the space-fixed coordinate system, the experimentally relevant quantity is the spatial average of eq. (174). The spatial average is obtained by integrating over all values of the Eulerian angles. Using the property

$$\frac{1}{8\pi^2} \int_0^{2\pi} \mathrm{d}\alpha \int_0^{\pi} \sin\beta\, \mathrm{d}\beta \int_0^{2\pi} \mathrm{d}\gamma\, D_{m_1' m_1}^{(j_1)*}(\omega)\, D_{m_2' m_2}^{(j_2)*}(\omega) = \delta(m_1', m_2')\, \delta(m_1, m_2)\, \delta(j_1, j_2) \frac{1}{2j_1+1}, \tag{175}$$

with

$$\begin{aligned}
m_1' &= -q_1', \qquad m_2' = q_2', \qquad j_1 = k_1, \\
m_1 &= -q_1, \qquad m_2 = q_2, \qquad j_2 = k_2,
\end{aligned}$$

and thus,

$$-q_1' = q_2' = q', \qquad -q_1 = q_2 = q, \qquad k_1 = k_2 = k,$$

one gets

$$\frac{1}{8\pi^2} \int_0^{2\pi} \mathrm{d}\alpha \int_0^{\pi} \sin\beta\, \mathrm{d}\beta \int_0^{2\pi} \mathrm{d}\gamma\, D_{-q_1' -q_1}^{(k_1)*}(\alpha,\beta,\gamma)\, D_{q_2' q_2}^{(k_2)*}(\alpha,\beta,\gamma) = \delta(-q_1', q_2')\, \delta(-q_1, q_2)\, \delta(k_1, k_2) \frac{1}{2k+1}. \tag{176}$$

Upon taking the spatial average, one finds

$$\begin{aligned}
&\left|\left\langle B\left|\hat{\boldsymbol{D}}_{\rho}^{(1)}\right|B'\right\rangle\right|^2 \\
&= (-1)^{\rho} \sum_{k,q,\lambda\,\text{even}} |A_{kq}|^2 \frac{1}{2k+1} (2\lambda_1+1)(2\lambda_2+1)\, \Xi(\lambda_1,k_1)\, \Xi(\lambda_2,k_2) \\
&\quad \times \sum_{q'} (-1)^{q'} \begin{pmatrix} 1 & \lambda_1 & k \\ \rho & -q'-\rho & q' \end{pmatrix} \begin{pmatrix} 1 & \lambda_2 & k \\ \rho & -q'-\rho & q' \end{pmatrix} \\
&\quad \times \begin{pmatrix} J & \lambda_1 & J' \\ -M & q'+\rho & M' \end{pmatrix} \begin{pmatrix} J' & \lambda_2 & J \\ -M & q'+\rho & M' \end{pmatrix} \left\langle l^N \psi J \left\| U^{(\lambda_1)} \right\| l^N \psi' J' \right\rangle \left\langle l^N \psi J \left\| U^{(\lambda_2)} \right\| l^N \psi' J' \right\rangle,
\end{aligned} \tag{177}$$

with

$$|A_{kq}|^2 = A_{kq}^* A_{kq} = (-1)^q A_{k,-q} A_{kq}. \tag{178}$$

The introduction of the factor $1/(2k+1)$ in eq. (177) is due to the random orientation of the molecules. Moreover, the properties of the 3-j symbols imply $\lambda_1 = \lambda_2$.

7.1.3. *Effect of random orientation on the transition operator*

The electric dipole operator $\hat{\boldsymbol{D}}_{\rho}^{(1)}$ is a tensor of rank 1, with components $\rho = +1, -1, 0$. The same considerations as developed in sect. 7.1.2 lead to a factor $\frac{1}{3}$, allowing for the random orientation of the rare-earth ions. In fact, this factor is introduced in the expression relating $\int \varepsilon \, \mathrm{d}\overline{\nu}$ to the dipole strength D (eq. 28).

7.1.4. *Summation over all components of the ground state and the excited state and over all ρ's*

Now, one has to sum over all crystal-field levels of the ground state and over all crystal-field levels of the excited state. This is a sum over all M and M' of the ground and final states, as well as a sum over the polarization numbers $\rho = -1$, 0 and +1.

Because of the properties of the 3-j symbols,

$$\sum_{m_1, m_2, m} \begin{pmatrix} j_1 & j_2 & j \\ m_1 & m_2 & m \end{pmatrix} \begin{pmatrix} j_1 & j_2 & j \\ m_1 & m_2 & m \end{pmatrix} = 1, \tag{179}$$

the sum over all ρ, q and q' values is equal to 1:

$$\sum_{\rho} (-1)^{\rho} \sum_{k,q,\lambda\,\text{even}} \sum_{q'} (-1)^{q} \begin{pmatrix} 1 & \lambda & k \\ \rho & -q'-\rho & q' \end{pmatrix} \begin{pmatrix} 1 & \lambda & k \\ \rho & q'-\rho & -q' \end{pmatrix} = 1. \tag{180}$$

Because of the property

$$\sum_{m_1, m_2} \begin{pmatrix} j_1 & j_2 & j \\ m_1 & m_2 & m \end{pmatrix} \begin{pmatrix} j_1 & j_2 & j' \\ m_1 & m_2 & m' \end{pmatrix} = \frac{1}{2j+1} \delta_{jj'} \delta_{mm'}, \tag{181}$$

the sum over all M, M' and q' gives

$$\sum_{M,M'}\sum_{q'}\begin{pmatrix} J & \lambda & J' \\ -M & q'+\rho & M' \end{pmatrix}\begin{pmatrix} J' & \lambda & J \\ -M' & q'-\rho & M \end{pmatrix} = \frac{1}{2\lambda+1}. \tag{182}$$

7.1.5. *Dipole strength and oscillator strength for randomly-oriented systems in Judd's parametrization scheme*

The dipole strength of rare-earth ions in solution is

$$\begin{aligned} D &= e^2\left|\left\langle B\left|D_\rho^{(1)}\right|B'\right\rangle\right|^2 \\ &= e^2\sum_{k,q,\lambda\ \text{even}}(2\lambda+1)\,|A_{kq}|^2\,\frac{1}{2k+1}\,\Xi^2(k,\lambda)\left|\left\langle l^N\psi J\left\|U^{(\lambda)}\right\|l^N\psi' J'\right\rangle\right|^2, \\ &\quad [\text{dim: } e^2\mathrm{L}^2], \end{aligned} \tag{183}$$

with

$$\begin{aligned} \Xi(k,\lambda) = 2\sum_{n'l'}(2l+1)(2l'+1)(-1)^{l+l'}\begin{Bmatrix} 1 & \lambda & k \\ l & l' & l \end{Bmatrix}\begin{pmatrix} l & 1 & l' \\ 0 & 0 & 0 \end{pmatrix}\begin{pmatrix} l' & k & l \\ 0 & 0 & 0 \end{pmatrix} \\ \times\frac{\langle nl\,|\hat{r}|\,n'l'\rangle\,\langle nl\,|\hat{r}^k|\,n'l'\rangle}{\Delta(n'l')}. \end{aligned} \tag{184}$$

Since (see eq. 50)

$$P_{\text{exp}} = \frac{\chi_{\text{ED}}}{2J+1}P = \frac{\chi_{\text{ED}}}{2J+1}\frac{8\pi^2 m_e c\bar{\nu}_0}{3he^2}D \qquad [D \text{ in esu}^2\,\text{cm}^2], \tag{185}$$

we have

$$P_{\text{exp}} = \frac{\chi_{\text{ED}}}{2J+1}\frac{8\pi^2 m_e c\bar{\nu}_0}{3he^2}e^2\sum_{k,q,\lambda\ \text{even}}(2\lambda+1)\,|A_{kq}|^2\,\frac{1}{2k+1}\,\Xi^2(k,\lambda)\left|\left\langle l^N\psi J\left\|U^{(\lambda)}\right\|l^N\psi' J'\right\rangle\right|^2 \tag{186}$$

[dim: /],

or

$$P_{\text{exp}} = \frac{\chi_{\text{ED}}}{2J+1}\frac{8\pi^2 m_e c\bar{\nu}_0}{3h}\sum_{k,q,\lambda\ \text{even}}(2\lambda+1)\,|A_{kq}|^2\,\frac{1}{2k+1}\,\Xi^2(k,\lambda)\left|\left\langle l^N\psi J\left\|U^{(\lambda)}\right\|l^N\psi' J'\right\rangle\right|^2. \tag{187}$$

Since $\bar{\nu}_0 = \nu_0/c$, we find

$$P_{\text{exp}} = \frac{\chi_{\text{ED}}}{2J+1}\frac{8\pi^2 m_e \nu_0}{3h}\sum_{k,q,\lambda\ \text{even}}(2\lambda+1)\,|A_{kq}|^2\,\frac{1}{2k+1}\,\Xi^2(k,\lambda)\left|\left\langle l^N\psi J\left\|U^{(\lambda)}\right\|l^N\psi' J'\right\rangle\right|^2 \tag{188}$$

[ν_0 in s^{-1}].

This last equation can be rewritten in parameter form:

$$P_{\text{exp}} = \sum_{\lambda=2,4,6} T_\lambda \nu_0 \left| \left\langle l^N \psi J \left\| U^{(\lambda)} \right\| l^N \psi' J' \right\rangle \right|^2 \qquad \text{[Judd 1962, eq. (16)]}, \tag{189}$$

where ν_0 is the frequency of the transition [dim: T^{-1}, units: s^{-1}], and T_λ ($\lambda = 2, 4, 6$) are adjustable parameters [dim: T, units: s]:

$$T_\lambda = \frac{\chi_{\text{ED}}}{2J+1} \frac{8\pi^2 m_e}{3h} (2\lambda+1) \sum_k (2k+1) B_k \Xi^2(k,\lambda) \quad \text{[Judd 1962, eq. (17)]}, \tag{190}$$

$$B_k = \sum_q |A_{kq}|^2 \frac{1}{(2k+1)^2} \qquad \text{[dim: } (\textit{energy}\, L^{-k})^2; \quad \text{Judd 1962, eq. (18)]}, \tag{191}$$

and

$$\Xi(k,\lambda) = 2 \sum_{n'l'} (2l+1)(2l'+1)(-1)^{l+l'} \begin{Bmatrix} 1 & \lambda & k \\ l & l' & l \end{Bmatrix} \begin{pmatrix} l & 1 & l' \\ 0 & 0 & 0 \end{pmatrix} \begin{pmatrix} l' & k & l \\ 0 & 0 & 0 \end{pmatrix} \times \frac{\langle nl | \hat{r} | n'l' \rangle \langle nl | \hat{r}^k | n'l' \rangle}{\Delta(n'l')} \qquad \text{[dim: } L^k\, (\textit{energy})^{-1}\text{]}. \tag{192}$$

Since the reduced matrix elements can be calculated if the free-ion wavefunctions are available, the T_λ parameters are determined semi-empirically from the experimental data. The T_λ parameters introduced by Judd are not the only parameters found in the literature to describe the intensities of transitions between $^{2S+1}L_J$ levels. The best known are the $\mathfrak{I}_\lambda$ parameters introduced by Carnall (see sect. 7.2) and the Ω_λ parameters introduced by Axe (see sect. 7.3). The intensity parameters used to describe transitions between crystal-field levels are discussed in sect. 6. Table 8 summarizes the dimensions and units of the different intensity parameters. Table 9 lists the relations between the intensity parameters.

Table 8
Dimensions and units of intensity parameters

Parameter	Dimensions	Units	Parameter	Dimensions	Units
$B_{\lambda,kq}$	L	cm	$\mathfrak{I}_\lambda$	L	cm
A^λ_{tp}	L	cm	Ω_λ	L^2	cm^2
T_λ	T	s			

Table 9
Relations between intensity parameters[a]

$$B_{\lambda kq} = A_{kq}\Xi(k,\lambda)$$

$$A^{\lambda}_{tp} = -B_{\lambda kq}\frac{2\lambda+1}{(2k+1)^{1/2}} = -A_{kq}\Xi(k,\lambda)\frac{2\lambda+1}{(2k+1)^{1/2}}$$

$$\mathfrak{I}_{\lambda} = (2J+1)\,c\,T_{\lambda}$$

$$\Omega_{\lambda} = \left(\frac{8\pi^2 m_e c}{3h}\chi_{\mathrm{ED}}\right)^{-1}\mathfrak{I}_{\lambda} = \left(1.085\times10^{11}\chi_{\mathrm{ED}}\right)^{-1}\mathfrak{I}_{\lambda}$$

$$\Omega_{\lambda} = \frac{1}{2\lambda+1}\sum_{t,p}\left|A^{\lambda}_{tp}\right|^2 = (2\lambda+1)\sum_{k,q}\left|A_{kq}\right|^2\Xi^2(k,\lambda)\frac{1}{2k+1}$$

$$\Omega_{\lambda} = (2\lambda+1)\sum_{k,q}\left|B_{\lambda kq}\right|^2\frac{1}{2k+1}$$

[a] The symbols are defined in the text.

7.2. *Carnall's $\mathfrak{I}_{\lambda}$ intensity parameters*

In order to make an intercomparison of parameters of different lanthanide ions easier, Carnall et al. (1965) introduced new parameters $\mathfrak{I}_{\lambda}$, writing the oscillator strength as

$$P_{\mathrm{exp}} = \sum_{\lambda=2,4,6}\mathfrak{I}_{\lambda}\frac{\overline{\nu}_0}{2J+1}\left|\left\langle l^N\psi J\left\|U^{(\lambda)}\right\|l^N\psi' J'\right\rangle\right|^2. \tag{193}$$

The parameters $\mathfrak{I}_{\lambda}$ can be related to the parameters T_{λ} by

$$\mathfrak{I}_{\lambda} = (2J+1)\,c\,T_{\lambda} \qquad [\mathrm{dim:\ L}]. \tag{194}$$

This is essentially only an extraction of the $(2J+1)^{-1}$ weighing factor out of the T_{λ} parameters. The factor c (speed of light) is used to convert the frequency ν_0 into the wavenumber $\overline{\nu}_0$ ($\nu_0 = c\overline{\nu}_0$). The dimension of $\mathfrak{I}_{\lambda}$ parameters is L [units: cm]. The $\mathfrak{I}_{\lambda}$ parameters are still used in the literature, especially by workers studying the absorption

spectra of lanthanide complexes in solutions. Sometimes the notation τ_λ is found instead of $\mathfrak{I}_\lambda$ (e.g., Henrie et al. 1976).

7.3. Ω_λ *intensity parameters*

7.3.1. *Definition*

Axe (1963) proposed a slightly modified parametrization scheme:

$$\begin{aligned} P_{\text{exp}} &= \frac{\chi_{\text{ED}}}{2J+1}\frac{8\pi^2 m_e c\bar{\nu}_0}{3h}\sum_{\lambda=2,4,6}\Omega_\lambda\left|\left\langle l^N\psi J\left\|U^{(\lambda)}\right\|l^N\psi' J'\right\rangle\right|^2 \\ &= 1.085\times 10^{11}\frac{\chi_{\text{ED}}}{2J+1}\bar{\nu}_0\sum_{\lambda=2,4,6}\Omega_\lambda\left|\left\langle l^N\psi J\left\|U^{(\lambda)}\right\|l^N\psi' J'\right\rangle\right|^2, \end{aligned} \tag{195}$$

where

$$\Omega_\lambda = (2\lambda+1)\sum_{k,q}|A_{kq}|^2\,\Xi^2(k,\lambda)(2k+1)^{-1} \qquad \text{[dim: L}^2\text{, units: cm}^2\text{]}. \tag{196}$$

The intensity parameters are now Ω_λ ($\lambda=2,4,6$) and they represent the square of the charge displacement due to the induced electric dipole transition. However, when transforming other parameters into the Ω_λ parameters one has to be very careful. One must check the expression for the oscillator or dipole strength to see which factors are included into the parameter and which not. In particular, see whether the factor $(2J+1)^{-1}$ is included or not. Some authors write T_λ when they mean $\mathfrak{I}_\lambda$. The conversion between the Ω_λ and $\mathfrak{I}_\lambda$ parameters is

$$\Omega_\lambda = \left(\frac{8\pi^2 m_e c}{3h}\chi_{\text{ED}}\right)^{-1}\mathfrak{I}_\lambda, \tag{197}$$

or

$$\Omega_\lambda = \left(1.085\times 10^{11}\chi_{\text{ED}}\right)^{-1}\mathfrak{I}_\lambda. \tag{198}$$

Note that the χ_{ED} correction factor is included in the $\mathfrak{I}_\lambda$ parameters, but not in the Ω_λ parameters. The advantage of the Ω_λ parameters is that only one set of parameters is needed for describing both the absorption and emission processes. Since the expression for χ_{ED} is different for both absorption and emission spectra (see sect. 3.5), it is better not to include the correction factor in the parameter. Moreover, with the Ω_λ parameters one has the possibility to take the dispersion into account.

The Ω_λ parameters can be related to the A^λ_{tp} parameters as follows:

$$\Omega_\lambda = \frac{1}{2\lambda+1}\sum_{t,p}\left|A^\lambda_{tp}\right|^2. \tag{199}$$

If the A^λ_{tp} parameters are known, the corresponding Ω_λ can be calculated. The reverse is not true however: knowledge of the Ω_λ parameters is not sufficient for calculating the

A_{tp}^{λ} parameters. This implies that the A_{tp}^{λ} parameters incorporate more information on the structure and on the lanthanide–ligand interaction.

The formalism of Axe can be expressed in terms of the dipole strength:

$$D_{\text{exp}} = \frac{\chi_{\text{ED}}}{2J+1} e^2 \sum_{\lambda=2,4,6} \Omega_\lambda \left| \left\langle l^N \psi J \left\| U^{(\lambda)} \right\| l^N \psi' J' \right\rangle \right|^2 . \tag{200}$$

The quantity

$$D_{\text{ED}} = e^2 \sum_{\lambda=2,4,6} \Omega_\lambda \left| \left\langle l^N \psi J \left\| U^{(\lambda)} \right\| l^N \psi' J' \right\rangle \right|^2 \tag{201}$$

is also known as the line strength (alternative notation: S_{ed}). For convenience, we will abbreviate the notation $\left| \left\langle l^N \psi J \left\| U^{(\lambda)} \right\| l^N \psi' J' \right\rangle \right|^2$ to $U^{(\lambda)}$. The (squares of the) reduced matrix elements have been tabulated for lanthanide ions in aqueous solution by Carnall and coworkers in four consecutive papers: Pr^{3+}, Nd^{3+}, Pm^{3+}, Sm^{3+}, Dy^{3+}, Ho^{3+}, Er^{3+} and Tm^{3+} (Carnall et al. 1968b), Gd^{3+} (Carnall et al. 1968c), Tb^{3+} (Carnall et al. 1968d) and Eu^{3+} (Carnall et al. 1968e). The matrix elements between the ground state and the excited state are listed, so that these matrix elements can be used for calculated dipole strengths extracted from absorption spectra. For Eu^{3+}, Carnall et al. (1968e) also list matrix elements for transitions starting from the $^7F_1$ state. Since these matrix elements can be considered in a first approximation as constants for a given lanthanide ion, they can be used for lanthanide ions in other media than water. The actual values of the matrix elements depends on the calculation scheme, but the differences are not significant. Values for the matrix elements in the intermediate coupling scheme for lanthanide ions doped into LaF_3 have been given by Carnall et al. (1977). This list is more extensive than the list of the matrix elements in aqueous solution in the sense that it can also be used for transitions in which the ground state is not necessarily involved (e.g. in luminescence spectra). Matrix elements for Pr^{3+} can be found in Weber (1968), for Gd^{3+} in Detrio (1971), for Ho^{3+} in Weber et al. (1972), and for Er^{3+} in Weber (1967b). A full set of reduced matrix elements has also been listed for Nd^{3+} in $Lu_3Sc_2Ga_3O_{12}$ by Kaminskii et al. (1994c) and for Er^{3+} in $YAlO_3$ by Kaminskii et al. (1995b).

The fact that the χ_{ED} factor is not absorbed in the Ω_λ intensity parameters has the disadvantage that the dependence of the spectral intensities on the refractive index is not reflected in these parameters. A higher refractive index results in more intense transitions. This is especially true for hypersensitive transitions (see sect. 8). Because of this disadvantage, one has to be cautious when comparing Ω_λ intensity parameters (see also sect. 9). Two systems with the same parameter set show different oscillator strengths if there is a difference in the refractive index of the media.

7.3.2. *Determination of Ω_λ intensity parameters*

The Ω_λ parameters for induced electric dipole transitions can be determined by writing down for each transition an expression of the form

$$D_{\text{exp}} = \frac{\chi_{\text{ED}}}{2J+1} e^2 \left(\Omega_2 U^{(2)} + \Omega_4 U^{(4)} + \Omega_6 U^{(6)} \right) \qquad [D \text{ in esu}^2\,\text{cm}^2]. \tag{202}$$

There are several numerical methods to determine the Ω_λ parameters; below we describe, as examples, the *standard least-squares method* and the *chi-square method.*

7.3.2.1. *Standard least-squares method.* The standard least-squares method minimizes the absolute differences between the experimental and the calculated values. The least-squares method is simpler than the chi-square method, but has the disadvantage that a small discrepancy in a large experimental value has the same influence as a large error in a small experimental value. Therefore the Ω_λ parameters depend largely on the relative magnitude of the oscillator (or dipole) strengths of the transitions used in the fit. However, the parameter set should be able to predict both small and large oscillator (or dipole) strengths.

We define:

$$\Delta^{\exp} := \frac{(2J+1)D_{\exp}}{e^2 \cdot \chi_{\mathrm{ED}}}; \tag{203}$$

then,

$$\Delta^{\exp} = \Omega_2 U^{(2)} + \Omega_4 U^{(4)} + \Omega_6 U^{(6)}. \tag{204}$$

It is possible to write down such an equation for each spectral transition, resulting in a system of n equations for n transitions:

$$\begin{aligned}
\Delta_1^{\exp} &= \Omega_2 U_1^{(2)} + \Omega_4 U_1^{(4)} + \Omega_6 U_1^{(6)}, \\
\Delta_2^{\exp} &= \Omega_2 U_2^{(2)} + \Omega_4 U_2^{(4)} + \Omega_6 U_2^{(6)}, \\
&\vdots \\
\Delta_n^{\exp} &= \Omega_2 U_n^{(2)} + \Omega_4 U_n^{(4)} + \Omega_6 U_n^{(6)}.
\end{aligned} \tag{205}$$

We want to find a good estimate for the parameter set $(\Omega_2', \Omega_4', \Omega_6')$. The set of equations (205) is of the form

$$\begin{aligned}
y_1 &= a_1 x_{11} + a_2 x_{12} + \cdots + a_k x_{1k}, \\
y_2 &= a_1 x_{21} + a_2 x_{22} + \cdots + a_k x_{2k}, \\
&\vdots \\
y_n &= a_1 x_{n1} + a_2 x_{n2} + \cdots + a_k x_{nk}.
\end{aligned} \tag{206}$$

The y_i are the values of the observations, the x_{ik} are coefficients and the a_i are unknowns (the parameters). The observational model is a general linear model, because the dependent variable y_i is described as a function of several independent variables x_{ik}. The function is a linear function (there are no terms of a degree higher than 1). The matrix method is used to solve the problem. This method is described in every good textbook

dealing with statistics. The system of eq. (206) can be written in terms of the response random vector, containing the response values of the n observations:

$$\boldsymbol{Y} = \begin{pmatrix} y_1 \\ y_2 \\ \vdots \\ y_n \end{pmatrix}, \tag{207}$$

the model parameter vector:

$$\boldsymbol{a} = \begin{pmatrix} a_1 \\ a_2 \\ \vdots \\ a_n \end{pmatrix}, \tag{208}$$

the vector of errors associated with the n observations:

$$\boldsymbol{E} = \begin{pmatrix} \varepsilon_1 \\ \varepsilon_2 \\ \vdots \\ \varepsilon_n \end{pmatrix}, \tag{209}$$

and the $n \times k$ design matrix:

$$X = \begin{pmatrix} x_{11} & x_{12} & \cdots & x_{1k} \\ x_{21} & x_{22} & \cdots & x_{2k} \\ \vdots & \vdots & \ddots & \vdots \\ x_{n1} & x_{n2} & \cdots & x_{nk} \end{pmatrix}. \tag{210}$$

The matrix representation for any set of observations $y_1, y_2, \ldots, y_n$ becomes

$$\boldsymbol{Y} = \boldsymbol{X}\boldsymbol{a} + \boldsymbol{E}. \tag{211}$$

Let the matrix

$$\hat{\boldsymbol{a}} = \begin{pmatrix} \hat{a}_1 \\ \hat{a}_2 \\ \vdots \\ \hat{a}_k \end{pmatrix} \tag{212}$$

represent the matrix of the least-squares estimates for the parameters of the general linear model. This matrix can be calculated as follows:

$$\hat{\boldsymbol{a}} = \left(\boldsymbol{X}^{\mathrm{T}}\boldsymbol{X}\right)^{-1} \boldsymbol{X}^{\mathrm{T}}\boldsymbol{Y}, \tag{213}$$

where $\boldsymbol{X}^{\mathrm{T}}$ is the transpose of $\boldsymbol{X}$. The matrix $\boldsymbol{X}$ is a $n \times k$ matrix, $\boldsymbol{X}^{\mathrm{T}}$ is a $k \times n$ matrix, and $\boldsymbol{X}^{\mathrm{T}}\boldsymbol{X}$ is a $k \times k$ matrix, with $n \geqslant k$. The matrix solution gives the set of parameter

estimates $\hat{a}_1, \hat{a}_2, \ldots, \hat{a}_k$ in the general linear model that minimizes $\sum_i (y_i - \hat{y}_i)^2$ for the data collected.

After the parameter estimates $\left(\hat{\Omega}_2, \hat{\Omega}_4, \hat{\Omega}_6\right)$ have been obtained, D^i_{ED} can be calculated:

$$D^i_{\mathrm{ED}} = e^2 \left(\hat{\Omega}_2 U^{(2)}_i + \hat{\Omega}_4 U^{(4)}_i + \hat{\Omega}_6 U^{(6)}_i\right). \tag{214}$$

The quantity $[\chi_{\mathrm{ED}}/(2J+1)]D^i_{\mathrm{ED}}$ is sometimes denoted as D^i_{calc}, and can be compared directly with the experimental dipole strength D^i_{exp} of transition i. The root mean square deviation error RMS is a measure for the goodness of the fit:

$$\mathrm{RMS} = \left[\frac{\text{sum of squares of deviations}}{\text{number of observations} - \text{number of parameters}}\right]^{1/2}. \tag{215}$$

For the dipole strengths, the RMS is given by

$$\mathrm{RMS} = \left[\frac{\sum_i \left(D^i_{\mathrm{exp}} - D^i_{\mathrm{calc}}\right)^2}{N-3}\right]^{1/2}, \tag{216}$$

where N is the number of transitions used in the fitting procedure. The number of parameters is three (Ω_2, Ω_4 and Ω_6). The ratio $D_{\mathrm{calc}}/D_{\mathrm{exp}}$ also gives useful information about the reliability of the calculations. The error on a parameter is given by the product of the square root of the respective diagonal matrix element of the matrix $\left(\boldsymbol{X}^{\mathrm{T}}\boldsymbol{X}\right)^{-1}$ and the RMS for the deviations between Δ_i^{exp} and Δ_i^{calc}.

7.3.2.2. *Chi-square method.* If one wants to weigh each value of the dipole strength by its own uncertainty, the *chi-square method* has to be chosen as the minimizing quantity (see, e.g., Caird et al. 1981, Seeber et al. 1995, Goldner and Auzel 1996). This method minimizes the relative differences between the experimental and the calculated values rather than the absolute differences. The uncertainty in the measured intensity of each transition is often difficult to estimate. Goldner and Auzel (1996) take a constant fraction of the experimental oscillator strength for the uncertainty. The RMS (eq. 216) of this method is independent of the number or the magnitude of the included transitions. The chi-square fitting method is analogous to the matrix calculation presented for the standard least-squares method, except that the design matrix $\boldsymbol{X}$ is now given by

$$\boldsymbol{X} = \begin{pmatrix} \frac{x_{11}}{\sigma_1} & \frac{x_{12}}{\sigma_1} & \cdots & \frac{x_{1k}}{\sigma_1} \\ \frac{x_{21}}{\sigma_2} & \frac{x_{22}}{\sigma_2} & \cdots & \frac{x_{2k}}{\sigma_2} \\ \vdots & \vdots & \ddots & \vdots \\ \frac{x_{n1}}{\sigma_n} & \frac{x_{n2}}{\sigma_n} & \cdots & \frac{x_{nk}}{\sigma_n} \end{pmatrix}, \tag{217}$$

and the vector $\boldsymbol{Y}$ with the observations is now given by

$$\boldsymbol{Y} = \begin{pmatrix} \frac{y_1}{\sigma_1} \\ \frac{y_2}{\sigma_2} \\ \vdots \\ \frac{y_n}{\sigma_n} \end{pmatrix}. \tag{218}$$

The fit is applied to the quantities $D^i_{\text{exp}}/\sigma_i$, where σ_i is the uncertainty in the experimental dipole strength D^i_{exp}. The error of a parameter is given by the square root of the respective diagonal matrix element of the matrix $\left(\boldsymbol{X}^{\text{T}}\boldsymbol{X}\right)^{-1}$.

7.3.3. *Additivity of intensity parameters*

The additivity of Ω_λ in eq. (202) has two major advantages. First of all, in the presence of several non-equivalent sites in the host matrix one obtains an average value for each of the Ω_λ parameters. The Ω_λ parametrization can therefore be used also for highly disordered systems, like glasses. Only when site selective spectroscopy is used are different Ω_λ values found for each site (Rodríguez et al. 1995). Secondly, in the case of overlapping bands, the matrix elements of each of the transitions contributing to the overlapping band can be summed. The complex band is integrated as a whole. For instance, if transition A and transition B overlap, one finds

$$D_{\text{ED}}(A+B) = e^2 \sum_{\lambda=2,4,6} \Omega_\lambda \left[U_A^{(\lambda)} + U_B^{(\lambda)}\right]. \tag{219}$$

7.3.4. *Mixed ED–MD transitions*

If the transition has partial MD character, the MD contribution D_{MD} has to be calculated first. The Ω_λ parameters are not fitted against D_{exp}, but against D^0_{exp}:

$$D^0_{\text{exp}} = D_{\text{exp}} - \frac{1}{2J+1}\chi_{\text{MD}} D_{\text{MD}}. \tag{220}$$

It is assumed that the experimental and calculated magnetic dipole strengths are equal.

7.4. *Successes and failures of the Judd–Ofelt theory*

The Ω_λ parametrization describes the intensity between J-levels. Each J-level is considered as $2J+1$-fold degenerate. This implies also that each of the M-levels of the ground state has an equal thermal population. If the crystal-field splitting of the ground state is not too large ($<500\,\text{cm}^{-1}$), the approximation is a good one at room temperature.

Even for larger splittings, the assumption is fairly good, since the crystal-field levels are often a linear combination of different M-levels (M-levels within one μ-matrix). However, the Judd–Ofelt theory with Ω_λ parameters cannot be used for low-temperature absorption spectra, especially not at 4.2 K, a temperature at which (in most cases) only the lowest crystal-field level of the ground state is populated. For europium, low-temperature spectra can be treated by the Judd–Ofelt theory, since the $^7F_0$ ground state is non-degenerate. At 77 K and lower, only the ground state is populated, while at higher temperatures the $^7F_1$ level has also a non-negligible thermal population (at room temperature ~35% of the total population). One can deal with this difference in thermal population by using the $X_A(T)$ fractional thermal population factor (as described in sect. 3.8).

An extensive list of Ω_λ intensity parameter sets for different (lanthanide ion)–(host matrix) systems is given in tables 10–21. Although we do not claim completeness, we have tried to compose a list which covers a broad range of different hosts. The data are covering lanthanide ions in solutions, glasses, polycrystalline samples and single crystals. The parameter sets have been classified within one lanthanide ion according to increasing values of Ω_2.

Over the years, the Judd–Ofelt theory has been proved to be quite successful for the intensity analysis of the trivalent lanthanide ions. A lot of pioneering work concerning the determination of experimental intensities of the f–f transitions over the lanthanide series and the systematic intensity parametrization has been done by Carnall and coworkers (Carnall et al. 1965, 1968a, see also Carnall 1979). They studied the spectra of the trivalent lanthanide ions in aqueous solution (diluted $HClO_4$). In order to extend the range of measurements to the near-infrared, spectra were also recorded in diluted $DClO_4$. The intensity of the transitions between J-multiplets in the spectrum can be rationalized in terms of only three parameters Ω_λ. One can make predictions about the intensity of transitions which cannot be observed experimentally (e.g. infrared 4f–4f transitions in aqueous solution). The parameter sets are a useful tool to compare the f–f intensity properties of different lanthanide systems. They may be used to derive relationships between spectral and structural properties for different kinds of lanthanide complexes.

For Pr^{3+}, the Judd–Ofelt theory does not seem to work well (Goldner and Auzel 1996). Difficulties are experienced if one tries to fit both the $^3F_3, ^3F_4 \leftarrow {}^3H_4$ and the $^3P_{2,1,0}, ^1I_6 \leftarrow {}^3H_4$ transition groups with the same set of Ω_λ intensity parameters (Carnall et al. 1968a). Instead of determining a parameter set with the inclusion of all transitions, the $^3F_3, ^3F_4 \leftarrow {}^3H_4$ transitions can be excluded. Of course, agreement will then be worse between the experimental and calculated dipole strengths for the latter transitions. Other authors prefer to exclude the $^3P_2 \leftarrow {}^3H_4$ transition (e.g., Eyal et al. 1985, Quimby and Miniscalco 1994, Seeber et al. 1995). It is also found that the Ω_6 parameter is appreciably larger than the value extrapolated from the other lanthanide ions in the same matrix (Peacock 1975). The problems with Pr^{3+} are due to the fact that assumptions in the theory are not valid in the proper case of Pr^{3+} (Carnall et al. 1968a, Peacock 1975). First of all, it has been assumed that the configurations which are mixed into the $4f^N$ configuration are degenerate. Only the barycenters of these excited configurations are considered. The $4f^15d^1$ configuration of Pr^{3+} starts about 45 000 cm^{-1} above the ground state, while those

Table 10
Phenomenological intensity parameters Ω_λ for Pr^{3+} in various host matrices; the host matrices are classified according to increasing values of Ω_2

Matrix	Ω_2 (10^{-20} cm^2)	Ω_4 (10^{-20} cm^2)	Ω_6 (10^{-20} cm^2)	Reference(s)
$Y_3Al_5O_{12}:Pr^{3+}$ (crystal)	−1.34	12.20	8.27	Malinowski et al. (1990)
ZBLA:Pr^{3+} glass	−1.0±4.8	4.4±2.2	7.8±2.1	Eyal et al. (1985)
ZBLA:Pr^{3+} glass	−0.76	4.91	8.54	McDougall et al. (1994a)
ZBLALi:Pr^{3+} glass	−0.65	5.54	8.95	McDougall et al. (1994c)
Pr^{3+} in Li_2CO_3–H_3BO_3 glass	−0.461	5.854	7.477	Devi and Jayasankar (1996b)
ZBLAN:Pr^{3+} glass	−0.37	5.36	0.54	McDougall et al. (1994c)
$30InF_3$–$30BaF_2$–$10ThF_4$–$9ZnF_2$–$20KF$–$1PrF_3$ glass	−0.37	13.19	3.61	Amaranath et al. (1990b); Amaranath and Buddhudu (1992)
$30InF_3$–$30BaF_2$–$10ThF_4$–$9ZnF_2$–$10NaF$–$10KF$–$1PrF_3$ glass	−0.11	14.56	4.41	Amaranath et al. (1990b) Amaranath and Buddhudu (1992)
Pr^{3+} in $30CaO$–$70B_2O_3$ glass	−0.10	4.75	5.12	Takebe et al. (1995)
$LiYF_4:Pr^{3+}$ (crystal)	0	8.07	7.32	Adam et al. (1985)
Pr^{3+} in $33.3ZnO$–$66.6TeO_2$ glass	0	9.96	21.47	Kanoun et al. (1990)
Pr^{3+} in PbO–PbF_2 glass	0.02	7.88	4.81	Nachimuthu and Jagannathan (1995a)
Pr^{3+} in ZBLAN glass	0.04	4.99	13.06	Binnemans et al. (1997b)
Pr^{3+} in $30Li_2O$–$30B_2O_3$ glass	0.10	4.71	5.28	Takebe et al. (1995)
$LaF_3:Pr^{3+}$ (crystal)	0.12±0.91	1.77±0.81	4.78±0.52	Krupke (1966)
Pr^{3+} in $52HfF_4$–$18BaF_2$–$3LaF_3$–$2AlF_3$–$25CsBr$ glass	0.212	5.82	6.68	Cases and Chamarro (1991)
ZBLA:Pr^{3+} glass	0.24±0.97	4.51±0.45	5.37±0.44	Eyal et al. (1985)
Pr^{3+} in lithium sodium sulphate glass	0.27	12.54	9.01	Ratnakaram (1994)
$KPrP_4O_{12}$ crystal	0.34	4.36	1.81	Kornienko et al. (1990)
Pr^{3+} in $SrCO_3$–Li_2CO_3–H_3BO_3 glass	0.357	5.091	6.335	Devi and Jayasankar (1996b)
ZBLYAN:Pr^{3+} glass	0.47	3.73	4.09	Ohishi et al. (1992)
Pr^{3+} in $30BaO$–$70B_2O_3$ glass	0.50	4.98	5.00	Takebe et al. (1995)
InF_3–BaF_2–SrF_2–PbF_2–ZnF_2–PrF_3 glass	0.523	3.82	4.92	Ohishi et al. (1992)
InF_3–BaF_2–SrF_2–CdF_2–PrF_3 glass	0.601	4.18	5.07	Ohishi et al. (1992)

continued on next page

Table 10, *continued*

Matrix	Ω_2 (10^{-20} cm^2)	Ω_4 (10^{-20} cm^2)	Ω_6 (10^{-20} cm^2)	Reference(s)
$35ZnF_2$–$15CdF_2$–$25BaF_2$–$12LiF$–$7AlF_3$–$5.5LaF_3$–$0.5PrF_3$ glass	0.72	4.80	7.93	Buñuel et al. (1992)
BIGaZLuTZrPb:Pr^{3+} glass	0.73	4.74	4.97	Adam et al. (1991)
Pr^{3+} in Li_2O–$2B_2O_3$ glass	0.77±1.38	3.84±0.58	3.58±0.61	Hormadaly and Reisfeld (1979)
Pr^{3+} in Na_2O–$2B_2O_3$ glass	0.77±1.45	4.13±0.62	3.07±0.65	Hormadaly and Reisfeld (1979)
ZBLAN:Pr^{3+} glass	0.84	4.79	9.13	Wetenkamp et al. (1992)
Pr^{3+} in $20ZnF_2$–$20SrF_2$–$20BaF_2$–$40InF_3$ glass	0.85	4.13	12.33	Arauzo et al. (1994)
Pr^{3+} in ZBLAN glass	0.94	6.54	3.84	Binnemans et al. (1997b)
Pr^{3+} in potassium sodium sulphate glass	0.97	3.32	3.15	Ratnakaram (1994)
Pr^{3+} in $30Na_2O$–$70B_2O_3$ glass	0.98	4.76	4.86	Takebe et al. (1995)
$48(NaPO_3)_6$–$20BaCl_2$–$10ZnCl_2$–$10LiCl$–$10NaCl$–$2PrCl_3$ glass	1.056	0.965	0.912	Subramanyam Naidu and Buddhudu (1992b)
$30InF_3$–$30BaF_2$–$10ThF_4$–$9ZnF_2$–$20NaF$–$1PrF_3$ glass	1.11	13.98	3.44	Amaranath et al. (1990b) Amaranath and Buddhudu (1992)
Pr^{3+} in magnesium sodium sulphate glass	1.16	5.60	3.62	Ratnakaram (1994)
$48(NaPO_3)_6$–$20BaCl_2$–$10ZnCl_2$–$10KCl$–$10LiCl$–$2PrCl_3$ glass	1.233	1.684	0.473	Subramanyam Naidu and Buddhudu (1992b)
$48(NaPO_3)_6$–$20BaCl_2$–$10ZnCl_2$–$20NaCl$–$2PrCl_3$ glass	1.317	2.082	0.714	Subramanyam Naidu and Buddhudu (1992b)
AlF_3–SrF_2–CaF_2–MgF_2–P_2O_5 glass (3 mol% PrF_3)	1.4±2.7	4.2±1.4	5.2±1.1	Seeber et al. (1995)
ZBLAN:Pr^{3+} glass	1.431	4.221	4.872	Ohishi et al. (1991)
ZBLAN:Pr^{3+} glass	1.46	4.89	4.85	Remillieux et al. (1996)
$48(NaPO_3)_6$–$20BaCl_2$–$10ZnCl_2$–$20KCl$–$2PrCl_3$ glass	1.549	1.344	1.034	Subramanyam Naidu and Buddhudu (1992b)
$48(NaPO_3)_6$–$20BaCl_2$–$10ZnCl_2$–$10NaCl$–$10KCl$–$2PrCl_3$ glass	1.557	1.044	1.102	Subramanyam Naidu and Buddhudu (1992b)
Pr^{3+} in $60ZrF_4$–$30BaF_2$–$7LaF_3$ glass	1.56	5.81	5.45	Hirao et al. (1994)
ZBLAN:Pr^{3+} glass	1.60	5.06	4.79	Adam et al. (1991)
Pr^{3+} in $MgCO_3$–Li_2CO_3–H_3BO_3 glass	1.796	3.575	6.915	Devi and Jayasankar (1996b)
Pr^{3+} in AlF_3–SrF_2–CaF_2–MgF_2–P_2O_5 glass (10 mol% PrF_3)	1.8±2.4	4.7±1.3	5.2±1.4	Seeber et al. (1995)
$LiPrP_4O_{12}$ (crystal)	1.82	2.83	6.54	Mazurak et al. (1984)
$YAlO_3$:Pr^{3+} (crystal)	2.00	6.00	7.00	Reisfeld (1976)

continued on next page

Table 10, *continued*

Matrix	Ω_2 (10^{-20} cm^2)	Ω_4 (10^{-20} cm^2)	Ω_6 (10^{-20} cm^2)	Reference(s)
Pr^{3+} in $30Na_2O$–$60P_2O_5$–$10Al_2O_3$ glass	2.06	6.41	5.61	Takebe et al. (1995)
Pr^{3+} in K_2O–$2B_2O_3$ glass	2.14±0.94	2.91±0.41	1.67±0.43	Hormadaly and Reisfeld (1979)
$30InF_3$–$30BaF_2$–$10ThF_4$–$9ZnF_2$–$10KF$–$10LiF$–$1PrF_3$ glass	2.20	17.27	6.93	Amaranath et al. (1990b) Amaranath and Buddhudu (1992)
Pr^{3+} in $30K_2O$–$70B_2O_3$ glass	2.33	4.65	3.84	Takebe et al. (1995)
Pr^{3+} in $30Li_2O$–$60P_2O_5$–$10Al_2O_3$ glass	2.41	5.89	5.60	Takebe et al. (1995)
ZBLAN:Pr^{3+} glass	2.5±3.2	5.4±1.8	6.0±1.2	Seeber et al. (1995)
Pr^{3+} in cadmium sodium sulphate glass	2.57	3.00	3.57	Ratnakaram (1994)
Pr^{3+} in $35ZnO$–$65TeO_2$ glass	2.59±1.97	7.26±0.84	5.45±0.90	Hormadaly and Reisfeld (1979)
Pr^{3+} in $20Li_2O$–$20CaO$–$60SiO_2$ glass	2.69	6.01	4.70	Takebe et al. (1995)
AlF_3–SrF_2–CaF_2–MgF_2–P_2O_5 glass (20 mol% PrF_3)	2.7±2.9	5.3±1.6	5.0±1.5	Seeber et al. (1995)
Pr^{3+} in $20Na_2O$–$80TeO_2$ glass	2.83±1.86	6.50±0.79	4.60±0.83	Hormadaly and Reisfeld (1979)
ZBLAN:Pr^{3+} glass	2.9±1.4	6.4±1.8	5.5±0.7	Simons (1995)
Pr^{3+} in saturated $MgCl_2$ solution	2.95	3.48	2.43	Lakshman and Buddhudu (1982)
Pr^{3+} in $BaCO_3$–Li_2CO_3–H_3BO_3 glass	2.991	6.713	11.868	Devi and Jayasankar (1996b)
Pr^{3+} in fluoroindate glass	3.2±3.4	4.5±1.1	6.5±1.4	Seeber et al. (1995)
Pr^{3+} in zinc sodium sulphate glass	3.44	15.19	10.22	Ratnakaram (1994)
Pr^{3+} in $30BaPO_3$–$60P_2O_5$–$10Al_2O_3$ glass	3.53	5.66	4.77	Takebe et al. (1995)
$75NaPO_3$–$24CaF_2$–$1PrF_3$ glass	3.67±3.58	5.75±3.93	5.59±1.45	Binnemans et al. (1997c)
Pr^{3+} in $20Na_2O$–$20CaO$–$60SiO_2$ glass	3.91	5.72	3.82	Takebe et al. (1995)
$48(NaPO_3)_6$–$20BaCl_2$–$10ZnCl_2$–$20LiCl$–$2PrCl_3$ glass	4.382	1.867	1.281	Subramanyam Naidu and Buddhudu (1992b)
Pr^{3+} in $40Na_2O$–$60SiO_2$ glass	4.81	4.71	3.01	Takebe et al. (1995)
Pr^{3+} in BaO–TeO_2 glass	4.95±2.40	6.46±1.09	5.44±1.09	Hormadaly and Reisfeld (1979)
Pr^{3+} in $20K_2O$–$20CaO$–$60SiO_2$ glass	5.16	5.21	2.50	Takebe et al. (1995)
Pr^{3+} in $30CaO$–$60P_2O_5$–$10Al_2O_3$ glass	5.28	5.20	4.34	Takebe et al. (1995)
$30InF_3$–$30BaF_2$–$10ThF_4$–$9ZnF_2$–$20LiF$–$1PrF_3$ glass	5.64	13.32	4.15	Amaranath et al. (1990b) Amaranath and Buddhudu (1992)

continued on next page

Table 10, *continued*

Matrix	Ω_2 (10^{-20} cm^2)	Ω_4 (10^{-20} cm^2)	Ω_6 (10^{-20} cm^2)	Reference(s)
ZBLAK:Pr^{3+} glass	6.10	0.36	6.57	McDougall et al. (1994c)
Pr^{3+} in saturated $CaCl_2$ solution	6.11	1.30	3.85	Lakshman and Buddhudu (1982)
Pr^{3+} in $30MgO–60P_2O_5–10Al_2O_3$ glass	6.44	4.52	3.95	Takebe et al. (1995)
ZBLA:Pr^{3+} glass	6.68	5.05	6.92	Adam and Sibley (1985)
$La_3Ga_5SiO_{14}:Pr^{3+}$ (crystal)	6.89	2.76	6.24	Kaminskii et al. (1990)
Pr^{3+} in saturated NH_4Cl solution	7.04	2.57	2.78	Lakshman and Buddhudu (1982)
Pr^{3+} in saturated $CdCl_2$ solution	7.12	3.33	3.05	Lakshman and Buddhudu (1982)
Pr^{3+} in $70Ga_2S_3–30La_2S_3$ glass	7.3±0.9	6.2±0.6	3.9±0.2	Hewak et al. (1994a)
Pr^{3+} in $CaCO_3–Li_2CO_3–H_3BO_3$ glass	7.361	1.031	12.105	Devi and Jayasankar (1996b)
Pr^{3+} in $LiNO_3–KNO_3$ melt	8.63±0.4	6.30±1.1	6.48±1.5	Carnall et al. (1978)
$PrCl_3$ in water	9.25	3.56	2.18	Lakshman and Buddhudu (1982)
Pr(benzoylacetonate)$_3$ in DMF	9.42	12.83	20.81	Tandon and Mehta (1970)
Pr(acetylacetonate)$_3$ in DMF	9.57	12.90	12.98	Tandon and Mehta (1970)
Pr^{3+} in $80GeS_2–20Ga_2S_3$ glass	9.6±3.9	15.4±4.7	4.4±1.9	Simons et al. (1995)
Pr^{3+} in $Zn(PO_3)_2$ glass	10.0	2.0	7.0	Ingeletto et al. (1991)
Pr^{3+} in $80GeS_3–20Ga_2S_3$ glass	11.6±2.2	5.6±2.6	6.0±1.1	Simons (1995)
Pr^{3+} in $91GeS_{2.5}–9Ga_2S_3$ glass	12.8	4.3	7.7	Wei et al. (1995)
Pr^{3+} in $GeS_2–20Ga_2S_3$ glass	13.2±3.4	8.6±4.1	6.1±1.7	Simons (1995)
Pr^{3+} in $Pb(PO_3)_2$ glass	14.8	9.7	26.9	Ingeletto et al. (1991)
$Y_2O_3:Pr^{3+}$ (crystal)	17.21±0.162	19.80±0.14	4.88±0.09	Krupke (1966)
Pr(thenoyltrifluoroacetonate)$_3$ in DMF	23.12	16.09	22.69	Tandon and Mehta (1970)
$K_7[PrW_{10}O_{35}]$	26.97±60.28	5.10±2.09	36.94±2.47	Peacock (1973)
Pr^{3+} (aquo)	28.0±72	5.89±2.50	32.2±3.0	Carnall et al. (1983)
Pr(α-picolinate) in water	46±72	7.0±2.5	39.5±3.0	Bukietynska and Choppin (1970)
Pr(acetylacetonate)$_3$ in methanol	51.79	14.38	18.35	Tandon and Mehta (1970)

continued on next page

Table 10, *continued*

Matrix	Ω_2 (10^{-20} cm^2)	Ω_4 (10^{-20} cm^2)	Ω_6 (10^{-20} cm^2)	Reference(s)
$50(NaPO_3)_6$–$18BaF_2$–$10ZnF_2$–$20KF$–$2PrF_3$ glass	57	1.23	2.81	Ranga Reddy et al. (1991)
Pr(benzoylacetonate)$_3$ in methanol	62.60	15.16	20.61	Tandon and Mehta (1970)
Pr(thenoyltrifluoroacetonate)$_3$ in methanol	70.54	13.22	22.79	Tandon and Mehta (1970)
$50(NaPO_3)_6$–$18BaF_2$–$10ZnF_2$–$20NaF$–$2PrF_3$ glass	88	2.16	3.74	Ranga Reddy et al. (1991)
$50(NaPO_3)_6$–$18BaF_2$–$10ZnF_2$–$10LiF$–$10NaF$–$2PrF_3$ glass	97	1.73	4.03	Ranga Reddy et al. (1991)
$50(NaPO_3)_6$–$18BaF_2$–$10ZnF_2$–$20LiF$–$2PrF_3$ glass	117	1.91	4.19	Ranga Reddy et al. (1991)
$Sr_xBa_{1-x}Nb_2O_6$:Pr^{3+} (crystal)	145.7310	0.68210	1.58810	Zhang et al. (1994)
$50(NaPO_3)_6$–$18BaF_2$–$10ZnF_2$–$10NaF$–$10KF$–$2PrF_3$ glass	160	2.30	2.94	Ranga Reddy et al. (1991)
$50(NaPO_3)_6$–$18BaF_2$–$10ZnF_2$–$10LiF$–$10KF$–$2PrF_3$ glass	188	2.23	4.05	Ranga Reddy et al. (1991)

Table 11
Phenomenological intensity parameters Ω_λ for Nd^{3+} in various host matrices; the host matrices are classified according to increasing values of Ω_2

Matrix	Ω_2 (10^{-20} cm^2)	Ω_4 (10^{-20} cm^2)	Ω_6 (10^{-20} cm^2)	Reference(s)
$Lu_3Sc_2Ga_3O_{12}$:Nd^{3+} (crystal)	0.082	2.844	3.137	Kaminskii et al. (1994c)
$58BeF_2$–$40KF$–$2NdF_3$ glass	0.1±0.2	2.7±0.3	3.2±0.1	Stokowski et al. (1981b)
$47BeF_2$–$10AlF_3$–$14CaF_2$–$27LiF$–$2NdF_3$ glass	0.1±0.3	3.7±0.5	3.8±0.2	Stokowski et al. (1981b)
$47BeF_2$–$10AlF_3$–$14CaF_2$–$27NaF$–$2NdF_3$ glass	0.1±0.3	3.7±0.4	4.3±0.2	Stokowski et al. (1981b)
$58BeF_2$–$20KF$–$20CsF$–$2NdF_3$ glass	0.1±0.2	4.0±0.3	5.0±0.1	Stokowski et al. (1981b)
$58.59BeF_2$–$40.41KF$–$1NdF_3$ glass	0.1±0.2	4.4±0.4	5.3±0.2	Stokowski et al. (1981b)
$47BeF_2$–$27KF$–$14CaF_2$–$10AlF_3$–$2NdF_3$ glass	0.2±0.3	3.9±0.4	4.6±0.2	Stokowski et al. (1981b)
$58BeF_2$–$20KF$–$20LiF$–$2NdF_3$ glass	0.2±0.2	3.9±0.3	5.1±0.1	Stokowski et al. (1981b)
$Y_3Al_5O_{12}$:Nd^{3+} (crystal)	0.2	2.7	5.0	Krupke (1971)
$Y_3Sc_2Al_3O_{12}$:Nd^{3+} (crystal)	0.23	2.87	4.78	Allik et al. (1990)
SrF_2:Nd^{3+} (crystal)	0.24	1.24	1.72	Payne et al. (1991)
BaF_2:Nd^{3+} (crystal)	0.25	0.41	0.43	Payne et al. (1991)
$LiYF_4$:Nd^{3+} (crystal)	0.25	4.09	4.83	Kaminskii et al. (1994b)
$58BeF_2$–$20KF$–$20KCl$–$2NdF_3$ glass	0.3±0.2	3.0±0.3	3.7±0.1	Stokowski et al. (1981b)
$49BeF_2$–$30KF$–$14CaF_2$–$5AlF_3$–$2NdF_3$ glass	0.3±0.2	3.4±0.3	4.3±0.1	Stokowski et al. (1981b)
LaF_3:Nd^{3+} (crystal)	0.35	2.6	2.5	Krupke (1966)
$LiYF_4$:Nd^{3+} (crystal)	0.362	4.02	4.84	Ryan and R. Beach (1992)
YAG:Nd^{3+} (crystal)	0.37	2.29	5.97	Kaminskii and Li (1974)
$46BeF_2$–$20NaF$–$2.5MgF_2$–$10CaF_2$–$20AlF_3$–$1.5NdF_3$ glass	0.4±0.2	2.8±0.3	3.5±0.1	Stokowski et al. (1981b)
$47BeF_2$–$10AlF_3$–$14CaF_2$–$27RbF$–$2NdF_3$ glass	0.4±0.2	3.9±0.4	4.8±0.2	Stokowski et al. (1981b)
$NdGaO_3$ (crystal)	0.46	3.6	2.6	Orera et al. (1995)
(CaF_2,LaF_3):Nd^{3+} (crystal)	0.48	2.53	3.74	Payne et al. (1991)
$49BeF_2$–$15KF$–$20AlF_3$–$14CaF_2$–$2NdF_3$ glass	0.5±0.2	3.1±0.3	4.0±0.1	Stokowski et al. (1981b)
$47BeF_2$–$10AlF_3$–$27KF$–$14MgF_2$–$2NdF_3$ glass	0.5±0.2	3.5±0.3	4.6±0.2	Stokowski et al. (1981b)
$45BeF_2$–$20AlF_3$–$15KF$–$18SrF_2$–$2NdF_3$ glass	0.5±0.2	3.5±0.3	4.6±0.2	Stokowski et al. (1981b)
$45AlF_3$–$34CaF_2$–$20BaF_2$–$1NdF_3$ glass	0.6±0.3	3.7±0.5	4.1±0.1	Tesar et al. (1992)

continued on next page

Table 11, *continued*

Matrix	Ω_2 (10^{-20} cm^2)	Ω_4 (10^{-20} cm^2)	Ω_6 (10^{-20} cm^2)	Reference(s)
Y_2SiO_5:Nd^{3+} (crystal)	0.67	6.19	2.71	Tkachuk et al. (1986)
$49PbF_2$–$25MnF_2$–$25GaF_3$–$1NdF_3$ glass	0.7±0.3	3.7±0.4	3.8±0.2	Tesar et al. (1992)
$K_7[NdW_{10}O_{53}]$	0.77±0.39	5.56±0.63	7.06±0.30	Peacock (1973)
$Ca_2Ga_2SiO_7$:Nd^{3+} (crystal)	0.82	4.41	6.44	Kaminskii et al. (1992)
$La_3Lu_2Ga_5O_{12}$:Nd^{3+} (crystal)	0.84	2.64	2.61	Allik et al. (1988)
KYF_4:Nd^{3+} (crystal)	0.85	2.38	3.93	Kaminskii et al. (1994b)
KYF_4:Nd^{3+} (crystal)	0.86	2.39	3.93	Allik et al. (1993)
CaF_2:Nd^{3+} (crystal)	0.87	3.44	9.47	Sardar et al. (1993)
$30ZnF_2$–$20BaF_2$–$14AlF_3$–$14YF_3$–$21ThF_4$–$1NdF_3$ glass	0.9±0.3	3.8±0.5	4.0±0.2	Tesar et al. (1992)
$GdGaGe_2O_7$:Nd^{3+} (crystal)	0.907	2.773	5.981	Kaminskii et al. (1987)
$LiKYF_5$:Nd^{3+} (crystal)	0.92	3.21	4.26	Kaminskii et al. (1994a)
AlF_3–ZrF_4–MgF_2–CaF_2–SrF_2–BaF_2–YF_3–NdF_3 glass	1.0±0.3	3.6±0.5	4.2±0.2	Tesar et al. (1992)
AlF_3–BeF_2–MgF_2–CaF_2–SrF_2–BaF_2–YF_3–LaF_3–NdF_3 glass	1.0±0.3	3.7±0.5	4.1±0.2	Tesar et al. (1992)
$45BeF_2$–$20AlF_3$–$15KF$–$18CaF_2$–$2NdF_3$ glass	1.0±0.4	4.7±0.6	5.9±0.3	Stokowski et al. (1981b)
YSZ:Nd^{3+}	1.1	1.24	1.23	Merino (1993) Orera et al. (1995)
$30AlF_3$–$27BeF_2$–$27CaF_2$–$15BaF_2$–$1NdF_3$ glass	1.1±0.3	3.2±0.4	3.9±0.2	Tesar et al. (1992)
Nd^{3+} in magnesium sodium sulphate glass	1.12	2.81	3.67	Ratnakaram (1994)
$Nd(ClO_4)_3$ in DMF	1.2	8.9	8.4	Bünzli and Vuckovic (1984)
$Nd(ClO_4)_3$ in CH_3CN	1.2	7.7	9.8	Bünzli and Vuckovic (1984)
AlF_3–BeF_2–MgF_2–CaF_2–SrF_2–BaF_2–YF_3–NdF_3 glass	1.2±0.3	3.7±0.4	4.3±0.2	Tesar et al. (1992)
CLAP:Nd^{3+} glass	1.2±0.3	3.9±0.5	4.7±0.2	Tesar et al. (1992)
ZBLA:Nd^{3+} glass	1.23	3.37	3.20	McDougall et al. (1994a)
$YAlO_3$:Nd^{3+} (crystal)	1.24	4.68	5.85	Weber and Varitimos (1971)
$Ba_{0.25}Mg_{2.75}Y_2Ge_3O_{12}$:$Nd^{3+}$ (crystal)	1.25	3.23	3.26	Sardar and Stubblefield (1995)
BIGaZYTZrPb:Nd^{3+} fluoride glass	1.26	2.74	4.01	Adam et al. (1991)

continued on next page

Table 11, *continued*

Matrix	Ω_2 (10^{-20} cm^2)	Ω_4 (10^{-20} cm^2)	Ω_6 (10^{-20} cm^2)	Reference(s)
BIGaZLuTMn:Nd^{3+} fluoride glass	1.26	2.58	4.08	Azkargorta et al. (1994)
$LuAlO_3$:Nd^{3+} (crystal)	1.28	4.45	4.88	Kaminskii et al. (1991)
ZBLALi:Nd^{3+} glass	1.28	3.91	3.78	McDougall et al. (1994c)
$10Al(PO_3)_3$–$59BaF_2$–$30MgF_2$–$1Nd_2O_3$ glass	1.3±0.3	4.7±0.4	5.1±0.2	Stokowski et al. (1981b)
BIGaZYTZr fluoride glass	1.31	2.71	4.01	Elejalde et al. (1992)
$23ZrF_4$–$15AlF_3$–$9YF_3$–$12SrF_2$–$15BaF_2$–$25ZnF_2$–$1NdF_3$ glass	1.38±0.22	2.58±0.25	3.86±0.19	Binnemans et al. (1998)
$98BeF_2$–$2NdF_3$ glass	1.4±0.2	2.9±0.2	3.6±0.1	Stokowski et al. (1981b)
Nd^{3+} in $35ZnF_2$–$15CdF_2$–$25BaF_2$–$12LiF$–$7AlF_3$–$6LaF_3$ glass	1.40	2.77	5.77	Cases et al. (1991)
ZBLAK:Nd^{3+} glass	1.40	3.477	3.08	McDougall et al. (1994c)
$29AlF_3$–$20BaF_2$–$29YF_3$–$21ThF_4$–$1NdF_3$ glass	1.5±0.3	3.3±0.4	3.6±0.2	Tesar et al. (1992)
PZG:Nd^{3+} fluoride glass	1.53	3.19	4.93	Balda et al. (1994)
ZBLAN:Nd^{3+} glass	1.54	3.66	3.50	McDougall et al. (1994c)
$34BeF_2$–$19MgF_2$–$10CaF_2$–$14BaF_2$–$22AlF_3$–$1NdF_3$ glass	1.6±0.2	3.6±0.3	3.9±0.1	Tesar et al. (1992)
$2.67Al(PO_3)_3$–$37.33AlF_3$–$1.0YF_3$–$10MgF_2$–$30CaF_2$–$10SrF_2$–$8BaF_2$–$1.0NdF_3$ glass	1.6±0.2	3.8±0.3	4.5±0.1	Stokowski et al. (1981b)
ZBT:Nd^{3+} glass	1.7±0.4	4.0±0.6	4.2±0.3	Tesar et al. (1992)
ZBAT:Nd^{3+} glass	1.7±0.3	3.8±0.4	3.8±0.2	Tesar et al. (1992)
$53ZrF_4$–$20BaF_2$–$3AlF_3$–$3LaF_3$–$20NaF$–$1NdF_3$ glass	1.76±0.22	3.08±0.30	3.67±0.32	Binnemans et al. (1996)
$57HfF_4$–$33BaF_2$–$9ThF_4$–$1NdF_3$ glass	1.8±0.3	4.0±0.4	3.9±0.2	Tesar et al. (1992)
$55HfF_4$–$31BaF_2$–$4AlF_3$–$9ThF_4$–$1NdF_3$ glass	1.8±0.5	4.3±0.8	4.3±0.3	Tesar et al. (1992)
$2Al(PO_3)_3$–$38AlF_3$–$10MgF_2$–$30CaF_2$–$10SrF_2$–$10BaF_2$–$1NdF_3$ glass	1.8±0.2	3.2±0.3	4.5±0.1	Stokowski et al. (1981b)
$8Ba(PO_3)_2$–$40AlF_3$–$5BaF_2$–$10MgF_2$–$16CaF_2$–$10SrF_2$–$10NaF$–$1.0NdF_3$ glass	1.8±0.3	3.8±0.4	4.6±0.2	Stokowski et al. (1981b)
$5Al(PO_3)_3$–$25AlF_3$–$10NaF$–$10MgF_2$–$10CaF_2$–$10SrF_2$–$10BaF_2$–$1NdF_3$ glass	1.8±0.2	3.8±0.3	4.9±0.1	Stokowski et al. (1981b)
$24.69MgF_2$–$18.25AlF_3$–$29.39LiF$–$27.17NaPO_3$–$0.5Nd_2O_3$ glass	1.8±0.3	5.3±0.5	5.6±0.2	Stokowski et al. (1981b)
$Ca_3Ga_2Ge_4O_{14}$:Nd^{3+} (crystal)	1.88	3.65	5.65	Kaminskii et al. (1984)

continued on next page

Table 11, *continued*

Matrix	Ω_2 (10^{-20} cm^2)	Ω_4 (10^{-20} cm^2)	Ω_6 (10^{-20} cm^2)	Reference(s)
ZBALBe:Nd^{3+} glass	1.9±0.3	3.5±0.4	3.7±0.2	Tesar et al. (1992)
$51HfF_4$–$34BaF_2$–$4LaF_3$–$10ThF_4$–$1NdF_3$ glass	1.9±0.4	3.7±0.5	4.2±0.2	Tesar et al. (1992)
ZrF_4–BaF_2–NdF_3 glass	1.95±0.26	3.65±0.38	4.17±0.17	Lucas et al. (1978)
Nd^{3+}-trifluoroacetate in water	1.96	2.34	5.38	Surana et al. (1980)
$60ZrF_4$–$34BaF_2$–$5LaF_3$–$1NdF_3$ (ZBL:Nd^{3+}) glass	2.0±0.5	3.9±0.8	3.8±0.3	Tesar et al. (1992)
$57ZrF_4$–$34BaF_2$–$4LaF_3$–$4AlF_3$–$1NdF_3$ (ZBLA:Nd^{3+}) glass	2.0±0.3	3.6±0.4	3.8±0.2	Tesar et al. (1992)
ZBLAN:Nd^{3+} glass	2.0±0.3	3.9±0.4	4.3±0.2	Tesar et al. (1992)
$45ZrF_4$–$36BaF_2$–$8AlF_3$–$10YF_3$–$1NdF_3$ (ZBAY:Nd^{3+}) glass	2.0±0.3	3.7±0.8	4.0±0.2	Tesar et al. (1992)
$57HfF_4$–$34BaF_2$–$4AlF_3$–$4LaF_3$–$1NdF_3$ (HBLA:Nd^{3+}) glass	2.0±0.3	3.7±0.4	4.0±0.2	Tesar et al. (1992)
$28NaF$–$47LiF$–$24Mg(PO_3)_2$–$1Nd_2O_3$ glass	2.0±0.2	4.7±0.4	5.3±0.2	Stokowski et al. (1981b)
$48(NaPO_3)_6$–$20BaCl_2$–$10ZnCl_2$–$10LiCl$–$10KCl$–$2NdCl_3$ glass	2.02	1.41	4.21	Subramanyam Naidu and Buddhudu (1992a)
$10BaCO_3$–$39Li_2CO_3$–$50H_3BO_3$–$1Nd_2O_3$ glass	2.02	10.62	4.94	Devi and Jayasankar (1995)
$LaGaO_3$:Nd^{3+} (crystal)	2.1	2.4	2.3	Orera et al. (1995)
$57ZrF_4$–$33BaF_2$–$9ThF_4$–$1NdF_3$ (HBT) glass	2.1±0.4	3.6±0.6	4.1±0.3	Tesar et al. (1992)
ZBLAN:Nd^{3+} glass	2.10	3.71	4.62	Wetenkamp et al. (1992)
$48(NaPO_3)_6$–$20BaCl_2$–$10ZnCl_2$–$10NaCl$–$10KCl$–$2NdCl_3$ glass	2.19	1.61	4.20	Subramanyam Naidu and Buddhudu (1992a)
ZBLAN:Nd^{3+} glass	2.20	2.82	3.94	Adam et al. (1991)
$10Mg(PO_3)_2$–$25AlF_3$–$13MgF_2$–$23CaF_2$–$14SrF_2$–$14BaF_2$–$1NdF_3$ glass	2.2±0.2	4.2±0.3	4.9±0.2	Stokowski et al. (1981b)
Nd^{3+} in $50ZnCl_2$–$50KI$ glass	2.20	8.10	5.00	Weber et al. (1982)
$40ZrF_4$–$25BaF_2$–$25LiF$–$10ThF_4$–$1NdF_3$ (ZBTLi) glass	2.2±0.5	3.3±0.7	4.8±0.3	Tesar et al. (1992)
$36HfF_4$–$10ZrF_4$–$4CsF$–$30BaF_2$–$4YF_3$–$5LaF_3$–$10ThF_4$–$1NdF_3$ (HZBYLTCs:Nd^{3+}) glass	2.2±0.5	3.8±0.7	4.3±0.3	Tesar et al. (1992)
Nd^{3+} (aquo)	2.25±1.7	4.08±0.80	9.47±1.3	Carnall et al. (1983)
$Sr_3Ga_2Ge_4O_{14}$:Nd^{3+}	2.32	1.63	4.74	Kaminskii et al. (1984)
$65Al(PO_3)_3$–$23.44BaF_2$–$18.75CaF_2$–$14.06MgF_2$–$37.5AlF_3$ glass (1 mol% Nd_2O_3)	2.33	2.78	4.43	Balda et al. (1996a)

continued on next page

Table 11, *continued*

Matrix	Ω_2 (10^{-20} cm^2)	Ω_4 (10^{-20} cm^2)	Ω_6 (10^{-20} cm^2)	Reference(s)
Nd^{3+} in $52HfF_4$–$18BaF_2$–$3LaF_3$–$2AlF_3$–$25CsBr$ glass	2.36	4.48	4.72	Cases and Chamarro (1991)
$75NaPO_3$–$24SrF_2$–$1NdF_3$ glass	2.39±0.34	4.02±0.40	6.10±0.30	Binnemans et al. (1998)
$46HfF_4$–$4CsF$–$30BaF_2$–$4YF_3$–$5LaF_3$–$10ThF_4$–$1NdF_3$ (HBYLTCs:Nd^{3+}) glass	2.4±0.4	4.1±0.6	4.3±0.3	Tesar et al. (1992)
$La_3Ga_5SiO_{14}$:Nd^{3+} (crystal)	2.4	4.6	3.4	Kaminskii et al. (1983)
$66.6NaPO_3$–$33.3ZnCl_2$–$0.1Nd_2O_3$ glass	2.4	5.9	6.2	Weber and Almeida (1981)
$75NaPO_3$–$24BaF_2$–$1NdF_3$ glass	2.41±0.28	3.27±0.32	5.19±0.25	Binnemans et al. (1998)
Nd^{3+}-trichloroacetate in water	2.42	1.55	5.88	Surana et al. (1980)
Nd:ODA (1:3 in water)	2.42±0.45	3.92±0.55	8.56±0.39	Devlin et al. (1988)
$16Al(PO_3)_3$–$50LiF$–$33NaF$–$1Nd_2O_3$ glass	2.5±0.3	5.3±0.5	5.6±0.2	Stokowski et al. (1981b)
Nd^{3+} in La_2O_3–PbO–TeO_2–SiO_2–B_2O_3–$Ba_3Y_3WO_9$ glass	2.54±0.18	0.97±0.26	1.88±0.12	Bullock et al. (1997)
Nd^{3+} in $Pb(PO_3)_2$ glass	2.6	3.5	4.3	Marion and Weber (1991)
$20Al(PO_3)_3$–$47LiF$–$14Li_2O$–$18BaF_2$–$1.0Nd_2O_3$ glass	2.6±0.3	5.4±0.4	5.7±0.2	Stokowski et al. (1981b)
Nd^{3+} in potassium sodium sulphate glass	2.61	4.57	5.45	Ratnakaram (1994)
ZBLAN:Nd^{3+} glass	2.66	3.05	4.08	Balda et al. (1994)
Nd^{3+}-tribromoacetate in water	2.66	1.26	5.64	Surana et al. (1980)
$79.5LiF$–$20Al(PO_3)_3$–$0.5NdF_3$ glass	2.7±0.2	4.8±0.4	5.1±0.2	Stokowski et al. (1981b)
$75NaPO_3$–$24CaF_2$–$1NdF_3$ glass	2.78±0.31	4.16±0.36	5.56±0.24	Binnemans et al. (1998)
$48(NaPO_3)_6$–$20BaCl_2$–$10ZnCl_2$–$10LiCl$–$10NaCl$–$2NdCl_3$ glass	2.85	0.30	4.49	Subramanyam Naidu and Buddhudu (1992a)
$48InF_3$–$24BaF_2$–$7AlF_3$–$20KF$–$1NdF_3$ glass	2.86	1.61	1.30	Annapurna et al. (1992)
$48(NaPO_3)_6$–$20BaCl_2$–$10ZnCl_2$–$20KCl$–$2NdCl_3$ glass	2.87	0.49	3.97	Subramanyam Naidu and Buddhudu (1992a)
$49.96P_2O_5$–$35.47K_2O$–$13.99MgO$–$0.58Nd_2O_3$ glass	2.9±0.3	4.6±0.4	5.1±0.2	Stokowski et al. (1981a)
$48(NaPO_3)_6$–$20BaCl_2$–$10ZnCl_2$–$20LiCl$–$2NdCl_3$ glass	2.95	0.40	4.06	Subramanyam Naidu and Buddhudu (1992a)
$58.73SiO_2$–$27.47Li_2O$–$11.45MgO$–$2.01Al_2O_3$–$0.34Nd_2O_3$ glass	3.0±0.3	4.6±0.4	4.5±0.2	Stokowski et al. (1981a)

continued on next page

Table 11, *continued*

Matrix	Ω_2 (10^{-20} cm^2)	Ω_4 (10^{-20} cm^2)	Ω_6 (10^{-20} cm^2)	Reference(s)
Nd^{3+}-dichloroacetate in water	3.01	2.42	5.89	Surana et al. (1980)
$48(NaPO_3)_6$–$20BaCl_2$–$10ZnCl_2$–$20NaCl$–$2NdCl_3$ glass	3.09	0.86	4.24	Subramanyam Naidu and Buddhudu (1992a)
ZBAN:Nd^{3+} glass	3.09	3.65	5.74	Petrin et al. (1991)
$88.65TeO_2$–$11.08P_2O_5$–$0.27NdF_3$ glass	3.1±0.1	4.0±0.2	3.9±0.1	Stokowski et al. (1981b)
$50SiO_2$–$2.5Al_2O_3$–$27.5Li_2O$–$20CaO$–$0.16CeO_2$–$0.8Nd_2O_3$ glass	3.1±0.2	4.6±0.3	5.1±0.1	Stokowski et al. (1981a)
Nd^{3+}-monofluoroacetate in water	3.10	1.45	5.62	Surana et al. (1980)
$75NaPO_3$–$24NaF$–$1NdF_3$ glass	3.19±0.29	3.73±0.34	5.55±0.26	Binnemans et al. (1998)
$75NaPO_3$–$24CdF_2$–$1NdF_3$ glass	3.19±0.27	3.88±0.31	5.73±0.24	Binnemans et al. (1998)
Nd(α-picolinate) in water	3.2±0.85	10.4±1.2	10.3±0.6	Bukietynska and Choppin (1970)
Nd^{3+}-dibromoacetate in water	3.21	1.62	5.78	Surana et al. (1980)
Nd^{3+}:DPA (1:1 in water)	3.26±0.49	4.27±0.45	9.67±0.62	Mondry and Starynowicz (1995)
Nd^{3+}:MIDA (1:3 in water)	3.29±0.51	4.62±0.62	8.36±0.44	Devlin et al. (1988)
$45P_2O_5$–$25Li_2O$–$4.3Al_2O_3$–$15Na_2O$–$10CaO$–$0.7Nd_2O_3$ glass	3.3±0.2	4.7±0.3	5.4±0.2	Stokowski et al. (1981a)
$50.01P_2O_5$–$32.95K_2O$–$16.51BaO$–$0.53Nd_2O_3$ glass	3.3±0.2	5.0±0.4	5.6±0.2	Stokowski et al. (1981a)
$65.0SiO_2$–$15.0Li_2O$–$20BaO$–$0.3Nd_2O_3$ glass	3.3±0.1	3.5±0.2	4.0±0.1	Stokowski et al. (1981a)
Nd^{3+}:IDA (1:3 in water)	3.31±0.60	5.08±0.72	9.30±0.51	Devlin et al. (1988)
$30Li_2O$–$55P_2O_5$–$10CaO$–$4.3Al_2O_3$–$0.7Nd_2O_3$ glass	3.4	4.8	5.4	Marion and Weber (1991)
$50P_2O_5$–$30Li_2O$–$15CaO$–$4.3Al_2O_3$–$0.7Nd_2O_3$ glass	3.4±0.2	4.4±0.3	5.1±0.1	Stokowski et al. (1981a)
$40P_2O_5$–$35Li_2O$–$20CaO$–$4.3Al_2O_3$–$0.7Nd_2O_3$ glass	3.4±0.2	4.6±0.3	5.3±0.1	Stokowski et al. (1981a)
$Li_6Y_5(BO_3)_3$:Nd^{3+} (crystal)	3.44	3.99	4.67	Huang et al. (1992b)
$75NaPO_3$–$24LiF$–$1NdF_3$ glass	3.44±0.36	4.14±0.42	6.28±0.32	Binnemans et al. (1998)
Nd^{3+}-monoiodoacetate in water	3.50	2.07	6.17	Surana et al. (1980)
$88.01TeO_2$–$10.44Nb_2O_5$–$1.55Nd_2O_3$ glass	3.5±0.1	3.5±0.2	3.5±0.1	Stokowski et al. (1981b)
$50P_2O_5$–$30Li_2O$–$5SiO_2$–$4.3Al_2O_3$–$10CaO$–$0.7Nd_2O_3$ glass	3.5±0.2	4.4±0.3	5.2±0.1	Stokowski et al. (1981a)
$81.3NaPO_3$–$18.6ZnCl_2$–$0.1Nd_2O_3$ glass	3.5	5.4	6.6	Weber and Almeida (1981)

continued on next page

Table 11, *continued*

Matrix	Ω_2 (10^{-20} cm^2)	Ω_4 (10^{-20} cm^2)	Ω_6 (10^{-20} cm^2)	Reference(s)
$68TeO_2$–$31ZnO$–$1Nd_2O_3$ glass	3.6±0.2	4.6±0.3	4.3±0.1	Stokowski et al. (1981b)
$79TeO_2$–$20Li_2O$–$1Nd_2O_3$ glass	3.6±0.2	4.9±0.3	4.6±0.2	Stokowski et al. (1981b)
$55P_2O_5$–$25Li_2O$–$4.3Al_2O_3$–$15CaO$–$0.7Nd_2O_3$ glass	3.6±0.2	4.7±0.3	5.4±0.1	Stokowski et al. (1981a)
$66.5SiO_2$–$33Li_2O$–$0.5Nd_2O_3$ glass	3.6±0.2	3.9±0.3	4.3±0.1	Stokowski et al. (1981a)
$87GeO_2$–$12.43Li_2O$–$0.57Nd_2O_3$ glass	3.6±0.2	3.6±0.2	4.1±0.1	Stokowski et al. (1981b)
$75NaPO_3$–$24KF$–$1NdF_3$ glass	3.61±0.30	3.81±0.35	5.83±0.27	Binnemans et al. (1998)
Nd^{3+} in $25Na_2O$–$65P_2O_5$–$10Al_2O_3$ glass	3.62	4.73	5.68	Nageno et al. (1993)
Nd^{3+} in $20Li_2O$–$20CaO$–$60SiO_2$ glass	3.63	4.21	4.94	Takebe et al. (1995)
$30Na_2O$–$55P_2O_5$–$10CaO$–$4.3Al_2O_3$–$0.7Nd_2O_3$ glass	3.7	4.0	4.4	Marion and Weber (1991)
Nd^{3+}-monochloroacetate in water	3.70	1.79	5.18	Surana et al. (1980)
$65SiO_2$–$15Na_2O$–$20BaO$–$0.3Nd_2O_3$	3.7±0.1	3.2±0.2	3.6±0.1	Stokowski et al. (1981a)
$52CaO$–$36Al_2O_3$–$6Na_2O$–$6SrO$ glass (0.5 mol% Nd_2O_3)	3.71±0.3	5.03±0.5	2.90±0.2	Uhlmann et al. (1994)
Nd^{3+} in $30Li_2O$–$60P_2O_5$–$10Al_2O_3$ glass	3.71	4.70	5.15	Takebe et al. (1995)
Nd^{3+} in $60PbO$–$20Bi_2O_3$–$20Ga_2O_3$ glass	3.72	4.48	4.33	Takebe et al. (1996)
$75NaPO_3$–$24ZnF_2$–$1NdF_3$ glass	3.75±0.40	4.05±0.47	5.99±0.36	Binnemans et al. (1998)
$48ZrF_4$–$24BaF_2$–$7AlF_3$–$20KF$–$1NdF_3$ glass	3.75	5.45	8.95	Hanumanthu et al. (1991)
$75NaPO_3$–$24.5ZnO$–$0.5Nd_2O_3$ glass	3.76±0.25	3.27±0.29	5.23±0.22	Binnemans et al. (1998)
Nd^{3+} in $NaPO_3$ glass	3.8	5.3	6.0	Weber and Almeida (1981); Marion and Weber (1991)
Nd^{3+} in $30Na_2O$–$60P_2O_5$–$10Al_2O_3$ glass	3.82	4.74	5.53	Takebe et al. (1995)
Nd^{3+} in $80PbO$–$20Ga_2O_3$ glass	3.84	3.87	4.07	Takebe et al. (1996)
Nd^{3+} in $40PbO$–$40Bi_2O_3$–$20Ga_2O_3$ glass	3.88	4.24	4.30	Takebe et al. (1996)
Nd^{3+} in $70PbO$–$10Bi_2O_3$–$20Ga_2O_3$ glass	3.89	4.07	4.31	Takebe et al. (1996)
$49P_2O_5$–$33.33K_2O$–$16.67ZnO$–$1Nd_2O_3$ glass	3.9±0.2	4.8±0.4	5.5±0.2	Stokowski et al. (1981a)
$73.08SiO_2$–$13.02BaO$–$12.71K_2O$–$1.19Nd_2O_3$ glass	3.9±0.1	2.3±0.2	2.2±0.1	Stokowski et al. (1981a)
Nd^{3+} in $Cd(PO_3)_2$ glass	3.9	4.2	4.6	Marion and Weber (1991)

continued on next page

Table 11, *continued*

Matrix	Ω_2 (10^{-20} cm^2)	Ω_4 (10^{-20} cm^2)	Ω_6 (10^{-20} cm^2)	Reference(s)
$40BaO–55P_2O_5–4.7La_2O_3–0.3Nd_2O_3$ glass	3.9	4.3	5.1	Marion and Weber (1991)
Nd^{3+}-monobromoacetate in water	3.90	2.00	5.72	Surana et al. (1980)
Nd:DPA (1:2 in water)	3.92±0.52	4.32±0.48	10.37±0.67	Mondry and Starynowicz (1995)
Nd^{3+} in $50PbO–30Bi_2O_3–20Ga_2O_3$ glass	3.94	4.09	4.31	Takebe et al. (1996)
$58CaO–36Al_2O_3–6Na_2O$ glass (0.5 mol% Nd_2O_3)	3.95±0.3	4.81±0.4	3.20±0.2	Uhlmann et al. (1994)
$NdCl_6^{3-}$ in acetonitrile	3.95±0.29	1.23±0.33	0.72±0.25	Henrie and Henrie (1977)
$30K_2O–55P_2O_5–10CaO–4.3Al_2O_3–0.7Nd_2O_3$ glass	4.0	5.1	5.9	Marion and Weber (1991)
Nd^{3+} in $Ba(PO_3)_2$ glass	4.0	5.4	5.6	Weber et al. (1981)
$75SiO_2–25Na_2O–0.3Nd_2O_3$ glass	4.0±0.1	3.2±0.2	3.0±0.1	Stokowski et al. (1981a)
$82TeO_2–17BaO–1Nd_2O_3$ glass	4.0±0.2	5.1±0.2	4.8±0.1	Stokowski et al. (1981b)
$65SiO_2–35Na_2O–0.3Nd_2O_3$ glass	4.1±0.1	3.2±0.2	3.3±0.1	Stokowski et al. (1981a)
$70SiO_2–30Na_2O–0.3Nd_2O_3$ glass	4.1±0.1	3.2±0.1	3.3±0.1	Stokowski et al. (1981a)
$79TeO_2–20Na_2O–1Nd_2O_3$ glass	4.1±0.2	4.8±0.2	4.6±0.1	Stokowski et al. (1981b)
$80SiO_2–20Na_2O–0.3Nd_2O_3$ glass	4.2±0.1	2.8±0.2	2.8±0.1	Stokowski et al. (1981a)
$65SiO_2–15K_2O–20BaO–0.3Nd_2O_3$ glass	4.2±0.1	2.5±0.2	2.7±0.2	Stokowski et al. (1981a)
$66.5SiO_2–33.0Na_2O–0.5Nd_2O_3$	4.2±0.1	3.3±0.2	3.1±0.1	Stokowski et al. (1981a)
$20.41Bi_2O_3–37.1CdO–41.99SiO_2–0.50Nd_2O_3$ glass	4.2±0.3	4.0±0.5	4.9±0.2	Stokowski et al. (1981a)
Nd^{3+} in $30Li_2O–70B_2O_3$ glass	4.20	3.89	4.74	Takebe et al. (1995)
Nd^{3+} in $33.3ZnO–66.6TeO_2$ glass	4.24	0.88	7.05	Kanoun et al. (1990)
$74.70SiO_2–24.89K_2O–0.41Nd_2O_3$ glass	4.3±0.2	1.7±0.2	1.8±0.1	Stokowski et al. (1981a)
$73.18SiO_2–11.27CaO–8.66Na_2O–5.64K_2O–1.07BaO–0.19Nd_2O_3$ glass	4.3±0.1	2.7±0.2	2.9±0.1	Stokowski et al. (1981a)
Nd^{3+} in $Sr(PO_3)_2$ glass	4.3	4.3	5.0	Weber et al. (1981)
$40SrO–55P_2O_5–4.7La_2O_3–0.3Nd_2O_3$ glass	4.3	4.4	5.0	Marion and Weber (1991)
Nd^{3+} in $30CaO–70B_2O_3$ glass	4.36	3.74	4.64	Takebe et al. (1995)
Nd^{3+} in $30BaO–60P_2O_5–10Al_2O_3$ glass	4.37	4.05	4.82	Takebe et al. (1995)
$74.72SiO_2–24.91Na_2O–0.37Nd_2O_3$ glass	4.4±0.1	2.6±0.2	3.0±0.1	Stokowski et al. (1981a)

continued on next page

Table 11, *continued*

Matrix	Ω_2 (10^{-20} cm^2)	Ω_4 (10^{-20} cm^2)	Ω_6 (10^{-20} cm^2)	Reference(s)
$65SiO_2$–$15K_2O$–$20SrO$–$0.3Nd_2O_3$ glass	4.4±0.2	2.8±0.2	2.9±0.1	Stokowski et al. (1981a)
Nd^{3+} in $67SiO_2$–$15K_2O$–18BaO glass	4.4±0.1	2.5±0.1	2.6±0.1	Stokowski et al. (1981a)
$30Rb_2O$–$55P_2O_5$–$10CaO$–$4.3Al_2O_3$–$0.7Nd_2O_3$ glass	4.4	5.5	6.2	Marion and Weber (1991)
$52CaO$–$36Al_2O_3$–$6Na_2O$–6BaO glass (0.5 mol% Nd_2O_3)	4.46±0.4	5.18±0.5	2.73±0.2	Uhlmann et al. (1994)
Nd^{3+} in $Ca(PO_3)_2$ glass	4.5	4.8	4.9	Weber et al. (1981)
$66.5SiO_2$–$33K_2O$–$0.5Nd_2O_3$ glass	4.5±0.1	2.2±0.1	2.0±0.1	Stokowski et al. (1981a)
$99NaPO_3$–$1NdF_3$ glass	4.52±0.39	3.94±0.45	5.93±0.34	Binnemans et al. (1998)
$99.5La(PO_3)_3$–$0.5Nd_2O_3$ glass	4.6±0.3	3.9±0.4	4.0±0.2	Stokowski et al. (1981a)
$99.5Al(PO_3)_3$–$0.5Nd_2O_3$ glass	4.6±0.3	4.1±0.5	4.3±0.2	Stokowski et al. (1981a)
Nd^{3+} in $20Na_2O$–$20CaO$–$60SiO_2$ glass	4.64	3.81	4.17	Takebe et al. (1995)
Nd^{3+} in $30BaO$–$70B_2O_3$ glass	4.65	3.56	4.74	Takebe et al. (1995)
$40CaO$–$55P_2O_5$–$4.7La_2O_3$–$0.3Nd_2O_3$ glass	4.7	4.2	4.7	Marion and Weber (1991)
$89TeO_2$–$10Cs_2O$–$1Nd_2O_3$ glass	4.7±0.2	4.9±0.3	4.4±0.1	Stokowski et al. (1981b)
Nd:DPA (1:3 in water)	4.70±0.98	4.78±1.17	11.31±0.83	Devlin et al. (1988)
$Nd(PO_3)_3$ glass	4.8	3.2	3.7	Weber et al. (1981)
$65SiO_2$–$15K_2O$–$20CaO$–$0.3Nd_2O_3$ glass	4.8±0.2	3.2±0.2	3.1±0.1	Stokowski et al. (1981a)
$89TeO_2$–$10K_2O$–$1Nd_2O_3$ glass	4.8±0.2	5.3±0.3	5.0±0.1	Stokowski et al. (1981b)
Nd^{3+} in $40Na_2O$–$60SiO_2$ glass	4.83	3.07	3.37	Takebe et al. (1995)
$64CaO$–$36Al_2O_3$ glass (0.5 mol% Nd_2O_3)	4.87±0.2	5.50±0.3	3.42±0.1	Uhlmann et al. (1994)
$89.99SiO_2$–$9.54Na_2O$–$0.48Nd_2O_3$ glass	4.9±0.1	2.9±0.2	2.9±0.1	Stokowski et al. (1981a)
Nd^{3+} in $30Na_2O$–$70B_2O_3$ glass	4.91	3.28	4.51	Takebe et al. (1995)
Nd^{3+} in $30K_2O$–$70B_2O_3$ glass	4.94	3.10	3.42	Takebe et al. (1995)
Nd^{3+} in $Zn(PO_3)_2$ glass	5.1	4.4	4.7	Marion and Weber (1991)
$23.05Ta_2O_5$–$36.73SiO_2$–$17.07B_2O_3$–$22.15BaO$–$1.0Nd_2O_3$	5.1±0.5	4.1±0.7	4.1±0.3	Stokowski et al. (1981b)
$79TeO_2$–$20Rb_2O$–$1Nd_2O_3$ glass	5.1±0.2	5.1±0.4	4.4±0.2	Stokowski et al. (1981b)
$74.5SiO_2$–$15Na_2O$–$5BaO$–$5ZnO$–$0.5Nd_2O_3$ glass	5.1±0.2	3.2±0.2	3.6±0.1	Stokowski et al. (1981a)

continued on next page

Table 11, *continued*

Matrix	Ω_2 (10^{-20} cm^2)	Ω_4 (10^{-20} cm^2)	Ω_6 (10^{-20} cm^2)	Reference(s)
$48.85P_2O_5$–$37.5MgO$–$12.5MnO$–$1.16Nd_2O_3$ glass	5.1±0.1	3.7±0.2	4.2±0.1	Stokowski et al. (1981a)
$39.16SiO_2$–$24.75BaO$–$35.36TiO_2$–$0.73Nd_2O_3$ glass	5.2±0.1	3.9±0.1	3.2±0.1	Stokowski et al. (1981a)
Nd^{3+} in sodium β''-alumina	5.19	0.973	0.971	Alfrey et al. (1988)
Nd^{3+} in $20K_2O$–$20CaO$–$60SiO_2$ glass	5.23	3.10	3.14	Takebe et al. (1995)
Nd^{3+} in $30CaO$–$60P_2O_5$–$10Al_2O_3$ glass	5.27	3.69	4.31	Takebe et al. (1995)
Nd^{3+} in $Mg(PO_3)_2$ glass	5.3	4.7	4.3	Weber et al. (1981)
$24.21Bi_2O_3$–$43.93CdO$–$31.29SiO_2$–$0.56Nd_2O_3$ glass	5.4±0.3	5.1±0.5	5.9±0.2	Stokowski et al. (1981a)
$NdBr_6^{3-}$ in acetonitrile	5.46±2.10	3.15±3.22	1.08±1.25	Henrie and Henrie (1977)
$21.87P_2O_5$–$77.02MgO$–$0.33As_2O_3$–$0.78Nd_2O_3$ glass	5.7±0.2	4.1±0.3	4.5±0.2	Stokowski et al. (1981a)
$79TeO_2$–$20K_2O$–$1Nd_2O_3$ glass	5.7±0.2	5.0±0.3	4.7±0.1	Stokowski et al. (1981b)
Nd^{3+} in $BiCl_3$–40KCl glass	5.70	6.60	4.40	Weber et al. (1982)
Nd^{3+} in $30MgO$–$60P_2O_5$–$10Al_2O_3$ glass	5.72	3.69	4.31	Takebe et al. (1995)
$80H_3BO_3$–$10Na_2CO_3$–$9LiF$–$1NdF_3$ glass	5.758	1.702	5.484	Ratnakaram and Buddhudu (1996)
$65SiO_2$–$15K_2O$–$20MgO$–$0.3Nd_2O_3$ glass	5.8±0.2	3.3±0.2	3.1±0.1	Stokowski et al. (1981a)
$95.13SiO_2$–$4.45Na_2O$–$0.41Nd_2O_3$ glass	5.8±0.2	3.4±0.2	3.0±0.1	Stokowski et al. (1981a)
YVO_4:Nd^{3+} (crystal)	5.88	4.08	5.11	Lomheim and DeShazer (1978)
$40MgO$–$55P_2O_5$–$4.7La_2O_3$–$0.3Nd_2O_3$ glass	6.0	4.0	4.7	Marion and Weber (1991)
$99.91SiO_2$–$0.09Nd_2O_3$ glass	6.0±0.3	4.7±0.4	4.1±0.2	Stokowski et al. (1981a)
$89Al(PO_3)_3$–$10Zn_2P_2O_7$–$1.0Nd_2O_3$ glass	6.1±0.2	3.3±0.3	3.8±0.1	Stokowski et al. (1981a)
$74.605P_2O_5$–$25.0Al_2O_3$–$0.395Nd_2O_3$ glass	6.2±0.2	3.6±0.3	4.2±0.2	Stokowski et al. (1981a)
Nd^{3+} in $Al(PO_3)_3$ glass	6.3	4.0	4.6	Marion and Weber (1991)
$10MgCO_3$–$39Li_2CO_3$–$50H_3BO_3$–$1Nd_2O_3$ glass	6.30	33.17	9.51	Devi and Jayasankar (1995)
$67.83P_2O_5$–$16.67Nd_2O_3$ glass	6.4±0.3	4.7±0.4	5.3±0.2	Stokowski et al. (1981a)
$10SrCO_3$–$39Li_2CO_3$–$50H_3BO_3$–$1Nd_2O_3$ glass	6.52	5.00	6.16	Devi and Jayasankar (1995)
$48InF_3$–$24BaF_2$–$7AlF_3$–$20NaF$–$1NdF_3$	6.56	2.31	2.81	Annapurna et al. (1992)
Nd^{3+} in cadmium sodium sulphate glass	6.61	3.97	6.65	Ratnakaram (1994)

continued on next page

Table 11, *continued*

Matrix	Ω_2 (10^{-20} cm^2)	Ω_4 (10^{-20} cm^2)	Ω_6 (10^{-20} cm^2)	Reference(s)
Ga_2S_3–La_2S_3–Nd_2S_3 glass	6.65	4.39	4.67	Bornstein and Reisfeld (1982)
$40BeO$–$55P_2O_5$–$4.7La_2O_3$–$0.3Nd_2O_3$ glass	6.7	3.3	3.8	Marion and Weber (1991)
$Nd(NO_3)_3$ in DMF	6.7	5.0	7.6	Bünzli and Vuckovic (1984)
$49.31SiO_2$–$25.06Na_2O$–$25.07TiO_2$–$0.56Nd_2O_3$ glass	6.7±0.2	3.7±0.2	3.8±0.1	Stokowski et al. (1981a)
$64.19SiO_2$–$15.08Na_2O$–$20.11TiO_2$–$0.62Nd_2O_3$ glass	6.8±0.1	3.5±0.2	3.4±0.1	Stokowski et al. (1981a)
Nd^{3+} in zinc sodium sulphate glass	6.80	5.50	6.96	Ratnakaram (1994)
Nd^{3+} in $30K_2O$–$70Ga_2O_3$ glass	6.95	4.76	5.34	Takebe et al. (1996)
Nd:CDA (1:3 in water)	6.99±0.26	7.09±0.38	12.28±1.68	Devlin et al. (1988)
$17Ta_2O_5$–$31.5MgO$–$38SiO_2$–$13BaO$–$0.5Nd_2O_3$ glass	7.0±0.3	4.6±0.4	4.7±0.2	Stokowski et al. (1981a)
$99.98GeO_2$–$0.02Nd_2O_3$ glass	7.0±0.7	4.8±1.0	5.4±0.4	Stokowski et al. (1981b)
$80H_3BO_3$–$10Na_2CO_3$–$9ZnF_2$–$1NdF_3$ glass	7.020	1.504	6.413	Ratnakaram and Buddhudu (1996)
Nd:DPA (1:3 in water)	7.13±0.80	3.78±0.74	13.21±1.01	Mondry and Starynowicz (1995)
Nd:DPA (1:4 in water)	7.19±0.79	3.98±0.73	13.38±1.00	Mondry and Starynowicz (1995)
$Ba_3LaNb_3O_{12}$:Nd^{3+} (crystal)	7.226	1.402	2.845	Antonov et al. (1986)
$80H_3BO_3$–$10Na_2CO_3$–$9KF$–$1NdF_3$ glass	7.499	1.921	7.695	Ratnakaram and Buddhudu (1996)
$48ZrF_4$–$24BaF_2$–$7AlF_3$–$20LiF$–$1NdF_3$ glass	7.57	2.54	13.85	Hanumanthu et al. (1991)
$Na_3[Nd(DPA)_3]\cdot 14H_2O$ (crystal)	7.57±0.62	3.14±0.57	8.15±0.79	Mondry and Starynowicz (1995)
$10CaCO_3$–$39Li_2CO_3$–$50H_3BO_3$–$1Nd_2O_3$ glass	7.85	6.75	7.61	Devi and Jayasankar (1995)
$48InF_3$–$24BaF_2$–$7AlF_3$–$20LiF$–$1NdF_3$ glass	7.89	5.18	2.12	Annapurna et al. (1992)
Nd:CDO (1:3 in water)	7.95±2.28	5.62±3.33	11.23±1.47	Devlin et al. (1988)
Nd^{3+} in $30K_2O$–$10Ta_2O_5$–$60Ga_2O_3$ glass	8.64	5.18	5.47	Takebe et al. (1996)
$80H_3BO_3$–$10Na_2CO_3$–$9BaF_2$–$1NdF_3$ glass	8.702	5.586	14.390	Ratnakaram and Buddhudu (1996)
Nd^{3+} in $30K_2O$–$20Ta_2O_5$–$50Ga_2O_3$ glass	9.16	5.06	5.90	Takebe et al. (1996)
$Nd(NO_3)_3$ in ethylacetate	9.2±0.4	5.4±0.3	7.7±0.45	Carnall et al. (1965)
$48ZrF_4$–$24BaF_2$–$7AlF_3$–$20NaF$–$1NdF_3$ glass	9.42	2.31	19.42	Hanumanthu et al. (1991)
$0.13Nd_2S_3$–$0.87La_2S_3$–$3Al_2S_3$ glass	9.45	4.84	6.54	Reisfeld (1982)

continued on next page

Table 11, *continued*

Matrix	Ω_2 (10^{-20} cm^2)	Ω_4 (10^{-20} cm^2)	Ω_6 (10^{-20} cm^2)	Reference(s)
Nd^{3+} in $30K_2O$–$30Ta_2O_3$–$40Ga_2O_3$ glass	9.46	4.27	5.34	Takebe et al. (1996)
Nd^{3+} in $35K_2O$–$20Ta_2O_5$–$45Ga_2O_3$ glass	10.4	4.89	5.53	Takebe et al. (1996)
Nd^{3+} in $LiNO_3 + KNO_3$ melt	11.20±0.3	2.62±0.3	4.14±0.4	Carnall et al. (1978)
Nd^{3+} in $40K_2O$–$20Ta_2O_5$–$40Ga_2O_3$ glass	11.4	5.04	5.57	Takebe et al. (1996)
$Nd(NO_3)_3$ in TBP	11.5	3.2	8.9	Henrie and Smysen (1977)
$Nd(NO_3)_3$ in CH_3CN	11.8	2.1	6.6	Bünzli and Vuckovic (1984)
Nd^{3+} in BaS–CdS–GeS_2 glass	11.9	7.7	5.4	Meresse (1996)
$49Li_2CO_3$–$50H_3BO_3$–$1Nd_2O_3$ glass	12.21	16.38	7.53	Devi and Jayasankar (1995)
Nd^{3+} in lithium sodium sulphate glass	12.22	3.65	9.19	Ratnakaram (1994)
Nd(acetylacetonate)$_3$ in methanol/ethanol	15.7	0.73	7.4	Sinha et al. (1972)
Nd(acetylacetonate)$_3$ in methanol	16.95	0.89	11.74	Mehta and Tandon (1970)
$NdCl_3$–$(AlCl_3)_x$ vapor complex	18.00	4.8	3.9	Øye and Gruen (1969)
$(Me_4N)_2Nd(NO_3)_5$ in CH_3CN	18.7	1.0	4.9	Bünzli and Vuckovic (1984)
Nd(thenoyltrifluoro-acetonate)$_3$ in methanol	22.16	0.34	10.65	Mehta and Tandon (1970)
Nd(acetylacetonate)$_3$ in DMF	22.62	0.65	11.96	Mehta and Tandon (1970)
Nd(acetylacetonate)$_3$ in DMF	24.5	0.71	9.1	Sinha et al. (1972)
Nd(benzoylacetonate)$_3$ in methanol	26.20	1.23	11.67	Mehta and Tandon (1970)
Nd(thenoyltrifluoro-acetonate)$_3$ in DMF	30.38	0.38	10.66	Mehta and Tandon (1970)
Nd(benzoylacetonate)$_3$ in DMF	33.71	0.26	11.96	Mehta and Tandon (1970)
Nd(dibenzoylacetyl-acetonate)$_3$ in methanol/ethanol	34.1	2.5	9.1	Sinha et al. (1972)
$Nd(DBM)_3 \cdot H_2O$ (powder)	44.7	11.9	1.25	Kirby and Palmer (1981b)
$Nd(DBM)_3$ in methanol	47.52	5.25	12.36	Mehta and Tandon (1970)
$Nd(DBM)_3$ in DMF	55.39	2.46	21.10	Mehta and Tandon (1970)
$CsNdI_4$ vapor	130	–	–	Liu and Zollweg (1974)
$NdBr_3$ vapor	180	9	9	Gruen et al. (1967)
NdI_3 vapor	275	9	9	Gruen et al. (1967)

Table 12
Phenomenological intensity parameters Ω_λ for Pm^{3+} in various host matrices; the host matrices are classified according to increasing values of Ω_2

Matrix	Ω_2 (10^{-20} cm^2)	Ω_4 (10^{-20} cm^2)	Ω_6 (10^{-20} cm^2)	Reference
LaF_3:Pm^{3+} (crystal)	0.5	1.9	2.2	Leavitt and Morrison (1980)
$LaCl_3$:Pm^{3+} (crystal)	0.97	1.63	1.66	Morrison and Leavitt (1982)
Pm^{3+} (aquo)	1.30±0.26	4.36±0.48	3.94±0.34	Carnall et al. (1983)
Pm^{3+} in $LiNO_3$–KNO_3 melt	12.50±0.5	3.78±0.8	4.14±0.4	Carnall et al. (1978)

Table 13
Phenomenological intensity parameters Ω_λ for Sm^{3+} in various host matrices; the host matrices are classified according to increasing values of Ω_2

Matrix	Ω_2 (10^{-20} cm^2)	Ω_4 (10^{-20} cm^2)	Ω_6 (10^{-20} cm^2)	Reference
$32ZnF_2$–$28CdF_2$–$20BaF_2$–$11LiF$–$5AlF_3$–$3.9LaF_3$–$0.1SmF_3$ glass	0.68	3.77	2.15	Rodríguez et al. (1992)
$LaF_3:Sm^{3+}$ (crystal)	1.0	0.5	1.5	Leavitt and Morrison (1980)
Sm^{3+} (aquo)	1.08±0.42	3.67±0.70	2.87±0.56	Carnall et al. (1983)
Sm^{3+} in $52HfF_4$–$18BaF_2$–$3LaF_3$–$2AlF_3$–$25CsBr$ glass	1.44	2.87	1.44	Cases and Chamarro (1991)
ZBLA:Sm^{3+} glass	1.66	1.69	1.24	McDougall et al. (1994a)
ZBLALi:Sm^{3+} glass	1.95	2.38	1.64	McDougall et al. (1994c)
ZBLAN:Sm^{3+} glass	2.06	2.55	1.63	McDougall et al. (1994c)
$75NaPO_3$–$24CaF_2$–$1SmF_3$ glass	2.18±0.32	3.80±0.28	2.15±0.18	Binnemans et al. (1997c)
ZBLALi:Sm^{3+} glass	2.37	4.24	2.99	Canalejo et al. (1988)
Sm^{3+} in borate glass	2.42	4.62	4.16	Reisfeld (1976)
$75NaPO_3$–$20CaF_2$–$5SmF_3$ glass	2.76±0.24	4.11±0.21	2.52±0.14	Binnemans et al. (1997c)
Sm^{3+} in tellurite glass	3.17	3.65	1.61	Boehm et al. (1979)
Sm^{3+} in germanate glass	3.97	3.33	2.85	Reisfeld (1976)
Sm^{3+} in phosphate glass	4.31	4.28	5.78	Boehm et al. (1979)
ZBLAK:Sm^{3+} glass	4.88	–0.35	1.65	McDougall et al. (1994c)
Sm^{3+} in borate glass	6.36	6.02	3.51	Boehm et al. (1979)
Sm^{3+} in germanate glass	6.48	4.98	3.18	Boehm et al. (1979)
Sm^{3+} in $LiNO_3 + KNO_3$ melt	8.10±1.8	4.52±0.5	3.74±0.5	Carnall et al. (1978)
Sm^{3+}:ODA (1:3 in water)	30.17±24.99	4.37±0.27	5.96±0.45	Yoon et al. (1992)
Sm^{3+}:IDA (1:3 in water)	33.10±77.84	4.57±0.85	6.58±1.45	Yoon et al. (1992)
Sm^{3+}:MIDA (1:3 in water)	33.91±70.97	5.14±0.77	7.02±1.28	Yoon et al. (1992)
Sm^{3+}:DPA (1:3 in water)	44.16±56.11	4.28±0.61	5.79±1.01	Yoon et al. (1992)
Sm(α-picolinate) in water	82±27	5.9±0.4	3.7±0.4	Bukietynska and Choppin (1970)
$K_7[SmW_{10}O_{35}]$	119.78±33.70	3.85±0.34	2.32±0.39	Peacock (1973)

Table 14
Phenomenological intensity parameters Ω_λ for Eu^{3+} in various host matrices; the host matrices are classified according to increasing values of Ω_2

Matrix	Ω_2 (10^{-20} cm^2)	Ω_4 (10^{-20} cm^2)	Ω_6 (10^{-20} cm^2)	Reference
ZBLAN:Eu^{3+} glass	0.05	1.34	1.61	McDougall et al. (1994c)
ZBLALi:Eu^{3+} glass	0.09	1.51	1.79	McDougall et al. (1994c)
ZBLAK:Eu^{3+} glass	0.11	1.04	1.16	McDougall et al. (1994c)
ZBLA:Eu^{3+} glass	0.10	1.54	1.71	McDougall et al. (1994a)
ZBLA:Eu^{3+} glass	0.49±0.29	4.15±1.44	2.76±0.16	Dejneka et al. (1995)
$60ZrF_4$–$33BaF_2$–$5LaF_3$–$2EuF_3$ (ZBL) glass	0.93	2.61	2.17	Blanzat et al. (1980)
ZBANK:Eu^{3+} glass	1.07	0.52	0.75	Harinath et al. (1990)
LaF_3:Eu^{3+} (crystal)	1.19	1.16	0.39	Weber (1967a)
KY_3F_{10}:Eu^{3+}	1.22	1.26	8.55	Porcher and Caro (1980)
ZBANLi:Eu^{3+} glass	1.27	0.61	0.88	Harinath et al. (1990)
Eu^{3+} (aquo)	1.46	6.66	5.40	Carnall et al. (1983)
Eu^{3+} (aquo)	1.62	5.65	5.02	Binnemans et al. (1997a)
$30PbO$–$70PbF_2$ glass	2.641	2.288	1.405	Nachimuthu and Jagannathan (1995b)
$YAlO_3$:Eu^{3+} (crystal)	2.66	6.33	0.80	Weber et al. (1973)
ZBLAN:Eu^{3+} glass	2.89	3.87	2.88	Binnemans (1996)
$60NaPO_3$–$15BaF_2$–$10YF_3$–$15EuF_3$ glass	3.24	5.11	2.89	Balda et al. (1996b)
EuP_5O_{14} (crystal)	3.66	1.43	3.07	Blanzat et al. (1980)
Eu^{3+} in $70PbO$–$30PbF_2$ glass	3.765	3.086	1.190	Nachimuthu and Jagannathan (1995b)
$75NaPO_3$–$24BaF_2$–$1EuF_3$ glass	4.07	5.09	3.74	Binnemans et al. (1997c)
Eu^{3+} in phosphate glass	4.12	4.69	1.83	Blanzat et al. (1980)
$48InF_3$–$24BaF_2$–$7AlF_3$–$20KF$–$1EuF_3$ glass	4.90	0.78	1.60	Annapurna and Buddhudu (1993)
Eu^{3+}:DPA (1:1) in water	5.02	5.65	5.52	Binnemans et al. (1997a)
$75NaPO_3$–$24CaF_2$–$1EuF_3$ glass	5.12	5.45	4.12	Binnemans et al. (1997c)
$K_7[EuW_{10}O_{35}]$	5.18	0.91	4.61	Peacock (1973)
$48InF_3$–$24BaF_2$–$7AlF_3$–$20NaF$–$1EuF_3$ glass	5.35	1.18	1.30	Annapurna and Buddhudu (1993)
$75NaPO_3$–$20CaF_2$–$5EuF_3$ glass	5.52±1.52	4.21±0.93	3.58±0.10	Binnemans et al. (1997c)

continued on next page

Table 14, *continued*

Matrix	Ω_2 (10^{-20} cm^2)	Ω_4 (10^{-20} cm^2)	Ω_6 (10^{-20} cm^2)	Reference
$48InF_3$–$24BaF_2$–$7AlF_3$–$20LiF$–$1EuF_3$ glass	6.01	2.30	1.50	Annapurna and Buddhudu (1993)
$58NaPO_3$–$11BaF_2$–$30YF_3$–$1EuF_3$ glass	6.18	3.42	3.94	Binnemans (1996)
Y_2O_3:Eu^{3+} (crystal)	6.31	0.66	< 0.48	Krupke (1966)
Eu^{3+} in $30K_2O$–$10MgO$–$60SiO_2$ glass	6.36	3.94	0.51	Nageno et al. (1994)
$75NaPO_3$–$24MgF_2$–$1EuF_3$ glass	6.50	5.36	3.87	Binnemans et al. (1997c)
Eu^{3+} in $35K_2O$–$5MgO$–$60SiO_2$ glass	6.54	3.57	0.28	Nageno et al. (1994)
$75NaPO_3$–$24ZnF_2$–$1EuF_3$ glass	6.75	6.18	4.23	Binnemans et al. (1997c)
Eu^{3+} in $25K_2O$–$20MgO$–$60SiO_2$ glass	6.86	4.10	0.55	Nageno et al. (1994)
Eu^{3+} in $5K_2O$–$35MgO$–$60SiO_2$ glass	8.65	–	1.66	Nageno et al. (1994)
$Eu(picNO)_3$*o*-phen (powder)	8.7	5	–	de Sá et al. (1994)
Eu^{3+} in $10K_2O$–$30MgO$–$60SiO_2$ glass	8.98	–	1.52	Nageno et al. (1994)
Eu^{3+} in $20K_2O$–$20MgO$–$60SiO_2$ glass	9.28	4.81	0.88	Nageno et al. (1994)
Eu^{3+} in $10K_2O$–$30MgO$–$60SiO_2$ glass	9.65	6.68	1.15	Nageno et al. (1994)
Eu^{3+}:DPA (1:3) in water	10.50	5.31	8.32	Binnemans et al. (1997a)
Eu^{3+} in germanate glass	14.83	1.93	4.67	Reisfeld (1976)
$Eu(picNO)_3$Terpy (powder)	22.8	8.3	–	de Sá et al. (1994)
Eu^{3+} in $LiNO_3$–KNO_3 melt	26	–	4.60	Carnall et al. (1978)
$Eu(DBM)_3 \cdot 3H_2O$ (powder)	78.8	–	–	Kirby and Palmer (1981b)

Table 15
Phenomenological intensity parameters Ω_λ for Gd^{3+} in various host matrices; the host matrices are classified according to increasing values of Ω_2

Matrix	Ω_2 (10^{-20} cm^2)	Ω_4 (10^{-20} cm^2)	Ω_6 (10^{-20} cm^2)	Reference
$LiYF_4:Gd^{3+}$ (crystal)	0.32	–	1.8	Ellens (1996)
$LaF_3:Gd^{3+}$ (crystal)	1.1	1.2	0.5	Leavitt and Morrison (1980)
Gd^{3+} (aquo)	1.94±0.43	5.27±1.7	4.46±1.1	Carnall et al. (1983)
ZBLA:Gd^{3+} glass	2.44	–	2.12	McDougall et al. (1994a)
ZBLAN:Gd^{3+} glass	2.49	–	2.30	McDougall et al. (1994c)
ZBLALi:Gd^{3+} glass	2.58	–	2.34	McDougall et al. (1994c)
ZBLA:Gd^{3+} glass	2.7	–	2.5	Alonso et al. (1988)
ZBLALi:Gd^{3+} glass	2.7	–	2.5	Alonso et al. (1988)
ZBLAN:Gd^{3+} glass	3.35±0.62	–	2.81±0.08	Binnemans et al. (1997d)
ZBLAK:Gd^{3+} glass	4.66	–	1.88	McDougall et al. (1994c)
Gd^{3+} in lanthanum borate glass	7.27	–	4.11	Verwey et al. (1989)

Table 16
Phenomenological intensity parameters Ω_λ for Tb^{3+} in various host matrices; the host matrices are classified according to increasing values of Ω_2

Matrix	Ω_2 (10^{-20} cm^2)	Ω_4 (10^{-20} cm^2)	Ω_6 (10^{-20} cm^2)	Reference
Tb^{3+} in $40Na_2O$–$60SiO_2$ glass	–	0.48	0.78	Takebe et al. (1995)
Tb^{3+} in $20K_2O$–$20CaO$–$60SiO_2$ glass	–	0.61	1.05	Takebe et al. (1995)
$75NaPO_3$–$20CaF_2$–$5TbF_3$ glass	–	0.62±0.17	2.78±0.04	Binnemans et al. (1997c)
Tb^{3+} in $20Na_2O$–$20CaO$–$60SiO_2$ glass	–	0.68	1.39	Takebe et al. (1995)
Tb^{3+} in $30K_2O$–$70B_2O_3$ glass	–	0.73	1.76	Takebe et al. (1995)
Tb^{3+} in $20Li_2O$–$20CaO$–$60SiO_2$ glass	–	0.75	2.11	Takebe et al. (1995)
ZBLAK:Tb^{3+} glass	–0.20	3.53	1.88	McDougall et al. (1994c)
ZBLALi:Tb^{3+} glass	0	2.02	2.30	McDougall et al. (1994c)
ZBLA:Tb^{3+} glass	0.03	2.20	1.75	McDougall et al. (1994a)
ZBLAN:Tb^{3+} glass	0.03	1.88	2.48	McDougall et al. (1994c)
LaF_3:Tb^{3+} (crystal)	1.1	1.4	0.9	Leavitt and Morrison (1980)
$56NaPO_3$–$8BaF_2$–$36TbF_3$ glass	2.75	3.21	3.36	Duhamel-Henry et al. (1996)
Tb^{3+} (aquo)	2.76±5.3	7.95±6.2	2.87±1.0	Carnall et al. (1983)
$YAlO_3$:Tb^{3+} (crystal)	3.25	7.13	2.00	Weber et al. (1973)
$32ZnF_2$–$28CdF_2$–$20BaF_2$–$11LiF$–$5AlF_3$–$3LaF_3$–$1TbF_3$ glass	4.9	4.0	1.6	Martín et al. (1992)
Tb^{3+} in $30Li_2O$–$70B_2O_3$ glass	5.56	1.33	3.22	Takebe et al. (1995)
Tb^{3+} in $30Li_2O$–$60P_2O_5$–$10Al_2O_3$ glass	6.44	1.05	2.21	Takebe et al. (1995)
Tb^{3+} in $30BaO$–$70B_2O_3$ glass	6.72	0.95	2.81	Takebe et al. (1995)
Tb^{3+} in $30Na_2O$–$60P_2O_5$–$10Al_2O_3$ glass	6.80	1.11	2.27	Takebe et al. (1995)
Tb^{3+} in $30CaO$–$70B_2O_3$ glass	6.95	1.28	2.91	Takebe et al. (1995)
Tb^{3+} in $30BaO$–$60P_2O_5$–$10Al_2O_3$ glass	7.26	0.90	2.03	Takebe et al. (1995)
Tb^{3+} in $30CaO$–$70B_2O_3$ glass	7.51	0.79	1.60	Takebe et al. (1995)
Tb^{3+} in $30MgO$–$60P_2O_5$–$10Al_2O_3$ glass	8.41	0.86	1.31	Takebe et al. (1995)
Tb^{3+} in $30Na_2O$–$70B_2O_3$ glass	8.82	0.85	2.80	Takebe et al. (1995)
$30BaF_2$–$30InF_3$–$10ThF_4$–$9ZnF_2$–$20KF$–$1TbF_3$ glass	10.95	1.75	3.95	Amaranath et al. (1990a)
$30BaF_2$–$30InF_3$–$10ThF_4$–$9ZnF_2$–$10LiF$–$10KF$–$1TbF_3$ glass	12.27	2.04	4.31	Amaranath et al. (1990a)

continued on next page

Table 16, *continued*

Matrix	Ω_2 (10^{-20} cm^2)	Ω_4 (10^{-20} cm^2)	Ω_6 (10^{-20} cm^2)	Reference
$30BaF_2$–$30InF_3$–$10ThF_4$–$9ZnF_2$–$20NaF$–$1TbF_3$ glass	12.32	1.90	4.32	Amaranath et al. (1990a)
$30BaF_2$–$30InF_3$–$10ThF_4$–$9ZnF_2$–$20LiF$–$1TbF_3$ glass	13.40	2.15	4.90	Amaranath et al. (1990a)
$30BaF_2$–$30InF_3$–$10ThF_4$–$9ZnF_2$–$10NaF$–$10KF$–$1TbF_3$ glass	13.73	2.29	4.85	Amaranath et al. (1990a)
$30BaF_2$–$30InF_3$–$10ThF_4$–$9ZnF_2$–$10LiF$–$10NaF$–$1TbF_3$ glass	14.42	2.45	5.18	Amaranath et al. (1990a)
Tb^{3+} in $LiNO_3$–KNO_3 melt	15	2.86±2.6	5.24±0.7	Carnall et al. (1978)
$TbCl_3$–$(AlCl_3)_x$ vapor complex	20.5±1.2	2.30±0.96	3.0±0.17	Caird et al. (1981)

Table 17
Phenomenological intensity parameters Ω_λ for Dy^{3+} in various host matrices; the host matrices are classified according to increasing values of Ω_2

Matrix	Ω_2 (10^{-20} cm^2)	Ω_4 (10^{-20} cm^2)	Ω_6 (10^{-20} cm^2)	Reference
$K_7[DyW_{10}O_{35}]$	−23.01±6.65	4.95±0.66	3.28±0.32	Peacock (1973)
Dy^{3+} (aquo)	0.584±6.3	3.54±0.74	3.90±0.62	Carnall et al. (1983)
LaF_3:Dy^{3+} (crystal)	1.10	1.40	0.90	Xu et al. (1984)
Dy^{3+}:ODA (1:3 in water)	1.030±0.235	0.271±0.265	1.211±0.127	Jung et al. (1992)
Dy^{3+}:MIDA (1:3 in water)	1.292±0.338	−0.333±0.381	1.277±0.182	Jung et al. (1992)
Dy^{3+}:IDA (1:3 in water)	1.298±0.250	0.177±0.282	1.192±0.135	Jung et al. (1992)
$Dy_2(C_5H_8NO_4)_2(ClO_4)_4 \cdot 9H_2O$	1.35±0.80	2.67±0.35	3.82±0.37	Csöreg et al. (1989)
Dy(α-picolinate) in water	1.37±0.55	3.44±0.38	4.70±0.46	Bukietynska and Choppin (1970)
Dy^{3+} in $35ZnF_2$–$15CdF_2$–$25BaF_2$–$12LiF$–$7AlF_3$–$6LaF_3$ glass	1.38	1.05	2.35	Cases et al. (1991)
Dy^{3+} in Na_2O–P_2O_5 glass	1.46±1.99	1.16±0.21	1.97±0.10	Hormadaly and Reisfeld (1979)
Dy^{3+}:DPA (1:3 in water)	1.767±0.216	0.735±0.243	1.402±0.116	Jung et al. (1992)
ZBLAN:Dy^{3+} glass	1.86	1.42	2.37	Wetenkamp et al. (1992)
$DyCl_3 \cdot xH_2O$ in CH_3OH	2.02±0.54	2.69±0.19	2.67±0.25	Legendziewicz et al. (1984)
ZBLALi:Dy^{3+} glass	2.60	1.13	1.91	McDougall et al. (1994c)
ZBLA:Dy^{3+} glass	2.65	1.29	1.72	McDougall et al. (1994a)
ZBLALi:Dy^{3+} glass	2.7	1.8	2.0	Orera et al. (1988)
ZBLAN:Dy^{3+} glass	3.03	1.32	2.06	McDougall et al. (1994c)
Dy^{3+} in $POCl_3/ZrCl_4$ (solution)	3.09±0.19	2.23±0.21	3.33±0.09	Bukietynska and Radomska (1981)
ZBLAK:Dy^{3+} glass	3.13	1.14	1.87	McDougall et al. (1994c)
Dy^{3+} in $52HfF_4$–$18BaF_2$–$3LaF_3$–$2AlF_3$–$25CsBr$ glass	3.12	2.07	2.48	Cases and Chamarro (1991)
Dy^{3+} in BaO–TeO_2 glass	3.20±0.86	1.35±0.09	2.47±0.04	Hormadaly and Reisfeld (1979)
ZBLA:Dy^{3+} glass	3.22	1.35	2.38	Adam et al. (1988)
$75NaPO_3$–$24CaF_2$–$1DyF_3$ glass	3.63±0.34	2.03±0.32	1.89±0.19	Binnemans et al. (1997c)
Dy^{3+} in Na_2O–TeO_2 glass	3.70±1.35	1.15±0.14	2.22±0.07	Hormadaly and Reisfeld (1979)
$DyCl_3 \cdot xH_2O$ in C_2H_5OH	4.27±0.44	2.20±0.20	1.74±0.21	Legendziewicz et al. (1984)
Dy^{3+} in ZnO–TeO_2 glass	4.28±1.36	1.32±0.14	2.53±0.07	Hormadaly and Reisfeld (1979)

continued on next page

Table 17, *continued*

Matrix	Ω_2 (10^{-20} cm^2)	Ω_4 (10^{-20} cm^2)	Ω_6 (10^{-20} cm^2)	Reference
Dy^{3+} in $20Li_2O$–$20CaO$–$60SiO_2$ glass	5.87	1.94	1.22	Takebe et al. (1995)
Dy^{3+} in $30Li_2O$–$70B_2O_3$ glass	5.90	1.82	2.02	Takebe et al. (1995)
Dy^{3+} in $30CaO$–$70B_2O_3$ glass	5.99	2.01	1.96	Takebe et al. (1995)
Dy^{3+} in $40Na_2O$–$60SiO_2$ glass	6.04	0.90	0.24	Takebe et al. (1995)
Dy^{3+} in $30Li_2O$–$60P_2O_5$–$10Al_2O_3$ glass	6.19	1.80	1.50	Takebe et al. (1995)
Dy^{3+} in $20Na_2O$–$20CaO$–$60SiO_2$ glass	6.42	1.46	0.65	Takebe et al. (1995)
Dy^{3+} in $30BaO$–$71B_2O_3$ glass	6.44	1.66	1.84	Takebe et al. (1995)
Dy^{3+} in $30K_2O$–$70B_2O_3$ glass	6.62	0.99	0.63	Takebe et al. (1995)
$Dy_2(CH_3COO)_6 \cdot 4H_2O$ (crystal)	6.69±0.70	1.89±0.30	3.67±0.32	Mondry and Bukietynska (1996)
Dy^{3+} in $30Na_2O$–$60P_2O_5$–$10Al_2O_3$ glass	6.70	1.98	1.73	Takebe et al. (1995)
Dy^{3+} in $20K_2O$–$20CaO$–$60SiO_2$ glass	6.81	1.39	0.43	Takebe et al. (1995)
Dy^{3+} in $30Na_2O$–$70B_2O_3$ glass	6.85	1.64	1.61	Takebe et al. (1995)
Dy^{3+} in $30BaO$–$60P_2O_5$–$10Al_2O_3$ glass	7.11	1.75	1.47	Takebe et al. (1995)
$DyCl_3 \cdot xH_2O$ in C_3H_7OH	7.39±0.37	2.42±0.16	2.00±0.18	Legendziewicz et al. (1984)
Dy^{3+} in $30CaO$–$60P_2O_5$–$10Al_2O_3$ glass	8.13	1.48	1.21	Takebe et al. (1995)
Dy^{3+} in $30MgO$–$60P_2O_5$–$10Al_2O_3$ glass	8.21	1.38	1.14	Takebe et al. (1995)
$LiNbO_3$:Dy^{3+} (crystal)	9.57	2.63	2.52	Malinowski et al. (1996)
Dy^{3+} in $Ge_{30}As_{10}S_{60}$ glass	10.53	3.17	1.17	Heo and Shin (1996)
Dy^{3+} in $Ge_{25}Ga_5S_{70}$ glass	11.86	4.00	1.47	Heo and Shin (1996)
Dy^{3+} in $70Ga_2S_3$–$30La_2S_3$ glass	11.3	1.0	1.3	Hewak et al. (1994b); Schweizer et al. (1996)
Dy^{3+} in $Ge_{25}Ga_5O_{70}$ glass	11.90	3.58	2.17	Wei et al. (1994)
Dy^{3+} in $LiNO_3$–KNO_3 melt	14.4±0.3	1.4±0.4	3.16±0.2	Carnall et al. (1978)

Table 18
Phenomenological intensity parameters Ω_λ for Ho^{3+} in various host matrices; the host matrices are classified according to increasing values of Ω_2

Matrix	Ω_2 (10^{-20} cm^2)	Ω_4 (10^{-20} cm^2)	Ω_6 (10^{-20} cm^2)	Reference
$Ho(NO_3)_3 \cdot 6H_2O$ in phtalic acid	0.697	6.146	7.086	Buddhudu et al. (1991)
Ho^{3+} (*aquo*)	0.791±0.79	3.13±0.40	2.86±0.26	Carnall et al. (1983)
Ho^{3+} in $32ZnF_2$–$28CdF_2$–$20BaF_2$–$11LiF$–$5AlF_3$–$4LaF_3$ glass	0.8	2.6	2.0	Villacampa et al. (1991a)
LaF_3:Ho^{3+} (crystal)	1.16	1.38	0.88	Weber et al. (1972)
$Ho(NO_3)_3 \cdot 6H_2O$ in benzoic acid	1.191	9.040	7.908	Buddhudu et al. (1991)
$Y_3Al_5O_{12}$:Ho^{3+} (crystal)	1.2	5.29	1.48	Antipenko and Tomashevich (1978)
Ho^{3+}:NTA (1:1) in water	1.56±0.30	3.70±0.43	3.39±0.30	Bukietynska and Mondry (1987)
$Ho(NO_3)_3 \cdot 6H_2O$ in salicylic acid	1.643	6.273	8.228	Buddhudu et al. (1991)
$50(NaPO_3)_6$–$18BaF_2$–$10ZnF_2$–$20KF$–$2HoF_3$ glass	1.660	2.894	0.632	Ranga Reddy et al. (1993)
Ho^{3+} in BZYTZ fluoride glass	1.73±0.25	1.89±0.39	1.43±0.26	Eyal et al. (1987a)
Ho^{3+}:NTA (1:3 in water)	1.76±0.37	4.33±0.54	3.89±0.38	Bukietynska and Mondry (1987)
$La_3Ga_5SiO_{14}$:Ho^{3+} (crystal)	1.78	2.74	1.16	Kaminskii et al. (1990)
Ho^{3+} in AlF_3–ZrF_4–MgF_2–CaF_2–SrF_2–BaF_2–NaF–$NaCl$ glass	1.86	1.90	1.32	Peng and Izumitani (1995)
Ho^{3+}:NTA (1:4 in water)	1.87±0.31	4.43±0.46	4.02±0.32	Bukietynska and Mondry (1987)
ZBLAN:Ho^{3+} glass	1.90	2.09	1.56	McDougall et al. (1994c)
Ho^{3+}:NTA (1:2 in water)	1.94±0.33	4.26±0.48	3.67±0.33	Bukietynska and Mondry (1987)
Ho^{3+}:(12-crown-4) (1:1 in acetonitrile)	1.968±0.242	0.799±0.371	0.784±0.242	Kang et al. (1995)
ZBLALi:Ho^{3+} glass	1.99	2.34	1.70	McDougall et al. (1994c)
Ho^{3+} in P_2O_5–AlF_3–YF_3–MgF_2–CaF_2–SrF_2–BaF_2–NaF glass	2.1	3.5	2.5	Peng and Izumitani (1995)
$48ZrF_4$–$23BaF_2$–$8AlF_3$–$5NaF$–$15KF$–$1HoF_3$ glass	2.12	0.50	0.73	Buddhudu and Bryant (1988)
$48(NaPO_3)_6$–$20BaCl_2$–$10ZnCl_2$–$20LiCl$–$2HoCl_3$ glass	2.14	9.91	0.27	Subramanyam Naidu and Buddhudu (1992d)
ZBLAN:Ho^{3+} glass	2.14	2.22	2.05	Binnemans (1996)
Ho^{3+}:(15-crown-15) (1:1) in acetonitrile	2.154±0.214	0.713±0.314	0.784±0.214	Kang et al. (1995)
$50(NaPO_3)_6$–$18BaF_2$–$10ZnF_2$–$20LiF$–$2HoF_3$ glass	2.169	4.930	0.985	Ranga Reddy et al. (1993)
$48(NaPO_3)_6$–$20BaCl_2$–$10ZnCl_2$–$20NaCl$–$2HoCl_3$ glass	2.18	5.92	0.96	Subramanyam Naidu and Buddhudu (1992d)

continued on next page

Table 18, *continued*

Matrix	Ω_2 (10^{-20} cm^2)	Ω_4 (10^{-20} cm^2)	Ω_6 (10^{-20} cm^2)	Reference
ZBLAK:Ho^{3+} glass	2.20	1.91	1.38	McDougall et al. (1994c)
$75NaPO_3$–$24CaF_2$–$1HoF_3$ glass	3.23±0.20	2.71±0.30	1.82±0.11	Binnemans et al. (1997c)
ZBLA:Ho^{3+} (glass)	2.28	2.38	1.79	McDougall et al. (1994a)
ZBLA:Ho^{3+} (glass)	2.28	2.08	1.73	Tanimura et al. (1984)
ZBLAN:Ho^{3+} glass	2.30	2.30	1.71	Wetenkamp et al. (1992)
$50(NaPO_3)_6$–$18BaF_2$–$10ZnF_2$–$10LiF$–$10NaF$–$2HoF_3$ glass	2.419	6.219	0.758	Ranga Reddy et al. (1993)
ZBLA:Ho^{3+} (glass)	2.43±0.08	1.67±0.15	1.84±0.06	Reisfeld et al. (1985)
$50(NaPO_3)_6$–$18BaF_2$–$10ZnF_2$–$20KF$–$2HoF_3$ glass	2.720	2.518	0.771	Ranga Reddy et al. (1993)
$48(NaPO_3)_6$–$20BaCl_2$–$10ZnCl_2$–$20KCl$–$2HoCl_3$ glass	2.82	3.92	0.67	Subramanyam Naidu and Buddhudu (1992d)
$48(NaPO_3)_6$–$20BaCl_2$–$10ZnCl_2$–$10LiCl$–$10KCl$–$2HoCl_3$ glass	2.90	5.13	1.32	Subramanyam Naidu and Buddhudu (1992d)
$50(NaPO_3)_6$–$18BaF_2$–$10ZnF_2$–$10NaF$–$10KF$–$2HoF_3$ glass	3.099	4.363	0.635	Ranga Reddy et al. (1993)
$48(NaPO_3)_6$–$20BaCl_2$–$10ZnCl_2$–$10NaCl$–$10LiCl$–$2HoCl_3$ glass	3.11	7.12	0.77	Subramanyam Naidu and Buddhudu (1992d)
Ho:DPA (1:1, pH = 2.93)	3.14±0.30	3.52±0.44	3.74±0.31	Mondry (1989)
$48ZrF_4$–$23BaF_2$–$8AlF_3$–$15NaF$–$5KF$–$1HoF_3$ glass	3.15	0.74	1.09	Buddhudu and Bryant (1988)
$50(NaPO_3)_6$–$18BaF_2$–$10ZnF_2$–$10KF$–$10LiF$–$2HoF_3$ glass	3.195	3.549	0.457	Ranga Reddy et al. (1993)
Ho^{3+} in GeO_2–BaO–K_2O glass	3.30	1.14	0.14	Peng and Izumitani (1995)
Ho^{3+} in $52HfF_4$–$18BaF_2$–$3LaF_3$–$2AlF_3$–25CsBr glass	3.30	2.22	1.93	Cases and Chamarro (1991)
Ho^{3+} in P_2O_5–Al_2O_3–MgO–BaO–K_2O glass	3.33	3.01	0.61	Peng and Izumitani (1995)
$K_7[HoW_{10}O_{35}]$	3.52±0.13	2.33±0.19	2.60±0.14	Peacock (1973)
Ho^{3+} in SiO_2–Al_2O_3–Li_2O–Na_2O–SrO glass	3.60	2.30	0.65	Peng and Izumitani (1995)
$48(NaPO_3)_6$–$20BaCl_2$–$10ZnCl_2$–$10NaCl$–$10KCl$–$2HoCl_3$ glass	3.64	3.36	0.84	Subramanyam Naidu and Buddhudu (1992d)
Ho:ODA (1:3 in water)	3.88±0.28	4.02±0.41	4.24±0.23	Devlin et al. (1988)

continued on next page

Table 18, *continued*

Matrix	Ω_2 (10^{-20} cm^2)	Ω_4 (10^{-20} cm^2)	Ω_6 (10^{-20} cm^2)	Reference
Ho^{3+} in $20Li_2O$–$20CaO$–$60SiO_2$ glass	4.03	2.47	1.07	Takebe et al. (1995)
$48ZrF_4$–$23BaF_2$–$8AlF_3$–$10NaF$–$10KF$–$1HoF_3$ glass	4.09	0.97	1.41	Buddhudu and Bryant (1988)
Ho:IDA (1:3 in water)	4.09±0.34	5.01±0.50	4.18±0.28	Devlin et al. (1988)
Ho^{3+} in $40Na_2O$–$60SiO_2$ glass	4.24	1.09	0.47	Takebe et al. (1995)
Ho^{3+} in $20Na_2O$–$20CaO$–$60SiO_2$ glass	4.44	1.51	0.71	Takebe et al. (1995)
Ho^{3+} in $30Li_2O$–$70B_2O_3$ glass	4.56	3.14	1.78	Takebe et al. (1995)
Ho(α-picolinate) in water	4.62±0.62	4.07±0.88	3.88±0.73	Bukietynska and Choppin (1970)
$Ho(NO_3)_3 \cdot 6H_2O$ in anthrolinic acid	4.628	1.116	7.978	Buddhudu et al. (1991)
Ho:MIDA (1:3 in water)	4.64±0.23	3.76±0.34	3.32±0.19	Devlin et al. (1988)
Ho^{3+} in $56PbO$–$27Bi_2O_3$–$17Ga_2O_3$ glass	4.77	2.18	1.22	Shin et al. (1995)
Ho^{3+} in Al_2O_3–CaO–MgO–BaO glass	4.90	2.50	0.68	Peng and Izumitani (1995)
Ho^{3+} in $30CaO$–$70B_2O_3$ glass	4.90	3.29	1.74	Takebe et al. (1995)
Ho^{3+} in $30Li_2O$–$60P_2O_5$–$10Al_2O_3$ glass	4.92	2.28	1.54	Takebe et al. (1995)
Ho^{3+} in $30BaO$–$70B_2O_3$ glass	4.96	2.99	1.61	Takebe et al. (1995)
Ho^{3+}:DPA (1:2, pH = 3.17)	5.14±0.55	3.84±0.81	3.71±0.57	Mondry (1989)
Ho^{3+} in $20K_2O$–$20CaO$–$60SiO_2$ glass	5.19	1.35	0.61	Takebe et al. (1995)
Ho^{3+} in $30K_2O$–$70B_2O_3$ glass	5.29	1.40	0.78	Takebe et al. (1995)
Ho^{3+} in $30Na_2O$–$70B_2O_3$ glass	5.30	2.52	1.53	Takebe et al. (1995)
Ho^{3+} in $30Na_2O$–$60P_2O_5$–$10Al_2O_3$ glass	5.31	2.62	1.62	Takebe et al. (1995)
$48ZrF_4$–$23BaF_2$–$8AlF_3$–$10LiF$–$10NaF$–$1HoF_3$ glass	5.32	1.26	1.84	Buddhudu and Bryant (1988)
Ho^{3+}:DPA (1:4, pH = 3.33)	5.35±0.46	3.97±0.67	4.28±0.47	Mondry (1989)
Ho^{3+} in $30BaO$–$60P_2O_5$–$10Al_2O_3$ glass	5.36	2.39	1.33	Takebe et al. (1995)
Ho^{3+} in $NaPO_3$ glass	5.60±0.28	2.72±0.41	1.87±0.26	Reisfeld and Hormadaly (1976)
Ho^{3+} in Ga_2O_3–K_2O–CaO–SrO–BaO glass	5.70	3.10	0.37	Peng and Izumitani (1995)
Ho^{3+} in $30CaO$–$60P_2O_5$–$10Al_2O_3$ glass	6.23	1.56	1.21	Takebe et al. (1995)

continued on next page

Table 18, *continued*

Matrix	Ω_2 (10^{-20} cm^2)	Ω_4 (10^{-20} cm^2)	Ω_6 (10^{-20} cm^2)	Reference
Ho:DPA (1:3 in water)	6.39±0.45	4.03±0.67	4.11±0.37	Devlin et al. (1988)
Ho^{3+} in $30MgO–60P_2O_5–10Al_2O_3$ glass	6.58	1.57	1.09	Takebe et al. (1995)
$48ZrF_4–23BaF_2–8AlF_3–5LiF–15NaF–1HoF_3$ glass	6.77	1.31	1.87	Buddhudu and Bryant (1988)
Ho^{3+} in $CaO–Li_2O–B_2O_3$ glass	6.83±0.29	3.15±0.42	2.53±0.31	Reisfeld and Hormadaly (1976)
Ho^{3+} in $20Na_2O–80TeO_2$ glass	6.92±0.22	2.81±0.33	1.42±0.20	Reisfeld and Hormadaly (1976)
Ho^{3+} in $Ge_{30}As_{10}S_{60}$ glass	6.98	2.53	0.78	Shin et al. (1995)
Ho^{3+}:DPA (1:4, pH = 7.10)	7.72±0.60	3.80±0.89	5.32±0.63	Mondry (1989)
Ho^{3+}:DPA (1:4, pH = 11.17)	7.54±0.60	3.91±0.88	5.25±0.62	Mondry (1989)
Ho^{3+} in $La_2S_3–3Al_2S_3$ glass	8.1	3.8	1.4	Reisfeld (1982)
$48ZrF_4–23BaF_2–8AlF_3–15LiF–5NaF–1HoF_3$ glass	8.13	1.58	2.24	Buddhudu and Bryant (1988)
$Na_3[Ho(dpa)_3]·NaClO_4·10H_2O$ (crystal)	9.27±0.42	3.49±0.61	4.55±0.43	Mondry (1989)
$81B_2O_3–10Na_2O–8AlF_3–1HoF_3$ glass	9.934	22.989	3.096	Sathyanarayana et al. (1996)
Ho^{3+}:CDA (1:3 in water)	10.11±0.62	5.07±0.93	4.81±0.52	Devlin et al. (1988)
Ho^{3+}:CDO (1:3 in water)	11.09±0.57	5.17±0.86	4.86±0.48	Devlin et al. (1988)
$81B_2O_3–10Na_2O–8LiF–1HoF_3$ glass	11.920	17.025	2.964	Sathyanarayana et al. (1996)
$81B_2O_3–10Na_2O–8NaF–1HoF_3$ glass	12.174	18.895	4.745	Sathyanarayana et al. (1996)
$81B_2O_3–10Na_2O–4NaF–4AlF_3–1HoF_3$ glass	12.861	12.770	7.141	Sathyanarayana et al. (1996)
$81B_2O_3–10Na_2O–4LiF–4AlF_3–1HoF_3$ glass	12.989	10.206	8.160	Sathyanarayana et al. (1996)
Ho^{3+} in $LiNO_3–KNO_3$ melt	16.4±0.2	3.6±0.3	2.3±0.2	Carnall et al. (1978)
$10Li_2SO_4·H_2O–40ZnSO_4·7H_2O–49B_2O_3–1Ho_2(SO_4)_3·8H_2O$ glass	18.95	7.25	10.45	Rukmini and Jayasankar (1995)
$10Na_2SO_4·H_2O–40ZnSO_4·7H_2O–49B_2O_3–1Ho_2(SO_4)_3·8H_2O$ glass	20.32	10.34	11.31	Rukmini and Jayasankar (1995)
$10K_2SO_4·H_2O–40ZnSO_4·7H_2O–49B_2O_3–1Ho_2(SO_4)_3·8H_2O$ glass	21.92	7.45	11.23	Rukmini and Jayasankar (1995)
$50ZnSO_4·7H_2O–49B_2O_3–1Ho_2(SO_4)_3·8H_2O$ glass	22.42	5.19	12.33	Rukmini and Jayasankar (1995)
$Ho(DBM)_3·H_2O$ (powder)	42.8	<0.01	1.95	Kirby and Palmer (1981b)

Table 19
Phenomenological intensity parameters Ω_λ for Er^{3+} in various host matrices; the host matrices are classified according to increasing values of Ω_2

Matrix	Ω_2 (10^{-20} cm^2)	Ω_4 (10^{-20} cm^2)	Ω_6 (10^{-20} cm^2)	Reference
$Y_3Al_5O_{12}:Er^{3+}$ (crystal)	0.19	1.68	0.62	Wang et al. (1986)
$Y_3Al_5O_{12}:Er^{3+}$ (20.57% Er^{3+}) (crystal)	0.32	1.19	0.80	Wang et al. (1993)
$Y_3Al_5O_{12}:Er^{3+}$ (29.06% Er^{3+}) (crystal)	0.40	0.65	0.75	Wang et al. (1993)
$Y_3Al_5O_{12}:Er^{3+}$	0.45	0.98	0.62	Kaminskii et al. (1982)
$Y_3Al_5O_{12}:Er^{3+}$ (17.38% Er^{3+}) (crystal)	0.56	0.99	0.78	Wang et al. (1993)
$KCaF_3:Er^{3+}$ (crystal)	0.74	0.87	0.57	Chen et al. (1989)
$LiErP_4O_{12}$ (crystal)	0.85±0.09	0.96±0.19	0.72±0.09	Ryba-Romanowski et al. (1980)
$YAlO_3:Er^{3+}$ (crystal)	0.95	0.58	0.55	Kaminskii et al. (1995a,b)
$LiYF_4:Er^{3+}$ (crystal)	0.97	1.21	1.37	Wu et al. (1986)
$BaYb_2F_8:Er^{3+}$ (crystal)	1.062	0.409	0.946	Kaminskii et al. (1996)
$Y_3Al_5O_{12}:Er^{3+}$ (0.52% Er^{3+}) (crystal)	1.07	1.61	1.14	Wang et al. (1993)
$LaF_3:Er^{3+}$ (crystal)	1.16	1.38	0.88	Weber et al. (1972)
$36AlF_3$–$7.5YF_3$–$2LaF_3$–$50(MgF_2$–CaF_2–SrF_2–$BaF_2)$–$4.5ErF_3$ glass	1.28	1.35	1.01	Yanagita et al. (1991)
Er^{3+} in $32ZnF_2$–$28CdF_2$–$20BaF_2$–$11LiF$–$5AlF_3$–$4LaF_3$ glass	1.3	1.6	0.9	Villacampa et al. (1991a)
$10MgCO_3$–$39Li_2CO_3$–$50H_3BO_3$–$1Er_2O_3$ glass	1.33	0.39	0.62	Devi and Jayasankar (1996a)
Er^{3+} (aquo)	1.34±0.37	2.19±0.25	1.88±0.11	Carnall et al. (1983)
$Y_3Al_5O_{12}$ (0.79% Er^{3+}) (crystal)	1.43	1.64	1.28	Wang et al. (1993)
$LiYF_4:Er^{3+}$ (crystal)	1.48	0.92	1.00	Hubert et al. (1991)
AlF_3–MgF_2–CaF_2–SrF_2–$Sr(PO_3)_2$–ErF_3 glass	1.48	0.78	1.07	Ledig et al. (1990)
$48(NaPO_3)_6$–$20BaCl_2$–$10ZnCl_2$–$10KCl$–$10LiCl$–$2ErCl_3$ glass	1.50	7.21	4.15	Subramanyam Naidu and Buddhudu (1992c)
Er^{3+} in yttria-stabilized zirconia (crystal)	1.50	0.50	0.22	Merino et al. (1991)
Er^{3+} in PbZnGaLa fluoride glass	1.54±0.25	1.13±0.40	1.19±0.20	Reisfeld et al. (1982)
$Bi_4Ge_3O_{12}:Er^{3+}$ (crystal)	1.66	0.46	0.21	Kaminskii et al. (1979)
ErP_5O_{14} (crystal)	1.68±0.17	2.07±0.12	0.98±0.21	Ryba-Romanowski et al. (1980)
Er^{3+} in $55ZnF_2$–$30BaF_2$–$15YF_3$ glass	1.78	1.48	1.12	Tanabe et al. (1995b)

continued on next page

Table 19, *continued*

Matrix	Ω_2 (10^{-20} cm^2)	Ω_4 (10^{-20} cm^2)	Ω_6 (10^{-20} cm^2)	Reference
$33CdCl_2$–$17CdF_2$–$34NaF$–$13BaF_2$–$3KF$ glass (0.15 mol% Er^{3+})	1.80	2.62	1.35	Adam et al. (1994,1995)
$10CaCO_3$–$39Li_2CO_3$–$50H_3BO_3$–$1Er_2O_3$ glass	1.80	0.28	0.90	Devi and Jayasankar (1996a)
$YAlO_3$:Er^{3+} (crystal)	1.82	2.38	1.53	Weber et al. (1972)
ZBLAK:Er^{3+} glass	1.86	0.94	0.73	McDougall et al. (1994c)
BZYTZ:Er^{3+} fluoride glass	1.89±0.10	1.54±0.15	0.95±0.10	Eyal et al. (1987a)
$LiYF_4$:Er^{3+}	1.92	0.26	1.96	Tkachuk et al. (1985)
ZBLALi:Er^{3+} glass	2.06	1.42	0.87	McDougall et al. (1994c)
$25AlF_3$–$13ZrF_4$–$6YF_3$–$46(MgF_2$–CaF_2–SrF_2–$BaF_2)$–$3NaCl$–$5ErF_3$ glass	2.08	1.29	1.15	Yanagita et al. (1991)
Er^{3+} in $45InF_3$–$40BaF_2$–$15YF_3$ glass	2.10	1.59	1.10	Tanabe et al. (1995b)
Er^{3+} in $45ScF_3$–$40BaF_2$–$15YF_3$ glass	2.17	1.45	1.09	Tanabe et al. (1995b)
$20ZnF_2$–$20SrF_2$–$2NaF$–$16BaF_2$–$6GaF_3$–$35InF_3$–$1ErF_3$ glass	2.17	2.31	0.89	Flórez et al. (1995)
$48(NaPO_3)_6$–$20BaCl_2$–$10ZnCl_2$–$20KCl$–$2ErCl_3$ glass	2.18	3.97	4.71	Subramanyam Naidu and Buddhudu (1992c)
$20ZnF_2$–$20SrF_2$–$2NaF$–$16BaF_2$–$6GaF_3$–$33InF_3$–$3ErF_3$ glass	2.18	1.68	1.10	Flórez et al. (1995)
$30BaF_2$–$20ZnF_2$–$30InF_3$–$8YbF_3$–$10ThF_4$–$2ErF_3$ glass	2.19	1.52	0.91	Yeh et al. (1989)
ZBLAN:Er^{3+} glass	2.20	1.40	0.91	McDougall et al. (1994c)
$75NaPO_3$–$24CaF_2$–$1ErF_3$ glass	2.25±0.13	1.01±0.18	0.80±0.07	Binnemans et al. (1997c)
Er^{3+} in $45AlF_3$–$30BaF_2$–$25YF_3$ glass	2.27	1.31	0.98	Tanabe et al. (1995b)
$48(NaPO_3)_6$–$20BaCl_2$–$10ZnCl_2$–$20NaCl$–$2ErCl_3$ glass	2.27	2.23	4.98	Subramanyam Naidu and Buddhudu (1992c)
Er^{3+} in $45GaF_3$–$30BaF_2$–$25YF_3$ glass	2.33	1.51	1.00	Tanabe et al. (1995b)
$48(NaPO_3)_6$–$20BaCl_2$–$10ZnCl_2$–$20LiCl$–$2ErCl_3$ glass	2.39	1.43	0.85	Subramanyam Naidu and Buddhudu (1992c)
BZYTL:Er^{3+} fluoride glass	2.44	1.55	1.18	Eyal et al. (1987a)
$20ZnF_2$–$20SrF_2$–$2NaF$–$16BaF_2$–$6GaF_3$–$32InF_3$–$4ErF_3$ glass	2.45	1.47	1.22	Flórez et al. (1995)

continued on next page

Table 19, *continued*

Matrix	Ω_2 (10^{-20} cm^2)	Ω_4 (10^{-20} cm^2)	Ω_6 (10^{-20} cm^2)	Reference
$20ZnF_2$–$20SrF_2$–$2NaF$–$16BaF_2$–$6GaF_3$–$34InF_3$–$2ErF_3$ glass	2.46	1.63	1.23	Flórez et al. (1995)
$48(NaPO_3)_6$–$20BaCl_2$–$10ZnCl_2$–$10KCl$–$10LiCl$–$2ErCl_3$ glass	2.51	4.15	4.70	Subramanyam Naidu and Buddhudu (1992c)
$10SrCO_3$–$39Li_2CO_3$–$50H_3BO_3$–$1Er_2O_3$ glass	2.53	0.39	1.10	Devi and Jayasankar (1996a)
ZBLA:Er^{3+} glass	2.54	1.39	0.965	Shinn et al. (1983)
$LiYF_4$:Er^{3+} (crystal)	2.56	0.35	2.05	Kaminskii et al. (1995a)
ZBLA:Er^{3+} glass	2.59	1.30	0.85	McDougall et al. (1994a)
$50(NaPO_3)_6$–$18BaF_2$–$10ZnF_2$–$10KF$–$10LiF$–$2ErF_3$ glass	2.7295	1.6522	2.6806	Ranga Reddy et al. (1992b)
Er^{3+} in $50HfF_4$–$30BaF_2$–$20YF_3$ glass	2.84	1.52	1.01	Tanabe et al. (1995b)
Y_2SiO_5:Er^{3+} (crystal)	2.84	1.42	0.82	Li et al. (1992)
Er^{3+} in fluorophosphate glass	2.88	1.40	1.27	Yanagita et al. (1991)
ZBLAN:Er^{3+}	2.91	1.78	1.00	Wetenkamp et al. (1992)
$53ZrF_4$–$20BaF_2$–$4LaF_3$–$3AlF_3$–$20NaF$–$1ErF_3$ (ZBLAN-20) glass	2.91	1.27	1.11	Zou and Izumitani (1993)
$10PO_{2.5}$–$33AlF_3$–$4YF_3$–$48(MgF_2$–CaF_2–SrF_2–$BaF_2)$–$5NaF$–$1ErO_{1.5}$ glass	2.91	1.63	1.26	Zou and Izumitani (1993)
Er^{3+} in $50ZrF_4$–$30BaF_2$–$20YF_3$ glass	2.93	1.52	1.02	Tanabe et al. (1995b)
ZBLAN:Er^{3+}	2.97	1.23	1.17	Yanagita et al. (1991)
Er^{3+}:NTA (1:1 in water)	3.16±0.29	2.35±0.47	2.04±0.26	Bukietynska and Mondry (1987)
$ErCl_3 \cdot 6H_2O$ in methanol	3.20±0.22	3.25±0.16	0.8±0.3	Keller et al. (1982)
Er^{3+} in $52HfF_4$–$18BaF_2$–$3LaF_3$–$2AlF_3$–$25CsBr$ glass	3.20	1.65	1.23	Cases and Chamarro (1991)
$49Li_2CO_3$–H_3BO_3–$1Er_2O_3$ glass	3.24	0.92	0.82	Devi and Jayasankar (1996a)
$Er(CCl_3COO)_3.2H_2O$ (crystal)	3.31±0.15	1.12±0.23	1.10±0.12	Legendziewicz et al. (1991)
$50(NaPO_3)_6$–$18BaF_2$–$10ZnF_2$–$20KF$–$2ErF_3$ glass	3.4001	5.9560	2.4358	Ranga Reddy et al. (1992b)
$Er_2(CH_3COO)_6 \cdot 4H_2O$ (crystal)	3.58±0.33	1.24±0.51	1.36±0.27	Mondry and Bukietynska (1996)
$10CaCO_3$–$39Li_2CO_3$–$50H_3BO_3$–$1Er_2O_3$ glass	3.68	0.76	1.52	Devi and Jayasankar (1996a)
$NaPO_3$–$1Er_2O_3$ glass	3.73	1.00	0.72	McDougall et al. (1996)

continued on next page

Table 19, *continued*

Matrix	Ω_2 (10^{-20} cm^2)	Ω_4 (10^{-20} cm^2)	Ω_6 (10^{-20} cm^2)	Reference
Er^{3+} in La_2S_3–$3Al_2O_3$ glass	3.74	4.33	0.90	Reisfeld (1982)
$CaYAlO_4$:Er^{3+} (crystal)	3.78	2.52	1.91	Souriau et al. (1994)
Er^{3+}:NTA (1:2 in water)	3.84±0.33	2.31±0.52	2.16±0.30	Bukietynska and Mondry (1987)
$Ca_2Al_2SiO_7$:Er^{3+} (crystal)	3.85	1.85	1.00	Simondi-Teisseire et al. (1996)
Er^{3+}:MAL (1:3 in water)	3.88±0.42	1.95±0.56	2.15±0.64	Devlin et al. (1987a)
Y_2O_2S:Er^{3+} (crystal)	3.90	0.91	0.97	Timofeev et al. (1990)
$48(NaPO_3)_6$–$20BaCl_2$–$10ZnCl_2$–10LiCl–10NaCl–$2ErCl_3$ glass	4.04	1.17	3.67	Subramanyam Naidu and Buddhudu (1992c)
Er^{3+}:NTA (1:3) in water	4.05±0.37	2.35±0.54	2.32±0.31	Bukietynska and Mondry (1987)
$50(NaPO_3)_6$–$18BaF_2$–$10ZnF_2$–20LiF–$2ErF_3$ glass	4.2009	3.2677	2.6256	Ranga Reddy et al. (1992b)
$50SiO_2$–$5AlO_{1.5}$–$36(LiO_{0.5}$–$NaO_{0.5})$–9SrO–$1ErO_{1.5}$ silicate glass	4.23	1.04	0.61	Zou and Izumitani (1993)
$50(NaPO_3)_6$–$18BaF_2$–$10ZnF_2$–10KF–10NaF–$2ErF_3$ glass	4.5285	0.8512	2.5104	Ranga Reddy et al. (1992b)
Y_2O_3:Er^{3+} (crystal)	4.59	1.21	0.48	Krupke (1966)
$88.92TeO_2$–$10.04Na_2O$–$1.04Er_2O_3$ glass	4.65	1.21	0.87	McDougall et al. (1996)
Er^{3+} in potassium sodium sulphate glass	4.74	0.96	2.36	Ratnakaram (1994)
Er^{3+} in phosphate glass	4.76	1.14	0.86	Yanagita et al. (1991)
$ErCl_3 \cdot 6H_2O$ in ethanol	5.0±0.2	2.5±0.2	0.6±0.3	Keller et al. (1982)
Er^{3+} in phosphate glass	5.08	1.10	0.87	Qi et al. (1992)
Er^{3+} in $55GeO_2$–20PbO–10BaO–10ZnO–$5K_2O$ glass	5.14±0.25	1.24±0.15	0.68±0.10	Pan et al. (1996)
$78.40GeO_2$–$8.79Bi_2O_3$–$11.79PbO$–$1.02Er_2O_3$ glass	5.26	1.41	0.88	McDougall et al. (1996)
Er^{3+}:ODA (1:3 in water)	5.26±0.48	1.61±0.64	3.23±0.74	Devlin et al. (1987a)
Er^{3+}:IDA (1:3 in water)	5.33±0.77	2.17±1.03	2.44±1.18	Devlin et al. (1987a)
$50(NaPO_3)_6$–$18BaF_2$–$10ZnF_2$–20NaF–$2ErF_3$ glass	5.3335	4.7130	2.6256	Ranga Reddy et al. (1992b)
Er^{3+} in $30GeO_2$–30PbO–$30TeO_2$–10CaO glass	5.44±0.27	1.36±0.20	0.97±0.15	Pan et al. (1996)
$ErCl_3 \cdot 6H_2O$ in *n*-propanol	5.5±0.2	2.5±0.2	0.7±0.3	Keller et al. (1982)
Er^{3+} in $48AlO_{1.5}$–36CaO–8MgO–8BaO glass	5.60	1.60	0.61	Zou and Izumitani (1993)

continued on next page

Table 19, *continued*

Matrix	Ω_2 (10^{-20} cm^2)	Ω_4 (10^{-20} cm^2)	Ω_6 (10^{-20} cm^2)	Reference
Er^{3+} in $85.6TeO_2$–$8.4BaO$–$4Na_2O$–$1MgO$–$1ZnO$ glass	5.66	1.75	0.96	Ryba-Romanowski (1990)
Er^{3+} in $50GaO_{1.5}$–$8KO_{0.5}$–$14CaO$–$19SrO$–$9BaO$ glass	5.71	0.96	0.72	Zou and Izumitani (1993)
$50(NaPO_3)_6$–$18BaF_2$–$10ZnF_2$–$10NaF$–$10LiF$–$2ErF_3$ glass	5.7202	1.6227	3.0597	Ranga Reddy et al. (1992b)
$57GeO_2$–$26.1KO_{0.5}$–$16.5BaO$–$1ErO_{1.5}$ glass	5.81	0.85	0.28	Zou and Izumitani (1993)
Er^{3+} in tellurite glass	6.05	1.78	1.07	Yanagita et al. (1991)
Er^{3+} in $Pb(PO_3)_2$ glass	6.30	2.00	1.10	Ingeletto et al. (1991)
Er^{3+} in magnesium sodium sulphate glass	6.39	3.92	2.22	Ratnakaram (1994)
$65.2PO_{2.5}$–$8.6AlO_{1.5}$–$7.5(BaO$–$MgO)$–$18.7KO_{0.5}$–$1ErO_{1.5}$ glass	6.65	1.52	1.11	Zou and Izumitani (1993)
Er^{3+} in $66.7CaO$–$33.3Al_2O_3$ glass (1 mol% Er^{3+})	6.87	1.50	0.70	Tanabe et al. (1993c)
$K_7[ErW_{10}O_{35}]$	7.02±0.20	2.24±0.31	1.44±0.19	Peacock (1973)
$La_3Ga_5SiO_{14}$:Er^{3+} (crystal)	7.05	1.53	0.73	Kaminskii et al. (1990)
TeO_2–BaO–ZnO–Y_2O_3–Tm_2O_3–Er_2O_3 glass	7.14	1.75	0.918	Tanabe et al. (1994)
$LiNbO_3$:Er^{3+} (crystal)	7.29±1.50	2.24±0.48	1.27±0.35	Amin et al. (1996)
Er^{3+} in lithium sodium sulphate glass	7.40	0.98	2.17	Ratnakaram (1994)
Er^{3+} in $66.7CaO$–$33.3Al_2O_3$ glass (0.1 mol% Er^{3+})	7.67	1.86	0.40	Tanabe et al. (1993d)
Er^{3+}:DPA (1:3 in water)	7.81±0.69	1.67±0.92	3.23±1.05	Devlin et al. (1987a)
$KY(WO_4)_2$:Er^{3+} (crystal)	7.96	2.31	1.40	Huang et al. (1992a)
Er^{3+} in cadmium sodium sulphate glass	9.42	2.37	3.09	Ratnakaram (1994)
Er^{3+} in $Zn(PO_3)_2$ glass	9.90	1.60	1.80	Ingeletto et al. (1991)
Er^{3+} in zinc sodium sulphate glass	9.99	2.25	1.77	Ratnakaram (1994)
Er^{3+}:CDO (1:3 in water)	10.45±0.26	2.06±0.29	3.41±0.34	Devlin et al. (1987a)
Er^{3+}:CDA (1:3 in water)	12.03±0.18	2.55±0.20	3.56±0.23	Devlin et al. (1987a)
Er^{3+} in $CaSO_4$–K_2SO_4–$ZnSO_4$ glass	15.18	1.65	6.69	Subramanyam et al. (1990)
Er^{3+} in $LiNO_3$–KNO_3 melt	15.8±1.2	2±2	1.4±0.9	Carnall et al. (1978)
Er(α-picolinate) in water	17.63±4.74	2.77±0.79	2.94±4.40	Bukietynska and Choppin (1970)

continued on next page

Table 19, *continued*

Matrix	Ω_2 (10^{-20} cm^2)	Ω_4 (10^{-20} cm^2)	Ω_6 (10^{-20} cm^2)	Reference
Er^{3+} in $BaSO_4$–K_2SO_4–$ZnSO_4$ glass	18.37	1.36	9.39	Subramanyam et al. (1990)
Er^{3+} in $MgSO_4$–K_2SO_4–$ZnSO_4$ glass	18.68	2.35	7.15	Subramanyam et al. (1990)
$10K_2SO_4 \cdot H_2O$–$39ZnSO_4 \cdot 7H_20$–$50B_2O_3$–$1Er_2(SO_4)_3 \cdot 7H_2O$ glass	21.10	3.08	11.94	Ravi Kanth Kumar et al. (1996)
$10Li_2SO_4 \cdot H_2O$–$39ZnSO_4 \cdot 7H_20$–$50B_2O_3$–$1Er_2(SO_4)_3 \cdot 7H_2O$ glass	21.31	4.90	9.61	Ravi Kanth Kumar et al. (1996)
$10Na_2SO_4 \cdot H2O$–$39ZnSO_4 \cdot 7H_20$–$50B_2O_3$–$1Er_2(SO_4)_3 \cdot 7H_2O$ glass	25.82	0.43	11.33	Ravi Kanth Kumar et al. (1996)
Er(acetylacetonate)$_3$ in methanol	26.11±0.28	1.56±0.40	2.09±0.23	Isobe and Misumi (1974)
Er(acetylacetonate)$_3$ in DMF	26.40±0.43	2.49±0.63	1.09±0.36	Isobe and Misumi (1974)
$49ZnSO_4 \cdot 7H_20$–$50B_2O_3$–$1Er_2(SO_4)_3 \cdot 7H_2O$ glass	27.85	0.68	8.92	Ravi Kanth Kumar et al. (1996)
$ErCl_3$–$(AlCl_3)_x$ vapor complex (400°C)	28.5	4.38	2.09	Carnall et al. (1978)
$1Gd_2(SO_4)_3 \cdot 7H_2O$–$38ZnSO_4 \cdot 7H_20$–$50B_2O_3$–$1Er_2(SO_4)_3 \cdot 7H_2O$ glass	31.77	4.53	9.18	Ravi Kanth Kumar et al. (1996)
Er(thenoyltrifluoro-acetonate)$_3$ in DMF	32.36±0.01	2.55±0.01	1.96±0.01	Isobe and Misumi (1974)
Er(thenoyltrifluoro-acetonate)$_3$ in methanol	34.72±0.40	1.32±0.59	2.70±0.33	Isobe and Misumi (1974)
Er(DBM)$_3 \cdot H_2O$	35.1	1.11	6.64	Kirby and Palmer (1981b)
Er(DBM)$_3$ in methanol	42.39±0.54	1.37±0.80	3.31±0.46	Isobe and Misumi (1974)
Er(DBM)$_3$ in DMF	43.24±0.41	1.09±0.60	2.59±0.34	Isobe and Misumi (1974)
Er(DBM)$_3$ vapor	46	2.7	3.7	Gruen et al. (1967)
$ErBr_3$ vapor	60	1.47	1.66	Gruen et al. (1967)
ErI_3 vapor	100	–	–	Gruen et al. (1967)

Table 20
Phenomenological intensity parameters Ω_λ for Tm^{3+} in various host matrices; the host matrices are classified according to increasing values of Ω_2

Matrix	Ω_2 (10^{-20} cm^2)	Ω_4 (10^{-20} cm^2)	Ω_6 (10^{-20} cm^2)	Reference
LaF_3:Tm^{3+} (crystal)	0.52	0.59	0.22	Leavitt and Morrison (1980)
$Tm(C_2H_5SO_4)_3 \cdot 9H_2O$ (crystal)	0.593	2.248	1.251	Krupke and Gruber (1965)
Tm^{3+} (aquo)	0.646±1.0	2.31±0.60	1.47±0.20	Carnall et al. (1983)
$YAlO_3$:Tm^{3+} (crystal)	0.67	2.30	0.74	Weber et al. (1973)
YAG:Tm^{3+} (crystal)	0.7	1.2	0.5	Weber et al. (1973)
BZYT:Tm^{3+} fluoride glass	1.14	1.57	1.13	Yeh et al. (1988)
$AlPO_4$–AlF_3–PbF_2–CaF_2–YbF_3–TmF_3 glass	1.3	1.0	1.5	Özen et al. (1993)
$AlPO_4$–AlF_3–PbF_2–CaF_2–TmF_3 glass	1.38	0.75	0.92	Özen et al. (1995)
$K_7[TmW_{10}O_{35}]$	1.58	5.78	0.83	Peacock (1973)
Tm^{3+} in PZG fluoride glass	1.71	1.46	1.06	Eyal et al. (1987b)
AlF_3–CaF_2–BaF_2–YF_3–TmF_3 glass	1.75	1.33	1.27	Tanabe et al. (1993a,b)
Tm^{3+} in $40ZnF_2$–$15AlF_3$–$15BaF_2$–$15SrF_2$–$15YF_3$ glass	1.83	1.70	1.12	Tanabe et al. (1996)
BIGaZYTZr fluoride glass (1 mol% Tm^{3+})	1.89	1.56	1.09	Joubert et al. (1995)
Tm^{3+} in AlF_3–ZrF_4–MgF_2–CaF_2–SrF_2–BaF_2–NaF–NaCl glass	1.92	1.68	1.13	Peng and Izumitani (1995)
ZBLA:Tm^{3+} glass	1.94	1.63	0.74	McDougall et al. (1994a)
ZBLAK:Tm^{3+} glass	1.98	1.54	0.56	McDougall et al. (1994c)
AlF_3–CaF_2–BaF_2–YF_3–TmF_3 glass	1.98	1.32	1.07	Hirao et al. (1993)
Tm^{3+} in BaF_2–ThF_4 glass	2.02	1.56	1.1	Yeh et al. (1989)
$75NaPO_3$–$24CaF_2$–$1TmF_3$ glass	2.03±0.62	1.09±0.48	1.17±0.18	Binnemans et al. (1997c)
BIZYT:Tm^{3+} fluoride glass	2.05	1.58	1.12	Guéry et al. (1988)
BIZYT:Tm^{3+} glass	2.07	1.54	1.12	Guéry (1988)
ZBLALi:Tm^{3+} glass	2.09	1.74	0.91	McDougall et al. (1994c)
Tm^{3+} in $32ZnF_2$–$28CdF_2$–$20BaF_2$–$11LiF$–$5AlF_3$–$4LaF_3$ glass	2.1	1.5	1.3	Villacampa et al. (1991a)

continued on next page

Table 20, *continued*

Matrix	Ω_2 (10^{-20} cm^2)	Ω_4 (10^{-20} cm^2)	Ω_6 (10^{-20} cm^2)	Reference
ZBLAN glass 2% Tm^{3+}	2.21	1.71	0.92	McDougall et al. (1994c)
ZBLAN glass 0.5% Tm^{3+}	2.33	1.44	0.82	McDougall et al. (1994b,1995)
ZBLAN glass 1% Tm^{3+}	2.38	1.82	0.86	McDougall et al. (1994b,1995)
Tm^{3+} in ZrBTmA glass	2.39	1.60	0.89	Oomen (1992)
$LiYF_4$:Tm^{3+} (crystal)	2.42	1.28	0.90	Razumova et al. (1995)
$LiYF_4$:Tm^{3+} (crystal)	2.43±0.10	1.08±0.12	0.67±0.04	Dulick et al. (1991)
Y_2SiO_5:Tm^{3+} (crystal)	2.43	1.74	0.66	Li et al. (1994)
BATY:Tm^{3+} glass	2.46	1.41	1.13	Guéry (1988)
Tm^{3+} in PbO–PbF_2 glass	2.50	2.35	1.16	Nachimuthu and Jagannathan (1995a)
ZBLAN:Tm^{3+} glass (0.2 mol% Tm^{3+})	2.57	1.90	0.84	Oomen (1992)
ZBLAN:Tm^{3+} glass	2.70	1.59	1.09	Wetenkamp et al. (1992)
ZBLA:Tm^{3+} glass	2.72	1.82	0.99	Guéry (1988)
$65ZrF_4$–$32BaF_2$–$2.5LaF_3$–$0.5TmF_3$ glass	2.73	1.75	0.96	Tanabe and Hanada (1994)
Tm^{3+} in $60HfF_4$–$33BaF_2$–$7LaF_3$ glass	2.73	1.35	0.98	Tanabe et al. (1996)
Tm^{3+} in P_2O_5–AlF_3–YF_3–MgF_2–CaF_2–SrF_2–BaF_2–NaF glass	2.75	2.28	1.18	Peng and Izumitani (1995)
ZBLAN glass 4.32% Tm^{3+}	2.75	0.95	1.02	McDougall et al. (1994b,1995)
$LiYF_4$:Tm^{3+} (crystal)	2.79	0.45	0.98	Razumova et al. (1996)
ZBLALi:Tm^{3+} glass	2.80	1.91	1.01	Sanz et al. (1987)
ZBLA:Tm^{3+}	2.8	1.9	1.0	Villacampa et al. (1991b)
Tm^{3+} in $52HfF_4$–$18BaF_2$–$3LaF_3$–$2AlF_3$–25CsBr glass	2.81	2.07	0.96	Cases and Chamarro (1991)
$65ZrF_4$–$29BaF_2$–$3BaCl_2$–$2.5LaF_3$–$0.5TmF_3$ glass	2.99	1.83	0.96	Tanabe et al. (1994)
Tm^{3+} in germanate glass	3.22	1.25	0.65	Reisfeld and Eckstein (1975)
$65ZrF_4$–$26BaF_2$–$6BaCl_2$–$2.5LaF_3$–$0.5TmF_3$ glass	3.31	2.03	0.93	Tanabe and Hanada (1994)

continued on next page

Table 20, *continued*

Matrix	Ω_2 (10^{-20} cm^2)	Ω_4 (10^{-20} cm^2)	Ω_6 (10^{-20} cm^2)	Reference
Tm^{3+} in SiO_2–Al_2O_3–Li_2O–Na_2O–SrO glass	3.31	1.21	0.48	Peng and Izumitani (1995)
$65ZrF_4$–$23BaF_2$–$9BaCl_2$–$2.5LaF_3$–$0.5TmF_3$ glass	3.57	1.80	1.03	Tanabe and Hanada (1994)
Tm^{3+} in $56PbO$–$27Bi_2O_3$–$17Ga_2O_3$ glass	3.59±0.11	0.76±0.03	1.27±0.15	Heo et al. (1995)
$65ZrF_4$–$20BaF_2$–$12BaCl_2$–$2.5LaF_3$–$0.5TmF_3$ glass	3.87	2.00	1.02	Tanabe and Hanada (1994)
Tm^{3+} in GeO_2–BaO–K_2O glass	4.05	1.01	0.28	Peng and Izumitani (1995)
Y_2O_3:Tm^{3+} (crystal)	4.07	1.46	0.61	Krupke (1966)
Tm^{3+} in $60GeO_2$–30BaO–10ZnO glass	4.08	0.95	0.59	Tanabe et al. (1996)
Tm^{3+} in fluorophosphate glass	4.12	1.47	0.72	Kermanoui et al. (1984)
Tm^{3+} in $60TeO_2$–30BaO–10ZnO glass	4.23	0.83	0.74	Tanabe et al. (1996)
MgF_2–CaF_2–SrF_2–AlF_3–$Sr(PO_3)_2$–TmF_3 glass	4.27	2.63	1.22	Seeber and Ehrt (1992)
Tm(α-picolinate) in water	4.82±4.46	7.56±7.29	2.89±2.24	Bukietynska and Choppin (1970)
Tm^{3+} in P_2O_5–Al_2O_3–MgO–BaO–K_2O glass	4.86	1.68	0.77	Peng and Izumitani (1995)
Tm^{3+} in Al_2O_3–CaO–MgO–BaO glass	4.91	1.65	0.63	Peng and Izumitani (1995)
$LiNbO_3$:Tm^{3+} (crystal)	4.91	0.48	0.31	Núñez et al. (1993)
Tm^{3+} in Ga_2O_3–K_2O–CaO–SrO–BaO glass	4.98	1.54	0.60	Peng and Izumitani (1995)
Tm^{3+} in magnesium sodium sulphate glass	4.99	3.08	0.14	Ratnakaram (1994)
TeO_2–BaO–ZnO–Y_2O_3–Tm_2O_3 glass	5.01	1.36	0.84	Tanabe and Hanada (1994)
Tm^{3+} in tellurite glass	5.04	1.36	1.22	Spector et al. (1977)
$LiNbO_3$(MgO):Tm^{3+} (crystal)	5.30	0.34	0.42	Núñez et al. (1993)
Tm^{3+} in borate glass	5.42	2.78	1.66	Reisfeld and Eckstein (1975)
Tm^{3+} in Na_2SO_4–$ZnSO_4 \cdot 7H_2O$–B_2O_3 glass	5.81	7.87	10.75	Rukmini and Jayasankar (1994)
Tm^{3+} in phosphate glass	5.88	2.88	0.71	Reisfeld and Eckstein (1975)
TeO_2–BaO–ZnO–Y_2O_3–Er_2O_3–Tm_2O_3 glass	6.15	1.89	0.835	Tanabe et al. (1994)

continued on next page

Table 20, *continued*

Matrix	Ω_2 (10^{-20} cm^2)	Ω_4 (10^{-20} cm^2)	Ω_6 (10^{-20} cm^2)	Reference
Tm^{3+} in germanate glass	6.70	1.04	0.53	Reisfeld (1976)
Tm^{3+} in cadmium sodium sulphate glass	6.75	3.49	0.56	Ratnakaram (1994)
$50(NaPO_3)_6$–$18BaF_2$–$10ZnF_2$–$20KF$–$2TmF_3$ glass	7.611	0.396	6.619	Ranga Reddy et al. (1992a)
GeO_2–BaO–ZnO–Y_2O_3–Tm_2O_3 glass	7.70	1.39	0.91	Tanabe and Hanada (1994)
Tm^{3+} in potassium sodium sulphate glass	7.83	5.97	0.22	Ratnakaram (1994)
Tm^{3+} in phosphate glass	8.08	3.05	1.66	Spector et al. (1977)
$50(NaPO_3)_6$–$18BaF_2$–$10ZnF_2$–$20NaF$–$2TmF_3$ glass	8.520	0.561	4.721	Ranga Reddy et al. (1992a)
$50(NaPO_3)_6$–$18BaF_2$–$10ZnF_2$–$20LiF$–$2TmF_3$ glass	8.618	0.752	5.737	Ranga Reddy et al. (1992a)
Tm^{3+} in K_2SO_4–$ZnSO_4 \cdot 7H_2O$–B_2O_3 glass	9.04	6.89	10.67	Rukmini and Jayasankar (1994)
Tm^{3+} in borate glass	9.18	2.91	1.87	Reisfeld (1976)
Tm^{3+} in $LiNO_3$–KNO_3 melt	10.4±2	2.8±0.7	1.7±0.4	Carnall et al. (1978)
Tm^{3+} in lithium sodium sulphate glass	10.67	3.63	2.07	Ratnakaram (1994)
Tm^{3+} in Li_2SO_4–$ZnSO_4 \cdot 7H_2O$–B_2O_3 glass	12.63	8.92	7.57	Rukmini and Jayasankar (1994)
Tm^{3+} in $ZnSO_4 \cdot 7H_2O$–B_2O_3 glass	12.65	6.99	10.55	Rukmini and Jayasankar (1994)
Tm^{3+} in zinc sodium sulphate glass	15.95	3.30	2.46	Ratnakaram (1994)

Table 21
Phenomenological intensity parameters Ω_λ for Yb^{3+} in various host matrices; the host matrices are classified according to increasing values of Ω_2 [a]

Matrix	Ω_2 (10^{-20} cm^2)	Ω_4 (10^{-20} cm^2)	Ω_6 (10^{-20} cm^2)	Reference
Yb^{3+} (aquo)	0.93	1.76	1.89	Carnall et al. (1965)
Yb^{3+} (aquo)	0.8	(1.6)	(1.6)	Bel'tyukova et al. (1977)
Yb^{3+}:EDTA (1:2)	5.5	(1.6)	(1.6)	Bel'tyukova et al. (1977)
Yb^{3+}:antipyrine (1:5)	6.0	(1.6)	(1.6)	Bel'tyukova et al. (1977)
Yb^{3+}:EDTA (1:3)	9.2	(1.6)	(1.6)	Bel'tyukova et al. (1977)
Yb^{3+}:NTA (1:5)	9.6	(1.6)	(1.6)	Bel'tyukova et al. (1977)
Yb^{3+}:MAL (1:5)	11.1	(1.6)	(1.6)	Bel'tyukova et al. (1977)
Yb^{3+}:sulfosalicylic acid (1:2)	11.9	(1.6)	(1.6)	Bel'tyukova et al. (1977)
Yb^{3+}:citric acid (1:5)	13.6	(1.6)	(1.6)	Bel'tyukova et al. (1977)
Yb^{3+} in $LiNO_3$–KNO_3 melt	13.1	2.32	1.55	Carnall et al. (1965, 1978)
Yb^{3+}:maleic acid (1:5)	13.1	(1.6)	(1.6)	Bel'tyukova et al. (1977)
Yb^{3+}:nitriloacetic acid (1:2)	15.6	(1.6)	(1.6)	Bel'tyukova et al. (1977)
Yb^{3+}:trihydroxyglutatic acid (1:5)	19.3	(1.6)	(1.6)	Bel'tyukova et al. (1977)
Yb^{3+}:malic acid (1:5)	20.0	(1.6)	(1.6)	Bel'tyukova et al. (1977)
Yb^{3+}:tartaric acid (1:5)	20.0	(1.6)	(1.6)	Bel'tyukova et al. (1977)
Yb^{3+}:acetylacetone (1:10)	26.7	(1.6)	(1.6)	Bel'tyukova et al. (1977)
Yb^{3+}:benzoylacetone (1:10)	28.9	(1.6)	(1.6)	Bel'tyukova et al. (1977)
Yb^{3+}:thenoyltrifluoro-acetone (1:10)	30.9	(1.6)	(1.6)	Bel'tyukova et al. (1977)
Yb^{3+}:DBM (1:10)	32.8	(1.6)	(1.6)	Bel'tyukova et al. (1977)
Yb^{3+}:sulfosalicylic acid (1:40)	36.9	(1.6)	(1.6)	Bel'tyukova et al. (1977)

[a] Values in parentheses were not varied during the fitting procedure.

of other lanthanide ions (except Tb^{3+}) start above 60 000 cm^{-1}. It has been argued that the low energetic position of the disturbing excited configuration is the main reason for the anomalous behavior of Pr^{3+}. A second assumption is that the energy difference between the ground J-level of the $4f^N$ configuration and the barycenter of the excited disturbing configuration can be considered to be equal to the energy difference between the excited J'-level of the $4f^N$ configuration and the barycenter of the same excited disturbing configuration. This approximation is good only if the barycenter is situated at a very high energy. Once again, this is not the case for Pr^{3+}. Since this approximation enables to cancel out the part of the intensity from terms with odd λ values, we can expect parameters with an odd λ value to give a non-negligible contribution to the intensity of the 4f–4f transitions of Pr^{3+}. Eyal et al. (1985) have included the Ω_3 and Ω_5 parameters in the intensity fitting of Pr^{3+} in ZBLA glass. Flórez et al. (1996) also fitted the intensities of f–f transitions in Pr^{3+}-doped fluoroindate glasses in terms of odd intensity parameters. They found that it was necessary for a good fit to incorporate the $^1I_6 \leftarrow {}^3H_4$ transition in the fitting procedure. Odd $U^{(\lambda)}$ matrix elements ($\lambda = 1, 3, 5$) have been listed. Levey (1990) assumed that the $4f^15d^1$ configuration dominates as the perturbing configuration in the induced electric dipole transitions and calculated the energy denominators in eq. (185) explicitly. Three additional odd Ω_λ parameters have to be considered. Levey applied his method to the calculation of the lifetime from $^1S_0$ in LaF_3:Pr^{3+}.

It should be mentioned also that the hypersensitive transition $^3F_2 \leftarrow {}^3H_4$ has to be included in the fit of Pr^{3+} systems, because otherwise a negative value for the Ω_2 parameter is found (just as is sometimes observed by inclusion of the $^3P_2 \leftarrow {}^3H_4$ transition in the fit). An intensity parameter with a negative value has no physical significance. Extraction of a reliable Ω_2 parameter is often a problem for Pr^{3+}, since the $^3F_2 \leftarrow {}^3H_4$ transition is situated in the infrared spectral region and cannot be observed in an aqueous solution (it is masked by vibrational transitions). In order to find more reliable intensity parameters for Pr^{3+}, Quimby and Miniscalco (1994) introduced a modified Judd–Ofelt theory in which the luminescence branching ratios are included in the fit (see sect. 7.7).

Kornienko et al. (1990) have tried to take into account the influence of the excited state of Pr^{3+} on the dipole strength:

$$D = e^2 \sum_{\lambda = 2, 4, 6} \Omega_\lambda \left[1 + 2\alpha \left(E_J + E_{J'} - 2E_f^0\right)\right] \left| \left\langle l^N \psi J \left\| U^{(\lambda)} \right\| l^N \psi' J' \right\rangle \right|^2, \tag{221}$$

with E_J the energy of the ground state $^{2S+1}L_J$, $E_{J'}$ the energy of the excited state $^{2S+1}L_{J'}$, E_f^0 the energy of the center of gravity of the $4f^2$ configuration ($\approx 10\,000\ cm^{-1}$), and $\alpha = \frac{1}{2}[E(4f5d) - E(4f)]$.

The parameter α has a value of $\sim 10^{-5}\ cm^{-1}$, but in practice is treated as an additional fitting parameter. The method of Kornienko has been applied to Pr^{3+}-doped glasses by Buñuel et al. (1992), Alcalá and Cases (1995) and Medeiros Neto et al. (1995). Goldner and Auzel (1996) have pointed out the fact that the α-parameter has to be set to a value which is inconsistent with experiment. If reasonable values for the energy of the $4f^15d^1$

configuration are taken into account, the modified theory of Kornienko et al. (1990) does not improve the fit, but the intensity parameters and the calculated intensities are modified. The authors propose to set α to a reasonable value and not to let α vary.

A possible breakdown of the Judd–Ofelt theory was suggested by Henrie and Henrie (1977) for the absorption spectrum between 18 400 cm^{-1} and 22 600 cm^{-1} for $NdBr_6^{3-}$ in acetonitrile. In this region the observed intensities are much larger than the calculated ones. But in general, the Judd–Ofelt theory works very well for Nd^{3+}. The Judd–Ofelt theory is not very suitable for the *ab initio* calculation of intensity parameters. Especially the so-called hypersensitive transitions give problems (see sect. 8). Therefore, a number of refinements of the intensity theory have been published after the original papers of Judd and Ofelt. These models are discussed in detail in sections 6.2 and 8.2.

The dependence of the intensity parameters on the host matrix is discussed in sections 8 and 9.

The variation of the intensity parameter across the lanthanide series has been studied by Peacock (1973, 1975). If the intensity is produced by a static perturbation (Judd–Ofelt theory), a monotonous decrease of the Ω_λ parameters from Pr^{3+} to Tm^{3+} is predicted. It is assumed that the lanthanide ions have been doped into the same host matrix or that an isostructural series of lanthanide complexes is considered. A change in symmetry would result in an abrupt change of the parameters. To a good approximation, a linear variation was found for the Ω_6 parameter of $[RW_{10}O_{35}]^{7-}$ with the number of 4f electrons. The same behavior was found for Ω_4, but there was more scatter due to a larger uncertainty on the values of this parameter. The Ω_2 parameters appeared to vary randomly.

7.5. *Ab initio calculation of intensity parameters*

In general, the Ω_λ intensity parameters are determined semi-empirically by fitting calculated dipole strengths (or oscillator strengths) against experimental dipole strengths (or oscillator strengths) (see sect. 7.3). However, some authors have tried to calculate the intensity parameters from first principles (*ab initio*).

The first attempt to calculate the intensity parameters by *ab initio* methods was undertaken by Judd in his classical paper (Judd 1962). He calculated the T_λ parameters of the Nd^{3+} and Er^{3+} ions in aqueous solutions by a point charge electrostatic model. The positional coordinates of the water oxygens were derived from the known positions of the oxygen molecules in $GdCl_3 \cdot 6H_2O$. As perturbing configurations, the excited configurations $4f^{N-1}5d$ and $4f^{N-1}n'g$ were chosen. Configurations of the type $4f^{N-1}n'd$ with $n' \geq 6$ were not considered. The radial integral involving the latter configurations is very small, because of the reduced overlap with the 4f eigenfunctions. The calculated parameters are a factor 2 too small for Nd^{3+} and 8 times too small for Er^{3+}. It was shown that g orbitals have to be taken into account for explaining the observed intensity, although the $4f^{N-1}n'g$ configurations are at a high energy.

Krupke (1966) calculated the Ω_λ parameters for Pr^{3+}, Nd^{3+}, Eu^{3+}, Er^{3+} and Tm^{3+} in Y_2O_3, for Pr^{3+} and Nd^{3+} in LaF_3, and for Er_2O_3, Tm_2O_3 and Yb_2O_3. The calculated values for $\Xi(k, \lambda)$ are given in table 22. He argued that the phenomenological

Table 22
Free ion $\Xi(k,\lambda)$ values for selected lanthanide ions[a,b]

Ion	$\Xi(1,2)$	$\Xi(3,2)$	$\Xi(3,4)$	$\Xi(5,4)$	$\Xi(5,6)$	$\Xi(7,6)$
Pr^{3+}	−1.78	1.54	1.75	−2.26	−5.45	4.54
Nd^{3+}	−1.58	1.35	1.50	−1.98	−4.62	3.96
Eu^{3+}	−1.08	0.88	0.90	−1.27	−2.70	2.58
Tb^{3+}	−0.83	0.64	0.64	−0.89	−1.84	1.78
Er^{3+}	−0.57	0.36	0.37	−0.44	−0.92	0.71
Tm^{3+}	−0.40	0.30	0.29	−0.30	−0.66	0.43

[a] After Krupke (1966).
[b] $\Xi(1,2)$ is expressed in 10^{-6} cm^2 erg^{-1}, $\Xi(3,2)$ and $\Xi(3,4)$ are expressed in 10^{-22} cm^4 erg^{-1}, $\Xi(5,4)$ and $\Xi(5,6)$ in 10^{-38} cm^6 erg^{-1} and finally, $\Xi(7,6)$ is in units of 10^{-54} cm^8 erg^{-1}.

Ω_λ parameters incorporate both contributions from the static crystal field and from the vibronic–electronic interaction involving single phonons. Calculations reveal that the static contributions to the phenomenological parameters decrease monotonically with increasing number of 4f electrons. For Y_2O_3, only the experimental curve of the Ω_2 parameter shows such a behavior. The experimental curves of the Ω_4 and Ω_6 parameters can be decomposed into two parts, one with a slope similar to the curve of the Ω_2 parameter and another with a slope which increases from the beginning of the lanthanide series until Gd^{3+} and which then decreases again towards the end of the lanthanide series. This composition of the Ω_4 and Ω_6 curves is consistent with the experimental facts that Pr^{3+} and Tm^{3+} show intense vibronic structure in their absorption spectra, Nd^{3+} and Er^{3+} show much less vibronic structure, and Eu^{3+} exhibits virtually no vibronic structure. Calculated values of the Ω_4 and Ω_6 parameters of lanthanide ions in Y_2O_3 on the basis of an electrostatic model can be compared only directly with the experimental values of Eu^{3+}. The calculated values of the Ω_2 parameter can be compared with the experimental values for all lanthanide ions, since only the static crystal-field interaction contributed to the Ω_2 parameter. The experimental and calculated Ω_2 curves show, however, a large difference in slope. For Y_2O_3:Eu^{3+}, the calculated value of Ω_4 is a factor 12.5 larger than the experimental value, while the calculated value of Ω_6 is underestimated by a factor 8.9. Krupke discussed the discrepancies in terms of crystal-field shielding and distortion of the radial free-ion wave functions. He concluded that the excited $4f^{N-1}ng$ configurations contribute to the observed intensities an order of magnitude more than is indicated by free-ion calculations, and that the excited $4f^{N-1}5d$ configuration contributes an order of magnitude less than indicated by free-ion calculations.

Intensity parameters for the lanthanide ions Ce^{3+} through Yb^{3+} doped into single-crystal LaF_3 have been calculated by Leavitt and Morrison (1980). They used wave-functions generated by k = even crystal-field parameters determined from a point-charge model. The k = odd crystal-field parameters have been calculated on the basis of the same

point-charge model. The procedure for the calculation of the radial integrals is based on that of Krupke (1966). The quantities

$$\frac{\langle nl\,|r|\,n'l'\rangle\,\langle nl\,|r^k|\,n'l'\rangle}{\Delta(n'l')}$$

necessary for the calculation of $\Xi(k,\lambda)$ (see sect. 6.1) have been tabulated for $l' = d$ and for $l' = g$. The intensity parameters were used to calculate radiative lifetimes and branching ratios (see also sect. 7.7). Morrison et al. (1983) reported calculated parameters for the Y_2O_3 host matrix. Allik et al. (1988) calculated by the same method the Ω_λ parameters for the lanthanide ions doped into lanthanum lutetium gallium garnet ($La_3Lu_2Ga_5O_{12}$), and Deb et al. (1981) calculated the parameters for the lanthanide ions in cubic LaOF. Calculated Ω_λ parameters for Tm^{3+} in rare-earth garnets were reported by Morrison et al. (1991). The k = odd crystal-field parameters have been calculated by Garcia et al. (1983) for $LiYF_4$:Nd^{3+}, YOBr:Eu^{3+}, YOCl:Eu^{3+}, BaFCl:Sm^{2+}, SrFCl:Sm^{2+}, $BaTiO_3$:Eu^{3+}, $NdAlO_3$, $LaAlO_3$:Eu^{3+}, Nd_2O_3, Nd_2O_2S, LaF_3:Nd^{3+}, $LaCl_3$:Nd^{3+}, Y_2O_3:Eu^{3+} and KY_3F_{10}:Eu^{3+}. (Notice that the divalent Sm^{2+} ion has a $4f^6$ configuration, so Sm^{2+} is iso-electronic with Eu^{3+}). The calculations included contributions from point charges, consistent dipoles and quadrupoles induced in the crystalline matrix. Some Ω_λ parameters have been calculated on the basis of those crystal-field parameters, using the $\Xi(k,\lambda)$ values reported by Krupke (1966). k-odd crystal-field parameters for $LiYF_4$:Pr^{3+} based on a lattice sum calculation were presented by Estorowitz et al. (1979). da Gama and de Sá (1982) calculated the intensity parameters for Nd^{3+} in $LiYF_4$, LaF_3 and Y_2O_3, using a combination of the standard Judd–Ofelt theory and pseudo-multipolar field mechanisms (ignoring interference effects) and using two different sets of radial integrals.

Carnall et al. (1983) calculated the Ω_4 and Ω_6 parameters for the trivalent lanthanide ions in aqueous solution. They used radial integrals based on *relativistic Hartree–Fock* calculations. The energies of the excited configurations were those given by Brewer (1971a,b), but corrected for the energy lowering of 15–20 000 cm^{-1} due to the effects of the condensed phase. Only the lowest $n'd$ configuration is considered as the perturbing configuration. The results of Carnall et al. (1983) for the intensity parameters of Nd^{3+} and Er^{3+} did not differ importantly from the values calculated by Judd (1962), although the radial parameters used by Carnall et al. were considerably smaller than those used by Judd. The Ω_λ parameters have been predicted to decrease in magnitude from f^2 to f^7, to increase from f^7 to f^8, and again to decrease from f^8 through f^{12}.

Model calculations for intensity parameters have been reported for a series of Nd^{3+}, Ho^{3+} complexes (E.M. Stephens et al. 1984) and for Er^{3+} complexes (Devlin et al. 1987b) with trigonal symmetry. The ligands in the complexes are oxydiacetate (ODA), dipicolinate (DPA), iminodiacetate (IDA) and (methylimino)diacetate (MIDA). In addition, chelidonate (CDO) and chelidamate (CDA) complexes were studied for Er^{3+}. The calculations take into account the static-coupling [SC] and dynamic-coupling [DC] mechanisms as well as contributions arising from interferences between transition

moments by the static and dynamic coupling models [SC, DC] (see sect. 6.2). The [SC] and [DC] contributions are always positive, whereas the contributions from [SC, DC] may be either positive or negative in sign, depending on the relative phases of the SC and DC electric dipole transition moments. The phase relationships depend on the geometrical distributions of ligand charge and polarizability around the lanthanide ion. Expressions for the different contributions are given. The authors found that the calculated Ω_2 parameters are dominated by [DC] and [SC, DC] contributions, and that the calculated Ω_6 parameters are dominated by [SC] contributions. The calculated Ω_4 parameters were found to vary considerably from complex to complex and from the choice of the radial integrals $\Xi(k,4)$ and $\langle r^4 \rangle$. The greater sensitivity of the experimental Ω_2 parameter for the ligand environment was also reflected by the calculations for Ω_2. Calculated Ω_λ parameters for rare-earth ions in the eight-coordinate tetrakis(diethyldithiocarbamate) complexes $Na[R(Et_2DTC)_4]$ have been given by Mason and Tranter (1983) and by Mason (1984, 1986). The relative importance of crystal-field and ligand-polarization contributions to the total calculated dipole strength were considered. It was shown that the ligand-polarization contribution to $\Omega_\lambda(total)$ decreases from 66% to 17% and to 0.1% for Ω_2, Ω_4 and Ω_6, respectively. The corresponding crystal-field contribution increases from 5% to 57% and to 98.5% respectively. The remaining fractions were contributed to pseudoscalar cross-term components between the static and the dynamic components of the first-order electric dipole transition moment.

Discrepancies between experimental and calculated Ω_λ intensity parameters can be due to (1) J-mixing, (2) linear and non-linear shielding of the electrons from the electrostatic crystalline electric field resulting from the distortion of the closed 5s and 5p shell outside the 4f shell by the lattice charges, (3) relativistic effects, and (4) effects of electron correlation. Detrio (1971) found that the effects of J-mixing are negligible. However, a modified Judd–Ofelt theory for taking into account the effects of J-mixing was proposed by Shangda and Yimin (1984). Krupke (1966) reported that not all discrepancies between experimental and calculated intensity parameters can be attributed to shielding effects. Jankowski and Smentek-Mielczarek (1979) studied the effect of electron correlation on the intensities of induced electric dipole transitions. They introduced effective operators to take into account the modifications of the Judd–Ofelt theory. These effective operators can be represented by a sum of one- and two-electron effective operators. The two-electron operators do not occur in the standard Judd–Ofelt theory. One-particle operators on unit tensor operators of odd rank are also not included in the original theory. Jankowski and Smentek-Mielczarek showed that the empirical Ω_λ intensity parameters incorporate some correlation effects (i.e. those effects arising from one-particle operators of even rank). Their model was applied to $LaCl_3:Pr^{3+}$ (Smentek-Mielczarek and Jankowski 1979, Jankowski and Smentek-Mielczarek 1981) and to $LaCl_3:Eu^{3+}$ (Jankowski and Smentek-Mielczarek 1981).

For non-stoichiometric and amorphous systems (e.g. liquids, glasses, polymers, ...), where the local structure cannot be determined by diffraction methods, the Judd–Ofelt theory can be combined with *molecular-dynamics* simulations for the calculation of intensity parameters (Edvardsson et al. 1992, 1996, Wolf et al. 1993, Klintenberg et al.

1997). *Molecular dynamics* is a computer-simulation method in which the motion of N particles (ions) is treated by classical dynamics. The interaction between the particles is expressed through potential functions. The *simulation box* contains a limited number of particles (from a few hundred to several thousands of ions). Starting from the initial positional coordinates (the crystallographic coordinates for crystalline compounds), the ions are allowed to move and the new positional coordinates are evaluated for a succession of time steps, each typically a few femtoseconds. Velocities and positions are obtained by solving Newton's equation of motion for each particle in the simulation box. Molecular dynamics generates a number of representative environments in the simulation box. At each step of the simulation, the positions of the surrounding ions are used to calculate the instantaneous k-odd crystal-field parameters and subsequently the Ω_λ intensity parameters and oscillator strengths. This enables to investigate how ions in different structural situations contribute to the absorption spectrum and how the various transitions are affected by fluctuations in the local environment. Each of the environments produces a transition with a slightly different energy and intensity. A summation over the different environments gives the total absorption band. The authors applied this method to Nd^{3+} in Nd_2O_3, Na^+/Nd^{3+} β''-alumina and YAG:Nd^{3+}. Some authors prefer a direct calculation of the intensity of transitions between J-multiplets, i.e. without using phenomenological intensity parameters. Oganesyan et al. (1990) introduced a method in which the oscillator strengths are expressed in terms of the polarizability of the lanthanide ion. The method was applied for intensity calculations of Er^{3+} in LaF_3 single crystal.

7.6. *Simulation of absorption spectra*

Although the calculated dipole strength can be compared directly with the experimental dipole strength, it is also possible to simulate the spectrum with the aid of the calculated dipole strength and to compare it with the experimental spectrum. A spectrum is a plot of the molar absorptivity ε as a function of the wavenumber $\bar{\nu}$. The molar absorptivity $\varepsilon(\bar{\nu})$ can be related to the dipole strength D:

$$\varepsilon(\bar{\nu}) = 108.9 \times 10^{36} \times D \times \bar{\nu}_0 \times f(\bar{\nu}) \qquad [D \text{ in esu}^2\,\text{cm}^2], \qquad (222)$$

where $f(\bar{\nu})$ is a normalized line shape function. For $\bar{\nu}_0$, one can take the calculated energy of the free ion level. Alternatively, one can take the experimental barycenter or the peak maximum of the absorption band. Determination of $\bar{\nu}_0$ is not a problem if the band is symmetric, because then the barycenter and the peak maximum coincide. In many cases the absorption band is asymmetric or is a superposition of overlapping bands. It is then better not to report the band maximum, but the barycenter. The barycenter $\bar{\nu}_0^b$ can be considered as an average wavenumber, so that the area under the absorption band left and right of this barycenter is the same:

$$\bar{\nu}_0^b = \frac{\sum_i D_{\text{exp}}^i \bar{\nu}_0^i}{\sum_i D_{\text{exp}}^i}. \qquad (223)$$

The summation runs over all the absorption bands (with wavenumber $\bar{\nu}_0^i$ and experimental dipole strength D_{exp}^i) which contribute to the complex band structure. $\sum_i D_{\text{exp}}^i$ is the total dipole strength of the complex band. In practice, $\bar{\nu}_0^b$ is determined by curve-fitting software by placing a line shape function under the complex band. $\bar{\nu}_0^b$ is equal to the sum of the peak maxima $\bar{\nu}_0^i$ weighted by the fractional contribution x_i ($0 \leqslant x_i \leqslant 1$, $\sum_i x_i = 1$) of each single band i to the total absorption band:

$$\bar{\nu}_0^b = \sum_i x_i \bar{\nu}_0^i. \tag{224}$$

As the line shape function $f(\bar{\nu})$, a Gauss, Lorentz or Voigt function can be chosen. The mathematical expressions for these functions have $\bar{\nu}$ as the variable and have two parameters: the band center $\bar{\nu}_0$ (wavenumber at which the function reaches its maximum value) and the curve width Γ (half width at half height). Sometimes Δ (half width at height 1/e) is used instead of Γ. The relation between both quantities is: $\Delta = (\ln 2)^{-1/2}\,\Gamma$. All these line shape functions are symmetric around the band center $\bar{\nu}_0$. The expressions for the functions are:

Gauss function:

$$f_{\text{G}}(\bar{\nu}, \bar{\nu}_0) = \frac{1}{\Gamma_{\text{G}}} \frac{\sqrt{\ln 2}}{\sqrt{\pi}} \exp\left[-\frac{(\bar{\nu} - \bar{\nu}_0)^2 \ln 2}{\Gamma_{\text{G}}^2}\right], \tag{225}$$

Lorentz function:

$$f_{\text{L}}(\bar{\nu}, \bar{\nu}_0) = \frac{\Gamma_{\text{L}}}{\pi\left[\Gamma_{\text{L}}^2 + (\bar{\nu} - \bar{\nu}_0)^2\right]}. \tag{226}$$

Voigt function: the Voigt function is the convolution of a Lorentz function with a Gauss function:

$$f_{\text{V}}(\mu, \xi) = \frac{1}{\Gamma_{\text{G}}} \frac{\sqrt{\ln 2}}{\sqrt{\pi}} \int_{-\infty}^{+\infty} \frac{\exp\left(-\zeta^2\right)}{\mu^2 + (\xi - \zeta)^2}\, \mathrm{d}\zeta, \tag{227}$$

where

$$\xi = \frac{\bar{\nu} - \bar{\nu}_0}{\Gamma_{\text{G}}} \sqrt{2 \ln 2}, \tag{228}$$

and

$$\mu = \frac{\Gamma_{\text{L}}}{\Gamma_{\text{G}}} \sqrt{2 \ln 2}. \tag{229}$$

A Lorentz function is smaller than a Gauss function near the peak maximum, but the principal distinguishing characteristic of a Lorentz function is that it has significant

wings. The Voigt function has broader wings than a Gauss function, but smaller than a Lorentz function. The line shape of a crystal-field transition is described by a Lorentz function. For glasses and solutions, the absorption bands are broadened by inhomogeneous line-broadening. The band shape of an inhomogeneously broadened absorption band is described by a Gauss function (a Gaussian band can be seen as a superposition of many Lorentzian bands). The curve width Γ is an adjustable parameter, since the curve width cannot be calculated from first principles. Γ can be changed within a reasonable range, in order to get the best agreement between the calculated and experimental absorption peaks. The total spectrum is the sum of the different simulated absorption bands.

7.7. *Luminescence spectra*

For emission (or luminescence) spectra, the spontaneous emission coefficient (also called probability for spontaneous emission or the Einstein coefficient for spontaneous emission) $A(\Psi J, \Psi' J')$ is often reported instead of the oscillator or dipole strength:

$$A(\Psi J, \Psi' J') = \frac{64\pi^4 \bar{\nu}^3}{3h(2J+1)} \left[n^3 D_{\mathrm{MD}} + \frac{n(n^2+2)^2}{9} D_{\mathrm{ED}} \right] \qquad [\mathrm{dim:\ T^{-1}}]. \tag{230}$$

As for absorption spectra, it is assumed implicitly that all the crystal-field components of the initial state are equally populated. If the lifetime of the state is long compared to the rate at which it is populated in the excitation process, thermal equilibrium at the temperature of the system can be achieved before emission takes place (Carnall 1979). Because an excited state ΨJ is relaxed to several lower-lying states $\Psi' J'$, the radiative branching ratio β_{R} is defined

$$\beta_{\mathrm{R}}(\Psi J, \Psi' J') = \frac{A(\Psi J, \Psi' J')}{\sum_{\Psi' J'} A(\Psi J, \Psi' J')} \qquad [\mathrm{dim:\ /}]. \tag{231}$$

The branching ratios can be used to predict the relative intensities of all emission lines originating from a given excited state. The experimental branching ratios can be found from the relative areas of the emission lines.

Once all emission probabilities that depopulate an initial level ${}^{2S+1}L_J$ have been calculated, they can be used to determine how fast that level is depopulated. This rate is given by the radiative lifetime $\tau_{\mathrm{R}}(\Psi J)$:

$$\tau_{\mathrm{R}}(\Psi J) = \frac{1}{\sum_{\Psi' J'} A(\Psi J, \Psi' J')} \qquad [\mathrm{dim:\ T}]. \tag{232}$$

Stronger emission probabilities and more transitions from a level lead to faster decay and shorter lifetimes. The theoretical radiative lifetime $\tau_{\mathrm{R}}(\Psi J)$, calculated from the

knowledge of the Ω_λ intensity parameters, can be compared with the measured lifetime $\tau_{\text{meas}}(\Psi J)$. The discrepancy between theoretical and calculated lifetimes can be attributed to non-radiative relaxation (multiphonon decay and energy transfer). The measured lifetime includes all relaxation processes (both radiative and non-radiative processes). The quantum efficiency η is a measure of the number of photons emitted per excited ion and is given by

$$\eta = \frac{\tau_{\text{meas}}(\Psi J)}{\tau_{\text{R}}(\Psi J)} \qquad \text{[dim: /]}. \tag{233}$$

The peak stimulated emission cross-section $\sigma(\Psi J, \Psi' J')$ between the states ΨJ and $\Psi' J'$ having a probability $A(\Psi J, \Psi' J')$ is given by (Weber et al. 1982):

$$\sigma(\Psi J, \Psi' J') = \frac{\lambda_{\text{p}}^4}{8\pi c n^2 \Delta\lambda_{\text{eff}}} A(\Psi J, \Psi' J') \qquad \text{[dim: L}^2\text{]}, \tag{234}$$

where λ_{p} is the wavelength of peak emission (in nm), $\Delta\lambda_{\text{eff}}$ is the effective linewidth of the transition (in nm) and n is the refractive index of the host. The effective linewidth $\Delta\lambda_{\text{eff}}$ is defined by

$$\Delta\lambda_{\text{eff}} = \int \frac{I(\lambda)}{I_{\max}} \, \mathrm{d}\lambda \qquad \text{[dim: L]}, \tag{235}$$

where $I(\lambda)$ is the intensity at wavelength λ and $I_{\max}$ is the maximum intensity of the emission band.

The luminescence intensities of lanthanide ions in aqueous solution have been discussed in detail by Carnall (1979) and Carnall et al. (1983). Quimby and Miniscalco (1994) introduced a modified Judd–Ofelt theory in which the branching ratios are incorporated into the calculation of the Ω_λ parameters. In this way, the reliability of the intensity parameters can be increased by an increase of the number of measured transitions. The procedure was applied to Pr^{3+}-doped ZBLAN fluorozirconate glass. The best improvement of the fit was obtained by considering the branching ratios, but by excluding the $^3P_2 \leftarrow {}^3H_4$ transition from the data of the absorption spectra. Quimby and Miniscalco (1994) suggest that the method can be useful for lanthanide-doped chalcogenide glasses, where host absorption in the visible spectral region makes the determination of a sufficient number of oscillator (or dipole) strengths difficult.

In Nd^{3+}, luminescence from the metastable $^4F_{3/2}$ to the $^4I_{J'}$ ($J' = 9/2, \ldots$) manifolds of the ground term ^4I can be observed. Since the matrix elements $\langle {}^4F_{3/2} | U^{(2)} | {}^4I_{J'} \rangle$ are nearly equal to zero, since the magnetic dipole contributions to these transitions can be neglected, and since the dispersion is often small in the spectral region of interest (900–2000 nm), the branching ratio $\beta_{\text{R}}({}^4F_{3/2}, {}^4I_{J'})$ for the transitions from $^4F_{3/2}$ are a function of the ratio Ω_4/Ω_6 and do not depend on the parameters Ω_4 and Ω_6 separately (Kaminskii and Li 1974, Denisenko 1987). The ratio Ω_4/Ω_6 is called *spectroscopic quality factor* or *spectroscopic quality parameter*. From the knowledge of Ω_4/Ω_6, one can predict by

which channel the ions from the metastable state $^4F_{3/2}$ relax by luminescence, without the need to calculate the branching ratios explicitly. For the majority of the Nd^{3+} compounds $\Omega_4 < \Omega_6$ (see table 6) and the most intense transition is to the $^4I_{11/2}$ state. If $\Omega_4 > \Omega_6$, the $^4F_{3/2} \rightarrow {}^4I_{9/2}$ transition has the highest intensity. For other lanthanide ions than Nd^{3+}, the spectroscopic quality factor is not usable, since in general the branching ratio cannot be reduced to a function of the Ω_4/Ω_6 ratio.

8. Hypersensitivity

8.1. *Definition and experimental evidence*

The intensities of the induced electric dipole transitions in lanthanide ions are not much affected by the environment. The dipole strength of a particular transition of a lanthanide ion in different matrices will not vary more than a factor two or three. However, a few transitions are very sensitive to the environment, and these are usually more intense for a complexed lanthanide ion than for the lanthanide ion in aqueous solution. The intensity increases up to a factor 200 (Gruen and DeKock 1966, Gruen et al. 1967). Only in a few cases has a lower intensity than in the aqueous solution been reported for these transitions (e.g. Krupke 1966). Jørgensen and Judd (1964) have called such transitions *hypersensitive transitions*. They noted that all known hypersensitive transitions obey the selection rules $|\Delta S| = 0$, $|\Delta L| \leqslant 2$ and $|\Delta J| \leqslant 2$. These selection rules are the same as the selection rules of a pure quadrupole transition, but calculations have revealed that the intensities of hypersensitive transitions are several orders of magnitude too large for these transitions to have a quadrupole character. Therefore, hypersensitive transitions have been called also *pseudo-quadrupole transitions*. No quadrupole transitions have been observed for lanthanide ions, although Chrysochoos and Evers (1973) stated that the intensity of the hypersensitive transitions $^5D_2 \leftarrow {}^7F_0$ (in the absorption spectrum) and $^5D_0 \rightarrow {}^7F_2$ (in the luminescence spectrum) of Eu^{3+} are mainly quadrupolar in nature.

Much attention has been given to the explanation of the phenomenon *hypersensitivity* and to chemical applications of this effect. Hypersensitivity has been discussed in review articles by Peacock (1975), Henrie et al. (1976), Judd (1980b), Misra (1985) and Misra and Sommerer (1991). Selwood (1930) noticed a sensitivity of certain transitions in the aqueous spectra of Nd^{3+}, Eu^{3+}, Ho^{3+} and Er^{3+} nitrates at different concentrations. The high sensitivity of the spectral intensities to the ligand environment as a general phenomenon was first noticed by Moeller and coworkers during a spectroscopic study of complexes of Nd^{3+}, Ho^{3+} and Er^{3+} with EDTA and β-diketonates (Moeller and Brantley 1950, Moeller and Jackson 1950, Moeller and Ulrich 1956). Hypersensitive transitions have been observed for nearly every lanthanide ion. A list of the hypersensitive transitions is given in table 23. It should be noted that there is a disagreement concerning the hypersensitivity of some transitions. For instance, the $^3P_2 \leftarrow {}^3H_4$ and $^1D_2 \leftarrow {}^3H_4$ transitions of Pr^{3+} and the $^4G_{7/2}, {}^2K_{13/2} \leftarrow {}^4I_{9/2}$ transition of Nd^{3+} are considered as hypersensitive transitions by Henrie et al. (1976), but not by Peacock (1975). Misra and

Table 23
Hypersensitive transitions for trivalent lanthanide ions[a]

Ion	Transition	Approximate wavenumber (cm^{-1})	Ion	Transition	Approximate wavenumber (cm^{-1})
Pr^{3+}	$^3F_2 \leftarrow {}^3H_4$ [b]	5200	Dy^{3+}	$^6F_{11/2} \leftarrow {}^6H_{15/2}$ [e]	7700
Nd^{3+}	$^4G_{5/2} \leftarrow {}^4I_{9/2}$ [c,d]	17300	Ho^{3+}	$^5G_6 \leftarrow {}^5I_8$	22100
Pm^{3+}	$^5G_2, {}^5G_3 \leftarrow {}^5I_4$	18000		$^3H_6 \leftarrow {}^5I_8$	27700
Sm^{3+}	$^4F_{1/2}, {}^4F_{3/2} \leftarrow {}^6H_{5/2}$	6400	Er^{3+}	$^2H_{11/2} \leftarrow {}^4I_{15/2}$	19200
Eu^{3+}	$^5D_1 \leftarrow {}^7F_1$	18700		$^4G_{11/2} \leftarrow {}^4I_{15/2}$	26400
	$^5D_2 \leftarrow {}^7F_0$	21500	Tm^{3+}	$^3F_4 \leftarrow {}^3H_6$	5900
	$^5D_0 \rightarrow {}^7F_2$	16300		$^3H_4 \leftarrow {}^3H_6$	12700
Gd^{3+}	$^6P_{5/2}, {}^6P_{7/2} \leftarrow {}^8S_{7/2}$	32500		$^1G_4 \leftarrow {}^3H_6$	21300
Tb^{3+}	None reported				

[a] After Peacock (1975).
[b] According to Henrie et al. (1976), the transitions $^3P_2 \leftarrow {}^3H_4$ (22500 cm^{-1}) and $^1D_2 \leftarrow {}^3H_4$ (17000 cm^{-1}) are also hypersensitive transitions for Pr^{3+}.
[c] The $^4G_{5/2} \leftarrow {}^4I_{9/2}$ transition overlaps with the transition $^2G_{7/2} \leftarrow {}^4I_{9/2}$.
[d] The transition $^4G_{7/2}, {}^3K_{13/2} \leftarrow {}^4I_{9/2}$ (19200 cm^{-1}) has been mentioned as a hypersensitive transition by Henrie et al. (1976).
[e] Hypersensitivity of the transition $^4G_{11/2}, {}^4I_{15/2} \leftarrow {}^6H_{15/2}$ (23400 cm^{-1}) has been reported by Henrie et al. (1976).

coworkers (Misra et al. 1990, 1994a,b, Misra and Sommerer 1991, 1992a,b, Misra and John 1993) argue that these transitions show hypersensitivity only in the presence of some particular ligands. They use the term *ligand-mediated pseudo-hypersensitivity* for this phenomenon, because the coordination number and coordinating power, the hapticity, the bite angle and the size of the chelate ring of the different ligands affect the sensitivity of these non-hypersensitive transitions to a different degree. Other ligand-mediated pseudo-hypersensitive transitions are $^4F_{7/2} \leftarrow {}^4I_{9/2}$, $^4F_{5/2} \leftarrow {}^4I_{9/2}$ and $^4F_{3/2} \leftarrow {}^4I_{9/2}$ for Nd^{3+}. For Eu^{3+}, in addition to the $^5D_2 \leftarrow {}^7F_0$ and $^5D_1 \leftarrow {}^7F_1$ transitions, the $^5D_0 \leftarrow {}^7F_0$ transition is indicated as hypersensitive by Katzin (1969).

Karraker has studied the hypersensitive transitions of Nd^{3+}, Ho^{3+} and Er^{3+} in detail (Karraker 1967, 1968). In his first paper, Karraker (1967) considered the absorption spectra of six-, seven- and eight-coordinated β-diketonates in non-aqueous solutions to determine the effects of the coordination number on the intensity and fine structure of the spectra. He selected the lanthanide β-diketonates for investigation, since all the ligands are bonded through oxygen atoms, so that coordination number and geometry of the bonding groups were the major experimental variables. He chose organic liquids with low polarity as solvents in order to avoid solvent effects to the crystal-field splitting of the lanthanide ions. The hypersensitive transitions under consideration were: $^4G_{5/2}, {}^2G_{7/2} \leftarrow {}^4I_{9/2}$ for Nd^{3+}, $^5G_6, {}^5F_1 \leftarrow {}^5I_8$ for Ho^{3+}, and $^2H_{11/2} \leftarrow {}^4I_{15/2}$ for Er^{3+}. He concluded that the hypersensitive transitions show differences that are characteristic

for the coordination and the symmetry of the lanthanide ion. The conclusion was based on the following findings: (1) there is a difference between the appearance of the absorption bands for hypersensitive transitions between six-, seven- and eight-coordinated lanthanide ions; (2) addition of the unidentate ligand hexafluoroacetylacetone (HFAA) to solutions of six- and seven-coordinated complexes results in changing the spectra to spectra resembling those of seven- and eight-coordinated complexes; (3) the removal of water from solutions of hydrated complexes results in changing the spectra to spectra resembling spectra of lower coordination; (4) there is a correlation between the intensity of hypersensitive transitions and the coordination number. In his second paper, Karraker (1968) investigated the effects of strong aqueous chloride and perchlorate solutions on the hypersensitive transitions. The change in the band shape was used to recognize changes in the coordination. He found that the shape of all Nd^{3+} absorption bands (both hypersensitive and non-hypersensitive transitions) changes as the electrolyte concentration or the temperature was increased, but there is no change in shape for the absorption bands of Ho^{3+} and Er^{3+}. The intensity of the hypersensitive transitions of Nd^{3+}, Er^{3+} and Ho^{3+} increases as electrolyte or temperature is increased. The change in shape for Nd^{3+} is attributed to a change in the coordination number from 9 (dilute solutions) to 8 (concentrated solutions). The increase in intensity in concentrated solutions is due to an enhancement of the electric field acting on the lanthanide ions as water in the secondary hydratation layer is replaced with anions or hydrated cations. The anions will increase the electric field on the ion by electrostatic interactions and the hydrated cations will increase the electric field by inversing the direction of the water molecules from their direction in diluted aqueous solutions. Temperature effects in concentrated solutions are attributed to entropy differences between lanthanide ions and other cations.

Choppin et al. (1966) suggested that the band shape and intensity of hypersensitive transitions could be used as a qualitative indication of the site symmetry. They studied the absorption spectra of Nd^{3+} with different anions. Choppin and Fellows (1973) found on the basis of the spectra of lanthanide ions in diluted perchloric acid at various ionic strength that the hypersensitivity is independent of ion pairing (between the lanthanide cation and the perchlorate anion) in the outer sphere at high ionic strength conditions. According to these authors, oscillator strengths are, in first approximation, not dependent on the ionic strength of the solution.

The first case of a hypersensitive transition in Pr^{3+} was reported by Peacock (1970). Fellows and Choppin (1974) reported a study of the relationship between the ligand pK_a and the oscillator strength of the hypersensitive transitions of Nd^{3+} and Ho^{3+} with dibasic and polybasic ligands. For aminopolycarbonate ligands, the order of the oscillator strengths is EDTA > HEDTA > DTPA > DCTA > NTA in the case of Nd^{3+}, and HEDTA > DTPA > NTA > EDTA > DCTA in the case of Ho^{3+}. It was not possible to give an explanation for these sequences, nor why the sequence differs for Nd^{3+} and Ho^{3+}. The oscillator strength of the hypersensitive transitions shows only a moderate variation for the different ligands and no correlation exists between the oscillator strength and the sum of the ligand pK_a values. Fellows and Choppin found, however, a good correlation between the oscillator strength and the sum of the ligand pK_a values for

dibasic ligands. The variation of the oscillator strength with basicity is less for dibasic than for monobasic ligands. With ligands containing both nitrogen and oxygen donor atoms, the correlation holds when only the basicity of the oxygen sites is considered. Fellows and Choppin suggest that the metal–nitrogen interaction has little influence on the spectral intensities when compared to the metal–oxygen bonding. Sinha (1966) also found that the lanthanide–nitrogen donor interaction has little effect on the electronic spectra of lanthanide complexes in solution. The existence of such a correlation between the oscillator strength and the basicity for monodentate as well as for polydentate ligands could indicate that differences in symmetry are less important than the variation in metal–ligand bond covalency (Fellows and Choppin 1974). The similarity of oscillator strengths for fumarate complexes (monodentate) and maleate complexes (bidentate) is a good example that the ligand basicity has a much greater influence on the oscillator strengths than symmetry. This experimental relation between ligand basicity and hypersensitivity was treated in detail by the same group of authors in a review article (Henrie et al. 1976). They state three generalizations concerning the intensity of the hypersensitive transitions: (1) an increasingly basic character of the coordination ligand results in increasing ligand absorption intensity, (2) decreasing metal–ligand bond distances result in intensity enhancement, (3) the greater the number of (more basic) ligands, the greater the enhancement of intensity. With these rules many qualitative explanations can be given. Organometallic complexes, such as complexes with cyclopentadiene, show very high intensities for the hypersensitive transitions (Pappalardo 1968). These high intensities can be attributed to the high basicity of the cyclopentadienide ion, although aqueous pK_a values are not known because of the instability of the ligand in water. A self-consistent series of increasing hypersensitivity with increasing ligand basicity is given by the β-diketones hexafluoroacetylacetone < trifluoroacetylacetone < acetylacetone < di(tertiarybutyl)acetylacetone and benzoylacetylacetone < thenoyltrifluoroacetylacetone < dibenzoylacetylacetone (Karraker 1967, Kononenko et al. 1971, Isobe and Misumi 1974). Another example is the series of 5,7-dihalogenated oxine derivatives: 5,7-dichloro < 5-chloro,7-iodo < 5,7-dibromo < 5,7-diiodo (Gupta et al. 1970, Bratzel et al. 1972). The intensity increase by a decrease in metal–ligand bond length was used by Henrie et al. (1976) to explain the order of the intensity of the hypersensitive transition of Nd^{3+} for the series $Y_3Al_5O_{12} < YAlO_3 < Y_2O_3$.

Other authors have tried to correlate the intensity of hypersensitive transitions with the site symmetry of the rare-earth ion. Krupke (1966) attributed the difference in intensity for Nd^{3+} doped into the crystalline host matrices Y_2O_3 to a difference in symmetry. In general, it is assumed that the higher the site symmetry, the lower the intensity. This thought is based on the fact that in theory the intensity of the hypersensitive transition is zero when the lanthanide ion is at a center of symmetry (just as for other induced electric dipole transitions). Intensity can in this case only be gained by vibronic coupling (see sect. 11). Low intensities are found for Eu^{3+} at the S_6 site of Y_2O_3 (Kisliuk et al. 1964) and at the O_h site of $Cs_2NaEuCl_6$ (Schwartz 1975). According to Bel'tyukova et al. (1981), the increase of the intensity ratio $I(^5D_0 \rightarrow {}^7F_2)/I(^5D_0 \rightarrow {}^7F_1)$ of the hypersensitive electric dipole transition $^5D_0 \rightarrow {}^7F_2$ to the magnetic dipole transition

$^5D_0 \rightarrow {}^7F_1$ in Eu^{3+} of complexes in solution relative to those for the solid compounds is due both to the solvatation of the complexes in solution, to a change in the symmetry of the environment, and to the coordination number of Eu^{3+}. If the ligand field strength is strong, the solvatation has a larger influence on the intensity of hypersensitive transitions. Bel'tyukova et al. (1981) have also shown that on passing from the solid state to solutions, the intensity of hypersensitive transitions increase. According to Kandpal and Joshi (1988) the intensity of the hypersensitive transition $^5D_0 \rightarrow {}^7F_2$ in Eu^{3+}-doped glasses is enhanced by a high asymmetry of the Eu^{3+} site. Asymmetry increases in the order borate < phosphate < silicate < germanate < tellurite.

Poluéktov et al. (1972) have shown for a series of phenol-like derivatives of Nd^{3+}, Ho^{3+} and Er^{3+} that the intensity of hypersensitive bands increases with increasing number of coordinated ligands. Choppin and Fellows made similar observations for a broader range of ligands (Choppin and Fellows 1973, Fellows and Choppin 1974). Changes in the coordination number have been suggested also by Katzin and Barnett (1964) as a possible cause for intensity and fine-structure differences. Surana et al. (1975) found that the intensity of hypersensitive transitions in Nd^{3+} complexes follows the order of the ligands: oxygen donor > nitrogen–oxygen donor > nitrogen donor > sulfur donor > aquo ion.

Misra and Mehta (1991) described the pseudo-hypersensitivity in complexes of Nd^{3+} with fluorinated nucleic bases and with fluorinated nucleosides. Pr^{3+} complexes with haloacetate, fluorocarboxylate, β-diketonates, diols and orthophenanthroline derivatives have been considered by Misra and Mehta (1992). The fluorocarboxylates of Pr^{3+} tend to have lower intensities for the f–f transitions with the increased number of fluorine ligands. This is understandable in terms of the electron withdrawing capacity of different fluoroalkyl groups (lower covalency). The increase in intensity in the order butane-1,4-diol < butene-1,4-diol < butyne-1,4-diol has been ascribed to the interaction of the π electron density of the multiple bond with some sort of linear combination of Pr^{3+} 5d, 6s, 6p and 4f orbitals. Misra et al. (1994a) studied 27 Nd^{3+} complexes with the identical chromophore NdO_6N_2 (CN 8) in methanol, DMF, acetonitrile, and isopropanol.

8.2. *Theoretical models for hypersensitivity*

Judd (1962) noticed that hypersensitive transitions are associated with large values of the $U^{(2)}$ reduced matrix element in eq. (189). Hypersensitivity is described by the Ω_2 parameter if the $U^{(4)}$ and $U^{(6)}$ matrix elements for the hypersensitive transition are small. Poluéktov et al. (1977) proposed a power law between the oscillator strength and the matrix element $U^{(2)}$. It can be mentioned that Henrie and Henrie (1974) did not consider the absolute magnitude of the Ω_2 parameter as a measure for hypersensitivity, but the relative magnitude of Ω_2 with respect to Ω_4 and Ω_6.

As long as the Ω_2 parameter is treated as an adjustable parameter, the Judd–Ofelt theory gives good agreement between experimental and calculated dipole strengths for hypersensitive transitions. However, the original Judd–Ofelt theory cannot give a theoretical explanation for the hypersensitivity effect (Peacock 1975). If it is assumed that the radial integrals in eq. (196) are not largely affected by the ligand environment of the lanthanide ion,

and if the intensity parameters Ω_4 and Ω_6 have to remain unaltered, the Ω_2 parameter can be changed only through the A_{1q} crystal-field parameters. Judd (1962) did not include the A_{1q} crystal-field parameters in the expression for Ω_2, because their presence implies a non-zero electric field at the nucleus of the lanthanide ion. In this case, the lanthanide ion is not in equilibrium with its surroundings. Equilibrium of the lanthanide ion with the environment is a basic requirement in a static perturbation model. Later, Judd (1966a) stated that for certain point groups the A_{1q} parameter could be included in the lattice sum, without violating the basic assumption of the static model. These point groups are: C_s, C_1, C_2, C_3, C_4, C_6, C_{2v}, C_{3v}, C_{4v} and C_{6v}. In these point groups, the electrons of the lanthanide ion can produce a non-vanishing electric field at the nucleus which is cancelled by the crystal field. According to Judd, hypersensitivity is thus related to symmetry. In theory, hypersensitivity can be observed only for the point groups mentioned above. Several examples seem to confirm the theory. For instance, the Ω_2 parameter for Nd^{3+} in $Y_3Al_5O_{12}$ (D_2) and in $YAlO_3$ (D_{3h}) is much smaller than for the same ion in Y_2O_3 (C_2) and in the $Nd(NO_3)_9^{6-}$ complex (C_3). There are however many exceptions. Although the symmetry of Nd^{3+} in the gaseous compounds $NdBr_3$ and NdI_3 is D_{3h}, these systems show the highest intensities ever observed for Nd^{3+} (Peacock 1975). Pappalardo has shown that the crystal-field fine structure of the hypersensitive transition in the holmium tris(methylcyclopentadienyl) complex is not compatible with point groups having a A_{1q} coefficient in the expansion of the odd crystal-field potential (Pappalardo 1969).

It was argued by Jørgensen and Judd (1964) that inhomogeneities in the dielectric surrounding of the lanthanide ion could enhance the intensity. According to this model, the electric field induces oscillating dipole moments in the ligands, which become secondary sources of radiation. Since the ligands are close to the central lanthanide ion, they produce an electric field that is very different from the plane wave that the lanthanide ions would feel in the absence of the dipoles in the medium. Since the dimension of a lanthanide ion is much smaller than the wavelength of visible and even ultraviolet radiation, there is only little spatial variation of the electric field in the neighborhood of the lanthanide ion, if only a homogeneous dielectric is considered. In an *inhomogeneous dielectric* with the asymmetric distribution of oscillating dipoles, the electric field possesses a strong quadrupole component. These quadrupole components are then assumed to induce f–f transitions according to an electric quadrupole transition mechanism. As pointed out by Peacock (1975), this theory has been criticized by many authors. For instance, Bell et al. (1969) argue that if the inhomogeneous dielectric is responsible for the intensity of hypersensitive transitions, the intensity of a hypersensitive transition should decrease as the temperature is increased, because of an increase in homogeneity of the solvent dielectric at higher temperatures. No intensity decrease is found at higher temperatures. In a later paper, Judd (1979) has shown that the model of the inhomogeneous dielectric is formally identical with the dynamic coupling model of Mason et al. (see further in this section). Both models give alternative descriptions for the same physical phenomenon.

Peacock (1970) argued that any theory which ascribes hypersensitivity to a vibronic mechanism is dubious. He arrived at this conclusion by variable-temperature measurements of the hypersensitive transition $^5D_2 \leftarrow {}^7F_0$ in $K_{13}[Eu(SiW_{11}O_{39})]$. Earlier,

Jørgensen and Judd (1964) and Gruber et al. (1969) had also reached that conclusion. Such a vibronic mechanism was for instance proposed by Gruen and DeKock (1966) for explaining the large intensities for the hypersensitive transitions in the gaseous molecules $NdBr_3$ and NdI_3. Henrie and Choppin (1968) explained the hypersensitivity of various Nd^{3+} complexes by means of a vibronic mechanism with the inclusion of covalency. However, Judd (1980a) has shown that the strongest vibronic lines in rare-earth spectra should be associated with hypersensitive transitions (see also sect. 11).

A covalency model of hypersensitivity was developed by Henrie et al. (1976). The idea for that model came from the observation of charge-transfer transitions in lanthanide complexes. The energies and intensities of these charge-transfer transitions are very sensitive to the type of ligand and to the lanthanide ion. In fact, the energy of the ligand-to-metal charge transition is a function of the metal orbital energy, the interelectronic repulsion energy and the ligand energy. For one particular metal ion, the charge-transfer energy will vary only with the nature of the ligand (Peacock 1977). In fact, the charge-transfer energy may be expressed as a function of the difference between the optical electronegativities of the ligand and the metal (Jørgensen 1962). There is a non-monotonic variation of the charge-transfer energy over the lanthanide series (Peacock 1977). In comparison with the charge-transfer transitions, the $5d \leftarrow 4f$ transitions are relatively insensitive to the ligand type. Barnes and Pincott (1966) not only showed that the energies of the charge-transfer transitions depend on the nature of the coordinating ligands, but also that the energies increase with an increase in the number of ligands. As already mentioned in this section, the intensity of hypersensitive transitions increases with an increase in the number of coordinating ligands. Henrie et al. (1976) argued that sensitivity to ligand environment is intrinsically built into a model for hypersensitivity, if the hypersensitive transitions gain some charge-transfer character. Barnes and Pincott (1966) modified the Judd–Ofelt theory by including charge-transfer states as perturbing states to be mixed with the $4f^N$ configuration, in addition to the perturbing configurations $4f^{N-1}5d^1$ and $4f^{N-1}5g^1$. They considered charge-transfer states which arise from one-electron transfers from the ligand orbitals to the f orbitals of the lanthanide ion.

The covalency model describing the mixing of charge-transfer states into the f^N configurations provides a theoretical basis for the correlation of the intensity of hypersensitive transitions with the ligand pK_a. The hypersensitive transition $^5D_2 \rightarrow {}^7F_0$ of Eu^{3+} is more sensitive to the environment than any other transition of a trivalent lanthanide ion. This is due to the relatively low energy of the charge-transfer transition, combined with the relatively high value of the energy of the hypersensitive transition: the intensity is inversely proportional to the square of the energy difference between the hypersensitive transition and the charge-transfer transition (Henrie et al. 1976). On the basis of the same arguments, it is possible to explain the greater sensitivity for Ho^{3+} than for Nd^{3+}. Blasse (1976) also found a correlation between the intensity of the hypersensitive transition $^5D_2 \rightarrow {}^7F_0$ and the charge-transfer energy.

Henrie et al. (1976) found a direct relation between the hypersensitivity and the nephelauxetic effect. The *nephelauxetic effect* is observed as a red-shift of the f–f

transitions and increases with increasing degree of covalency. The charge-transfer states with the same parity as the $4f^N$ states and being mixed with $4f^N$ via configuration interaction lie lower for more covalent ligands. This explains why the triplet levels of Pr^{3+} show a greater nephelauxetic effect than the singlet levels for several series of compounds. Indeed, charge-transfer transitions from ligand to metal give rise, for Pr^{3+}, to singlets with a barycenter at a higher energy than the triplets. Therefore, a larger red-shift is found for the triplets of the $4f^2$ configuration of Pr^{3+} than for the singlets. The same model could also be used to interpret the variation in the nephelauxetic effect for lanthanide and actinide ions as a function of the atomic number.

However, by considering the variation of the charge-transfer energy and of the intensity parameter Ω_2 across the isostructural series $Y_2O_3:R^{3+}$, Peacock (1977) concluded that charge-transfer mixing is of negligible importance in accounting for the intensity of the hypersensitive transitions. He argued that if the charge-transfer mixing is the major contribution to Ω_2, the variation of the parameter should mirror the variation of the charge-transfer energy, raised to the power –3, since

$$\Omega_2 \propto P_{CT} E_{CT}^{-3}, \tag{236}$$

where P_{CT} is the charge-transfer oscillator strength and E_{CT} is the charge-transfer energy. P_{CT} is known to vary more or less monotonically across the lanthanide series (Jørgensen 1962, Ryan and Jørgensen 1966). However, the charge-transfer energy shows a non-monotonical variation over the lanthanide series, whereas the Ω_2 parameter values lie close to a smooth decreasing curve. According to Peacock (1977), the relationship between the pK_a of the ligand and the Ω_2 parameter can be easily rationalized by the ligand-polarization theory, just as it can be rationalized by charge-transfer mixing. Since the charge-transfer energy is proportional to the optical electronegativity $\chi(L)$ of the ligand and since the Ω_2 parameter according to the ligand-polarization theory is proportional to $1/\chi(L)^4$ for a particular metal ion, it seems to be possible to relate the Ω_2 parameter to the charge-transfer energy. Peacock also gave an explanation alternative to that of Henrie et al. (1976) for the greater sensitivity of Eu^{3+} to the ligand environment in comparison with Nd^{3+}. The hypersensitive transition $^5D_2 \leftarrow {}^7F_0$ of Eu^{3+} is proportional to the $\Omega_2(Eu)$ parameter, whereas the hypersensitive transition $^4G_{5/2}, {}^2G_{7/2} \leftarrow {}^4I_{9/2}$ of Nd^{3+} is proportional to both $\Omega_2(Nd)$, $\Omega_4(Nd)$ and $\Omega_6(Nd)$. Because of the non-zero value of the reduced matrix elements $U^{(4)}$ and $U^{(6)}$, it is sufficient to double the dipole strength of the Eu^{3+} transition in order to double $\Omega_2(Eu)$, whereas an increase by a factor five is needed to double the $\Omega_2(Nd)$ parameter. The non-negligible contribution of $\lambda=4$ and $\lambda=6$ terms to the intensity of the hypersensitive transition $^4G_{5/2}, {}^2G_{7/2} \leftarrow {}^4I_{9/2}$ of Nd^{3+} has been discussed also by Malta and de Sá (1980). Poluéktov et al. (1984) correlated the intensity of hypersensitive transitions to the ground-state L and J quantum numbers. Jankowski and Smentek-Mielczarek (1981) reported that electron correlation effects could be one of the most important mechanisms contributing to the intensity of hypersensitive transitions.

The hypersensitive transitions are not well described by the original Judd–Ofelt theory, because not all the metal–ligand interactions can be taken into account. In the Judd–Ofelt theory, the lanthanide ion is perturbed by the ligands. The ligands produce a static potential of odd parity ($D_q^{(k)}$ with k odd) around the lanthanide ion. In this way, 4f states of mixed parity are produced. Transitions between these states can be induced directly by the electric dipole component of the light. Eventually, the ligands can be isotropically polarized by the lanthanide ion. However, it is assumed that the ligands are not influenced by the radiation field of the incident light. Therefore, the Judd–Ofelt theory is also called a *static-coupling (SC) model.* The perturbing wavefunctions Ψ_s^0 are localized on the central metal ion.

In order to give a more accurate description for the intensity of hypersensitive transition, Mason et al. (1974, 1975) have developed a new theoretical model: the *dynamic-coupling model* (*ligand-polarization model*). The model has been discussed also by Peacock (1975, 1978) and Mason (1980). In this model, dipoles are induced by the charge distribution caused by the f–f transition. Thus, the f electrons polarize the ligands. The ligand wavefunctions are perturbed by the lanthanide ion. The dynamic coupling mechanism gives a contribution to the Ω_2 parameter if the expansion of the odd part of the crystal-field potential contains the terms A_{3q}. These terms are present if the point group contains no center of symmetry. In this case the induced dipoles can combine into a non-vanishing dipole moment. This dipole moment can interact with the radiation field. The point groups in question are C_s, C_n, C_{nv}, C_{3h}, D_n, D_{3h}, D_{2d}, S_4, T and T_d. Therefore, the model can give an explanation for the hypersensitivity of the trihalides $NdCl_3$ and NdI_3 in the vapor phase. These complexes possess D_{3h} symmetry. Newman and Balasubramanian (1975) published a complementary theory in order to take also non-hypersensitive transitions into account. Reid and Richardson (1983a–c, 1984a–c) brought both ideas together in a general intensity model (see also sect. 6.2).

Kuroda et al. (1980, 1981) demonstrated that the intensity of the hypersensitive $^5D_2 \leftarrow {}^7F_0$ transition of Eu^{3+} in different systems with D_3 symmetry can be described adequately only if anisotropic ligand polarization is considered. They ignored J-mixing. The dynamic coupling model predicts the sequence $I^- > Br^- > Cl^- > H_2O > F^-$ for the intensity of hypersensitive transitions. The sequence is identical to the ligand polarizability order. Kirby and Palmer (1981a) investigated the hypersensitive transition $^4G_{5/2}, {}^2G_{7/2} \leftarrow {}^4I_{9/2}$ of Nd^{3+} in $Nd(DBM)_3 \cdot H_2O$, and calculated the oscillator strengths in the context of the dynamic-coupling model. The same authors reported an intensity study of $Eu(DBM)_3 \cdot H_2O$, $Ho(DBM)_3 \cdot H_2O$ and $Er(DBM)_3 \cdot H_2O$ (Kirby and Palmer 1981b). They found that the Ω_2 parameter does not vary in the $R(DBM)_3 \cdot H_2O$ series as predicted by the dynamic-coupling model. They remarked also that the $^5G_5 \leftarrow {}^5I_8$ transition of Ho^{3+}, which is formally not a hypersensitive transition, is unusually intense in $Ho(DBM)_3 \cdot H_2O$. Richardson et al. (1981) calculated the intensity of hypersensitive transitions in nine-coordinate $R(ODA)_3^{3-}$ with trigonal symmetry. A combined static-coupling/dynamic-coupling theory was used and the intensities were calculated directly, without the introduction of intensity parameters.

8.3. *Application of hypersensitivity*

Hypersensitivity has been used for the study of the coordination polyhedron (coordination number and site symmetry) around the rare-earth ion. As already mentioned in sect. 8.1, Karraker used the shape of a hypersensitive transition to study the coordination of rare-earth β-diketonates in non-aqueous solution (Karraker 1967) and the coordination of rare-earth ions in strong chloride and perchlorate aqueous solution (Karraker 1968). Since the profile of the band due to the $^2H_{9/2}, {}^4F_{5/2} \leftarrow {}^4I_{9/2}$ and the $^4G_{5/2}, {}^2G_{7/2} \leftarrow {}^4I_{9/2}$ transitions in the spectrum of Nd^{3+}(aquo) resembles the profile for the same transitions in solid $Nd(BrO_3)_3 \cdot 9H_2O$ (9-coordination for Nd^{3+}), Karraker suggested a coordination number 9 for Nd^{3+} in water: $Nd(OH_2)_9{}^{3+}$. On the basis of the shape of the hypersensitive transition $^4G_{5/2}, {}^2G_{7/2} \leftarrow {}^4I_{9/2}$ of Nd^{3+} in sodium borate glasses with Na_2O content varying between 7.5 and 40 mol%, Gatterer et al. (1994) correlated the immediate neighborhood of Nd^{3+} ions with an existing model of eight-fold coordination around the rare-earth with non-bridging oxygens in oxide glasses. It was concluded that the Nd^{3+} ions in the glass have a strong tendency to create an environment similar to that in pure oxides.

Hypersensitive transitions can be useful for the study of structure, conformation and binding modes of biomolecules, and of reaction mechanism of biochemical reactions involving calcium ions. Birnbaum et al. (1970, 1976, 1977) have used changes in the shape and intensity of the hypersensitive transition $^4G_{5/2} \leftarrow {}^4I_{9/2}$ of Nd^{3+} in absorption difference spectra as a spectral probe for exploring the binding of Nd^{3+} with bovine trypsin and bovine serum albumin. The possibility of probing the binding characteristics of biomolecules via hypersensitive transitions has been reviewed by Misra and John (1993).

A practical application of the spectral intensity of hypersensitive transitions in lanthanide ions is the determination of stability constants. Bukietynska et al. (1977, 1981a,b) have evaluated the stability constants of lanthanide complexes from the changes of the oscillator strength of hypersensitive transitions as a function of the ligand concentration. The method was applied to acetate, propionate, glycolate, lactate and α-hydroxyisobutyrate complexes of Nd^{3+}, Ho^{3+} and Er^{3+}. Bukietynska et al. claim that this spectrophotometric method is superior to the potentiometric method, since the best results for the latter method can be obtained only for the first complexation steps. The stability constants evaluated at several temperatures have been used also to calculate the thermodynamic quantities ΔG, ΔH and ΔS.

9. Compositional dependence of the intensity parameters

Since the intensity of f–f transitions in rare-earth complexes is ligand dependent, several authors have tried to correlate the intensity parameters with the chemical nature of the metal–ligand bond, with the properties of the ligand itself, or with the structure of the complex. Of course, most attention has been paid to the hypersensitive transitions (see sect. 8). Indeed, the intensity of these transitions shows a large variation with

ligand type. However, the discussion can go beyond the results obtained by the study of the hypersensitive transitions, although the range for the experimental values of the Ω_2 parameter (describing hypersensitivity) is much larger than the range for the experimental values of the parameters Ω_4 and Ω_6. It should be noted that a correlation between the intensity of the f–f transitions and the chemical nature of the rare-earth complex is more difficult to establish than a correlation between spectroscopic and structural properties for d-group transition metal complexes, because the f orbitals are much better shielded from the environment than the d orbitals.

In the view of the discussion of hypersensitivity, the Ω_2 parameter can be seen as an indicator for covalent binding (Reisfeld and Jørgensen 1977). A large value for the Ω_2 parameter is found if the chemical bond shows a substantial covalent character. The interest in the variation of the parameters Ω_4 and Ω_6 with the composition and properties of the host matrix is from a rather recent date. Until the beginning of the 1980s it was believed that the small variation of the Ω_4 and Ω_6 parameters was not predictable. A comparative study of the intensity parameters for complexes containing Er^{3+} allowed Jørgensen and Reisfeld (1983) to conclude that the Ω_6 parameter is related to the rigidity of the medium in which the lanthanide ions are embedded. The parameter value increases over a series of increasing mean displacements from equilibrium distances to the nearest-neighbor nuclei, or in other words, the parameter increases with increasing vibrational amplitude of the R–X distance. Rigid matrices show low values for the Ω_6 parameter. The rigidity increases in the order crystalline mixed oxides < glasses < viscous solutions < hydrated ions < halide vapors < complexes of organic ligands. A few years later, Reisfeld and Jørgensen (1987) stated that the Ω_4 parameter follows the same trend as the Ω_6 parameter. The Ω_4 and Ω_6 parameters were considered as indicators of viscosity (for rare-earth ions in glasses). The compositional dependence of the Ω_λ intensity parameters has been studied extensively in vitreous matrices, because a glass offers the advantage of a large compositional space.

Tanabe et al. (1993a) have reported that the Ω_6 parameter is sensitive to the overlap integral of the 4f and 5d orbitals, $\langle 4f | \hat{r}^k | 5d \rangle$. They arrived at that conclusion by a study of the relation between the Ω_λ intensity parameters of Er^{3+} in oxide glasses and the isomer shift of ^{151}Eu Mössbauer spectra in glasses of the same compositions. The Ω_6 parameter decreases when the isomer shift increases (negative correlation). The shift reflects the 6s electron density of the rare-earth ions. The overlap integral of the 4f and 5d orbitals is supposed to decrease when the 6s electron density is large, because the 6s electron density shields the 5d electron orbital or to repulse the 5d electron. If the radial integrals dominate the Ω_λ parameters, the parameters are assumed to decrease with an increase of the 6s electron density. The Ω_6 parameter ($k = 5$ or 7) is more sensitive to the radial integral than the Ω_2 parameter ($k = 1$ or 3) or the Ω_4 parameter ($k = 3$ or 5). They also found a negative correlation between the Ω_6 parameters of Nd^{3+} and Er^{3+} and the 6s electron density (Tanabe et al. 1993b). Alternatively, the 6s electron density can be seen as a measure of the σ character of the R–X bond, and this is a measure for the covalency. Tanabe et al. (1995a) concluded that whereas the Ω_2 parameter increases with increasing covalency, the opposite trend is found for the

Ω_6 parameter. For Dy^{3+}-doped glasses, they found that the Ω_2 value showed the order sulfide > tellurite > fluorozirconate > fluoroindate. For the Ω_6 parameter, this order is reversed. However, Tanabe et al. (1995b) found no correlation between the Ω_6 parameter and the isomer shift in fluoride glasses. This is probably due to the small covalency in fluoride glasses (low 6s electron density).

Weber et al. (1981) indicated that the Ω_2 parameter decreased and the Ω_4 and Ω_6 parameters increased with increasing ion size of the glass modifier. They also stated that these intensity parameters depend on the covalence of the Nd–O bond in Nd^{3+}-doped metaphosphate glass. Izumitani et al. (1982) believe that the Ω_4 and Ω_6 parameters are a measure of the distortion in the ligand field of Nd^{3+}-ions in phosphate and silicate glasses. Zahir et al. (1985) reported that Ω_2 depends on the asymmetry of the rare-earth ligand field in the range of 10–25 mol% Na_2O and on the asymmetry and the Eu–O covalency in the range of 25–30 mol% Na_2O in Eu^{3+}-doped sodium borate glasses. According to Oomen and van Dongen (1989), the Ω_2 parameter depends on *short-range effects,* i.e. the covalency of the ligand field and/or structural changes in the vicinity of the lanthanide ion. The Ω_4 parameter seems to be mainly dependent upon *long-range effects,* and this parameter can be related to the bulk properties of the glass. They have studied the dependence of the Eu^{3+} emission spectrum upon glass composition (for silicate, germanate, borate and phosphate glasses). A study of Er^{3+}-doped alkali borate glasses was reported by Tanabe et al. (1992). They found that the variation of the Ω_2 parameter with the alkali content was related to the change in the asymmetry of the rare-earth ligand field due to structural mixing of borate groups. The variations of the Ω_4 and Ω_6 parameters were related to the local basicity of the rare-earth sites. A study of Eu^{3+}-doped silicate glasses by Nageno et al. (1994) indicated that the Ω_2 parameter depends on the covalency of the Eu–O bond and structural changes around the Eu^{3+} ions, whereas the Ω_4 and Ω_6 parameters are only related to the covalency of the Eu–O bond. Nageno et al. (1993) concluded that the ionic packing ratio of the glass hosts greatly affects the intensity parameters Ω_4 and Ω_6. The parameter values increase with increasing ionic packing ratio. The ionic packing ratio is related to the rigidity of the matrix. Nageno et al. (1993) also mentioned that the Ω_4 and Ω_6 parameters depend on the covalency of the Nd–O bond. The intensity parameter Ω_2 in silicate and borate glasses depends on the asymmetry around the Nd^{3+} ion when the type and content of the modifier are varied. The Ω_2 parameter is rather independent of the covalency of the Nd–O bond. In phosphate glasses, Ω_2 varies systematically with the ionic radius of the network modifier. Uhlmann et al. (1994) found that the Ω_λ values for Nd^{3+}-doped calcium aluminate glasses vary randomly with the glass composition. It can be shown that the Ω_2 parameter increases as the cationic strength of the network-forming ions increases (Tanabe et al. 1995b). The cationic strength is defined as the charge divided by the ionic radius. Flórez et al. (1995) correlated the small variation of the Ω_2 parameter with the Er^{3+} concentration in fluoroindate glass with the micro-structural homogeneity around the Er^{3+} ion. The effect of the PbO content in lead borate glasses on the intensity parameters of Nd^{3+}, Sm^{3+} and Dy^{3+} was been studied by Saisudha and Ramakrishna (1996). The variation of the Ω_2 parameter with PbO content for Nd^{3+} and Sm^{3+} implies that both the asymmetry of the

crystal field at the rare-earth site and the covalency of the R–O bond play an important role in determining the intensity, whereas only the covalency plays a dominant role in Dy^{3+}-doped glasses. The variation of the Ω_6 parameter has been related to a variation in the covalency of the R–O bond. In the lead borate glasses, the covalency of the R–O bond increases with an increase in PbO content. Stokowski et al. (1981a) mention that although small compositional changes of a few percent may significantly change the characteristic temperatures of the glass (glass transition temperature, crystallization temperature and melting temperature) and other physical properties, these changes cause generally only small variations in the intensity parameters. These changes are often within the experimental uncertainties.

Keller et al. (1982) have shown that within the limits of experimental error, the intensities of the transitions of both anhydrous and hydrated rare-earth chlorides in different alcohols are the same. For the Ho^{3+} and Er^{3+} systems, the Ω_2 parameter increases in the order methanol < ethanol < *n*-propanol, whereas for Nd^{3+} the sequence methanol < *n*-propanol < ethanol was found (Bukietynska et al. 1981c). This difference was interpreted in terms of the symmetry and the number of alcohol molecules in the first coordination sphere.

Poluéktov and Bel'tyukova (1974) and Tishchenko et al. (1976) have shown that the intensity of transitions of a series of ionic complexes increases with an increase of the dielectric constant of the solvent. Strek (1979) has given a general theory on the influence of the solvent on the intensity of f–f transitions in lanthanide complexes. The model is based on the dynamic coupling between non-overlapping chromophoric units between which a Coulombic interaction exists. The pairwise interactions between the metal ion and the ligand and between the metal ion and the solvent are considered. The effects on the ligands and many-body interactions are neglected. The intensity of induced electric dipole transitions depends on the permanent dipole moment of the solvent, whereas the intensity of hypersensitive transitions depends on the polarizability of the solvent. Strek suggests that the intensity analysis of f–f transitions in lanthanide complexes may be a useful method for the investigation of intermolecular interactions in liquids. Bukietynska et al. (1995) reported that increase in ligand polarizability enhanced the spectral intensities of neodymium complexes in water. However, Chrysochoos (1974) found that the intensity of the hypersensitive transition $^5D_1 \leftarrow {}^7F_1$ in Eu^{3+} increases as the dielectric constant of the solvent decreases; the author could not assign this transition correctly and the paper was commented upon by Peacock (1974). The intensity of the magnetic dipole transition $^5D_1 \leftarrow {}^7F_0$ remains constant in the different solvents (as expected). For europium perchlorate in non-aqueous solutions, Jezowska-Trzebiatowska et al. (1984) found a positive correlation between the measured values of the square roots of the oscillator strengths for the hypersensitive transition $^5D_2 \leftarrow {}^7F_0$ and the mean molar refractivity of the solutions.

Auzel (1969) plotted the values of the T_λ parameters for Er^{3+}-doped glasses as functions of χ_{ED}. The χ_{ED} factor can be considered as a measure of the polarizability of the medium by the incident electromagnetic radiation. The author remarks that if n would have been chosen instead of χ_{ED}, there would be a minor regroupment of the points in

the curves, because χ_{ED} increases less than n between 1 and 1.5, but increases faster between 1.5 and 2. Finally, $\chi_{ED} = n = 2$. He found that the T_2 parameter tends to increase with increasing values for the refractive index of the glass host, whereas the T_4 and T_6 parameters stay rather independent of the glass host. He stated that for Er^{3+} ions in glasses, it is possible to characterize the intensities by the T_2 parameter only, while fixing the values of T_4 and T_6. The increase of T_2 with n gives an indication for the polarizability of the surrounding ligands.

The last word about the meaning of the intensity parameters has not been said yet, and further research is necessary. A problem for a rigorous comparison is the relatively large error in the Ω_λ parameter (more than 5% or sometimes up to 10–20%). Parameter sets for the same system, but determined by different authors, may be substantially different. This is partially due to the fact that the values of the parameters depend on the transitions chosen for the fitting procedure (as the standard least-squares fitting procedure is chosen). Comparison between fits is only possible if the chi-square method is used to determine the parameters (Goldner and Auzel 1996).

10. Two-photon spectra

In a two-photon transition, a simultaneous absorption of two photons takes place. The molecule, atom or ion is excited to a state with an energy equal to the sum of the two photon energies. When the two photons have the same energy, the transition is called a *one-color two-photon absorption* (OCTPA). If the two photons have a different energy, one has a *two-color two-photon absorption* (TCTPA). In one-photon absorption (OPA), light is absorbed from an initial state to a final state. No other states have to be considered, because the perturbation of the wavefunctions by the radiation field is very weak. A strong radiation field will cause a superposition of a third level with both the initial and final state, producing a non-stationary intermediate state. The non-stationary intermediate state provides a bridge for the completion of the transition to the final state (Denning 1991). A two-photon absorption spectrum has been reported for $LiYF_4:Tb^{3+}$ (Huang et al. 1989). As early as 1931, Maria Göppert-Mayer created a second-order perturbation theory that predicted the phenomenon of two-photon absorption (Göppert-Mayer 1931). However, one had to wait until the availability of intense laser sources in the early 1960s before multi-photon spectroscopy was possible.

The first observed two-photon absorption was the $4f^6 5d^1 \leftarrow 4f^7$ transition in a europium-doped CaF_2 crystal by Kaiser and Garrett (1961) using a pulsed ruby laser. Moreover, this was one of the very first experiments in which a laser was applied for spectroscopic measurements. The sharp parity-allowed $4f^N \leftarrow 4f^N$ two-photon absorption transitions could be observed after the development of tuneable dye lasers. The absorption of the first photon to the non-stationary intermediate state in a two-photon process has to compete with one-photon absorption to an energy level with an energy equal to the photon energy. A two-photon transition is a second-order process and has a much smaller probability than a first-order absorption process. Therefore, a

two-photon transition can be observed only if there is a large energy gap between the initial and final state, so that competition with one-photon absorption to an intermediate state is excluded. The best candidates among the lanthanide ions are Eu^{3+}, Gd^{3+} and Tb^{3+}, although two-photon absorption transitions have been observed also for other lanthanide ions. A list of lanthanide-doped single crystals investigated by two-photon spectroscopy is given in table 24. Two-photon absorption (TPA) is especially advantageous in lanthanide ions in a centrosymmetric environment (Denning 1991) for the following reasons: (1) one has access to most f^N states, without vibronic clutter (as in the case of one-photon absorption), (2) the TPA spectra are polarized so that one can identify the irreducible representations in cubic materials, (3) TPA allows the determination of *gerade* vibronic modes, (4) the intensities reflect the static and vibronic interactions in the intermediate states, (5) parity-conserving states can be found in regions of intense one-photon absorption, and (6) the small lattice dispersion in *gerade* vibronic modes can sharpen the spectra in relation to one-photon absorption.

Axe (1964) developed a theory for the calculation of the intensities of two-photon absorption transitions. The calculation of the intensities is straightforward for second-order mechanisms. He predicted that the intensities of all 4f–4f two-photon transitions between J-manifolds can be explained by fitting only one parameter. Just as Judd did, Axe assumes that all the crystal-field levels of the ground state are equally populated. However, the Axe theory failed in explaining the two-photon excitation spectra of Gd^{3+} in LaF_3, $Gd(OH)_3$ and $GdCl_3$ and of Eu^{2+} in CaF_2 and SrF_2 (Downer et al. 1982, 1983, Downer and Bivas 1983, Judd and Pooler 1982, Jacquier et al. 1987). In particular, the Axe theory is inadequate for the description of two-photon transitions which violate the selection rules $\Delta J \leqslant 2$, $\Delta S = 0$ and $\Delta L \leqslant 2$. Moreover, some transitions were much more intense than predicted by the second-order theory of Axe. A strong host dependence is also in conflict with the theory of Axe, just as the strong polarization of the line transitions. To explain the spin-forbiddenness, Judd and Pooler (1982) suggested that the half-filled shell character of the Gd^{3+} and Eu^{2+} ions plays an important role in the failure of the second-order theory of Axe. They proposed a third-order mechanism in which the spin–orbit coupling is responsible for the perturbation of the intermediate levels. They applied the technique of *second quantization* to lanthanide spectroscopy. In second quantization the eigenfunctions are transformed in operators. The fundamentals for second quantization were introduced by Judd (1966b). The second quantization is a very powerful and convenient method to simplify complicated transition operators. By translating all expressions into the language of second quantization, the expressions for the operators are simplified via several recoupling and anti-commutation relationships. Vandenberghe (1995) has recalculated the third-order mechanism of Judd and Pooler and his results differ by a phase factor from those of Judd and Pooler. Downer et al. (1982) proposed a third-order mechanism in which the crystal-field interaction is considered as a perturbation of the intermediate level. The second-quantization expression of this operator was published by Downer (1989). By introducing a 9-j symbol, Ceulemans and Vandenberghe (1993) were able to reduce the expression of Downer to a more compact transition operator. Moreover, an important phase error was detected in Downer's expression for the crystal-

Table 24
Literature references of two-photon spectroscopy of lanthanide ions in host single crystals

Crystal	Reference(s)
$CaF_2:Ce^{3+}$	Gayen and Hamilton (1983); Gayen et al. (1986); Leavitt (1987)
$LiYF_4:Ce^{3+}$	Gâcon et al. (1995)
$LaCl_3:Pr^{3+}$	Rana et al. (1984)
$Y_3Al_5O_{12}:Pr^{3+}$	Gayen et al. (1992); Xie et al. (1993)
$SrMoO_4:Pr^{3+}$	de Mello Donegá and Meijerink (1993)
$YAlO_3:Pr^{3+}$	Malinowski et al. (1995)
$LiYF_4:Nd^{3+}$	Chase and Payne (1986)
$Y_3Al_5O_{12}:Nd^{3+}$	Chase and Payne (1986)
$CaF_2:Eu^{3+}$	Kholodenkov and Makhanek (1982)
$Y_3Al_5O_{12}:Eu^{3+}$	Kholodenkov and Makhanek (1984)
$LaF_3:Eu^{3+}$	Kholodenkov et al. (1984)
$CaF_2:Eu^{2+}$	Fritzler (1977); Fritzler and Schaack (1976); Downer et al. (1983)
$SrF_2:Eu^{2+}$	Fritzler (1977); Fritzler and Schaack (1976); Downer et al. (1983)
$LaF_3:Gd^{3+}$	Dagenais et al. (1981)
$GdCl_3$	Mahiou et al. (1983)
$Gd(OH)_3$	Jacquier et al. (1987,1989)
GdODA	Kundu et al. (1990)
$LiYF_4:Tb^{3+}$	Huang et al. (1989)
$Cs_2NaTbCl_6$	Denning (1991); Berry et al. (1996)
Cs_2NaTbF_6	Berry et al. (1996)
$CaF_2:Ho^{3+}$	Rao et al. (1983); Apanasevich et al. (1973)
$CdF_2:Ho^{3+}$	Rao et al. (1983)
$SrF_2:Ho^{3+}$	Rao et al. (1983)
$CaF_2:Er^{3+}$	Apanasevich et al. (1973)
$La_2O_2S:Tm^{3+}$	Bleijenberg et al. (1980)

field potential. In order to explain the orbit- and spin-forbidden $A_{1g} \leftarrow A_{1g}$ transition in the $^5D_4 \leftarrow {}^7F_6$ manifold of the two-photon spectrum of $Cs_2NaTbCl_6$, Ceulemans and Vandenberghe (1993) introduced a fourth-order mechanism in which both the spin–orbit coupling and the crystal field are perturbations of the intermediate level. The complicated fourth-order term could be simplified greatly by application of the closure approximation and by application of second quantization. The expression contains a 12-*j* symbol which describes the coupling of five angular momenta. Their model was tested by calculation of the intensity for the two-photon transition between the two highest M components of the $^8S_{7/2}$ ground state and the $^6I_{17/2}$ excited state of Gd^{3+} in the cubic elpasolite matrix (Ceulemans and Vandenberghe 1994). Reid and Richardson (1984d) estimated the importance of dynamic ligand-polarization contributions to two-photon absorption within the f^7configuration of Gd^{3+} in CaF_2. Smentek-Mielczarek and Hess (1987, 1989)

considered the influence of excited configurations on the two-photon transitions via the crystal-field potential. The influence of the spin–orbit interaction on the two-photon f–f absorption intensities has been discussed by Smentek-Mielczarek (1993a,b) and Smentek and Hess (1996).

Gâcon et al. (1987, 1989) reported two-photon spectra of Sm^{2+} in BaClF single crystals. The intensities of the individual crystal-field transitions between the $^7F_0$ and $^5D_2$ multiplets were calculated in the framework of the Axe theory (second-order terms). A satisfactory agreement between theory and experiment was found. Intensity calculations for two-photon transitions in GdODA were reported by Kundu et al. (1990). The two-photon spectra of the uranyl ion in $Cs_2UO_2Cl_4$ were given by Denning (1991). Daoud and Kibler (1992) developed a theory for describing the polarization dependence of an interconfigurational two-photon transition between the crystal-field components arising from the configurations nl^N and $nl^{N-1}n'l'$ of opposite parity. They applied their model to the Ce^{3+} ion in CaF_2 and in $LuPO_4$ ($5d^1 \leftarrow 4f^1$ transitions). Many-body perturbation theory calculations of two-photon transition intensities in Gd^{3+} have been published by Burdick and Reid (1993a,b). Burdick et al. (1993) pointed out the interplay between Coulomb and spin–orbit contributions to two-photon transition intensities. Reid et al. (1994) demonstrated the equivalence between direct calculation (Burdick and Reid 1993a,b), many-body perturbation and Judd–Pooler-type calculations (Judd and Pooler 1982).

11. Vibronic transitions

In centrosymmetric systems, electric dipole transitions can be induced only by a vibronic coupling mechanism between the f electrons and *ungerade* vibrational modes. A *vibronic transition* involves a simultaneous change in the electronic and vibrational states of the system. Vibronic transitions in rare-earth spectroscopy have been reviewed by Hüfner (1978) and by Blasse (1992). The intensities of vibronic transitions in the spectra of Eu^{3+} have been described in detail by Blasse (1990), the vibronic transitions of Gd^{3+} by Blasse and Brixner (1990), and those of Tm^{3+} by Ellens et al. (1996). The vibronic intensities show a host dependence: higher covalency for the metal–ligand bond gives higher vibronic intensities (Meijerink et al. 1996). This has been illustrated for Pr^{3+} in several host lattices (de Mello Donegá et al. 1992, 1995). It is worth mentioning that the vibronic intensities for Gd^{3+} are much lower than for Pr^{3+} (Blasse et al. 1995). Ellens and coworkers have studied the variation of the electron–phonon coupling strength over the lanthanide series (Ellens 1996, Ellens et al. 1997b). Their results show that the electron–phonon coupling is strong at the beginning (Pr^{3+}) and at the end of the series (Tm^{3+}), but small at the center (Eu^{3+}, Gd^{3+}, Tb^{3+}). Intense vibronic transitions are expected if strong electron–phonon coupling is available. This trend is explained by two effects: the lanthanide contraction and the decrease of 4f electron shielding, which influence the electron–phonon coupling strength through the lanthanide series in an opposite way. Ellens studied the lanthanide ions in $LiYF_4$ as host crystal. Earlier observations for this behavior were

provided by Hellwege (1941), who performed measurements on $R_2(SO_4)_3 \cdot 8H_2O$ salts, and by Krupke (1966), who considered Y_2O_3 as host matrix. The temperature-dependent line broadening can be used as a probe of the electron–phonon coupling strength of lanthanide ions (Ellens et al. 1997a): broader lines are found for ions with a strong electron–phonon coupling than for ions with a weak coupling.

In the X-ray excited emission spectrum of $Gd(ClO_4)_3 \cdot 6H_2O$, Blasse and Brixner (1989) found the first example of a vibronic line in a trivalent lanthanide ion emission spectrum which is due to coupling with the second coordination sphere (in this case the perchlorate ion). Blasse and coworkers (de Mello Donegá et al. 1994, Blasse et al. 1995) have shown that concentration dependence of vibronic intensities does not exist. In the past, several authors had claimed an enhancement of the intensity of vibronic transitions by a concentration enhancement, e.g. on $La_{2-x}Pr_xO_3$ (de Mello Donegá et al. 1993), on $Y_{2-x}Eu_xO_2S$ (Hoshina et al. 1977, 1979) and on $[(C_4H_9)_4N]_3Y_{1-x}Eu_x(NCS)_6$ (Auzel et al. 1980). They were all misled by saturation effects. Vibronic transitions in the luminescence spectrum of $Eu(DBM)_3 \cdot H_2O$ have been discussed by Kirby and Richardson (1983). Vibronic components in the spectra of single crystals of lanthanide complexes (R = Pr, Nd, Eu) with isoleucine have been analyzed by Legendziewicz et al. (1993).

Faulkner and Richardson (1978a) have developed a theory on the intensity of vibronically induced electric dipole transitions of lanthanide complexes with octahedral symmetry (O_h, CN 8). The model places emphasis on the direct calculation of the vibronic intensities. No parameters have to be determined, but explicit assumptions have to be made with respect to the lanthanide–ligand interaction, the vibrational force fields of the complex, the vibronic interactions involving the 4f electrons of the lanthanide ion, and the odd-parity vibrational modes. The theory is based on a model in which both static (point-charge crystal field) and dynamic coupling (transient ligand dipoles) between the metal ion and the ligands are included. The metal ion and the ligand are treated as independent subsystems to zeroth order. The charge distribution of the subsystems are assumed to interact through electrostatic (Coulombic) force, but overlap is neglected (no exchange interaction). The interactions between the subsystems and the influence of these interactions upon the f–f transitions are treated by first-order perturbation theory. The model is applied to the spectral intensities of Eu^{3+} in the elpasolite host matrix $Cs_2NaEuCl_6$. The *ungerade* skeletal vibrations of the $EuCl_6^{3-}$ clusters are considered as vibrations. Good agreement is found between the calculated and the experimental intensities of the vibronically induced electric dipole transitions, both for the total intensity and for the relative intensity for the crystal-field transitions between two $^{2S+1}L_J$ manifolds. In a subsequent paper (Faulkner and Richardson 1978b), an intensity analysis of the $^5D_4 \rightarrow {}^7F_J$ ($J = 2, 3, 4, 5, 6$) transitions of the emission spectrum of Tb^{3+} in $Cs_2NaTbCl_6$ was performed on the basis of the same theory. Good agreement was found between experimental and calculated intensities of vibronically induced electric dipole transitions, except for the $^5D_4 \rightarrow {}^7F_4$ transitions. Some transitions ($\Delta J = \pm 1$), have a pure magnetic dipole character. The transitions with $\Delta J = 0, \pm 2$ have both a magnetic dipole and a vibronically induced electric dipole character. Later, calculations of vibronic intensities based on the model have been reported by the

same authors for several other lanthanide ions in the elpasolite host matrix Cs_2NaRCl_6: Pr^{3+} (Morley et al. 1982a), again Eu^{3+} (Morley et al. 1982b), Ho^{3+} (Morley et al. 1981), Er^{3+} (Hasan and Richardson 1982), and Tm^{3+} (Faulkner et al. 1979). Although some agreement between experimental and calculated vibronic intensities was obtained, rationalization of the relative intensities associated with large numbers of transitions was not possible. Because not all the interactions involved are known, trying to improve the direct calculation proved to be useless. Reid and Richardson (1984a,b) developed a general parametrization scheme for the electric dipole intensities of one-electron, one-phonon vibronic interactions in rare-earth complexes. This parametrization scheme can be related to the general parametrization scheme proposed by the same authors (see sect. 6.2) for one-electron, no-phonon transitions (pure electric dipole transitions). The parametrization scheme assumes that the vibronic interactions have a linear dependence on the normal coordinates of the system, but are independent of the detailed nature of the lanthanide–ligand–radiation interaction, except for the one-electron, one-photon, one-phonon interaction. Whereas the parametrization model of Faulkner and Richardson was only applicable to centrosymmetric systems with O_h symmetry, the model of Reid and Richardson is applicable to both centrosymmetric and non-centrosymmetric systems. In non-centrosymmetric systems, the pure electronic transitions (no-phonon) and the vibronic transitions (one-phonon) are parametrized by two different sets of intensity parameters. The parameters for the pure electronic transitions are the A^{λ}_{tp} parameters (see sect. 6.2), and the parameters for the vibronic transitions are $A^{\lambda}_{tc^*\gamma^*}$. Contrary to the empirically determined vibronic intensity parameters, the calculation of intensity parameters by *ab initio* methods requires a knowledge of the physical details of the active vibrational modes, as well as an explicit knowledge about the lanthanide–ligand–radiation field interaction. The authors give also expressions for the *ab initio* calculation of the parameters.

Judd (1980a) studied the vibronic transitions of octahedral rare-earth complexes in the elpasolite matrix, but with emphasis on the use of tensor techniques. For non-centrosymmetric systems, he concluded that vibronic contributions are important for explaining the intensity of hypersensitive transitions. Stavola et al. (1981) studied cooperative vibronic spectra involving lanthanide ions and water molecules in dilute aqueous solutions and in hydrated salts. Special attention was given to the Tb^{3+} ion. In a cooperative vibronic transition, an electronic transition within the 4f shell of the lanthanide ion occurs simultaneously with a vibrational transition within the ligand. The excitation is thus localized on spatially separated ionic and molecular centers. Selection rules were derived. The theory of Stavola et al. (1981) predicts a zero intensity for the vibronic spectra of the $^5D_0 \rightarrow {}^7F_0$ and $^5D_1 \rightarrow {}^7F_0$ transitions of Eu^{3+}. The occurrence of these transitions in many vibronic spectra of europium complexes has been discussed by Tanaka and Kushida (1993) in terms of J-mixing. They have worked out the example of $Ca(PO_3)_2$:Eu^{3+} glass. Cooperative vibronic lines in Yb^{3+} complexes with OH^- and H_2O ligands were studied by Dexpert-Ghys and Auzel (1984). They compared the approaches of Faulkner and Richardson (1978a), Judd (1980a) and Stavola et al. (1981). Stewart

(1993) has shown that ligand polarizability anisotropies and polarizability derivatives make a major contribution to the vibronic emission of the $^5D_0 \rightarrow {}^7F_2$, ν_3 transition in the elpasolite $Cs_2NaEuCl_6$. Measured oscillator strengths for the vibronic transitions of the $^5D_0 \leftarrow {}^7F_0$ absorption spectrum of $Cs_2NaEuCl_6$ have been reported by Tanner et al. (1994). Sztucki (1994) has presented a theory of two-photon vibronic transitions in centrosymmetric lanthanide systems.

12. Color of lanthanide ions

As a consequence of the selective absorption of light in the visible spectral region by the lanthanide ions, solutions or solids containing lanthanide ions have a particular color. With the relatively constant value of the energetic position of the free-ion levels in mind, it is surprising that different papers and textbooks are not consistent concerning the color of some lanthanide ions. Binnemans and Görller-Walrand (1995) have considered in detail the color caused by the 4f–4f transitions of lanthanide ions. The color of each lanthanide ion was predicted on the basis of the position and the intensity of the absorption bands of the lanthanide perchlorates in aqueous solution. The results have a general validity for solutions containing lanthanide ions at a moderate concentration if the lanthanide ions are not luminescent and if the ligands do not absorb light in the visible region. Solids may show a deviant behavior. In this section the color of lanthanide ions is considered.

People usually associate a color with a particular wavelength of visible light. Visible light is the part of the electromagnetic spectrum to which the human eye is sensitive, i.e. between 400 and 700 nm (25 000–14 286 cm^{-1}). However, the range differs from person to person and can even go from 380 to 770 nm. Since the response curve of the eye can be slightly different for different people, color is a subjective phenomenon. Although a given wavelength corresponds to a color, there is no one-to-one relation between color and wavelength. Some colors are not present in the spectrum of visible light (for instance purple, brown and pink). Colors are not identified with a unique wavelength, but by a wavelength interval (table 25). Visible light can be broken up into its components by a dispersing element, such as a prism or a grating. The intensity of the light has also an influence on the color perception: light of a particular wavelength can appear red at a low light intensity, but orange at a higher light intensity. Most colors are not monochromatic, but composed of a mixture of light of different wavelengths, each with its own intensity. An observed color can be described by three quantities: hue, saturation (or chroma) and value (of lightness). *Hue* distinguishes one spectral color from another. The colors can be classified as red, yellow, green, blue, ... Hue can thus be considered as the color name. Hue is specified by the dominant wavelength in an intensity distribution curve. *Saturation* describes the extent to which a color has been diluted with white light. It is a measure for the purity of a color. Monochromatic spectral colors have the highest saturation, while an unsaturated color also contains contributions from many other wavelengths. White light is completely unsaturated, because it contains all wavelengths without a dominant one. It can be considered as composed by mixing equal amounts

Table 25
The spectral colors

Spectral color	Wavelength (nm)	Wavenumber (cm^{-1})	Energy (eV)
violet	400–420	25000–23810	3.10–2.95
violet-blue	420–460	23810–21739	2.95–2.70
blue	460–480	21739–20833	2.70–2.58
blue-green	480–495	20833–20202	2.58–2.50
green	495–530	20202–18868	2.50–2.34
green-yellow	530–570	18868–17544	2.34–2.18
yellow	570–590	17544–16949	2.18–2.10
orange	590–630	16949–15873	2.10–1.97
red	630–700	15873–14286	1.97–1.77

of red, green and blue light. Pink is unsaturated red. It is thus a mixture of saturated red with white light. The saturation is described in terms of *light* (or *pale*) and *dark*. *Value* is related to the fraction of incident light reflected on a surface. It describes the amount of achromatic grey or black which has been mixed into the color. The more reflecting the surface, the greater its *lightness*. Instead of lightness, one sometimes speaks of brightness. *Brightness* is the sensation of the overall intensity of a light and is described in terms of *dim* and *bright*.

The question is why objects have a particular color. An object is colored when it selectively absorbs some parts of the visible spectrum. The transmitted or reflected light contains the complementary color of the absorbed color. Two colors are complementary if they give white light by mixing additively equal proportions of them. *The observed color is thus the complementary color of the absorbed color.* Complementary colors can be identified in the color rosette of Newton (Brill 1980) or in the CIE 1931 chromaticity diagram (Judd 1950, 1952). The complementary colors are summarized in table 26. The green colors between 495 and 565 nm have no complementary spectral color. Their complements are various purple colors, from reddish purple to bluish purple. Solutions act very much like filters, since there is only little reflection. Light is transmitted through the solution with some wavelengths absorbed more than others. The color is produced by a subtractive process determined by the transmittance (or absorbance) curve. If there is more than one absorption band in the visible part of the spectrum, the resulting colors seen in transmission will be combined by *subtractive mixing*. It is as if several color filters are placed over each other. Each color filter shows a selective absorption which corresponds to one absorption band. The result obtained when white light passes through the absorbing medium can be found by multiplying the transmittance curves of the filters. Let us illustrate this with an example. A yellow filter removes the blue from white light, leaving green and red. A cyan filter (blue-green) removes the red from white light, leaving blue and green. If a yellow and a cyan filter are combined, the transmitted light will be green. Because solutions and solids do not behave as ideal filters, it is very

Table 26
Spectral colors and their complements

Wavelength (nm)	Spectral color	Complementary color
400–420	violet	green-yellow
420–460	violet-blue	yellow
460–480	blue	orange
480–495	blue-green	red
495–530	green	purple
530–570	green-yellow	violet
570–590	yellow	violet-blue
590–630	orange	blue
630–700	red	blue-green

difficult to predict the result of subtractive color mixing. There is not only a selective absorption of the wavelengths at the place of an absorption peak, one can also notice an intensity decrease of all wavelengths due for instance to scattering by the matrix or impurity absorption spread over the whole spectrum. This intensity decrease will saturate the color, by removing white light. If the background absorption is not constant over the spectrum, the hue of the color may even change by longer path lengths of the light through the absorbing solution. If the compound (for instance a solid) has a high refractive index, reflection may become important. In addition to the color determined by the selective absorption, the color is also determined by a subtractive process ruled by the reflectance curve (which may be different from the transmittance curve). For powders, the particle size has an influence on the observed color. A fine powder gives a lighter, more unsaturated color than a coarse powder. The color of a compound also depends on the light source. Therefore an object may have a different color when it is illuminated with incandescent light or fluorescent light instead of daylight. A complication in the color description is observed if the compound shows a strong luminescence. Luminescence can be a color cause for some lanthanide ions, such as europium. This will be discussed in detail below. Finally, two observers may give different descriptions for one particular color. For additional reading about color theory, the reader is referred to Judd (1952), Nassau (1983), Falk et al. (1986), and Billmeyer and Saltzman (1967).

Since the intensities of the 4f–4f transitions of lanthanide ions are weak, it can be expected that solutions with a low or moderate concentration of lanthanide ions will show only unsaturated colors compared to solutions with transition metal ions in the same concentration. Indeed, many lanthanide compounds show pastel colors. Based on the absorption spectra of the trivalent lanthanides in perchlorate solution (Binnemans and Görller-Walrand 1995) and the assignments of the energy levels of the lanthanides in LaF_3 (Carnall et al. 1988), the colors of the trivalent lanthanide ions can be predicted. This color prediction is simple, if only one absorption band is observed in the visible part of the spectrum or if there is no visible absorption at all. Especially in cases where several

Table 27
Color of trivalent lanthanide ions

Ion	Electron configuration	Color
La^{3+}	$[Xe]4f^0$	colorless
Ce^{3+}	$[Xe]4f^1$	colorless
Pr^{3+}	$[Xe]4f^2$	yellow-green
Nd^{3+}	$[Xe]4f^3$	lilac, violet-blue[a]
Pm^{3+}	$[Xe]4f^4$	pink, lilac
Sm^{3+}	$[Xe]4f^5$	pale yellow
Eu^{3+}	$[Xe]4f^6$	colorless[b]
Gd^{3+}	$[Xe]4f^7$	colorless
Tb^{3+}	$[Xe]4f^8$	colorless
Dy^{3+}	$[Xe]4f^9$	pale yellow
Ho^{3+}	$[Xe]4f^{10}$	yellow, brownish pink[a]
Er^{3+}	$[Xe]4f^{11}$	pink
Tm^{3+}	$[Xe]4f^{12}$	pale green
Yb^{3+}	$[Xe]4f^{13}$	colorless
Lu^{3+}	$[Xe]4f^{14}$	colorless

[a] The colors of Nd^{3+} and Ho^{3+} are very dependent on the light source.
[b] For Eu^{3+} complexes with a strong luminescence, a pale pink hue color can be observed.

absorption bands are spread over the spectrum, it is very hard to say which color will be observed. The color of one ion can even change from compound to compound and depends also on the light source used. It is however possible to deduce general trends. The colors of the trivalent lanthanide ions due to f–f transitions are summarized in table 27.

Binnemans and Görller-Walrand (1995) have considered only intraconfigurational 4f–4f transitions, because these transitions are responsible for the color of the trivalent lanthanide ions. The allowed f–d transitions have no influence on the color of the trivalent lanthanide ions, since the $4f^{N-1}5d^1$ configuration starts only at more than $50\,000\,cm^{-1}$ above the ground state ($4f^N$ configuration) (Dieke 1968). The only exceptions are Ce^{3+} and Tb^{3+}, but their f–d bands are found in the ultraviolet spectral region. For the divalent lanthanide ions, the f–d transitions can be important. The strong colors of the sesquisulfides R_2S_3 are not due to 4f–4f transitions, but to transitions involving energy bands. This mechanism can be explained by band theory (Nassau 1983). The colors reported for some of the sesquisulfides in the cubic γ form are: La_2S_3 yellow, Ce_2S_3 red, Pr_2S_3 green, Nd_2S_3 light green, Gd_2S_3 purple, Tb_2S_3 light yellow, and Dy_2S_3 orange (Maestro and Huguenin 1995). Rhône-Poulenc Chimie, France, has patented these vivid colored rare-earth sulfides for use as pigments in plastics or paints (Rhône-Poulenc 1985). Especially cerium sesquisulfide (Ce_2S_3) in the γ form is useful as a non-toxic, environmentally safe substitute for the cadmium reds. The dark color of mixed-valence compounds (e.g. Pr_6O_{11} and Tb_4O_7) is caused by intervalence charge transfer (Nassau

1983). The colors of the divalent lanthanide ions are: orange-yellow to brown-red for Sm^{2+}, colorless or yellow for Eu^{2+}, brick red for Tm^{2+}, green or yellow for Yb^{2+}.

La^{3+} ($4f^0$). Lanthanum is the first element of the lanthanide series. Since La^{3+} has no 4f electrons, no 4f–4f transitions can occur. La^{3+} shows no color. Solutions and single crystals containing La^{3+} are *colorless,* powdered samples will be white. Some examples of colored lanthanum compounds have been published, but this color is due to impurity absorption: a yellow-brown color for *A*-La_2O_3 (Huber and Holley 1953), a cream color for $LaCl_3$ (Carter and Murray 1972) and a greyish lilac color for LaOF (Popov and Knudson 1954).

Ce^{3+} ($4f^1$). The 4f configuration of Ce^{3+} consists of only two multiplets: the ground state $^2F_{5/2}$ and the excited state $^2F_{7/2}$, which is about 2000 cm^{-1} above the ground state. The $^2F_{7/2} \leftarrow {}^2F_{5/2}$ transition absorbs only infrared radiation and no visible light, so the Ce^{3+} ion is *colorless.* Powders containing Ce^{3+} will be white. Ce^{3+} has however a strong UV absorption (Carnall 1979). If traces of Ce^{4+} are present, color can be produced by intervalence charge transfer. CeO_2 itself is pale yellowish in a pure state. Ce^{4+} can show an orange color in solutions, because of a shift of the tail of the strong ultraviolet absorption band to longer wavelengths. These bands are charge-transfer bands. f–d transitions cannot occur, since Ce^{4+} has no 4f electrons. Ce^{3+} may show a broad band luminescence from the lowest crystal-field level of the excited configuration $5d^1$ to the levels $^2F_{5/2}$ and $^2F_{7/2}$ of the ground configuration $4f^1$. Usually, the Ce^{3+} emission is in the ultraviolet or in the blue spectral region, but for $Y_3Al_5O_{12}$:Ce^{3+} it is in the green and red, and for CaS:Ce^{3+} it is in the red spectral region (Blasse and Grabmaier 1994).

Pr^{3+} ($4f^2$). The absorption spectrum of Pr^{3+} shows a complex structure of intense absorption bands between 21 000 and 22 800 cm^{-1}(476–439 nm). These bands are transitions of the $^3H_4$ ground state to the $^3P_0$, $^3P_1$, $^1I_6$ and $^3P_2$ excited states. The most intense transition is $^3P_2 \leftarrow {}^3H_4$. Since this absorption is in the violet-blue part of the spectrum, a *yellow-green* color is observed. The weak $^1D_2 \leftarrow {}^3H_4$ transition around 17 000 cm^{-1} (588 nm) has no influence on the color. All authors report a green or yellow-green color for solutions or solids containing trivalent praseodymium ions. If solids contain traces of Pr^{4+}, the color will be darker, e.g. brown for PrOF (Popov and Knudson 1954). The mixed oxide Pr_6O_{11} is nearly black. As already mentioned, this color is due to intervalence charge transfer. Pr^{3+} is sometimes used to color glass (Riker 1981). Cr^{3+} is however preferred in most cases, because chromium compounds are much cheaper than pure praseodymium compounds. The luminescence color of Pr^{3+} strongly depends on the host lattice. If the emission originates from the $^3P_0$ level, it may be green, like in Gd_2O_2S:Pr^{3+} (due to the $^3P_0 \rightarrow {}^3H_4$ transition), but a red color can also be observed, like in $LiYF_4$:Pr^{3+} (due to the transition $^3P_0 \rightarrow {}^3H_6, {}^3F_2$). Emission originating from the $^1D_2$ level is found in the red (and in the near-infrared) (Blasse and Grabmaier 1994).

Nd^{3+} ($4f^3$). The color of the trivalent neodymium ion is caused by two intense absorption bands in the visible part of the spectrum: the $^4G_{5/2}, {}^4G_{7/2} \leftarrow {}^4I_{9/2}$ transition at about 17 400 cm^{-1} (575 nm) and a complex band consisting of the $^4G_{7/2} \leftarrow {}^4I_{9/2}$ transition at 19 200 cm^{-1} (521 nm) and the $^2K_{13/2}, {}^4G_{9/2} \leftarrow {}^4I_{9/2}$ transition at 19 700 cm^{-1}

(508 nm). The 575 nm absorption in the yellow gives a purplish-blue color to Nd^{3+} and the 521 nm absorption in the green region adds a reddish-purple component to it. The observed color will depend on the light source, the concentration and the matrix in which the neodymium ions are embedded. Colors reported for Nd^{3+} ions are reddish (Moeller 1963), red-violet (Remy 1956), violet (Kolthoff et al. 1963), and lilac (Cotton et al. 1987). The oxide Nd_2O_3 shows a light blue color (Douglass 1956). If the light source is not rich in the yellow component of the spectrum (e.g. some fluorescent lamps), the neodymium compound may even look nearly colorless. It may seem poetic, but the color of neodymium ions can be compared very well to the color of the flowers of the lilac tree (*Syringa* sp.). In the same way as the varieties of these flowers can be blue, violet-blue, reddish violet, or in one word *lilac,* the neodymium ion can also show all these different colors, depending on the compound in which it is embedded. In oxide glasses, the $(^4G_{5/2}, ^4G_{7/2}) \leftarrow {}^4I_{9/2}$transition may show its absorption maximum at longer wavelengths, up to 589 nm, due to the nephelauxetic effect. In this case, the Nd^{3+} ions will very effectively absorb the light emitted by Na^+ ions (the sodium D lines). Nd^{3+}-containing glasses are therefore used in glassmaker's goggles to protect the eyes against the yellow glow of sodium in molten glass. Nd^{3+} is also a component of lilac and bluish-purple colored glasses (Riker 1981). Since the color depends on the thickness of the glass, neodymium colored crystal glass can even show more than one color within one workpiece. In thin pieces, a bluish purple color can be noticed. In thicker pieces, a more reddish purple will appear. This was also noticed by Ctyroký (1940), who also discussed the color change of neodymium ions in sun light or under an incandescent lamp. Neodymium oxide can be used as a physical decolorizer for silicate and lead glasses (Riker 1981). It provides the complementary color to that of ferrous or ferric oxide, hence provides a neutral transmittance of the glass.

Pm^{3+} ($4f^4$). Because promethium is a radioactive element and its isotopes have relatively short decay times, spectroscopic data of Pm^{3+} are very sparse in the literature. Some authors give the same color for Pm^{3+} as for Ho^{3+} (Moeller 1963). The color of Pm^{3+}-containing compounds is pink, e.g. PmOF (Weigel 1969), or blue-violet, e.g. $PmCl_3$ (Weigel and Scherer 1967). An aqueous solution absorption spectrum of Pm^{3+} has been published by Carnall (1979). The strongest absorption bands in the visible part of the spectrum are due to the transitions $^5G_2 \leftarrow {}^5I_4$ (17 605 cm^{-1} or 568 nm), $^5G_4 \leftarrow {}^5I_4$ (18 235 cm^{-1} or 548 nm) and $^5G_3, {}^3K_7 \leftarrow {}^5I_4$ (18 315 cm^{-1} or 546 nm). The color of the Pm^{3+} ions is predicted to be intermediate between the colors of the Nd^{3+} and Er^{3+} ions, thus from lilac to pink. Pm^{3+} will show no yellow color like Ho^{3+}, in contradiction to some earlier predictions (Main Smith 1927, Moeller 1963).

Sm^{3+} ($4f^5$). Sm^{3+} has only detectable transitions above 20 000 cm^{-1} (500 nm), of which the $^6P_{3/2} \leftarrow {}^6H_{5/2}$ transition (about 25 000 cm^{-1} or 400 nm) has the highest intensity. As a consequence of this absorption in the blue and violet region, the trivalent samarium ion has a *(pale) yellow* color. All authors report a yellow color for solutions containing Sm^{3+}. Exceptions for the color of solids are pink (Staritzky and Asprey 1957) for SmF_3 and greyish green for SmOF (Popov and Knudson 1954). Sm^{3+} ions are often luminescent.

The orange-red luminescence is due to transitions from the $^4G_{5/2}$ level to the ground state $^6H_{5/2}$ and to other J-manifolds of the ^6H term (Blasse and Grabmaier 1994).

Eu^{3+} ($4f^6$). Although Eu^{3+} shows several absorption peaks in the visible part of the spectrum, e.g. $^5D_2 \leftarrow {}^7F_0$, $^5D_1 \leftarrow {}^7F_0$, $^5D_1 \leftarrow {}^7F_1$ and $^5D_0 \leftarrow {}^7F_1$, they are too weak to give a distinct color to Eu^{3+} ions. The intense $^5L_6 \leftarrow {}^7F_0$ transition around 25 400 cm^{-1} (394 nm) is already at the UV border of the spectrum. Solutions and single crystals containing Eu^{3+} are therefore *colorless,* powders are white. Some authors report however a pale pink color for the europium ion (Cotton et al. 1987, Main Smith 1927, Lagowski 1973, Shriver et al. 1994). This pink color is not due to an absorption of electromagnetic radiation, but is caused by the luminescence of Eu^{3+}. It is well known that solid Eu^{3+} compounds are strong emitting phosphors, which find application in television screens to generate the red color: YVO_4:Eu^{3+}, Y_2O_3:Eu^{3+} or Y_2O_2S:Eu^{3+} (McColl and Palilla 1981). Europium ions chelated by large organic ligands also show a strong luminescence. This luminescence can already be noticed by irradiation with daylight or with an artificial light source. In this case, not a red, but a pink color is observed. Pink is not a spectral color. It is in fact red diluted with a lot of white light. The pink color is especially easy to observe on a white background matrix, namely the color of europium containing powders. If europium compounds are irradiated by ultraviolet light, a strong orange or red luminescence can be observed. $EuCl_3$ shows a yellow color (Stubblefield and Eyring 1955), which is caused by the Eu^{2+} ion. Eu^{2+} has intense broad absorption bands in the UV, violet and blue region of the spectrum. These absorption bands are not forbidden 4f ← 4f transitions, but allowed $4f^{N-1}5d^1 \leftarrow 4f^N$ transitions. For the same reason, LaF_3:Eu^{3+} crystals can be yellow.

Gd^{3+} ($4f^7$). Trivalent gadolinium ions only absorb UV radiation with an energy greater than 32 000 cm^{-1} (wavelengths smaller than 311 nm). Gd^{3+} is *colorless* in solutions and single crystals, powders are white.

Tb^{3+} ($4f^8$). Except for the very weak $^5D_4 \leftarrow {}^7F_6$ transition around 20 550 cm^{-1} (487 nm), the trivalent terbium ion has no absorption bands in the visible part of the spectrum. The intensity of this transition is too low to have an influence on the color of the Tb^{3+} ion. Solutions and single crystals containing Tb^{3+} are *colorless,* powders are white. The pale pink color reported by some authors (Cotton et al. 1987, Main Smith 1927) can be theoretically explained by the $^5D_4 \leftarrow {}^7F_6$ transition, although that seems unlikely considering the intensities. An alternative explanation is the presence of impurities: erbium ions or fluorescent europium ions. The mixed oxide Tb_4O_7 has a dark brown color, due to intervalence charge transfer. Terbium ions may show a strong luminescence, which is due to the transitions $^5D_4 \rightarrow {}^7F_6$ and $^5D_4 \rightarrow {}^7F_5$, which are mainly in the green spectral region. In cases where there is considerable contribution to the luminescence from the $^5D_3 \rightarrow {}^7F_J$ transitions, the luminescence color can have a more bluish tinge. Tb^{3+} finds application in green emitting phosphors (Blasse and Grabmaier 1994).

Dy^{3+} ($4f^9$). Because of the weak transitions $^4F_{9/2} \leftarrow {}^6H_{15/2}$, $^4I_{15/2} \leftarrow {}^6H_{15/2}$, $^4I_{11/2} \leftarrow {}^6H_{15/2}$ and $^4M_{21/2} \leftarrow {}^6H_{15/2}$ (between 21 000 cm^{-1} and 25 000 cm^{-1} or 476–400 nm) in the blue and violet part of the visible spectral region, the Dy^{3+} ion will be nearly *colorless*

in low concentrations and *pale yellow* or *yellow-green* in higher concentrations. A yellow color is reported by most authors. Luminescence with a whitish to yellow color can be observed. This luminescence is due to transitions from the $^4F_{9/2}$ level to $^6H_{15/2}$ and $^6H_{13/2}$ (Blasse and Grabmaier 1994).

Ho^{3+} ($4f^{10}$). The color of the trivalent holmium ion is determined by the relative contributions of the $^5F_4, ^5S_2 \leftarrow {}^5I_8$ transition at about 18 700 cm^{-1} (535 nm) and the $^5G_6 \leftarrow {}^5I_8$ transition at 22 350 cm^{-1} (447 nm). The latter transition is additionally a hypersensitive transition. The color of Ho^{3+} can be *yellow*, *brownish yellow* or *brownish pink*. Which color will be observed differs from compound to compound and depends also on the light source used. The trivalent holmium ion shows a color-changing effect in the sense that it can be yellow under one light source or pink under another. The $^5F_5 \leftarrow {}^5I_8$ transition at 15 600 cm^{-1} (641 nm) in the red part of the spectrum has no influence on the color, because the complementary color which would be seen by this absorption is absorbed itself by a complex band which represents the transitions from $^5I_8$ to $^5F_3$ (20 800 cm^{-1} or 481 nm), to $^5F_2$ (21 250 cm^{-1} or 471 nm) and to $^3K_8$ (21 500 cm^{-1} or 465 nm). Farok et al. (1996) have studied the color-changing effect of Ho^{3+} in metaphosphate glass $(Ho_2O_3)_{0.22}(P_2O_5)_{0.78}$. This effect is compared with the *alexandrite effect,* referring the color-changing gemstone alexandrite. The color changes from dark salmon pink in artificial light to yellow in daylight. The authors conclude that the light transmission through optical windows in the Ho^{3+} absorption spectrum is the dominating effect in determining the color. The color change is thus not due to fluorescence induced by the light source.

Er^{3+} ($4f^{11}$). Although Er^{3+} has several relatively intense absorption peaks in the visible part of the spectrum, its *pink* color is almost entirely due to the $^2H_{11/2} \leftarrow {}^4I_{15/2}$ transition at 19 300 cm^{-1} (518 nm) in the green region. At higher concentration and low light intensities, the color may appear more reddish. The other transitions have less influence on the color, for the same reason as for Ho^{3+}. The $^4F_{7/2} \leftarrow {}^4I_{15/2}$ transition (20 700 cm^{-1} or 483 nm) absorbs the complementary color of the $^4F_{9/2} \leftarrow {}^4I_{15/2}$ transition (15 450 cm^{-1} or 647 nm). Since the absorption peaks in the violet region of the spectrum are less intense than those of Ho^{3+}, the color of Er^{3+} contains no yellow component. Trivalent erbium ions are added to glass compositions to give a pink color to the glass (Riker 1981). Most authors report a pink color for erbium compounds. Sometimes, a lilac color is mentioned (Cotton et al. 1987). A yellow color for *C*-Er_2O_3 has been reported (Noguchi and Mizuno 1967).

Tm^{3+} ($4f^{12}$). In the visible part of the absorption spectrum of trivalent thulium ions, three absorption bands can be observed: $^3F_3 \leftarrow {}^3H_6$ (14 500 cm^{-1} or 690 nm), $^3F_2 \leftarrow {}^3H_6$ (15 200 cm^{-1} or 658 nm) and $^1G_4 \leftarrow {}^3H_6$ (21 350 cm^{-1} or 468 nm). The most intense transition is the one at 14 500 cm^{-1} in the red region of the spectrum, although the intensity is not very strong. For low concentrations of Tm^{3+}, solutions and single crystals containing this ion are *nearly colorless.* Powders will be white. For higher concentrations, a *pale green* color can be observed. The green color can be more pronounced in glasses with a high thulium concentration. It is confusing to report the color of Tm^{3+} just as green

(Cotton et al. 1987, Shriver et al. 1994, Moeller 1970). Tm^{3+} compounds may show a blue luminescence.

Yb^{3+} ($4f^{13}$). The 4f configuration of Yb^{3+} has the same energy levels as the 4f configuration of Ce^{3+} ($4f^1$), but here $^2F_{7/2}$ is the ground state and $^2F_{5/2}$ the excited state. Since the $^2F_{5/2} \leftarrow {}^2F_{7/2}$ transition absorbs only infrared radiation (about 10 500 cm^{-1} or 952 nm) and no visible light, the Yb^{3+} ion is *colorless* in solutions and single crystals, while Yb^{3+}-containing powders are white.

Lu^{3+} ($4f^{14}$). Since the trivalent lutetium ion has a filled 4f shell, no $4f \leftarrow 4f$ transitions can occur. Lu^{3+} is *colorless* in solutions and single crystals, white in powdered samples.

In many textbooks on inorganic chemistry it is pointed out that the color of a lanthanide ion with N 4f electrons is the same as the color of the lanthanide ion with $14-N$ 4f electrons. This concept was introduced by Main Smith (1927). It is even adhered to by Moeller (1963) in his authoritative work *Chemistry of the Lanthanides* and later in *J. Chem. Educ.* (Moeller 1970), although he is somewhat cautious. Indeed, this conformity is only accidental. Although $4f^N$ and $4f^{14-N}$ systems have the same $^{2S+1}L_J$ free-ion levels, the relative sequence of the J-levels within one term is reversed and the energetic positions are not the same. The splitting of the energy levels changes because of an increase of the spin–orbit coupling over the lanthanide series. Only when two systems have absorption peaks at the same wavenumbers and the intensities and bandwidths of the peaks are the same, will their respective colors be identical. The absorption spectra for the different lanthanide ions differ strongly from ion to ion. Consider, for instance, Pr^{3+} and Tm^{3+}. Whereas the color of Pr^{3+} is a rather strong yellow-green, the color of Tm^{3+} is only a pale green. The green color of the Pr^{3+} ion is due to a selective absorption in the blue-violet region of the spectrum. The color of Tm^{3+} is however caused by an absorption band at the red end of the spectrum. The reason for this apparent periodicity in color over the lanthanide series, is the fact that the energy gap between the barycenter of the ground term and the first excited term becomes larger towards the center of the lanthanide series. Therefore, Pr^{3+}, Nd^{3+}, Pm^{3+}, Ho^{3+}, Er^{3+} and Tm^{3+} have absorption bands in the blue, yellow and red parts of the spectrum. They will show a noticeable color (except for Tm^{3+}). Sm^{3+} and Dy^{3+} only have absorption bands at the violet end of the visible region and will therefore show a yellow color. The most intense absorption bands of Eu^{3+} and Tb^{3+} are already in the ultraviolet, so that these ions are colorless. The energy gap is the largest for Gd^{3+}, which has no absorption bands in the visible part of the electromagnetic spectrum and is thus colorless.

13. Intensities of transitions in actinide ions

Studies of transition intensities are sparser for actinide ions than for lanthanide ions. A reason for this is of course the radioactivity of the actinides, which makes their manipulation troublesome. Special safety precautions are necessary during the manipulation of these compounds. Actinide-doped crystals are darkened by radiation damage of the crystal lattice, and solutions containing actinide ions are often subject to

Table 28
Intensity parameters Ω_λ for the heavy trivalent actinide ions[a]

Ion	Ω_2 (10^{-20} cm^2)	Ω_4 (10^{-20} cm^2)	Ω_6 (10^{-20} cm^2)
Cm^{3+}	15.2	16.8	38.1
Bk^{3+}	6.96	12.2	18.7
Cf^{3+}	3.39	15.4	16.6
Es^{3+}	1.32	15.8	18.5

[a] After Carnall et al. (1983).

radiolysis. This solvent decomposition leads to broad absorption bands in the ultraviolet. Several of the transuranium elements are available only in very limited quantities, since all these elements have to be prepared artificially.

The intensity analysis of trivalent actinide ions in an aqueous solution of $HClO_4$ (or $DClO_4$) has been reviewed by Carnall and coworkers (Carnall et al. 1983, Carnall and Crosswhite 1985, 1986). Since the f^N states of the actinides occur in a smaller energy range than the f^N states of the lanthanides, the density of states in the optical region of interest is high for the actinides. It is difficult to assign a $^{2S+1}L_J$ free-ion label to the transitions in the spectra of the trivalent actinide ions in aqueous solution. This is especially a problem for U^{3+}, Np^{3+} and Pu^{3+}, so that it was not possible to make a detailed intensity analysis for these ions in water. The oscillator strengths for the trivalent actinide ions in aqueous solution are a factor 10–100 greater than the oscillator strengths of the corresponding trivalent lanthanide ions in aqueous solution. This increase in intensity is not only reflected by the intensity parameters, but also by the reduced matrix elements $U^{(\lambda)}$. In comparison with the corresponding lanthanide ions, the reduced matrix elements are a factor 6–10 larger for the actinide ions. However, it should be noted that because of the broader bandwidths for actinide ions, the molar absorptivity increases less drastically. The average intensity of a transition decreases with increasing atomic number. It reaches a minimum for Cm^{3+} and remains rather constant over the second half of the actinide series. The Judd–Ofelt theory gives a satisfactory agreement between the experimental and calculated oscillator strengths for the heavy 5f elements. The Ω_λ intensity parameters for these heavy trivalent actinide ions are given in table 28. For actinide ions, Ω_2 has no significant influence on the observed intensities, so that the intensity of each transition in the spectrum could be described rather adequately in terms of only two parameters: Ω_4 and Ω_6. Reduced matrix elements $U^{(\lambda)}$ for trivalent actinide ions have been published by Carnall and coworkers: Pu^{3+} (Carnall et al. 1970), Cm^{3+} (Carnall and Rajnak 1975), Bk^{3+} (Carnall et al. 1984), and Es^{3+} (Carnall et al. 1973). Carnall et al. (1983) reported model calculations for the Ω_4 and Ω_6 intensity parameters.

Carnall et al. (1970) have performed an intensity analysis on thin films of sublimed $PuCl_3$ at 4 K and at 298 K. Since it was impossible to determine the concentration and the optical pathlength exactly, they did not report Ω_λ parameters, but t_λ parameters (in which the concentration and the optical pathlength are excluded). The intensity calculations

Table 29
Hypersensitive transitions of trivalent actinide ions[a]

Ion	Transition	Energy (cm^{-1})	Ion	Transition	Energy (cm^{-1})
U^{3+}	$^4F_{5/2} \leftarrow {}^4I_{9/2}$	9500	Bk^{3+}	$^7F_5 \leftarrow {}^7F_6$	5000
	$^4G_{5/2} \leftarrow {}^4I_{9/2}$	11100	Cf^{3+}	$^6F_{11/2} \leftarrow {}^6H_{15/2}$	6500
Np^{3+}	$(J=2) \leftarrow {}^5I_4$	7600		$^6H_{13/2} \leftarrow {}^6H_{15/2}$	8000
	$(J=2) \leftarrow (J=4)$	11700	Es^{3+}	$(J=6) \leftarrow (J=8)$	13100
Pu^{3+}	$^6F_{3/2} \leftarrow {}^6H_{5/2}$	6800		$(J=6) \leftarrow (J=8)$	20100
	$^6F_{1/2} \leftarrow {}^6H_{5/2}$	7100			
Am^{3+}	$^7F_2 \leftarrow {}^7F_0$	5300			
	$^5G_2 \leftarrow {}^7F_0$	21000			

[a] After Henrie et al. (1976).

gave only a moderate agreement between the experimental and the calculated oscillator strengths. The authors conclude that in this case intensity calculations cannot be used as a reliable tool for energy level assignments.

One could expect that some transitions in actinide ions would show hypersensitivity. Until now, hypersensitivity has only been demonstrated clearly for Am^{3+}, although several hypersensitive transitions in trivalent actinide ions have been listed by Henrie et al. (1976) (see table 29). A very high intensity has been found for the hypersensitive transition $^7F_2 \leftarrow {}^7F_0$ in $AmCp_3$ (Pappalardo et al. 1969a). Intensity data are available for Am^{3+} in other media: in molten LiCl–KCl and $LiNO_3$–KNO_3 (Carnall and Fields 1962), chloride complexes in organic solutions (Marcus and Shiloh 1969), aqueous nitrate, carbonate, bromide and iodide solutions (Shiloh et al. 1969), in the crystalline trihalides $AmCl_3$, $AmBr_3$ and AmI_3 (Pappalardo et al. 1969b), and in fluorozirconate glass (Valenzuela and Brundage 1990, Brundage et al. 1991, Williams and Brundage 1992, Brundage 1994). Beitz (1994) discussed the luminescence of Am^{3+} in aqueous solution. Simoni et al. (1995) performed a parametrization of the intensities in terms of $B_{\lambda kq}$ parameters of the transitions between crystal-field levels of U^{3+} in $LiYF_4$. The exact site symmetry S_4 was approximated by a D_{2d} symmetry, so that the number of intensity parameters could be reduced to six. A rather good agreement between experimental and calculated oscillator strengths was found. The authors showed that the excited $5f^26d^1$ configuration contributes only weakly in the parity mixing with the $5f^3$ configuration. The proximity of the $5f^26d^1$ configuration, which extends from 20000 cm^{-1} to 33000 cm^{-1}, does not seem to introduce any errors in the applicability of the Judd–Ofelt theory. Another proof of the reliability of the theoretical model was the consistency between the experimental radiative lifetime of the lowest emitting crystal-field level of the $^4I_{11/2}$ multiplet and the lifetime calculated from the intensity parameters.

Auzel et al. (1982) calculated the absolute oscillator strengths between J-manifolds of U^{4+} ($5f^2$) in an aqueous hydrobromic solution and in $ThBr_4$. The oscillator strengths

were found to be two orders of magnitude larger than the oscillator strengths of the corresponding 4f–4f transitions of the $4f^2$ configuration of Pr^{3+} and one order of magnitude larger than the oscillator strengths for U^{3+}. A negative value for the Ω_6 parameter was obtained and there were similar discrepancies as for Pr^{3+}. Because of the proximity of the $5f^16d^1$ configuration, the authors introduced odd $U^{(\lambda)}$ matrix elements in the calculation and a variable energy denominator with respect to the degenerate $5f^16d^1$ configuration. However, this did not improve the fit, which indicates that the 5f6d configuration has only limited influence on the intensities of the $5f^2$ configuration. The odd $U^{(\lambda)}$ matrix elements have been tabulated by Auzel et al. (1982). For Cs_2UCl_6 (O_h symmetry), only vibronic transitions are observed and no zero phonon line (Johnson et al. 1966). Satten et al. (1983) have dealt with the vibronic transitions in the centrosymmetric system UCl_6^{2-} (O_h symmetry). They focused primarily on the intensities associated with the high-frequency ν_3 (t_{1u}) symmetric mode (~260 cm^{-1}) observed in the absorption spectrum of $[(CH_3)_4N]_2UCl_6$ single crystals. The vibronic lines are expressed in terms of two different sets of parameters, namely $G_i^{(J)}$ and P_i. Reid and Richardson have applied their general parametrization scheme for vibronic transitions (see sect. 11) to the intensity data reported by Satten et al. (1983).

Pa^{2+}, Th^{2+}, U^{2+}, Cm^{2+} and Np^{2+} have no f^N ground state, but a $f^{N-1}d^1$ ground state. Bk^{2+}, Pu^{2+} and Am^{2+} have f–f transitions in the IR region (Brewer 1971a,b). Spectroscopic results for divalent actinide ions are still fragmentary. Moreover, it is possible that the f–f transitions are masked by broad intense f–d transitions or charge-transfer transitions. The observed transitions in UF_6 and in uranyl (UO_2^{2+}) are not f–f transitions, but have been interpreted as involving the excitation of a bonding electron into a non-bonding f orbital of uranium(VI). These charge-transfer transitions show a very strong symmetry dependence. For uranyl ions, a band is found around 25 000 cm^{-1} with fine structure due to vibronic coupling of O–U–O stretching vibrations to charge-transfer transitions. The electronic structure of the uranyl ion has been the subject of a review article by Denning (1992). In hexavalent actinide compounds, f–f transitions have been detected in NpF_6 and PuF_6 (Beitz et al. 1982). Ekstrom et al. (1968) compared the spectra of plutonyl (PuO_2^{2+}) in different solvents.

14. Conclusions

A study of the intensities of intraconfigurational f–f transitions of trivalent lanthanide ions is of both academic and technological interest. The technological interest is especially focused on the field of rare-earth lasers. The intensities are of academic interest, because the spectral intensities can help to understand the interactions between the lanthanide ions and the surrounding ions. The Judd–Ofelt theory gives a tractable expression for the induced electric dipole matrix element. Although this theory already dates from the beginning of the 1960s, the papers by Judd (1962) and Ofelt (1962) remain very popular among rare-earth spectroscopists. Several improvements have been added to the Judd–Ofelt theory, but the basic idea remains the same. Moreover, the formula used nowadays

to determine the intensity parameters for transitions between J-manifolds in solutions and glasses is still based on the formula presented by Judd (1962).

The Ω_λ intensity parameters provide a convenient way to describe the intensities of f–f transitions in terms of only three parameters. Although a large number of parameter sets is available to date, comparison of the parameters sets is not always easy. This is partly due to the rather large error in the determination of these parameters (10–20% or more). These large errors are not only due to inadequacies of the intensity theory, but also to the difficulty of obtaining accurate dipole (or oscillator) strengths, especially in the case of overlapping bands. Moreover, large differences are found for the parameters of the same system, but determined by different authors. This problem is also discussed by Goldner and Auzel (1996). Because of these uncertainties, some trends in the parameters may not look very obvious. The physical significance of the intensity parameters is still not fully understood, although several hypotheses have been launched.

The limited number of studies of the intensities between crystal-field levels are in deep contrast with the number of papers dealing with the Ω_λ intensity parameters. The determination of the A_{tp}^{λ} parameters is difficult, because a set of non-linear equations has to be solved. The final parameter set depends to a large extent on the chosen starting values. A sign uncertainty is inherent in this problem. In general, the number of independent intensity parameters is large. Sets of A_{tp}^{λ} parameters are even more difficult to compare with each other than sets of Ω_λ parameters. On the other hand, the A_{tp}^{λ} parameters are more subtle than the Ω_λ parameters, in the sense that the former reflect clearer the interaction between the lanthanide ion and the surrounding ions.

The study of intensities of f–f transitions is not limited to absorption and luminescence spectra, neither to pure electronic transitions. Therefore, we have included vibronic and two-photon spectroscopy in our discussion. Theoretical work on these spectroscopies is of a more recent date than the original Judd–Ofelt theory, and progress can be expected here. In these fields, much more experimental data are desirable to make comparisons or to test theories. Since the color is an intensity-related phenomenon which can be observed by the naked eye, the color of the lanthanide ions has been reviewed in this chapter. We have pointed to inconsistencies of colors reported in the literature and have tried to clarify this problem. Although this handbook deals with rare earths, we have also discussed the intensities of the actinide ions. More particularly, the 5f–5f transitions of the actinide ions can also be described by the Judd–Ofelt theory, just as the 4f–4f intensities of the lanthanide ions.

Acknowledgments

K. Binnemans is Postdoctoral Fellow of the F.W.O. – Flanders (Belgium). Financial support from the Geconcerteerde Onderzoeksakties (Konventie Nr. 87 93-110) and from the I.I.K.W. (4.0007.94 and G.0124.95) is gratefully acknowledged. We wish to thank J.L. Adam (University of Rennes, France) for critically reading the manuscript and for his help in collecting the literature dealing with Judd–Ofelt parameters of lanthanide ions in

glasses. L. Fluyt (K.U. Leuven, Belgium) is acknowledged for a reading of the manuscript. The proof reading was done with the help of I. Couwenberg and H. De Leebeeck (K.U. Leuven, Belgium). The authors wish to thank G. Burdick (La Sierra University, Riverside, CA) for useful comments.

References

Adam, J.L., and W.A. Sibley, 1985, J. Non-Cryst. Solids **76**, 267.

Adam, J.L., W.A. Sibley and D.R. Gabbe, 1985, J. Lumin. **33**, 391.

Adam, J.L., A.D. Docq and J. Lucas, 1988, J. Solid State Chem. **75**, 403.

Adam, J.L., N. Rigout, E. Dénoue, F. Smektala and J. Lucas, 1991, in: Fiber Laser Sources and Amplifiers III, SPIE Proc. **1581**, 155.

Adam, J.L., M. Matecki, H. L'Helgoualch and B. Jacquier, 1994, Eur. J. Solid State Inorg. Chem. **31**, 337.

Adam, J.L., M. Matecki and J. Lucas, 1995, J. Non-Cryst. Solids **184**, 119.

Alcalá, R., and R. Cases, 1995, Adv. Mater. 7, 190.

Alfrey, A.J., O.M. Stafsudd, B. Dunn and D.L. Lang, 1988, J. Chem. Phys. **88**, 707.

Allik, T.H., S.A. Stewart, D.K. Sardar, G.J. Quarles, R.C. Powell, C.A. Morrison, G.A. Turner, M.R. Kokta, W.W. Hovis and A.A. Pinto, 1988, Phys. Rev. B **37**, 9129.

Allik, T.H., C.A. Morrison, J.B. Gruber and M.R. Kokta, 1990, Phys. Rev. B **41**, 21.

Allik, T.H., L.D. Merkle, R.A. Utano, B.H.T. Chai, J.L.V. Lefaucheur, H. Voss and G.F. Dixon, 1993, J. Opt. Soc. Am. B **10**, 633.

Alonso, P.J., V.M. Orera, R. Cases, R. Alcalá and V.D. Rodríguez, 1988, J. Lumin. **39**, 275.

Amaranath, G., and S. Buddhudu, 1992, J. Non-Cryst. Solids **143**, 252.

Amaranath, G., S. Buddhudu and F.J. Bryant, 1990a, J. Non-Cryst. Solids **122**, 66.

Amaranath, G., S. Buddhudu, F.J. Bryant, L. Xi, B. Yu and S. Huang, 1990b, Mater. Res. Bull. **25**, 1317.

Amin, J., B. Dussardier, T. Schweizer and M. Hempstead, 1996, J. Lumin. **69**, 17.

Annapurna, K., and S. Buddhudu, 1993, Spectrochim. Acta A **49**, 73.

Annapurna, K., M. Hanumanthu and S. Buddhudu, 1992, Spectochim. Acta A **6**, 791.

Antipenko, B.M., and Yu.V. Tomashevich, 1978, Opt. Spectrosc. (USSR) **44**, 157.

Antonov, V.A., P.A. Arsenev, A.A. Evdokimov, E.K. Kopylova, A.M. Starikov and Kh.G. Tadzhi-Aglaev, 1986, Opt. Spectrosc. (USSR) **60**, 57.

Apanasevich, P.A., R.I. Gintoft, V.S. Korolkov, A.G. Makhanek and G.A. Skripko, 1973, Phys. Status Solidi A **58**, 745.

Arauzo, A.B., R. Cases and R. Alcalá, 1994, Phys. Chem. Glasses **35**, 202.

Atkins, P.W., 1983, Molecular Quantum Mechanics (Oxford University Press, Oxford).

Atkins, P.W., 1988, Quanta: A Handbook of Concepts (Clarendon Press, Oxford).

Auzel, F., 1969, Ann. Telecom. **24**, 199.

Auzel, F., G.F. de Sá and W.M. de Azevedo, 1980, J. Lumin. **21**, 187.

Auzel, F., S. Hubert and P. Delanoye, 1982, J. Lumin. **26**, 251.

Axe Jr, J.D., 1963, J. Chem. Phys. **39**, 1154.

Axe Jr, J.D., 1964, Phys. Rev. A **136**, 42.

Azkargorta, J., I. Ipparraguirre, R. Balda, J. Fernández, E. Dénoue and J.L. Adam, 1994, IEEE J. Quantum Electron. **QE-30**, 1862.

Balda, R., J. Fernández, A. Mendioroz, J.L. Adam and B. Boulard, 1994, J. Phys.: Condens. Matter **6**, 913.

Balda, R., J. Fernández, A. de Pablos, J.M. Fdez-Navarro and M.A. Arriandiaga, 1996a, Phys. Rev. B **53**, 5181.

Balda, R., J. Fernández, J.L. Adam and M.A. Arriandiaga, 1996b, Phys. Rev. B **54**, 12076.

Banks, C.V., and D.W. Klingman, 1956, Anal. Chim. Acta **15**, 356.

Barnes, J.C., and H. Pincott, 1966, J. Chem. Soc. A, 842.

Bebb, H.B., and A. Gold, 1966, Phys. Rev. **143**, 1.

Becker, P.C., N. Edelstein, B.R. Judd, R.C. Leavitt and G.M.S. Lister, 1985, J. Phys. C **18**, L1063.

Becker, P.J., 1971, Phys. Status Solidi B **43**, 583.

Beitz, J.V., 1994, J. Alloys & Compounds **207/208**, 41.

Beitz, J.V., C.W. Williams and W.T. Carnall, 1982, J. Chem. Phys. **76**, 2756.

Bell, J.T., C.C. Thompson and D.M. Helton, 1969, J. Phys. Chem. **73**, 3338.

Bel'tyukova, S.V., N.S. Poluéktov, V.N. Drobyazko, N.A. Nazarenko and L.I. Kononenko, 1977, Dokl. Akad. Nauk SSSR **235**, 107.

Bel'tyukova, S.V., N.A. Nazarenko, T.L. Gritsai and E.V. Lozanova, 1981, Russ. J. Inorg. Chem. **55**, 117.

Berry, A.J., C.S. McCaw, I.D. Morrison and R.G. Denning, 1996, J. Lumin. **66&67**, 272.

Berry, M.T., and F.S. Richardson, 1986, J. Less-Common Met. **126**, 251.

Berry, M.T., C. Schwieters and F.S. Richardson, 1988, Chem. Phys. **122**, 105.

Biedenharn, L., 1953, J. Math. Phys. **31**, 287.

Billmeyer Jr, F.W., and M. Saltzman, 1967, Principles of Color Technology (Interscience, New York).

Binnemans, K., 1996, Ph.D. Thesis (K.U. Leuven, Heverlee, Belgium).

Binnemans, K., and C. Görller-Walrand, 1995, Chem. Phys. Lett. **235**, 163.

Binnemans, K., D. Verboven, C. Görller-Walrand, J. Lucas, N. Duhamel-Henry and J.L. Adam, 1996, J. Non-Cryst. Solids **204**, 178.

Binnemans, K., K. Van Herck and C. Görller-Walrand, 1997a, Chem. Phys. Lett. **266**, 297.

Binnemans, K., D. Verboven, C. Görller-Walrand, J. Lucas, N. Duhamel-Henry and J.L. Adam, 1997b, J. Alloys & Compounds **250**, 321.

Binnemans, K., R. Van Deun, C. Görller-Walrand and J.L. Adam, 1997c, unpublished results.

Binnemans, K., C. Görller-Walrand and J.L. Adam, 1997d, Chem. Phys. Lett. **280**, 333.

Binnemans, K., R. Van Deun, C. Görller-Walrand and J.L. Adam, 1998, J. Alloys Compounds, in press.

Birnbaum, E.R., D.W. Darnall and J.E. Gomeze, 1970, J. Am. Chem. **92**, 5287.

Birnbaum, E.R., F. Abou, J.E. Gomez and D.W. Darnall, 1976, Biochemistry **50**, 17.

Birnbaum, E.R., F. Abou, J.E. Gomez and D.W. Darnall, 1977, Arch. Biochem. Biophys. **179**, 469.

Blanzat, B., L. Boehm, C.K. Jørgensen, R. Reisfeld and N. Spector, 1980, J. Solid State Chem. **32**, 185.

Blasse, G., 1976, Struct. Bonding **26**, 43.

Blasse, G., 1990, Inorg. Chim. Acta **167**, 33.

Blasse, G., 1992, Int. Rev. Phys. Chem. **11**, 71.

Blasse, G., and A. Bril, 1966, Philips Res. Rep. **21**, 379.

Blasse, G., and L.H. Brixner, 1989, Inorg. Chim. Acta **161**, 13.

Blasse, G., and L.H. Brixner, 1990, Inorg. Chem. Acta **169**, 25.

Blasse, G., and B.C. Grabmaier, 1994, Luminescent Materials (Springer, Berlin).

Blasse, G., A. Meijerink and C. de Mello Donegá, 1995, J. Alloys & Compounds **225**, 24.

Bleijenberg, K.C., F.A. Kellendonk and C.W. Struck, 1980, J. Chem. Phys. **73**, 3586.

Boehm, L., R. Reisfeld and N. Spector, 1979, J. Solid State Chem. **28**, 75.

Bornstein, A., and R. Reisfeld, 1982, J. Non-Cryst. Solids **50**, 23.

Bratzel, M.P., J.J. Aaron, J.D. Winefordner, S.G. Schulman and H. Gershon, 1972, Anal. Chem. **44**, 1240.

Brewer, L., 1971a, J. Opt. Soc. Am. **61**, 1101.

Brewer, L., 1971b, J. Opt. Soc. Am. **61**, 1666.

Brill, T.B., 1980, J. Chem. Educ. **57**, 259.

Broer, L.J.F., C.J. Gorter and J. Hoogschagen, 1945, Physica **11**, 231.

Brown, C.A., M. Gerloch and R.F. McMeeking, 1988a, Mol. Phys. **64**, 771.

Brown, C.A., M.J. Duer, M. Gerloch and R.F. McMeeking, 1988b, Mol. Phys. **64**, 793.

Brown, C.A., M.J. Duer, M. Gerloch and R.F. McMeeking, 1988c, Mol. Phys. **64**, 825.

Brundage, R.T., 1994, J. Alloys & Compounds **213/214**, 199.

Brundage, R.T., M.M. Svatos and R. Grinbergs, 1991, J. Chem. Phys. **95**, 7933.

Buddhudu, S., and F.J. Bryant, 1988, Spectrochim. Acta A **44**, 1381.

Buddhudu, S., V.N. Rangarajan, G. Amaranath and R. Harinath, 1991, Phys. Chem. Liq. **23**, 61.

Bukietynska, K., and G.R. Choppin, 1970, J. Chem. Phys. **52**, 2875.

Bukietynska, K., and A. Mondry, 1987, Inorg. Chim. Acta **130**, 271.

Bukietynska, K., and B. Radomska, 1981, Chem. Phys. Lett. **79**, 162.

Bukietynska, K., A. Mondry and E. Osmedo, 1977, J. Inorg. Nucl. Chem. **39**, 483.

Bukietynska, K., A. Mondry and E. Osmedo, 1981a, J. Inorg. Nucl. Chem. **43**, 1311.

Bukietynska, K., A. Mondry and E. Osmedo, 1981b, J. Inorg. Nucl. Chem. **43**, 1321.

Bukietynska, K., B. Jezowska-Trzebiatowska and B. Keller, 1981c, J. Inorg. Nucl. Chem. **43**, 1065.

Bukietynska, K., A. Mondry, Phan Ngoc Thuy and P. Starynowicz, 1995, J. Alloys & Compounds **225**, 52.

Bullock, S.R., B.R. Reddy, C.L. Pope and S.K. Nash-Stevenson, 1997, J. Non-Cryst. Solids **212**, 85.

Buñuel, M.A., R. Cases, M.A. Chamarro and R. Alcalá, 1992, Phys. Chem. Glasses **33**, 16.

Bünzli, J.C., and M.M. Vuckovic, 1984, Inorg. Chim. Acta **95**, 105.

Burdick, G.W., and M.C. Downer, 1991, Eur. J. Solid State Inorg. Chem. **28**, 217.

Burdick, G.W., and M.F. Reid, 1993a, Phys. Rev. Lett. **70**, 2491.

Burdick, G.W., and M.F. Reid, 1993b, Phys. Rev. Lett. **71**, 3892.

Burdick, G.W., M.C. Downer and D.K. Sardar, 1989, J. Chem. Phys. **91**, 1511.

Burdick, G.W., H.J. Kooy and M.F. Reid, 1993, J. Phys.: Condens. Matter **5**, L323.

Burdick, G.W., C.K. Jayasankar, F.S. Richardson and M.F. Reid, 1994, Phys. Rev. B **50**, 16309.

Burdick, G.W., F.S. Richardson, M.F. Reid and H.J. Kooy, 1995, J. Alloys & Compounds **225**, 115.

Caird, J.A., W.T. Carnall and J.P. Hessler, 1981, J. Chem. Phys. **74**, 3225.

Canalejo, M., R. Cases and R. Alcalá, 1988, Phys. Chem. Glasses **29**, 187.

Carnall, W.T., 1979, The absorption and fluorescence spectra of rare earth ions in solution, in: Handbook on the Physics and Chemistry of Rare Earths, Vol. 3, eds K.A. Gschneidner Jr and L. Eyring (North-Holland, Amsterdam) ch. 24, p. 171.

Carnall, W.T., and H.M. Crosswhite, 1985, Argonne Nat. Lab. Rep. ANL-84-90.

Carnall, W.T., and H.M. Crosswhite, 1986, Optical spectra and electronic structure of actinide ions in compounds and solutions, in: The Chemistry of the Actinide Elements, 2nd Ed., Vol. 2, eds J.J. Katz, G.T. Seaborg and L.R. Morss (Chapman and Hall, London) ch. 16, p. 1235.

Carnall, W.T., and P.R. Fields, 1962, Dev. Appl. Spectrosc. **1**, 233.

Carnall, W.T., and K. Rajnak, 1975, J. Chem. Phys. **63**, 3510.

Carnall, W.T., P.R. Fields and B.G. Wybourne, 1965, J. Chem. Phys. **42**, 3797.

Carnall, W.T., P.R. Fields and K. Rajnak, 1968a, J. Chem. Phys. **49**, 4412.

Carnall, W.T., P.R. Fields and K. Rajnak, 1968b, J. Chem. Phys. **49**, 4424.

Carnall, W.T., P.R. Fields and K. Rajnak, 1968c, J. Chem. Phys. **49**, 4443.

Carnall, W.T., P.R. Fields and K. Rajnak, 1968d, J. Chem. Phys. **49**, 4447.

Carnall, W.T., P.R. Fields and K. Rajnak, 1968e, J. Chem. Phys. **49**, 4450.

Carnall, W.T., P.R. Fields and R.G. Pappalardo, 1970, J. Chem. Phys. **53**, 2922.

Carnall, W.T., D. Cohen, P.R. Fields, R.K. Sjablom and R.F. Barnes, 1973, J. Chem. Phys. **59**, 1785.

Carnall, W.T., H.M. Crosswhite and H. Crosswhite, 1977, Energy level structure and transition probabilities of the trivalent lanthanide ions in LaF_3 (Chemistry Division, Argonne National Laboratory, Argonne, IL).

Carnall, W.T., J.P. Hessler and F. Wagner, 1978, J. Phys. Chem. **82**, 2152.

Carnall, W.T., J.V. Beitz, H. Crosswhite, K. Rajnak and J.B. Mann, 1983, Spectroscopic properties of the f-elements in compounds and solutions, in: Systematics and Properties of the Lanthanides, ed. S.P. Sinha (Reidel, Dordrecht, Netherlands) p. 389.

Carnall, W.T., J.V. Beitz and H. Crosswhite, 1984, J. Chem. Phys. **80**, 2301.

Carnall, W.T., G.L. Goodman, K. Rajnak and R.S. Rana, 1988, A systematic analysis of the spectra of the lanthanides doped into single crystal LaF_3, Report ANL-88-8 (Chemistry Division, Argonne National Laboratory, Argonne, IL).

Carter, F.L., and J.F. Murray, 1972, Mater. Res. Bull. **7**, 519.

Carter, R.C., C.E. Miller, R.A. Palmer, P.S. May, D.H. Metcalf and F.S. Richardson, 1986, Chem. Phys. Lett. **131**, 37.

Cases, R., and M.A. Chamarro, 1991, J. Solid State Chem. **90**, 313.

Cases, R., M.A. Chamarro, R. Alcalá and V.D. Rodríguez, 1991, J. Lumin. **48&49**, 509.

Ceulemans, A., and G.M. Vandenberghe, 1993, J. Chem. Phys. **98**, 9372; erratum: 1995, **102**, 7762.

Ceulemans, A., and G.M. Vandenberghe, 1994, J. Alloys & Compounds **207/208**, 102.

Chan, D.K., and M.F. Reid, 1989, J. Less-Common Met. **148**, 207.

Chase, L.L., and S.A. Payne, 1986, Phys. Rev. B **34**, 8883.

Chen, C.Y., W.A. Sibley, D.C. Yeh and C.A. Hunt, 1989, J. Lumin. **43**, 185.

Chertanov, M., O.K. Moune, B. Biriou, J. Dexpert-Ghys, M. Faucher and M. Guittard, 1994, J. Lumin. **59**, 231.

Choppin, G.R., and R.L. Fellows, 1973, J. Coord. Chem. **3**, 209.

Choppin, G.R., D.E. Henrie and K. Buijs, 1966, Inorg. Chem. **5**, 1743.

Christensen, H.P., 1979, Phys. Rev. B **19**, 6573.

Chrysochoos, J., 1974, J. Chem. Phys. **60**, 1110.

Chrysochoos, J., and A. Evers, 1973, Chem. Phys. Lett. **18**, 115.

Cotton, F.A., G. Wilkinson and P.L. Gaus, 1987, Basis Inorganic Chemistry, 2nd Ed. (Wiley, New York).

Csöreg, I., M. Czugler, P. Kierkegaard and J. Legendziewicz, 1989, Acta Chem. Scand. **43**, 735.

Ctyroký, V., 1940, Glastechn. Ber. **18**, 1.

da Gama, A.A.S., and G.F. de Sá, 1982, J. Phys. Chem. Solids **43**, 845.

Dagenais, M., M. Downer, R. Neumann and N. Bloembergen, 1981, Phys. Rev. Lett. **46**, 561.

Daoud, M., and M. Kibler, 1992, Laser Phys. **2**, 704.

de Mello Donegá, C., and A. Meijerink, 1993, J. Lumin. **55**, 315.

de Mello Donegá, C., A. Meijerink and G. Blasse, 1992, J. Phys.: Condens. Matter **4**, 8889.

de Mello Donegá, C., A. Ellens, A. Meijerink and G. Blasse, 1993, J. Phys. Chem. Solids **54**, 293.

de Mello Donegá, C., A. Meijerink and G. Blasse, 1994, J. Lumin. **62**, 189.

de Mello Donegá, C., G.J. Dirksen, H.F. Folkerts, A. Meijerink and G. Blasse, 1995, J. Phys. Chem. Solids **56**, 267.

de Sá, G.F., F.R.G. e Silva and O.L. Malta, 1994, J. Alloys & Compounds **207/208**, 457.

Deb, K.K., R.G. Buser, C.A. Morrison and R.P. Leavitt, 1981, J. Opt. Soc. Am. **71**, 1463.

Dejneka, M., E. Snitzer and R.E. Riman, 1995, J. Lumin. **65**, 227.

Delsart, C., and N. Pelletier-Allard, 1971, J. Phys. Paris **32**, 507.

Denisenko, G.A., 1987, Indian J. Phys. **61A**, 295.

Denning, R.G., 1991, Eur. J. Solid State Inorg. Chem. **28**, 33.

Denning, R.G., 1992, Structure and Bonding **79**, 215.

Detrio, J.A., 1971, Phys. Rev. B **4**, 1422.

Devi, A.R., and C.K. Jayasankar, 1995, Mater. Chem. Phys. **42**, 106.

Devi, A.R., and C.K. Jayasankar, 1996a, J. Non-Cryst. Solids **197**, 111.

Devi, A.R., and C.K. Jayasankar, 1996b, Phys. Chem. Glasses **37**, 36.

Devlin, M.T., E.M. Stephens, F.S. Richardson, T.C. Van Cott and S.A. Davis, 1987a, Inorg. Chem. **26**, 1204.

Devlin, M.T., E.M. Stephens, M.F. Reid and F.S. Richardson, 1987b, Inorg. Chem. **26**, 1208.

Devlin, M.T., E.M. Stephens and F.S. Richardson, 1988, Inorg. Chem. **27**, 1517.

Dexpert-Ghys, J., and F. Auzel, 1984, J. Chem. Phys. **80**, 4003.

Dexter, D.L., 1958, Theory of the optical properties of imperfections in nonmetals, in: Solid State Physics, Advances in Research and Applications, Vol. 6, eds F. Seitz and D. Turnbull (Academic Press, New York) p. 353.

Dieke, G.H., 1968, Spectra and Energy Levels of Rare Earth Ions in Crystals (Interscience, New York).

Dirckx, V., 1995, Ph.D. Thesis (K.U. Leuven, Heverlee, Belgium).

Douglass, R.M., 1956, Anal. Chem. **28**, 551.

Downer, M.C., 1989, Topics Appl. Phys. **65**, 29.

Downer, M.C., and A. Bivas, 1983, Phys. Rev. B **28**, 3677.

Downer, M.C., A. Bivas and N. Bloembergen, 1982, Opt. Commun. **41**, 335.

Downer, M.C., C.D. Cordero-Montalvo and H. Crosswhite, 1983, Phys. Rev. B **28**, 4931.

Downer, M.C., G.W. Burdick and D.K. Sardar, 1988, J. Chem. Phys. **89**, 1787.

Duhamel-Henry, N., J.L. Adam, B. Jacquier and C. Linarès, 1996, Opt. Mater. **5**, 197.

Dulick, M., G.E. Faulkner, N.J. Cockroft and D.C. Nguyen, 1991, J. Lumin. **48&49**, 517.

Edmonds, A.R., 1974, Angular Momentum in Quantum Mechanics (Princeton University Press, Princeton, NJ).

Edvardsson, M., M. Wolf and J.O. Thomas, 1992, Phys. Rev. B **45**, 10919.

Edvardsson, M., M. Klintenberg and J.O. Thomas, 1996, Phys. Rev. B **54**, 17476.

Ekstrom, A., M.S. Farrell and J.J. Lawrence, 1968, J. inorg. nucl. Chem. **30**, 660.

Elejalde, M.J., R. Balda, J. Fernández, E. Macho and J.L. Adam, 1992, Phys. Rev. B **46**, 5169.

Ellens, A., 1996, Ph.D. Thesis (Utrecht University, Utrecht, Netherlands).

Ellens, A., S. Schenker, A. Meijerink and G. Blasse, 1996, J. Lumin. **69**, 1.

Ellens, A., H. Andres, A. Meijerink and G. Blasse, 1997a, Phys. Rev. B **55**, 173.

Ellens, A., H. Andres, M.L.H. ter Heerdt, R.T. Wegh, A. Meijerink and G. Blasse, 1997b, Phys. Rev. B **55**, 180.

Elliot, J.P., 1953, Proc. Roy. Soc. (London) **A218**, 345.

Estorowitz, L., F.J. Bartoli, R.E. Allen, D.E. Wortman, C.A. Morrison and R.P. Leavitt, 1979, Phys. Rev. B **19**, 6442.

Eyal, M., E. Greenberg, R. Reisfeld and N. Spector, 1985, Chem. Phys. Lett. **117**, 108.

Eyal, M., R. Reisfeld, C.K. Jørgensen and B. Bendow, 1987a, Chem. Phys. Lett. **139**, 395.

Eyal, M., R. Reisfeld, A. Schiller, C. Jacoboni and C.K. Jørgensen, 1987b, Chem. Phys. Lett. **140**, 595.

Falk, D.S., D.R. Brill and D.G. Stork, 1986, Seeing the Light. Optics in nature, photography, vision, and holography (Wiley, New York).

Farok, H.M., G.A. Saunders, W.A. Lambson, R. Krüger, H.B. Senin, S. Barlett and S. Takel, 1996, Phys. Chem. Glasses **37**, 125.

Faulkner, T.R., and F.S. Richardson, 1978a, Mol. Phys. **35**, 1141.

Faulkner, T.R., and F.S. Richardson, 1978b, Mol. Phys. **36**, 193.

Faulkner, T.R., R.W. Schwartz and F.S. Richardson, 1979, Mol. Phys. **38**, 1767.

Fellows, R.D., and G.R. Choppin, 1974, J. Coord. Chem. **4**, 79.

Flórez, A., Y. Messaddeq, O.L. Malta and M.A. Aegerter, 1995, J. Alloys & Compounds **227**, 135.

Flórez, A., O.L. Malta, Y. Messaddey and M.A. Aegerter, 1996, in: Extended Abstracts, 10th Int. Symp. on Non-Oxide Glasses, June 19–22 1996 (Corning, NY, USA) p. 252.

Fluyt, L., K. Binnemans and C. Görller-Walrand, 1995, J. Alloys & Compounds **225**, 71.

Fluyt, L., I. Couwenberg, H. Lambaerts, K. Binnemans, C. Görller-Walrand and M.F. Reid, 1996, J. Chem. Phys. **105**, 6117.

Fluyt, L., H. De Leebeeck, E. Hens and C. Görller-Walrand, 1997, J. Alloys & Compounds, in press.

Fowler, W.B., and D.L. Dexter, 1962, Phys. Rev. **128**, 2154.

Freeth, C.A., G.D. Jones and R.W.G. Syme, 1982, J. Phys. C **15**, 5667.

Fritzler, U., 1977, Z. Phys. B **27**, 289.

Fritzler, U., and G. Schaack, 1976, J. Phys. C **9**, L23.

Gâcon, J.C., J.F. Marcerou and B. Jacquier, 1987, Inorg. Chim. Acta **139**, 295.

Gâcon, J.C., J.F. Marcerou, M. Bouazaoui and B. Jacquier, 1989, Phys. Rev. B, **40**, 2070.

Gâcon, J.C., J. Baudry, C. Garapon and G.W. Burdick, 1995, Radiat. Eff. Defects Solids **135**, 41.

Gajek, Z., 1993, Acta Phys. Pol. A **84**, 875.

Garcia, D., and M. Faucher, 1992, J. Alloys & Compounds **180**, 239.

Garcia, D., M. Faucher and O.L. Malta, 1983, Phys. Rev. B **27**, 7386.

Gatterer, K., G. Pucker, H.P. Fritzer and S. Arafa, 1994, J. Non-Cryst. Solids **176**, 237.

Gayen, S.K., and D.S. Hamilton, 1983, Phys. Rev. B **28**, 3706.

Gayen, S.K., D.S. Hamilton and R.H. Bartram, 1986, Phys. Rev. B **34**, 7517.

Gayen, S.K., B.Q. Xie and Y.M. Cheung, 1992, Phys. Rev. B **45**, 20.

Goldner, P., and F. Auzel, 1996, J. Appl. Phys. **79**, 7972.

Göppert-Mayer, M., 1931, Anw. Phys. **9**, 273.

Görller-Walrand, C., 1985, Chem. Phys. Lett. **115**, 333.

Görller-Walrand, C., and K. Binnemans, 1996, Rationalization of crystal-field parametrization, in: Handbook on the Physics and Chemistry of Rare Earths, eds K.A. Gschneidner Jr and L. Eyring, Vol. 23 (North-Holland, Amsterdam) ch. 155, p. 121.

Görller-Walrand, C., and L. Fluyt-Adriaens, 1985, J. Less-Common Met. **112**, 175.

Görller-Walrand, C., and J. Godemont, 1977, J. Chem. Phys. **66**, 48.

Görller-Walrand, C., M. Behets, P. Porcher and W.T. Carnall, 1986, J. Less-Common Met. **126**, 271.

Görller-Walrand, C., L. Fluyt, P. Porcher, A.A.S. da Gama, G.F. de Sá, W.T. Carnall and G.L. Goodmann, 1989, J. Less-Common Met. **148**, 339.

Görller-Walrand, C., L. Fluyt, A. Ceulemans and W.T. Carnall, 1991, J. Chem. Phys. **95**, 3099.

Görller-Walrand, C., L. Fluyt, J. D'Olieslager, M.P. Gos and I. Hendrickx, 1992, J. Chem. Phys. **99**, 3182.

Görller-Walrand, C., L. Fluyt, P. Verhoeven, E. Berghmans and G.M. Vandenberghe, 1993, Bull. Soc. Chim. Belg. **102**, 99.

Görller-Walrand, C., P. Verhoeven, J. D'Olieslager, L. Fluyt and K. Binnemans, 1994a, J. Chem. Phys. **100**, 815; erratum: **101**, 7189.

Görller-Walrand, C., E. Huygen, K. Binnemans and L. Fluyt, 1994b, J. Phys.: Condens. Matter **6**, 7797.

Griffith, J.S., 1960, Mol. Phys. **3**, 477.

Gruber, J.B., E.R. Menzel and R.L. Ryan, 1969, J. Chem. Phys. **51**, 3816.
Gruen, D.M., and C.W. DeKock, 1966, J. Chem. Phys. **45**, 455.
Gruen, D.M., C.W. DeKock and R.L. McBeth, 1967, Adv. Chem. Ser. **71**, 102.
Guéry, C., 1988, Ph.D. Thesis (Université de Rennes I, France).
Guéry, C., J.L. Adam and J. Lucas, 1988, J. Lumin. **42**, 181.
Gupta, R.D., G.S. Manku, A.N. Bhat and B.D. Jain, 1970, Z. Anorg. Allg. Chem. **379**, 312.
Hanumanthu, M., K. Annapurna and S. Buddhudu, 1991, Solid State Comm. **80**, 315.
Harinath, R., S. Buddhudu, F.J. Bryant and L. Xi, 1990, Solid State Commun. **74**, 1147.
Hasan, Z., and F.S. Richardson, 1982, Mol. Phys. **45**, 1299.
Hellwege, K.H., 1941, Ann. Phys. **40**, 529.
Henrie, D.E., and G.R. Choppin, 1968, J. Chem. Phys. **49**, 477.
Henrie, D.E., and B.K. Henrie, 1974, J. Inorg. Nucl. Chem. **36**, 2125.
Henrie, D.E., and B.K. Henrie, 1977, J. Inorg. Nucl. Chem. **39**, 1583.
Henrie, D.E., and C.E. Smysen, 1977, J. Inorg. Nucl. Chem. **39**, 625.
Henrie, D.E., R.L. Fellows and G.R. Choppin, 1976, Coord. Chem. Rev. **18**, 199.
Hens, E., 1996, Ph.D. Thesis (K.U. Leuven, Heverlee, Belgium).
Hens, E., and C. Görller-Walrand, 1995, J. Alloys & Compounds **225**, 66.
Heo, J., and Y.B. Shin, 1996, J. Non-Cryst. Solids **196**, 162.
Heo, J., Y.B. Shin and J.H. Jang, 1995, Appl. Optics **34**, 4284.
Hewak, D.W., J.A. Medeiros Neto, B. Samson, R.S. Brown, K.P. Jedrzejewski, J. Wang, E. Taylor, R.I. Laming, G. Wylangowski and D.N. Payne, 1994a, IEEE Photonics Techn. Lett. **6**, 609.
Hewak, D.W., B.N. Samson, J.A. Medeiros Neto, R.I. Laming and D.N. Payne, 1994b, Electron. Lett. **30**, 968.
Hirao, K., K. Tamai, S. Tanabe and N. Soga, 1993, J. Non-Cryst. Solids, **160**, 261.
Hirao, K., M. Higuchi and N. Soga, 1994, J. Lumin. **60&61**, 115.
Hollebone, B.R., 1993, Spectrochim. Acta Rev. **6**, 493.
Hölsä, J., P. Porcher and J. Huang, 1990, Ber. Bunsenges. Phys. Chem. **94**, 583.
Hormadaly, J., and R. Reisfeld, 1979, J. Non-Cryst. Solids **30**, 337.
Hoshina, T., S. Imanaga and S. Yokono, 1977, J. Lumin. **15**, 455.
Hoshina, T., S. Imanaga and S. Yokono, 1979, J. Lumin. **18&19**, 88.
Huang, J., G.K. Liu and R.L. Cone, 1989, Phys. Rev. B **39**, 6348.
Huang, Y., Z. Luo and G. Wang, 1992a, Opt. Commun. **88**, 42.
Huang, Y., C. Tu, Z. Luo and G. Chen, 1992b, Opt. Commun. **92**, 57.
Huber, E.J., and C.E. Holley, 1953, J. Am. Chem. Soc. **75**, 3594.
Huber, M.C.E., and R.J. Sandeman, 1986, Rep. Prog. Phys. **49**, 397.
Hubert, S., D. Meichenin, B.W. Zhou and F. Auzel, 1991, J. Lumin. **50**, 7.
Hüfner, S., 1978, Optical Spectra of Transparent Rare Earth Compounds (Academic Press, New York).
Ingeletto, M., M. Bettinelli, L. Di Sipio, F. Negrisolo and C. Aschieri, 1991, Inorg. Chim. Acta **188**, 201.
Isobe, T., and S. Misumi, 1974, Bull. Chem. Soc. Jpn. **47**, 281.
Izumitani, T., H. Toratani and H. Kuroda, 1982, J. Non-Cryst. Solids, **47**, 87.
Jacquier, B., Y. Salem, C. Linarès, J.C. Gâcon, R. Mahiou and R.L. Cone, 1987, J. Lumin. 38, 258.
Jacquier, B., J.C. Gâcon, Y. Salem, C. Linarès and R.L. Cone, 1989, J. Phys.: Condens. Matter **1**, 7385.
Jankowski, K., and L. Smentek-Mielczarek, 1979, Mol. Phys. **38**, 1445.
Jankowski, K., and L. Smentek-Mielczarek, 1981, Mol. Phys. **43**, 371.
Jezowska-Trzebiatowska, B., J. Legendziewicz and W. Strek, 1984, Inorg. Chim. Acta **95**, 157.
Johnson, D.R., R.A. Satten, C.L. Schneiber and E.Y. Wang, 1966, J. Chem. Phys. **44**, 3141.
Jørgensen, C.K., 1962, Mol. Phys. **5**, 271.
Jørgensen, C.K., and B.R. Judd, 1964, Mol. Phys. **8**, 281.
Jørgensen, C.K., and R. Reisfeld, 1983, J. Less-Common Met. **93**, 107.
Joubert, M.F., S. Guy, C. Linarès, B. Jacquier and J.L. Adam, 1995, J. Non-Cryst. Solids **184**, 98.
Judd, B.R., 1962, Phys. Rev. **127**, 750.
Judd, B.R., 1963, Operator Techniques in Atomic Spectroscopy (McGraw-Hill, New York).
Judd, B.R., 1966a, J. Chem. Phys. **44**, 839.

Judd, B.R., 1966b, Second Quantization and Atomic Spectroscopy (The Johns Hopkins Press, Baltimore, MD).

Judd, B.R., 1979, J. Chem. Phys. **70**, 4830.

Judd, B.R., 1980a, Phys. Scr. **21**, 543.

Judd, B.R., 1980b, in: ACS Symposium Series, Lanthanide and Actinide Chemistry and Spectroscopy, ed. N. Edelstein (American Chemical Society) p. 267.

Judd, B.R., and D.R. Pooler, 1982, J. Phys. C **15**, 591.

Judd, D.B., 1950, Colorimetry, NSRDS-NBS Circular No. 478 (US GPO, Washington).

Judd, D.B., 1952, Color in Business, Science and Industry, 1st Ed. (Wiley, New York).

Jung, S.H., S.K. Yoon, J.G. Kim and J.G. Kang, 1992, Bull. Korean Chem. Soc. **13**, 650.

Kaiser, W., and C.G.B. Garrett, 1961, Phys. Rev. Lett. **7**, 229.

Kaminskii, A.A., and L. Li, 1974, Phys. Status Solidi A **26**, K21.

Kaminskii, A.A., S.E. Sarkisov, T.I. Butaeva, G.A. Denisenko, B. Hermoneit, J. Bohm, W. Grosskreutz and D. Schultze, 1979, Phys. Status Solidi A **56**, 725.

Kaminskii, A.A., A.G. Petrosyan, G.A. Denisenko, T.I. Butaeva, V.A. Federov and S.E. Sarkisov, 1982, Phys. Status Solidi A **71**, 291.

Kaminskii, A.A., I.M. Silvestrova, S.E. Sarkisov and G.A. Denisenko, 1983, Phys. Status Solidi A **80**, 607.

Kaminskii, A.A., E.L. Belokoneva, B.V. Mill, Yu.V. Pisarevskii, S.E. Sarkisov, I.M. Silvestrova, A.V. Butashin and G.G. Khodzhabagyan, 1984, Phys. Status Solidi A **86**, 345.

Kaminskii, A.A., B.V. Mill, A.V. Butashin, E.L. Belokoneva and K. Kurbanov, 1987, Phys. Status Solidi A **103**, 575.

Kaminskii, A.A., B.V. Mill, A.V. Butashin, K. Kurbanov and L.A. Polyakova, 1990, Phys. Status Solidi A **120**, 253.

Kaminskii, A.A., A.G. Petrosyan, A.A. Markosyan and G.O. Shironyan, 1991, Phys. Status Solidi A **125**, 353.

Kaminskii, A.A., V.A. Karasev, V.D. Dubrov, V.P. Yakunin, A.V. Butashin and A.F. Konstantinova, 1992, Neorg. Mater. **28**, 1034.

Kaminskii, A.A., V.S. Mironov, S.N. Bagaev, N.M. Khaidukov, M.F. Joubert, B. Jacquier and G. Boulon, 1994a, Phys. Status Solidi A **145**, 177.

Kaminskii, A.A., V.S. Mironov, S.N. Bagaev, G. Boulon and N. Djeu, 1994b, Phys. Status Solidi B **185**, 487.

Kaminskii, A.A., G. Boulon, M. Buoncristiani, B. Di Bartolo, A. Kornienko and V. Mironov, 1994c, Phys. Status Solidi A **141**, 471.

Kaminskii, A.A., V.S. Mironov and S.N. Bagaev, 1995a, Phys. Status Solidi A **148**, K107.

Kaminskii, A.A., V.S. Mironov, A. Kornienko, S.N. Bagaev, G. Boulon, A. Brenier and B. Di Bartolo, 1995b, Phys. Status Solidi A **151**, 231.

Kaminskii, A.A., A.V. Butashin, V.S. Mironov, S.N. Bagaev and H.J. Eichler, 1996, Phys. Status Solidi B **194**, 319.

Kandpal, H.C., and K.C. Joshi, 1988, J. Non-Cryst. Solids, **101**, 243.

Kang, J.G., S.K. Yoon, E.J. Kim, J.G. Kim and Y.D. Kim, 1995, Bull. Korean Chem. Soc. **16**, 232.

Kanoun, A., S. Alaya and H. Maaref, 1990, Phys. Status. Solidi B **162**, 523.

Karraker, D.G., 1967, Inorg. Chem. **6**, 1863.

Karraker, D.G., 1968, Inorg. Chem. **7**, 473.

Katzin, L.I., 1969, Inorg. Chem. **8**, 1649.

Katzin, L.I., and M.L. Barnett, 1964, J. Chem. Phys. **68**, 3779.

Keller, B., K. Butiekynska and B. Jezowska-Trzebiatowska, 1982, Chem. Phys. Lett. **92**, 541.

Kermanoui, A., C. Barthou, J.P. Denis and B. Blanzat, 1984, J. Lumin. **29**, 5799.

Kholodenkov, L.E., and A.G. Makhanek, 1982, Phys. Status Solidi B **112**, K149.

Kholodenkov, L.E., and A.G. Makhanek, 1984, Phys. Status Solidi B **125**, 365.

Kholodenkov, L.E., A.G. Makhanek and A.A. Kaminskii, 1984, Phys. Status Solidi B **126**, 659.

Kirby, A.F., and R.A. Palmer, 1981a, Inorg. Chem. **20**, 1030.

Kirby, A.F., and R.A. Palmer, 1981b, Inorg. Chem. **20**, 4219.

Kirby, A.F., and F.S. Richardson, 1983, J. Phys. Chem. **87**, 2544.

Kisliuk, P., W.F. Krupke and J.B. Gruber, 1964, J. Chem. Phys. **40**, 3606.

Klintenberg, M., S. Edvardsson and J.O. Thomas, 1997, Phys. Rev. B **55**, 10369.

Klochkov, A.A., U.V. Valiev and A.S. Moskvin, 1991, Phys. Status Solidi B **167**, 337.

Kolthoff, I.M., P.J. Evling and E.B. Sandell, 1963, Treatise on Analytical Chemistry, Part II, Vol. 8 (Interscience, New York).

Kononenko, L.I., M.A. Tishchenko and U.N. Drobyazko, 1971, Zh. Anal. Khim. **26**, 729.
Kornienko, A.A., A.A. Kaminskii and E.B. Dunina, 1990, Phys. Status Solidi A **157**, 267.
Krupke, W.F., 1966, Phys. Rev. **145**, 325.
Krupke, W.F., 1971, IEEE J. Quantum Electron. **QE-7**, 153.
Krupke, W.F., and J.B. Gruber, 1965, Phys. Rev. A **139**, 2008.
Kundu, T., A.K. Banerjee and M. Chowdhury, 1990, Phys. Rev. B **41**, 10911.
Kuroda, R., S.F. Mason and C. Rosini, 1980, Chem. Phys. Lett. **70**, 11.
Kuroda, R., S.F. Mason and C. Rosini, 1981, J. Chem. Soc. Faraday Trans. II, **77**, 2125.
Ladenburg, R., 1921, Z. Phys. **4**, 451.
Lagowski, J.J., 1973, Modern Inorganic Chemistry (Marcel Dekker, New York).
Lakshman, S.V.J., and S. Buddhudu, 1982, J. Phys. Chem. Solids **43**, 849.
Leavitt, R.C., 1987, Phys. Rev. B **35**, 9271.
Leavitt, R.P., and C.A. Morrison, 1980, J. Chem. Phys. **73**, 749.
Ledig, M., E. Heumann, D. Ehrt and W. Seeber, 1990, Opt. Quantum Electron. **22**, S107.
Legendziewicz, J., G. Oczko and G. Meyer, 1991, Polyhedron **10**, 1921.
Legendziewicz, J., Z. Ciunik, P. Gawryszewska and J. Sokolnicki, 1993, Acta Phys. Pol. A **84**, 917.
Legendziewicz, L., G. Oczko and B. Keller, 1984, Polyhedron **3**, 161.
Levey, G.C., 1990, J. Lumin. **45**, 168.
Li, C., C. Wyon and R. Moncorgé, 1992, IEEE J. Quantum Electron. **28**, 1209.
Li, C., A. Lagriffoul, R. Moncorge, J.C. Souriau, C. Borel and C. Wyon, 1994, J. Lumin. **62**, 157.
Liu, C.S., and R.J. Zollweg, 1974, J. Chem. Phys. **60**, 2384.
Livshits, M.A., 1972, Opt. Spectrosc. (USSR) **33**, 603.
Lomheim, T.S., and L.G. DeShazer, 1978, J. Appl. Phys. **49**, 5517.
Lucas, J., M. Chanthanasinh, M. Poulain, P. Brun and M.J. Weber, 1978, J. Non-Cryst. Solids **27**, 273.
Maestro, P., and D. Huguenin, 1995, J. Alloys & Compounds **225**, 520.
Mahiou, R., B. Jacquier and C. Linarès, 1983, J. Opt. Soc. Am. **73**, 1383.
Main Smith, J.D., 1927, Nature **120**, 583.
Malinowski, M., R. Wolski and W. Wolinski, 1990, Solid State Commun. **74**, 17.
Malinowski, M., C. Garapon, M.F. Joubert and B. Jacquier, 1995, J. Phys.: Condens. Matter **7**, 199.
Malinowski, M., P. Myziak, R. Piramidowicz, I. Pracka, T. Lukasiewicz, B. Surma, S. Kaczmarek, K. Kopzynski and Z. Mierczyk, 1996, Acta Phys. Pol. A **90**, 181.
Malta, O.L., 1981, Mol. Phys. **42**, 65.
Malta, O.L., and G.F. de Sá, 1980, Chem. Phys. Lett. **74**, 101.
Malta, O.L., S.J.L. Ribeiro, M. Faucher and P. Porcher, 1991, J. Phys. Chem. Solids **52**, 587.
Marcus, Y., and M. Shiloh, 1969, Isr. J. Chem. **7**, 31.
Marion, J.E., and M.J. Weber, 1991, Eur. J. Solid State Inorg. Chem. **28**, 271.
Martín, I.R., V.D. Rodríguez, R. Alcalá and R. Cases, 1992, Bol. Soc. Esp. Ceram. Vid. **31C**, 351.
Mason, S.F., 1980, Struct. Bond. **39**, 43.
Mason, S.F., 1984, Inorg. Chim. Acta **94**, 313.
Mason, S.F., 1986, J. Indian Chem. Soc. **63**, 73.
Mason, S.F., and G.E. Tranter, 1983, Chem. Phys. Lett. **94**, 29.
Mason, S.F., R.D. Peacock and B. Stewart, 1974, Chem. Phys. Lett. **29**, 149.
Mason, S.F., R.D. Peacock and B. Stewart, 1975, Mol. Phys. **30**, 1829.
May, P.S., M.F. Reid and F.S. Richardson, 1987, Mol. Phys. **61**, 1471.
May, S.P., C.K. Jayasankar and F.S. Richardson, 1989, Chem. Phys. **138**, 139.
Mazurak, Z., E. Lukowiak, B. Jezowska-Trzebiatowska, D. Schultze and C. Waligora, 1984, J. Phys. Chem. Solids **45**, 487.
McColl, J.R., and F.C. Palilla, 1981, Am. Chem. Soc. Symp. Ser. **164**, 177.
McDougall, J., D.B. Hollis, X. Liu and M.J.B. Payne, 1994a, Phys. Chem. Glasses **35**, 145.
McDougall, J., D.B. Hollis and M.J.B. Payne, 1994b, Phys. Chem. Glasses **35**, 229.
McDougall, J., D.B. Hollis and M.J.B. Payne, 1994c, Phys. Chem. Glasses **35**, 258.
McDougall, J., D.B. Hollis and M.J.B. Payne, 1995, Phys. Chem. Glasses **36**, 139.
McDougall, J., D.B. Hollis and M.J.B. Payne, 1996, Phys. Chem. Glasses **37**, 73.
Medeiros Neto, J.A., D.W. Hewak and T. Tate, 1995, J. Non-Cryst. Solids **183**, 201.
Mehta, P.C., and S.P. Tandon, 1970, J. Chem. Phys. **53**, 414.
Meijerink, A., G. Blasse, J. Sytsma, C. de Mello Donega and J. Ellens, 1996, Acta Phys. Pol. A **90**, 109.

Meresse, Y., 1996, Ph.D. Thesis (Université de Rennes I, France).
Merino, R.I., 1993, Ph.D. Thesis (University of Zaragoza, Spain).
Merino, R.I., V.M. Orera and M.A. Chamarro, 1991, J. Phys.: Condens. Matter **3**, 8491.
Misra, S.N., 1985, J. Sci. Ind. Res. **44**, 366.
Misra, S.N., and K. John, 1993, Appl. Spectrosc. Rev. **28**, 285.
Misra, S.N., and S.B. Mehta, 1991, Bull. Chem. Soc. Jpn. **64**, 3653.
Misra, S.N., and S.B. Mehta, 1992, Ind. J. Pure Appl. Chem. **30**, 159.
Misra, S.N., and S.O. Sommerer, 1991, Appl. Spectrosc. Rev. **26**, 151.
Misra, S.N., and S.O. Sommerer, 1992a, Can. J. Chem. **70**, 46.
Misra, S.N., and S.O. Sommerer, 1992b, Rev. Inorg. Chem. **12**, 157.
Misra, S.N., K.J. Shah, G. Joseph, K. Anjaiah and Venkatasubramanian, 1990, Indian J. Chem. A **29**, 266.
Misra, S.N., S.B. Mehta, K.G. Chaudhari and C.M. Suveerkumar, 1994a, Indian J. Chem. A **33**, 893.
Misra, S.N., I. Devi, C.M. Suveerkumar and S.N. Mathew, 1994b, Rev. Inorg. Chem. **14**, 347.
Moeller, T., 1963, The Chemistry of the Lanthanides (Reinhold, New York).
Moeller, T., 1970, J. Chem. Educ. **47**, 417.
Moeller, T., and J.C. Brantley, 1950, J. Am. Chem. Soc. **72**, 5447.
Moeller, T., and D.E. Jackson, 1950, Anal. Chem. **22**, 1393.
Moeller, T., and W.F. Ulrich, 1956, J. Inorg. Nucl. Chem. **2**, 164.
Mondry, A., 1989, Inorg. Chim. Acta **162**, 131.
Mondry, A., and K. Bukietynska, 1996, Acta Phys. Pol. A **90**, 233.
Mondry, A., and P. Starynowicz, 1995, J. Alloys & Compounds **225**, 367.
Moran, D.M., and F.S. Richardson, 1990, Phys. B **42**, 3331.
Moran, D.M., A. De Piante and F.S. Richardson, 1989, J. Less-Common Met. **148**, 297.
Morley, J.P., T.R. Faulkner, F.S. Richardson and R.W. Schwartz, 1981, J. Chem. Phys. **75**, 539.
Morley, J.P., T.R. Faulkner and F.S. Richardson, 1982a, J. Chem. Phys. **77**, 1710.
Morley, J.P., T.R. Faulkner, F.S. Richardson and R.W. Schwartz, 1982b, J. Chem. Phys. **77**, 1734.
Morrison, C.A., and R.P. Leavitt, 1982, Spectroscopic properties of trivalent lanthanides in transparent host crystals, in: Handbook on the Physics and Chemistry of Rare Earths, Vol. 5, eds K.A. Gschneidner Jr and L. Eyring (North-Holland, Amsterdam) ch. 46, p. 461.
Morrison, C.A., R.P. Leavitt, J.B. Gruber and N.C. Chang, 1983, J. Chem. Phys. **79** (1983) 4758.
Morrison, C.A., E.D. Filer and N.P. Barnes, 1991, Report HDL-TR-2196 (Harry Diamond Laboratories, Adelphi, MD).
Nachimuthu, P., and R. Jagannathan, 1995a, Phys. Chem. Glasses **36**, 77.
Nachimuthu, P., and R. Jagannathan, 1995b, Proc. Indian Acad. Sci. (Chem. Sci.) **107**, 59.
Nageno, Y., H. Takebe and K. Morinaga, 1993, J. Am. Chem. Soc. **76**, 3081.
Nageno, Y., H. Takebe, K. Morinaga and T. Izumitani, 1994, J. Non-Cryst. Solids **169**, 288.
Nassau, K., 1983, The Physics and Chemistry of Color – the fifteen causes of color (Wiley, New York).
Newman, D.J., 1971, Adv. Phys. **20**, 197.
Newman, D.J., 1978, Aust. J. Phys. **31**, 79.
Newman, D.J., and G. Balasubramanian, 1975, J. Phys. C **8**, 37.
Newman, D.J., and B. Ng, 1989, Rep. Prog. Physics **52**, 699.
Nielson, C.W., and J.F. Koster, 1964, Spectroscopic Coefficients for the p^N, d^N and f^N configurations (M.I.T. Press, Cambridge, MA).
Nieuwpoort, W.C., and G. Blasse, 1966, Solid State Commun. **4**, 227.
Nishimura, G., and T. Kushida, 1988, Phys. B **37**, 9075.
Nishimura, G., and T. Kushida, 1991, J. Phys. Soc. Jpn. **60**, 683.
Nishimura, G., M. Tanaka, A. Kurita and T. Kushida, 1991, J. Lumin. **48&49**, 473.
Noguchi, T., and M. Mizuno, 1967, Sol. Energy **11**, 90.
Núñez, L., J.O. Tocho, J.A. Sanz-García, E. Rodríguez, F. Cussó, D.C. Hanna, A.C. Topper and A.C. Lange, 1993, J. Lumin. **55**, 253.
Ofelt, G.S., 1962, J. Chem. Phys. **37**, 511.
Oganesyan, S.S., G.G. Demirkhanyan and F.P. Safarsyan, 1990, Opt. Spectrosc. (USSR) **68**, 333.
Ohaka, T., and Y. Kato, 1983, Bull. Chem. Soc. Jpn. **56**, 1289.
Ohishi, Y., T. Kanamori, S. Takahashi, E. Snitzer and G.H. Sigel Jr, 1991, Opt. Lett. **16**, 1747.

Ohishi, Y., T. Kanamori, T. Nishi, Y. Nishida and S. Takahashi, 1992, Bol. Soc. Esp. Ceram. **31C**, 73.

Oomen, E.W.J.L., 1992, J. Lumin. **50**, 317.

Oomen, E.W.J.L., and A.M.A. van Dongen, 1989, J. Non-Cryst. Solids **111**, 205.

Orera, V.M., P.J. Alonso, R. Cases and R. Alcalá, 1988, Phys. Chem. Glasses **29**, 59.

Orera, V.M., L.E. Trinkler, R.I. Merino and A. Larrea, 1995, J. Phys.: Condens. Matter **7**, 9657.

Øye, H.A., and D.M. Gruen, 1969, J. Am. Chem. Soc. **91**, 2229.

Özen, G., X. Wu, J.P. Denis, A. Kermaoui, F. Pellé and B. Blanzat, 1993, J. Phys. Chem. Solids **54**, 1533.

Özen, G., A. Kermaoui, J.P. Denis, X. Wu, F. Pelle and B. Blanzat, 1995, J. Lumin. **63**, 85.

Pan, Z., S.H. Morgan, K. Dyer, A. Ueda and H. Liu, 1996, J. Appl. Phys. **79**, 8906.

Pappalardo, R., 1968, J. Chem. Phys. **49**, 1545.

Pappalardo, R., 1969, J. Mol. Spectrosc. **29**, 13.

Pappalardo, R., W.T. Carnall and P.R. Fields, 1969a, J. Chem. Phys. **51**, 842.

Pappalardo, R., et al., 1969b, Cited in section 13. Please add??

Pasternak, S., 1940, Astrophys. J. **92**, 129.

Payne, S.A., J.A. Caird, L.L. Chase, L.K. Smith, N.D. Nielsen and W.F. Krupke, 1991, J. Opt. Soc. Am. B **8**, 726.

Peacock, R.D., 1970, Chem. Phys. Lett. **7**, 187.

Peacock, R.D., 1973, Mol. Phys. **4**, 817.

Peacock, R.D., 1974, J. Chem. Phys. **61**, 2483.

Peacock, R.D., 1975, Struct. Bond. **22**, 83.

Peacock, R.D., 1977, Mol. Phys. **33**, 1239.

Peacock, R.D., 1978, J. Mol. Struct. **48**, 203.

Peng, B., and T. Izumitani, 1995, Opt. Mater. **4**, 797.

Petrin, R.B., M.L. Kliewer, J.T. Beasley, R.C. Powell, I.D. Aggarwal and R.C. Ginther, 1991, IEEE J. Quantum Electron. **QE-27**, 1031.

Piepho, S.B., and P.N. Schatz, 1983, Group Theory in Spectroscopy. With Applications to Magnetic Circular Dichroism (Wiley, New York).

Pink, H., 1975, Ph.D. Thesis (University of Syracuse, New York).

Poluéktov, N.S., and S.V. Bel'tyukova, 1974, Dopov. Akad. Nauk Ukr. RSR Ser. B **10**, 451.

Poluéktov, N.S., L.A. Alakaeva and M.A. Tishchenko, 1972, Zh. Prikl. Spektrosk. **17**, 819.

Poluéktov, N.S., S.V. Bel'tyukova and V.T. Mischenko, 1977, Dokl. Akad. Nauk. SSSR **235**, 1107.

Poluéktov, N.S., N.A. Nazarenko, V.T. Mischenko and S.V. Bel'tyukova, 1984, in: Proc. Int. Symp. on Rare Earth Spectroscopy, Wroclaw, Poland, September 1984, eds B. Jezowska-Trzebiatowska, J. Legendziewicz and W. Strek, p. 363.

Popov, A.I., and G.E. Knudson, 1954, J. Am. Chem. Soc. **76**, 3921.

Porcher, P., and P. Caro, 1978, J. Chem. Phys. **68**, 4176.

Porcher, P., and P. Caro, 1980, J. Lumin. **21**, 207.

Qi, C., X. Zhang, Yasi Jiang and Yanyan Jiang, 1992, Chin. Phys. **12**, 344.

Quagliano, J.R., G.W. Burdick, D.P. Glover-Fischer and F.S. Richardson, 1995, Chem. Phys. **201**, 321.

Quimby, R.S., and W.J. Miniscalco, 1994, J. Appl. Phys. **75**, 613.

Racah, G., 1942, Phys. Rev. **62**, 438.

Racah, G., 1943, Phys. Rev. **63**, 367.

Racah, G., 1949, Phys. Rev. **76**, 1352.

Rana, R.S., C.D. Cordero-Montalvo and N. Bloembergen, 1984, J. Chem. Phys. **81**, 2951.

Ranga Reddy, A.V., T. Balaji and S. Buddhudu, 1991, Phys. Chem. Glasses **32**, 263.

Ranga Reddy, A.V., T. Balaji and S. Buddhudu, 1992a, Spectrochim. Acta A **48**, 1515.

Ranga Reddy, A.V., K. Annapurna, G. Amaranath, A.S. Jacob, A. Suresh Kumar and S. Buddhudu, 1992b, Ferroelectrics Lett. **14**, 145.

Ranga Reddy, A.V., K. Annapurna, A.S. Jacob and S. Buddhudu, 1993, Ferroelectrics Lett. **15**, 33.

Rao, D.N., J. Prasad and P.N. Prasad, 1983, Phys. Rev. B **28**, 20.

Ratnakaram, Y.C., 1994, Phys. Chem. Glasses **35**, 182.

Ratnakaram, Y.C., and S. Buddhudu, 1996, Solid State Commun. **97**, 651.

Ravi Kanth Kumar, V.V., C.K. Jayasankar and R. Jagannathan, 1996, Phys. Status Solidi B **195**, 287.

Razumova, I., A. Tkachuk, A. Nikitichev and D. Mironov, 1995, J. Alloys & Compounds **225**, 129.

Razumova, I.K., A.M. Tkachuk, D.I. Mironov and A.A. Nikitichev, 1996, Opt. Spectrosc. **81**, 205.

Reid, M.F., 1981, Ph.D. Thesis (University of Canterbury, Christchurch, New Zealand).

Reid, M.F., 1987, J. Chem. Phys. **87**, 6388.

Reid, M.F., and F.S. Richardson, 1983a, Chem. Phys. Lett. **95**, 501.

Reid, M.F., and F.S. Richardson, 1983b, J. Chem. Phys. **79**, 5735.

Reid, M.F., and F.S. Richardson, 1983c, J. Less-Common Metals **93**, 113.
Reid, M.F., and F.S. Richardson, 1984a, J. Phys. Chem. **88**, 3579.
Reid, M.F., and F.S. Richardson, 1984b, Mol. Phys. **541**, 1077.
Reid, M.F., and F.S. Richardson, 1984c, in: Proc. Int. Symp. on Rare Earth Spectroscopy, Wroclaw, Poland, September 1984, eds B. Jezowska-Trzebiatowska, J. Legendziewicz and W. Strek, p. 298.
Reid, M.F., and F.S. Richardson, 1984d, Phys. Rev. B **29**, 2830.
Reid, M.F., and F.S. Richardson, 1984e, J. Lumin. **31&32** 207.
Reid, M.F., J.J. Dallara and F.S. Richardson, 1983, J. Chem. Phys. **79**, 5743.
Reid, M.F., B. Ng and D.J. Newman, 1988, J. Lumin. **40&41**, 115.
Reid, M.F., G.W. Burdick and H.J. Kooy, 1994, J. Alloys & Compounds **207/208**, 78.
Reisfeld, R., 1976, Colloq. Int. C.N.R.S. **255**, 149.
Reisfeld, R., 1982, Ann. Chim. Fr. **7**, 147.
Reisfeld, R., and Y. Eckstein, 1975, J. Chem. Phys. **63**, 4001.
Reisfeld, R., and J. Hormadaly, 1976, J. Chem. Phys. **64**, 3207.
Reisfeld, R., and C.K. Jørgensen, 1977, Laser and Excited States of Rare Earths (Springer, Berlin).
Reisfeld, R., and C.K. Jørgensen, 1987, Excited state phenomena in vitreous materials, in: Handbook on the Physics and Chemistry of Rare Earths, Vol. 9, eds K.A. Gschneidner Jr and L. Eyring (North-Holland, Amsterdam) ch. 58, p. 1.
Reisfeld, R., G. Katz, N. Spector, C.K. Jørgensen, C. Jacoboni and R. De Pape, 1982, J. Solid State Chem. **41**, 253.
Reisfeld, R., M. Eyal, E. Greenberg and C.K. Jørgensen, 1985, Chem. Phys. Lett. **118**, 25.
Remillieux, A., B. Jacquier, C. Linarès, C. Lesergent, S. Artigaud, D. Bayard, L. Hamon and J.L. Beylat, 1996, J. Phys. D **29**, 963.
Remy, H., 1956, Treatise on Inorganic Chemistry, Vol. II (Elsevier, Amsterdam).
Rhône-Poulenc, 1985, French Patent 85 06546.
Richardson, F.S., J.D. Saxe, S.A. Davis and T.R. Faulkner, 1981, Mol. Phys. **42**, 1401.
Riker, L.W., 1981, Am. Chem. Soc. Symp. Ser. **164**, 81.
Rodríguez, V.D., I.R. Martín, R. Alcalá and R. Cases, 1992, J. Lumin. **54**, 231.
Rodríguez, V.L., U.R. Rodríguez-Mendoza, I.R. Martín and P. Nuñez, 1995, Radiat. Eff. Defects Solids **135**, 105.
Rotenberg, M., R. Bivens, N. Metropolis and J.K. Wooten, 1959, The 3-*j* and 6-*j* Symbols (MIT Press, Cambridge, MA).
Rukmini, E., and C.K. Jayasankar, 1994, J. Non-Cryst. Solids **176**, 213.
Rukmini, E., and C.K. Jayasankar, 1995, Opt. Mater. **4**, 529.
Ryan, J.L., and C.K. Jørgensen, 1966, J. Phys. Chem. **70**, 2845.
Ryan, J.R., and R. Beach, 1992, J. Opt. Soc. Am. B **9**, 1883.
Ryba-Romanowski, W., 1990, J. Lumin. **46**, 163.
Ryba-Romanowski, W., Z. Masurak, B. Jezowska-Trzebiatowska, D. Schultze and C.W. Waligora, 1980, Phys. Status Solidi A **62**, 75.
Saisudha, M.B., and J. Ramakrishna, 1996, Phys. Rev. B **53**, 6186.
Sanz, J., R. Cases and R. Alcalá, 1987, J. Non-Cryst. Solids **93**, 377.
Sardar, D.K., and S.C. Stubblefield, 1995, Phys. Status Solidi A **152**, 549.
Sardar, D.K., R.C. Velarde-Montecinos and S. Vizcarra, 1993, Phys. Status Solidi A **136**, 555.
Sathyanarayana, J.V., T. Balaji, K. Annapurna and S. Buddhudu, 1996, Phys. Chem. Glasses **37**, 41.
Satten, R.A., C.L. Schreiber and E.Y. Wong, 1983, J. Chem. Phys. **78**, 79.
Schwartz, R.W., 1975, Mol. Phys. **30**, 81.
Schweizer, T., D.W. Hewak, B.N. Samason and D.N. Payne, 1996, Optics Lett. **21**, 1594.
Seeber, W., and D. Ehrt, 1992, Phys. Status Solidi A **130**, K215.
Seeber, W., E.A. Downing, L. Hesselink, M.M. Fejer and D. Ehrt, 1995, J. Non-Cryst. Solids **189**, 218.
Selwood, P.W., 1930, J. Am. Chem. Soc. **52**, 4308.
Shangda, X., and C. Yimin, 1984, J. Lumin. **31&32**, 204.
Shiloh, M., M. Givon and Y. Marcus, 1969, J. Inorg. Nucl. Chem. **31**, 1807.
Shin, Y.B., J.N. Yang and J. Heo, 1995, Opt. Quantum Electronics **27**, 379.
Shinn, M.D., W.A. Sibley, M.G. Drexhage and R.N. Brown, 1983, Phys. Rev. B **27**, 6635.
Shortley, G.H., 1940, Phys. Rev. **57**, 225.
Shriver, D.F., P.W. Atkins and C.H. Langford, 1994, Inorganic Chemistry, 2nd Ed. (Oxford University Press, Oxford).

Simondi-Teisseire, B., B. Viana, D. Vivien and A.M. Lejus, 1996, Phys. Status Solidi A **155**, 249.

Simoni, E., M. Louis, S. Hubert and M.F. Reid, 1995, J. Phys. II France **5**, 755.

Simons, D.R., 1995, Ph.D. Thesis (TU Eindhoven, Netherlands).

Simons, D.R., A.J. Faber and H. de Waal, 1995, Optics Lett. **20**, 468.

Sinha, S.P., 1966, Spectrochim. Acta **22**, 57.

Sinha, S.P., P.C. Mehta and S.S.L. Surano, 1972, Mol. Phys. **23**, 807.

Smentek, L., and B.A. Hess Jr, 1996, Mol. Phys. **88**, 783.

Smentek-Mielczarek, L., 1993a, Phys. Rev. B **48**, 9273.

Smentek-Mielczarek, L., 1993b, Phys. Rev. Lett. **71**, 3891.

Smentek-Mielczarek, L., and B.A. Hess, 1987, Phys. Rev. B **36**, 1811.

Smentek-Mielczarek, L., and B.A. Hess, 1989, J. Chem. Phys. **90**, 1390.

Smentek-Mielczarek, L., and K. Jankowski, 1979, Mol. Phys. **38**, 1459.

Souriau, J.C., C. Borel, C. Wyon, C. Li and R. Moncorgé, 1994, J. Lumin. **59**, 349.

Spector, N., R. Reisfeld and L. Boehm, 1977, Chem. Phys. Lett. **49**, 49.

Staritzky, E., and L.B. Asprey, 1957, Anal. Chem. **29**, 855.

Stavola, M., L. Isganitis and M. Sceats, 1981, J. Chem. Phys. **74**, 4228.

Stephens, E.M., M.F. Reid and F.S. Richardson, 1984, Inorg. Chem. **23**, 4611.

Stephens, P.J., 1970, J. Chem. Phys. **52**, 3489.

Stephens, P.J., 1976, Adv. Chem. Phys. **25**, 197.

Stewart, B., 1983, Mol. Phys. **50**, 161.

Stewart, B., 1993, Chem. Phys. Lett. **206**, 106.

Stewart, D.C., and D. Kato, 1958, Anal. Chem. **30**, 164.

Stokowski, R.E., R.A. Saroyan and M.J. Weber, 1981a, Nd-Doped Laser Glass Spectroscopic and Physical Properties, M-095, Rev. 2, Vol. 1 (Lawrence Livermore National Laboratory, Livermore, CA).

Stokowski, R.E., R.A. Saroyan and M.J. Weber, 1981b, Nd-Doped Laser Glass Spectroscopic and Physical Properties, M-095, Rev. 2, Vol. 2 (Lawrence Livermore National Laboratory, Livermore CA).

Strek, W., 1979, Theor. Chim. Acta **52**, 45.

Stubblefield, C.T., and L. Eyring, 1955, J. Am. Chem. Soc. **77**, 3004.

Subramanyam, Y., L.R. Moorthy and S.V.J. Lakshman, 1990, Mater. Lett. **9**, 277.

Subramanyam Naidu, K., and S. Buddhudu, 1992a, J. Quant. Spectrosc. Radiat. Transfer **47**, 515.

Subramanyam Naidu, K., and S. Buddhudu, 1992b, J. Mater. Sci. Lett. **11**, 386.

Subramanyam Naidu, K., and S. Buddhudu, 1992c, Mater. Lett. **13**, 299.

Subramanyam Naidu, K., and S. Buddhudu, 1992d, Mater. Lett. **14**, 355.

Surana, S.S.L., R.C. Mathur, P.C. Mehta and S.P. Sandon, 1975, Appl. Phys. **6**, 363.

Surana, S.S.L., M. Singh and S.N. Misra, 1980, J. Inorg. Nucl. Chem. **42**, 61.

Sztucki, J., 1994, J. Lumin. **60&61**, 681.

Takebe, H., Y. Nageno and K. Morinaga, 1995, J. Am. Chem. Soc. **78**, 116; erratum: **78**, 2287.

Takebe, H., T. Murata, H. Nishida, D.W. Hewak and K. Morinaga, 1996, J. Ceram. Soc. Jpn. **104**, 243.

Tanabe, S., and T. Hanada, 1994, J. Appl. Phys. **76**, 3730.

Tanabe, S., T. Ohyagi, N. Soga and T. Hanada, 1992, Phys. Rev. B **46**, 3305.

Tanabe, S., T. Ohyagi, S. Todoroki, T. Hanada and N. Soga, 1993a, J. Appl. Phys. **73**, 8451.

Tanabe, S., T. Hanada, T. Ohyagi and N. Soga, 1993b, Phys. Rev. B, **48**, 10591.

Tanabe, S., K. Tamai, K. Hirao and N. Soga, 1993c, Phys. Rev. B, **47**, 2507.

Tanabe, S., T. Ohyagi, T. Hanada and N. Soiga, 1993d, J. Ceram. Soc. Jpn. **101**, 78.

Tanabe, S., K. Suzuki, N. Soga and T. Hanada, 1994, J. Opt. Soc. Am. B **11**, 933.

Tanabe, S., T. Hanada, M. Watanabe, T. Hayashi and N. Soga, 1995a, J. Am. Ceram. Soc. **78**, 2917.

Tanabe, S., K. Takahara, M. Takahashi and Y. Kawamoto, 1995b, J. Opt. Soc. Am. B **12**, 786.

Tanabe, S., K. Tamai, K. Hirao and N. Soga, 1996, Phys. Rev. B **53**, 8358.

Tanaka, M., and T. Kushida, 1993, J. Alloys & Compounds **193**, 183.

Tanaka, M., G. Nishimura and T. Kushida, 1994, Phys. Rev. B **49**, 16917.

Tandon, S.P., and P.C. Mehta, 1970, J. Chem. Phys. **52**, 4313.

Tanimura, K., M.D. Shinn, W.A. Sibley, M.G. Drexhage and R.N. Brown, 1984, Phys. Rev. **30**, 2429.

Tanner, P.A., Y.-L. Liu, M. Chua and M.F. Reid, 1994, J. Alloys & Compounds **207/208**, 83.

Tesar, A., J. Campbell, M. Weber, C. Weinzapfel, Y. Lin, H. Meissner and H. Toratani, 1992, Optical Mater. **1**, 217.

Timofeev, Y.P., N.K. Tkhan and S.A. Fridman, 1990, Opt. Spectrosc. **69**, 220.

Tishchenko, M.A., G.I. Gerasimenko and N.S. Poluéktov, 1976, Dopov. Akad. Nauk. Ukr. RSR Ser. B **12**, 1107.

Tkachuk, A.M., A.V. Poletimova and M.V. Petrov, 1985, Opt. Spectrosc. **59**, 680.

Tkachuk, A.M., A.K. Przhevusskii, L.G. Morozova, A.V. Poletimova, M.V. Petrov and A.M. Korovkin, 1986, Opt. Spectrosc. (USSR) **60**, 176.

Uhlmann, E.V., M.C. Weinberg, N.J. Kreidl, L.L. Burgner, R. Zanoni and K.H. Church, 1994, J. Non-Cryst. Solids **178**, 15.

Valenzuela, R.W., and R.T. Brundage, 1990, J. Chem. Phys. **93**, 8469.

Valiev, U.V., A.A. Klochkov, A.A. Moskvin and P. Shiroki, 1990, Opt. Spectrosc. USSR **69**, 68.

Van Vleck, J.H., 1937, J. Chem. Phys. **41**, 67.

Vandenberghe, G.M., 1995, Ph.D. Thesis (K.U. Leuven, Heverlee, Belgium).

Verwey, J.W.M., G.F. Imbusch and G. Blasse, 1989, J. Phys. Chem. Solids **50**, 813.

Villacampa, B., V.M. Orera, R.I. Merino, R. Cases, P.J. Alonso and R. Alcalá, 1991a, Mater. Res. Bull. **26**, 741.

Villacampa, B., R.I. Merino, V.M. Orera, R. Cases, P.J. Alonso and R. Alcalá, 1991b, Mater. Sci. Forum **67&68**, 527.

Wang, Q., S. Zhang, S. Wu, Y. Ren and X. Dong, 1986, Acta Opt. Sinica 307.

Wang, Q.Y., S.Y. Zang and Y.Q. Jia, 1993, J. Alloys & Compounds **202**, 1.

Weber, M.J., 1967a, in: Optical Properties of Ions in Crystals, eds H.M. Crosswhite and H.W. Moos (Wiley-Interscience, New York).

Weber, M.J., 1967b, Phys. Rev. **157**, 262.

Weber, M.J., 1968, J. Chem. Phys. **48**, 4774.

Weber, M.J., and R.M. Almeida, 1981, J. Non-Cryst. Solids **43**, 99.

Weber, M.J., and T.E. Varitimos, 1971, J. Appl. Phys. **42**, 4996.

Weber, M.J., B.H. Matsinger, V.L. Donlan and G.T. Surratt, 1972, J. Chem. Phys. **57**, 562.

Weber, M.J., T.E. Varitimos and B.H. Matsinger, 1973, Phys. Rev. B **8**, 47.

Weber, M.J., R.A. Saroyan and R.C. Ropp, 1981, J. Non-Cryst. Solids **44**, 137.

Weber, M.J., D.C. Ziegler and C.A. Angell, 1982, J. Appl. Phys. **53**, 4344.

Wei, K., D.P. Machewirth, J. Wenzel, E. Snitzer and G.H. Sigel Jr, 1994, Opt. Lett. **19**, 904.

Wei, K., D.P. Machewirth, J. Wenzel and G.H. Sigel Jr, 1995, J. Non-Cryst. Solids **182**, 257.

Weigel, F., 1969, Fortschr. Chem. Forsch. **12**, 539.

Weigel, F., and V. Scherer, 1967, Radiochem. Acta **7**, 46.

Weissbluth, M., 1978, Atoms and Molecules (Academic Press, New York).

Wetenkamp, L., G.F. West and H. Tobben, 1992, J. Non-Cryst. Solids **140**, 35.

Williams, M.C., and R.T. Brundage, 1992, Phys. Rev. B **45**, 4561.

Wolf, M., S. Edvardsson, M.A. Zendejas and J.O. Thomas, 1993, Phys. Rev. B. **48**, 10129.

Wu, S., S. Zhang and Q. Wang, 1986, Chinese J. Lumin. **7**, 252.

Wybourne, B.G., 1967, in: Optical Properties of Ions in Crystals, eds H.M. Crosswhite and H.H. Moos (Wiley-Interscience, New York) p. 35.

Xie, B.Q., Y.M. Cheung and S.K. Gayen, 1993, Phys. Rev. B **47**, 5557.

Xu, L.W., H.M. Crosswhite and J.P. Hessler, 1984, J. Chem. Phys. **81**, 698.

Yanagita, H., K. Okada, K. Miura, H. Toratani and T. Yamashita, 1991, Mater. Sci. Forum **67&68**, 521.

Yeh, D.C., W.A. Sibley and M.J. Suscavage, 1988, J. Appl. Phys. **63**, 4644.

Yeh, D.C., R.R. Petrin, W.A. Sibley, V. Madigou, J.L. Adam and M.J. Suscavage, 1989, Phys. Rev. B **39**, 80.

Yoon, S.K., S.S. Yun and J.G. Kang, 1992, Bull. Korean Chem. Soc. **13**, 54.

Zahir, M., R. Olazcuaga, C. Parent, G. Le Flem and P. Hagenmuller, 1985, J. Non-Cryst. Solids **69**, 221.

Zhang, G., X. Ying, L. Yao, T. Chen and H. Chen, 1994, J. Lumin. **59**, 315.

Zou, X., and T. Izumitani, 1993, J. Non-Cryst. Solids **162**, 68.

Handbook on the Physics and Chemistry of Rare Earths
Vol. 25
edited by K.A. Gschneidner, Jr. and L. Eyring

Chapter 168

ORGANOMETALLIC π COMPLEXES OF THE f-ELEMENTS

Gabriella BOMBIERI* and Gino PAOLUCCI#
**Istituto di Chimica Farmaceutica, Università di Milano, Viale Abruzzi 42, 20131 Milano, Italy; #Dipartimento di Chimica, Università di Venezia, Calle Larga S. Marta 2137, 30123 Venezia, Italy*

Contents

List of Abbreviations

An	actinide	dmpe	1,2-bis(dimethylphosphino)ethane
bpy	2,2′-bipyridine	ind	indenyl
^{n}Bu	*n*-butyl	Ln	lanthanide
^{s}Bu	*sec*-butyl	Me	methyl
^{t}Bu	*tert*-butyl	Me-THF	methyltetrahydrofuran
Cg	center of gravity	Ph	phenyl
Cp	η^5-C_5H_5	phen	1,10-phenanthroline
Cp^0	η^5-C_5H_4–CH_2CH_2OMe	^{i}Pr	*iso*-propyl
Cp^*	η^5-C_5Me_5	^{n}Pr	*n*-propyl
diglyme	diethylene glycol dimethyl ether	THF	tetrahydrofuran
DME	1,2-dimethoxyethane	tmeda	*N,N,N′,N′*-tetramethylethylenediamine

1. Introduction

There were several unsuccessful attempts to prepare organolanthanide compounds in the first half of the 20th century, but the first syntheses of tricyclopentadienyl derivatives of scandium, yttrium and of almost all of the lanthanides were made by Wilkinson and Birmingham in 1954. The first organoactinide to be prepared was Cp_3UCl obtained by Reynolds and Wilkinson in 1956. In 1968 the first indenyl (Tsutsui and Gysling 1968) and, one year later, the first cyclooctatetraenyl uranium complexes (Hayes and Thomas 1969) were isolated. In the past two decades organolanthanide and organoactinide chemistry developed tremendously as a consequence of the increased availability of pure elements and of the applications of these compounds in many fields. This extensive research work has been widely reviewed in several books (Marks and Fragalà 1985, Bochkarev et al. 1989), in a series of comprehensive and specialized review articles (Marks and Ernst 1982, Palenik 1983, Evans and Hosborn 1987, Marks et al. 1989, Green 1989, Burns and Bursten 1989, Ephritikhine 1992, Schaverien 1994a, Edelmann 1995a, Schumann et al. 1995a, Cloke 1995, Richter and Edelmann 1996, Deacon and Shen 1996). Along the

Table 1
Oxidation states and E^0 values of some common f-elements in aqueous solution[a]

State	E^0	State	E^0	State	E^0
Pr^{4+}/Pr^{3+}	+3.2 V	Tb^{4+}/Tb^{3+}	+3.1 V	Ce^{4+}/Ce^{3+}	+1.74 V
Eu^{3+}/Eu^{2+}	−0.35 V	Yb^{3+}/Yb^{2+}	−1.15 V	Sm^{3+}/Sm^{2+}	−1.55 V
Tm^{3+}/Tm^{2+}	−2.1 V				
UO_2^{2+}/UO_2^{+}	+0.05 V	UO_2^{+}/U^{4+}	+0.62 V	UO_2^{2+}/U^{4+}	+0.33 V

[a] Available oxidation states: Ln^{4+} (Ce, Tb, Pr); Ln^{3+} (main oxidation state for all lanthanides); Ln^{2+} (Eu, Sm, Yb, Lu); U (U^{3+}, U^{4+}, U^{5+}, U^{6+}).

lanthanide series, the 4f orbitals are completely buried inside the inner core and their r^6 electron-probability dependence prevents them from penetrating inside the $n=4$ shell. Thus they do not experience as great an effective nuclear charge as the 5p, 6s, or 5d orbitals. Although well shielded, the 4f orbitals become more attractive as Z increases, and a smooth decrease in radius, known as the "lanthanide contraction", is observed.

The tendency to attain the stable electronic configurations of La or Xe by removal of 4f electrons, makes the trivalent oxidation state the most favorable. However, other oxidation states are available when $4f^0$, $4f^7$ or $4f^{14}$ configurations are achieved or at least approached. Thus La^{3+} ($4f^0$), Gd^{3+} ($4f^7$) and Lu^{3+} ($4f^{14}$) represent reference elements for some regular changes in the chemical behavior such as an abnormal valency state. In fact Ce ($4f^5d^6s^2$) and Tb ($4f^96s^2$), following La ($5d^6s^2$) and Gd ($4f^75d^6s^2$) respectively, can easily become tetravalent, while Eu ($4f^76s^2$) and Yb ($4f^{14}6s^2$), preceding Gd ($4f^75d^6s^2$) and Lu ($4f_5^{15}d^6s^2$) respectively, can become bivalent. Thus, in addition to the Ln^{3+}, the most common (and stable) species to be found are Ce^{4+} ($4f^0$), Eu^{2+} ($4f^7$), Sm^{2+} ($4f^6$) and Yb^{2+} ($4f^{14}$), although Pr^{4+} ($4f^1$) and Tb^{4+} ($4f^7$), among others, are also accessible under more restricted conditions. However all 4+ species are strong oxidizing agents, and all 2+ species are strong reducing agents. Ce^{4+} is widely used as a powerful one-electron oxidizing agent. Despite its high oxidizing power, some organometallic compounds of cerium(IV) have been obtained (Alcock et al. 1992). The oxidation states and E^0 values of some common f-elements are reported in table 1.

While the lanthanide series is due to the successive filling of the 4f orbitals, it is generally assumed that they do not contribute significantly to bonding due to their limited radial extension and the shielding from the valence shell by the filled 5s and 5p orbitals. However, these f-orbitals (filled or empty) should be able to modulate some electronic properties of the metal center. In the ubiquitous oxidation state 3+, the lanthanide ions reach an inert gas core configuration by the loss of one 4f electron. It is for this reason that yttrium and scandium complexes are included in discussions of lanthanide chemistry; i.e., in their predominant 3+ oxidation states, these elements have an inert gas core configuration ([Kr] and [Ar], respectively) and empty d orbitals. Indeed, due to the lanthanide contraction, the size of Y^{3+} falls between Ho^{3+} and Er^{3+}, whereas scandium is considerably smaller than the lanthanides.

Table 2
D^0_{298} values for the gas phase dissociation of M–O (M = Ln, An)

Rare earth	D^0_{298}	Rare earth	D^0_{298}
La	799.7 kJ/mol	Tm	510.8 kJ/mol
Ce	795.5 kJ/mol	Th	854.1 kJ/mol
Eu	510.8 kJ/mol	U	761.6 kJ/mol
Sm	569.4 kJ/mol	Yb	397.7 kJ/mol

Lanthanides and actinides show a strong affinity for oxygen and an indirect measure of the oxophilicity of f-elements is the bond strength D^0_{298} for the gas phase dissociation of the diatomic species MO (Murad and Hildenbrand 1980) (table 2).

The chemical differences between lanthanide and actinide derivatives are mainly due to some differences in their electronic structures. The 5f orbitals of early actinides are incompletely shielded from external influences by the 6s and 6p electrons, thus they have sufficient radial expansion for some overlap with ligand orbitals. As a consequence, organoactinides show a consistent covalent contribution to bonding, even though the prevalent ionic character remains. In the later actinides the increased nuclear charge causes contraction of 5f orbitals so that the metal–ligand overlap decreases and the trivalent oxidation state dominates in the more ionic derivatives.

The combination of above mentioned properties has important consequences for the organometallic chemistry of these elements:

(i) organometallic compounds are largely ionic, due to the inability of the f-orbitals to overlap effectively ligand molecular orbitals;
(ii) unlike transition metal chemistry, oxidative–addition reactions are expected to be unfavorable due to the strength of the trivalent oxidation state (lanthanides);
(iii) the large radii of f-elements require sterically demanding ligands to form discrete, monomeric compounds (mainly for lanthanides);
(iv) in contrast to transition metals, all lanthanides display similar chemical behavior, differing only in degree due to changes in size. This provides the possibility of tuning the reaction site for a given reaction simply by changing the lanthanide and hence the radius of the central atom;
(v) the very low covalent contributions in bonding in conventional lanthanide chemistry offer possibilities for new reactivities not observed for d-transition elements, without the restrictions imposed by the need for compatible orbital symmetries;
(vi) unlike the transition elements, f-elements (either 4f and 5f) complexes are characterized by high coordination numbers (up to 12), thus making coordinatively unsaturated species, which are extremely reactive as catalysts, very easy to obtain.

Most organometallic derivatives of Ln and An contain at least one ligand of the π-donor/π-acceptor type, chiefly cyclopentadienyl and related species (including cyclooctatetraenes). While these ligands represent a sort of protective sheath around the metal center, the other ligands present (halides, hydrides, alkyls, etc.) are the reactive centers in organometallic stoichiometric and catalytic reactions. Thus, we will discuss

classes of organolanthanides and organoactinides apparently different in their oxidation states but similar in their reactivities.

Without trying to exhaustively cover this field due to its enormous development, several interesting structural and synthetic aspects differentiating or unifying the 4f and 5f element derivatives are here considered from 1982 onwards and referring to the rest by previous important reviews. The organization of the chapter is by ligand type. Ln and An derivatives are consecutive and separated when numerous, otherwise they are discussed in the same section.

2. Main classes of organolanthanides and organoactinides

2.1. *Cyclopentadienyls*

2.1.1. *Cp_4M (lanthanides and actinides)*

Cerium is the only lanthanide element forming tetravalent compounds, stable in aqueous solutions, because the ion Ce^{4+} has the electron configuration of the ideal gas xenon. Despite the very strong oxidizing power of the Ce^{IV} cation, several organometallic compounds have been reported to have an astonishingly high stability.

The synthesis of tetrakis- (or tetra-) cyclopentadienyl cerium was reported first by reaction of bis(pyridinium)hexachlorocerate and sodium cyclopentadienide (Kalsotra et al. 1971); the same reaction has been extended to other π-ligands such as indenyls and fluorenyls. However, in 1983 it was reported that the reaction of sodium cyclopentadienide with bis(pyridinium)hexachlorocerate in THF yields tricyclopentadienyl cerium(III) instead of tetrakiscyclopentadienyl cerium(IV) (Deacon et al. 1983).

The first approach to the synthesis of actinide tetracyclopentadienyls, Cp_4Th (Fischer and Tribner 1962) and Cp_4U (Fischer and Hristidu 1962), was made by reacting the actinide tetrachlorides and KCp in benzene. These compounds, due to their low solubility, required purification by Soxhlet extraction. Some other alternative synthetic approaches to tetracyclopentadienyl derivatives included the reaction of the metal tetrafluorides with dicyclopentadienyl magnesium in the absence of solvent (Reid and Wailes 1966) and, in the case of M = U, the reaction of uranium tetradiethylamide and freshly distilled cyclopentadiene (Paolucci et al. 1985a):

$$M(NEt_2)_4 + 4CpH \xrightarrow{\text{benzene}} MCp_4 + 4HNEt_2, \quad M = U, Th.$$

The X-ray crystal structure determination of Cp_4U (Burns 1974) and of the isostructural Cp_4Th (Mayer and Rebizant 1993) shows an overall S_4 molecular symmetry, thus confirming the pseudotetrahedral (η^5-cyclopentadienyl) structures previously proposed on the basis of their IR and solution dipole moments (fig. 1).

The reaction of Cp_4U with halogenated hydrocarbons yields a series of compounds either with insertion of the halogenated hydrocarbons into one of the cyclopentadienyl ligands or by substitution of one Cp ligand:

$$2Cp_4U + CCl_4 \rightarrow Cp_3UCl + Cp_3U(C_5H_4CCl_3) + \cdots,$$
$$2Cp_4U + CHCl_3 \rightarrow Cp_3UCl + Cp_3U(C_5H_4CHCl_2) + \cdots.$$

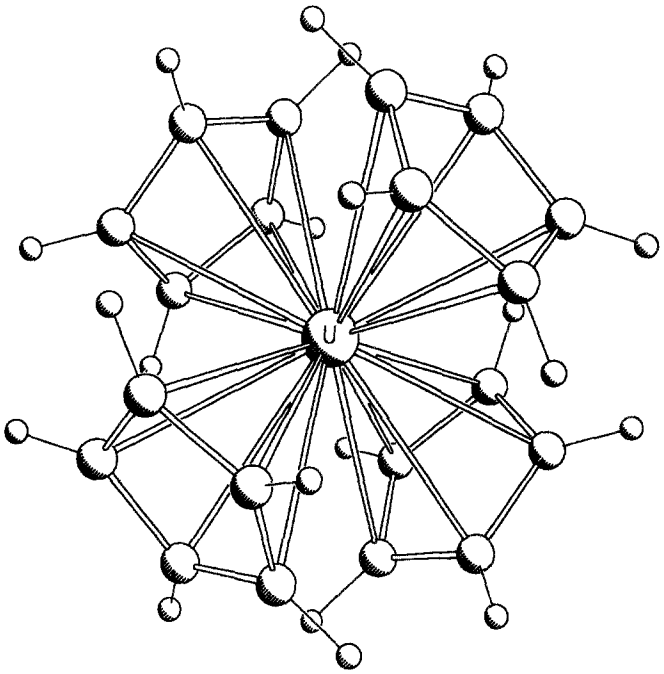

Fig. 1. Crystal structure of [Cp_4U] (Burns 1974).

Thus, Cp_3U–^{n}Bu is obtained by reaction of Cp_4U with ^{n}Bu–Cl, while $Cp_3UCH_2CHMe_2$ and $Cp_3UCH_2CMe_2Cl$ are obtained from the reactions with Me_2CHCH_2Cl and Me_3CCl, respectively (Leonov et al. 1990).

2.1.2. *Cp_3M, Cp_3ML and Cp_3ML_2*

2.1.2.1. *Lanthanides.* The triscyclopentadienyl derivatives of the lanthanides, isolated in 1954 by Birmingham and Wilkinson, were the first organolanthanide species to be unambiguously characterized (Wilkinson and Birmingham 1954). These air and moisture sensitive, solvent-free compounds were prepared by reaction of anhydrous $LnCl_3$ (Ln = Sc, Y, La, Ce Pr, Nd, Sm, Gd, Dy, Er, Yb) with sodium cyclopentadienide in THF at room temperature and isolated by sublimation at 200–250°C of the crude THF adduct formed. The same syntheses can be used to obtain Cp_3U derivatives (Kanellakopulos and Bagnall 1971), alternatively to the reduction reactions of several U^{IV} derivatives such as Cp_4U with potassium or U metals.

Cp_3Sm has been obtained by ligand exchange reactions of $(C_6F_5)_2Sm$ with CpH (Zhongwen et al. 1986). Unsolvated Cp_3Ln (Ln = Er, Yb) has been prepared by reaction of the lanthanide trichlorides with TlCp in THF or DME (Deacon et al. 1987a, 1989a–c). Optimized preparative routes to $Cp_3Ln(THF)$ have been achieved by reaction of powdered

lanthanide metals, thallium(I) cyclopentadienide and a trace of mercury metal which aids initiation of transmetallation (Kaesz 1989):

$$Ln(s) + 3TlCp \xrightarrow[Ln = Nd, Sm]{THF} LnCp_3 \cdot THF + 3Tl.$$

The same reaction with Yb metal in 1,2-dimethoxyethane forms the $Cp_2Yb(DME)$ complex (Deacon et al. 1989a).

Attempts have been made to prepare Ce^{+4} complexes of cyclopentadienide by the reaction of NaCp with $[NH_4]_2[Ce(NO_3)_6]$. By carrying out the reaction with molar ratio 1:1 of the reagents, the reduction of Ce^{+4} to Ce^{+3} takes place, and with molar ratio 6:1, $Cp_3Ce(THF)$ in high yield is obtained (Gradeff et al. 1989, Jacob et al. 1988). The same product can be obtained with La, Ce and Nd by reacting $LnCl_3$ and four equivalents of NaCp (Jacob et al. 1989). IR and NMR data suggest the formulation $[(\eta^5Cp)_3Ln(\mu\text{-}\eta^1\text{-}Cp)Na(THF)_n]$. The air and moisture sensitive Cp_3Ln are soluble in polar solvents like THF with formation of the corresponding solvates (see $Cp_3Ln{\cdot}L$) and insoluble or sparingly soluble in aliphatic and aromatic hydrocarbons respectively. The volatility of Cp_3Ln increases with increasing atomic number (Borisov et al. 1973, 1975, Duncan and Thomas 1964, Haug 1971, Devyatykh et al. 1972).

The same trend has been observed from mass spectral and thermochemical studies for the enthalpies of combustion and formation. A decrease of the mean energies of Cp–Ln bonds (Ln = Sc, Y, La, Pr, Tm and Yb) with increasing atomic number has been observed, being approximately 244±21 kJ/mol for ytterbium from mass spectral data (Devyatykh et al. 1973) and ranging from 323 kJ/mol for lanthanum to 214 kJ/mol for ytterbium from thermochemical measurements (Devyatykh et al. 1974). The observation of non-zero dipole moments for unsolvated Cp_3Ln excludes structures with a symmetrical disposition of the three cyclopentadienyl rings around the central lanthanide metal.

The crystal structures of several solvent-free Cp_3Ln (Ln = La, Eggers et al. 1986a, Rebizant et al. 1988; Pr, Hinrichs et al. 1983; Er, Eggers et al. 1986b; Tm, Yb, Eggers et al. 1987; Lu, Eggers et al. 1986c) have been determined by X-ray diffraction analysis. They show, besides a few monomeric structures (Er, Tm, Yb derivatives), different types of polymeric structures (La, Pr, Sm, Lu, Sc). The two forms of Cp_3La, obtained by different purification methods, differ in the crystal packing, one having (Eggers et al. 1986a) La···C short contacts between adjacent molecules in the form of $(\eta^5\text{-}C_5H_5)_2La(\mu\text{-}\eta^5{:}\eta^2\text{-}C_5H_5)$ units, while the second form (Rebizant et al. 1988) can be described as $(\eta^5\text{-}C_5H_5)_2La(\mu\text{-}\eta^5{:}\eta^1\text{-}C_5H_5)$ having one La···C short contact for the bridging Cp to the adjacent molecule (fig. 2).

Structures of compounds with the smaller Sc and Lu are isomorphous and polymeric of a new type represented by $[\eta^5\text{-}C_5H_5)_2Ln(\mu\text{-}\eta^1{:}\eta^1\text{-}C_5H_5]_\infty$. Recrystallization of Cp_3Sm from diethyl ether gave a new modification of Cp_3Sm, containing two crystallographically independent molecules which are bonded to each other by non-valence interactions in a contact dimer (Bel'skii et al. 1991d).

The molecular structure of sublimed Cp_3Pr (Hinrichs et al. 1983) confirms the presence of a singular polymeric chain in the solid involving η^5-coordination of each Pr with three

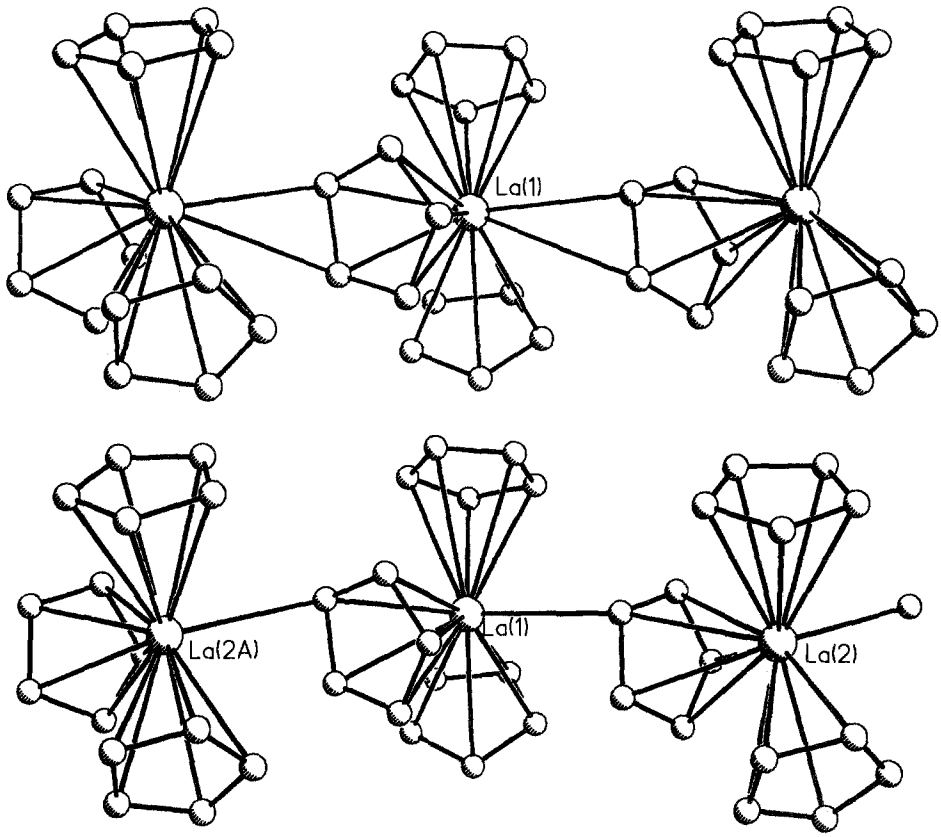

Fig. 2. Crystal structures of the two forms of $[Cp_3La]$ (Eggers et al. 1986a, Hinrichs et al. 1983).

neighboring Cp ligands and η^x-coordination ($1 < x < 2$) with a fourth bridging Cp ligand. These unusual interactions in the solid state are related more to ionicity than to covalency, as confirmed by physical and chemical data that are in favor of a predominance of ionic character. The isostructural Y (Adam et al. 1991), Er and Tm (Eggers et al. 1986b) compounds are monomeric with the closest Ln···C contacts, outside the three rings, greater than 3.14 Å, while Cp_3Yb (Eggers et al. 1987) is mononuclear but not isostructural with Tm and Lu complexes, even though they have ionic radii very close to Yb. The minimum contact distance with the adjacent Cp_3Yb unit of 4.139 Å seems to exclude "chemical" interaction between the metal ion and carbon of adjacent Cp_3Yb molecules, making this compound a rare example of almost ideal D_{3h} molecular symmetry on Yb.

The high degree of ionicity of Cp_3Ln, as shown by their magnetic moments whose values are very similar to those of the corresponding free ions, is due to the contracted nature of the 4f orbitals and their shielding by the 5s and 5p electrons (Tsutsui et al. 1966).

Optical spectra of f^n ions and compounds are characterized by relatively sharp lines due to transitions between energy levels within the f^n configuration and are indicative of

interactions between the f electrons of the ion and their surrounding ligands. The energy level structures of many tricyclopentadienyl lanthanides derived from their optical spectra (Carnall 1979), either in coordinating solvents such as THF and methyltetrahydrofurane or from a sublimed polycrystalline film or glassy melt, show a smaller nephelauxetic effect for the Cp_3Ln than for the transition elements, but a larger nephelauxetic effect than for the corresponding lanthanide chlorides.

The Raman spectra of Cp_3Ln (Ln = Y, Pr, Gd, Tb, Ho, Er and Lu) at room temperature, at 77 K, and in the molten state, show Cp ring vibrations typical for η^5-coordinated ligands, with the intensities of the bands reflecting considerable ionic character of the lanthanide metal to Cp ring bonds (Aleksanyam et al. 1977).

NMR spectroscopy has been widely applied in elucidating the magnetic and dynamic behavior of the Cp_3Ln systems. All the organometallic derivatives of the lanthanides in the oxidation state +3, except Sc, Y, La and Lu, are paramagnetic because of the unpaired f-electrons. Due to their paramagnetism the organolanthanide ^1H NMR spectra give rise to broadened and shifted signals. The extreme line broadening as a consequence of their very long relaxation times precludes the detection of resonances in Gd^{3+} and Er^{3+} species. The isotropic shifts of the organolanthanide compounds are the result of two contributions,

$$\Delta_{iso} = \Delta_{con} + \Delta_{dip}.$$

Δ_{con} is caused by contact interactions of unpaired f-electron spin density with the ligand, while Δ_{dip} is due to the magnetic anisotropy of the molecule, where geometric factors are important. Normally the isotropic shift of the organolanthanide compounds is due mainly to the dipolar contribution (Δ_{dip}) (or pseudo-contact contribution) as the contact contribution (Δ_{con}) is very low because of the very contracted nature of the lanthanide f-orbitals.

The reduction of olefins by Cp_3Ln/NaH systems has shown a decrease in reactivity correlating with the decrease of the ionic radius of the lanthanide ion (Qian et al. 1987). The reductive dehalogenation of aryl and vinyl halides with Cp_3Ln/NaH (Ln = La, Sm, Gd, Y, Lu) systems affords, respectively, the corresponding aromatics and alkenes in excellent yields under mild conditions. However, by using alkyl halides alkylated compounds were obtained, which yield alkyl cyclopentadienes after hydrolysis. A mechanistic hypothesis has been proposed involving a $[Cp_3Ln(\mu\text{-}H)LnCp_3]$ anion which makes a nucleophilic attack on the RX substrate to give the corresponding dimers containing a R-substituted cyclopentadienyl (Qian et al. 1991).

Cp_3Ln compounds (Ln = La, Ce, Pr, Nd, Sm, Eu) in the presence of sodium naphthalenide in THF have been used to reduce N_2 to ammonia (Bochkarev et al. 1987).

Triscyclopentadienyllanthanides readily form stable formally ten-coordinate adducts $Cp_3Ln{\cdot}L$, with many Lewis bases. Normally these adducts are monomeric; the coordinated base molecule prevents the formation of polynuclear species, satisfying the requirement for the metal ion to be coordinatively saturated.

The $Cp_3Ln{\cdot}THF$ adducts (Ln = Y, La, Pr, Nd, Gd and Lu) are isostructural (Rogers et al. 1980, 1981, Benetollo et al. 1984, Fan et al. 1984, Ni et al. 1985), the Cp ligands are η^5 bound to the metal. THF adducts with 2 and 3 THF molecules coordinated are also known (Suleimanov et al. 1982).

The reaction between activated Sm metal and Cp_2Hg in THF produces $Cp_3Sm(THF)$ and not $Cp_2Sm(THF)_2$. In order to obtain a compound of lower oxidation state, it is necessary to treat the Sm^{III} species with potassium in THF, with $KSmCp_3$ formed as a soluble complex. Reinvestigation of the reaction between Cp_2Hg and activated samarium metal in THF/ether revealed the formation of $Cp_3Sm{\cdot}THF$ (Deacon et al. 1985a). Thallous cyclopentadienides (TlC_5H_4–R, R = H, Me) in THF or DME have been used to prepare $Cp_3Ln{\cdot}THF$ (Ln = Ce, Nd, Sm, Gd, Er), Cp_3Ln (Ln = Er, Yb), (Me–C_5H_4)Ln (Ln = Nd, Sm, Gd), Cp_2Yb, $Cp_2Yb{\cdot}DME$ and $(Me–C_5H_4)_2Yb{\cdot}THF$. For Yb, it was observed that Cp_3Yb is reduced by Yb^0 to Cp_2Yb, and Cp_2Yb can be oxidized to Cp_3Yb by TlCp (Deacon et al. 1984a).

The crystal structure of $Cp_3Dy{\cdot}THF$, obtained by the usual method from $DyCl_3$ and NaCp in THF at room temperature, shows that the complex is isostructural with the analogous compounds of La, Pr, Nd, Gd. The THF molecule is coordinated to the dysprosium atom at a Dy–O distance of 2.522(5) Å and the Dy–C(Cp) bond distances range from 2.649(2) to 2.816(9) Å (Ye et al. 1990, Maier et al. 1992a, Wu et al. 1994a).

By using propionitrile as Lewis base, 1:1 and 1:2 adducts Cp_3LnL_n (Ln = La, Pr, Yb; L = CH_3CH_2CN; $n = 1, 2$) have been prepared and characterized by X-ray diffractometry. The Ln ion is η^5 bonded to three Cp ligands and to a propionitrile nitrogen atom. The site symmetry around the trivalent lanthanide ion is approximately C_{3v}. This arrangement is typical of most Cp_3LnX derivatives with ring centroid–metal–ring centroid angles (Cg–M–Cg) in the range 112° to 119°. A significant feature observed in these complexes is the deviation from linearity of the Ln–N≡C–CH_2CH_3 arrangement, the angle Ln–N≡C being 168.3(4)° for La and 171.0(5)° for Yb (fig. 3). As expected, the pseudo-tetrahedral $Cp_3Ln–NCCH_2CH_3$ system is able to accommodate an additional propionitrile molecule to give 1:2 adducts where the stereochemistry of the Ln atom is trigonal bipyramidal with D_{3h} pseudo symmetry for the Ln atom site. The three Cp ligands occupy the equatorial plane and the propionitrile ligands the *trans*-diaxial positions. A bending of about 14° is observed for the axial ligands probably due to steric reasons (Spirlet et al. 1987a,b). The crystal structure of $Cp_3Sm(NCCD_3)$ has also been reported (Rebizant et al. 1990).

Transmetallation reactions of TlCp and $LnCl_3$ have been studied in pyridine, acetonitrile and ether to give $Cp_3Ln{\cdot}L$ (Ln = Nd, Sm, Eu, Yb; L = pyridine) (Ln = Nd, Sm, Yb; L = acetonitrile) (Deacon et al. 1987b). The complex Cp_3Sm(pyridine) was also prepared by ligand exchange, and $Cp_3Eu(THF)$ was synthesized from Eu and $HgCp_2$ in THF. The crystal structures of Cp_3Ln(pyridine) (Ln = Sm, Nd) (Deacon et al. 1987b) differ in pyridine coordination.

The crystal and molecular structures of $Cp_3Pr{\cdot}BA$ (BA = *n*-butylacetate) and $Cp_3Tb{\cdot}$NCMe adducts were determined. In the case of $Cp_3Pr{\cdot}BA$ the individual molecules may be easily oriented in a static magnetic field or in the electric field vector of linearly polarized radiation giving rise to an absorption spectrum of the spin allowed transitions (Schulz et al. 1992a,b).

The absorption spectrum of $(Cp\text{-}d^5)_3Nd{\cdot}THF\text{-}d^8$ has been measured at room and low temperatures. The bands were assigned based on calculations assuming the crystal field parameters of the Nd complex were the same as for the previously analyzed

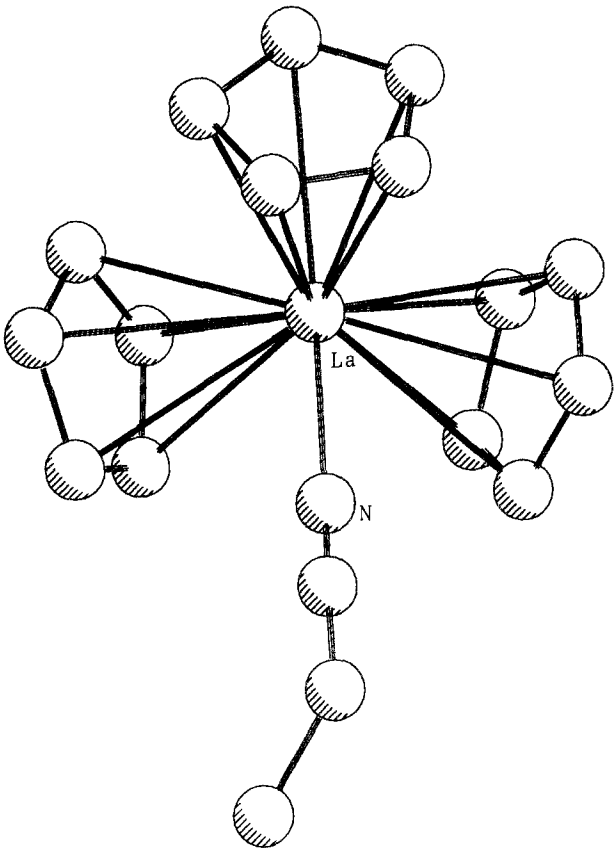

Fig. 3. Crystal structure of $[Cp_3LaNCCH_2CH_3]$ (Spirlet et al. 1987a).

$Cp_3Pr{\cdot}MeTHF$. Making use of the calculated wave functions and eigenvalues, the experimentally determined temperature dependence of μ_{eff} of powdered $Cp_3Nd{\cdot}THF$ and of an oriented single crystal of $Cp_3Nd{\cdot}NCMe$ could be simulated. Assuming that the methyl protons of the γ-picoline ligand of $Cp_3Nd{\cdot}\gamma$-pic and $(MeCp)_3Nd{\cdot}\gamma$-pic, respectively, experience only an NMR shift of dipolar type, the paramagnetic anisotropy was estimated (Reddmann et al. 1991).

The electric dipole moments of a series of organolanthanide compounds including $Cp_3Pr{\cdot}NCC_2H_5$, with a quasi-C_{3v} molecular symmetry and $Cp_3La(NCC_2H_5)_2$ with D_{3h} molecular symmetry were measured in benzene solutions. As expected, the compounds with D_{3h} symmetry do not exhibit a dipole moment, while the compounds with C_{3v} symmetry show a dipole moment higher than 4 D. The experimental values are in good agreement with the values calculated from crystallographic data (Maier et al. 1992b).

The first examples of sterically congested complex type $Cp_3Ln(NCR)_2$ resulted in the molecular structures of the three isomorphous compounds $Cp_3Ln(NCCH_3)_2$ (Ln = La, Ce, Pr) (Li et al. 1985). The complexes show a trigonal bipyramidal coordination geometry

around the metal ion which approximates a D_{3h} symmetry for the Ln atom: the three Cp rings are η^5 bonded in the equatorial plane. The two nitrogen bonded acetonitrile ligands occupy the *trans* diaxial positions.

$Cp_3Ln{\cdot}L$ adducts show a significantly higher solubility in organic solvents than the corresponding base-free species. The THF coordinated molecule of $Cp_3Ln{\cdot}THF$ can be removed in high vacuum from all the complexes except for $Cp_3Eu{\cdot}THF$. Solubility data in THF indicate that the early lanthanides have the greatest solubility.

Extensive ^1H NMR studies have been done with the cyclohexyl isocyanide adducts of Cp_3Ln. In the case of the praseodymium complex, while at room temperature rapid inversion of the cyclohexyl ring gives rise to 7 discrete cyclohexyl proton resonances, by lowering the temperature (−70°C) it has been possible to detect all 13 possible signals for the two slowly inverting conformers (ΔG for the ring inversion = 282±15 cal/mole) (Von Ammon et al. 1971). The electronic structure of Cp_3Ln adducts has been studied by Amberger and Schultze (1987).

^{139}La-NMR studies of oxygen adducts of $Cp_3La{\cdot}L$ (L = DMSO, DMF, $OP(OMe)_3$, and $OCMe_2$) and $[Cp_3LaL_x]^q$ (L = monodentate ligand; $x = 0$–2; $q = 0, -1$) have been reported (Adam et al. 1990a). Magnetic susceptibility measurements and EPR spectra for $Cp_3Yb{\cdot}L$ (L = THF, γ-picoline) were used to determine the spin–orbit coupling constant and crystal field parameters (Amberger et al. 1989). Significant changes in the ligand-to-metal charge-transfer transitions and the f–f transitions in the electronic spectra of Cp_3Yb are observed, when Lewis bases like pyrrolidine, triethylphosphine, THF or tetrahydrothiophene are added to the complex in benzene solution (Schlesener and Ellis 1983). Extensive studies of the absorption spectra of adducts of Cp_3Yb with a number of organic phosphines and isocyanides demonstrate that the shifting of the long-wave charge-transfer band as well as the changes of the $^2F_{5/2}$ term appear to be governed less by the basicity of the ligands than by essentially steric influences. Vibronic coupling in $Cp_3NdMe(THF)$ was studied in order to separate the vibronic and electronic transitions in $Cp_3Yb(CNC_6H_{11})$ and $Cp_3Yb{\cdot}(MeTHF)$ (Amberger et al. 1989).

The absorption spectrum of a $Cp_3Nd(NCCH_3)_2$ single crystal has been measured using liquid N_2 as coolant. From these data a truncated crystal field splitting pattern could be derived. The parameters of an empirical Hamiltonian were fitted the energies of 41 levels to give an r.m.s. deviation of 26 cm^{-1} (Schulz et al. 1992a,b). Some organolanthanide complexes with anions bridging two neutral Cp_3Ln unities such as $[Na(THF)_6][Cp_3Lu{-}H{-}LuCp_3]$ (Schumann et al. 1986a), $[Li(DME)_3][Cp_3Sm{-}Cl{-}SmCp_3]$ (Schumann et al. 1988a), $[NR_4][Cp_3Pr{-}X{-}PrCp_3]$ with $X = NCBH_3$ and NCS (Jahn et al. 1984), $[Li(DME)_3][Cp_3Nd{-}H{-}NdCp_3]$ (Sun et al. 1991) could be included in the general class $Cp_3Ln{\cdot}L$. By reacting $Cp_3Sm{\cdot}THF$ with lithium azide in dimetoxyethane (DME), the dimeric $[Li(DME)_3][(Cp_3Sm)_2(\mu{-}N_3)]$ (fig. 4) obtained has the azido group bridging the two Cp_3Sm units, as determined by X-ray crystallography (Schumann et al. 1988b).

2.1.2.2. *Actinides.* The synthesis of trivalent uranium Cp_3U can be carried out by different methods (Marks and Ernst 1982), for example by reduction of several U^{IV} derivatives or by photo-induced β-hydride elimination of tris-cyclopentadienyl uranium(IV)isopropyl

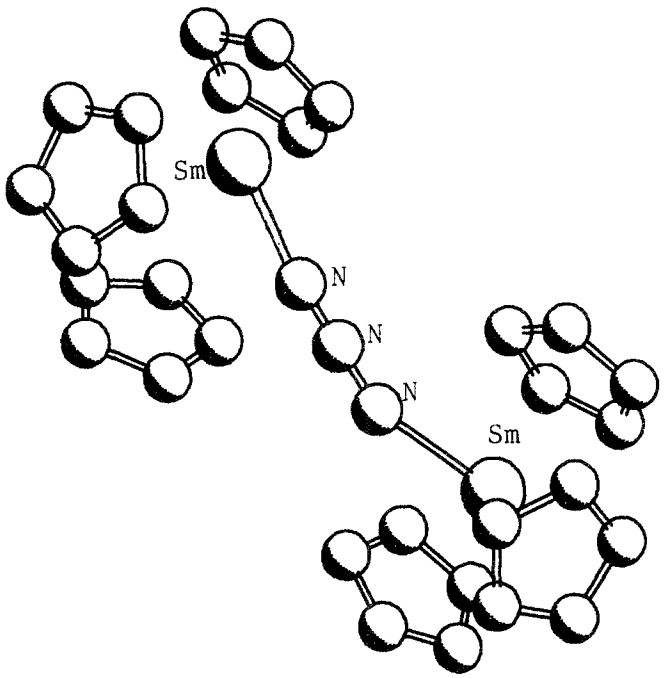

Fig. 4. Crystal structure of the anion $\{[Cp_3Sm]_2(\mu\text{-}N_3)\}^-$ (Schumann et al. 1988b).

(Bruno et al. 1982a,b). The high Lewis acidity of Cp_3U favors the formation of adducts with a variety of Lewis bases analogously to the corresponding lanthanide derivatives. Crystals of $Cp_3U{\cdot}THF$, suitable for a X-ray structure determination, have been obtained by reaction of $U[N(SiEt_3)_2]Cl_2$ with two equivalents of NaCp in THF (Wasserman et al. 1983). The THF adduct is isostructural to the analogous lanthanides $Cp_3Ln{\cdot}THF$ and shows, as usual for this class of compounds, distorted tetrahedral arrangement of THF and η^5-Cp ligands. From the value of U–O distance of 2.551(10) Å the authors suggest a radius for U^{3+} of 1.20 Å, in this class of compounds. In the reaction with $Cp_3U{\cdot}THF$, the potentially bidentate chelating phosphine, $Me_2PCH_2CH_2PMe_2$, acts as a bridging monodentate ligand towards each trivalent U atom, probably for steric reasons. In fact the molecular structure (fig. 5) shows that "the molecule is economically arranged in this *trans* conformation of the phosphine ligand". The U–P distance is 3.022(2) Å (Zalkin et al. 1987a). The synthesis of Cp_3Th with thorium in the rather unusual trivalent oxidation state has been made, as for Cp_3U, by reduction of Th^{IV} derivative with various reductant reagents (Marks and Ernst 1982) or from Cp_3Th–^{i}Pr (or Cp_3Th–^{n}Bu) in benzene solution via the photochemical β-hydride elimination with the sequence of reactions as for the uranium derivative (Bruno et al. 1982a,b). The green Cp_3Th was completely characterized by a series of physico-chemical measurements including the oxidative additions of iodine to form the known Cp_3ThI

$$Cp_3Th + \tfrac{1}{2}I_2 \xrightarrow{\text{benzene}} Cp_3ThI,$$

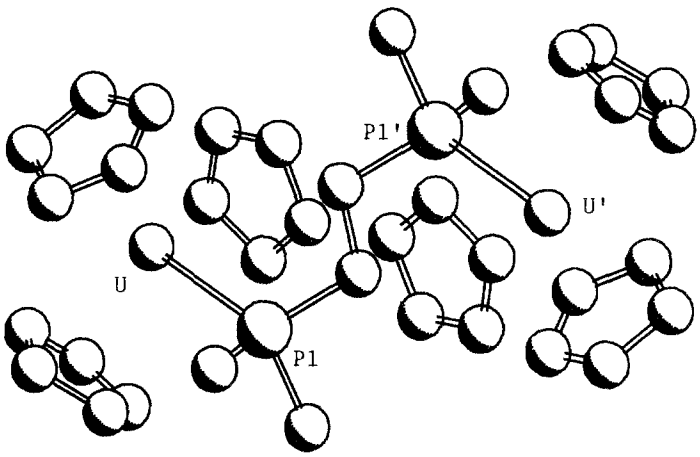

Fig. 5. Crystal structure of $[(Cp_3U)_2(Me_2P(CH_2)_2PMe_2)]$ (Zalkin et al. 1987a).

and of MeOH to form $Th(OMe)_4$ with the liberation of 0.5 mole of H_2. Magnetic measurements at room temperature show $\mu_{eff} = 0.404\mu_B$.

Quasi-relativistic Xα-scattered wave calculations on $Cp_3An{\cdot}L$ compounds with L = H, CO, NO, OH, led to the conclusion that sigma bonding to the π-neutral, π-acidic, and π-basic ligands has essentially the same donation of electron density from the sigma orbital of the L ligand into a uranium orbital that is primarily $6d_{z^2}$ in character. The 5f orbitals are responsible for back donation into the π^* orbitals of CO and NO. Acceptance of electron density from the π orbitals of OH involves the 6d orbitals (Bursten et al. 1989).

Results for Cp_3An (An = Pa, Np, Pu, Am, Cm, Bk, Cf) (Strittmatter and Bursten 1991) show that the 5f-orbital energy drops across the series while the 6d-orbital energy rises. Due to the greater radial extension of the 6d orbitals, the metal 6d orbitals are more important in bonding the Cp ligands than the 5f orbitals.

2.1.3. *Cp'_3M and Cp'_3ML (with substituted cyclopentadienyls)*

2.1.3.1. *Lanthanides.* Several studies have been done with the aim of reducing the molecularity of the triscyclopentadienyllanthanides by introducing alkyl substituents of increasing steric hindrance into the cyclopentadienyl rings. The Cp'_3Ln compounds, where Cp′ is an alkyl substituted cyclopentadienyl ring, have been prepared by following the same synthetic approach as those containing unsubstituted cyclopentadienyls:

$$LnCl_3 + 3Cp'Na \rightarrow Cp'_3Ln + 3NaCl.$$

Reaction of $LaCl_3$ with excess of Na(MeCp) in THF, followed by vacuum sublimation, yields $(MeCp)_3La$, which crystallizes as tetramer (Xie et al. 1991a). This structure differs significantly from that of Cp_3La. The methyl substituent on the cyclopentadienyl ring forces the mode of coordination from an $\eta^2{:}\eta^5$ polymer for Cp_3La to an $\eta^1{:}\eta^5$ tetramer

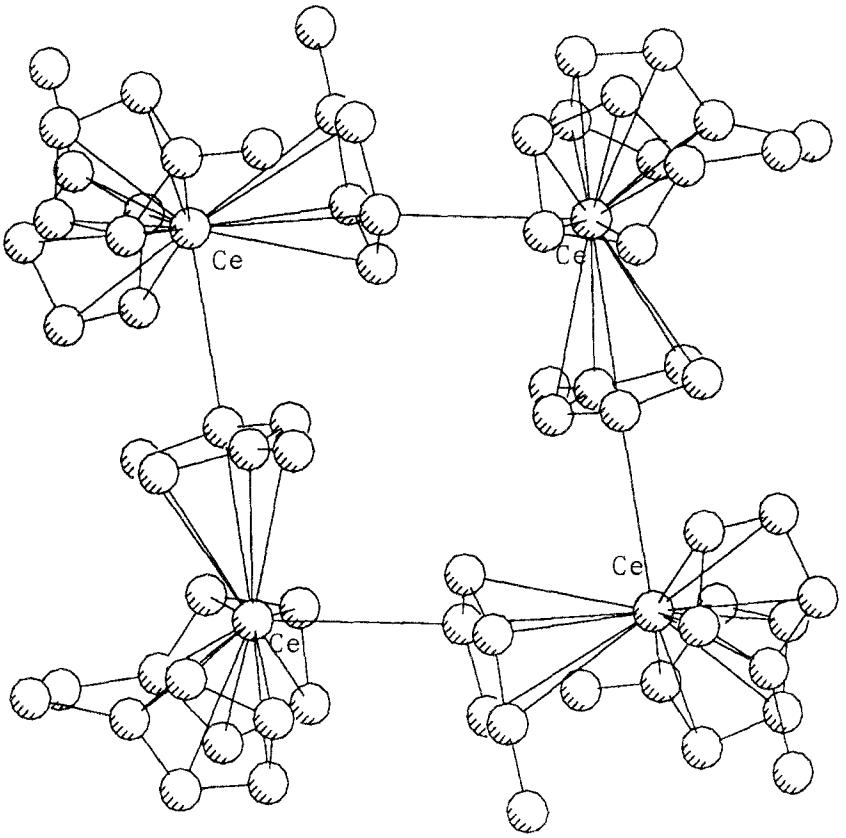

Fig. 6. Crystal structure of the tetramer $[(MeCp)_3Ce]_4$ (Stults et al. 1990a).

for $(MeCp)_3La$. The geometry of tetrameric $(MeCp)_3La$ is nearly identical with those of its cerium (Stults et al. 1990a) (fig. 6) and neodymium (Burns et al. 1974) analogs. The η^1-C–Ln distance is 3.018(7) Å for La, 3.03(3) Å for Ce and 2.984(3) Å for Nd. In contrast, $(MeCp)_3Yb$ is a monomer (Hammel et al. 1989). $(MeCp)_3Yb$ was used as a source of Yb in the growth of highly doped InP:Yb layers by organometallic vapor phase epitaxy (Weber et al. 1988).

A complete mass spectral fragmentation pattern common to base-free Cp'_3Ln, where $Cp' = MeC_5H_4$ and Ln = La, Pr, Nd, Tm, or Yb, shows the easy intramolecular migration of a methyl H atom to Ln or a Ln-bonded C_5H_4, resulting possibly in ring enlargement to C_6H_6 (Paolucci et al. 1988).

All the binary metallocenes $(RCp)_3Ln$ form 1:1 complexes with isocyanides and organocyanides and the structures of $(MeCp)_3Ce(CNCMe_3)$ and $[(Me_3Si)_2C_5H_3]_3Ce(CNCMe_3)$ have been determined (Stults et al. 1990a).

The trimethylphosphine adduct, $(MeCp)_3Ce{\cdot}PMe_3$, has been prepared by reaction of $(MeCp)_3Ce(THF)$ with PMe_3 in diethyl ether and recrystallized from diethylether at

253 K (Stults and Zalkin 1987). The structure consists of Ce-centered mononuclear units in which the Ce atom is η^5-coordinated to three cyclopentadienyl rings and to the phosphorus atom of the trimethylphosphine molecule. The compound is isomorphous with the uranium(III) analog (Brennan and Zalkin 1985) even though there are significant structural differences among the two complexes. The phosphite adduct, $(MeCp)_3Ce[P(OCH_2)_3C_2H_5]$, is also isostructural with the uranium(III) analog (Brennan et al. 1988a) and shows the usual coordination geometry, close to tetrahedral with three sites occupied by the ring centroids and the fourth position by the Lewis base. There is also analogy in the bond distances and angles confirming that the ionic radii of trivalent uranium and cerium are identical for molecules with the same coordination number. The main difference between the uranium and cerium complexes is the existence of a π bonding contribution in the U–P bond.

$(RCp)_3Gd$ (R = isopropyl), prepared by reaction of $GdCl_3$ and the sodium salt of the ligand, was used in the synthesis of high purity Gd_2O_3 (Makhaev et al. 1990). The Er analog was used to grow Er doped indium phosphide layers (J. Weber et al. 1990). With more sterically demanding substituents, the binary metallocenes $(Me_3SiCp)_3Ce$, $(^tBuCp)_3Ce$ and $[(Me_3Si)_2C_5H_3]_3Ce$ are monomeric in the gas phase and in the solid state.

The structure of the latter compound is based upon a trigonal-planar geometry (Stults et al. 1990a). Other complexes of monosubstituted cyclopentadienide ligands include $(^tBu\text{-}C_5H_4)_3La(THF)$, $(^tBu\text{-}C_5H_4)_3Sm$, which have been prepared according to the equation (Wayda 1989):

$$LnCl_3 + 3Na^tBu\text{–}C_5H_4 \xrightarrow{THF} \left(^tBu\text{–}C_5H_4\right)_3 Ln \cdot (THF)_x + 3NaCl,$$

where Ln = La; $x = 1$; Ln = Sm; $x = 0$.

By reacting SmI_2 and $Na^tBu\text{-}C_5H_4$ the compound $Na[(\eta^5{:}\eta^2\text{-}Cp^tBu)_3Sm{\cdot}THF]$ has been obtained, whose crystal structure is a polymer (average Sm–C bond distances: 2.89 Å) (Bel'skii et al. 1990).

The introduction of the Me_3Si substituent in the Cp ligand as in $(Me_3Si)_2C_5H_3$ (Lappert et al. 1981a) allowed, with its steric bulkiness and solubility, the development of the early lanthanide chemistry. Structural characterizations of the complexes $[(Me_3Si)_2C_5H_3]_3M$ (M = Th, Sm, Ce) show for all the complexes a trigonal arrangement of the ligand centroids around the metal ion (Evans et al. 1990a). Th and Sm complexes are also isostructural. The Sm–C(Cp) distance varies from 2.698(5) to 2.807(5) Å (the longest distance involves the carbon atom between the two carbons bearing the substituents Me_3Si). This trend is not observed in the Th analogs where the Th–C(Cp) range is 2.77(3)–2.85(2) Å and in particular no regular pattern is associated to the carbon sterically crowded positions. All of the binary metallocenes form 1:1 complexes with isocyanides and organocyanides, and the crystal structures of two of them have been determined: $(MeCp)_3Ce(CNCMe_3)$ and $[(Me_3Si)_2C_5H_3]_3Ce(CNCMe_3)$ (Stults et al. 1990a).

The $[(Me_3C)_2C_5H_5]_3Ce$ analog (Sofield and Andersen 1995) has been obtained from cerium triflate and $[(Me_3C)_2C_5H_3]_2Mg$ (in ratio 1:1.5). The same reaction with

$[(Me_3C)_2C_5H_3]_2Mg$ gives also the described Me_3Si ring-substituted Ce derivative. The two compounds are not isomorphous but the coordination geometries around Ce are the same. $LaCl_3$ reacts with $TlC_5H_4PPh_2$ ($TlCp'$) and NaCp in the molar ratio 1:2:1 to give the bidentate, monomeric tris(cyclopentadienyl)lanthanum derivative $CpLa(C_5H_4PPh_2)_2(THF)$. The X-ray crystal structure of the complex indicates a distorted tetrahedral geometry around the La atom (Schumann et al. 1992a).

An even more crowded system is present in the first tris-pentamethylcyclopentadienyl lanthanide complex Cp^*_3Sm obtained (Evans et al. 1991a) as byproduct of the reaction

$$2\,(C_5Me_5)_2\,Sm + COT \rightarrow (C_5Me_5)_3\,Sm + (C_5Me_5)\,Sm\,(COT).$$

In the solid state the complex is monomeric as is the less crowded complex $(C_5Me_4H)_3La$ (Schumann et al. 1993d). An improved synthesis (Evans et al. 1996) makes use of $(C_5Me_5)_2Sm(OEt_2)$ and $(C_5Me_5)_2Pb$ for obtaining Cp^*_3Sm in >90% yield. This route allowed also the synthesis of the crowded $(C_5Me_4Et)_3Sm$ derivative

$$(C_5Me_4Et)_2\,Sm\,(OEt)_2 + (C_5Me_5)_2\,Pb \rightarrow (C_5Me_4Et)_3\,Sm + Pb.$$

The crystal structure of the latter is characterized by a trigonal planar geometry around Sm as in Cp^*_3Sm, with a $Sm–C_{(C_5Me_4H)}$ average distance of 2.834 Å, the largest to date for $Sm^{III}(C_5R_5)_3$ derivatives.

The introduction of the modified Cp with a pendant chain containing one oxygen donor atom as $H_3COCH_2CH_2C_5H_4$ ($=Cp^0$) (Qian et al. 1992, Deng et al. 1993) allows the synthesis of Ln derivative Cp^0_3Ln (Ln = La, Pr, Nd, Sm, Gd) due to the possibility to saturate the metal ion with the oxygen additional coordination position. The crystal structure of the La derivative (Deng et al. 1993) shows a trigonal bipyramidal coordination geometry around the metal ion with formal coordination number 11.

2.1.3.2. *Actinides.* Trivalent uranium forms compounds of the type $(R\text{-}C_5H_4)_3U(L)$ where R is either H or CH_3 and L is a Lewis base such as THF (Wasserman et al. 1983), tetrahydrothiophene (Zalkin and Brennan 1985), 4-dimethylaminopyridine (Zalkin and Brennan 1987), trimethylphosphine (Brennan and Zalkin 1985), or 1,2-bis(dimethylphosphino)ethane (Zalkin et al. 1987a, Brennan et al. 1987a). All of the molecules may be described with a distorted tetrahedral stereochemistry. $(MeCp)_3U{\cdot}PMe_3$ represents an example of a short U^{III}–P bond distance, 2.972(6) Å, and of considerable distorted geometry of the three pentahapto-coordinated MeCp ligands. The Cg–U–Cg angles are 106.0, 109.8 and 119.4°; while in the $(MeCp)_3U{\cdot}THF$ derivative, the Cg–U–Cg angles are close to 118° (Zalkin et al. 1985).

In $(MeCp)_3U{\cdot}P(OCH_2)_3CC_2H_5$ (Brennan et al. 1988a) the short U–P bond distance of 2.988(6) Å, comparable to 2.972(6) Å in $(MeCp)_3U{\cdot}PMe_3$, has been rationalized in terms of U–P π-back bonding.

The structures of $(MeCp)_3U{\cdot}NH_3$ (Rosen and Zalkin 1989), $(MeCp)_3U{\cdot}N(CH_2CH_2)_3$-CH (Brennan et al. 1988a) and $(MeCp)_3U(NC_5H_4\text{-}4\text{-}NMe_2)$ (Zalkin and Brennan 1987)

represent other examples of pseudotetrahedral geometry around the U atom. The large variation in the U–N bond distances in the order $2.61(2)_{av.}$, 2.764(4) and $2.64(2)_{av.}$ Å reflects the different steric demands of the ligands. The Cg–U–Cg angular values (117° on average) reflect the tendency towards a trigonal pyramidal geometry for these compounds, increasing the size of the substituent on the cyclopentadienyl ring to Me_3Si the monomeric base-free $(Me_3Si\text{-}C_5H_4)_3U$ derivative has been obtained (Zalkin et al. 1988a) whose crystal structure shows the U atom η^5-bonded to the three cyclopentadienyl rings and in the plane of the ring centroids.

Reduction of $[\{(Me_3Si)_2C_5H_3\}_2ThCl_2]$ with Na–K in toluene produces $[(Me_3Si)_2\text{-}C_5H_3]_3Th^{III}$, which is monomeric in the solid state (Blake et al. 1986a, Blake et al. 1987) and different from the dimeric structure of $(Cp_3Th)_2$ (Baker et al. 1974). Its EPR spectrum suggests that the Th^{III} has a $6d^1$ ground state (Kot et al. 1988).

The first preparation at a normal temperature of a molecular carbonyl complex of uranium has been reported, and the IR stretches of ^{12}CO $\nu CO = 1976\,cm^{-1}$ and ^{13}CO $\nu CO = 1935\,cm^{-1}$ support the formulation $(Me_3SiC_5H_4)_3U(CO)$ (Brennan et al. 1986a). The compound, Cp'_3U, reversibly absorbs CO in solution and in the solid state. Calculations for the species $Cp_3U(CO)$ and $[Cp_3U(CO)]^+$ show that there is extensive $5f^2$ π-back bonding (Bursten and Strittmatter 1987). The relative affinity of Lewis bases towards $(MeCp)_3U$ indicated the trend: $PMe_3 > P(OMe)_3 > NC_5H_5 > SC_4H_8 \approx THF \approx N(CH_2H_2)_3CH > CO$.

2.1.4. *Cp_3MX (lanthanides and actinides)*

2.1.4.1. *X = halide.* Triscyclopentadienyl cerium(IV) chloride has been prepared by reaction of sodium cyclopentadienide and bis(pyridinium)hexachlorocerate in THF or benzene, or by ligand redistribution between bis(pyridinium)hexachlorocerate and tetracyclopentadienyl cerium (Kalsotra et al. 1971). These brown compounds, described as stable in water, act as starting materials for Cp_3CeZ (Z = alkyl, aryl, pseudohalide, mercaptide, carboxylate) (Marks and Ernst 1982).

The red-brown Cp_3UCl has been the first organoactinide compound to be synthesized (Reynolds and Wilkinson 1956) by reacting uranium tetrachloride and sodium cyclopentadienide in THF:

$$UCl_4 + 3NaCp \xrightarrow{THF} Cp_3UCl + 3NaCl.$$

Although uranium metal does not react directly with TlCp in THF, transmetallation may occur with uranium activated in situ by reaction with $HgCl_2$ to give Cp_3UCl. Alternatively, Cp_3UCl can be obtained from uranium metal and $HgCp_2/HgCl_2$ (Deacon and Tuong 1988).

$$2U + 6TlCp + HgCl_2 \xrightarrow{THF} 2Cp_3UCl + Hg + 6Tl,$$

$$2U + 3HgCp_2 + HgCl_2 \xrightarrow{THF} 2Cp_3UCl + 4Hg.$$

Cp_3UCl is one of the most widely used starting material for the preparation of many other Cp_3U–Z derivatives (Z = alkyl, aryl, alkynyl, allyl, alkoxide, amide, etc.). In contrast to the

behavior of Cp_3Ln, it has been shown that Cp_3UCl does not react with $FeCl_2$ to produce ferrocene, thus suggesting a greater covalency in the U^{IV}–C(ring) bonding.

The reaction of Cp_3UCl and $K[L_2ReH_6]$ affords $L_2ReH_6UCp_3$ ($L = PPh_3$, $P(p\text{-}FPh)_3$) containing hydride bridged heterobinuclear compounds (Baudry and Ephritikhine 1986) (see sect. 2.5.2). There is a large difference between the chemical shifts for the ^1H NMR of Cp_3UCl in the solid state and in solution, which implies a difference in molecular geometry in the two states (McGarvey and Nagy 1987).

The X-ray crystal structure of Cp_3UCl (Wong et al. 1965) showed a tetrahedral distorted geometry around the metal ion of approximate C_{3v} symmetry, with a U–Cl bond distance of 2.559(16) Å in the direction of the three-fold axis. The neutron diffraction crystal structure of Cp_3UCl shows disorder of the Cp rings and crystallographic phase transition between 80 and 100 K (Delapalme et al. 1988, 1994). Cp_3UBr is geometrically equivalent to Cp_3UCl but not isostructural (Spirlet et al. 1989) although both have the same pseudo-tetrahedral coordination geometry around the uranium atom as well as the analogous fluorine (Ryan et al. 1975) and iodine (Rebizant et al. 1992a) derivatives. No variation is observed in the coordination geometry and in the U–C bond distances ($2.73(4)_{av.}$ Å) when the halide is substituted with thiocyanate in $Cp_3U(NCS)$ (Spirlet et al. 1993a). The crystal field splitting pattern of $(\eta^5\text{-}C_5D_5)_3UCl$ has been determined from the absorption and magnetic circular dichroism spectra at room temperature (Amberger et al. 1988). The ^1H NMR spectra of solid powders of Cp_3UCl from 90 to 298 K showed that anisotropy in the line shape became more evident as the temperature was lowered. Below 140 K rotation of the Cp rings appeared to cease (McGarvey and Nagy 1987).

Cyclic voltammetry on Cp_3UCl ($E_{1/2} = -1.80$ V vs Fc/Fc+) and Cp_3NpCl ($E_{1/2} = -1.29$ V vs Fc/Fc+) shows a single reduction wave exhibiting the characteristics of a one-electron reversible process. The more negative the M^{IV}/M^{III} couple, the greater the stability of the M^{IV} state with respect to M^{III} (Sonnenberger and Gaudiello 1988). The bridging complexes $Cp_3U(\mu\text{-}Cl)_2AlCl_2$ and $Cp_3U(\mu\text{-}Cl)_2AlCl_2(THF)$ have been prepared by reaction of Cp_3UCl and $AlCl_3$ (Chang et al. 1987). The $[Na(18\text{-crown-}6)(THF)_2][(Cp_3U)_2Cl_2]$ compound was prepared by amalgam reductions of Cp_3UX (X = Cl, BH_4, Me, ^{n}Bu). The crystal structure of the anion revealed a symmetrical bent chloro bridge (Le Maréchal et al. 1989a).

The average heats of formation and U–Cl, U–C, and U–O bond cleavage for the Cp_3UX compounds (X = Cl, CH_2CHMe_2, OBu) have been determined (Tel'noi et al. 1989).

By oxidative addition of organic halides RX to $Cp_3U(THF)$, an equimolar mixture of Cp_3UX and Cp_3UR compounds was obtained:

$$2Cp_3U(THF) + RX \xrightarrow{THF} Cp_3UX + Cp_3UR,$$

where R = Me; X = I; R = ^{n}Bu; X = Cl, Br, I; R = ^{i}Pr; X = Cl; R = $PhCH_2$; X = Cl; R = $CH_2{=}CHCH_2$; X = Cl.

The alkyl derivatives were also prepared by reaction of Cp_3UCl with RX in the presence of Na/Hg (Villiers and Ephritikhine 1990).

2.1.4.2. *X = hydrocarbyl.* Dark brown compounds $Cp_3Ce–R$ (R = hydrocarbyl) have been prepared by reaction of the triscyclopentadienylcerium chloride and either organolithium or Grignard reagents in THF (Marks and Ernst 1982). It seems surprising that reduction to cerium(III) did not occur in these reactions in spite of the severe conditions used (prolonged reflux) and of the instability of the products formed.

The anionic triscyclopentadienylneodymium(III) phenyl, $[Cp_3Nd(C_6H_5)][Li(DME)_3]$ has also been isolated (Gao et al. 1989) by reaction of $NdCl_3 \cdot 2LiCl$ with 2 equivalents of NaCp and successive reaction of the $Cp_2NdCl \cdot 2LiCl$ formed with one equivalent of phenyllithium at −78°C. Differently from the anionic $[Cp_3Pr–{}^nBu]^-$, obtained by reacting Cp_3Pr and *n*-butyllithium in THF, the reaction of $Cp_3Nd \cdot THF$ with phenyllithium shows only the reactants. The X-ray crystal structure of $[Cp_3Nd(C_6H_5)][Li(DME)_3]$ at −80°C shows that the complex consists of disconnected ion pairs of $[Li(DME)_3]^+$ and $[\eta^5\text{-}C_5H_5)_3NdC_6H_5]^-$. The neodymium atom is connected to three η^5-bonded cyclopentadienyls and one σ-bonded phenyl in a distorted tetrahedral arrangement with Nd–C(σ) 2.593(17) (Gao et al. 1992).

Alkylation and arylation of Cp_3UCl with lithium or Grignard reagents afford tricyclopentadienyluranium(IV) hydrocarbyls (Marks and Ernst 1982):

$$Cp_3UCl + RMgX \text{ (or } RLi) \rightarrow Cp_3UR + MgXCl \text{ (or } LiCl),$$

where R = Me, ^{n}Pr, ^{i}Pr, ^{n}Bu, ^{t}Bu, neopentyl, ferrocenyl, allyl, 2-methallyl, vinyl, Ph, C_6F_5, *p*-$C_6H_4UCp_3$, C≡CH, C≡CPh, *p*-tolyl, benzyl, 2-*cis*-2-butenyl, 2-*trans*-2-butenyl, $(C_5H_4)Fe(C_5H4)UCp_3$.

The reaction of Cp_3UCl with an equimolar amount of $Li(CH_2)(CH_2)PMe_2Ph$ affords the green complex $Cp_3UCHPMe_2Ph$ in good yield (Cramer et al. 1981). The unusual mode of ylide–metal bonding suggested by this formulation differs from other structurally characterized uranium–phosphoylid complexes (Cramer et al. 1978, 1980) in that the carbon atom attached to the uranium is tri- rather than tetra-coordinated. The peculiarity of this structure is the short U–C(1) bond 2.29(3) Å which is the shortest uranium to carbon reported, suggesting for it a multiple-bond character as in the analogous $Cp_3UCHPMe_3$ (Cramer et al. 1988a) with a U–C(σ) bond distance of 2.274(8) Å. The activation of CO by the U–C double bond in Cp_3UCHPR_3 is a confirmation of the multiple character of this bond (Gilje and Cramer 1987). A neutron diffraction study at 20 K on the same compound (Stevens et al. 1990) confirms the results of the previous X-ray study. In particular, allowing the location of the α-hydrogen H(1), there is no indication of agostic interaction with the uranium atom.

Analogous triscyclopentadienyl thorium(IV) hydrocarbyls were prepared (Marks and Ernst 1982) by reaction of Cp_3ThCl with lithium or Grignard reagents. Triscyclopentadienyl uranium(IV) and thorium(IV) hydrocarbyls are extremely air sensitive but very thermally stable compounds.

Magnetic susceptibility studies on Cp_3UR derivatives show approximate Curie–Weiss behavior down to 70 K, while at lower temperatures, temperature-independent paramagnetism is observed. This behavior could be assigned to appreciable distortion

of the U^{IV} environment from tetrahedral symmetry (splitting of the triply degenerate ground state energy level) and is in contrast to the results obtained for Cp_4U. In the case of the bimetallic derivative Cp_3U-*p*-C_6H_4-UCp_3, levelling off of the susceptibility at low temperatures is not observed. Probably this phenomenon could be due to fortuitous equality of the ligand field strengths of the four groups around the uranium ion or to an exchange coupling between the metal ions occurring through the bridging ligands. NMR spectroscopy is extremely useful in structural and dynamic studies and provides extensive information on 5f spin delocalization in Cp_3UR derivatives (Marks and Ernst 1982). Variable temperature ^1H NMR spectra of Cp_3U(allyl) indicate the presence of an instantaneous η^1-allyl structure and also that a very low barrier ($\Delta G^{\neq} \approx 34\,kJ\,mol^{-1}$) exists for sigmatropic rearrangement of this structure. Variable temperature ^1H NMR experiments on Cp_3U^iPr provide quantitative information on the degree of steric congestion around the uranium ion. In fact at room temperature the three Cp ligands are magnetically equivalent, while at low temperature they are split in two signals with a ratio 2:1. This behavior could be explained in terms of restricted rotation around the U–C σ-bond (the energy barrier for this process is ca. $42\,kJ\,mol^{-1}$). The results for the Cp_3UR compounds indicate that the ligand molecular orbitals bearing the unpaired spin density in the uranium organometallics are predominantly the same as those bearing the unpaired spin density in the free radicals.

In comparative alcoholysis reactions of triscyclopentadienyl-uranium and -thorium hydrocarbyls, no cleavage of η^5-bonds is observed in the thorium system until η^1 cleavage is complete, while for uranium, η^5 and η^1 cleavages are competitive.

A detailed study of thermolysis pathway(s) in solution (Marks and Ernst 1982) has shown that the Cp_3ThR complexes are more stable than the corresponding uranium(IV) complexes. The general order of stability as a function of R is primary > secondary > tertiary. The $R = C_6F_5$ complexes are some of the least thermally stable. In the U and Th derivatives intramolecular abstraction of a ring hydrogen atom occurs with retention of stereochemistry at the carbon atom bound directly to the actinide ion.

The absence of the β-hydride elimination reaction as a thermolysis pathway is a striking feature of Cp_3UR and Cp_3ThR chemistry, and is an important contributing factor to their high thermal stability. Indeed, when the saturation is reduced as in the "MR_4" and $Cp^*_2MR_2$ ($Cp^* = \eta^5$-pentamethyl cyclopentadienyl) compounds, the β-hydride elimination reaction is thermally accessible. These reactivity constraints do not extend to photochemical activation, and Cp_3MR compounds undergo facile β-hydride elimination under photolytic conditions (Paolucci et al. 1984):

$$Cp_3MCHMe_2 \xrightarrow{h\nu,\ \text{benzene}} Cp_3MH + CH_2{=}CHMe,$$

$$Cp_3MH + Cp_3MCHMe_2 \rightarrow 2Cp_3M + C_3H_8 \quad (M = Th,\ U).$$

For the complexes Cp_3ThR ($R = {}^i$Pr or ^{n}Bu), $(MeC_5H_4)_3Th({}^n$Bu), and (indenyl)Th(^{n}Bu), UV photolysis in aromatic solvents produces 1:1 mixtures of alkane:alkene and Cp_3Th, and a photoinduced β-hydrogen elimination mechanism is proposed. In the corresponding

U compounds a similar β-hydrogen elimination with Cp_3U formation also occurs but H-abstraction from C_5H_5 rings constitutes the major pathway to decomposition (Bruno et al. 1982a,b).

By reacting $Cp_3U^{IV}R$ (R = ^{n}Bu or Ph) with R′Li (R′ = Me, ^{n}Bu, Ph) the corresponding anion $[Cp_3U^{III}–R']^-$ with lithium inserted in a macrocycle in the stoichiometry 1:1 is formed (Arnaudet et al. 1986). Crystals of $[Cp_3U^{III}\text{-}C_4H_9]^-[LiC_{14}H_{28}N_2O_4(2.1.1)]^+$ suitable for X-ray structure determination were obtained by slow diffusion in a small volume of THF of two separate solutions of Cp_3U-^{n}Bu Li and $C_{14}H_28N_2O_4(2.1.1.)$ through porous sintered glass. The U^{III} atom lies at the center of a distorted tetrahedron with three π-bonded η^5-cyclopentadienyls and σ-bonded to the *n*-buthyl group. Cg–U–Cg (av.) angle is 117°, greater than the ideal tetrahedral values, whereas Cg–U–U–C(^{n}Bu) angles range from 97° to 101°. These angular distortions are considered a consequence of the Cp ligands steric hindrance. Similar distorted tetrahedral coordination geometries are reported for $Cp_3U(CH_2\text{-}C_6H_4\text{-}p\text{-}CH_3)$ and Cp_3U–^{n}Bu.

A systematic molecular orbital study of the electronic and geometric structures of Cp_3U complexes suggests (Tatsumi and Nakamura 1984) a strong covalency in U–C(alkyl) σ bonds and weak covalency in the case of U–Cp π bonds consistent with the observations of Hoffmann and Tatsumi (Tatsumi and Hoffmann 1984) on the systems $[Cp_3UMe]^{2+}$ and $[Cp_3UCO]^{3+}$, where, although no strong π back-donation is expected for an actinide carbonyl interaction, there is a good chance of obtaining such compounds. Partial multiple bond character was indicated in Cp_3U–$CHPR_3$ and Cp_3U–CCR bonds.

In the case of Cp_3U(THF), LiR can be used reversibly to add alkyl groups or exchange one for another in Cp_3UR. Dihydrogen can also be used in conjunction with a terminal alkene ($R'CH_2$) to achieve this replacement of one alkyl group (R) by another ($R'CH_3$) (Foyentin et al. 1987a,b). The alkyne complex Cp_3U–C≡CPh was obtained by reaction of Cp_3U(THF) with HC≡CPh.

When Cp_3UMe is treated with BPh_3 a 1:1 adduct is formed in which the BPh_3Me unit is loosely coordinated. A similar adduct, Cp_3UBPh_4, can be obtained by the dehydration of $[Cp_3U(H_2O)_2][BPh_4]\cdot xH_2O$ (Aslan et al. 1988a).

Anionic complexes [Na(18-crown-6)][Cp_3UR] (R = Me, ^{n}Bu) were obtained by Na/Hg reduction of Cp_3UR (Le Maréchal et al. 1988).

To evaluate the geometric control in organometallic f-element compounds, the steric hindrance on the structure and chemistry of Cp_3M compounds has been studied, by using Cp_3UMe as model (Li et al. 1986).

2.1.4.3. *X = non-halide, non-hydrocarbyl.* Cp_3CeCl has been used as starting material for the synthesis of a number of triscyclopentadienyl cerium(IV) derivatives (Marks and Ernst 1982):

$$Cp_3CeCl + MZ \rightarrow Cp_3CeZ + MCl,$$

where M = Na or K; Z = N_3, NCS, CN, NCO; or NO_2, ONO_2; or SCH_3, SC_2H_5, SC_3H_7, $SCHMe_2$, Sn^{n}Bu, Si^{i}Bu, Si^{i}Pent; or O_2CH, O_2CCH_3, $O_2CC_2H_5$, $O_2CC_3H_7$, O_2CPh.

An improved synthesis of $Cp_3Ce(O^iPr)$ (69% yield) makes use of cerium(IV) isopropoxide and Me_3SnCp (Gulino et al. 1988):

$$Ce\left(O^iPr\right)4.HO^iPr + 3R_3SnCp \xrightarrow[65°C]{\text{toluene}} Cp_3Ce\left(O^iPr\right) + 3R_3Sn\left(O^iPr\right).$$

Electronic structure calculations at the nonrelativistic Xα-DVM level suggest non-negligible Ce–Cp f-orbital covalency and yield transition state ionization energies in good agreement with He^I/He^{II} photoelectron spectra. The reaction of $Ce(OCMe_3)(NO_3)_3(THF)_2$ with NaCp yields a mixture of $Cp_2Ce(OCMe_3)_2$ and $Cp_3Ce(OCMe_3)$. The latter compound can be isolated by recrystallization from *n*-hexane at −34°C. The three Cp ring centroids and the alkoxide oxygen atom form a distorted tetrahedron around the cerium(IV), while the comparable $Cp_3U(Z)$ has a near C_{3v} symmetry at the uranium (Evans et al. 1989a). The chloride substitution reactions on Cp_3AnCl by different nucleophiles (Z) afford a number of Cp_3An-derivatives:

$$Cp_3AnCl + MZ \rightarrow Cp_3AnZ + MCl,$$

where An = U, Th; Z = OR, OAr, NR_2, NAr_2, $NPPh_3$, $(CH_2)(CH_2)PR_2Ph$, $(CH_2)(CH_2)PRPh_2$, PPh_2, NCS, $NCBH_3$.

The reaction of Cp_3UCl with NaOR in THF affords Cp_3U–OR (R = CH_2CF_3, $C(CF_3)_2CH_3$, $C(CF_3)_2CCl_3$, $C(CF_3)_2CF(CF_3)_2$, C_6F_5; Knösel et al. 1987). The crystal structures of R = $C(CF_3)_2CCl_3$ derivative and of Cp_3U–OPh have been reported and show the usual distorted tetrahedral geometry around U, common for all the Cp_3AnX derivatives. The value of the bond distance (U–O = 2.119(7) Å and the angle U–O–C = 159.4(5)°; Spirlet et al. 1990a) in Cp_3UOPh differs significantly (taking into account the difference of the sulfur and oxygen covalent radii) from the value of U–S 2.695(4) Å and U–S–C angle of 107.2(5)° found in Cp_3U–SMe (Leverd et al. 1996) reflecting a stronger ligand to metal π donation in actinide alkoxide bonding. The U^{III}-thiolates and -selenates [Na(THF)][$Cp_3U(SR)$] R = Me, ^{i}Pr, ^{t}Bu or Ph and [Na(THF)][$(C_5H_4SiMe_3)_3USeMe$] (Leverd et al. 1996) has been obtained by sodium amalgam reduction of the tetravalent precursor.

High-yielding preparative routes to various actinide diethylamino-derivatives proceed according to the equation:

$$An(NEt_2)_4 + CpH \rightarrow Cp_nAn(NEt_2)_{4-n},$$

where $n = 1$, 2 or 3; however, n does not take the value 1 for Th. The reactions are under stoichiometric and kinetic control (Ossola et al. 1986b).

The uranium(IV) compounds $Cp_2U(NEt_2)_2$ and $Cp_3U(NEt_2)$ undergo U–N bond cleavage reactions with alcohols and phenols:

$$Cp_nAn(NEt_2)_{4-n} + nROH \rightarrow Cp_nU(OR)_{4-n},$$

where $n = 2$ or 3.

The product yields are controlled by the bulk of the new ligand, and the bis-alkoxide can disproportionate or decompose to give the mono-derivative (Berton et al. 1986).

A very short U–N bond distance (2.07(2) Å) has been observed in the crystal structure of Cp_3UNPPh_3, obtained by reaction of Cp_3AnCl (An = Th, U) with $LiNPPh_3$, suggesting the presence of a U–N triple bond further supported by molecular orbital calculations on several Cp_3U–N and Cp_3U–O derivatives (Cramer et al. 1988b).

Rare examples of electron transfer from U^{III} to a nitrile molecule are represented by the compounds [Cp_3UNCR] (R = Me, ^{n}Pr, ^{i}Pr, ^{t}Bu) obtained from Cp_3U and the corresponding RCN moiety and characterized by NMR spectroscopy and two of them the NC^nPr and NC^iPr derivatives also by X-ray analysis (Adam et al. 1993). The two compounds have the classical geometry of the $Cp_3U{\cdot}L$ complexes with single U–N σ bonds of 2.61(1) and 2.551(9) Å for the NC^nPr and NC^iPr derivatives, respectively.

Extended Hückel molecular orbital calculations on a series of analogous complexes Cp_3UNPH_3, Cp_3UNPh_2 (Brennan and Andersen 1985), $Cp_3UNCHCHPh_3$, Cp_3UNH_2 and $Cp_3UNH_3^+$ and on the corresponding ones with O-donor ligands indicate the important role of covalency in the bonding of actinide complexes. The very short U–N bond is in marked contrast to the very long U–O bond in the triphenylphosphineoxide analog and the difference is rationalized in terms of the bonding abilities of the two ligands. The U–N bond distance 2.29(1) Å, assignable to a bond order 2, characterizes the structure of the amide complex Cp_3UNPh_2 (Cramer et al. 1987a) prepared according to the following reaction:

$$Cp_3U{=}CHPMePh_2 + HNPh_2 \xrightarrow{\text{toluene}} Cp_3UNPh_2 + CH_2PMePh_2.$$

The same product was obtained via an acid-base reaction of Cp_3UPPh_3 and $HNPh_2$ (Paolucci et al. 1985b). In the phosphido complex Cp_3UPPh_2, the mass spectrometric, IR, VIS and ^{1}H NMR spectroscopic data indicate a free electron pair on P.

Cp_3UAlH_4 has been obtained by reaction of Cp_3UBH_4 and $LiAlH_4$ in Et_2O. A polymeric structure with trigonal planar Cp_3U moieties bridged by AlH_4 groups was proposed (Ossola et al. 1986a). The interesting reactivity of the polymeric Cp_3UAlH_4 has been studied towards a series of reagents, i.e. pyridine, MeCN, Me_3CNC, Me_3CNCO, THF, ROH, RCHO, MeCOMe, $BH_3{\cdot}SMe_2$, and MeI (Ossola et al. 1990) (Scheme 1).

The electronic structures of a series of closely related Cp_3U–Z (Z = Me, NH_2, BH_4, NCS) complexes have been studied using the SCF Hartree–Fock–Slater first-principles discrete variational Xα method in combination with He^I and He^{II} UV photoelectron spectroscopy (Gulino et al. 1992). The stringent necessity of maintaining the uranium center in a particularly stable electronic configuration causes larger covalency in the bonds of ancillary Z and an increased ($Z = NH_2 < CH_3 < NCS < BH_4$) ionic character of the U–Cp bonds.

By dehydration of $[Cp_3U(OH_2)_2][BPh_4]{\cdot}nH_2O$ or by addition of BPh_3 to Cp_3UMe the complexes Cp_3UBPh_4, $Cp_3UMeBPh_3$ and their MeCp-derivatives were obtained (Aslan et al. 1988a). Spectroscopic and chemical evidence suggested cation/anion interactions such as U–Me–B bridges.

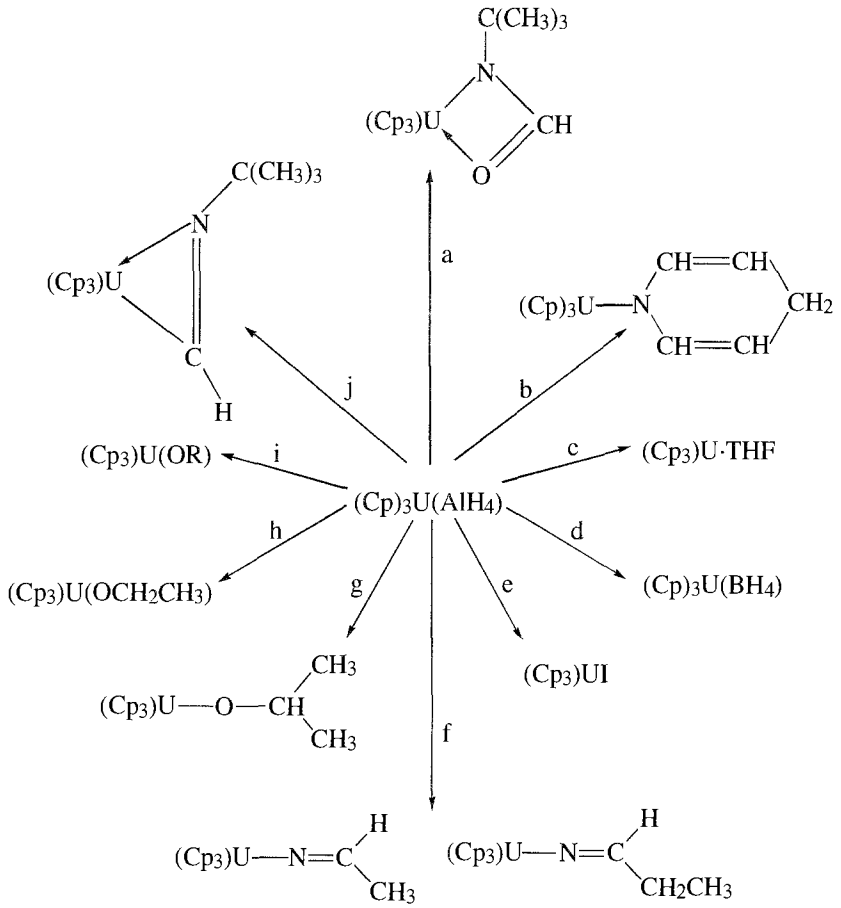

Scheme 1. (a) $(CH_3)_3CNCO$; (b) C_5H_5N; (c) (THF); (d) $BH_3{\cdot}S(CH_3)_2$; (e) CH_3I; (f) CH_3CN; (g) CH_3COCH_3; (h) CH_3CHO; (i) ROH; (j) $(CH_3)_3CNC$.

The reaction of Cp_3U–Z (Z = Cl, Me, ^{n}Bu, Ph) in toluene with tetracyanoethylene and 7,7,8,8-tetracyanoquinodimethane yields Cp_3U-ketoiminates. Spectral data indicated bipyramidal metal coordination (Rossetto et al. 1987). An interesting series of Cp_3An-derivatives with a rather unusual coordination geometry is represented by the complexes of the type Cp_3UXY where X and Y can be either neutral or anionic ligands. $[Ph_4As][Cp_3U(NCS)_2]$ (Bombieri et al. 1983a) and $Cp_3U(NCBH_3)(NCMe)$ (Adam et al. 1990b) have the same trigonal bipyramidal (tbp) stereochemistry with the three pentahapto-Cp located in the equatorial and the extra ligands in the axial positions (fig. 7).

A tbp coordination geometry around U was suggested by spectral data for the anion of the complex salts $A^+[Cp_3An(NCS)_2]^-$ where A = $[KCrypt]^+$ (Crypt = cryptofix) or Me_4N^+ and An = U, and also when A = Ph_4As^+ and An = U, Np or Pu (Bagnall et al. 1982).

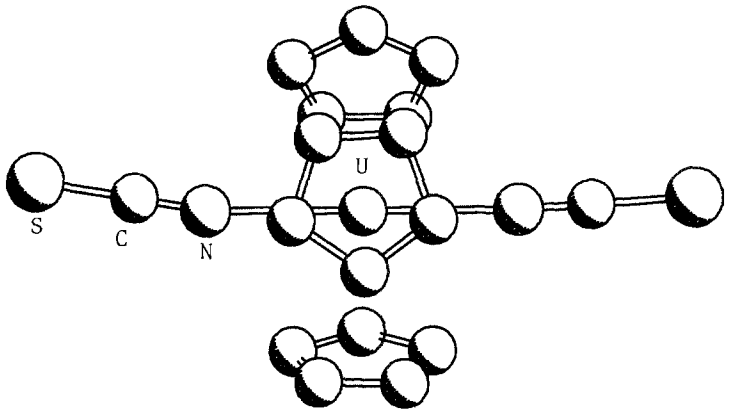

Fig. 7. Crystal structure of the anion $[Cp_3U(NCS)_2]^-$ (Bombieri et al. 1983a).

The salts $[Cp_3U(CNR)_2][BPh_4]$ and $[Cp_3U(CNR)(CNR')][BPh_4]$ (R = Me, ^{n}Pr, $^cC_6H_{11}$) have been prepared by reaction of the tetraphenylborate salt of $[Cp_3U(OH_2)_n]^+$ and $[Cp_2(CpMe)U(NCR)_2]^+$ with alkyl isocyanides (Aslan and Fischer 1986).

Treatment of Cp_3UCl in MeCN with gaseous butadiene (X) and traces of O_2 gives a green solid, identified by X-ray diffraction analysis as $[Cp_3U(NCMe)_2]_2[UO_2Cl_4]\cdot 2X$ (Bombieri et al. 1983b). The complex cation unit $[Cp_3U(NCMe)_2]^+$ is of about D_{3h} symmetry and the anion $[UO_2Cl_4]^-_2$ of approximate D_{2h} symmetry. This is an interesting example of the coexistence in the same crystal of uranium in two oxidation states +4 and +6. From the structural parameters of this trigonal bipyramidal derivative can be deduced that with respect to Cp_3UX compounds the addition of the fifth ligand of little steric hindrance does not significantly influence the U-ligands bond distances.

Other $[Cp_3U(NCR)_2][BPh_4]$ (R = Me, Et, ^{n}Pr, Ph) compounds have been reported (Aslan et al. 1988b). The X-ray analysis of the $[Cp_3U(NCMe)_2][BPh_4]$ derivative shows a complex cation structure analogous to those previously described.

The crystal structure of the complex $[Cp_3U(NCMe)_2]^+[CpThCl_4\cdot NCMe]^-$ (Rebizant et al. 1987) is unique since it contains simultaneously the well known cation complex of tbp geometry $[Cp_3U(NCMe)_2]^+$ with, as the counter anion, an organothorium component of octahedral coordination geometry.

The absorption and MCD spectra for Cp_3UY_2 ($Y = D_2O$, SCN^-, $NCBH_3^-$) derivatives have been reported (Amberger et al. 1986) and the parametrization of the crystal field splitting patterns of $[Cp_3U(NCS)_2]^-$ and $[Cp_3U(NCBH_3)_2]^-$ has been discussed (Amberger et al. 1987). The fragmentation patterns of a series of Cp_3U–Y compounds ($Y = NEt_2$, η^2-CMe=N(C_6H_{11}), and η^2-CMe=N^{n}Bu) under Electron Impact suggest the formation in these conditions of Cp_xU–hydride species and a mechanism for the β-hydride rearrangement was discussed (Paolucci et al. 1986).

An interesting series of insertion reactions into U–C, U–N, U–P, U–Si and U–Ge bonds have been studied. The insertion of CO into U–C and U–N bonds in Cp_3U–Z derivatives (Z = Me, Et, ^{i}Pr, ^{n}Bu, NEt_2, PPh_2, $NCBH_3$ or NEt_2; Paolucci et al. 1984) at room

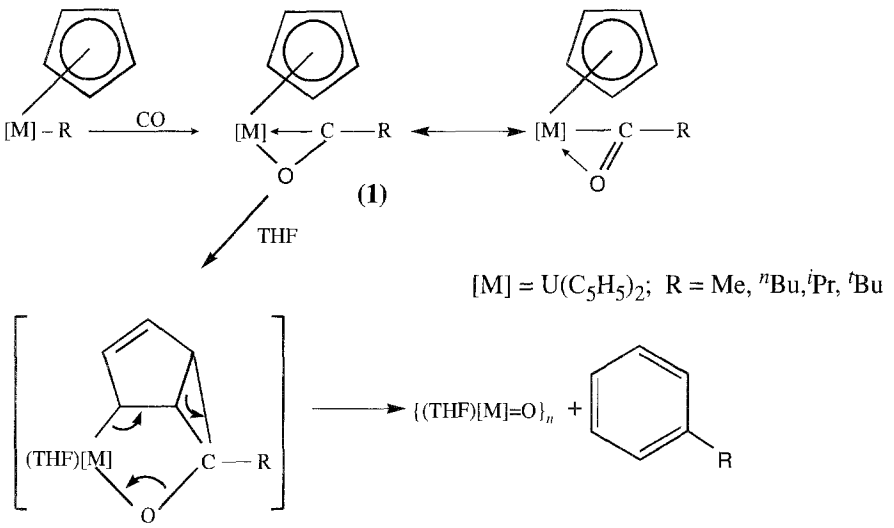

Scheme 2.

temperature gives $Cp_3U(\eta^2\text{-OCZ})$. In the case of Z = Me, through ^1H NMR experiments, the reversible CO insertion and elimination temperature dependent processes have been observed. Spectroscopic data agree with a dihapto-acyl or dihapto-carbamoyl formation.

Triscyclopentadienyluranium alkyl complexes react with CO in THF solution to give, via the intermediacy of the corresponding η^2-acyl compound, alkylbenzenes (C_6H_5R) (Villiers et al. 1992) by deoxygenation of the acyl group and through the ring enlargement of a cyclopentadienyl ligand as shown in scheme 2.

A synthetic and kinetic study of CO migratory insertion for Cp_3ThR (R = ^{i}Pr, ^{s}Bu, neopentyl, ^{n}Bu, CH_2SiMe_3, Me, CH_2Ph) (Sonnenberger et al. 1984) showed that the reactions were first order in Cp_3ThR and in CO. Dihaptoacyls were isolated for R = Me, ^{i}Pr, ^{n}Bu, neopentyl, and ^{s}Bu. Enolate rearrangement products were isolated for R = ^{i}Pr and CH_2SiMe_3. A comparative study of CO_2 migratory insertion was discussed. CO is easily inserted in the U–C multiple bond of $Cp_3U{=}CHPR_3$ ($PR_3 = PMePh_2$, PMe_2Ph) to give $Cp_3U(\eta^2\text{-OCCHPR}_3)$ (Cramer et al. 1982) its crystal structure shows a roughly tetrahedral coordination geometry around uranium if we consider the Cp centroids and the mid point of the C–O bond as the vertices of the tetrahedron.

Dihaptoiminoalkyl insertion products have been obtained by (Dormond et al. 1984) the reaction of isocyanides with Cp_3UR and Cp^*_2URCl (R = alkyl). Spectroscopic evidence pointed toward an η^2-structure with strong U–N bonding. Cp_3UMe did not react; however Cp_3U^nBu reacted at low temperature to yield $Cp_3U[\eta^2\text{-C}(^n\text{Bu})\text{NR}]$ (R = ^{t}Bu, C_6H_{11}, $C_6H_3Me_2$-2,6). Reaction of $Cp^*_2UMe_2$ with CN^tBu gave $Cp^*_2UX[\eta^2\text{-C(Me)N}^t\text{Bu}]$. The insertion of CNC_6H_{11} into the $U\text{–C}_{(methyl)}$ bond of Cp_3UMe affords $Cp_3U[\eta^2\text{-CMeN}(C_6H_{11})]$, characterized by IR, ^1H NMR and X-ray crystal structure (fig. 8). ^1H NMR double resonance experiments allowed the complete assignments of the eleven cyclohexyl protons (Zanella et al. 1985).

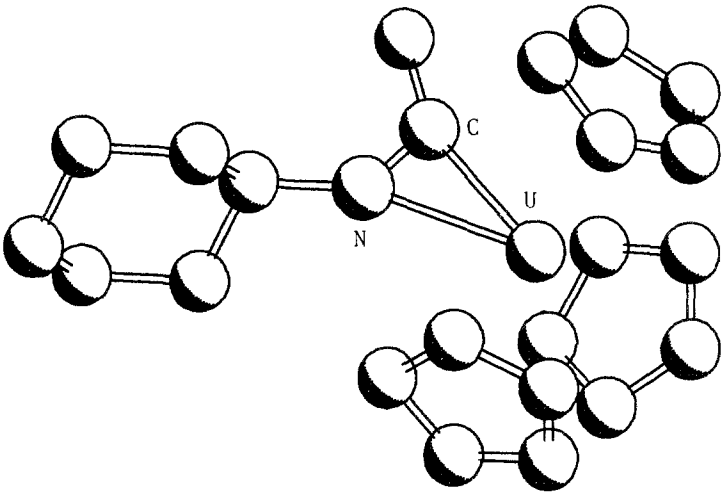

Fig. 8. Crystal structure of $Cp_3U[\eta^2CMeN(C_6H_{11})]$ (Zanella et al. 1985).

Isonitriles readily insert into the U–Ge bond of Cp_3UGePh_3 in the expected way (Porchia et al. 1987a,b, Zanella et al. 1987) and into the U–N bonds of Cp_3UNEt_2 and $Cp_2U(NEt_2)_2$. There is also some indication of insertion into the U–P of Cp_3UPPh_2. The X-ray structure of $[Cp_3U(C(NEt_2)=NC_6H_3Me_2\text{-}2,6)]$ represents the first example of the insertion of an isocyanide molecule into a U–N bond. The iminocarbamoyl ligand is bound via carbon and nitrogen to the uranium atom with equal values (2.35 Å) for the U–C and U–N distances, suggesting (for these distances) a partial double bond character.

The insertion product $Cp_3U[\eta^2\text{-}CN(C_6H_{11})CHPMePh_2]$ is prepared by reaction of CNC_6H_{11} and $Cp_3U=CHPMePh_2$. A multiple bond character of the U–N bond (2.31(2) Å (Cramer et al. 1984a) has been found by X-ray analysis. The Ph–N=C=O can be inserted into the uranium–carbon bond of $Cp_3U=CHPMe_2Ph$ in toluene solution at −58°C for 5 h (Cramer et al. 1987b):

$$Cp_3U{=}CHPMe_2Ph + PhNCO \rightarrow Cp_3U(NPh)(O)CCHPMe_2Ph.$$

The X-ray crystal structure of the insertion product shows a η^2-coordination (O and N) of the neutral ligand with the U–O bond distance of 2.34(1) Å and U–N of 2.45(1) Å consistent with single bonds. The structure of this compound represents the first *cis*-Cp_3UXY derivative with four membered chelate ring. The insertion of CO_2 into $U\text{–}C_{(allyl)}$ bond of $Cp_3U(allyl)$ affords $Cp_3U(CO_2CH_2CH{=}CH_2)$ (Karova et al. 1985). $Cp_3UCl(COMe)$ has been isolated as intermediate in the oxidative addition of Cp_3U with MeCOCl at 6°C, and characterized by ^1H NMR, electrochemical data and its chemical reactivity (Chang and Sung-Yu 1986). The insertion of acetonitrile into $Cp_3UCHPMePh_2$ produces $Cp_3UNC(Me)CHPMePh_2$ where multiple bond character for the U–N interaction (2.06(1) Å and a highly delocalized π system (Cramer et al. 1984a–d) have been detected by X-ray analysis.

2.1.5. *Cp′3MX (with substituted cyclopentadienyls). Actinides*

Lanthanide(IV) derivatives with modified Cp are as yet unknown so this section reports only on actinide derivatives

2.1.5.1. *X = halide.* The first example of intermolecular C–F activation of a saturated fluorocarbon is the reaction of $(MeCp)_3U(^tBu)$ with hexafluorobenzene at room temperature giving $[(MeCp)_3UF]$ (Weydert and Andersen 1993). The steric congested $(Me_4Cp)_3AnCl$ (An = U, Th) (Cloke et al. 1994) has been synthesized from $Li(C_5Me_4H)$ and $AnCl_4$. The X-ray structure of the U derivative presents the usual distorted tetrahedral coordination geometry with U–C bond lengths (av. 2.79 Å) close to that of the related Cp* derivatives. Cyclic voltammetry measurements indicate a very electron rich uranium center.

2.1.5.2. *X = hydrocarbyl.* Absolute uranium–ligand bond disruption enthalpies in the series Cp'_3UR ($Cp' = Me_3SiC_5H_4$, R = ^{n}Bu, Bz, CH_2SiMe_3, Me, vinyl, C≡CPh), which increase from 29(2) for ^{n}Bu to 86.7 (kJ mol^{-1}) for C≡CPh, have been measured by halogenolytic isoperibol titration calorimetry of $Cp'_3U/Cp'_3UI/Cp'_3UR$ (Schock et al. 1988). The magnitude of the D(U–R) values appear to reflect a combination of steric and electronic factors and suggest that D(U–I) is less sensitive to ancillary ligation than D(U–alkoxide). The X-ray structure of Cp'_3U–CH=CH_2 complex has the usual pseudotetrahedral Cp_3MX configuration. The introduction of the vinyl group into the Cp'_3U moiety induces a shrinking in the Cg–U–Cg angles as expected, while the U–C(Cp) distances are somewhat shortened. The relatively short U–C distance 2.435(4) Å and the relatively large U–C–C angle, 137.7(3)°, have been attributed to non-bonded repulsions and to α-C–H···metal interactions (the U···H(1) distance is 2.93(4) Å).

The absolute uranium–ligand bond-disruption enthalpies (kJ mol^{-1}) of the series $[(RC_5H_4)_3UX]$ (X = H or I; R = ^{t}Bu or $SiMe_3$) have been measured by iodinolysis batch-titration solution calorimetry in toluene: R = ^{t}Bu, 246.3±5.3 (X = I), 249.7±5.7 (X = H); R = $SiMe_3$, 265.6±4.3 (X = I), 251.7±5.1 (X = H) (Jemine et al. 1992).

An unusual molecule $[Li(tmed)_2]\{[Li(tmed)]_2(\mu\text{-}MeC_5H_4)\}\{[(MeC_5H_4)_3U]_2(\mu\text{-}Me)\}$ (Stults et al. 1989) (tmed = *N*,*N*,*N*′,*N*′-tetramethylethylendiamine) is obtained by reacting LiMe, $(MeC_5H_4)_3U{\cdot}THF$, tmed in diethyl ether. The linear methyl bridging in the U fragment (U–C–U angle 176.9(11)°) may be considered as a model for the bimolecular transition state in electrophilic substitution at unsaturated and saturated carbon centers. The MeCp ligand has a higher solubility in hydrocarbon solvent with respect to the analogous unsubstituted ligand and presents a more advantageous NMR spectrum (three sets of resonances). These characteristics make its use preferred. Very recently (Weydert et al. 1995) the reactions of $(MeCp)_3U(^tBu)$ with Lewis bases (L = PMe_3, THF, ^{t}BuCN and EtNC) giving the $(MeCp)_3U^{III}(L)$ derivatives, have been investigated. The adducts were identified by NMR spectroscopy.

Carbon monoxide undergoes migratory insertion into the metal tertiary alkyl bond

$$(MeCp)_3\,U\,(^tBu) + CO \xrightarrow{\text{toluene}} (MeCp)_3\,UC\,(O) - {}^tBu,$$

while under ethylene (210 psi) the mono insertion product $(MeCp)_3U(CH_2CH_2)$-*t*-Bu is obtained. IR and NMR data support these results.

The first spectroscopic evidence of the formation of the $(Me_3SiC_5H_4)_3UCO$ compound is reported (Brennan et al. 1986a) while with the highly sterically congested $(C_5Me_4H)^-$ ligand the first isolable carbonyl complex $(C_5Me4H)_3UCO$ (Parry et al. 1995) by reduction of $(C_5Me_4H)_3UCl$ has been obtained according to the equation:

$$(C_5Me_4H)_3\,UCl \xrightarrow[NaC_{10}H_8]{THF} (C_5Me_4H)_3\,U + NaCl,$$

successive treatment with CO (1 atm) gives $(C_5Me_4H)_3UCO$. The IR solid state spectrum shows an intense band at 1880 cm^{-1} suggesting a strong U–CO π back bonding interaction. The X-ray structure shows an about linear U–C–O angle 175.2(6)° and a relative short U–C(O) bond (2.383(6) Å) in agreement with IR data.

2.1.5.3. *X = non-halide, non-hydrocarbyl.* The first organouranium(V) complexes $(MeCp)_3UNR$ (R = Ph, $SiMe_3$) were obtained by oxidation of the trivalent uranium derivative $(MeCp)_3U(THF)$ with the organic azides (Me_3SiN_3 and PhN_3; Brennan and Andersen 1985). Crystallographic characterization of $(MeCp)_3UNPh$ shows a U–N triple bond of 2.019(6) Å and a linear U–N–C angle (167.4(6)°). This suggests that both the nitrogen lone pairs of electrons are involved in bonding to uranium. The pentavalent uranium organoimide derivatives with evolution of either nitrogen or carbon monoxide is an important synthetic reaction for these species. In contrast with organic isocyanates the 2:1 complex $[(MeCp)_3U]_2[PhNCO]$ was obtained. The $[PhNCO]^{2-}$ anion bridges two $[(MeCp)_3U]^+$ fragments in an η^1–η^2 fashion. Important distances include U–N = 2.36(2) Å, U–C = 2.42(2) Å, U–O = 2.11(1) Å.

Antiferromagnetic coupling between uranium centers was observed in the bimetallic $[(MeCp)_3U]_2[\mu\text{-}1,4\text{-}N_2C_6H_4]$, while no coupling is observed when the bridging ligand between the two $(MeCp)_3U$ unities is $1,3\text{-}N_2C_6H_4$ (Rosen et al. 1990).

The synthesis and characterization of a series of $(C_5H_4SiMe_3)_3U$-azide compounds including mononuclear U^{III} and U^{IV} derivatives with terminal N_3 ligands, binuclear U^{III}–U^{III} and U^{IV}–U^{IV} compounds with 1,3-μ-azido-groups and the first mixed valence (U^{III}–U^{IV}) azido-bridged binuclear complex have been reported (Berthet et al. 1991a) (see reaction scheme 3).

The X-ray crystal structure of the anion in $[Na(18\text{-crown-}6)]^+[(C_5H_4SiMe_3)_3U\text{–}N_3\text{–}U(C_5H_4SiMe_3)_3]^-$ resembles that of the samarium(III) analog (Schumann et al. 1988b) and reveals the 1,3-μ-form of the linear azide ligand (U–N 2.40(2) Å, U–C(Cp) average 2.54(2) Å).

The compound $(Me_3SiC_5H_4)_3U$ reacts with CO_2 or N_2O to give $[(Me_3SiC_5H_4)_3U]_2$-[μ-O], the crystal structure of which reveals the presence of a linear U–O–U bridge with U–O distances of 2.1053(2) Å (Berthet et al. 1991b).

Tetravalent U hydroxocomplexes (Berthet et al. 1993) $[(C_5H_4R)_3UOH]$ (R = $SiMe_3$, ^{t}Bu) have been synthesized. They react with $(C_5H_4R)_3UH$ giving the $[(C_5H_4R)_3U]_2(\mu\text{-}O)]$

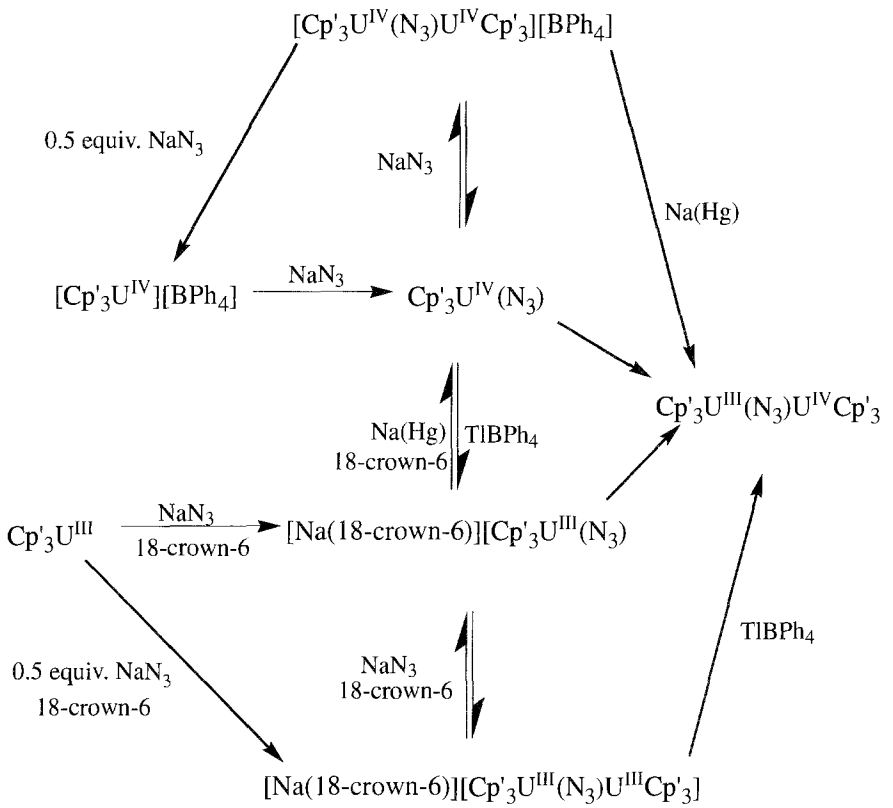

Scheme 3.

(R = $SiMe_3$) which by thermolysis produces the trinuclear derivative $[(C_5H_4SiMe_3)_3U]_2$-$(\mu\text{-}O)]_3$. The planar six-membered ring formed by U and O atoms and the average of the U–O bonds 2.08(4) Å similar to that of the dinuclear derivative (vide supra), reflect the strong π bonding between the metal and the oxygen atoms.

The trivalent uranium metallocenes $(MeC_5H_4)_3U(THF)$ and$(Me_3Si\text{-}C_5H_4)_3U$ react with CS_2 to form the dinuclear U^{IV} complexes $[(RC_5H_4)_3U]_2[\mu\text{-}\eta^1,\eta^2\text{-}CS_2]$ (R = Me, $SiMe_3$) (Brennan et al. 1986b). The crystal structure of R = Me shows disorder of the CS_2 ligand resulting in equivalent η^1,η^2 U–S distances of 2.792(3) Å. In fact the bridging CS_2 molecule acts with η^2-hapticity via C–S on one uranium and as η^1 (*via* the remaining sulphur atom) on the second uranium. The U–S distance of 2.792 Å is in between the values of 2.986(5) Å reported for $(MeCp)_3U$ (tetrahydrothiophene) (Zalkin and Brennan 1985) and 2.60(1) Å for the sulphur-bridged $[(MeCp)_3U]_2(\mu\text{-}S)$ derivative (Brennan et al. 1986c). NMR and susceptibility data, are consistent with two full one-electron transfers into the CS_2. There is no measurable magnetic interaction between the paramagnetic ions to 5 K.

Electron transfer reactions have been also observed by reacting $(MeC_5H_4)_3U{\cdot}THF$ with COS, $SPPh_3$, $SePPh_3$ or $TeP(^nBu)_3$ to form the bridging chalcogenide complexes $[(MeC_5H_4)_3U]E$ where E = S, Se or Te while the monomeric complex $(MeCp)_3U{\cdot}OPPh_3$ was isolated when triphenylphosphine oxide was utilized (Brennan et al. 1986a–c).

The complexes $(C_5H_4SiMe_3)_3U{-}SR$ and $(C_5H_4^tBu)_3U{-}SR$ (R = Et, ^{i}Pr, or ^{t}Bu) can be prepared by oxidation of the corresponding $(C_5H_4SiMe_3)_3U^{III}$ and $(C_5H_4^tBu)_3U^{III}$ precursors with RSSR. With diselenide MeSeSeMe the analogous selenium derivatives can be obtained (Leverd et al. 1996). The reaction of $(^tBuCp)_3U$ with HSPh led to the dimeric $(^tBuCp)_4U_2(\mu\text{-}SPh)_2$ which rearranges in solution to give $(^tBuCp)_3USPh$. When MeCp is used, the dimer cannot be detected and only the rearrangement products $(MeCp)_3U{-}OMe$, $(MeCp)_3U(OCHMe_2)$, $(MeCp)_3U(OPh)$ and $(MeCp)_3USCHMe_2$ were isolated (Stults et al. 1990b).

2.1.6. *Cp_2MX_2, Cp_2MXY, Cp_2MX*

2.1.6.1. *X = halide.*

2.1.6.1.1. *Lanthanides.* Several synthetic methods are available (Marks and Ernst 1982) for the preparation of dicyclopentadienyl lanthanide chlorides:

$$LnCl_3 + 2MCp \xrightarrow{THF} Cp_2LnCl + 2MCl,$$

where Ln = Y, Sm, Gd, Tb, Dy, Ho, Er, Tm, Yb, Lu; M = alkali metals.

$$LnCl_3 + 2Cp_3Ln \xrightarrow{THF} 3Cp_2LnCl,$$

where Ln = Sm, Gd, Dy, Ho, Er, Yb.

In the solid state, in the gas phase, in solution, in non-coordinating solvents, Cp_2LnCl is mainly dimeric but also different polynuclear species have been observed. In THF solution monomeric adducts are formed, from which by sublimation at 200–250°C under vacuum (10^{-3} torr), the solvent-free dimers are obtained.

The $[Cp_2LnCl]_2$ (Ln = Er, Lamberts et al. 1987a; Yb, Lueken et al. 1989, Akhnoukh et al. 1991) structure consists of well separated dimers where the two $(Cp_2Ln)^+$ units are doubly bridged by the chloride anions. This basic structure is common also to the Gd, Dy, Er and Yb bromides while tetrameric species are reported for the corresponding Gd chloride (Lamberts et al. 1987b) where two non-equivalent Gd^{3+} species with formal coordination numbers 8 and 9 are present (fig. 9) and the units are equal to the basic motif for the polymeric infinite double chains of $[Cp_2GdBr]_\infty$ (Lamberts et al. 1986).

A polymeric structure is shown also by $[Cp_2DyCl]_\infty$ (Lamberts and Lueken 1987). It is worth noting that despite the close similarity of the metal radii, the type of polynuclear units (Er, dinuclear; Gd, tetranuclear; Dy, infinite one-dimensional species) and their arrangements in the solid state differ widely. The formation of a distinct crystal structure depends on the species in the gaseous phase during sublimation. This has been proved to be the case for $[Cp_2GdBr]_2$ (Lamberts et al. 1986). With a low sublimation temperature the gaseous phase contains almost exclusively $[Cp_2GdBr]_2$. A higher sublimation temperature

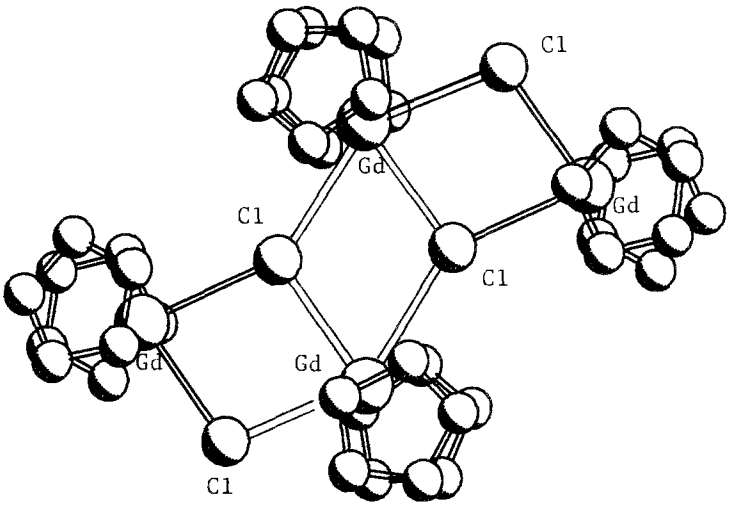

Fig. 9. Crystal structure of $[Cp_2GdCl]_4$ (Lamberts et al. 1987b).

shifts the equilibrium to monomeric Cp_2GdBr which condenses in a monodimensional polymeric structure. The temperature dependence of the gaseous phase equilibrium

$$[Cp_2GdBr]_2 \rightarrow 2[Cp_2GdBr]$$

is confirmed by mass spectra recorded at various ion source temperatures.

The only known $[Cp_2LnI]_2$ (Ln = Sm, Ye et al. 1986a; Er, Magin et al. 1963; Yb, Deacon et al. 1984b) complexes are poorly characterized, while the unique example of a fluoride derivative is the trimer $[Cp_2ScF]_3$ (Bottomley et al. 1985).

The reaction of the halide derivatives with Lewis bases causes in some cases, the cleavage of the dimeric structure, while in other cases the dimeric structure is maintained also after the coordination of the Lewis base.

The compounds $[Cp_2YCl]\cdot AlH_3\cdot OEt_2$, $[Cp_2YCl]_2\cdot 2(AlH_3NEt_3)$ and $[Cp_2Y(\mu Cl)]_2$-$(AlMe_2)$ (Lobkovskii et al. 1982, 1983) are prepared by reaction of $CpYCl_2$ and AlH_3OEt_2 or AlH_3NEt_3 or $(MeAlCl_2)_2$ in diethyl ether. The structure of the AlH_3OEt_2 derivative consists of a polymeric chain made up from $Cp_2Y(\mu\text{-}Cl)_2YCp_2$ fragments and $AlH_3\cdot OEt_2$ units linked together through Y–H–Al bridges, while the AlH_3NEt_3 derivative is formed by $[Cp_2YCl]_2$ dimers bonded to $AlH_3\cdot NEt_3$ by H bridges between Y and Al, as well as by weak Al–Cl bonds.

The monomeric adducts $Cp_2LnCl(THF)$ are known and in particular the Lu derivative obtained from $LuCl_3$ and 2NaCp in THF (Ni et al. 1986) characterized by X-ray analysis shows a distorted tetrahedral arrangement of the ligands around Lu, typical of the formally eight coordinate lanthanide metal ions. The isostructural dimers $[Cp_2LnCl(THF)]_2$ (Ln = Nd, Jin et al. 1988a; Yb, Jusong et al. 1992) in the solid state show asymmetrical chlorine bridges. The electronic structure of $Cp_2NdCl(THF)$ by INDO calculations showed the compound to be covalent with some ionic character (Z. Li et al. 1987). A cone

angle model has been proposed to calculate the structure pattern of cyclopentadienyl lanthanide compounds (X. Li et al. 1987).

2.1.6.1.2. *Actinides.* The very few actinide species of the type (Cp_2AnX) reflect the predominance of tetravalent over trivalent oxidation state in organoactinide chemistry (Marks and Ernst 1982).

While Cp_2MCl_2 (M = Ti, Zr, Hf) compounds are stable and extremely interesting in organometallic chemistry, the corresponding actinide derivatives are notably unstable towards intermolecular ligand redistribution processes. Thus "Cp_2UCl_2" obtained by the following reaction:

$$UCl_4 + 2TlCp \xrightarrow{DME} \text{“}Cp_2UCl_2\text{”} + 2TlCl,$$

is actually a mixture of Cp_3UCl and $CpUCl_3(DME)$ (Marks and Streitwieser 1986). By complexing "Cp_2UCl_2" with additional ligands to prevent ligand redistribution processes it is possible to isolate $[Cp_2UCl_2L]_2$ species only with $L = Ph_2P(O)CH_2CH_2P(O)Ph_2$ (Bagnall et al. 1978). The synthesis and the dynamic behavior of the complexes $[(Cp)_{4-n}UCl_n]$ ($n = 1$–3) in non-coordinating solvent and in absence of Lewis bases have been the object (Arliguie et al. 1994a) of a very interesting study, which results in the production of, among others ($CpUCl_3$ and Cp_3UCl), the species $U_5Cp_8Cl_{12}$; its X-ray crystal structure established the chemical formulation $\{[Cp_2U(\mu\text{-}Cl)]_3(\mu^3\text{-}Cl)_2\}[(CpUCl_2)_2(\mu\text{-}Cl)_3]$ (fig. 10). The latter when dissolved in THF affords ligand redistribution

$$2U_5(Cp)_8Cl_{12} \xrightarrow{THF} 7\,[CpUCl_3(THF)_2] + 3\,[(Cp)_3UCl].$$

The crystal structure of $Cp_2ThCl_2(dmpe)L$ (Zalkin et al. 1987b) shows hexa-coordination to the metal ion (Cp is considered as one coordination site). Among the two possible

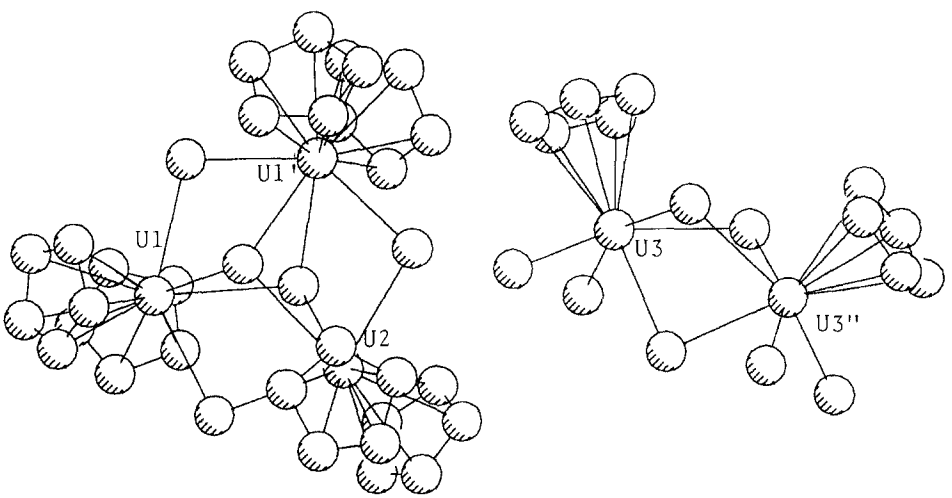

Fig. 10. Crystal structure of $[\{Cp_2U(\mu\text{-}Cl)]_3(\mu^3\text{-}Cl)_2\}(CpUCl_2)_2(\mu\text{-}Cl)_3]$ (Arliguie et al. 1994a).

idealized geometries, that is either the chlorine ligands or the Cp ligands are *trans* to dmpe, the Cp ligands resulted *trans* to the bidentate phosphine. This is in agreement with the Kepert rule (Kepert 1977) for this type of molecule, in which monodentate ligands with the shortest metal–ligand bonds occupy the less hindered sites *trans* to the bidentate ligand. The compound is isostructural with the $Cp_2ThX_2(dmpe)$ (X = Me, benzyl) derivatives (see sect. 2.1.6.2.2).

2.1.6.2. *X = hydrocarbyl.*

2.1.6.2.1. *Lanthanides.* Dicyclopentadienyl lanthanide alkyl and aryl derivatives were first reported in 1975 (see Marks and Ernst 1982), prepared according to the general method:

$$\tfrac{1}{2}\,[Cp_2LnCl]_2 + MR \xrightarrow{THF} Cp_2LnR + MCl,$$

where M = Li, Na; R = alkyl or aryl group.

The X-ray crystal structure of $Cp_2YbMe(THF)$ and its use in the synthesis of hydride species such as $[Cp_2YbH(THF)]_2$ and $[(Cp_2YbMe)_3H(THF)]Li(THF)$ have been reported (Evans et al. 1986a). The Yb–Me distance is 2.36(1) Å.

Thermally stable monometallic complexes have been prepared by using bulky alkyl anions such as Li^{t}Bu (Evans et al. 1981a):

$$\tfrac{1}{2}\,[Cp_2LnCl]_2 + Li^tBu \xrightarrow{THF} Cp_2Ln^tBu\,(THF) + LiCl,$$

where Ln = Er, Lu.

These complexes are particularly interesting for their high stability, unusual for species containing β-hydrogen atoms. The possible β-hydrogen extrusion destabilises complexes containing ethyl, isopropyl, *sec*-butyl ligands with respect to the methyl derivative. As in the case of the lutetium series, where only with bulky alkyl or aryl group the $Cp_2LuR{\cdot}THF$ compounds are isolable at room temperature. In fact when R = Me, Et, ^{i}Pr or ^{n}Bu, the corresponding compounds were only detected by NMR (Schumann et al. 1981, 1982, Evans et al. 1981c, 1982a). A distorted tetrahedral geometry of the ligands around the metal ion is typical for the compounds of this series and it can be obtained in monomeric species by additional coordination of a solvent molecule, of a stabilising heterometallic species such as in $Cp_2Yb(\mu\text{-}Me)_2AlMe_2$ (see below) or of a bidentate ligand, or even by dimerization as in $[Cp_2Y(\mu\text{-}Me)]_2$ (Holton et al. 1979).

Analogous geometries characterize two other alkyldicyclopentadienyl lutetium derivatives (Schumann et al. 1982) $Cp_2Lu(CH_2SiMe_3)(THF)$ and $Cp_2Lu(C_6H_4\text{-}4\text{-}Me)(THF)$.

Some other *p*-tolyl derivatives of Gd, Er and Yb as well as the *p*-chlorophenyl Er complexes were synthesized (Qian et al. 1983).

Several dicyclopentadienyl ytterbium hydrocarbyls were prepared by reaction of $Cp_2Yb(DME)$ with HgR_2 ($R = C_6F_5$, C_6Cl_5, C≡CPh) (Deacon and Wilkinson 1988).

Preparation and reactivity studies of Cp_2SmCH_2Ar (Ar = Ph, *o*-^{t}BuC$_5$H$_4$, 2,5-Me$_2$C$_5$H$_3$) have been reported (Collin et al. 1987).

The one-step reaction of $LuCl_3$, NaCp and $Li(CH_2)_3NMe_2$ in the molar ratio 1:2:1 affords the lutetium alkyl derivative $Cp_2Lu(CH_2)_3NMe_2$ containing a Me_2N–Lu intramolecular bond of 2.37(1) Å (Schumann et al. 1992b). The same reaction of $ErCl_3$ (or $LuCl_3$) in the presence of tmed affords $Cp_2Er(\mu\text{-}CH_3)_2Li(tmed)$ whose X-ray crystal structure has been determined (Schumann et al. 1985a).

The structure characterization of $Cp_2YbMe(THF)$ (Evans et al. 1986a) provides useful information about the reactivity of compounds of the same family, e.g., $Cp_2LnR(THF)$, $[Cp_2LnR]_2$ (Ln = Y, Er, Yb or Lu, and R = H or Me), in hydrogenolysis reactions. In fact, small differences in the metal, alkyl group and solvent sizes produce substantial changes in their reactivity. The Yb–C(σ) bond distance (2.362(11) Å) agrees with those of the Lu analog while in Lu'Bu derivative it is significantly longer (2.471(2) Å). The Yb–C(σ) distance in the methyl derivative is the first determined for an unsubstituted small sized alkyl ligand allowing the characterization of the steric crowding in related complexes.

Some bimetallic kinetically stable metal alkyls and bridging methyls $Cp_2LnR(\mu\text{-}R)AlR_2$ derivatives were reported in the 70's (Marks and Ernst 1982).

The pink erbium derivative $[Cp_2ErC{\equiv}CCMe_3]_2$ was synthesized by the halide-free reaction of $[Cp_2ErMe]_2$ with $HC{\equiv}CCMe_3$ in THF solution (Atwood et al. 1981). Its X-ray structural analysis confirms the dimeric formulation.

By reacting $Cp_2LnCl(phen)_n$ with alkynylsodium or alkyllithium reagents the corresponding $Cp_2LnC{\equiv}CPh(phen)$ (Ln = La, Nd), $Cp_2Ln(^tBu)(phen)$ (Ln = La, Nd) and $[Cp(CH_2)_3Cp]NdC{\equiv}CPh(phen)$ were obtained (Qian and Ge 1986).

Several reactions of Cp_2LnX (X = Cl or R) with phosphoylides or phosphoranes have been reported:

$$[Cp_2LuCl]_2 + 2LiCH_2PMe_2 \rightarrow 2Cp_2LuCH_2PMe_2 + 2LiCl.$$

The molecular structure of $Cp_2LuCH_2PMe_2$ is characterized by a three-membered Lu–C–P ring (Schumann et al. 1985b). The reaction of $[Cp_2LuCl]_2$ with $Li(CH_2)_2P(^tBu)_2$ yields a chelate complex (Schumann and Reier 1984):

$$[Cp_2LuCl]_2 + 2Li(CH_2)_2P(^tBu)_2 \rightarrow 2Cp_2Lu(CH_2)_2P(^tBu)_2 + 2LiCl.$$

The reaction of $[Cp_2YCl]_2$ with four equivalents of $LiCH_2SiMe_3$ in DME/dioxane yielded the bisanionic dimer $[Li_2(DME)_2(dioxane)]$ $[Cp_2Y(CH_2SiMe_3)_2]_2$ (Evans et al. 1985a). This complex was structurally characterized and consists of $[Cp_2Y(CH_2SiMe_3)_2]^-$ anions while the cations consist of two lithium ions bridged by dioxane and each containing one DME molecule and an interaction with the backside of a Cp ring. The reactions of $Cp_2Lu\text{-}R(THF)$ (R = ^tBu, CH_2SiMe_3)(THF) with $CH_2{=}PPh_3$ or $Me_3SiCH{=}PMe_3$ in toluene produces Cp_2LuR' (R' = methylene triorganophosphoranes; Schumann and Reier 1984). Mixed ligand complexes of the type $Cp_2LnInd{\cdot}THF$ (Ln = Sm, Dy, Ho, Er, Yb) have been prepared and characterized by analytical and spectroscopic data (Zhennan et al. 1989).

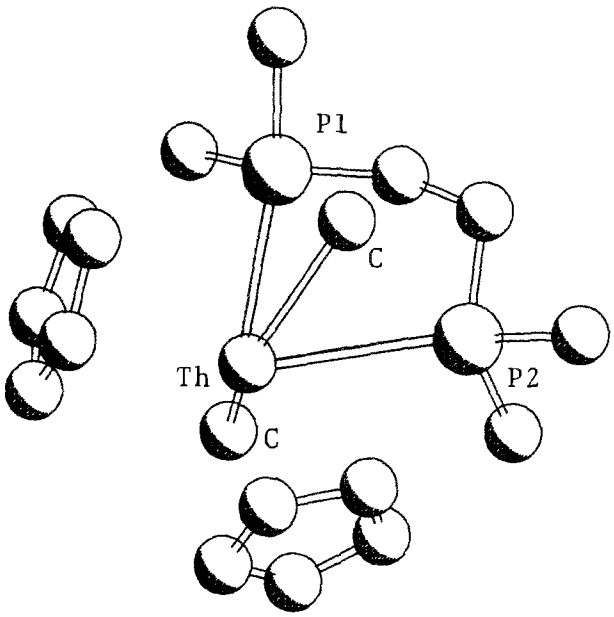

Fig. 11. Crystal structure of $[Cp_2ThMe_2(Me_2P(CH_2)_2PMe_2)]$ (Zalkin et al. 1987b).

Recently, the structure of the novel compound $[Na(diglyme)_2Cp_2Lu(C_{14}H_{10})]$, containing the bulky anthracene ligand, has been reported (Roitershtein et al. 1993).

2.1.6.2.2. *Actinides.* The electronic and geometric structures of dicyclopentadienyl actinide acyl complexes have been studied thoroughly (Tatsumi et al. 1985, Hoffmann et al. 1985). Comparison between η^2-aryls formed and η^1-coordination were discussed, as well as the unique reactivity of acyl ligands in $Cp_2An(COR)X$ compounds. A series of studies on the electronic structures of Cp_2AnR_2 (R = alkyl, butadiene, metallacyclopentadiene, cyclobutadiene), among other features, justify by molecular orbital analysis the observed deformation in Th–Cα–Cβ angles (Tatsumi and Nakamura 1987a,b). The crystal structure of the two compounds Cp_2ThX_2(dmpe) (X = Me; Zalkin et al. 1987b) and benzyl (Zalkin et al. 1987c) show that they are isomorphous and six-coordinated (fig. 11).

The chemistry of U^{IV} and Th^{IV}, usually similar, differs in the reaction of Cp_3AnCl with $Li(CH_2CH_2PPh_2)$ (Cramer et al. 1995a) (scheme 4). A methine carbon is coordinated with a multiple bond character in the U derivative, while with thorium two ylide anions chelate to the metal through methylene groups. This has been related to the difference in the electronic configuration of uranium(IV) and thorium(IV).

2.1.6.3. *X = non-halide, non-hydrocarbyl.*

2.1.6.3.1. *Lanthanides.* Dicyclopentadienyl lanthanide chlorides can be used to prepare a number of dicyclopentadienyl compounds containing Ln–O, Ln–S, Ln–N, Ln–P σ-bonds.

The reaction of Cp_2LnCl with sodium carboxylates yields the corresponding dicyclopentadienyl lanthanide carboxylates, which on the basis of their molecular weight

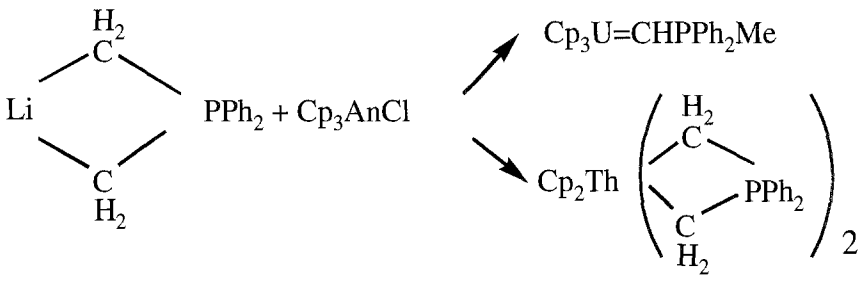

Scheme 4.

determinations in benzene are dimers with μ-carboxylate bridges (Marks and Ernst 1982).

A series of carboxylates of the type $Cp_2Yb(O_2CR)$ (R = Me, CF_3, Ph, C_6F_5, C_6Br_5, $MeO_2CC_6H_4$, C_6H_2-2,4,6-Me_3, NC_5H_4-2) have been prepared by oxidation of Cp_2Yb-(DME) with $M(O_2CR)_n$ ($M = Hg^{II}$, $n = 2$ or $M = Tl^{I}$, $n = 1$). The complexes with R = Me, CF_3, Ph or C_6F_5 appear to be dimeric (Deacon and Wilkinson 1989).

The compounds CpYb[CO(O)CH=CHC(O)O], CpYb[OC(O)$(CH_2)_n$C(O)O] ($n = 0$–2), CpYb[OC(O)C_6H_4C(O)O] (Wang and Ye 1985), Cp_2YbO_2CR (R = CMe_3, CCl_3, Et, CH_2Cl; Ye et al. 1984), $[Cp_2YbO_2C]_2R$ (R = CH_2, CH_2CH_2, *o*-C_6H_4, *p*-C_6H_4; Wang et al. 1986) were synthesized by reaction of Cp_3Yb or $[Cp_2YbCl]_2$ with the corresponding carboxylic acids or carbonyls. While acetates Cp_2Ln OAc (Ln = Sm, Gd, Tb, Dy, Ho, Tm, Lu) were prepared from $[Cp_2LnCl]_2$ and NaOAc in THF (Ye et al. 1986b). A different synthetic method, namely oxidative addition of Hg, Tl, Ag or Cu salts to Cp_2Yb(DME), produced $[Cp_2Yb–Z]$ (Z = O_2CMe, $O_2CC_6F_5$, $O_2CC_5H_4N$, Cl, Br, I, C≡CPh, C_6F_5, $(MeCO)_2CH$, $(PhCO)_2CH$; Deacon et al. 1984b). Very recently (Stuedel et al. 1996) optically active ligands have been used to synthesize the complexes $[Cp_2Sm(\mu\text{-}OC_{10}H_{19})]_2$ and $[Cp_2Sm\{\mu\text{-}OCH(Me)COO^tBu\}]_2$ which display significant circular dichroism (below 600 nm) of discrete f–f crystal field transition. The X-ray structure of the isomethoxide ($OC_{10}H_{19}$) derivative adopts a conformation with axial O–Sm and ^{i}Pr substituent. 1,10-phenanthroline adducts of Cp_2Ln trifluoroacetates (monodentate) were also prepared, $Cp_2LnOC(O)CF_3(phen)_n$ (Ln = Pr, Nd; $n = 1$ or 2; Ln = La, Ce; $n = 2$) by the reaction of $Cp_2LnCl(phen)_n$ with $NaOOCCF_3$ (Zhou et al. 1984). The complexes were characterized by elemental analysis, IR, NMR, and mass spectrometry.

Solvent free $[Cp_2Ln(triflate)]_2$ dimers were obtained by metathesis of $Ln(OSO_2CF_3)_3$ with NaCp (1:2) (Ln = Sc, Lu, Schumann et al. 1989a, 1992b; Yb, Stehr and Fischer 1992). The X-ray structure of the latter is in fig. 12.

Some *tert*-buthoxide derivatives, Cp_2LnO^tBu, were isolated (Ln = Sm, Schumann et al. 1982; Dy, Yb, Wu et al. 1994b; Lu, Schumann et al. 1988c).

The reaction of Cp_3Ln (Ln = Dy, Yb) with alcohols HOR (R = $(CH_2)_4CH_3$, $(CH_2)_2$-CHMe) in THF (Wu et al. 1996a) produces dinuclear dimers $[Cp_2Ln(\mu\text{-}OR)]_2$ with symmetrical alkoxide bridges (A) while with acetoxime the dimeric complexes $Cp_2Ln(\mu$-

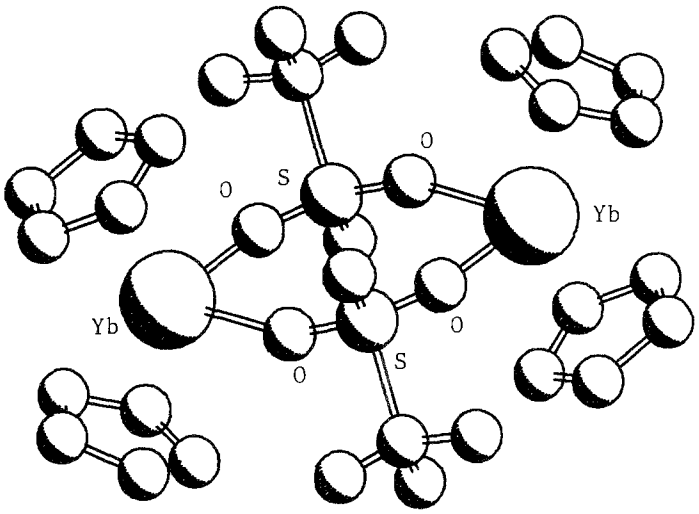

Fig. 12. Crystal structure of $[Cp_2YbOSO_2CF_3]_2$ (Stehr and Fischer 1992).

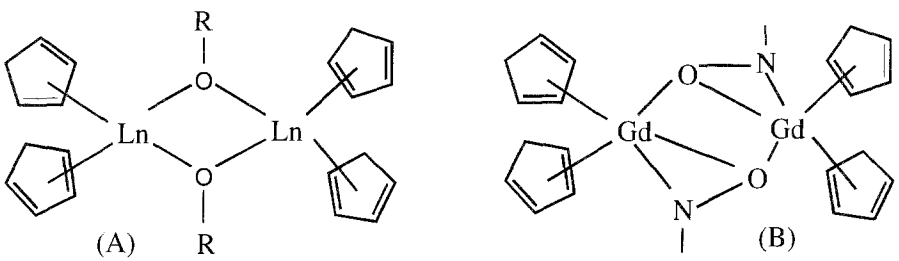

Scheme 5.

η^2-ONCMe) (Ln = Pr, Gd, Dy, Yb) are obtained. The X-ray structure of the Gd derivative (Wu et al. 1996b) shows that the N–O fragment of the oximato ligand acts as bridging and side-on donating group (B) (see scheme 5).

Mononuclear derivatives $Cp_2Ln(THF)(OR(F))$ are obtained with 2,4,6-tris(trifluoromethyl)phenol(RFOH) (Ln = Nd, Sm, Yb; Poremba et al. 1995).

By reaction of dicyclopentadienyl scandium chloride with Na(acac) (acac = acetylacetonate) the monomeric $Cp_2ScOC(Me)CHC(O)Me$ complex, bonded by the chelating acac group, was isolated. Mass spectra studies of twelve ytterbium compounds of Cp_2YbL and $CpYbL_2$ types (LH = acetylacetone; 2,2,6,6-tetramethylheptane-3,5-dione; 1,1,1-trifluoroacetylacetone, benzoylacetone, 4-benzoyl-3-methyl-1-phenyl-5-pyrazolone and trifluoroacetyl-α-thiophene) indicate that thermal disproportionation reactions occur when the compounds reach a certain evaporation temperature to give $Cp_3Yb^{\bullet+}$ and $L_3Yb^{\bullet+}$ products (Yang et al. 1989).

CO inserts at room temperature into the Lu–C bond of $Cp_2Lu–CMe_3(THF)$ to give the corresponding η^2-acyl compound, $Cp_2Lu[\eta^2–C(O)^tBu]$, characterized by IR and ^1H NMR

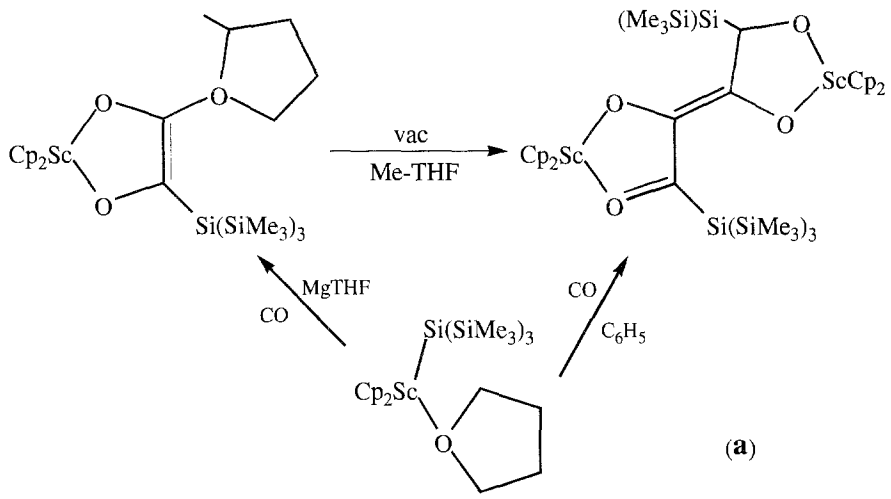

Scheme 6.

spectroscopies (Evans et al. 1981a). In the presence of an excess of CO, the η^2-acyl further reacts to give a purple compound $[Cp_2LuOC(^tBu)=C=O]_2$ containing two Cp_2Lu moieties bridged by the enedione diolate ligand 4,5-dihydroxy-2,2,7,7-tetramethyloct-4-ene-3,6-dionato which forms 6-membered metallocyclic rings with each Lu ion according to the crystallographic results. The use of ^{13}CO gave some evidence that ketene-carbene intermediates are involved in the formation of the final product.

Carbon dioxide activation has been carried out by $Cp_2Sc\text{-}SiR_3$ ($R_3=(SiMe_3)_3$, $^tBuPh_2$) to give the corresponding silanecarboxylate complexes, $[Cp_2Sc(\mu\text{-}O_2CSiR_3)]_2$ (Campion et al. 1990a). The dimeric nature of the complex with $R_3=(SiMe_3)_3$ was established by X-ray crystallography while $[Cp_2Sc(THF)Si(SiMe_3)_3]$ is a monomer (Campion et al. 1993; Sc–Si, 2.863(2) Å). The monomeric structure of the organoactinide silyl complex Cp_3USiPh_3 is also known (Porchia et al. 1989).

With carbon monoxide activation by $Cp_2Sc(ER_3)THF$ ($ER_3=Si(SiMe_3)_3$, $SiPh_2^tBu$, $Ge(SiMe_3)_3$) the compounds $Cp_2Sc[OC(ER_3)C(L)O]$ ($L=THF$, MeTHF, PMe_2Ph) or the enedionediolates $Cp_2SiSc[OC(ER_3)CO]_2$ have been isolated (Campion et al. 1993).

Generally, electron-deficient alkyl and silyl complexes of d^0 metals such as $Cp_2Sc\text{-}R'$, insert CO or isocyanides to form reactive η^2-acyl or η^2-iminoacyl derivatives (Campion et al. 1990a). In some cases, products of CO–CO or CNR–CNR coupling result. Thus, carbonylation of $Cp_2Sc\text{–}SiMe_3\cdot THF$ in methyltetrahydrofuran (Me–THF) (50 psi of CO) gave the orange complex (a, scheme 6), characterized by ^{13}C NMR spectroscopy in solution. The ^{13}C NMR spectrum of 2-$^{13}C_2$ (obtained by carbonylation with ^{13}CO) shows doublets at δ 142.21 and 158.57 ($^1J_{CC}=84$ Hz), indicating coupling of two CO molecules. Removal of the coordinated Me–THF affords the enediolate complex characterized by mass spectrometry and the ^{13}C NMR spectrum.

Hydrolysis of Cp_2Y^tBu in the presence of diphenylethylene gives the dimer hydroxide $[Cp_2Y(\mu\text{-}OH)]_2\cdot C_2Ph$ solvate (Evans et al. 1988a), while cleavage of THF in the

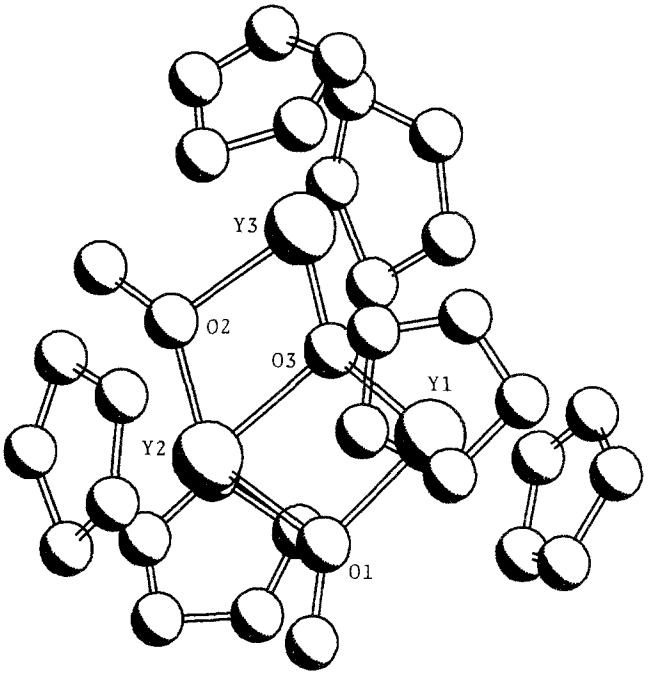

Fig. 13. Crystal structure of the anion $\{[Cp_2Y]_3(\mu\text{-}OMe)_2(\mu^3\text{-}O)\}^-$ (Evans et al. 1992a).

crystallization process from THF of $Cp_2LuPPh_2 \cdot THF$ produces the dimer $\{Cp_2Lu[\mu\text{-}O(CH_2)_4PPh_2]\}_2$ (Schumann et al. 1990a). A rare oxobridged dimer, $[Cp_2Lu(THF)]_2(\mu\text{-}O)$ with a linear Lu–O–Lu moiety (from X-ray results) is obtained by hydrolysis of $Cp_2LuAsPh_2(THF)$. A trinuclear anionic derivative containing μ-methoxo and μ-oxo bridges is revealed in the structure of $\{[Cp_2Y]_3(\mu\text{-}OMe)_2(\mu_3\text{-}O)\}^-$ (fig. 13) the cation being $[(Na(THF)_3)_2(\mu\text{-}Cp)]^+$ (Evans et al. 1992a).

The heavier **VIA** group elements like S and Se can coordinate the Cp_2Ln moiety, but with minor stability with respect to the oxygen donor ligands. The few known examples have the same geometry as the oxygen analogs. The first Se derivative, $Cp_2Lu(\mu\text{-}SePh)_2Li(THF)_2$, was obtained from $Cp_2Lu(\mu\text{-}Me)_2Li(THF)_2$ and benzeneselenol (Schumann et al. 1988c). The X-ray structure of $Cp_2Lu(\mu\text{-}SePh)_2Li(THF)_2$ is shown in fig. 14. The same reaction with 2-methylpropane-2-thiol affords the corresponding sulfur derivative of analogous structure. The monomer $Cp_2Lu(\mu\text{-}S^tBu)_2Li(THF)_2$ (Schumann et al. 1988c) derivative characterized by NMR data is also known as well as $Cp_2DySC_4H_9$ (Wu et al. 1994a) for which NMR data suggest a dimeric structure. Very recently (Wu et al. 1996c) a series of dimeric lanthanide thiolates $[Cp_2Ln(\mu\text{-}SR)]_2$ ($R = CH_2CH_2CH_3$ or $R = CH_2CH_2CH_2CH_3$, Ln = Dy, Yb) have been isolated by protonolysis of the corresponding Cp_3Ln with HSR (in THF at room temperature). The X-ray structure of $[Cp_2Yb(\mu\text{-}S(CH_2)_3CH_3)]_2$ (Wu et al. 1996d) shows the *n*-butyl group in *anti*-conformation relative to the Yb_2S_2 ring.

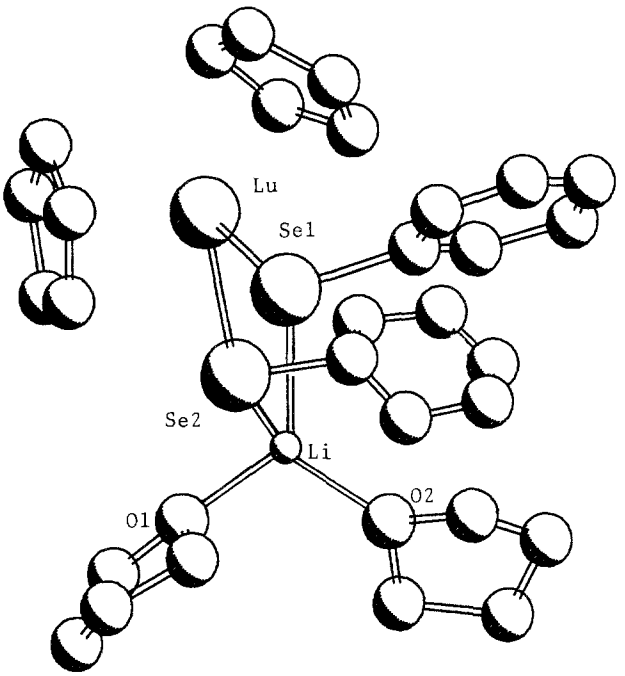

Fig. 14. Crystal structure of $[Cp_2Lu](\mu\text{-}SePh)_2Li(THF)_2$ (Schumann et al. 1988c).

The more hindering thiolate anion $[R(F)S]^-$ (R(F) = 2,4,6-tris(trifluoromethyl)phenyl) was used in the synthesis of the first mononuclear Yb(thiolate) derivative $Cp_2Yb(THF)$-SR(F) (Poremba et al. 1995) which was structurally characterized (Yb–S, 2.639(3)Å), the hindering RF ligand prevents dimerization.

Cp_2ErNH_2 was the first organolanthanide compound containing a Ln–N bond to be isolated (Magin et al. 1963). The insertion of *tert*-butylisocyanide into the Y–H bond of $[RCpYH(THF)]_2$ (R = H, Me) gives rise to the corresponding formimidoyl derivatives (Evans et al. 1983a, 1987a):

$$[RCp_2LnH(THF)]_2 + CN\text{–}{}^t\!Bu \rightarrow \left[RCp_2Ln\left(\mu, \eta^2\text{-}HC = NCMe_3\right)\right]_2,$$

where Ln = Y, Er; R = H, Me.

The two complexes with R = H, crystallographically characterized (fig. 15), are isostructural with $Y\text{–}C_{(Cp)} = 2.68(1)$ Å, $Y\text{–}C_{(\sigma)} = 2.553(8)$ Å, Y–N = 2.325(4) Å and $Er\text{–}C_{(Cp)} = 2.64(1)$ Å, $Er\text{–}C_{(\sigma)} = 2.52(2)$ Å and Er–N = 2.304(8) Å.

The X-ray dimeric structure of an other type of alkylideneamido lanthanide species $[Cp_2Y(\mu\text{-}N = CH{}^t\!Bu)]_2$ shows the two Cp_2Y units connected by two asymmetric Y–N bridges (Evans et al. 1984a) while with the diazadiene ligand DAB (^{t}Bu–N=CH–CH=N–^{t}Bu) the bimetallic compound $Cp_2Yb(\mu\text{-DAB})Li(DME)$ has been prepared, where the Cp_2Yb fragment is linked to the Li ion through two symmetric Yb–N bridges (Trifonov et al. 1994). Pyridine adducts Cp_2Ypy and Cp_2Ypy_2 (obtained in excess

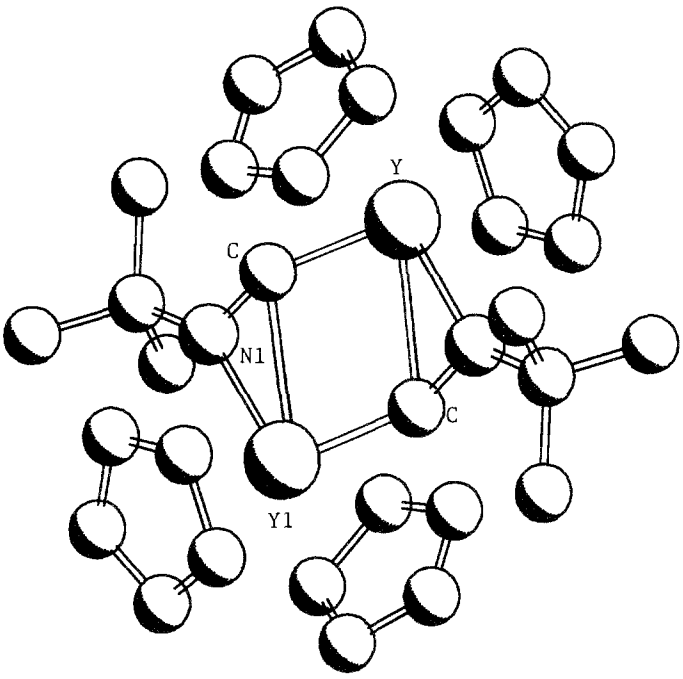

Fig. 15. Crystal structure of $[Cp_2Y(\mu\text{-}\eta^2\text{-}(HC{=}N^tBu)]_2$ (Evans et al. 1983a).

of py from the monoadduct) are also known (Evans et al. 1984a). A monomeric pseudotetrahedral structure is shown by the pyrrol derivative $Cp_2Lu(NC_4H_2Me_2)(THF)$ as demonstrated by the X-ray analysis of the compound with the pyrrole η^1-coordinated to the metal (with d transition metal it behaves also as a pentahapto ligand; Schumann et al. 1990b). The same type of geometry has been observed in the anion of the $[Cp_2Lu(NPh_2)]^-[Li(THF)_4]^+$ (Et_2O) complex (Schumann et al. 1990c). Recently (Campion et al. 1993) the blue $Cp_2ScN(C_6H_3Me_2\text{-}2,6)\text{-}C(SiMe_3){=}C\{NC_8H_9[Si(SiMe_3)_2]\}$ derivative was obtained from $Cp_2ScSi(SiMe_3)_3THF$ and $CNC_6H_3Me_2$-2,6 reacted in benzene. Unlike CO, isoelectronic $CN_{(xylyl)}$ affords an isolable monoinsertion product $Cp_2Sc\{\eta^2\text{-}C[Si(SiMe_3)_3]N(xylyl)\}$ (^{13}C NMR, iminoacyl carbon at δ 299.07) with $Cp_2Sc[Si(SiMe_3)_3](THF)$. Addition of a further equivalent of CN(xylyl) to the monoinsertion product results in the formation of the isocyanide coupling product, the crystal structure of which has been solved (scheme 7).

The chelate ring is derived from the two isocyanide groups and contains a Sc–N(1) single bond (2.133(7) Å), a longer (dative) Sc–N(2) bond (2.324(8), a C=C double bond (C(1)–C(2) = 1.375(12) Å; Campion et al. 1990b).

Dicyclopentadienyl lanthanide compounds containing Ln–P bonds were prepared by reaction of the corresponding chlorides and LiPRR′ (Marks and Ernst 1982). With lithium cyclohexylphosphide and lithium phenylphosphide, $[Cp_2YbPHC_6H_{11}]$ and $[Cp_2YbPHPh]$ are formed first but cannot be isolated as they decompose in solution to give polymeric

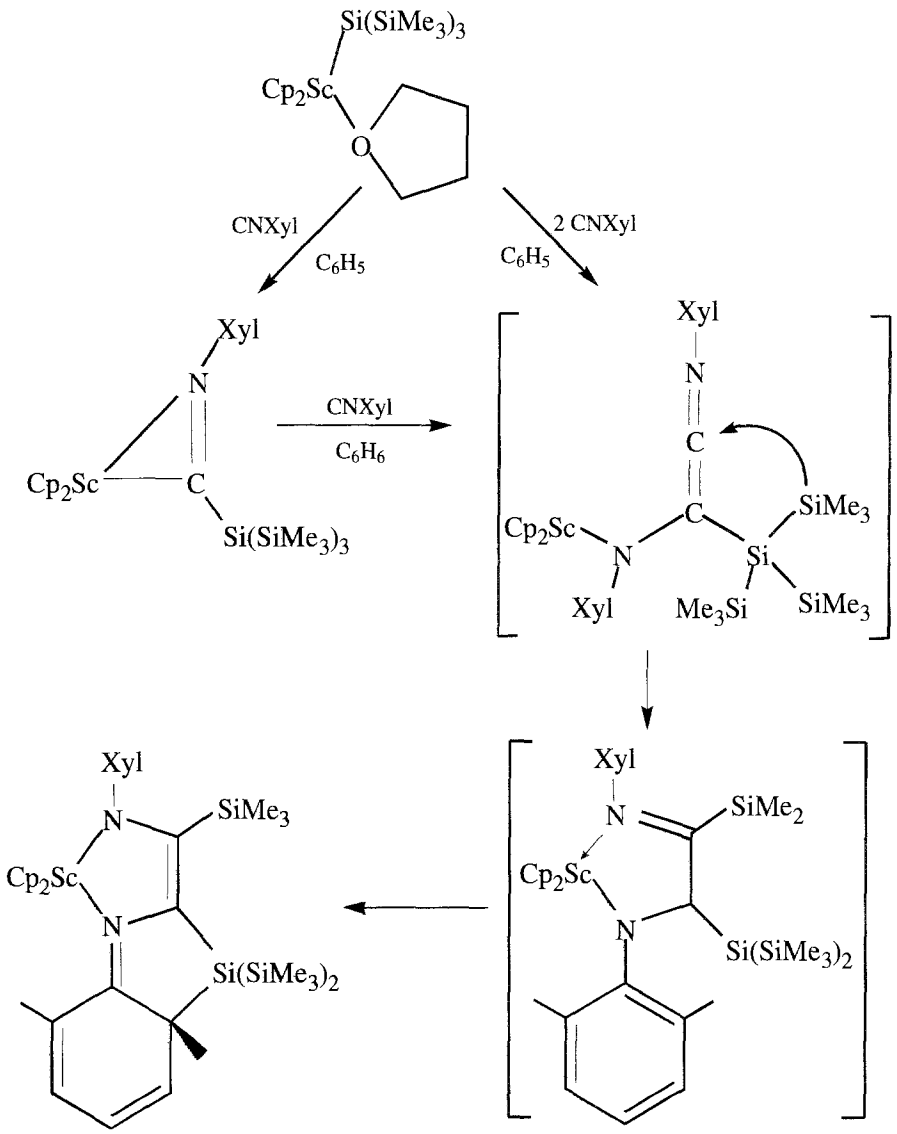

Scheme 7.

species $[CpYbPC_6H_{11}]_n$ and $[CpYbPPh]_n$, respectively. The first X-ray structural characterization of an organolanthanoid-phosphane $[Cp_2Lu(PPh_2)_2Li(tmed)\cdot 1/2toluene]$ was reported by Schumann et al. (1986b) (the Lu–P distances are 2.782(1) Å and 2.813(2) Å). The As analog (Schumann et al. 1988d) has the same structure.

Dicyclopentadienyl lanthanide chlorides react with $NaBH_4$ in THF solution to yield the corresponding monomeric borohydride complexes isolated as THF adducts (Schumann et al. 1982, Marks and Grynkewich 1976)

$$Cp_2LnCl \cdot (THF) + NaBH_4 \xrightarrow{THF} Cp_2LnBH_4 \cdot (THF) + NaCl,$$

where Ln = Sm, Er, Yb, Lu. The IR spectra of the Sm borohydride and borodeuteride suggest that the borohydride or borodeuteride groups act as tridentate bridges, while in the case of the smaller Er and Yb derivatives bidentate bridges are proposed. The Lu derivative reversibly loses the coordinated THF molecule upon heating in vacuo or in solution (toluene).

Two borohydride complexes were synthesized. The reaction of $[Cp_2YCl]_2$ with $NaBH_4$ in THF gave $Cp_2Y(BH_4)(THF)$ in 67% yield and in DME $Na[Cp_2Y(BH_4)_2]$ in 66% yield (Borisov et al. 1986).

2.1.6.3.2. *Actinides.* $Cp_2U(NEt_2)_2$ has been used as starting material for the synthesis of many other Cp_2UX_2 compounds by protolysis of the diethylamido ligands by a variety of protonic or electrophilic sterically crowded reagents (Marks and Ernst 1982). The protolysis of $Cp_2U(NEt_2)_2$ with ROH and ArOH yields the corresponding $Cp_2U(OR)_2$ derivatives only when the alcohol is sterically hindered, otherwise the usual ligand redistribution processes take place. $Cp_2U(NEt_2)_2$ was shown to react with 8-hydroxyquinoline to form Cp_2U(8-hydroxyquinolate)$_2$ (Zanella et al. 1984a). Attempts to prepare this compound by reacting UCl_2(8-hydroxyquinolate)$_2$ with TlCp produced Cp_3UCl instead.

With $ThCl_4$ and UCl_4 some tropolonate (trop) compounds have been prepared: $Cp_2U(trop)_2$, $CpU(trop)_3$, $CpU(trop)Cl_2$ and $CpU(trop)_2Cl$ (Zanella et al. 1984b). The Cp_2UX_2 formulation is also stabilized using the charged chelating triazenides and formamidides (Paolucci et al. 1985b):

$$Cp_2U(NEt_2)_2 + HL \rightarrow Cp_2UL_2 + 2HNEt_2,$$

where L = *N*,*N*′-di-*p*-tolyltriazenide, *N*,*N*′-di-*p*-tolylformamidide.

BH_4^- ligands have again been attached to organouranium moieties, as for example in $[Cp_2U(BH_4)]^-$ (Le Maréchal et al. 1988) and $CpU(BH_4)_3L_2$ where BH_4 group is bound to the uranium atom in a tridentate mode, and L is a neutral monodentate O-donor (Baudry et al. 1988a). Using different ligands, (η-2,4-dimethylpentadienyl)$U(BH_4)_3$ and (η-6,6-dimethyl-cyclohexadienyl)$_2U(BH_4)_2$ have been synthesized and their products investigated (Baudry et al. 1988b).

2.1.7. *Cp'_2MX with substituted cyclopentadienyls*

2.1.7.1. *X = halide.*

2.1.7.1.1. *Lanthanides.* The use of substituted Cp has been introduced in order to determine the structural and chemical and physical properties changes in the metal complexes depending on the number and the type of ring substituents. An important

class of derivatives has been obtained with modified RC_5H_4 ligands where the most common R groups are Me, ^{t}Bu, Me_3Si, Me_2PhSi, $MeOCH_2CH_2$ or 1,3-$R_2C_5H_4$ with R = ^{t}Bu and Me_2Si. The complexes show coordination geometry comparable to those of the unsubstituted parent even though better crystallization properties are determined by the reduced vibrational motion of the substituted Cp ligand.

Dimeric $[(^t BuCp)_2LnCl]_2$ (Ln = Sm, Lu) have been obtained by reacting the corresponding anhydrous lanthanide trichlorides with two equivalents of Na^{t}BuCp (Wayda 1989). The synthetic effect of monosubstitution of the Cp ring with a bulky *tert*-butyl group is minimal. The use of this ligand does not yield of mono- and bis(cyclopentadienide)-derivatives to the early lanthanides.

For the smallest lanthanide, Lu, the metal is apparently too small to permit three bulky ^{t}BuCp ligands to coordinate. Syntheses directed towards the isolation of the expected $(^t BuCp)_3Lu$ yield only the bis(cyclopentadienide)-derivative. For samarium, approximately in the middle of the series (on the basis of size) the metal is large enough to allow the isolation of $(^t BuCp)_3Sm$ and $[(^t BuCp)_2SmCl]_2$ but too large to support the stable coordination of one ligand without ligand redistribution. For lanthanum, as in the unsubstituted case, $(^t BuCp)_3La(THF)$ (see sect. 2.1.3.1) can be isolated but the corresponding bis(cyclopentadienide)complex cannot.

With disubstituted Cp ligands as (Cp** = 1,3-$^t Bu_2$-C_5H_3) the dimeric $[Cp^{**}_2Nd(\mu\text{-}Cl)]_2$ has been prepared by the reaction of $NdCl_3(THF)_2$ with two equivalent of KCp**. Significant structural parameters are: Nd–Cl, 2.837(1) and 2.841(1) Å; Nd–C(Cp)av, 2.760(1) Å; Nd–Cg, 2.486(1) Å (Cg = Cp ring centroid); Nd–Cl–Nd′, 106.0(1)°; and Cl–Nd–Cl′,74.0(1)° (Recknagel et al. 1991a).

The introduction of a bulky -$SiMe_3$ group into a cyclopentadienyl ligand made possible the isolation of early lanthanide dicyclopentadienyl chlorides either as solvated monomeric species or as dimers. A series of $[Cp'_2Ln(\mu\text{-}X)]_2$ and $[Cp'_2Ln(\mu\text{-}X)]_2Li(L)_2$ (Cp′ = Me_3Si–C_5H_4; Ln = Y, Yb, Lu; X = Cl, I; L = THF, tmed, Et_2O) were obtained (Marks and Ernst 1982). The X-ray structure of $[Cp'_2Yb(\mu\text{-}Cl)]_2$ has been investigated recently (Spirlet and Goffart 1995).

Another bulky substituted cyclopentadienyl ligand was introduced in the chemistry of organo-f-elements by Lappert et al. (1981a,b), the bis(trimethylsilyl)cyclopentadienyl anion, (Cp″ = $C_5H_3(Me_3Si)_2$). Organo-f-elements compounds containing this ligand show an increased solubility in aprotic solvents. The reaction of $LnCl_3$ with $Li[(Me_3Si)_2C_5H_3]$ in THF yields complexes of the type $[(Me_3Si)_2C_5H_3]_2Ln(\mu\text{-}Cl)_2Li(THF)_2$ (including early lanthanides) which by heating above 140°C under vacuum decompose to the corresponding solvent free species. The same solvent free compounds have been isolated after sublimation at 250–280°C 10^{-3} torr for the whole series of lanthanides from scandium to lutetium as crystalline solids. The X-ray crystal structures of isostructural $[Cp''_2Ln(\mu\text{-}Cl)]_2$ (Ln = Sc, Pr, Yb) show distorted tetrahedral coordination around the metal ions. The dimers $[Cp''_2Ln(\mu\text{-}Cl)]_2$ (Ln = Y, Pr, Nd, Dy, Tm) react with chlorides of large cations ZCl (Z = $N(PPh_3)_2$, PPh_4, $AsPh_4$, $PPh_3(CH_2Ph)$) to give stable $[Z][Cp''_2LnCl_2]$ which decompose on melting at about 165–175°C (Lappert et al. 1983a).

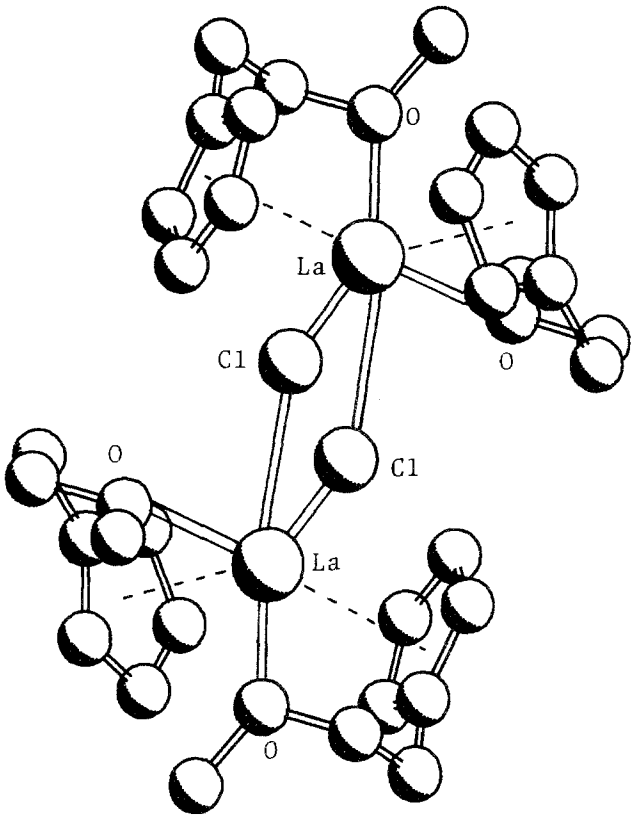

Fig. 16. Crystal structure of $[(MeOCH_2CH_2C_5H_4)_2LaCl]_2$ (Deng et al. 1990a).

The reaction of THF-solvated lanthanide triiodides with two equivalents of KCp″ yields $[K(THF)_x][Cp''_2LnI_2]$ which after extraction with toluene and successive treatment with MeCN produces $Cp''_2Ln(I)(NCMe)_2$ (Ln = La, Ce; Hazin et al. 1990). Significant changes in the coordination geometries occur with substituted Cp ligands containing coordinating side chains as in $[(MeOCH_2CH_2Cp)_2Ln(\mu\text{-}Cl)]_2$ (Ln = La, Pr, Nd; Deng et al. 1990a). The crystal structure of the lanthanum derivative revealed a chelating $MeOCH_2CH_2Cp$ ligand η^5-coordinated through the ring carbon atoms and forming an intramolecular Lewis acid/base adduct with the ethereal substituent (fig. 16) with a pseudo octahedral coordination geometry. The corresponding Ln = La, Nd, Gd, Ho, Er, Yb and Y derivatives were studied by X-ray photoelectron spectroscopy (Deng et al. 1990b) with smaller lanthanides (Nd, Dy, Er, Yb), and X = Cl (Chen et al. 1993) monomeric species $(MeOCH_2CH_2C_5H_4)_2LnX$ have been obtained of pseudo trigonal bipyramidal geometry as detected by X-ray crystallography. The same geometry and monomeric species can be obtained also with iodine when Ln = La, Nd, Y (Qian et al. 1994) of formal coordination number 9 (it was ten in the La dimer). The $(Me_2NCH_2CH_2Cp)_2NdCl$ compound (Herrmann et al. 1993) is also a monomer with the two nitrogen atoms

bonded to Nd and a formal coordination number 9. A review article on the synthesis and structure of organolanthanide complexes with the 2-methoxyethylcyclopentadienyl ligand was recently published (Wang et al. 1995).

2.1.7.1.2. *Actinides.* The complete series of dimers $[Cp''_2U^{III}X]_2$ [X = F, Cl, Br; Cp'' = η^5-1,3-$C_5H_3(SiMe_3)_2$] has been prepared by reduction of the corresponding $Cp''_2U^{IV}X_2$ halides with Na/Hg in toluene (Blake et al. 1986b). The fluoride was obtained by reduction of $[Cp''_2U(\mu\text{-}BF_4)(\mu\text{-}F)]_2$. The isostructural chloride and bromide derivatives are centrosymmetric dimers in the crystal. The symmetric halide bridge has the dimensions: U–Cl, 2.818(4) [2.94(1)] Å; U–Cl′, 2.802(4) [2.93(1)] Å. The Pr analog (Lappert et al. 1981a) is also isostructural to the two U halides and the geometrical parameters are almost identical to the chloride derivative.

Nine years later the same authors (Blake et al. 1995) report the synthesis, spectroscopic data and the X-ray crystal structure for the monomeric U^{IV} and Th^{IV} halide derivatives. Cp''_2AnX (An = Th, U; X = Cl; An = U, X = Br, I, BH_4). The structural motif is analogous to that of the anion $[Cp''_2UCl_2]$ (see below) with the Me_3Si groups staggered in the iodine derivative while they are eclipsed in the Cl, Br, BH_4 derivatives (U–Cl is 2.579(2) Å significantly shorter than in the U^{III} anionic derivative; Th–Cl is 2.632(2); U–Br, 2.734(1); U–I, 2.953(2) and U···B, 2.56(1) Å). From the Lappert group (Edelmann et al. 1995) a ligand which is new, for f element chemistry, $[C_5H_2(SiMe_3)_3]1,2,4]^-$ (= Cp‴) has been used for the synthesis of two Th^{IV} derivatives $[Cp'''_2ThCl_2(Et_2O)]$ and the unsolvated one, while the entirely new $[C_5H_3(SiMe_2{}^tBu)_2$ 1-2$]^-$(Cp^{1*}) ligand allowed the preparation of $[Cp^{1*}_2ThCl_2]$, $[Cp^{1*}_2ThCl_2(dmpe)]$, $[Cp^{1*}_2ThCl_2(acac)Cl]$ and $[Cp^{1*}_2ThClCH(SiMe_3)_2]$. They have been characterized by NMR and mass spectra and for the latter the X-ray structure determination showed the usual distorted tetrahedral coordination geometry of the bent metallocene (Th–Cl bond distance is 2.607(6) and Th–C_σ, 2.55(2) Å).

$Cp''_2U^{III}(\mu\text{-}Cl)_2Li(L)_n$, L = THF, n = 2; L = PMDETA, n = 1] are the first dichloro-bridged alkali metal complexes to be structurally characterized (Blake et al. 1988a). The PMDETA (PMDETA = *N,N,N′,N′,N″*-pentamethyldiethylenetriamine) adduct has been obtained by reduction of Cp''_2UCl_2 with $[Li(\mu\text{-}P(SiMe_3)_2(THF)_2]$ as reducing agent. The compound of usual distorted tetrahedral geometry around Li and U coordination spheres is characterized by U–Cl and Li–Cl bond lengths of 2.730(1) and 2.46(6) Å, respectively. The reaction of the starting chloride with LiX (X = Cl, Br) in THF or $[PPh_4]X$ in toluene yielded $Cp''_2U(\mu\text{-}Cl)(\mu\text{-}X)Li(THF)_2$ or $[PPh_4][Cp''_2UClX]$. The crystal structure of $[PPh_4][Cp''_2UCl_2]$ shows the usual distorted tetrahedral geometry around the uranium metal ion (U–Cl = 2.666(8) Å; Blake et al. 1988b).

The dimeric $[(^tBu_2Cp)_2UCl]_2$ (Zalkin et al. 1988b) shows small geometrical changes with respect to the Me_3Si substituted cyclopentadienyl derivative, attributed to the larger steric hindrance of Me_3C than Me_3Si group which hinders a closer approach to the uranium atom. The rings of the bent sandwich molecule are in staggered configuration with respect to each other.

The good donor properties of organic cyanides and isocyanides towards uranium metal centers appear in the three compounds of general formula Cp''_2UXL_2 (X = Cl, L = $CNC_6H_3Me_2$, Zalkin and Beshouri 1989a; L = $NCSiMe_3$, Zalkin and Beshouri 1989b;

and X = Br, L = CNMe, Beshouri and Zalkin 1989), obtained from the corresponding $[Cp''_2UX]_2$ derivatives and the appropriate isocyanide ligand. The uranium atom is formally five coordinated. The dimer, $[Cp''U(BF_4)F]_2$ was prepared by the reaction of $AgBF_4$ in OEt_2 with $Cp''UCl_2$ or $Cp''U(CH_2R)_2$ (R = $SiMe_3$, Ph) and structurally characterized (Hitchcock et al. 1984). The bridging fluorides are not symmetrical at 2.354(5) and 2.260(5) Å from U. The bridging BF_4^- ligands are 2.402(5) and 2.420(5) Å from the U atom.

2.1.7.2. *X = hydrocarbyl.*

2.1.7.2.1. *Lanthanides.* The great interest in the Cp ring substituted complexes is connected to their possible application in the homogeneous ethylene polimerization as the alkyl-bridged species $Cp'_2Ln(\mu\text{-}R)_2AlR_2$ and $Cp'_2Ln(\mu\text{-}R)_2LnCp'_2$ (R = CH_3, C_4H_9, C_8H_{17}, $C_5H_3CH_3$; Ln = Y, Ho, Er, Yb) containing methylcyclopentadienyl, trimethylsilylcyclopentadienyl, tetramethylcyclopentadienyl (Cp′) ligands (Ballard et al. 1978). Dimeric structures with symmetric methyl bridges have been found in $[(Me_2Cp)_2YMe]_2$ prepared by reacting $(Me_2Cp)_2YCl(THF)$ with LiMe. Y–C(σ) = 2.61(2) Å (Evans and Ulibarri 1987a) while in $[(^tBuCp)_2NdMe]_2$ the two $(^tBuCp)_2Nd$ units are connected by asymmetrical methyl bridges with independent Nd–C(σ) bond lengths of 2.70(2) and 2.53(2) Å and Nd–C(σ)–Nd angles of 94.7(9)° and 87.3(6)° (Shen et al. 1991). The analogous Ce derivative is also dimeric (Stults et al. 1993).

The bright orange complex $[(MeCp)_2Yb\text{–}C{\equiv}C\text{–}CMe_3]_2$ has been obtained by the halide-free reaction of $[(MeCp)_2YbCH_3]_2$ with $HC{\equiv}C\text{–}CMe_3$ in THF (Evans and Wayda 1980). The X-ray structure analysis of the analogous samarium compound $[(MeCp)_2Sm\text{–}C{\equiv}C\text{–}CMe_3]_2$ (Evans et al. 1983b) shows a centrosymmetric dimer where the two $(MeCp)_2Sm$ units are connected by alkynyl bridges with Sm–C distances of 2.55(1) Å and asymmetric Sn–C≡C angles with an overall geometry close to the Er analog, $[Cp_2ErC{\equiv}CCMe_3]_2$ (Atwood et al. 1981). The ν(C≡C) IR absorption of this compound falls at 2035 cm^{-1}. The complex appears to be monomeric in THF solution and it undergoes protolysis by Ph_2PH in toluene solution to yield $(MeCp)_2SmPPh_2$. The X-ray molecular structure $[^tBuCp_2Sm\text{–}C{\equiv}CPh]_2$ differs from the previous one only by a greater asymmetry in the alkynyl bridges, suggesting a little η^2-interaction of the triple bond π-orbitals with the samarium center (Shen et al. 1990a).

Other monomeric compounds $(MeC_5H_4)_2LnR$ (Ln = Lu, R = $CH_2CHMeCH_2NMe_2$ base free, Schumann et al. 1992b; Ln = Y, R = $CH_2CH{=}CH_2$, C(Et) = CHEt, Evans et al. 1984a; and CH_2SiMe_3, Evans et al. 1986a) as THF adducts have been synthesized.

The X-ray structure of the dihydroanthracene derivative $[Li(THF)_4]\{[(C_{14}H_{10})CMe_2\text{-}C_5H_4]_2Nd$ (Chauvin et al. 1993) is again a monomer of pseudotetrahedral coordination geometry.

Very recently the ligand 1,3-dithiane was introduced in organolanthanide chemistry with the synthesis of the bis(*tert*-butylcyclopentadienyl) complexes of Lu and Y with σ-bound η^2-coordinated 1,3-dithiane: $[(^tBuC_5H_4)_2Ln(C_4H_7S_2\text{-}1,3)]LiCl{\cdot}2THF$ (Vinogradov et al. 1995) characterized also by X-ray diffraction analysis. The two structures are of about the same type with pseudotetrahedral metal coordination. Interesting is the

unprecedented formation of a "pentagonal coordination ring" formed by Ln1,3-dithiane and a molecule of LiCl (generally the central core is tetragonal with bridging halogen or carbon atoms and metals in the opposite corners positions; Lu–C(19), 2.45(2); Lu–Cl, 2.570(5)Å; Y–C(19), 2.47(3); Y–Cl, 2.638(6)Å).

2.1.7.2.2. *Actinides.* Apart from the new thorium derivative $(C_5H_3(SiMe_2^tBu)_21,3)_2$-Th(Cl)CH$(SiMe_3)_2$ (Edelmann et al. 1995) and the $[(Me_3Si)_2C_5H_3]_2$UCl(CN-2,6-dimethylphenyl)$_2$ derivative (Zalkin and Beshouri 1989a) described in the halide section no other compounds apparently have been reported.

2.1.7.3. *X = non-halide, non-hydrocarbyl.*

2.1.7.3.1. *Lanthanides.* Few oxygen bonded derivatives are known and their structure is very often of dimeric type with the oxygen donor ligand bridging the bent metallocene Ln moieties. Enolate bridges are in the $[(MeCp)_2Y(\mu\text{-}OCH{=}CH_2)]_2$ derivative (Evans et al. 1986b), methoxide in $[(Me_3SiC_5H_4)_2Y(\mu\text{-}OMe)]_2$ (Evans et al. 1992a). The unusual structure of a chiral dimer $\{(MeCp)_2Yb[\mu\text{-}O(C_4H_7O)]\}_2$ is reported in fig. 17 (Masserwech and Fischer 1993). ^{t}Butyl-substituted cyclopentadiene Ce alkox-

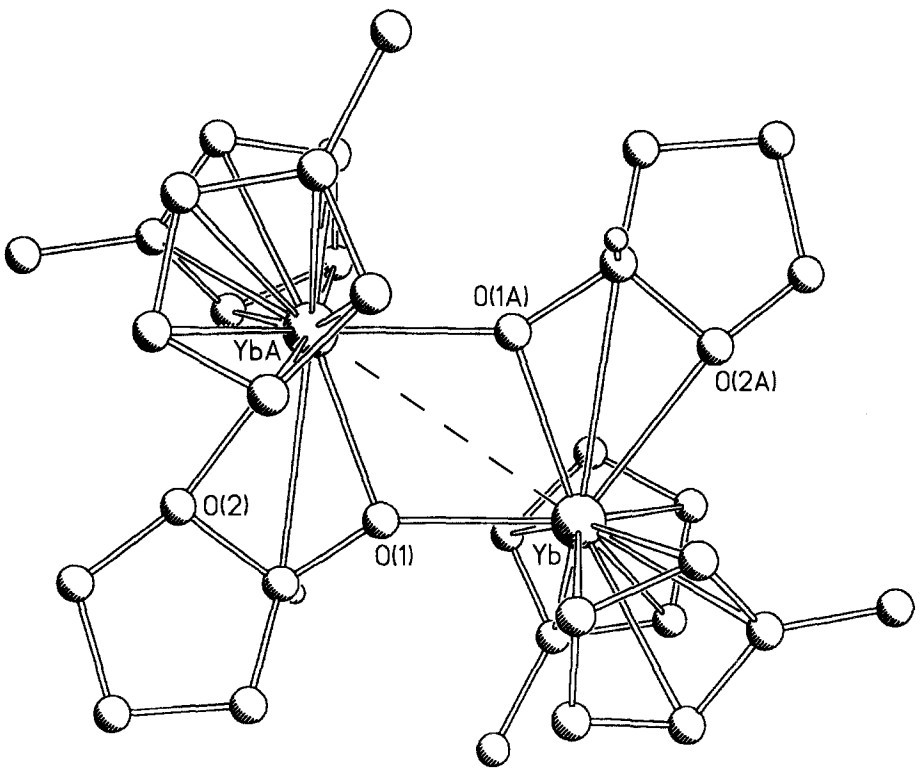

Fig. 17. Crystal structure of $\{(MeC_5H_4)_2Yb[\mu\text{-}O(C_4H_7O)]\}_2$ (Masserwech and Fischer 1993).

ide dimeric complexes $[(^tBuC_5H_4)_2Ce(\mu\text{-}OR)]_2$ (R = ^{i}Pr, Ph) with bridging alkoxide groups are known, they have the usual pseudotetrahedral geometry around Ce (Stults et al. 1990b).

With trimethylsilyl-substituted ligands pure hydroxide derivatives $\{[(Me_3Si)_2C_5H_3]_2\text{-}Ln(\mu\text{-}OH)\}_2$ have been obtained (Hitchcock et al. 1991) by hydrolysis of the corresponding bivalent samarocene and ytterbocene derivatives $[(Me_3Si)_2C_5H_3]_2Sm(THF)$ and $(Me_3SiC_5H_4)_2Yb(Et_2O)$. Their dimeric solid state structures as well as that of the lutetium homolog have been reported (Beletskaya et al. 1993a). Other related dimers of the type $[(^tBuC_5H_4)_2Ln(\mu\text{-}OH)]_2$ (Ln = Dy, Nd) were synthesized (Herrmann et al. 1992).

With the 2-methoxyethylcyclopentadienyl ligand (see sect. 2.1.7.1.1) the dimer $[(MeOCH_2CH_2Cp)_2Er(\mu\text{-}OH)]_2$ (Deng et al. 1990b) has been isolated by hydrolysis from the corresponding chloride derivative, the single crystal X-ray structure of which revealed the dimeric nature of the complex with bridging hydroxide groups. The Er–O(OH) bond distances are 2.258(5) and 2.216(5) Å, while the methoxyethyl group coordinated(O*) (Er–O*, 2.542(3) Å) is more loosely bonded.

Very recently the optically active Sm(II) and Yb(II) metallocene complexes of potential use in catalytic reactions (Molander et al. 1996) $\{Ln(S)\text{-}\eta^5\text{:}\eta^1\text{-}C_5H_4(CH_2CHROMe)\}_2$ (R = Me, Ln = Sm, Yb; R = Ph, Ln = Sm), $\{Ln(S)\text{-}\eta^5\text{:}\eta^1\text{-}C_5H_4(CH_2CH(Me)NMe_2)\}_2$ (Ln = Sm, Yb) and $\{Ln(S)\text{-}\eta^5\text{:}\eta^1\text{-}C_5H_4(CH(Ph)CH_2NMe_2)\}_2$ (Ln = Sm, Yb) have been synthesized and the monomeric structure of the Yb derivative of tetrahedral geometry determined.

Sulfur, selenium and tellurium derivatives have also been synthesized. From thiols and alkylcyclopentanedienyl lanthanides (Stults et al. 1990b) dimeric compounds have been obtained according to the equation

$$2(RC_5H_4)_3Ce + 2HSR' \rightarrow \left[(RC_5H_4)_2\,Ce\,(\mu\text{-}SR')\right]_2 + 2RC_5H_5,$$

where R = Me, R′ = ^{t}Bu; R = ^{t}Bu, R′ = ^{i}Pr, Ph, as confirmed by the X-ray crystallography of $[(^tBuC_5H_4)_2Ce(\mu\text{-}S^iPr)]_2$. Many other dimeric derivatives with sulfur and selenium of the type $[(^tBuC_5H_4)_2Ln(\mu\text{-}ER)]_2$ (Ln = Y, E = S, R = Ph, ^{t}Bu, ^{n}Bu, CH_2Ph and ER = SePh; Beletskaya et al. 1993b) have been obtained by cleavage of the Ln–Me bond in $[(^tBuC_5H_4)_2Ln(\mu\text{-}Me)]_2$ by R–E–E–R dichalcogenides.

A tellurium derivative $[(^tBuC_5H_4)_2Y(\mu\text{-}TeMe)]_2$ has been synthesized by reaction of metal with $[(^tBuC_5H_4)_2Y(\mu\text{-}Me)]_2$ (Beletskaya et al. 1993c).

As with the lighter chalcogenides (oxygen) analogous complexes containing nitrogen donor ligands can be synthesized, mainly by using the same methods of the corresponding unsubstituted Cp derivatives and they show the same typology in the crystal structures. The compound $[(MeCp)_2YbNH_2]_2$ was obtained as byproduct of the reaction of MeCpH and Yb metal in liquid ammonia (Hammel and Weidlein 1990). The X-ray structure shows a centrosymmetric dimer where the plane of the Yb_2N_2 fragment is about orthogonal to the plane of the two ring centroids and Yb atoms. Other dimeric species have been synthesized like $[(MeCp)_2Y(\mu\text{-}N{=}CMe)]_2$ (Evans et al. 1984a) and $\{(MeCp)_2Lu[\mu\text{-}\eta^2(HC{=}N^tBu)]\}_2$ (Ln = Y, Er; Evans et al. 1983a, 1987a) which have a structure analogous to that of the corresponding unsubstituted Cp.

Lanthanide iodide compounds of the type $Cp''_2LnI(NCMe)_2$ [Ln = Ce, La; $Cp'' = \eta^5$-$1,3(Me_3Si)_2C_5H_3$] are useful precursors for complexes containing the early-lanthanide fragments $[Cp''_2Ln^{III}]^+$ (Hazin et al. 1990), like the heterobimetallic non-emissive $[Cp''_2Ce(\mu\text{-}\eta^2OC)W(CO)Cp(\mu\text{-}\eta^2CO)]_2$ and the ionic compound $[Cp''_2La(NCMe)(DME)][BPh_4]\cdot 0.5DME$. The cation structure can be described as a bent metallocene with three equatorial ligands. The DME ligand is puckered and the nitrile ligand is essentially linear. Significant distances are La–C(Cp″)(av), 2.83 Å; La–O(1), 2.580(8) Å; La–O(2), 2.673(9) Å; La–N, 2.61(1) Å.

Recently an important series of chiral organolanthanides used as precatalyst for enantioselective or diasteroselective hydroamination/cyclization processes for the conversion of aminoolefins to chiral pyrrolidines and piperidines have been synthesized $[Me_2Si(Me_4C_5)(C_5H_3R)LnN(SiMe_3)_2]$ [Ln = Y, La, Sm, Lu; R = (+)neomenthyl, Sm; R = (–)menthyl, (+)neomenthyl, (–)phenylmenthyl]; Gagné et al. 1992, Girardello et al. 1994a, Wo et al. 1994).

2.1.7.3.2. *Actinides.* Several compounds of the type Cp''_2AnClZ (An = Th, U; $Z = OC_6H_3$-$2,6\text{-}^iPr_2$, OC_6H_3-2,6-Ph, SC_6H_2-$2,4,6\text{-}^tBu_3$) and $[Cp''_2U(OC_6H_3\text{-}2,6\text{-}^iPr_2)(THF)]$ have been prepared and characterized (Blake et al. 1987).

The dimeric species with bent metallocene were found in the μ-oxo derivative $[Cp''_2U(\mu\text{-}O)]_2$ $\{Cp'' = \eta^5\text{-}(Me_3Si)_2C_5H_3\}$ (Zalkin and Beshouri 1988); the U′···U separation is 3.2927(9) Å with rather symmetric bridges U–O, 2.096(6) Å and μ–O′, 2.1209(5) Å.

Tetravalent uranium complexes with bridging organoimide ligands $(MeC_5H_4)_4U_2(\mu\text{-}NR)_2$ have been obtained in THF solution by valence disproportionation and ligand redistribution reaction:

$$(MeC_5H_4)_3\,U\,(THF) + (MeC_5H_4)_3\,U\,(NR) \xrightarrow{THF} (MeC_5H_4)_4U_2(\mu - NR)_2,$$

where R = Ph, $SiMe_3$. The X-ray crystal structures of the two derivatives show that they are centrosymmetric dimers.

When $R = SiMe_3$ the compound is symmetrical (U–N lengths 2.217 and 2.230 Å), but with R = Ph the bridging is not symmetrical (U–N lengths 2.315 and 2.156 Å; Brennan et al. 1988b). This has been rationalized by considering the imide fragment acting as μ,η^3-bridging (scheme 8).

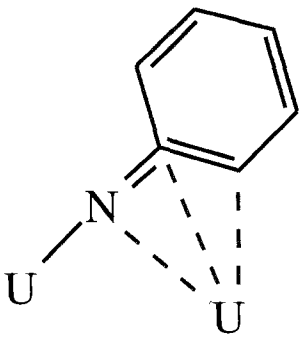

Scheme 8.

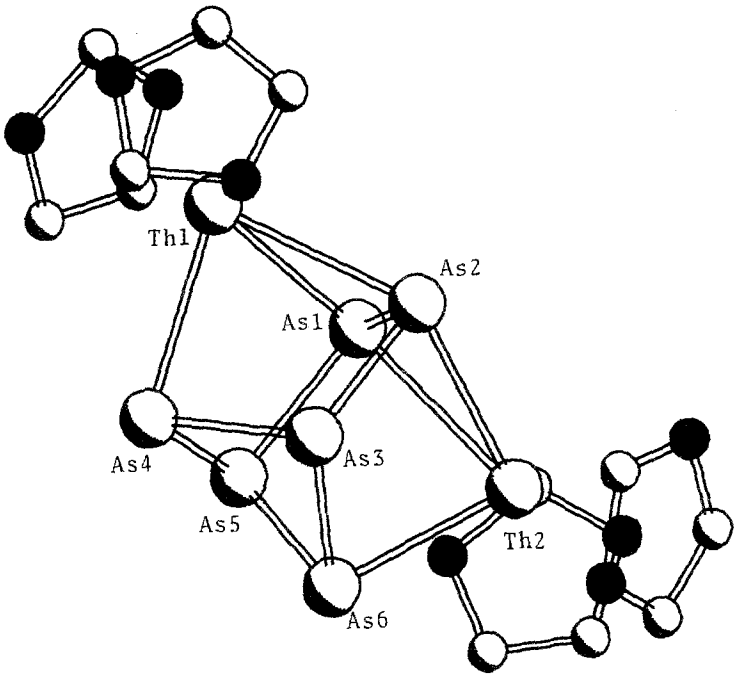

Fig. 18. Crystal structure of $[\{(^tBu)_2C_5H_3\}_2Th]_2As_6$ (solid circles are the carbons attached to ^tBu, omitted for clarity) (Scherer et al. 1994).

In compounds of the type Cp_2UX_2 the reactivity when $X=NEt_2$ is greater than that for other compounds, i.e., $X=BH_4$, O_2CCMe_2, and S_2CNEt_2. This is reflected in the photoelectron spectra of the compounds. The lowest energy ionization events are the removal of U 5f electrons, followed by a N 2p for the NEt_2 complex but by a π-ring electron for the others (Arduini et al. 1987).

An unusual example of a direct An–As bond is given by the dimer $\{[(^tBu)_2C_5H_3]_2Th\}$-$(\mu\text{-}\eta^{2:1:2:1}\text{-}As_6)$ obtained by reaction of $[(^tBu)_2C_5H_3]_2Th(C_4H_6)$ with As in boiling xylene (Scherer et al. 1994). The As_6 ligand according to the authors can be considered as "open-edged" As_6 benzvalene (Th–As range 2.913(2)–3.044(2)Å) (fig. 18).

The same reaction in toluene with $(P_6)^{4-}$ gives the analog with a cage of phosphorus with the same structure (Scherer et al. 1991) while in the presence of $MgCl_2$ $[(^tBu)_2C_5H_3]_2Th(\mu\text{-}\eta^3P_3)Th(Cl)[(^tBu_2)C_5H_3]_2$ is obtained (Th–P range 2.84–2.93 and 2.81–2.99 Å) in the two compounds (fig. 19).

2.1.8. *Cp_2Ln, $Cp_2Ln{\cdot}L_x$, Cp'_2Ln and $Cp'_2Ln{\cdot}L_x$*

The Cp_2Ln compounds (Ln = Yb, Eu) can be obtained either by dissolving Eu and Yb metals in liquid ammonia in the presence of cyclopentadiene (Calderazzo et al. 1966) and successive vacuum sublimation of the ammonia-solvated adducts at 400–420°C, or by reductive methods such as the reduction of Cp_2YbCl with either Na or Yb metal in THF,

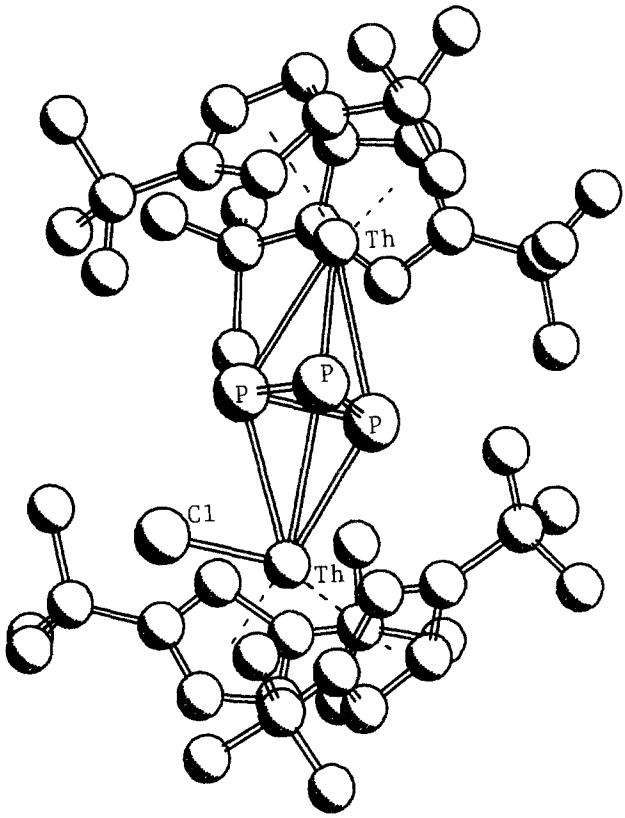

Fig. 19. Crystal structure of $[(('Bu)_2C_5H_3)_2Th(\mu\text{-}\eta^3P_3)Th(Cl)('Bu_2C_5H_3)_2]$ (Scherer et al. 1991).

followed by vacuum sublimation of the THF solvated species. The high degree of ionic character for these very air and moisture sensitive divalent organolanthanides has been derived from various physico-chemical measurements (IR, ^{151}Eu Mössbauer) (Marks and Ernst 1982). A phosphine oxide complex of Yb^{2+}, $Cp_2Yb(OPPh_3)_2$, has been prepared by reacting $Cp_2Yb(DME)$ and Ph_3PO (Deacon et al. 1989b). The X-ray structure of this compound reveals a pseudotetrahedral arrangement of the Cp and $OPPh_3$ ligands around the Yb^{2+} ion. The Yb–O distances are unusually short at 2.30(2) and 2.33(2) Å.

The equilibrium geometries of the metallocenes Cp_2M (M = Ca, Sr, Ba, Sm, Eu or Yb) have been studied by *ab initio* pseudopotential calculations at the Hartree–Fock (HF), MP_2 and CISD levels. In the HF calculations all molecules are found to favor regular sandwich-type equilibrium structures with increasingly shallow potential energy surfaces for the bending motions along the series M = Ca, Yb, Sr, Eu, Sm and Ba (Kaupp et al. 1992a).

Ab initio calculations show that the hypothetical organometallic cations Cp_2Ln^+ (Ln = Sc, La) have bent metallocene structures as a consequence of the covalent σ-bonding contributions involving the totally symmetric metal d_σ orbitals, which favor bent

geometries. Although the contribution to covalent bonding of these orbitals is lower than that of the d_π orbitals, their involvement is sufficient to give bent structures (Kaupp et al. 1992b).

By Na reduction of (^{t}BuCp)$_2$YbCl(THF) in THF, the (^{t}BuCp)$_2$Yb^{II}(THF)$_2$ compound was obtained (Makhaev et al. 1990). The molecule has an approximate C_2 symmetry with the average bond distances Yb–C(Cp), 2.722(16); Yb–O, 2.431(8) Å, and angles Cg–Yb–Cg, 134.0°; O(1)–Yb–O(2), 83.3(4)°. The ^{t}BuCp ligands are staggered.

Interaction of SmI_2 with the sterically hindered (^{t}Bu$_2$Cp)Na yields the monosolvate complex (^{t}Bu$_2$Cp)$_2$Sm·(THF) which is monomeric with a pseudotrigonal coordination environment around the Sm atom (Bel'skii et al. 1990). The wedge-like (^{t}Bu$_2$Cp)$_2$Sm sandwich is bound to THF with a Sm–O distance of 2.57(1) Å and a Cg–Sm–Cg angle of 132.5°. (^{t}BuCp)$_2$Sm(DME) was obtained by metallic sodium reduction of (^{t}BuCp)$_2$SmCl(DME) in THF at reflux (Shen et al. 1990b). In the same way, (^{t}BuCp)$_2$Yb(THF)$_2$ was prepared and when reacted with $OPPh_3$ it gives (^{t}BuCp)$_2$Yb(OPPh$_3$)(THF).

Cp$''_2$Sm (Cp$''$ = (Me$_3$Si)$_2$-1,3-C$_5$H$_3$) was obtained by desolvating Cp$''_2$Sm(THF), prepared in turn from SmI_2(THF)$_2$ and KCp$''$. The solvated complex is an active catalyst in the ethylene polymerization (Evans et al. 1990b). The polymeric lanthanocene(II) compounds [Cp$''_2$Ln] (Ln = Yb, Eu) were prepared by desolvation of the corresponding monomeric Et_2O-adduct (Yb) and THF-adduct (Eu), respectively (Hitchcock et al. 1992). Their crystal structures show a bent metallocene conformation with Cg–Yb–Cg, 138.0° and γ-methyl–metal agostic-like intermolecular interactions: the distance between the metal center of one Cp$''_2$Yb unit and a methyl group of a neighboring unit is Yb···C 2.872(7) Å while in the Eu complex the corresponding intermolecular contact is Eu···C 3.091(6) Å, with a metal–hydrogen distance Eu···H of 2.70 Å (Cg–Eu–Cg 122°) and an unprecedented conformation with a cyclopentadienyl ring bridging η^5:η^3 between two non-equivalent Eu atoms is present. The bis(ethyltetramethylcyclopentadienyl)(THF) complexes of Sm^{II} and Yb^{II} are more soluble reagents than the corresponding penthamethylated analogs but they have similar chemical reactivity (Schumann et al. 1995b). They have been prepared by the reaction

$$LnI_2(THF)_x + 2Na(C_5Me_4Et) \xrightarrow{THF} (C_5Me_4Et)_2Ln(THF) + 2NaI,$$

where Ln = Sm, Yb, and their structure is typically trigonal with bent metallocene moieties. They react with carbene ligand like CN(Me)CMe=CMeN(Me) according to

$$(C_5Me_4Et)_2Ln(THF) + (CHNRCH_2CH_2NR) \xrightarrow{THF} (C_5Me_4Et)_2Ln{-}(CHNRCH_2CH_2NR),$$

where R = Me, ^{i}Pr; Ln = Sm, Yb; giving the corresponding carbene derivatives.

2.1.9. *Monocyclopentadienyls*

2.1.9.1. *Lanthanides.* The advantage of synthesizing f element derivatives with only one bulky Cp ligand is to have compounds more reactive, as the other coordination positions are more accessible for substitution.

In the early studies only species of the heavier lanthanides solvated by three THF molecules could be isolated (Marks and Ernst 1982). Later in the '80s the synthesis of $CpLnCl_2(THF)_x$ complexes with lighter lanthanides (Ln = La, Tm, $x = 3$; Ln = Eu, $x = 2$; Ln = La, Sm, Eu, Tm and Yb, $x = 4$) containing a variable number of coordinated THF molecules was carried out (Chen et al. 1983).

The monomeric nature of $CpLnX_2L_3$ complexes has been shown by the crystal structures of the isostructural complexes $CpErCl_2(THF)_3$ (Day et al. 1982), $CpYbBr_2(THF)_3$ (Deacon et al. 1985b) and $CpYbCl_2(THF)_3$ which have a distorted octahedral geometry of the type *mer-trans* (*trans* chlorines and *mer* THF ligands) like the related $MeCpUCl_3(THF)_2$ (Ernst et al. 1979). All show as major distortions the bending of the equatorial ligands (two THF and two halides) in the opposite direction to the bulk Cp ligand, and the lengthening of the axial Ln–O(THF) with respect to the equatorial Ln–O(THF) bonds, associated with the steric effect of the Cp ligand *trans* to it.

The easy synthesis of $[Li(THF)_2]_2(\mu\text{-}Cl)_4[CpLn\cdot THF]$ (Ln = La, Nd) from $LnCl_3\cdot n LiCl\cdot n THF$ and CpNa has been reported (Jin et al. 1988b). The two compounds are isomorphous, the structure of the Nd derivative shows a distorted octahedral geometry around the metal ion with the *trans* positions filled by Cp and THF on one side and two bridging $(THF)_2Li(\mu\text{-}Cl)_2$ on the other side (significant bond distances are Nd–C(Cp) 2.77, Nd–O 2.52, Nd–Cl 2.78 Å and Cl–Nd–Cl(av)(chelate) angle is 82.0° (av). The Pr derivative has the same structure (Lin et al. 1992).

The octahedral coordination geometry is present also in the binuclear $CpSmCl(THF)_2$-$(\mu\text{-}Cl)_2SmCl_2(THF)_3$ derivative (Depaoli et al. 1990) in the "left half side" of the molecule containing the Cp ligand bonded to Sm connected via double chlorine bridges to the second "right" half of about pentagonal-bipyramidal coordination geometry around to the other Sm.

The dimers $[CpY(\mu\text{-}O^tBu)(O^tBu)]_2$ and $Cp_2Y(\mu\text{-}O^tBu)_2Y(O^tBu)Cp$ have been synthesized in the context of reactivity studies of the trimetallic yttrium alkoxides $Y_3(O^tBu)_7Cl_2$-$(THF)_2$ with alkali metal cyclopentadienyl reagents (Evans et al. 1993a) and their X-ray structure determined.

The reaction of $Cp_2YCl(THF)$ with desolvated KOMe in THF at 30°C affords dicyclopentadienylyttrium methoxide and a minor reaction product $(CpY)_5(\mu\text{-}OMe)_4(\mu^3\text{-}OMe)_4(\mu^5\text{-}O)$. The latter compound has been characterized crystallographically (fig. 20). This rather interesting structure consists of a square pyramid of yttrium atoms each coordinated to one Cp ligand. Each triangular face contains a triply bridging methoxide ligand and a doubly bridging methoxide group is attached to each base (Evans and Sollberger 1986). It is worth noticing the easy formation of cluster alkoxides with mono-Cp derivatives. Some heteroleptic complexes containing bidentate uninegative oxygen ligands of the types $Cp_nLn(sal)_{(3-n)}$ and $Cp_nLn(fur)_{(3-n)}$ (Ln = Nd, Yb, $n = 1,2$; salH = salicylaldehyde; furH = furfuryl alcohol) have been synthesized (Wu et al. 1989) and shown to be thermally unstable with respect to the following disproportionation equations:

$$2CpLnL_2 \rightarrow Cp_2LnL + LnL_3, \qquad 3Cp_2LnL \rightarrow Cp_3Ln + LnL_3,$$

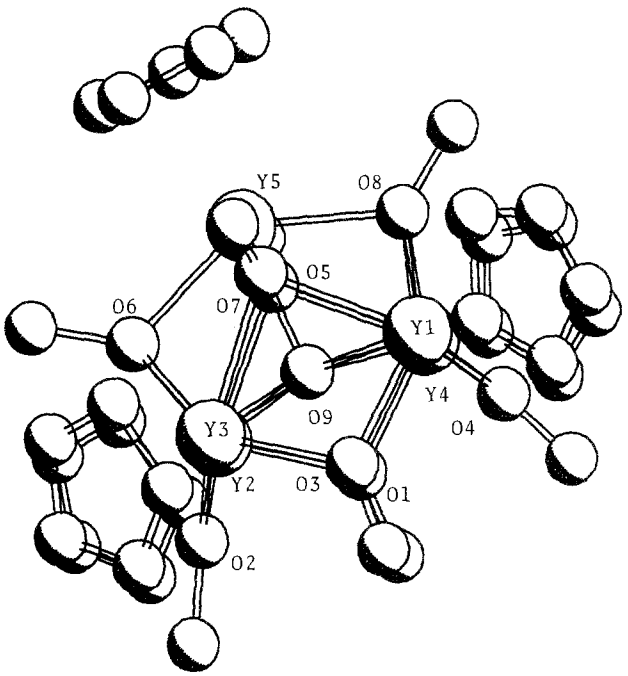

Fig. 20. Crystal structure of $[(CpY)_5(\mu\text{-}OMe)_4(\mu^3\text{-}OMe)_4(\mu^5\text{-}O)]$ (Evans and Sollberger 1986).

where L = sal or fur.

Non-solvated organolanthanide monocyclopentadienyls derivatives have been synthesized (Yu et al. 1991) of general formula $CpLn(Cl)[OCOC_6H_4(O\text{-}Z)]$ (Ln = Sm, Yb; Z = H, F, Br, I and OCH_3) for which a bridged dimeric structure has been postulated on the basis of IR, mass spectra and XPS results.

The lanthanide complexes $CpLu(OSO_2CF_3)_2(THF)_3$ and $Cp_2Lu(OSO_2CF_3)THF$ are potential precursors for new compounds due to the leaving group properties of the triflate anion (Schumann et al. 1989a). The molecular structure of the three THF adduct shows a pseudo-octahedral coordination geometry of the usual type *mer, trans.*

A dimeric structure is present in the $[Cp(THF)Yb]_2[N_2Ph_2]_2$ complex obtained by the reactive $Cp_2Yb(THF)$ treated with azobenzene in THF and toluene (Evans et al. 1988b) with an overall geometry similar to that of $[Cp^*(THF)Sm]_2(N_2Ph_2)_2$ (see sect. 2.1.11.5.1). The substitution of Cp^* with the less hindering Cp produces a shortening in some distances greater than the difference in the respective ionic radii. The scandium monocylopentadienyl moiety can be stabilised by the bulky dianion octaethylporphyrin (OEP), as proved by the successful synthesis and X-ray characterization of CpScOEP which presents a novel type of sandwich structure (Arnold and Hoffman 1990, Arnold et al. 1993).

To compensate for the low saturation of the reactive mono Cp ligand, bulky hydrocarbyl ligands have been introduced. $CpLnX_2 \cdot L_3$ compounds react with cyclooctate-

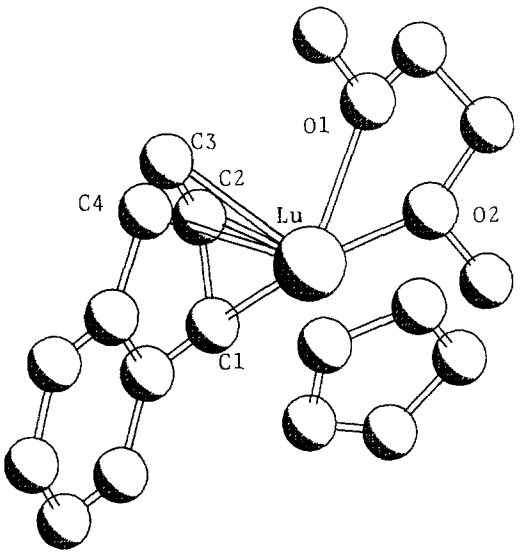

Fig. 21. Crystal structure of $[CpLu(\eta^4C_{10}H_8)\text{-}(MeO(CH_2)_2OMe)]$ (Protchenko et al. 1993).

traenide dianion or with the phenylacetylide anion to produce mixed ligand compounds CpLn(COT)(THF) (Ln = heavier lanthanides) and $CpHo(C{\equiv}C\text{–}Ph)_2$ (Marks and Ernst 1982).

Metathesis of $CpLuCl_2(THF)_3$ and $LiCH_2CH(Me)CH_2NMe$ or $Li(CH_2)_3NMe_2$ produces $CpLu[CH_2CH(Me)CH_2NMe_2](Cl)(THF)_2$ (**1**) and $CpLu[(CH_2)_3NMe_2]Cl(THF)_2$. The X-ray structure of (**1**) (Schumann et al. 1992c) with *mer trans* pseudo-octahedral geometry represents the first example of a monomeric lanthanide with a Lu–C σ-bond (Lu–C 2.411(7) Å. The same philosophy as the chelating effect guided the preparation of the thermally stable $CpY\{[C_5H_3(CH2NMe_2)]FeCp\}_2$ and $CpSm(Cl)[C_5H_3(CH_2NMe_2)]\cdot$ FeCp (Jacob et al. 1992, 1993) the bulky anthracene $(C_{14}H_{10})^{2-}$ (Protchenko et al. 1993) and naphtalide $(C_{10}H_8)^{2-}$ ligands are other stabilizing agents as shown by the crystal structure of $CpLu(\eta^4C_{10}H_8)(DME)$ (fig. 21). The reaction of $CpLu(C_{10}H_8)(DME)$ with diphenyl acetylene

$$2CpLuC_{10}H_8(DME) + 2PhC{\equiv}CPh \rightarrow$$
$$[CpLu(DME)]_2[\mu\text{-}(Ph)C(Ph)C{=}C(Ph)C(Ph)] + 2C_{10}H_8,$$

results in C–C coupling with the formation of the dinuclear complex shown in the equation. The X-ray data and the diamagnetism of the compound suggest the presence in the complex of a bridging dialkylidene type ligand.

An unusual tetranuclear Nd-cluster stabilized by an oxygen dianion, $[Li(DME)_3]_2\text{-}[(CpNd)_4(\mu^2\text{-}Me)_2(\mu4\text{-}O)(\mu^2\text{-}Cl)_6]$ has been synthesized (Jin et al. 1990).

$[CpLu(OSO_2CF_3)_2(THF)]_n$ ($n = 1, 2$) reacts with $R_2As(CH_2)_3MgCl$ ($R = {}^t$Bu, Me) to give $CpLu[(CH_2)_3AsR_2]_2$ (Schumann et al. 1992c). The chelating C–As system provides a stabilization of the compound.

2.1.9.2. *Actinides.* Monocyclopentadienyl derivatives are less common and the majority of the reported complexes are Lewis-base adducts of the type $CpAnX_3 \cdot Ln$ (X = halide). Their steric and electronic unsaturation make their synthesis challenging. The first $CpUCl_3 \cdot 2L$ compounds in ethereal solvents (DME or THF) were prepared by reacting UCl_4 with thallium cyclopentadienide (Marks and Ernst 1982).

The X-ray structures of the $CpUCl_3(OPPh_3)_2(THF)$ (Bombieri et al. 1978, Bagnall et al. 1984) and $CpUCl_3[OP(NMe_2)_3]_2$ show the uranium atom octahedrally coordinated with the two neutral ligands in *cis* positions, the chlorine atoms are in the *mer* arrangement and the Cp ligand is *trans* to one neutral ligand. The $CpNpCl_3(PMePh_2O)_2$ derivative (Bagnall et al. 1986a) shows the same overall conformation as the uranium analog (Np–Cl 2.65(2) Å and Np–O 2.27(5) Å). The occurrence of *cis* geometry with the Cp ligand *trans* to an oxygen donor ligand can be explained as *trans* effect.

Bagnall and his group made fundamental contributions to this area. The synthesis, IR and NIR spectra were recorded for $CpPuCl_3L_2$ [L = $HCONMe_2$, $MeCONMe_2$, $MeCON^iPr_2$, $EtCON^iPr_2$, $Me_3CCONMe_2$, $OPMe_3$, $OPMe_2Ph$, $OPMePh_2$, $OPPh_3$, $OP(NMe_2)_3$]. The analogous thiocyanate derivatives $CpAn(NCS)_3L_x$ ($x = 2$, An = Pu, L = $OPMe_3$; An = Np, Pu, L = $OPMePh_2$, $OPMe_2Ph$) have been isolated as well the halide and pseudohalide derivatives, $CpThX_3L_2$ [X = Cl, L = $MeCON^iPr_2$, $MeCON(C_6H_{11})_2$; X = Br, L = $Me_2CHCONMe_2$, $Me_2CHCON^iPr_2$, $EtCONEt_2$], $CpUCl_3L_2$ [L = $MeCON^iPr_2$, $EtCON^iPr_2$, $CO(NMe_2)_2$], $CpUCl_3[MeCON(C_6H_{11})_2]_2(THF)$, $CpAnCl_2(HBL_3)$ (An = Th, U; L = 3,5-dimethylpyrazolyl; Marçalo et al. 1986), $CpThCl_3L_x$ ($x = 2$, L = THF; $x = 3$, L = MeCN; Bagnall et al. 1983, 1984, 1986a,b). (MeCp)ThCl·THF, $CpUCl_3L_2$ (L = $OPMe_3$, $OPMe_2Ph$, $OPMePh_2$) and $CpU(NCS)_3L_3$ (L = $OPMe_2Ph$, $OPMePh_2$; Ahmed and Bagnall 1984).

The dynamic behavior in solution of some of these compounds $CpUCl_3L_2$ (L = hexamethylphosphoramide, THF, $OPPh_3$) has been reported by Le Maréchal et al. (1986). The stable structure in solution seemed to be a *mer* pseudo-octahedral configuration.

A pentagonal bipyramidal coordination around U, with the oxygen ligands in the equator and Cl and Cp in axial positions, has been detected in the uranium(IV) complex $CpUCl(acac)_2(OPPh_3)$ (Baudin et al. 1988).

An unusual oxygen bridged cluster structure containing both inorganic and organometallic uranium atoms is shown by the dimer $[Cp(Ac)_5U_2O]_2$ obtained from $[Cp_2U(AlH_4)_2] \cdot nEt_2O$ with acetic acid (Brianese et al. 1989). In the centrosymmetric tetranuclear dimer two $Cp(Ac)_5U_2O$ moieties are connected by chelating carboxylato and (μ^3-O) oxide bridges. The coordination geometry around the "organometallic" uranium atoms is about pentagonal bipyramidal while the "inorganic" uranium is eight coordinated. Significant distances are U–O(μ^3) 2.17(1) → 2.37(1) Å, U–Oacetate 2.33(1) → 2.69(1) Å. The tetrameric derivative $[CpU(Ac)_2]_4O_2$ (Rebizant et al. 1992b) is of pentagonal bipyramidal geometry around each U^{IV} with the Cp in the apical sites and acetate and oxide O bridging the uranium (U–O(μ^2) 2.03(1) → 2.10(2) Å).

An unprecedented cyclic hexanuclear complex $[CpTh_2(O\text{-}^iPr)_7]_3$ obtained from $ThBr_4(THF)_4$, TlCp and $K_2(O^iPr)$ (Barnhart et al. 1995) is formed by three $[CpTh_2(O\text{-}$

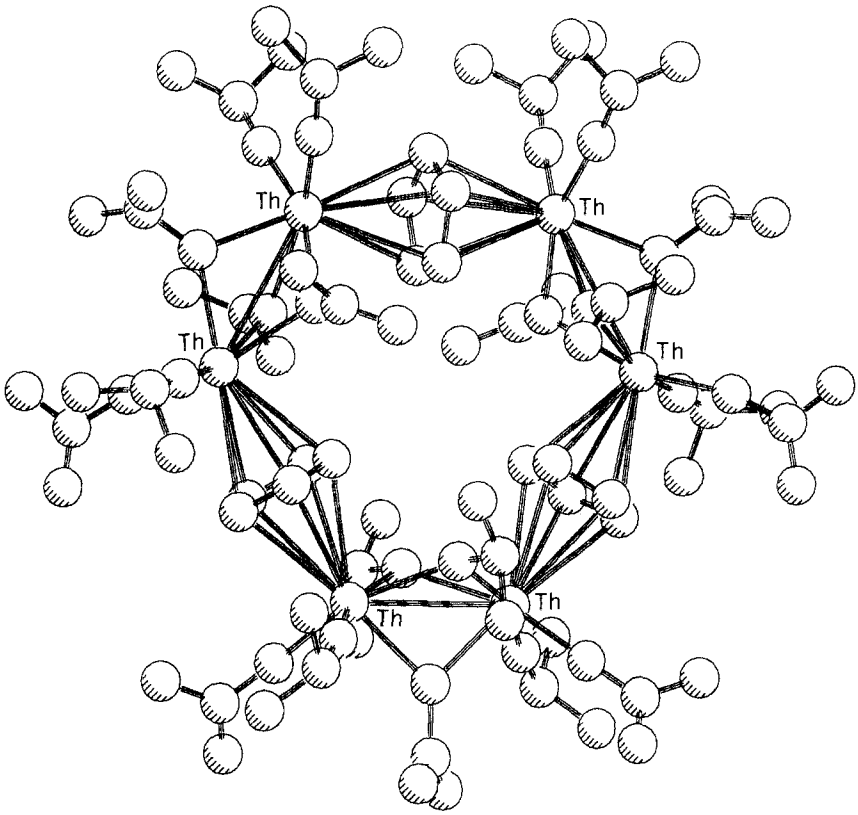

Fig. 22. Crystal structure of $[CpTh_2(O\text{-}^iPr)_7]_3$ (Barnhart et al. 1995).

$^iPr)_7$] unit bridged by Cp ligand (μ-η^5:η^5) with a distorted octahedral geometry around each Th (fig. 22).

The interaction of the powerful nucleophile ylide ligand $[(CH_2)(CH_2)PPh_2]$ with actinide ions has been examined from both a molecular orbital and an ionic point of view in the crystallographically characterized compound: $CpU[(CH_2)(CH_2)PPh_2]_3$ (Cramer et al. 1984b) of pentagonal bipyramidal geometry around uranium. The twelve independent U–C σ-bonds have an average value (2.66(3) Å) among the longest known. Molecular orbital calculations suggest a significant covalent character for the U–C σ-bond, but the authors conclude the long U–C σ-bonds can be also explained in terms of an ionic bonding model. The U–B distances (2.46(4) and 2.57(5) Å) of $CpU(BH_4)_3$ suggest tridentate coordination, although the hydrogen atoms were not located (Baudry and Ephritikhine 1988).

2.1.10. *$Cp'MX_2$ or $Cp'MXY$ (with substituted cyclopentadienyls)*

2.1.10.1. *Lanthanides.* The use of bulky ligands like differently substituted Cp which are more soluble and have higher thermal stability than the unsubstituted ones, allows the

synthesis of early lanthanide complexes. The most common RCp have R = Me, ^{t}Bu, C_5H_9, C_3H_5, Me_3Si, and recently $MeOCH_2CH_2$. By metathesis of the corresponding anhydrous $LnCl_3$ with respective sodium organyl many substituted cyclopentadienyl halide solvated complexes have been obtained. Alkyne metal halides when used in the reaction pot are very often incorporated as they stabilize the complex formation.

The reaction of $LnCl_3 \cdot 2LiCl$ with 1 eq of MeCpNa in THF produces the precursors $[(THF)_2Li]_2(\mu\text{-}Cl)_4[(MeCp)Ln(THF)]$ (Ln = Nd, La; Guan et al. 1992). The crystal structure of the Nd derivative has been determined. The $Li(\mu\text{-}Cl)_2Nd(\mu\text{-}Cl)_2Li$ cluster moiety is a stabilizing factor for the simple cyclopentadienyl chlorides of the light lanthanides. The ligands around the Nd ion are arranged in a distorted octahedral coordination geometry with a formal CN = 8.

Transmetallation reaction of $[(THF)_2\ Li(\mu\text{-}Cl)_2]_2\ [(MeCp)Ln(THF)]$ with $LiNPh_2$ produces $[Li(DME)_3][(MeCp)Ln(NPPh_2)_3]$ (Ln = La, Pr, Nd) derivatives which have been characterized by IR and NMR spectra and the crystal structure of La derivative shows well separated $[(MeCp)La(NPPh_2)_3]^-$ anions and $[Li(DME)_3]^+$ cations. A distorted tetrahedral geometry characterizes the central La ion. Steric congestion of the methyl Cp causes irregularities at the Cg–La–N angles (range 106.0 → 121.0°). The La–N distances average 2.459(7) Å and are the first example of La–N σ-bonds.

A different type of heterometallic bridge can stabilize an unsubstituted Cp ligand, an example is the synthesis and the X-ray structure of $(Me_3SiC_5H_4)Y[(\mu\text{-}O^tBu)(\mu\text{-}Me)AlMe_2]_2$ with a rather unusual tetragonal pyramidal coordination geometry around yttrium (Evans et al. 1993b).

$ErCl_3$ reacts with cyclopentane substituted cyclopentadienyl sodium salt ($C_5H_9C_5H_4Na$) (1:1) in THF at room temperature to give $[(C_5H_9C_5H_4)Er(THF)]_2(\mu^2\text{-}Cl)_3(\mu^3\text{-}Cl)_2[Na(THF)_2]$ (Jin et al. 1992). Its dimeric structure (Er···Er 3.876(2) Å) shows each erbium surrounded by one $C_5H_9C_5H_4$ ligand two μ^3-Cl, μ^2-Cl and one THF in a distorted octahedral arrangement. (The average bond length of Er-μ^3-Cl, 2.760 Å, is longer than Er-μ^2-Cl, 2.744 Å).

(^{t}BuCp)$SmI_2 \cdot 3THF$ (Bel'skii et al. 1991a) represents a rare example of iodide derivative. The Sm coordination polyhedron is a distorted octahedron. The Sm–I bond distances are 3.107(1), 3.186(2) Å as in the $Cp^0SmI_2 \cdot 2THF$ compound (Deng et al. 1994) where the chelating behavior of the 2-methoxyethylcyclo-pentadienyl ligand (Cp^0) forces the two iodine in *cis* position while they are in *trans* in the other Sm derivative. The use of the sterically congested ($Me_4C_5SiMe_2N^tBu$) ligand enhances the stability of metalloorganic lanthanide derivatives (Piers et al. 1990, Shapiro et al. 1990) and allows isolation of $[(Me_4C_5SiMe_2)(\eta^1\text{-}N^tBu)]ScCH(SiMe_3)_2$ and of the dimer $\{[(Me_4C_5SiMe_2)(\eta^1\text{-}N^tBu)]Sc(\mu^1\text{-}Pr)\}_2$ which was characterized also by X-ray crystallography (Shapiro et al. 1994). Other derivatives of the type $[(Me_4C_5SiMe_2)(\eta^1\text{-}N^tBu)]ScL$ (L = C_3H_7, $CH(SiMe_3)_2$; C_4H_9, C_6H_{11}, $CHPh(CH_3)Ph$) have also been reported.

The strong oxophilic character of lanthanides has been discussed in the previous sections, and the frequent occurrence of oxoderivatives is accidental as in the tetranuclear oxo species $[Li(THF)_4]_2\{[(MeC_5H_4)]NdCl(\mu^2\text{-}Cl)NdCl(\mu^2\text{-}Cl)NdCl_2[(MeC_5H_4)]_2(\mu^4\text{-}O)\}$

(Guan et al. 1990) obtained by metathesis of $NdCl_3(LiCl)_2(THF)_n$ with MeCpNa in THF. Another cluster has recently been synthesized (Zhou et al. 1995) from $YbCl_3$ and YbOCl reacted with MeCpNa in THF $(MeCp)_3Yb_4(\mu\text{-}Cl)_6(\mu^3\text{-}Cl)(\mu^4\text{-}O)(THF)_3$. Its crystal structure reveals an oxygen-centered tetrahedal arrangement of Yb atoms with μ-Cl bridging each edge and μ^3-Cl over the triangular face formed by the (MeCp)Yb moieties (Yb–O(μ^4-oxide) bond distance range 2.13(1)–2.29(1) Å).

2.1.10.2. *Actinides.* Also with actinides inclusion of NaCl and LiCl salts stabilizes the structures of the mono Cp derivatives as in the trimethyl-silyl substituted Cp derivative $[(Cp''')UCl_2(THF)(\mu\text{-}Cl)_2Li(THF)_2]$ (Edelmann et al. 1987) ($Cp''' = C_5H_2(SiMe_3)_3$-1,2,4). A typical octahedral coordination geometry has been found as in (MeC_5H_4)-$UCl_3 \cdot 2THF$ (Ernst et al. 1979). With the same ligand (Cp''') the Th derivative $[(Cp'''ThCl_3)_2NaCl(OEt_2)]_2$ has been synthesized (Edelmann et al. 1995); its X-ray structure is the first reported for mono $Cp'''Th^{IV}$chloride and is characterized by μ^2 and μ^3 bridging chlorides with average Th–Cl bond lengths of 2.860 Å and by a distorted octahedral coordination geometry. The synthesis of $\{Cp'''ThCl_3[MeN(CH_2CH_2NMe_2)_2]\}$ is also reported. The highly substituted Cp ligand has been selected in order to increase the lipophilicity of the complexes. A brief review of thorium and uranium chemistry with the 1,3-$C_5H_3(SiMe_3)_2$ ligand has been reported (Blake et al. 1987).

2.1.11. *Peralkylcyclopentadienyls*

As compared with the unsubstituted cyclopentadienyl, (Cp), the pentamethylcyclopentadienyl ligand C_5Me_5 (Cp*) shows the following special features:

- increased covalent character of the cyclopentadienyl–metal bond,
- stronger π-donor and weaker π-acceptor properties,
- kinetic stabilization effected by steric shielding of the metal ion,
- increased thermal stability of the metal complexes.

In addition, the Cp* ligand produces attenuation of intermolecular interactions, thus decreasing the tendency towards polymeric structures. Finally, the solubility in organic solvent and the vapor pressure are increased. All these features explain the wide use of the Cp* ligand in organolanthanide and organoactinide chemistry.

2.1.11.1. *Mixed valent or low valent Cp^*_2 lanthanides.* The pioneering work on low valent compounds in organolanthanide chemistry by Evans et al. (Evans et al. 1981b), has opened new routes to the synthesis of a wide variety of compounds, particularly as they provide access to soluble compounds. The metal vaporization technique has been widely used, in particular for the production of the first soluble $Cp^*_2Sm(THF)_2$ compound, that was also the first structurally characterized divalent organosamarium of pseudotetrahedral coordination geometry around Sm. In particular Sm yields a wide variety of compounds due to "relatively" easy access to the divalent state and to its high reactivity.

Cp^*_2Sm (Evans et al. 1984b) was obtained by metal vapor reaction of samarium with C_5Me_5H as a green complex, or from the red 2THF solvated species by desolvation and

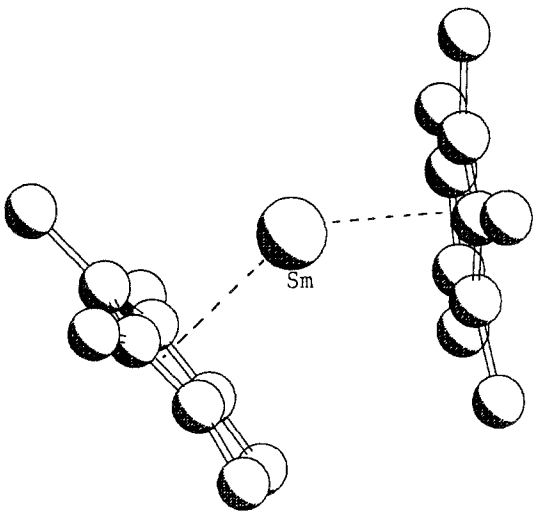

Fig. 23. Crystal structure of [Cp^*_2Sm] (Evans et al. 1984b).

sublimation. Crystallographic study on the green complex confirmed its formulation as a decamethylsamarocene of bent metallocene structure. The Cg–Sm–Cg angle is 140.1°, more open than in the disolvated analog (136.7°), this is accompanied by a reduction of the Sm–C bond distance 2.79(1) Å compared to 2.86(3) Å in the disolvated species (fig. 23).

By repeated sublimation at 70°C of $Cp^*_2Eu(THF)$ the red Cp^*_2Eu species isostructural to the Sm analog was obtained (Evans et al. 1986c). The unexpected bent structures observed, are best explained by the polarization argument: "a bent structure may optimize the polarization of a large cation by two anions and may give better total electrostatic bonding for the two rings". In fact, electrostatic considerations or molecular orbital calculations or steric effects do not support the bent structures observed, being instead in favor of parallel Me_5C_5 rings. A similar bent structure has been proposed for Cp^*_2Yb on the basis of electron diffraction studies (Andersen et al. 1986).

Cp^*_2Sm reacts with C_5H_6 forming a trivalent (see also sect. 2.1.11.3.1) and a mixed valent product: Cp^*_2SmCp (ruby-red) and $Cp^*_2SmCpSmCp^*_2$ (brown), respectively (Evans and Ulibarri 1987b). The formation of the second product appears with a deficiency of C_5H_6. In the mixed valent derivative $Cp^*_2Sm^{III}(\mu\text{-}Cp)Sm^{II}Cp^*_2$ the assignment of the two valence states made on the basis of spectroscopic results, is confirmed by the X-ray analysis on the compound. The Sm^{III} coordination geometry is still trigonal. The bridging Cp is symmetrically bound to Sm^{III} while only two atoms are closer to Sm^{II} at a distance of 2.986(8) and 3.180(9) Å, respectively. The characterization of this mixed valent complex elucidates the initial step of the Cp^*_2Sm interaction with a hydrocarbon (prior to activation).

The preparation and characterization of a soluble green Sm^{II} compound $Cp^*_2Sm(DME)$ obtained by metathetical reaction in refluxing DME of $SmCl_2$ and $NaCp^*$ (1:2) has been

reported (Swamy et al. 1988). The monomeric molecules show a pseudo tetrahedral ligand arrangement.

A novel synthesis (Evans et al. 1985b) of $Cp^*_2Sm(THF)_2$ has been devised by reacting SmI_2 with KCp^* (1:2). When the stoichiometry of the reaction is 1:1 the iodine derivative $[Cp^*Sm(\mu\text{-}I)(THF)_2]_2$ is formed. The latter, with the reactive side of the halide ligand, is suitable for enlarging the series of novel samarium compounds, particularly alkyl complexes.

Substitution of the solvent in $Cp^*_2Sm(THF)_2$ (Evans and Ulibarri 1989) with the appropriate neutral ligand, produces the two complexes $Cp^*_2Sm(dihydropyran)_2$ and $Cp^*_2Sm(tetrahydropyran)$ where the $Sm\text{–}C_{ring}$ average distance is, respectively, 2.842(4) Å and 2.816(3) Å, in agreement with the change of the formal coordination number for Sm from 8 to 7.

The solvate Cp^*_2YbL complexes (L = THF, Et_2O; Tilley et al. 1980) have been synthesized. The X-ray structure of the THF derivative shows a monomeric compound, whereas the corresponding $(MeCp)_2YbTHF$ in the solid state is a chain polymer with the Yb^{2+} ions connected by bridging MeCp ligands. The complex with pyridine $Cp^*_2Yb(py)_2$ (Tilley et al. 1982), characterized crystallographically, has approximately tetrahedral coordination geometry. Largely ionic character for the Cp^* binding mode in Yb^{II} complexes has been deduced from X-ray structure determinations, with the Cp^* radius close to the value 1.64(3) Å suggested by Raymond (Raymond and Eigenbrot 1980) for ionic bonding.

$Cp^*_2Ln(Me_2PCH_2CH_2PMe_2)$ (Ln = Eu, Yb; Tilley et al. 1983) complexes are hydrocarbon insoluble indicating possible polymeric structures while replacing the CH_2CH_2 bridge with CH_2 in the diphosphine ligand gives soluble compounds, the increase of steric hindrance between the Cp^* ligand prevents polymerization. The NMR data support this formulation.

The photophysics of the interaction between two $Cp_2Ln{\cdot}OEt_2$ compounds (Ln = Eu or Yb) in toluene shows that the Yb compound quenches the emission from its Eu analog. This is the first reported example of excited-state energy transfer between two organolanthanoid complexes (Thomas and Ellis 1985).

XPS spectral data and the results of molecular orbital calculation show that the Ln–L interactions in monomeric Cp^*_2Ln where Ln = Sm, Eu, or Yb are mainly ionic (Green et al. 1987). Cp^*_2Sm is a better reducing agent than SmI_2 for use in organic chemistry (Namy et al. 1987).

Wayda et al. (1984) reported the preparation of novel divalent Cp^*_2Eu and Yb, NH_3 adducts, by reacting the metal in liquid ammonia with C_5Me_5H in vacuum line. The ytterbium derivative has been characterized crystallographically.

$Cp^*_2YbOEt_2$ undergoes atom-abstractive oxidative addition with the alkyl and aryl halides RX (R = hydrocarbyl) to give Cp^*_2YbX and $Cp^*_2YbX_2$ along with Cp^*H and R–R, RH or R(-H), i.e., olefins (Finke et al. 1989). This reaction is 10^3–10^6 times faster than typical d-block atom abstraction reactions. Cp^*_2YbR is formed from radical trapping of R by the Yb^{II} compound, this reacts further with Cp^*_2YbX in a "Yb-Grignard" reaction.

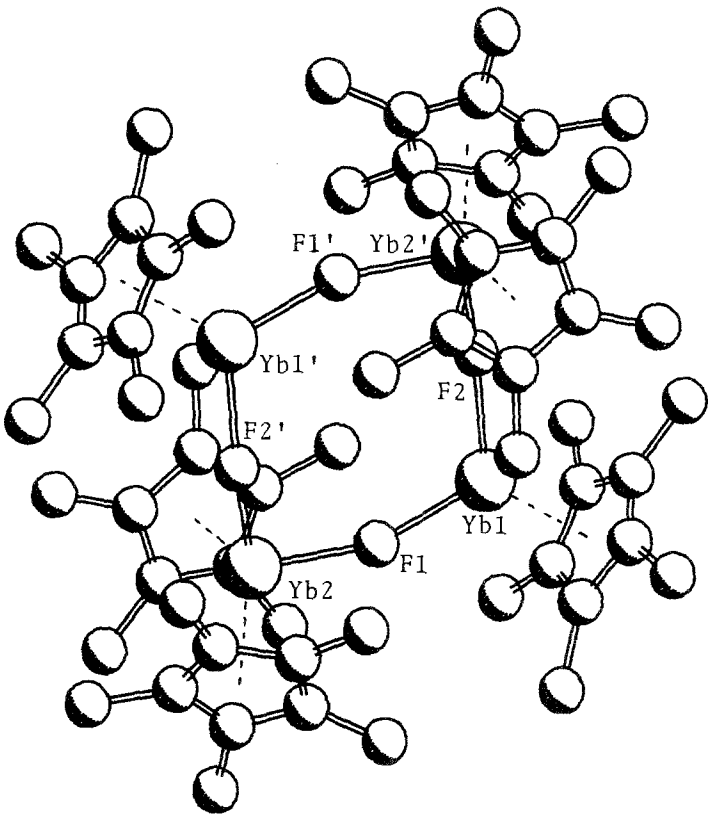

Fig. 24. Crystal structure of $[Cp^*_6Yb_4F_4]$ (Burns et al. 1987).

Mechanistic studies indicate the dominance of inner-sphere mechanisms in these reactions. The mixed valence compound $(Cp^*_2Yb)_2(\mu\text{-}F)$ (Burns and Andersen 1989) shows in the solid state a linear Yb^{II}–F–Yb^{III} asymmetric bridge [Yb(1)–F 2.317(2) and Yb(2)–F 2.084(2) Å] consistent with a Yb^{II}_1 and Yb^{III}_2 formulation; this is also supported by variable temperature measurements of magnetic susceptibility. The structure of the tetramer $Cp^*_6Yb_4(\mu\text{-}F)_4$ (Burns et al. 1987) is formed from two $Cp^*_2Yb(\mu\text{-}F)YbCp^*_2$ moieties centrosymmetrically related and connected via fluoro bridges; Yb^{III} is tetrahedral while Yb^{II} is trigonal (fig. 24). The anionic species $[Cp^*_2YbI_2][Li(ether)_2]$ and $[Cp^*_2YbMe_2][Li(ether)]$ have also been isolated (Watson 1980, Watson et al. 1981).

$Cp^*_2Yb(\eta^2\text{–}MeC{\equiv}CMe)$ (Burns and Andersen 1987a) characterized by spectroscopic and X-ray measurements, represents the first η^2-acetylene complex of a lanthanide. The structure has the acetylene plane, including Yb, about orthogonal (91.5°) to the centroids and Yb plane and a rather weak 2-butyne to Cp^*_2Yb interaction. $[K(THF)_n]_2[Cp^*_2NdCl_2]$, $[Cp^*_2NdCl(THF)]$, $[Cp^*_2Nd(S_2CNMe_2)]$ and $[Cp^*_2NdSe(mesityl)(THF)]$ are the first examples of Nd^{II} derivatives (Wedler et al. 1990).

2.1.11.2. *Cp^*_2M halide derivatives.*

2.1.11.2.1. *Lanthanides.* As already noticed, the size of the pentamethylcyclopentadienyl ligand gives stability to ligand redistribution, allowing the synthesis of the chloride derivatives of all lanthanides (except Pm) including Sc and Y. However, the majority of them is stabilized also by oligomerization or by the coordination of variety of Lewis bases and by coordination of alkali halides (in the anionic complexes). Cp^*_2ScCl was shown to be monomeric by cryoscopy (Thompson and Bercaw 1984) but also the dimeric species $[Cp^*_2ScCl]_2$ was obtained. A symmetric dimer has been revealed by the X-ray analysis of $Cp^*_2Y(\mu\text{-}Cl)Y(Cl)Cp^*_2$ where one Y center is formally 7 coordinate while the other is 8 coordinate containing one terminal chlorine (Evans et al. 1985c).

A rare example of cocrystallized species of THF disolvated and trisolvated (Evans et al. 1992b) is $Cp^*_2Y(\mu\text{-}Cl)_2Li(THF)_2$ (**1**) and $Cp^*_2YCl(\mu\text{-}Cl)Li(THF)_3$ (**2**), obtained by reacting $Cp^*_2YCl(THF)$ with 3 eq. of $LiOCMe_3$ in toluene. Compound **1** has the expected usual structure with two bridging chlorines to the $Li(THF)_2$ moiety, while compound **2** contains a terminal chlorine and a single bridging chlorine to the $Li(THF)_3$ moiety.

Other Lewis base derivatives are known as for example, with Et_2O, acetone, pyridine MeCN, ^{t}BuNC. In the X-ray structure of the complex $Cp^*_2YbCl(Me_2PCH_2PMe_2)$ (Tilley et al. 1983) where divalent Yb is oxidized by $YbCl_3$ to the trivalent metallocene, Yb is coordinated to the two Cp* ligands, to the chlorine and to one phosphorus of the dmpm ligand in a nearly tetrahedral arrangement. Yb–Cl bond length is 2.532(2), Yb–P is 2.941(3) Å.

$[Cp^*_2SmCl]_3$ (Evans et al. 1987b) is a nearly symmetric trimer (the uranium^{III} analog derivatives adopt the same structure). Electrostatic factors maximising the number of anions around Sm and steric factors explain the trimeric structure instead of the more common dimeric one. The three bridging chloride anions connect the three Cp^*_2Sm units, forming a planar six-membered ring. The structure of the tetraglyme derivative $Cp^*_{10}Sm_5Cl_5[Me(OCH_2CH_2)_4OMe]$ is characterized by four independent types of Cp^*_2Sm units: in the cation $[Cp^*_2ClSm(\mu\text{–}Cl)SmCp^*_2[\mu\text{-}\eta^4Me(OCH_2CH_2)_4OMe]SmCp^*_2]^+$ (fig. 25) we can distinguish two approximately tetrahedral Sm environments, while the remaining Cp^*_2Sm unit is bound to three oxygen atoms of the tetraglyme molecule. In the anion $[Cp^*_2ClSm(\mu\text{–}Cl)SmClCp^*_2]^-$ the Cp^*_2Sm units are twisted 90° with respect to each other. Interestingly, in the trimer $[Cp^*_2\cdot Sm(\mu\text{–}CN)(CN^cC_6H_{11})]_3$ (Evans and Drummond 1988a) the CN ligand which substitutes in position and function for the bridging chlorine, with consequently greater distance between the Sm ions, allows coordination of the additional $CN^cC_6H_{11}$ ligand to each samarium.

Cp* ligand has been useful for isolating a series of Yb and Lu halides derivatives (Watson et al. 1981) as $Li[Cp^*LnX_3]$ and $Li[Cp^*_2LnX_2]$ by oxidation of the corresponding metal with Cp*I in the presence of LiI or by reacting $LnCl_3$ with LiCp*. Cp^*_2LnX (Ln = Sm, Yb; X = Br; Ln = Sc, La, Ce, Sm, Yb; X = I) species have been synthesized generally with Lewis bases solvated (Marks and Ernst 1982).

Watson et al. (1990) reports the abstraction of fluorine atoms from perfluoroolefins by Cp^*_2LnL (Ln = Yb, Er, Sm; L = THF, Et_2O). The structures of $Cp^*_2YbF(OEt_2)$ and $Cp^*_2YbF(THF)$ show the usual tetrahedral coordination geometry around Yb with Yb–F

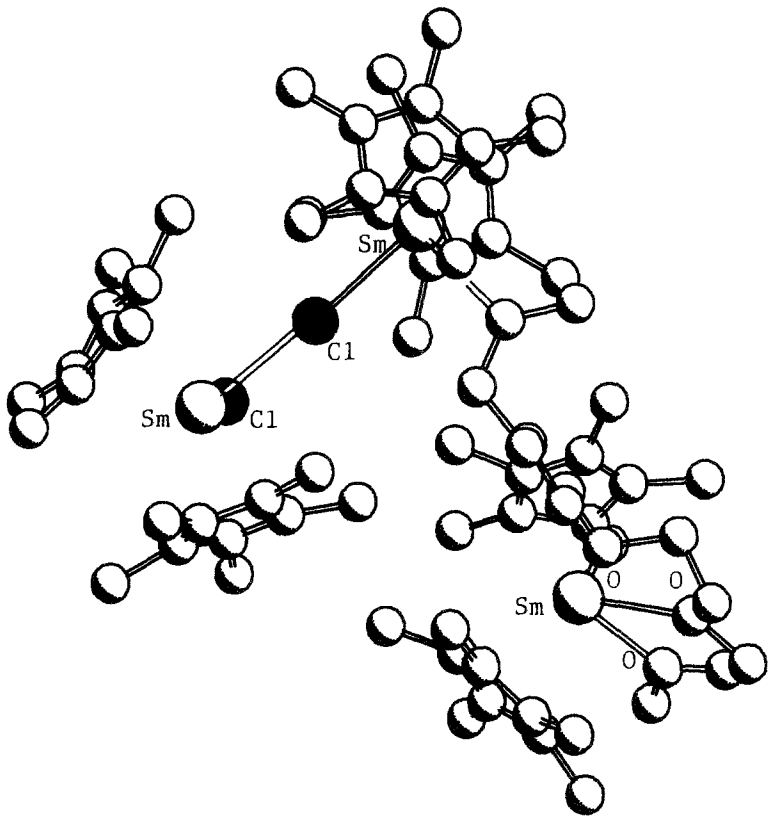

Fig. 25. Crystal structure of the cation $[Cp_2^*ClSm(\mu\text{-}Cl)SmCp_2^*(\mu\text{-}\eta^4\text{-}Me(OCH_2CH_2)_4OMe)SmCp_2^*]^+$ (Evans et al. 1987b).

distances of 2.015(4) Å and 2.026(2) Å, respectively. The reduction potentials M^{III}/M^{II} (M = Yb, Sm, Eu) have been measured for acetonitrile solvated complexes Cp_2^*M in CH_3CN by cyclic voltammetry: Cp_2^*Eu, −1.22 V; Cp_2^*Yb, −1.78 V; Cp_2^*Sm, −2.41 V. However, even if the reduction potentials are dominant factors for reactivity, steric factors play an important role in the inner-sphere atom abstraction due to the steric bulk of perfluorocarbons.

2.1.11.2.2. *Actinides.* Bis(pentamethylcyclopentadienyl) actinide dichlorides are important precursors for the organoactinide chemistry. Peralkylation of the Cp ligand with the consequent modification of the electronic and steric properties, limits the number of ligands which can enter in the metal coordination sphere, but also produces more stable, and more crystallizable compounds. The first organoactinides prepared were $Cp_2^*AnCl_2$ (An = Th, U) synthesized from MCl_4 and excess of $Me_5C_5^-$(Marks and Ernst 1982). The two $Cp_2^*AnCl_2$ (An = U, Th; Spirlet et al. 1992a) isostructural compounds have a distorted tetrahedral coordination geometry around An of C_{2v} symmetry.

A cyclic voltametric study has shown that $Cp^*_2UCl_2$ is reduced reversibly in THF with a half-wave potential corresponding to the 1-electron oxidation of $Na[Cp^*_2UCl_2 \cdot THF]$ (Finke et al. 1982).

The trimeric uranium(III) complex $[(Cp^*_2U)_2(\mu\text{-}Cl)]_3$ has been obtained by hydrogenolysis of the uranium (IV) alkyl complexes $[Cp^*_2U(R)Cl]$. Its structure consists of pseudotetrahedral (Cp^*_2U) units connected via bridging chloride ligands, the trimers are of approximate D_{3h} symmetry. The average U–C distance is 2.768(11) Å, U–Cl is 2.900(2) Å. The average Cl–U–Cl angle is 83.8(1)°. These values are close to those reported for the dimer $\{[(Me_3C)_2C_5H_3]_2U(\mu\text{-}Cl)\}$ (Zalkin et al. 1988b). The trimer is the precursor for a wide range of products: it forms adducts $Cp^*_2UCl \cdot L$ where L = THF, pyridine, PMe_3 and Et_2O.

The X-ray structure of the thorocene bromide $Cp^*_2ThBr_2(THF)$ (Edelmann et al. 1995) is the first for organothorium bromide with a coordination geometry around Th analogous to that of the pyrazole (see below) [Th–Br, 2.895(2) Å].

The dichloride derivatives $Cp^*_2AnCl_2$ (An = U, Th) are the progenitors of a series of complexes with dialkylamides. They react with carbon monoxide forming, via migratory insertion η^2 carbamoyl complexes like $Cp^*_2An(\eta^2\text{-}CONR_2)Cl$, $Cp^*_2An(\eta^2\text{-}CONR_2)NR$ and $Cp^*_2An(\eta^2\text{-}CONR_2)_2$ which were characterized by spectroscopic and (for two of them) crystallographic methods: the Th chloroderivative with R = Et and the U bis η^2-carbamoyl with R = Me (see sect. 2.1.11.3.2). The $Cp^*_2Th(\eta^2\text{-}CONEt_2)Cl$ derivative has the usual "bent sandwich" $Cp^*_2ThX_2$ configuration. Two isomers are present in the structure due to the two alternative positions of the η^2-bonded carbamoyl ligands (O and O′) in dynamic equilibrium according to variable temperature NMR studies. $Cp^*_2UCl_2$ reacts with pyrazole ($C_3H_4N_2$) giving $Cp^*_2UCl_2(C_3H_4N_2)$, $Cp^*_2UCl(C_3H_3N_2)$ and $Cp^*_2U(C_3H_3N_2)_2$ (Eigenbrot and Raymond 1982) (see for the latter sect. 2.1.11.4.2). The molecular structure of the dichloride derivative is highly symmetric with the uranium and the pyrazole nitrogen at the intersection of two orthogonal mirror planes. Its ^1H NMR spectrum shows fluxionality of the pyrazole ligand. In the $Cp^*_2UCl(C_3H_4N_2)$ derivative the absence of one chlorine (fig. 26), causes the coordination of both the pyrazole nitrogens maintaining the formal 9 coordination, with a significant reduction of the chlorine and nitrogen to uranium bond distances. Both compounds exhibit Curie–Weiss behavior with $\chi = 1.46$ [0.73], $O = 43.3$ [5.95] K and μ_{eff} 13.24 [2.42] BM (in brackets are the values for mono Cl derivative).

The reaction between $Cp^*_2UCl_2$ and the phosphineimine $HNPPh_3$ produces $Cp^*_2UCl_2(HNPPh_3)$ stable even in the presence of excess phosphineimine (Cramer et al. 1989b). The IR N–H stretching frequency at 3160 cm^{-1} is consistent with a hydrogen bonding to the chloride and an agostic interaction with U as shown by the X-ray structure of the compound (U–H, 2.2 Å). The overall geometry closely resembles that of $Cp^*_2UCl_2$ (pz) (vide supra), but unlike it the U–Cl bond distances differ by 0.052 Å, the longer bearing the hydrogen bond. The short U–N bond of 2.43(1) Å has been ascribed to the high polarity of the P–N bond. The X-ray structure of $Cp^*_2UCl_2(HNSPh_2)$ is analogous to the phosphineimine adduct (Cramer et al. 1995a,b).

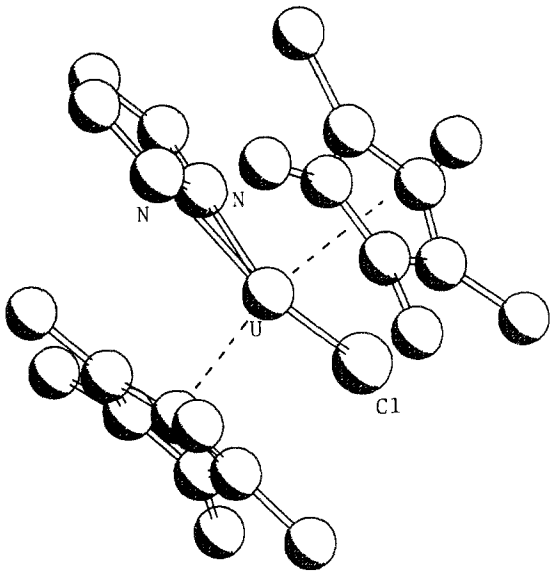

Fig. 26. Crystal structure of $[Cp_2^*U(\eta^2\text{–}C_3H_3N_2)Cl]$ (Eigenbrot and Raymond 1982).

Thermally stable chelating phosphorus ylide complexes (Cramer et al. 1989a) can be prepared as follows:

$$Cp_2^*AnCl_2 + Li\left[(CH_2)(CH_2)PRR^I\right] \rightarrow Cp_2^*AnCl\left[CH_2CH_2PRR^I\right] + LiCl,$$

where An = U, Th; R = Me; R^I = Ph; R = R^I = Ph or Me.

The ^1H NMR study on the diamagnetic Th(IV) shows fluxional behavior of the CH_2 groups. An unusual transformation process involving heterobimetallic C–H activation is shown by the heterobimetallic complex $Cp_2^*Th(Cl)Ru(Cp)(CO)_2$ (Sternal et al. 1987) which reacts with acetonitrile with formation of a novel diazathoracyclobutene (amidinate), shown in scheme 9.

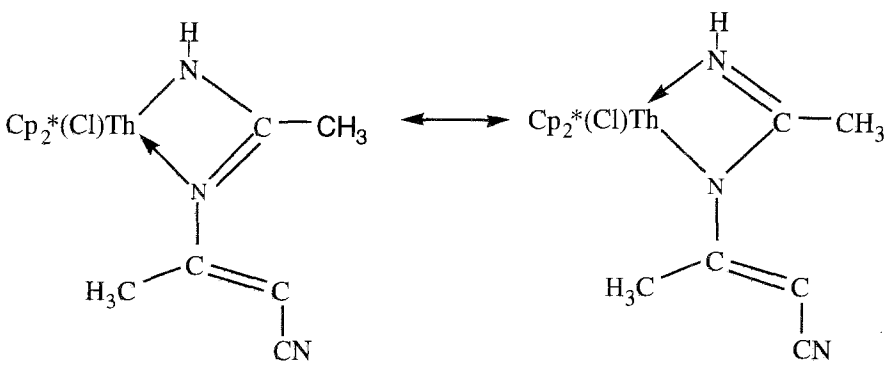

Scheme 9.

A possible mechanism involving heterolytic C–H scission and insertion of -C≡N into the Th–C bond has been postulated. The structural assignment has been made by NMR, IR, MS, elemental analysis and X-ray diffraction. The molecular structure shows the usual Cp^*_2ThCl fragment and a bidentate amidinate ligand. The equal values of the Th–N bond distances and the planarity of the resulting metallacycle are indicative of a highly delocalized system.

The characterization of the ylide product $Cp^*_2Th(Cl)O_2C_2[CH_2CMe_3][PMe_3]$ (Moloy et al. 1983) by an X-ray analysis suggests that the rate limit of its formation is the coupling of η^2-acyl with CO. This hypothesis is supported from IR and NMR studies on the isoelectronic isocyanides. The carbonylation of $Cp^*_2Th(Cl)(\eta^2$-$COCH_2$-^{t}Bu) in presence of phosphine (Moloy et al. 1986) produces the ylide complexes $Cp^*_2Th[OC(CH_2{}^tBu)C(PR_3)O](Cl)$ (R = Me, Ph). Isotopic ^{13}CO studies indicate the regiospecific insertion of the labeled carbon atom at the ylide α-carbon position. In absence of phosphines the dimer enedionediolate $[Cp^*_2Th[OC(CH_2{}^tBu)CO]Cl]_2$ is formed. The acyl complexes $Cp^*_2ThCl(COR)$ (R = CH_2Bu, CH_2Ph) react with isocyanides (RNC, R = ^{t}Bu, C_6H_{11}, -2,6-$Me_2C_6H_3$) forming the keteneimine derivatives.

2.1.11.3. *Cp^*_2M hydrocarbyl derivatives.*

2.1.11.3.1. *Lanthanides.* The pentamethylated cyclopentadienyl derivatives of this category constitute most of the compounds synthesized (over 180) ultimately for homogeneous catalytic reactions and C–H activation. The Zigler Natta-type catalyst $Cp^*_2LnMe(Et_2O)$ opens this large series (Watson and Roe 1982, Watson 1982). But the solvent-free electrophilic alkyl derivatives are the precursors of the majority of the compounds obtained, even though an important role is played by highly reactive divalent species (base solvated and unsolvated). Examples will be given for the different types of compounds with particular regard to their X-ray structures. Over forty samarium derivatives have been the best characterized from the structural point of view (the paramagnetism of the compounds makes the interpretation of their structure by NMR spectra difficult).

Reaction of samarium metal vapor (Evans 1985) with substituted cyclopentadienyl (between −110°C and −125°C) produces Cp^*_2Sm, $(C_5Me_4Et)_2Sm$. By dissolving these compounds in THF the corresponding biadducts are formed. While the reaction of $Cp^*_2Sm(THF)$ with $Hg(C_6H_5)_2$ gives the compound $Cp^*_2Sm(C_6H_5)THF$ (Evans et al. 1985d). The molecular structure of the latter consists of discrete molecules of typical bent metallocene structure.

The structural characterization of Cp^*_2SmCp (Evans and Ulibarri 1987b) represents the first example of a polyhapto ligand bound to a Cp^*_2Sm moiety. The samarium ion is trigonally coordinated to three cyclopentadienyl rings. The three ring centroids (Cg) are nearly coplanar with the metal ion. The two $Cg_{(Cp^*)}$–Sm–$Cg_{(Cp)}$ angles are equal (116.9 and 116.2°) and smaller than $Cg_{(Cp^*)}$–Sm–$Cg_{(Cp^*)}$ of 127°. The latter value is consistent with the increased steric hindrance. The methyl groups of the two C_5Me_5 ligands are staggered.

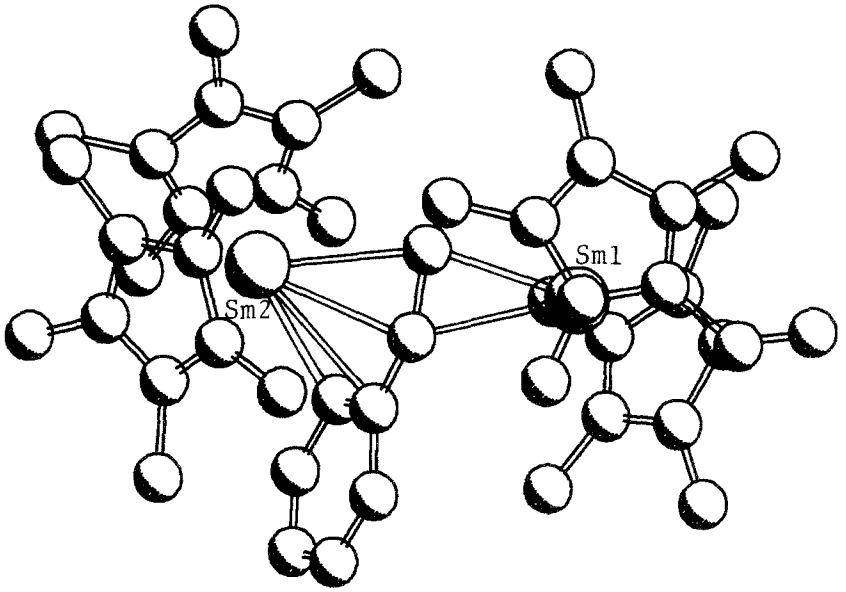

Fig. 27. Crystal structure of $[(Cp^*_2Sm)_2(\mu\text{-}\eta^2\text{:}\eta^4\text{-}CH_2CHPh)]$ (Evans et al. 1990c).

The reactive $Cp^*_2Sm(THF)_2$ (Evans et al. 1988c), reduces $AlMe_3$ (in toluene) giving the unusual tetrametallic $AlMe_4$ bridged complex $Cp^*_2Sm[(\mu\text{-}Me)AlMe_2(\mu\text{-}Me)]_2SmCp^*_2$. The two-metal system, is capable of metallating the C–H bonds of benzene, hexane, and pyridine, and of catalysing the polymerization of ethene. The X-ray structure shows the typical bent metallocene Cp^*_2Sm units, connected to two tetrahedral $(\mu\text{-}Me)_2AlMe_2$ moieties with approximately linear $Sm(\mu\text{-}Me)Al$ bridges. This may indicate an equatorial disposition of the bridging methyl hydrogens. The average Sm–C (bridging methyl distance) is 2.75(1) Å.

The high versatility of the unsaturated Cp^*_2Sm and $Cp^*_2Sm(THF)_2$ chemistry is further demonstrated by the isomerization of *cis*-stilbene to *trans*-stilbene with the production of the compound $[Cp^*_2Sm(\mu\text{-}\eta^2\text{:}\eta^4\text{-}PhCHCHPh)]$ (Evans et al. 1990c).

Cp^*_2Sm reacts with styrene to form the red-maroon complex $[Cp^*_2Sm]_2(CH_2CHPh)$. The single crystal X-ray analysis (fig. 27) shows the two Cp^*_2Sm units on opposite sides of the alkene bond, and the phenyl carbon atoms interacting with one of the samarium centers. The higher formal coordination number of Sm(2) (ten) due to the η^2-arene additional coordination, than for Sm(1) (eight) causes a lengthening in bond distances, with respect to the corresponding ones in Sm(1) (of about 0.07 Å for the $Sm–C_{ring}$ av). These structures demonstrate the possibility of a rather novel $\mu\text{-}\eta^2\text{:}\eta^4$ bimetallic coordination mode of Cp^*_2Sm to stilbene, styrene and dinitrogen.

$Cp^*_2Sm(THF)_2$ reacts with a wide variety of alkenes in hexane or toluene to form allyl complexes and alkene byproducts (Evans et al. 1990d). Binuclear Sm complexes can be obtained with the usual Cp^*_2Sm precursor and pyrene, anthracene, 2,3-benzanthracene,

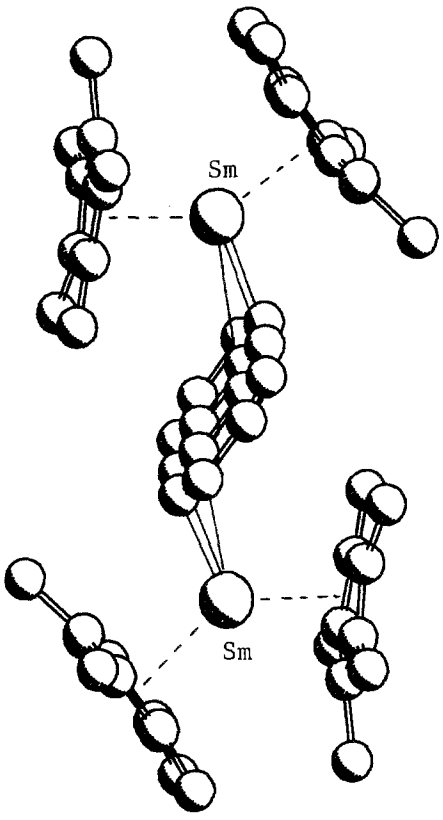

Fig. 28. Crystal structure of $[(Cp^*_2Sm)_2(\mu\text{-}\eta^3\text{:}\eta^3\text{-}C_{10}H_{14})]$ (Evans et al. 1994a).

9-methylanthracene and acenaphthylene-like $[(Cp^*_2Sm)_2(\mu\text{-}\eta^3\text{:}\eta^3\text{-}C_{10}H_{14})]$ (Evans et al. 1994a) (fig. 28).

The alkynide ligands RC≡C have often provided the first well characterized examples of f element compounds containing metal–carbon bonds, due to their strong σ-bonding and to the low steric congestion around the carbon donor atoms. They form strong three center M–C–M bridges as in the monosubstituted Cp derivative $[(MeCp)_2SmC{\equiv}C^tBu]_2$ (Evans et al. 1983b) and also heterobimetallic bridges as in the complex $Cp^*_2Y(\mu\text{-}C{\equiv}C^tBu)_2Li(THF)$ (Evans et al. 1989b). The η^2-attachment of a C=N to Ln is demonstrated by the insertion of the isonitrile 2,6-Me_2-C_6H_3NC into a (3,5-$C_6H_3CH_2$)–Y bond to give a dihapto-imine in $Cp^*_2Y[\eta^2\text{-}C(Ar){=}NAr']\cdot THF$, where Ar and Ar′ are the aryl groups already identified (Haan et al. 1987). The ^{t}BuNC ligand can be inserted into bridging Ln–H bonds, (Ln = Er or Y) to give $[Cp^*_2Ln(\mu,\eta^2\text{-}HC{=}NC^tBu)(THF)]_2$.

Many scandium and yttrium derivatives were also synthesized, but their characterization has been made mainly on the bases of spectroscopic data or by analogy with the corresponding Sm derivative. Nevertheless, Cp^*_2ScMe has been isolated and its X-ray structure is typical of a bent metallocene with a terminal methyl group (Thompson et al. 1987). Cp^*_2ScMe by σ-bond metathesis produces a variety of derivatives with

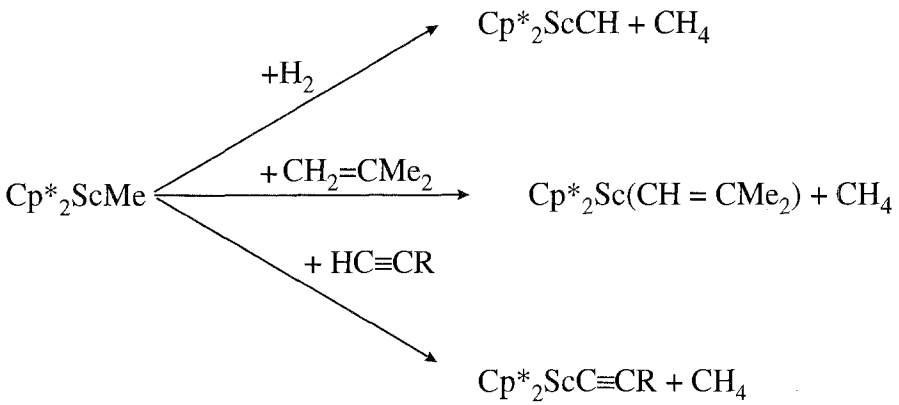

Scheme 10.

methane evolution (scheme 10), while by thermolysis in cyclohexane the dimer $[Cp^*_2Sc(\mu\text{-}\eta^1\text{:}\eta^5CH_2C_5Me_4)]_2$ identified by X-ray analysis was produced (Hajela et al. 1992). $[Cp^*_2LuMe]_2$ is an asymmetric dimer (Watson and Parshall 1985) where an agostic interaction between the bridging Me and Lu compensates the unsaturation of the Cp^*_2LuMe species. The reaction of $[Cp^*_2LnCl_2][Li(ether)_2]$ with $LiCH(SiMe_3)_2$ produces $Cp^*_2LnCH(SiMe_3)_2$ (Ln = La, Nd, Sm, Lu) derivatives. The structure of the Nd complex, besides the usual "bent sandwich" Cp^*_2Nd configuration (Cg–Nd–Cg 134.4°; Mauermann et al. 1985) shows a highly asymmetric $CH(SiMe_3)_2$ fragment with a Nd–C σ-bond distance of 2.517(7) Å and a secondary short contact Nd–C of 2.895(7)5 Å to a methyl carbon interpreted as γ-agostic interactions, as also suggested by spectroscopic data. The same γ-agostic interactions are present in the closely related $(C_5Me_4Et)_2SmCH(SiMe_3)_2$ derivative (Schumann et al. 1995e) where a little change in the hindrance of the $[C_5Me_5]^-$ ligand is produced by the substitution of a methyl with an ethyl group. $Cp^*_2LnCH(SiMe_3)_2$ compounds may increase their coordination sphere with small ligands such as NC^{t}Bu (with Ce) and CN^{t}Bu (with Y) (Heeres et al. 1988); while NC^{t}Bu, with the yttrium derivative is inserted into the Y–C bond giving the imide $Cp^*_2Y[N=C(^tBu)CH(SiMe_3)_2]NC^tBu$ (Haan et al. 1987).

A novel type of bridging ligand (Booij et al. 1991) characterizes the compound produced by thermolysis of $Cp^*_2CeCH(SiMe_3)_2$ in cyclohexane-d_{12} identified by X-ray analysis as $\{Cp^*_3[C_5Me_3(CH_2CH_2)]Ce_2\}_2$. Its structure consists of a centrosymmetric tetranuclear entity with a doubly metallated pentamethylcyclopentadienyl group η^5, η^1, η^1-$C_5(CH_2)_2Me_3$ shared between three cerium atoms. The unique structural feature of this compound arises from the steric unsaturation of the metal center combined with the flexibility of the Cp* ligand.

Dienelanthanides are of interest as model compounds for polymerization and hydrogenation of olefins (Scholz et al. 1991). By using "magnesium (butadiene)" as diene source the compound $Cp^*_2La(THF)(\mu\text{-}\eta^1, \eta^3\text{-}C_4H_6)LaCp^*_2$ has been obtained. The presence of four signals in the ^{13}C-NMR spectrum suggests an unsymmetrical charge distribution in the diene as confirmed by the results of an X-ray analysis. Cp^*_2 hydrido and alkyl

scandocene derivatives are effective catalysts for the polymerization of ethylene, with acetylene $Cp^*_2Sc–C{\equiv}CH$ is formed (Clair et al. 1991) which decomposes to the unusual acetylenediyl bridged dimer $Cp^*2Sc\,C{\equiv}C–ScCp^*_2$.

The diamagnetic $Yb[Sn(2,2\text{-dimethylpropyl})_2]_2(THF)_2$ (Cloke et al. 1991a) produces the novel mixed ligand complex $YbCp^*Sn(CH^t_2Bu)_3(THF)_2$ when treated with one equivalent of Cp^*. The compound was characterized by multinuclear NMR spectroscopy (^{119}Sn and ^{171}Yb).

Naphthalene ytterbium with $SnPh_4$ in THF produces $(Ph_3Sn_2)Yb(THF)_4$ and $Ph_3SnYb(THF)_2(\mu\text{-}Ph)_3Yb(THF)_3$ (Bochkarev et al. 1991). The structure of $Ph_3SnYb(THF)_2(\mu\text{-}Ph)_3Yb(THF)_3$ is characterized by a triple phenyl bridged dimer. The two Yb coordination spheres are different, one having a Ph_3–Sn moiety coordinated with Yb–Sn bond length of 3.379(1) Å and two THF molecules, the second three THF molecules. A distorted octahedral coordination is present in both. The compound is formally an association of two Yb units $Ph_3SnYbPh(THF)_2$ and $Ph_2Yb(THF)_3$. The $Yb–C_{bridge}$ is nearly symmetric with a range of distances from 2.60(1) to 2.66(1) Å.

2.1.11.3.2. *Actinides.* The pentamethylcyclopentadienyl ligand has proved very useful for the synthesis of trivalent uranium derivatives when associated with another encumbering ligand ($CH(SiMe_3)_2$ as in $Cp^*_2UCH(SiMe_3)_2$ (Fagan et al. 1982). Photoelectron spectra of the monomeric $Cp^*_2UCH[Si(Me)]_2$ derivative (Di Bella et al. 1996), when compared to those of analogous lanthanide complexes, show close similarity in the metal ligand bonding between the 4f and 5f M^{III} organometallics and the relative stability of the $5f^3$ configuration respect to the $5f^26d^1$ for the uranium ion configuration, explains the higher stability of U^{III} derivative than of the $Th^{III}(6d^1)$ analogs. Alkylation of $Cp^*_2AnCl_2$ (An = U, Th) derivatives with lithium reagent produces the corresponding monomeric air sensitive and thermally stable dialkyls (Fagan et al. 1981a)

$$Cp^*_2AnCl_2 + 2RLi \rightarrow Cp^*_2AnR_2 + 2LiCl,$$

where An = U, Th; R = Me, CH_2SiMe_3, CH_2Ph; An = Th; R = CH_2CMe_3, Ph.

The $Cp^*_2AnR_2$ where R are alkyls containing β-hydrogen atoms are unstable towards the alkene elimination. The $Cp^*_2An(NR_2)_2$ insert CO (Fagan et al. 1981a) giving the compounds $Cp^*_2An(c\eta^2\text{-}OCNR_2)(NR_2)$ (An = U, Th, R = Me; An = U, R = C_2H_5). A second insertion under more forcing conditions can happen as in $Cp^*_2U(\eta^2\text{-}OCNMe_2)_2$. The structure and the spectral data are indicative of dative nitrogen lone-pair donation to the carbenoid carbamoyl moiety.

Thermolysis of $Cp^*_2Th(CH_2MMe_3)_2$ (M = C, Si) in saturated hydrocarbon solvent yields the thoracyclobutane $Cp^*_2Th[(CH_2)_2MMe_2]$ (Bruno et al. 1982c). The X-ray structure of the $SiMe_2$ derivative indicates the usual pseudotetrahedral "bent sandwich" coordination geometry while $Cp^*_2Th(CH_2SiMe_3)_2$ (Bruno et al. 1983) shows a highly unsymmetric $Th\text{-}(CH_2SiMe_3)_2$ fragment with intramolecular contact of a methyl-H of one ligand approaching within 2.3 Å the α-carbon of the other.

The syntheses, structure, and cyclometallation reactions of Cp^*_2Th dialkyls were also investigated (Bruno et al. 1984). A neutron diffraction study at 50 K on $Cp^*_2Th(CH_2CMe_3)_2$

(Bruno et al. 1986) shows the usual bent metallocene pseudotetrahedral structure which contrasts with the highly unsymmetrical bonding of the neopentyl ligands where agostic interaction of α-hydrogen atom are present. A new synthetic procedure for $Cp^*_2Th(Ph)_2$ and $Cp^*_2Th(Me)(Aryl)$ compounds is the reaction of PhMgBr with $Cp^*_2ThCl_2$ in the presence of *p*-dioxane, by a similar method Cp^*_2ThMeL (L = O-$MeOC_6H_4$, O-MeC_6H_4, 2,5-MeC_6H_3) derivatives have been isolated (England et al. 1994). The tolyl and xylyl derivatives in solution exist as pair of rotamers.

Actinide diene complexes (Smith et al. 1986) can be prepared from Cp^*_2MCl (M = U, Th) and the appropriate Grignard reagent. The X-ray structure of the $Cp^*_2Th(\eta^4\text{-}C_4H_6)$ compound shows a "bent sandwich" Cp^*_2Th moiety coordinated to the butadiene ligand in s-*cis* conformation with an η^4 bonding mode. Thermochemical studies of the thorium–butadiene bond disruption enthalpy do not indicate particular Th–butadiene stabilization, it is comparable to that for Th to carbon σ-bonds. The compound adopts the familiar "bent sandwich" structure.

Cationic actinide alkyls species as possible catalytic agents for electron-deficient metal oxide supports ($\gamma\text{-}Al_2O_3$) are produced by protonolysis of actinide alkyls in non-coordinating solvents (Lin and Marks 1987). Recrystallization of one of the products i.d. $(Cp^*_2ThMe)^+(BPh_4)^-$ from THF/pentane yields the disolvated THF complex $[Cp^*_2Th(Me)(THF)_2][BPh_4]$. Its X-ray structure show a cation of "bent sandwich" structure with an unsymmetrical arrangement of the non Cp^* ligands. The different Th–O distances have been tentatively justified among other factors with "differing π-donation to thorium frontier orbitals".

Cationic actinide metallocene alkyls are key components among the catalysts for homogeneous olefin polymerization. Their reactivity is largely dependent on the nature of the counter-ion. The cationic actinide alkyl reactivity can be modulated by use of a large counterion as in $[Cp^*_2ThMe][B(C_6F_5)_4]$ (Yang et al. 1991) obtained by the reaction of $Cp^*_2ThMe_2$ with $(NH^nBu_3)B(C_6F_5)_4$. The crystal structure shows anion–cation interactions [Th–F 2.757(4), 2.675(5) Å]. The chelating binuclear fluoroaromatic $(ArF)^8$borane/species (Jia et al. 1994) should also increase the reactivity of the Cp^*_2Th-alkyl system by a reduced cation–anion interaction. The compound $(Cp^*_2ThMe)^+\{^tBuCH_2CH[B(C_6F_5)_2]_2H\}^-$ has been synthesized by the protonolytic reaction

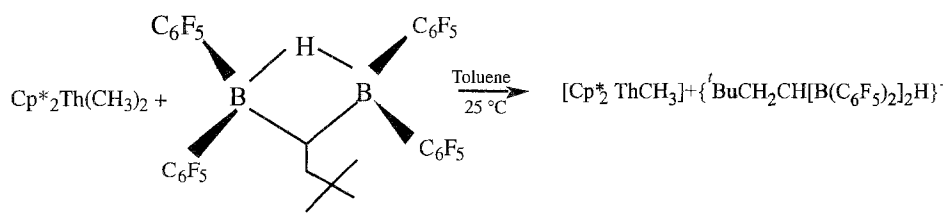

It is a catalyst for ethylene polymerization and 1-hexene hydrogenation.

The efficacy of uranium and thorium complexes of the type $Cp^*_2AnL_2$ (L = hydrocarbyl) as catalysts for decoupling silane has been also investigated (Aitken et al. 1989) while

$Cp^*_2ThMe_2$ selectively catalyses the dimerization of phenyl silane in diethylether the reaction with $Cp^*_2UMe_2$ is less selective and may involve U^{III} intermediates.

2.1.11.4. *Cp^*_2M non-halide non-hydrocarbyl derivatives.*

2.1.11.4.1. *Lanthanides.* The main synthetic routes for Cp^*_2Ln derivatives are, as already discussed, the use of highly reactive divalent species and alcoholysis of the corresponding alkyls or hydride derivatives.

$[Cp^*_2Sm]_2(\mu\text{-}O)$ is a common product (Evans et al. 1985e) in the reaction of Cp^*_2 Sm(THF) with oxygen-containing substrates like NO, N_2O, $CH_3CH_2CH_2CHO$ or C_5H_5NO but not with $OPPh_3$. (In the last case the adduct $Cp^*_2Sm^{II}(OPPh_3)THF$ is formed.) The compound contains linear Sm–O–Sm bridges. The dimeric molecule has perfect S_4 symmetry with the oxygen atoms lying at the center of the rotation axis and with the two bent metallocene units twisted 90° relative to each other. The Cp rings are in an eclipsed conformation on each samarium. $Cp^*_2Sm(OC_6HMe_4\text{-}2,3,5,6)$ is obtained by reacting $Cp^*_2Sm(THF)_2$ with 2,3,5,6-tetramethylphenol in toluene (Evans et al. 1985f). The compound is monomeric with the common bent metallocene structure and a nearly linear Sm–O–C(aryloxide) linkage [Sm–O 2.13(1) Å, Sm–O–C 172.3(13)°].

A cationic $[Cp^*_2Sm(THF)_2]^+$ moiety in the salt $[Cp^*_2Sm(THF)_2][BPh_4]$ is obtained again from $Cp^*_2Sm(THF)_2$ and $AgBPh_4$ in THF (Evans et al. 1990e). The most unusual feature of its X-ray structure is the eclipsed conformation of the Cp^* rings, which are staggered in the neutral bivalent $Cp^*_2Sm(THF)_2$ compound. The reaction of $[Cp^*_2Sm(THF)_2]$ with KCp^* occurs with THF ring opening to form the cyclopentadiene-substituted alkoxide $O(CH_2)_4C_5Me_5$ and generates the complex $Cp^*_2Sm[O(CH_2)_4Cp^*]THF$. This, according to the authors, may be considered as a prototype example of ligand reaction chemistry generated by coulombic attractions in a crowded lanthanide system. The structural details are as usual for $Cp^*_2SmL(THF)$ complexes. The pentamethylcyclopentadiene ring attached to the $(CH_2)_4$ chain has a localized diene structure.

The THF adduct $Cp^*_2Sm(THF)_2$ is also a CO and CH activating agent. It can assemble three CO molecules into a dimetal substituted ketenecarboxylate: $[Cp^*_2Sm_2(O_2CCCO)\text{-}(THF)]_2$ which crystallizes from THF solution as orange-brown crystals (Evans et al. 1985g). When reacted with $C_6H_5C{\equiv}CC_6H_5$, $Cp^*_2Sm(THF)_2$ forms $[Cp^*_2Sm]_2C_2(C_6H_5)_2$ which further reacts with CO giving the compound $[(Cp^*_2Sm)_2\text{-}\mu\text{-}\eta^2O_2C_{16}H_{10}]$ (Evans et al. 1988d). Its structure shows that the condensation of two CO molecules with one of diphenyl ethyne produces a tetracyclic dihydroindenoindene unit which bridges two Cp^*_2Sm units. The crystal structure of $[Cp^*_2Sm(CNCMe_3)]_2O$ was also reported.

The high reactivity of Sm-hydride is demonstrated by the bridged samarium siloxide $[Cp^*_2Sm(THF)]_2[\mu\text{-}\eta^2\text{-}(OSiMe_2OSiMe_2O)]$ compound (Evans et al. 1991b) obtained by dissolution of $[Cp^*_2Sm(\mu\text{-}H)]_2$ in THF distilled from glass were lubricated with high vacuum silicone grease. The initiation behavior of $[Cp^*_2SmH]_2$ for polymerization of methyl methacrylate (MMA) (Yasuda et al. 1992), suggested the preparation of 1:2 adduct of $[Cp^*_2SmH]_2$ with MMA. $Cp^*_2Sm(MMA)_2H$ crystallizes as air-sensitive orange crystals. One MMA unit binds to Sm as enolate and the other as C = O group (Sm–O(1) is 2.39(1) Å

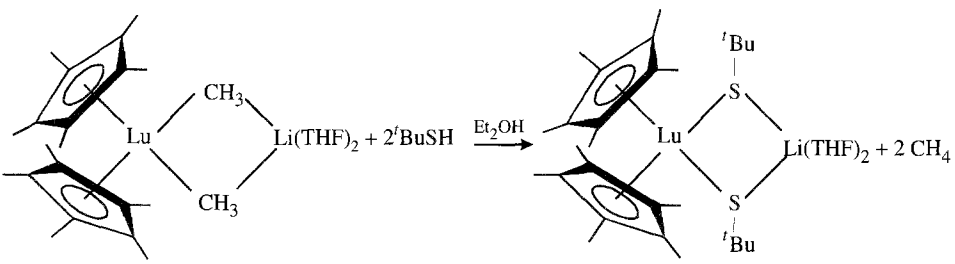

Scheme 11.

and Sm–O(2) is 2.188(9) Å. The excellent catalytic activity of the complex suggests this is the active species in the polymerization process.

The rapid interaction of $[Cp^*_2SmH]_2$ with CO in arene solvent generates a Ph_3PO adduct when crystallized by adding Ph_3PO (Evans et al. 1985h). The carbon monoxide is both reduced and dimerized yielding a bridging enediolate ligand of *cis* geometry, which rather easily isomerizes to *trans* bridge at room temperature. The *cis*$[Cp^*_2(Ph_3PO)Sm]_2(\mu$-OCH=CHO) derivative crystallizes as toluene solvate, while the *trans* is unsolvated. The isomerization of the *cis* enediolate unit to the *trans* isomer was not previously observed in CO/metal hydride chemistry.

The reactivity of the lanthanide carbyls $Cp^*_2LnCH(SiMe_3)_2$ (Ln = La, Ce) toward simple ketones such as acetone, 3-pentanone and di-*tert*-butylketone has been investigated (Heeres et al. 1992). No reaction occurs with di-*tert*-butylketone while with acetone the lanthanide aldolates $Cp^*_2LnOCMe_2CH_2C(=O)Me$ are formed. With 3-pentanone the enolate-ketone adducts $Cp^*_2LnOC(Et)\equiv C(H)Me\cdot O{=}CEt_2$ are produced. The difference in reactivity between acetone and 3-pentanone seems to be thermodynamic rather than kinetic. It appears that Cp^*_2Ln derivatives may serve as monomeric models for aldol condensation. The structure of the cerium aldol $Cp^*_2CeOCMe_2CH_2C(=O)Me$ has been reported. The two cerium oxygens distances differ significantly being Ce–O(2) 2.182(4) Å to the alkyl oxide and Ce–O(1) 2.506(4) to the carbonyl oxygen.

Organolanthanides with the heavier chalcogenides (S, Se, Te) are less common than those with oxygen due to the low stability of their bonds between "hard" lanthanides and "soft" donors (Pearson 1963). Zalkin et al. (1982), report the preparation and the structural characterization of the compound $Cp^*_2Yb(S_2CNEt_2)$ which represents the first example of determination of a Yb–S bond (2.70 Å), [S–Yb–S′ 67.1(3)°]. The magnetic behavior of $Cp^*_2Yb(O_2CCMe_3)$ and $Cp^*_2Yb(S_2CNEt_2)$ at low temperature (magnetic moment 3.29 and 3.39μ_B, 3–45 K, respectively) is independent of the ligand. A new versatile route for preparation of pentamethylcyclopentadienyl lutetium alkoxide and thiolates, is described (Schumann et al. 1985c), having as precursor $Cp^*_2Lu(\mu$-$CH_3)_2Li(THF)_2$. The product of the reaction with *tert*-butyl hydrosulfide $[Cp^*_2Lu(\mu$-$S^tBu)_2Li(THF)_2]$ has been characterized by X-ray crystallography (scheme 11).

The compound is a bis(*tert*-butylthio) bridged dinuclear Lu–Li complex, with a puckered LuS_2Li moiety. The Lu–S distances are 2.709(3) and 2.723(3) Å. The Cp^*_2Yb reactive moiety as hydrocarbon soluble source of a single electron, has been used for

the cleavage of molecules of the type REER (R is an organic group and E is O, S, Se or Te) to give the compounds $Cp^*_2Yb(ER)(L)$ (L = Lewis base). The structure of the compound Cp^*_2Yb ammine thiophenolato $[Cp^*_2Yb(SPh)(NH_3)]$ (Zalkin et al. 1987d) shows the Yb metal ion at the center of a distorted tetrahedron, consisting of one sulphur, one nitrogen and the ring centroids (Cg) of the two Cp* rings.

The crystal structure of $[Cp^*_2Yb(TePh)(NH_3)]$ (Berg et al. 1988) has an overall geometry similar to that of the sulphur analog, though the crystals are not isomorphous. The complex $(Cp^*_2Yb)_2Te_2$ was isolated by reacting $Cp^*_2Yb(C_2H_5)_2O$ with an excess of tellurium powder in hexane. Its structure consists of a centrosymmetric dimer (Zalkin and Berg 1988) where each Yb metal ion is about tetrahedrally bonded to the two Cp* ligands and to the Te_2^{2-} ion. $[Cp^*_2Yb]_2(\mu\text{-L})$ (L = S, Se, Te) have been prepared (Berg et al. 1989) and exhibit no magnetic exchange across the chalchogenide bridge. The X-ray structure of $[Cp^*_2Yb]_2(\mu\text{-Se})$ is characterized by a near linear Yb–Se–Yb bridge (171.1°) with the Cp^*_2Yb units mutually staggered about the bridge. The compound is formally seven coordinate.

The analogous samarium derivative with two additional THF ligands is also known (Evans et al. 1994b). The X-ray structures have been reported of (μ-Te) complexes of bisolvated THF Sm (Evans et al. 1994b), and of unsolvated Sc (Piers et al. 1994) and Yb (Zalkin and Berg 1988). The reactive $Cp^*_2Sm(THF)_2$, when treated with disulfides, diselenides and ditellurides organosamarium, produces complexes containing Sm–E bond (E = S, Se, Te; Recknagel et al. 1991b). Protolysis of $Cp^*_2CeCH(SiMe_3)_2$ by Et_3NHBPh_4 produces the cationic compounds $[Cp^*_2CeL_2][BPh_4]$ (L = THF, tetrahydrothiophene(THT); Heeres et al. 1991). The X-ray structure of the (THT) derivative is a rare example of X-ray characterization of a Ce–S dative bond in an organometallic derivative [Ce–S 3.058(1) and 3.072(1) Å].

The Cp^*_2Ln-amide derivatives $Cp^*_2LnN(SiMe_3)_2$ (Ln = Nd, Yb) were also synthesized (Tilley and Andersen 1981) while the X-ray structure of the yttrium derivative was reported later (Haan et al. 1986), the compound, of roughly trigonal planar coordination geometry, is coordinatively unsaturated, this favors the formation of weak γ-agostic Y–methyl contacts and a short Y–N distance due probably to the donation of the nitrogen lone-pair to the electron deficient yttrium center.

The analogous Y, Nd, Sm, Lu compounds were synthesized with the modified C_5Me_4Et ligand (Schumann et al. 1995c) and the X-ray structure of $(C_5Me_4Et)_2YN(SiMe_3)_2$ is comparable to that of the pentamethylated. The coordinative unsaturation favors the insertion of small molecules in alkyl derivatives as for example that of $^tBuC{\equiv}N$ in $Cp^*_2YCH(SiMe_3)_2$ giving $Cp^*2Y[N{=}C(^tBu)CH(SiMe_3)_2](NC^tBu)$ (Haan et al. 1987). An example of an 18 electron complex is given by the THF adduct of the iminoacyl derivative, i.e., $Cp^*_2Y\{\eta^2\text{-}[C(CH_2C_6H_3Me_2\text{-}3,5){=}NC_6H_3Me_2\text{-}2,6]\}THF$ whose X-ray structure shows a pseudotetrahedral coordination geometry around Y with a dihapto bonding mode of the iminoacyl ligand. Addition of acetonitrile to $Cp^*_2ScNHNR_2$ (R = H, Me; Shapiro et al. 1990) leads to $Cp^*_2ScNHCMeNNH_2$ and $Cp^*_2ScNHCMeNNMe_2$ derivatives. Their X-ray analyses established the given formulation with five membered and four membered metallacycles, respectively.

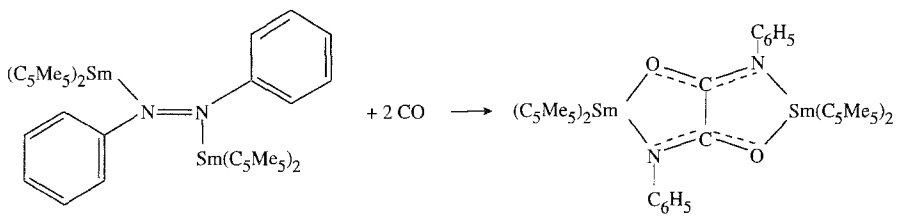

Scheme 12.

The reactive and soluble $Cp^*_2Sm(THF)_2$ precursor interacts also with nitrogen containing substrates; with azobenzene it forms the dimeric complex $[Cp^*_2Sm]_2(\mu\text{-}\eta^2\text{-}N_2Ph_2)$ (Evans et al. 1988b). The carbon monoxide insertion product $[Cp^*_2Sm]_2[\mu\text{-}\eta^4\text{-}(PhN)OCCO(NPh)]$, of this complex has been also prepared and structurally characterized (Evans and Drummond 1986). The N=N double bond of the azobenzene is broken and two N–C bonds and a C–C bond are formed in a single reaction with CO. Each Sm atom is bound to one O and one N of the new ligand formally a double deprotonated *N,N'*-diphenyloxamide (scheme 12).

Addition of azobenzene to $(Cp^*_2Sm)_2N_2Ph_2$ produces the monomeric derivative $(Cp^*_2Sm)N_2Ph_2$,

$$(Cp^*_2Sm)_2N_2Ph_2 + PhN{=}NPh \rightarrow 2(Cp^*_2Sm)N_2Ph_2,$$

while in THF the dimer slowly transforms into the orange $[Cp^*SmTHF]_2[\mu\text{-}\eta^2{:}\eta^2N_2Ph_2]_2$ compound with the rather unusual loss of a Cp^* unit from the Cp^*_2Sm moiety.

$$\underset{\text{blue}}{2\,[\,(\,Cp^*_2Sm\,)\,N_2Ph_2\,]} \xrightarrow{(THF)} \underset{\text{orange}}{[Cp^*(THF)Sm]_2[N_2Ph_2]_2} + 2Cp^* + 2Sm^{3+}.$$

In the X-ray structure of the monomer $(Cp^*_2Sm)(\eta^2\text{-}N_2Ph_2)(THF)$ the Cp^*_2Sm unit is bonded to the $\eta^2\text{-}N_2Ph_2$ ligand with the phenyl ring *cis* oriented and to a THF molecule. Magnetic and structural data indicate a trivalent oxidation state for the metal ion in the two complexes. The orange dimer $[Cp^*(THF)Sm]_2(N_2Ph_2)_2$ is characterized by two doubly bridging N_2Ph_2 units.

The reagent $Cp^*_2Sm(THF)_2$ induces facile multiple bond cleavage (Evans and Drummond 1988b) which produces rearrangement in unusual multiple bonded species. An example is the compound $Cp^*_2Sm[\mu\text{-}\eta^4(C_5H_4N)CH{=}C(O)C(O){=}CH(C_5H_4N)]SmCp^*_2$ which shows the unprecedented insertion of two CO molecules into a carbon–carbon double bond. Very recently a novel CO insertion product $(Cp^*_2Y)_2[\mu\text{-}\eta^2{:}\eta^2\text{-}CO(NC_5H_4)_2]$ has been reported (Deelman et al. 1994).

Studies of the reactivity of $Cp^*_2Sm(THF)_2$ compounds with CO, RC≡CR, RN=NR and $R_2C{=}CR_2$ (Evans and Drummond 1989) have shown the variety of useful transformations induced by Sm on these unsaturated substrates. In its reaction with azine (which contains a C=N double bond), in contrast to the two electron multiple bond reduction observed in the previously quoted substrates, the azines are reduced by one electron

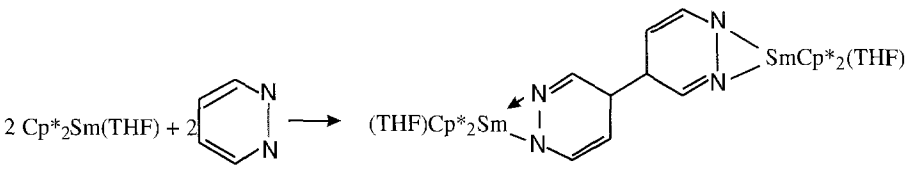

Scheme 13.

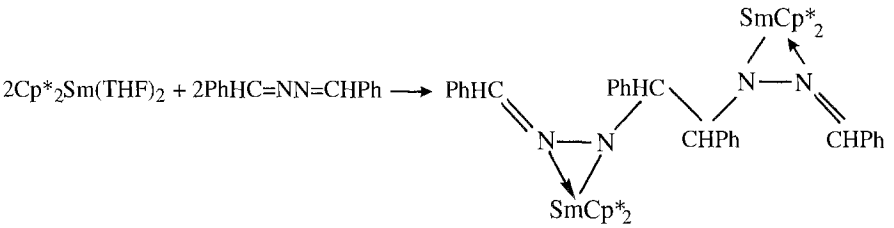

Scheme 14.

per substrate. $Cp^*_2Sm(THF)_2$ reacts with pyridazine, benzaldehydeazine and bipyridine giving well defined organosamarium (III) complexes, which have been characterized by complexometric analysis, NMR and IR spectroscopy and by X-ray diffraction methods. With pyridazine the complex $[Cp^*_2Sm(THF)]_2[\mu\text{-}\eta^4\text{-}(CH{=}NNCH{=}CHCH\text{-})_2]$ is obtained as orange crystals from toluene solution at –34°C. The X-ray analysis shows the formation of a bipyridazine unit according to the equation in scheme 13, where the two nitrogen atoms of each ring coordinate to a $Cp^*_2Sm(THF)$ moiety.

With benzaldehyde azine (PhHC=NN=CHPh) the unsolvated dimeric complex $[Cp^*_2Sm]_2[\mu\text{-}\eta^2\text{-}(PhCH{=}NNCHPh^-)_2]$ is formed. This is a further example of reductive coupling (scheme 14).

The samarium atom is eight coordinate and the structural parameters are in agreement with the corresponding ones in $Cp^*_2SmN_2Ph_2$. The reaction with bipyridine gives instead a monometallic complex $Cp^*_2Sm(\eta^2N_2C_{10}H_8)$. (This substrate can probably delocalize the electron density and the coordination of the bipyridyl anion to Sm can occur without coupling.) The ^{13}C NMR shifts for C_5Me_5 carbon atoms are characteristic of Sm^{III} complexes. $Cp^*_2Sm(THF)$ reacts also with 1,4-diazadienes (DAD) (Recknagel et al. 1991c) to give compounds of the type Cp^*_2SmDAD; with pyridinealdazine it produces the binuclear complex $(\mu\text{-}C_{12}H_{10}N_4)[Cp^*_2Sm]_2$ (scheme 15).

The molecular structure of $Cp^*_2Sm(^tBuN{=}CHCH{=}N^tBu)$ is monomeric. The dimeric dinitrogen complex $[Cp^*_2Sm]_2N_2$ is obtained as a secondary product in the synthesis of Cp^*_2Sm by metal vapor methods (Evans et al. 1988e). The dimer, of binary symmetry (the binary axis is coincident with the Sm(1)–Sm(2) vector) is a rare example of planar side-on bonding between a dinitrogen ligand and two metals. Spectral NMR results are consistent with Sm^{III} cations and reduced N_2 unit. The equilibrium

$$2Cp^*_2Sm + N_2 \xleftrightarrow{\text{toluene}} [Cp^*_2Sm]_2N_2,$$

explains the complex formation. (The enthalpy of dimerization is negative.)

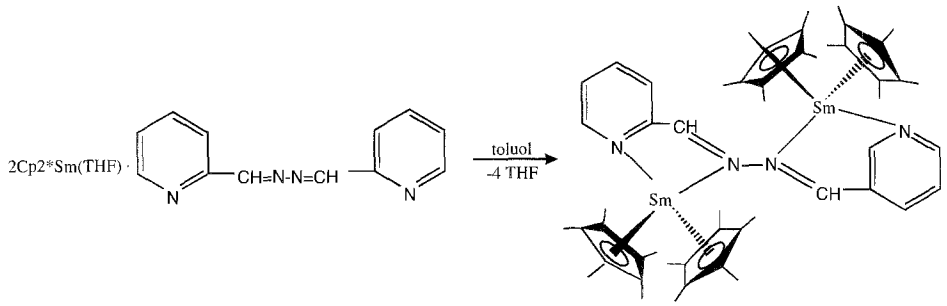

Scheme 15.

The crystal structure of the dimer $[Cp^*_2Sm(THF)]_2(\mu\text{-}\eta^2\text{:}\eta^2HNNH)$ is also known (Evans et al. 1992c). Very recently the Schumann group (Scholz et al. 1994) showed that N heterocyclic dianions of quinoxaline and phenazine also bridge two Cp^*_2La moieties as shown by the X-ray structure of $[Cp^*_2La]_2(C_{12}H_8N_2)$ (fig. 29). The selectivity of catalytic hydroamination/cyclization process of amino olefin assisted by the regiospecific

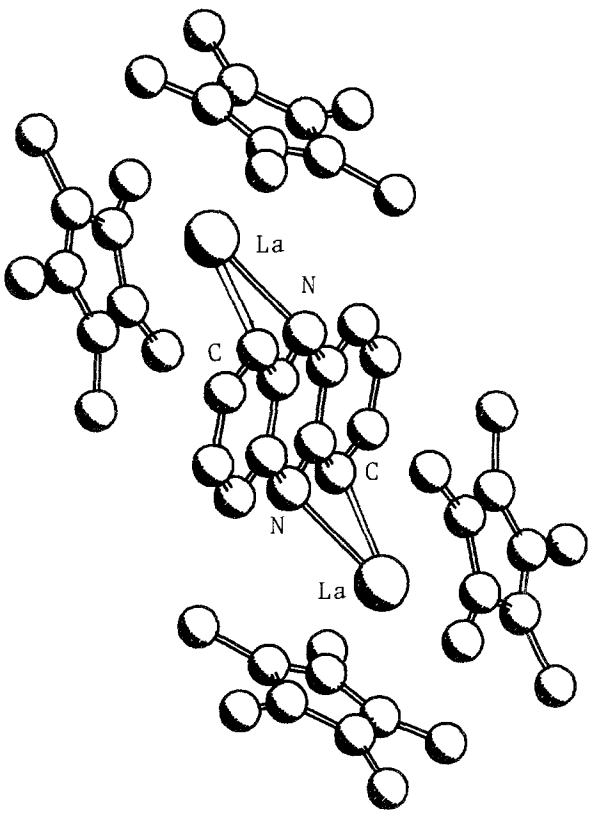

Fig. 29. Crystal structure of $[Cp^*_2La]_2$-$(C_{12}H_8N_2)]$ (Scholz et al. 1994).

Cp^*_2LnR compounds [R = H, $CH(TMS)_2$, η^3-C_3H_5, $N(TMS)_2$, Ln = La, Nd, Sm, Y, Lu] is widely described (Gagné et al. 1992) and the interpretation of the hydroamination/cyclization process involves comparable cyclization rate constant and kinetic isotope effects with different diasteroselectivities of ring closure where the lanthanide size, the ancillary ligand effects and the particular amino olefin play determinant roles. The complexes $Cp^*_2LnNHR(H_2NR)$ (Ln = La, R = CH_3, CH_2CH_3; Ln = Nd, R = CH_2CH_3) and $Cp^*_2LaNCH(CH_3)CH_2CR_2CH_2[HNCH(CH_3)CH_2CR_2CH_2]$ (R = H, CH_3) were synthesized as model species in the catalytic cycle. The structure of $Cp^*_2LaNHCH_3(H_2NCH_3)$ at −120°C is characterized by the presence of two distinct monomeric amine–amido complexes with large disparity in La–N bond distances between amido and amine (La–$N(HCH_3)$ 2.31(1) and La–$N(H_2CH_3)$ 2.70(1) Å in agreement with the different bonding environments noted in NMR spectra. The precatalyst activities for $Cp^*_2LnCH(TMS)_2$ are in the order La > Sm > Lu; $Et_2Si(C_5H_4)(Me_4C_5)LuCH(TMS)_2 > Me_2Si(Me_4C_5)_2LuCH(TMS)_2 > Cp^*_2LuCH(TMS)_2$ in agreement with olefin insertion reactivities.

The ability of the Cp^*_2Sm moiety to react with a variety of substrates has allowed the reaction (cyclohexane or benzene solution; Evans et al. 1991c)

$$4Cp^*_2Sm + 2BiPh_3 \rightarrow \left[Cp^*_2Sm\right]_2 \left(\mu\text{-}\eta^2 : \eta^2\text{-}Bi_2\right) + 2PhPh + 2\,(Cp^*_2)\,SmPh,$$

providing a new route to dibismuth compounds. The structure of $[(Cp^*_2)Sm]_2(\mu\text{-}\eta^2\text{:}\eta^2\text{-}Bi_2)$ is the first example of a dibismuth complex of an f element. The Bi_2 moiety coordinates planarly to two Sm. The formally dianionic Bi_2^{2-} unit has a Bi–Bi distance of 2.851(1) Å (suggesting a partial multiple bonding), and a distance of 3.29(2) Å to the Sm.

Cp^*_2Sm reacts also with $Sb(^tBu)_2$ in toluene (Evans et al. 1992d) to form the trimeric compound $Cp^*_2Sm(\mu\text{-}\eta^2\text{:}\eta^2\text{:}\eta^1\text{-}Sb_3)(THF)$, which contains a bent $(Sb_3)^{3-}$ anion (114.5(1)°) with an average Sb–Sb distance of 2.688(1) Å. Five of the six Sm–Sb distances are in the range 3.162(1)–3.205(1) Å while the sixth Sm–Sb distance, 3.686(1) Å, is considered too long for a significant interaction. The strategy which governed the synthesis of a substituted methane complex was to react MeBeCp* with Cp^*_2Yb as Lewis acid of bent structure, to receive the methyl counter part (Burns and Andersen 1987b). The structure of the complex obtained $Cp^*_2YbMeBeCp^*$ shows the moiety MeBeCp* linearly bridged (via Me) to the Cp^*_2Yb fragment.

The first compound containing a Ln–As bond, $Cp_2Lu(\mu\text{-}AsPh_2)_2Li$ (tmed) has been reported. The Lu–As lengths were found to be 2.896 and 2.870 Å (Schumann et al. 1986b, 1988d).

2.1.11.4.2. *Actinides.* The first report on Cp^*_2An derivatives with pnicogenides came from Fagan et al. (1981b).

The reaction of $Cp^*_2AnCl_2$ (An = U, Th with lithium dialkylamides (1:1) yields a series of monodialkylamido $Cp^*_2An(NR_2)Cl$ (An = U, Th; R = Me, Et) and bis-dialkylamido derivatives (1:2) $Cp^*_2An(NR)_2$ (An = U, Th; R = Me). They can be obtained also by protonolysis of the corresponding dialkyl derivatives:

$$Cp^*_2AnMe_2 + 2HNEt_2 \rightarrow Cp^*_2An(NEt_2)_2 + 2CH_4,$$

where An = U, Th.

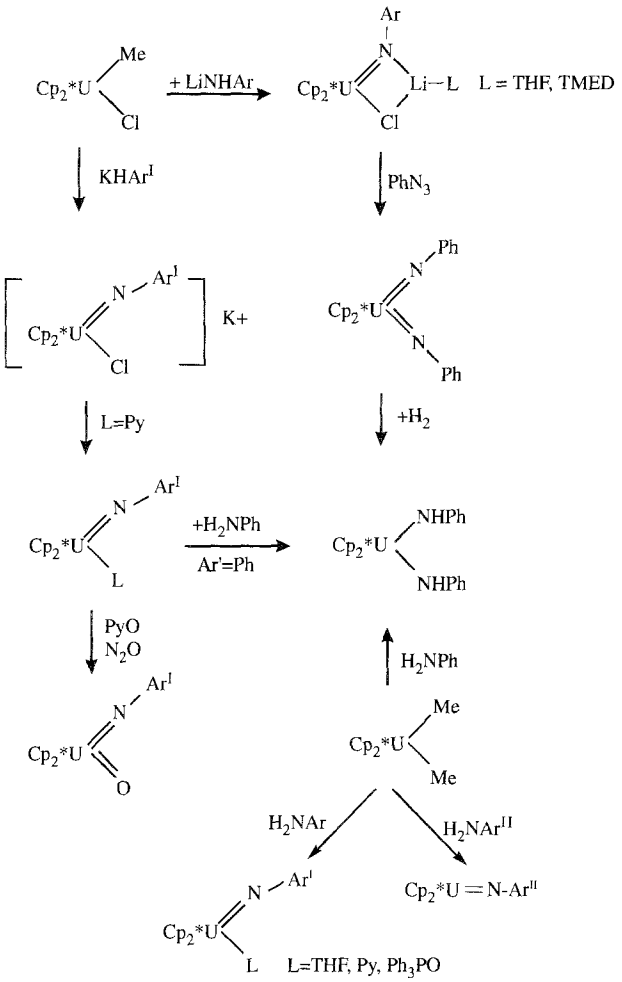

Ar = 2,6-^{i}Pr$_2$C$_6$H$_3$, C$_6$H$_5$ Ar^{II} = 2,4,6-^{t}Bu$_3$C$_6$H$_2$

Ar^{I} = 2,6-^{i}Pr$_2$C$_6$H$_3$, C$_6$H$_5$, 2,4,6-Me$_3$C$_6$H$_2$

Scheme 16.

The ^{1}H NMR spectra of the U^{IV} species show substantial isotropic shifts, and variable temperature experiments indicate restricted rotation around the U–N bond. The bis(dialkylamides) undergo stepwise migratory CO insertion to yield mono- and bis-carbamoyl derivatives. A large number of organouranium imido complexes with different uranium oxidation states IV and VI have been synthesized (Arney et al. 1992, Arney and Burns 1993, 1995) by both metathesis and direct protonation routes (scheme 16).

In the simplified scheme are shown some of the products obtainable from the $Cp^*_2UMe_2$ and $CP^*_2UMe(Cl)$ precursors. The U^{IV} organoimide derivatives in turn react

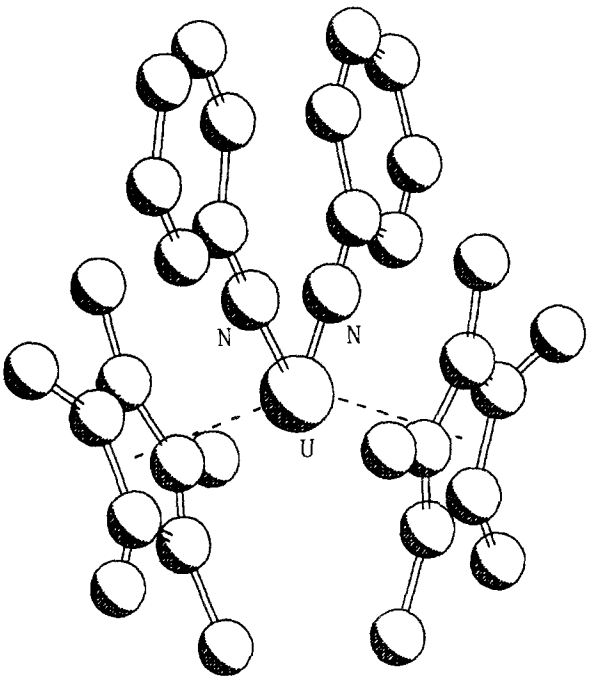

Fig. 30. Crystal structure of $[Cp^*_2U(NC_6H_5)_2]$ (Arney et al. 1992).

with 2-electron oxidative atom transfer reagents such as organic azides, NO and pyridine N-oxide as shown in the scheme, producing a new class of U^{IV} derivatives containing terminal imido and oxo functional group. The chemical stability of these complexes has been related to the formation of multiple uranium and oxo bonds. The first complex of uranium(VI) with metal carbon bonding in either a σ or π fashion, $Cp^*_2U(NC_6H_5)_2$, has been characterized by X-ray (−80°C), IR and NMR data which support the assignment of the formal 6+ oxidation state (Arney et al. 1992). (The NMR chemical shifts are outside the normal diamagnetic region; fig. 30) The uranium coordination is the usual pseudotetrahedral. The short U–N (1.952(7) Å) bond distance and the linear $U–N–C_{ipso}$ bond angle 177.8(6)° are consistent with organo imido ligands. The compound is also the first example of a bis (organoimido) uranium(VI) analog to UO_2^{2+} with an unexpected non linear geometry of the two organoimido ligands (N–U–N angle is 98.7(4)°).

The compounds, successively synthesized, $Cp^*_2U(OAr)(O)$ and $Cp^*_2U(NAr)(O)$ (Ar = 2,6-diisopropylphenyl; Evans et al. 1992c) are, respectively, the first U^V and U^{VI} complexes with terminal monoxofunctional groups as confirmed by the respective electron absorption spectra. The structure of $Cp^*_2U(O\text{-}2,6\text{-}Pr_2\text{-}C_6H_3)O$ (fig. 31) is analogous to that of the N derivative. The difference in the two U–O (terminal bond distances) 1.859(6) for the U^V species and 1.844(4) A for U^{VI} is consistent with the difference in the U^V and U^{VI} ionic radii (Shannon 1976).

In $Li(TMED)[Cp^*_2U(NC_6H_5)Cl]$ the U–N bond distance is 2.051(14) Å in the range 1.91(2)–2.07(2) Å characteristic for U–N terminal distances in U^V and U^{VI} complexes

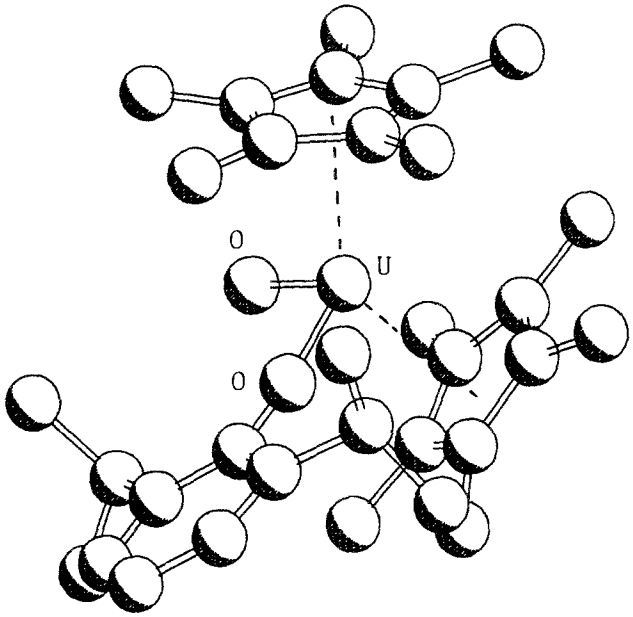

Fig. 31. Crystal structure of $[Cp_2^*U(O\text{-}2,6^iPr_2C_6H_3)O]$ (Evans et al. 1992c).

suggests again U–N multiple bond as in $Cp_2^*U(N\text{-}2,4,6\text{-}^tBu_3C_6H_2)$ of trigonal planar geometry around U, with an U–N linkage of 1.952(12) Å and an open U–N–C angle of 162.3(10)° (Arney and Burns 1995).

$Cp_2^*UMe_2$ reacts with primary aromatic or alifatic amines to give the monomeric U^{IV} complexes $Cp_2^*U(NHR)_2$ (R = 2,6-dimethylphenyl, Et and ^{t}Bu; Straub et al. 1996). The crystal structure of the bis-amido complex $Cp_2^*U[NH(C_6H_3Me\text{-}2,6)]_2$ shows the expected tetrahedral arrangement of the ligands. Subsequent reactions with σ-bond metathesis, of the bis(amido) and/or imido derivatives with alkynes generated the bis(acetylide) complexes $Cp_2^*U(C{\equiv}CR)_2$ (R = Ph, ^{t}Bu), which are useful in the regioselective oligomerization of terminal alkynes. The reaction of the cationic amide compound $[Cp_2^*U(NMe)_2(THF)][BPh_4]$ (Boisson et al. 1996) with THF using the free amine $NHEt_3BPh_4$ as catalyst gives the heterocyclic metallacycle

$$\left[Cp_2^*\overline{UO(CH_2)_4NMe_2(CH_2)_4O}\right][BPh_4]\cdot 0.5THF,$$

first example of a heterocyclic metallacycle containing both oxygen and nitrogen atoms.

The diorganophosphido actinide complexes, $Cp_2^*Th(PR_2)_2$ (R = Ph, Cy, Et) have been prepared by reaction of $Cp_2^*ThCl_2$ with $LiPPh_2$ in toluene (Wrobleski et al. 1986a). The unusual red-purple color of $Cp_2^*Th(PPh_2)_2$ was attributed to phosphido ligand-to-metal charge-transfer band (λ_{max} 570, 498 nm). Its X-ray crystal structure shows a pseudotetrahedral geometry around Th. The Th–P bond distances (Th–P 2.87(2) Å) does not show evidence for significant multiple bond character and the angles around P atoms are far from tetrahedral.

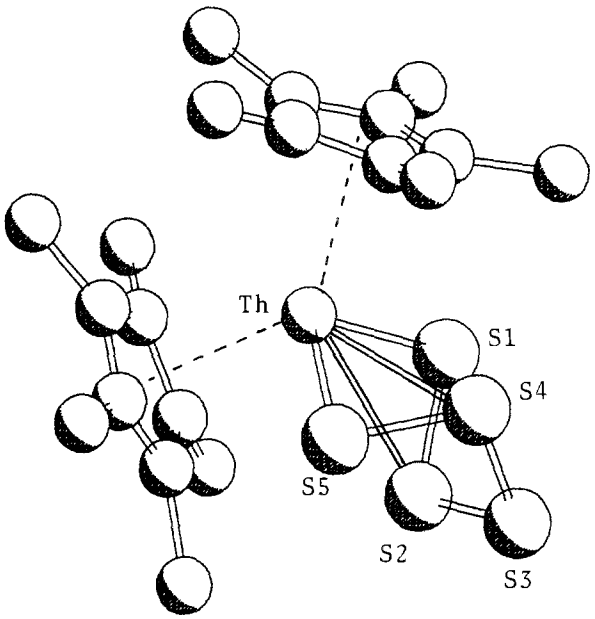

Fig. 32. Crystal structure of [Cp^*_2-ThS_5] (Wrobleski et al. 1986b).

The reaction chemistry of $[Cp^*_2AnH_2]_2$ with trimethyl phosphite has been reported (Duttera et al. 1984). The structure of the $[Cp_2U(OMe)]_2(\mu$-PH) dimer is characterized by a symmetric U–P–U bridge with U–P of 2.743(1) Å and U–P–U angle of 157.7(2)°. Recently, bis-(trimethylsilyl) phosphide compounds $Cp^*_2An(X)[P(SiMe_3)_2]$ (X = Cl, Me; An = U, Th) have been synthesized (Hall et al. 1993).

For the chalcogenides category alkylthiolate and polysulfide Th complexes have been reported.

The usual "bent sandwich" structure characterizes the organothorium alkylthiolate complex, $Cp^*_2Th[S(CH_2)_2Me]_2$. The Th–S bond distance is 2.718(3) Å. The actinide–thiolate bonding involves less ligand-to-metal π-donation than does actinide–alkoxide bonding (Lin et al. 1988). The first organoactinide polysulfide $Cp^*_2ThS_5$ (Wrobleski et al. 1986b) has been prepared from $Cp^*_2ThCl_2$ and Li_2S_5 as yellow crystals. The molecular structure (fig. 32) shows an unprecedented twist-boat ThS_5 ring conformation as "consequence of donor–acceptor bonding between the β-sulfur atoms of the S_5^{2-} chelate and the electron deficient thorium(IV) center", confirming the NMR data. The two different sets of Th–S bond distances could correspond to dative bond (Th–S(2) 3.036(3) Å) while Th–S(1) 2.768(4) Å is ionic.

2.1.11.5. *Cp*M derivatives.*

2.1.11.5.1. *Lanthanides.* The first synthesis of a mono Cp* ligand derivative was with Yb (Watson et al. 1981). The product $Cp^*Yb(\mu^2\text{-}I)_3Li(Et_2O)_2$ was obtained by reacting Yb metal with Cp*I and LiI in ether while the analogous chlorine derivative was produced by halide metathesis of $YbCl_3$ with Cp*Li. The latter method was subsequently used for

the preparation of a series of chlorine and iodine derivatives with different lanthanides mainly ether solvates. Monomeric solvent free species of the type Cp^*YbCl_2 have also been synthesized (Finke et al. 1986). Solvated species like $Cp^*CeI_2(THF)_3$ (Day et al. 1982) show a pseudooctahedral *mer, trans* geometry around the metal ion.

Reaction of SmI_2 in THF (1:1) gave $[Cp^*Sm(\mu\text{-}I)(THF)_2]_2$ (Evans et al. 1986d). Its molecular structure may be related to that of trivalent species, as for example $Cp^*_2Yb(\mu\text{-}I)_2Li(OEt_2)_2$ (see sect. 2.1.11.2.1) where a Cp^* ligand replaces two THF molecules. However, Sm^{2+} is more coordinatively unsaturated than any trivalent lanthanide due to its larger ionic radius and to the smaller space occupied by the two THF than by a Cp^* ligand. This increases its reactivity.

The reaction of $GdCl_3$ and $NaCp^*$ (1:1) produces either the monomer $Cp^*GdCl_2(THF)_3$ or the dimer $\{[Na(THF)][Cp^*Gd(THF)]_2Cl_5\}\cdot 6THF$ (Shen et al. 1990c), showing the relatively easy interchange in the metal coordination sphere for these labile derivatives. In the centrosymmetric dimer two $[Na(\mu^2\text{-}THF)][Cp^*Gd(THF)]_2(\mu^2\text{-}Cl)_3(\mu^3\text{-}Cl)_2]$ complex units are bridged via two THF molecules, with a rather complicated arrangement. However, a pseudo octahedral coordination geometry around each Gd ion, can be recognized (one ring centroid, one THF oxygen, two $\mu^2\text{-}Cl_2$ and two $\mu^3\text{-}Cl$).

Oligomeric species are very often obtained with halide derivatives for example $[K(DME)_3]\{K[(Cp^*Yb)_3Cl_8K(DME)_2]_2\}$ (Schumann et al. 1988e) with distorted octahedral geometry around Yb. The pentaytterbium cluster $[Yb_5Cp^*_6(\mu^4\text{-}F)(\mu^3\text{-}F)_2(\mu^2\text{-}F)_6]$ has been synthesized by defluorination with $Cp^*_2YbEt_2O$ of the fluoro carbonperfluoro-2,4-dimethyl-3-ethylpent-2-ene (Watson et al. 1990). Its X-ray structure is shown in fig. 33.

A cluster structure is shown (Zalkin and Berg 1989) by the Cp^*, chloro, oxo ether complex of Yb^{III}, $Cp^*_5Yb_5O(C_4H_{10}O)_2Cl_8$ isolated by reaction of $Cp^*_2Yb(OEt_2)$ with $YbCl_3$ impure for YbOCl. Metathesis of the chlorides of $LuCl_3(THF)_3$ with Cp^*Na and subsequent reaction with lithium alkyls, gave the synthesis of the first neutral $Cp^*Lu(alkyl)_2$ complex as $Cp^*Lu(CH_2SiMe_3)[CH(SiMe_3)_2](THF)$ which is also the first reported neutral "mixed" alkyl organolanthanide complex (Schaverien et al. 1989). The X-ray structures of its precursors $[Li(TMEDA)]Cp^*Lu[CH(SiMe_3)_2(\mu\text{-}Cl)_2$ (TMEDA = tetramethylethylene diamine) and $[Li(THF)_3][Cp^*Lu(CH_2SiMe_3)(CH(SiMe_3)_2)Cl]$ show for both lutetium atoms a three-legged piano-stool coordination geometry. In the first the lithium atom is linked to lutetium by two bridging chloride ligands while in the second it is linked by one.

Also the salt-free and solvent-free mono Cp^* lanthanide alkyl complex $Cp^*La[CH(SiMe_3)_2]_2$ has been synthesized and the X-ray structure together with that of its THF precursor show the stabilization of the unsaturated lanthanum center by unusual agostic Si–C bonds. The removal of THF produces a different conformation of the disylil ligands and pyramidalization of the $Cp^*La\ [CH(SiMe_3)_2]_2$ moiety.

$LnCl_3$ (Ln = La, Yb and Lu) reacts with $NaCp^*$ and LiMe or $LiCH_2SiMe_3$ in tetrahydrofuran giving a series of salts with $[Li(tmed)_2]^+$. In $[Li(tmed)_2][Cp^*LuMe_3]$ the Lu coordination geometry in the complex anion is approximately tetrahedral with

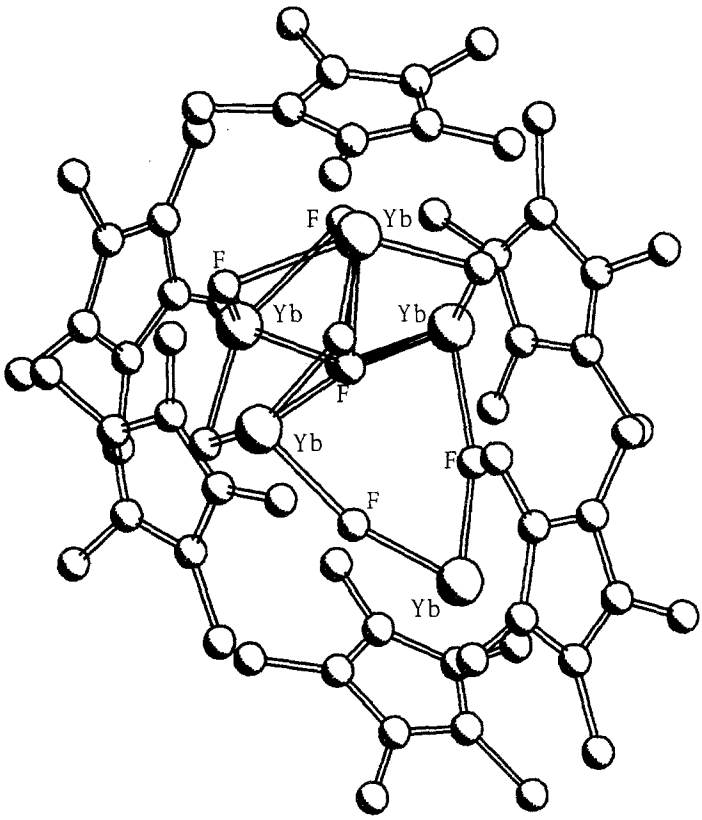

Fig. 33. Crystal structure of $[Cp^*_6Yb_5(\mu^4\text{-}F)(\mu^3\text{-}F)_2(\mu^2\text{-}F)_6]$ (Watson et al. 1990).

two long Lu–C (2.575Å) bonds and one short bond Lu–C (2.39(2) Å) (Schumann et al. 1984, Albrecht et al. 1985). The first examples of cationic lanthanide alkyl species and of an unprecedented BPh_4 coordination mode have been reported (Schaverien 1992b). By reacting $Cp^*La[CH(SiMe_3)_2]_2$ (**1**) with $[PhNMe_2H]BPh_4$ the zwitterion $Cp^*La[CH(SiMe_3)_2]BPh_4$ (**2**) is obtained. This reacts with THF affording the cationic alkyl complex $Cp^*La[CH(SiMe_3)_2](THF)_3BPh_4$, NMR and CPMASNMR data suggest that the electronic and steric unsaturation due to the **1** protonation allows η^6 coordination of two phenyl rings in **2** (scheme 17). The $[Cp^*Y(\mu\text{-}Me)_2]_3$ species have been synthesized from Cp*Y aryloxide and the trimer formation has been indicated in the NMR spectra (Schaverien 1994b).

Alcoholysis of the Ce–C bonds in $Cp^*CeH(SiMe_3)_2$ (Heeres et al. 1989a), constitutes a promising way to obtain cerium alkoxides and aryloxides. The compound $[Cp^*Ce(\mu\text{-}OCMe_3)_2]_2$ belongs to this category. The peculiarity of its dimeric structure is the *cis* configuration of the terminal $OCMe_3$ and Cp^* ligands, in order to minimize steric repulsions with the bridging $OCMe_3$ ligands. The geometry around Ce^{III} is a distorted tetrahedron.

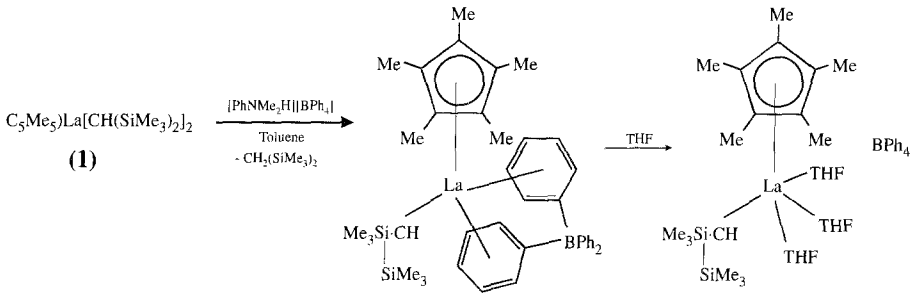

(2)

Scheme 17.

Alternative methods such as reaction of $Ln_3(O^tBu)_7Cl_2(THF)_2$ (Ln = Y, Evans et al. 1993a; Eu, Evans et al. 1994a–e) with NaCp* or KCp* in toluene give the appropriate $[Cp^*Ln(O\text{-}^tBu)_2]$ derivative.

The homoleptic aryloxides $Ln(OAr)_3$ are precursors for the synthesis of neutral mono Cp* lanthanide derivatives containing Ce–O, Ce–N and Ce–C bonds (Heeres et al. 1989b). A general feature for these compounds is the ease of disproportionation in Cp^*_2CeX and CeX_3 derivatives. $Ce(OAr)_3$ reacts with Cp*Li giving $Cp^*Ce(OAr)_2$ (OAr = 2,6-di-*tert*-butylphenoxo) which is the starting material for the preparation of $Cp^*Ce[CH(SiMe_3)_2]_2$ and $Cp^*Ce[N(SiMe_3)_2]_2$. The three complexes are monomeric, with Ce^{III} ions formally five-coordinated, the coordinative and electronic unsaturation of these compounds favors agostic interactions with the available C–H or Si–C bonds.

Mixed aryloxo Cp* lanthanide alkyl species have been synthetized. Solvent free monomeric species are obtained by metathesis of corresponding Cp*Ln aryloxides with $MCH(SiMe_3)_2$ (Ln = Y, Ce; M = Li, K), while dimeric oxobridged products can be obtained, for example, for Sc by reacting Cp*(alkoxo)Cl with LiMe (Schaverien 1994b).

Acetylacetonate monomers $Cp^*Sc(acac)_2$ (Piers et al. 1991) and $Cp^*Y(acac)_2$ (Schumann et al. 1993a) have been prepared by different methods. The X-ray analysis of the crystal found in an NMR tube containing $[(Cp^*_2Sm)_2(\mu = \eta^1{:}\eta^3\text{-}Se_3)THF]$ in toluene showed the formation of the polynuclear selenide $[(Cp^*Sm)_6Se_{11}]$ (Evans et al. 1994d).

Reaction of Cp^*_2Sm with excess hydrazine (Wang et al. 1992) produces a yellow material. The ^1H NMR spectra in toluene-d_8 was not structurally specific. X-ray analysis at low temperature shows a tetrameric structure for $[Cp^*Sm_4]_4(NHNH)_2(NHNH_2)_4(NH_3)_2$. The four Sm are tetrahedrally arranged with bridging hydrazido $(NHNH)^{2-}$ anions on each edge of the tetrahedron; significant distances are Sm···Sm 3.563(1) and 3.552(1) Å. Two ammonia molecules are coordinated to two Sm centers at a distance of 2.664(13) Å.

The dianionic carbollide ligand $[C_2B_9H_{11}]^{2-}$ prevents dimerization in alkyl or hydride-Cp*Sc derivatives which as monomers are catalytically active in α-olefin polymerization (Shapiro et al. 1990). The crystal structure has been determined for the $\{[Cp^*[(Me_3Si)_2CH]Sc(carbollide)]_2Li\}(Li(THF)_3)$ complex obtained by alkylation of $Cp^*(C_2B_9H_{11})Sc(THF)_3$ with $LiCH(SiMe_3)_2$ followed by pentane diffusion in toluene

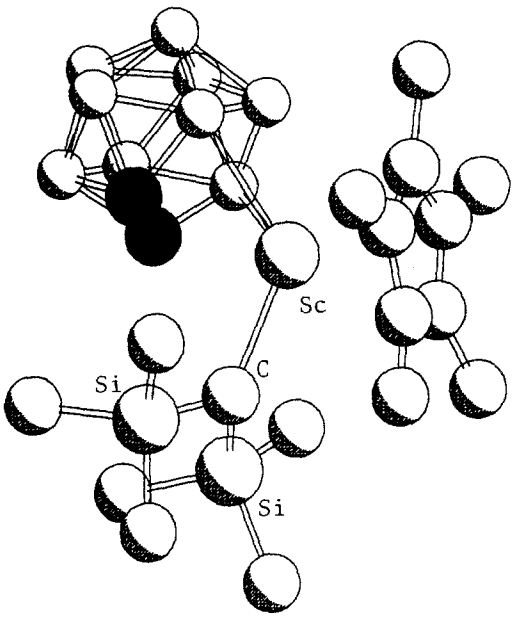

Fig. 34. Crystal structure of the fragment (Cp*-$(MeSi)_2CH$)Sc(carbollide) (Bazan et al. 1993) (solid circles are the carbons of the carbollide ligand).

(Marsh et al. 1992, Bazan et al. 1993). Each Sc is η^5-bonded to Cp*η^5 to one carbollide ligand (fig. 34) and to one -$CH(SiMe_3)_2$ group in the left. The angle at Sc with the centers of the two η^5 groups is 137.8°, two of these moieties share a Li atom to the B atoms of each carbollide creating a dimeric monoanion, the cation is $Li(THF)_3$ (Sc–$C_{[CH(SiMe_3)_2]}$ av. 2.278 Å).

2.1.11.5.2. *Actinides.* Actinide compounds containing a mono Cp* ligand are relatively rare when compared to the Cp^*_2An framework (Marks and Ernst 1982). Their steric and electronic unsaturation has recently attracted the synthesis of new products. Halide metathesis is the common route to introduce a single Cp* in the coordination sphere of the early actinides (Marsh et al. 1992, Bagnall et al. 1979, Mintz et al. 1982, Gilbert et al. 1989, Butcher et al. 1995). An alternative route has been devised by reacting (trifluoromethanesulfonic acid HOtf) with $Th[N(SiMe_3)_2]_3$(Otf) and Cp*H in toluene. The dimeric triflate-bridged complex Cp*$[(Me_3Si)_2N]Th(\mu^2$-$OSO_2CF_3)_3Th[N(SiMe_3)(SiMe_2CH_2)]$Cp* (Butcher et al. 1995) has a unique structure formed by two Cp*Th moieties joined by three bridging triflate ligands (fig. 35).

Very recently Cramer et al. (1995b) determined the X-ray structure of an unusual tetrauranium cluster obtained by hydrolysis of the $Cp^*_2UCl_2(HNSPh_2)$ with $HNSPh_2H_2O$ tentatively formulated, on the basis of the structural parameters as $[Cp^*(Cl)(HNSPh_2)U(\mu^3$-$O)(\mu^2$-$O)U(Cl)(HNSPh_2)]_2$. The cluster is centrosymmetric with U(1) and U(2) having formal coordination numbers eight and seven, respectively.

Relatively stable π-allylic complexes Cp*U(allyl)$_3$ (Cymbaluk et al. 1983) can be obtained from the precursor $Cp^*UCl_3(THF)_2$ reacted with (allyl)MgX (X = Br, Cl; allyl = C_3H_5 and 2–$CH_3C_3H_4$). The X-ray structure of Cp*U(2–$CH_3C_3H_4)_3$ shows

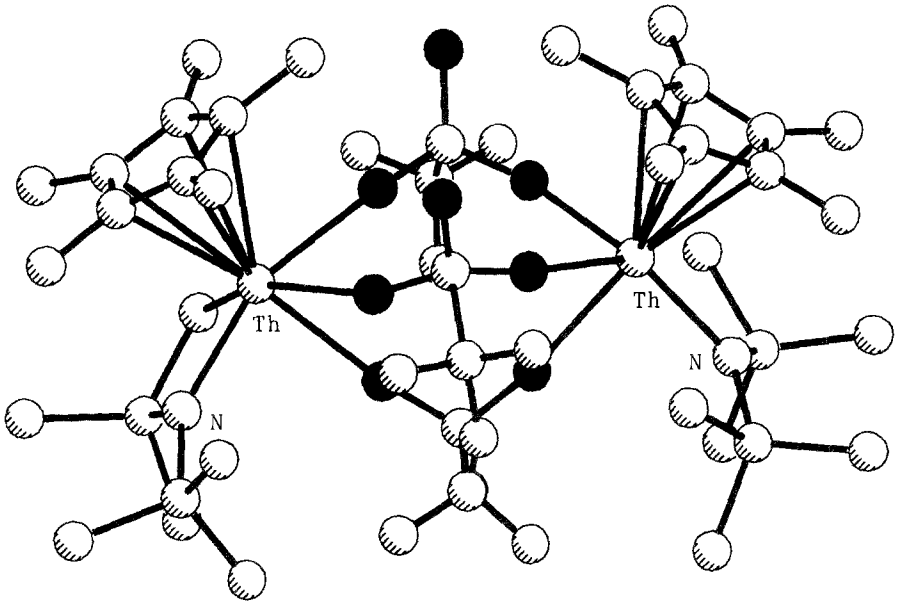

Fig. 35. Crystal structure of $Cp^*[(Me_3Si)_2N]Th(\mu^2\text{-}OSO_2CF_3)_3ThN(SiMe_3)(SiMe_2CH_2)]Cp^*$ (Butcher et al. 1995) (solid circles are oxygens).

a symmetric π-allyl structure. The coordination geometry around U is a distorted tetrahedron with two allyl groups in "downward" orientation and the third in "sideways" orientation. Monocyclopentadienyl derivatives of the type $Cp^*U(NEt_2)_3$ (Dormond 1983) can also be synthesized by metallation of Cp^*H with $U(NEt_2)_4$.

$[Cp^*U(NEt_2)_2(THF)_2]BPh_4$ and $[Cp^*U(COT)(THF)_2]BPh_4$ (Berthet et al. 1995) represent examples of monocationic and mixed ring complexes of uranium(IV). They have been obtained by protonolysis of their amide precursor according to the equation:

$$[Cp^*U(NEt_2)_3] + NHEt_3BPh_4 \xrightarrow{THF} [Cp^*U(NEt_2)_2(THF)_2]BPh_4 + NHEt_2 + NEt_3,$$

and characterized by NMR spectroscopy and by X-ray analysis. The five coordination of the $[Cp^*U(NEt_2)_2(THF)_2]$ cation is rather unusual in 5f chemistry and the geometry is a distorted trigonal bipyramid with the two THF units in *trans* position. The substitution of the two amide ligands with COT produced the usual tetrahedral arrangement of the coordinate ligands. The first reported mixed ring $Cp^*U(COT)(THF)$ and $Cp^*U(COT)(Me_2bpy)$ derivatives (Schake et al. 1993) are discussed in sect. 2.3.2.

2.1.12. *Ring bridged cyclopentadienyls*

2.1.12.1. *Lanthanides.* Dicyclopentadienyl lanthanide halides of the lighter lanthanides (La, Ce, Pr and Nd) cannot be isolated due to ligand redistribution reactions. For access to "$[Cp_2LnX]$" species of the lighter lanthanides, two possible routes have been found:

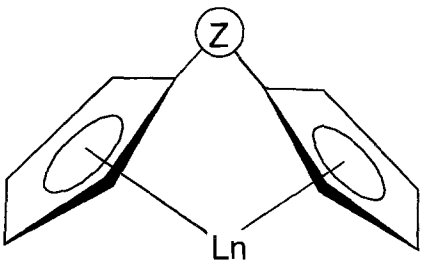

Scheme 18.

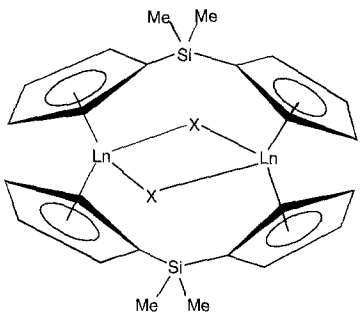

Form A

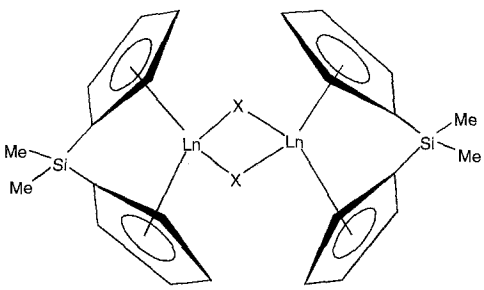

Form B

Scheme 19.

(i) increasing the steric hindrance around the Ln ion by mono- or poly-substitution of the Cp rings; (ii) reducing the Cp mobility by catenation.

Bridged cyclopentadienyl ligands of the type ZCp_2 ($Z = CH_2$, Me_2Si, $CH_2CH_2CH_2$) were first introduced (Secaur et al. 1976) as stabilizing agents with respect to the Cp redistribution reactions. The use of "tied-back" ligands reduces steric crowding of the central metal ion, with a shrinking of the Cg–Ln–Cg angle and consequent opening of the opposite metal coordination sphere, thus making approach of the substrate easier in catalytic reactions and increasing the reactivity of the system where $Z = CH_2$, $(CH_2)_n$, Me_2Si, etc. (scheme 18).

The synthesis of $Ln[1,3\text{-}(CH_2)_3(C_5H_4)_2]Cl$ (John and Tsutsui 1980; Ln = La and Ce), $[Cp(CH_2)_3Cp]LnR(THF)$ (R = Cl, Ln = Pr, Nd, Gd, Dy, Ho, Er, Lu; Qian et al. 1984) and the reactions of the THF adducts with aryllithium or alkyllithium produced several new Ln–C σ-bonded compounds where R = Ph (La, Pr), *p*-C_6H_4Me (La, Pr), CMe_3 (La, Nd, Y) and CH_2SiMe_3 (La) (Qian et al. 1986). In dimeric lanthanide derivatives the ligand $Cp(SiMe_2)Cp$ can in principle act either in the bridging (A) or chelating mode (B) (scheme 19).

Reaction of $YbCl_3$ or $YbBr_3$ with $Na_2[Cp(SiMe_2)Co]$ in THF led to the isolation of the A dimeric isomer $[Yb(\mu\text{-}X)(\mu\text{-}Me_2SiCp_2)]_2$ (where X = Cl or Br) in which the ligand bridges the two metal centers (Höck et al. 1986, Qiao et al. 1990, Akhnoukh et al. 1991). By reaction with NaH of $[Yb(\mu\text{-}Cl)(\mu\text{-}Me_2SiCp_2)]_2$ a mono-hydride, mono-chloride species $[\{(\mu\text{-}Me_2SiCp_2)Yb(THF)\}_2(\mu\text{-}H)(\mu\text{-}Cl)]$ has been isolated (Qiao

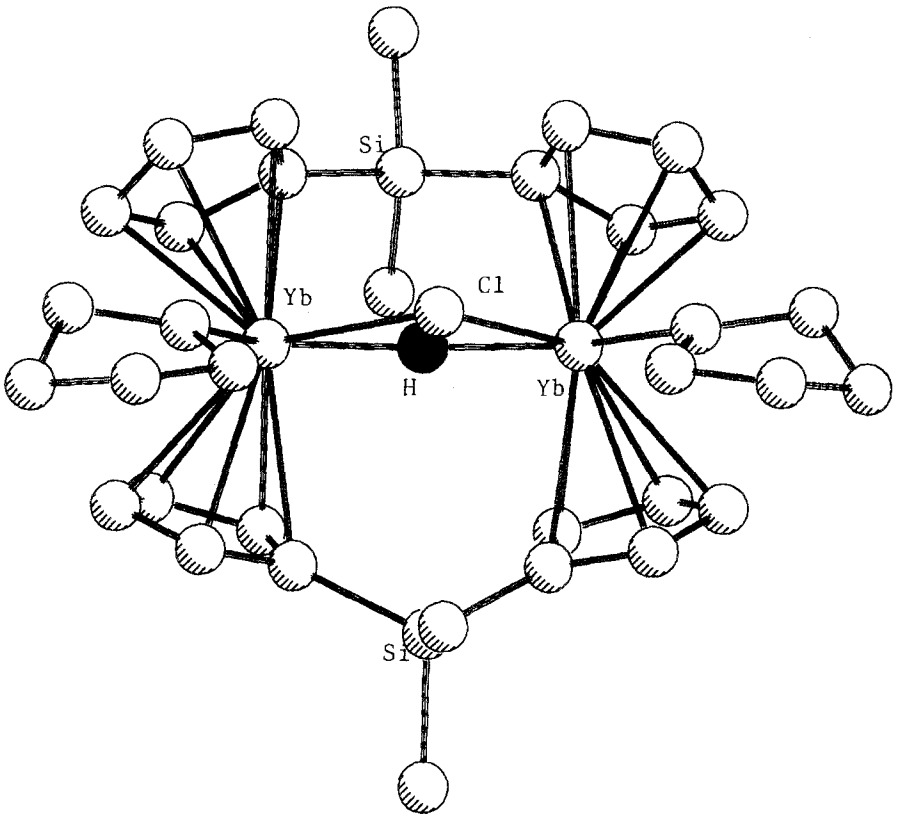

Fig. 36. Crystal structure of $[(Me_2SiCp_2)Yb(THF)]_2(\mu\text{-}H)(\mu\text{-}Cl)$ (Qiao et al. 1993).

et al. 1993) (fig. 36), while the corresponding Y derivative having the structural form B affords only the dimeric dihydride. By using unsymmetrical ^{t}Bu substituted Cp ligands as $Me_2Si(C_5H_3^tBu)_2^-$ in the $[Me_2Si(C_5H_3^tBu)_2Nd(\mu\text{-}Cl)_2Li(THF)_3]_2$ compound (Esser 1991) the bridging mode is preferred as with the methylated ligand $Me_2Si(C_5Me_4)_2^{2-}$ in the complex $[Me_2Si(C_5Me_4)_2Nd]_2(\mu\text{-}Cl)_3Li(THF)_2$ (Jeske et al. 1985b). The compounds $Me_2Si(C_5Me_4)_2Ln(\mu\text{-}Cl)_2Li(Et_2O)_2$ (Ln = Nd, Sm, Lu) have also been synthesized. Tetramethylethylene bridged dicyclopentadienyl $YbCl_2$ salt has been prepared (Yan et al. 1990) by reacting $YbCl_3$ with $Me_4C_2(C_5H_4)Mg_2Cl_2{\cdot}4THF$. In $\{[Me_4C_2(C_5H_4)_2]YbCl_2\}[(Mg_2Cl_3{\cdot}6THF)]{\cdot}THF$ the complex anion has a coordination geometry around the Yb atom which is pseudotetrahedral. The Cg–Yb–Cg angle is reduced to a smaller value (121.0°) than that in non-bridged Cp which results in a larger Cl–Yb–Cl angle 97.1(1)°. In the bridged ligand the Cp rings are almost eclipsed while the tetramethylethylene fragment has a distorted staggered conformation. The use of differently substituted Cp moieties which are R_2Si bridged, e.g., $[R_2Si(C_5H_4)(Me_4C_5]$ ligand (R = Me, Et), has shown a chemistry different from the A and B system with a substantial decrease in reactivity of "presumably steric and electronic origin" (Stern

et al. 1990). An explanation of the lack of catalytic activity of these species has been obtained from NMR studies, indicating that the intermediate hydride dimer is present as the isomeric form A (ligands in the bridging mode). This structure does not allow the alkene substrate to approach the Ln ion for the successive insertion into the Ln–H bond. In this context the X-ray structures of three Lu derivatives have been reported. The coordination geometry around Lu is of the expected Cp_2MX "bent-sandwich" type in the monomeric $[Me_2Si(C_5H_4)(Me_4C_5)]LuCH(SiMe_3)$ derivative. The shrinking of the Cg–Lu–Cg angle is from 134–140° found in Cp^*_2 organolanthanides to 125.2° with the lutetium ion equidistant from both C_5H_4 and Me_4C_5 ring (Lu–Cσ is 2.365(7) Å). An "agostic" Lu–CH_3–Si interaction is present and the disposition of the corresponding methyl hydrogens does not minimize the Lu–H distances but is "reminiscent of three-center, two-electron μ-alkyl groups".

$[Et_2Si(C_5H_4)(C_5Me_4)LuH]_2$ is a dimer, where a redistribution of the cyclopentadienyl ligation has occurred, according to the scheme

$$2R_2SiCpCp^*Lu \rightarrow [Lu(\mu\text{-}R_2SiCpCp^*)_2Lu],$$

where R = Me, Et (starting from a monometallic precursor). The short Lu···Lu distance 3.390(1) Å is attributed more to the constraints imposed by the Cp bridging ligand mode, than to metal–metal bonding.

The other dimer $[Et_2Si(C_5H_4)(Me_4C_5)Lu]_2(\mu\text{-}H)(\mu\text{-}C_2H_5)$ presents an unusual coordination geometry of the μ-ethyl ligand which is asymmetrically bridging the two Lu metal ions (fig. 37).

The R_2Si bridge which links equal Cp^* moieties should form Ln compounds of higher catalytic activity than the non-bridged ones (i.e., Cp^*_2Ln–C) due to the more open coordination sphere of the Ln ion (as previously described). They can be obtained from the halide precursor:

$$[Me_2SiCp_2]\,Ln\,(\mu\text{-}Cl)_2\,LiL_2 + LiCH\,(SiMe_3)_2 \xrightarrow{\text{toluene}} [Me_2SiCp^*_2]\,LnCH\,(SiMe_3)_2\,,$$

where L = Et_2O, THF; Ln = Sc (Piers et al. 1990), Nd, Sm, Lu (Piers et al. 1990). Their structure is of the type described for the monomeric Lu derivative (Jeske et al. 1985a).

The Si atoms in the bridge can be substituted by Ge (Schumann et al. 1991a) examples are the complexes $Me_2Ge(C_5Me_4)_2LnCH(SiMe_3)_2$ (Ln = Nd, Ho) characterized by mass, NMR spectra and X-ray analysis.

Recently the chiral asymmetric ligands $Me_2Si(C_5Me_4)(C_5H_3R^*)$ [R* = (–)-menthyl, (+)-neomenthyl, (–)-phenylmenthyl] have been used in the synthesis of the chiral $[Me_2Si(C_5Me_4)(C_5H_3R^*)]LnCH(SiMe_3)_2$ complexes (Ln = Y, La, Nd, Sm, Lu) which are precatalysts for catalytic enantioselective olefin hydrogenation (Conticello et al. 1992, Girardello et al. 1994a,b, Gagné et al. 1992). The complexes are stable at 60°C but they epimerize in the presence of primary alkyl amines.

The introduction of an oxygen atom in the carbon chain as in the ligand [1,1′-(3oxa-pentamethylene dicyclopentadienyl] $(O(CH_2CH_2C_5H_4)_2)$ can increase the saturation of

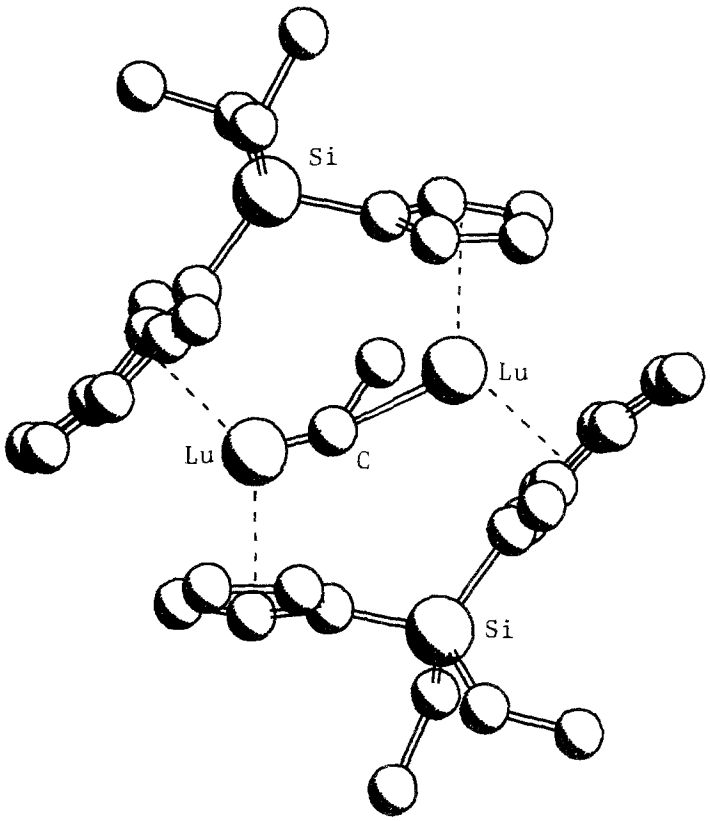

Fig. 37. Crystal structure of $[Et_2SiCp^*CpLu]_2(\mu\text{-H})(\mu\text{-Et})$ (Stern et al. 1990) (μ-H is missing).

the lanthanide ions as it offers an additional coordination position and an intramolecular stabilization.

This ligand was used in the synthesis of the complexes $[O(CH_2CH_2C_5H_4)_2]LnCl$ (Ln = Nd, Gd, Ho, Er, Yb, Lu, Y) (Qian et al. 1987, Fu et al. 1989). They are the precursors for the synthesis of 1,1′-(3-oxapentamethylene) dicyclopentadienyl lanthanide derivatives (Qian et al. 1990) according to the reactions

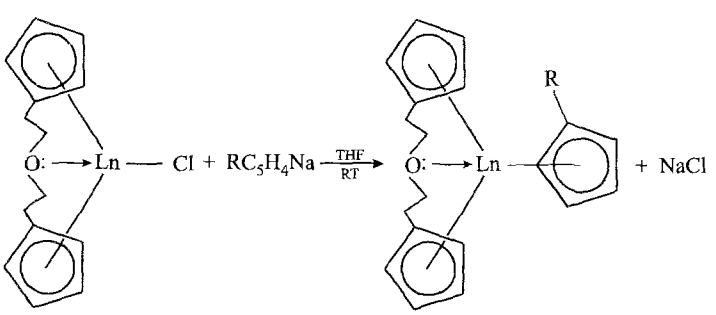

R = H; Ln = Nd, Gd, Er, Yb, Lu, Y. R = CH_3; Ln = Yb, Y.

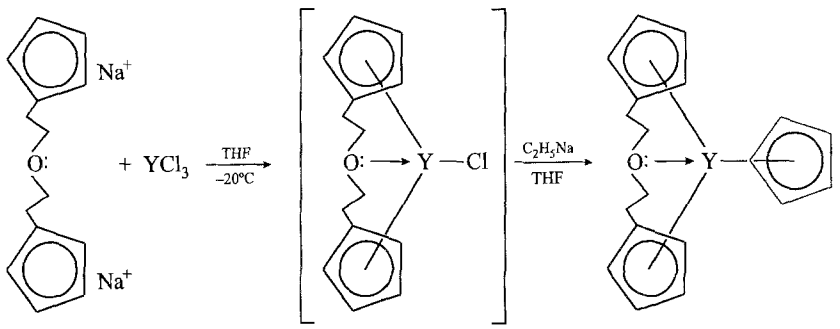

and for dimeric organolanthanide hydrides $\{[O(CH_2CH_2C_5H_4)_2]Ln(\mu\text{–}H)\}_2$ when reacted with NaH in THF (Xie et al. 1991b) (Ln = Gd, Er, Yb, Lu, Y)

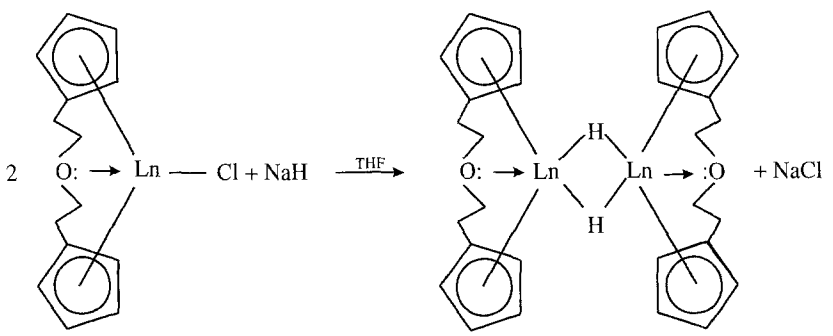

The hydrides can react with alkenes and alkynes. A more active system, organolanthanide hydride/NaH, is able not only to reduce specifically the terminal carbon–carbon double bond but also to catalyse dehalogenation of organic halides.

Monomeric species $\{[O(CH_2CH_2C_5H_4)_2]Ln(N_2C_3HMe_2)\}$ (Schumann et al. 1991b) are obtained with the Y and Lu pyrazolyl derivatives which undergo partial hydrolysis according to the reaction path with dimer formation of the type $\{[O(CH_2CH_2C_5H_4)_2]Ln\}(\eta^2\text{-}N_2C_3HMe_2)(\mu\text{-OH})$

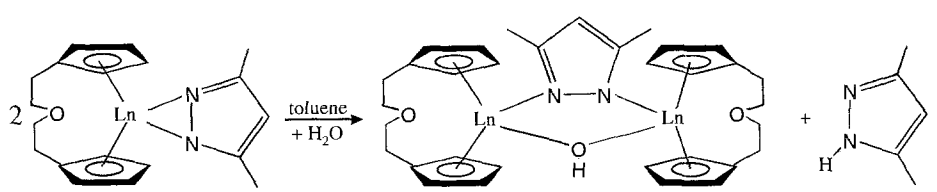

containing hydroxyl and pyrazolyl bridges, the ^1H NMR spectra for the diamagnetic derivatives are diagnostic for the type of structure.

Very recently (Qian et al. 1996) the bis-THF solvated divalent species Sm^{II} and Yb^{II}, stabilized through the previously quoted ligand $O(CH_2CH_2C_5H_4)_2$, have been

synthesized. The same stabilization has been obtained for the Sm^{II} and Yb^{II} species in the bisolvate THF derivative with the $CH_2(CH_2C_5H4)_2$ (Swamy et al. 1989) ligand.

The structure of $O(CH_2CH_2C5H_4)_2Yb(DME)$ of approximate trigonal bipyramidal geometry has an angle Cg–Yb–Cg of 132.7° as in the nonbridged derivative indicating a high conformational flexibility of the ligand.

Recently, several other ligands containing different bridging moieties between cyclopentadienyl rings such as $CH_3N(CH_2CH_2C_5H_4)_2$ (Qian and Zhu 1993) $(C_5H_4CMe_2$-$CMe_2C_5H_4)$ (Sun et al. 1986); 2,5-$(C_5H_4CH_2)_2C_4H_2O$ (Qian and Zhu 1994); 2,6-$(C_5H_4CH_2)_2C_5H_3N$ (Paolucci et al. 1994) and the disiloxane $(C_5H_4SiMe_2)_2O$ (Graper and Fischer 1994) have been used for the synthesis of new organometallic rare earth derivatives.

2.1.12.2. *Actinides.* Ring bridged Cp were devised with the aim of stabilizing the Cp_2AnX_2 configuration avoiding ligand redistribution. The first complexes of this type were obtained by metallation with buthyllithium and subsequent reaction with UCl_4. They crystallize as LiCl adducts (Secaur et al. 1976). The structure of $[Li(THF)_2]\{U_2[(C_5H_4)_2CH_2]_2Cl_5\}$ is a trinuclear derivative with μ^3 and μ^2 bridging chlorine with formally ten coordinated U ions.

Ring bridged C_5Me_5-like, $(C_5Me_4)_2Si(Me_2)$ (Fendrick et al. 1988) were prepared, taking advantage of the well-known properties of solubility, crystallizability, thermal stability of the C_5Me_5 ligand, to which is added a further stabilization due to the $SiMe_2$ bridge. By reacting the Cp^{II} ligand ($Cp^{II} = Me_4C_5$) with n-C_4H_9Li in 1,2-dimethoxyetane (DME), $Me_2Si(Cp^{II}Li)\cdot 2DME$ is obtained. By further reaction of the latter with $ThCl_4$ and alkylation of the resulting $Me_2SiCp^{II}ThCl_2\cdot 2LiCl\cdot 2DME$ with lithium reagents, the thermally stable $Me_2SiCp^{II}_2ThR_2$ complexes were obtained ($R = CH_2SiMe_3$, CH_2CMe_3, C_6H_5, n-C_4H_4 and $CH_2C_6H_5$).

$Me_2SiCp^{II}_2Th(CH_2SiMe_3)_2$ reacts with H_2 (2:1) giving the thorium hydride $[Me_2$-$SiCp^{II}_2ThH_2]_2$. The structure of the two compounds have similar peculiarities: in the monomer, the bridged Cp^{II} ligand produces the expected opening of the coordination sphere with contraction of the Cg–Th–Cg angle to 118.4 (compared with the values 135–138° found in Cp^*_2Th moieties) and a marked dispersion in Th–C ring distances (range 2.686(14)–2.917(17) Å). The $Th–C_{hydrocarbyl}$ distances are 2.54(2) and 2.49(2) Å. The dimer $(Me_2SiCp^{II}_2Th)_2(\mu$-H) shows Cg–Th–Cg angles of 118.1 and 117.1° with a distance Th–Th of 3.632(2) Å which suggests the given formulation. (Hydrogen atom positions were not detected in the X-ray study.) The opening of the metal coordination sphere over the Cp^*_2An analogs (as found for the trivalent lanthanides) produces an enhanced reactivity of metal–carbon and metal–hydrogen bonds.

Following the strategy of making optimum use of the metallocenophane effect (Paolucci et al. 1991) the 2,6-dimethylenepyridine group was introduced as a stabilizing, novel link for two C_5H_4 ligands coordinating a lanthanoid or actinoid ion. By reacting the new disodium salt $Na_2[2,6$-$C_5H_3N(CH_2C_5H_4)_2]$ with UCl_4 in THF the reddish green complex μ-$(2,6$-$CH_2C_5H_3NCH_2)(\eta^5$-$C_5H_4)_2UCl_2$ was obtained where the anion is chelating with a strong U–N interaction (2.62(1) Å) the X-ray structure is shown in fig. 38.

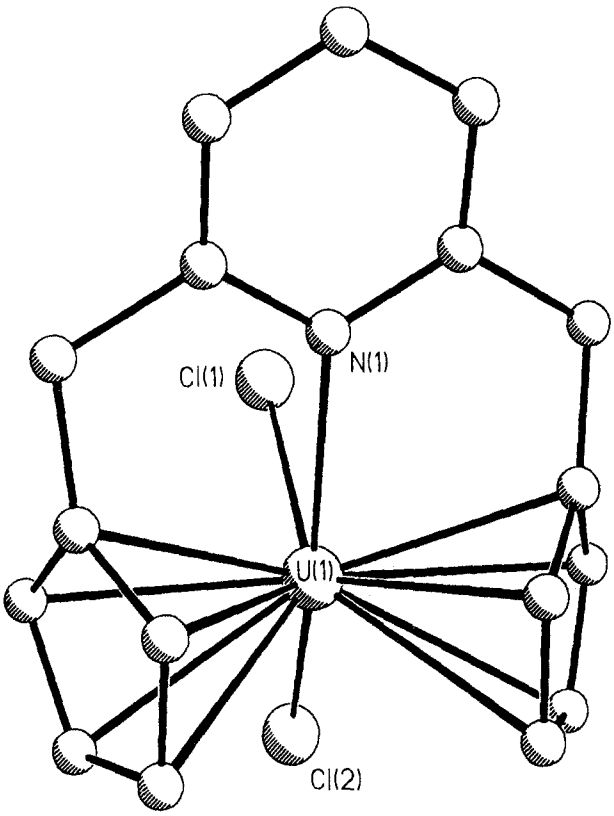

Fig. 38. Crystal structure of μ-(2,6-$CH_2C_5H_3NCH_2$)(η^5-C_5H_4)$_2UCl_2$(Paolucci et al. 1991).

2.2. *Indenyls (lanthanides and actinides)*

Both lanthanides and actinides give complexes with the indenyl ligand $(C_9H_7)^-$(Ind) which is formally analogous to $C_5H_5^-$, but makes a considerably greater steric demand. With the exception of cerium which forms both Ce^{IV} and Ce^{III} derivatives, and Sm, which forms both Sm^{II} and Sm^{III} derivatives, all lanthanides form Ln^{III} indenyl complexes.

The actinides (U and Th) form An^{IV} indenyl complexes preferentially although uranium(III) derivatives are also known. They are generally prepared by reaction of a metal halide or halometallate with an indenide or substituted indenide of a suitable cation (usually Na^+K^+) in an inert solvent. The metal ion:indenide mole ratio employed in the synthesis determines the stoichiometry of the resulting complex. Very often solvent molecules are incorporated in the complex. Mixed cyclopentadienyl–indenyl complexes of Ln have been prepared similarly from the Cp_2LnCl species and NaC_9H_7. The following examples are representative of the syntheses.

Trisindenyllanthanides, isolated as THF adducts (Tsutsui and Gysling 1969) were prepared by reaction of the anhydrous lanthanide trichlorides with sodium indenide:

$$3NaC_9H_7 + LnCl_3 \xrightarrow[THF]{} Ln(C_9H_7)_3THF + 3NaCl,$$

where Ln = La, Sm, Gd, Tb, Dy, Yb. The unsolvated samarium derivative has been prepared by reaction of $SmCl_3$ and $Mg(C_9H_7)_2$ in benzene (Atwood et al. 1973, Meunier-Piret et al. 1980a). Trisindenyl actinide halides have been prepared according to the equation:

$$AnX_4 + 3KC_9H_7 \rightarrow An(C_9H_7)_3X + 3KX,$$

where An = U, Th; X = Cl, Br, I. Like the analogous Cp_3AnX, the actinide trisindenyl halides are used as starting materials for the synthesis of the corresponding alkoxides $(C_9H_7)_3AnOR$ and tetrahydroborates (or tetradeuteroborates) (An = U, Th; R = Me, Et).

IR and Raman data analysis of $(C_9H_7)_3ThBH_4$ and $(C_9H_7)_3ThBD_4$ suggest that the tetrahydroborate group acts as a tridentate ligand. Vibrational spectra of the $(C_9H_7)_3An$ (An = U, Th) and the corresponding Lewis adducts (L = THF, CNCy) have been discussed, and the molecular structure of Ind_3U^{III} is known (Tsutsui et al. 1982) to have a trigonal coordination geometry analogous to that of Ind_3Sm.

The indenyl complexes exist in varieties of mono and polynuclear structures with the indenyl groups acting variably as penthapto, trihapto or even (for U^{IV}) monohapto ligands. The coordination number and the geometry of the metal center varies from complex to complex depending on the stoichiometry, the presence of the potentially bridging groups and the steric bulk of the indenyl ligands. The indenyl complexes of lanthanides and actinides series very often resemble the corresponding cyclopentadienyl compounds. The following examples show the structure types found in f block indenyl complexes.

The trisindenyl cerium pyridinate provides a clear example of trihapto indenyl coordination (Zazzetta and Greco 1979). A tetrahedral arrangement of the ligands around Ce is formed by the centroids of the π-bonded portion of the Ind ligands and the nitrogen of the σ-bonded pyridine. Trihapto indenyl coordination is also found in $(IndGdCl_2 \cdot 3THF)THF$ (Fuxing et al. 1992) and in $Ind_3Ln(THF)$ (Ln = Nd, Gd, Er; Xia et al. 1991a) with an octahedral and a tetrahedral arrangement of the ligands around the metal ion, respectively. A linear chlorine bridge and pentahapto indenyl coordination are the characteristic features of the structure of $[Na(THF)_6][NdInd_3(\mu\text{-}Cl)NdInd_3]$ (Chen et al. 1988).

The large Th^{IV} ion is linked to four Ind ligands with η^3-bonding mode in the compound $Th(Ind)_4$ (fig. 39) (Rebizant et al. 1986) the indenyl five membered rings are at the apices of a distorted tetrahedron. A trihapto bonding mode of the indenyl ligand and a pseudotetrahedral arrangement of the ligands around Th is found in the structure of chloro tris[1-3 η-(1,4,7-trimethyl indenyl)] thorium (Spirlet et al. 1982) which is isomorphous to the uranium analog (Meunier-Piret and van Meerssche 1984).

The non-methylated $(Ind)_3UCl$ (Burns and Lauberau 1971) is isomorphous with the bromide analog (Spirlet et al. 1987c), the absence of the methyl groups produces a

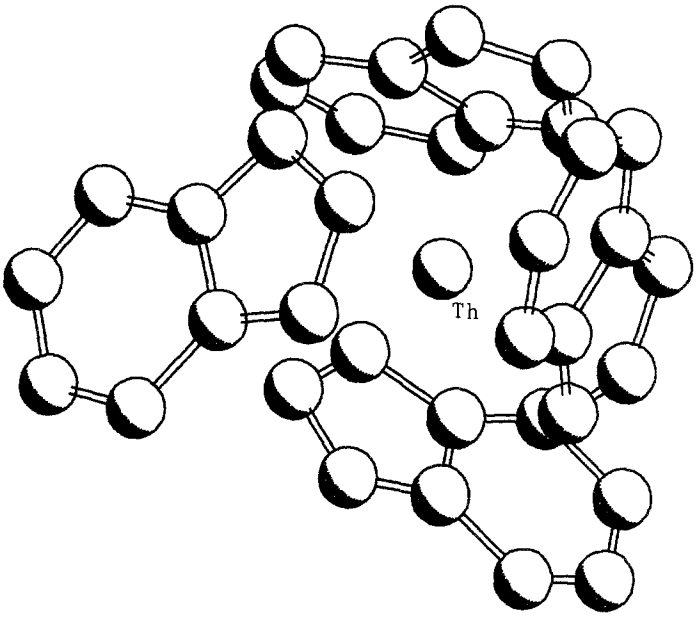

Fig. 39. Crystal structure of $[Th(Ind)_4]$ (Rebizant et al. 1986).

different reciprocal arrangement of the ligands, however, the coordination geometries and the bonding mode, are analogous to that of the previously described Ind compounds. The X-ray structure of the trifluoroethanolate derivative (Spirlet et al. 1993b) $[(C_9H_7)_3]U(OCH_2CF_2)$ is analogous to that of the corresponding halogen complex. The structure of $(Ind)_2U(BH_4)_2$ maintains the tetrahedral coordination geometry around U, but the relatively short range of the $U–C_{ring}$ distances suggests here a pentahapto covalent bonding ring to the indenyl ligands, indicating the importance also of steric factors for the indenyl bonding mode. The short U–B distances are characteristic of tridentate borohydride bonding (Rebizant et al. 1989).

The structural determination of the THF solvates shows that $(Ind)UX_3(THF)_2$ (X = Cl, Br) is isostructural (Rebizant et al. 1983, 1985). The coordination geometry around uranium is pseudooctahedral with one η^5-C_9H_7 ligand and one coordinated THF in the *trans* axial positions, the other THF and chlorine ligands are in the equatorial plane. The same coordination is found in $[(Ind)UBr_3(THF)(OPPh_3)]$ where the most hindering ligand $OPPh_3$ is in the *trans* axial position with respect to the Ind ligand (Meunier-Piret et al. 1980b). By treatment of the octahedral $(Ind)AnX_3 \cdot (THF)_2$ (An = U, Th; X = Cl, Br) with CH_3CN the complexes $[(Ind)AnX_2(CH_3CN)_4][AnX_6]$ are obtained (Beeckman et al. 1986). In an atmosphere of oxygen the biadduct $\{[(Ind)UX(CH_3CN)_4]_2(\mu\text{-}O)\}[UX_6]$ is formed. (Analogous compounds with substituted indenyl ligands 1-ethyl, 1,4,7-trimethyl or heptamethyl have been also prepared). The replacement of CH_3CN with butyronitrile and benzonitrile yields products which correspond to octahedral structures. The coordination geometry around U in both $[(Ind)UBr(CH_3CN)_4][UBr_6]^{2-}$ (Spirlet et al.

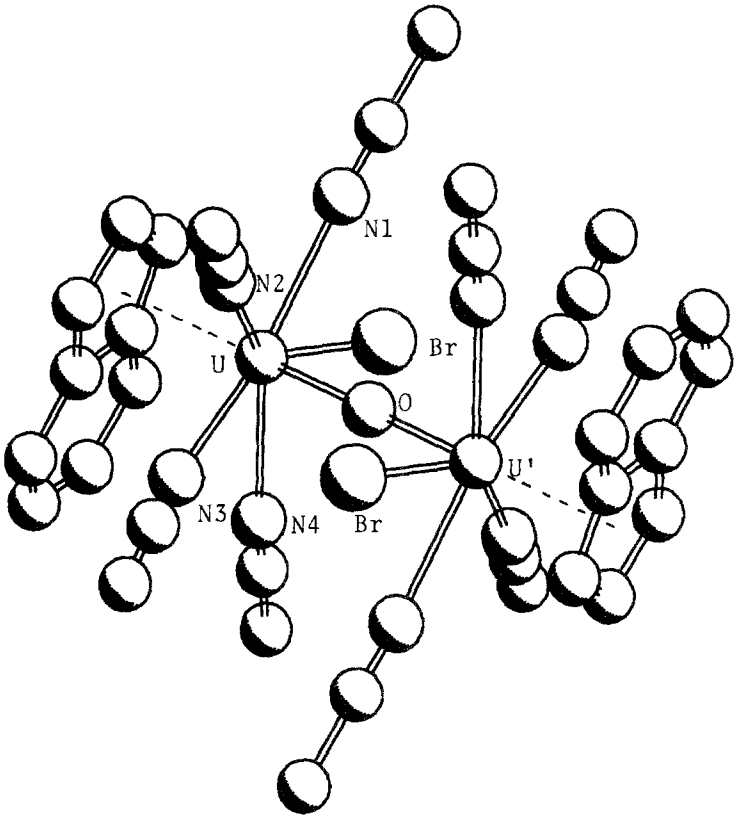

Fig. 40. Crystal structure of the cation $[(Ind)UBr(CH_3CN)_4]_2(\mu\text{-}O)]^{2+}$ (Beckman and Goffard 1988).

1986) and $\{[(Ind)UBr(CH_3CN)_4]_2(\mu\text{-}O)\}[UBr_6]^{2-}$ (Beeckman et al. 1986) cations is pentagonal bipyramidal (fig. 40). The apical positions are formed by the center of gravity of Ind *trans* to bromine in the monomer and *trans* to the bridging oxygen in the dimer. In both complexes the counter anion UBr_6^- has an octahedral geometry. The formation of the oxide bridged dimer could be considered (according to the authors) as one of the intermediate products in the oxidation of the actinide indenyl compounds.

Bond disruption enthalpies (Bettonville et al. 1989) for $(Ind)_3AnR$ and $(1\text{–}Et\text{–}Ind)_3AnR$ (An = U, Th; R = Me, $CH_2C_6H_5$, CH_2SiMe_3, $CHMe_2$, OCH_2CF_3) have also been measured. In $(Ind\text{–}Et)_3ThCl$ (Spirlet et al. 1990b) the three ethyl indenyl ligands are η^3-coordinated. The structure of chlorotris (1,2,4,5,6,7-hexamethylindenyl)U (Spirlet et al. 1992b) represents the first example of a monoapto σ-bonded indenyl ring to an U^{IV} metal ion of tetrahedral coordination geometry.

As expected, the indenyl hapticity is largely dependent on the steric hindrance in the An and Ln coordination spheres: four indenyl ligands $[(Ind)_4Th]$ or three indenyl derivative complexes generally determine a η^3-hapticity toward the metal ion. Pentahapto indenyl coordination is usually found in the mono indenyl derivatives, exceptions are the complex

cations. $\{[(Ind)UBr(CH_3CN)_4]_2(\mu\text{-}O)\}^{2+}$ with indenyl again η^3-bonded but in a crowded coordination sphere with a pentagonal bipyramidal coordination geometry around the metal ion. The difference in bond distances which differentiate η^3 from η^5-bonding mode are of the order of 0.2 Å.

Recently, in a study of the reactivity of $(Ind)_2Sm^{II}(THF)_x$ (Evans et al. 1995a), it has been pointed out that $(Ind)_2Sm(THF)_2$ could be used in organic syntheses as an alternative to the $Cp^*_2Sm(THF)_x$ complexes ($x=0$, 2), providing, as shown by the crystal structure of $(Ind)_2Sm(THF)_3$ (Evans et al. 1994e), a more open coordination environment of the two indenyl ligands than the Cp^*_2Sm unit which commonly adds two additional ligands.

2.3. *Cyclooctatetraenyls*

The aromatic dianion cyclooctatetraene $(C_8H_8)^{2-}$(COT) forms a variety of complexes with lanthanide and actinide ions due to their large ionic radii and possibly to the available f orbital of convenient symmetry. Some of the complexes isolated are of the sandwich type either monomeric as in uranocene COT_2U (Streitwieser and Müller-Westerhoff 1968a–c, Avdeef et al. 1972) or oligomeric with the COT units shared among equal or different metal ions. Mixed derivatives with Cp or Cp like ligands have been synthesized as well as mono-COT either with halides and neutral ligands or σ-bonded ligands such as alkyl, aryl, alkoxide, aryloxide, and amide. From the structural point of view a strict similarity exists between actinide and lanthanide derivatives, even though the lanthanides due to the more ionic nature of their bonding (Boussie et al. 1991) are more sensitive toward oxygen and can easily undergo ligand exchange (Hodgson and Raymond 1973) as shown by the nearly quantitative uranocene formation from [K(COT)Ce] when reacted with UCl_4. The structure of the mono-COT derivatives is usually monomeric and the number of the ligands is strongly related to their hindrance and to the ionic radii of the metal ions.

An unusual dimeric structure has recently been reported for Sm where the bridge is the COT unit (Schumann et al. 1993b) (see below) while, with halides, dimer formation has been known since 1971 (Mares et al. 1971).

2.3.1. *Lanthanides*

COT ligands, due to their steric and electronic properties, can in principle stabilize the three possible formal lanthanide oxidation states (II, III, IV). The first cyclooctatetraene lanthanide complexes isolated were the Ln(COT) species [$Ln=Eu^{II}$, Yb^{II}; $COT=(C_8H_8)^{2-}$; Hayes and Thomas 1969], prepared by direct reaction of the metals and cyclooctatetraene in liquid ammonia. Deep red-black crystals of $(COT)Yb(py)_3\cdot 0.5py$ (Wayda et al. 1987) obtained by treatment of Yb(COT) with excess pyridine have a crystal structure of the shape of a three-legged piano stool for the coordinated ligands. The first monomeric Sm^{II} (COT) complex has been obtained with the highly substituted 1,3,6-trimethylsilylCOT:

$$SmI_2(THF)_2 + K_2[(Me_3Si)_3C_8H_5] \rightarrow \left[(Me_3Si)_3\,C_8H_5\right] Sm\,(THF)_3 + 2KI,$$

characterized by spectroscopic methods (Edelmann 1995b). An anionic bis-cyclooctatetraenyl–lanthanide^{II} complex $[K(DME)_2]_2[Yb(COT)_2]$ (Kinsley et al. 1985), is obtained by stoichiometric reaction of COT, K and Yb in liquid ammonia solution. Its structure shows planar parallel eclipsed COT rings, sandwiching a centrosymmetric Yb (Yb–C 2.74±.03 Å). A K bound to DME is at the opposite side of each ring. By reacting *tert*-butylcyclooctatetraene instead of COT, the same authors (Kinsley et al. 1986) prepared the diglyme adduct (after diffusion into a diglyme solution) of dipotassium bis(*tert*-butylCOT)ytterbate(II). Its structure is similar to that of the DME adduct.

Most of the compounds synthesized are lanthanide(III) COT and substituted COT derivatives. In particular, a wide variety of half sandwich derivatives containing Ln to halide, chalcogenide, pnicogenide and hydrocarbyl bonds are known. A general approach to ionic lanthanocene derivatives is:

$$LnCl_3 + 2K_2(COT) \rightarrow K[Ln(COT)_2] + 3KCl,$$

where Ln = Y, La, Ce, Pr, Nd, Sm, Gd, Tb. The structure of [(diethylene glycol dimethyl ether)K][COT_2Yb^{III}] (Boussie et al. 1991) shows a shorter metal–ring carbon distance to the uncapped COT (Yb–Cg 1.843) than to the capped (Yb–Cg 1.902 Å). Comparison of the structural parameters of several COT complexes shows the importance of steric interactions, particularly with metals in higher oxidation states in determining the metal–ligand distances and with evidence for covalent bonding in these compounds. The tetranuclear nearly-linear complex (COT)Er(μ-COT)K(μ-COT)Er(μ-COT)K$(THF)_4$ (Xia et al. 1991b) was first synthesized by the reaction of benzylcyclopentadienyl erbium dichloride $(PhCH_2C_5H_4)ErCl_2 \cdot 3THF$ with cyclooctatetraenyl potassium, K_2COT, in 1:1 molar ratio in THF. A single crystal X-ray study has shown that the complex has a tetralayer-sandwich structure with adjacent Er^{3+} and K^+ ions bridged by η^8-cyclooctatetraenyl group (fig. 41).

The Er–C bond lengths range from 2.569(14)–2.660(19), while from $K–C_{COT}$ they range 3.024(16)–3.284(13) Å. In the dimeric Sc^{3+} derivative $\{[1,4(Me_3Si)_2(C_8H_6)]Sc\}_2$-$(\mu\text{-Cl})_2$(μ-THF) (Burton et al. 1989) the more sterically demanding substituted COT allows only bridging ligands: two chlorine and one THF molecule (O-bridging). Only monomeric species are synthesized with iodine $COTLnI(THF)_n$ (Mashima and Takaya 1989, Kilimann et al. 1994a,b, Mashima et al. 1994a) [Ln = La, Ce, Pr ($n = 3$), Nd ($n = 2$), Sm ($n = 1$)]. The X-ray structure of $COTCeI(THF)_3$ (Mashima and Takaya 1989) shows a four-legged piano stool geometry. These compounds are useful starting materials for the synthesis of mixed sandwich organolanthanides. Variously substituted Cp and COT ligands have been used for the synthesis of Ln complexes. An approximately linear arrangement (173°) of the ligand centroids around the metal is observed for unsolvated complexes as for example in the pentamethylated Cp*COTLu (Schumann et al. 1989b) shown in fig. 42. Its volatility and solubility is useful in CVD methods for the production of thin films (A. Weber et al. 1990).

The introduction of the cyclopentyl–cyclopentadienyl ($C_5H_9C_5H_4$) ligand (Jin et al. 1995) allowed the synthesis of the complexes $(COT)Ln(C_5H_9C_5H_4)(THF)_n$ (Ln = Nd, Gd; $n = 2$; Gd, $n = 1$) by reacting $LnCl_3$ with $C_5H_9C_5H_4Na$ and K_2COT.

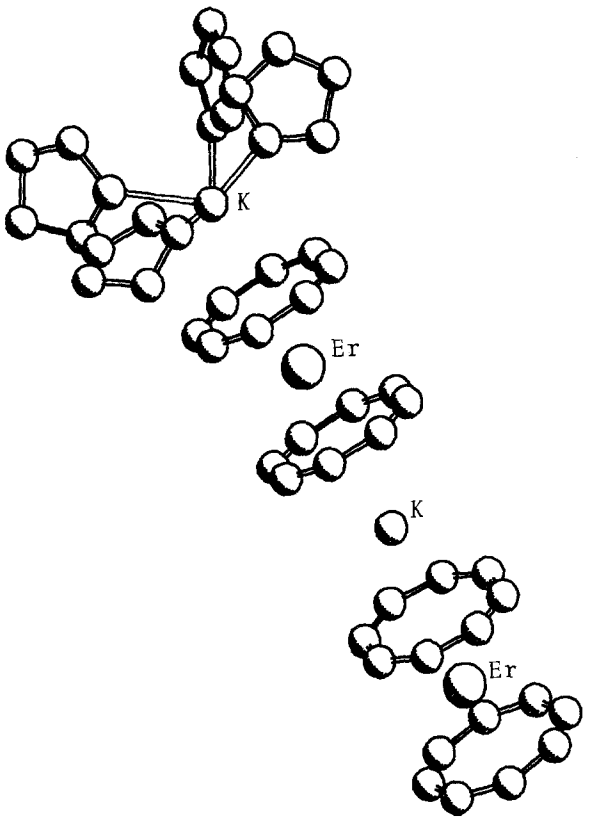

Fig. 41. Crystal structure of [(COT)-Er(μ-COT)K(μ-COT)Er(μ-COT)K $(THF)_4$] (Xia et al. 1991b).

The X-ray crystal structure of the Nd derivative shows the usual distorted tetrahedral geometry while in the Gd derivative the two forms with one and two THF molecules coexist in the same crystal, the coordination geometry being triangular for THF = 1 and tetrahedral when THF = 2. Also the 2,5-di-*tert*-butylpyrrolyl (pyr*) ligand (Schumann et al. 1996) has been used in association with COT to produce the mixed COTLnpyr*$(THF)_x$ derivative according to the equation

$$[COT(Ln)(\mu\text{-}Cl)(THF)]_2 + 2Na[pyr^*] \rightarrow 2[COTLn(pyr^*)(THF)_x] + 2NaCl,$$

where Ln = Sm, $x = 1$; Ln = Tm, Lu, $x = 0$. They are volatile and can be used in the "MOCVD processes" (Metal Organic Chemical Vapor Deposition) as precursors to the carbon-free lanthanide oxides. The X-ray crystal structure of the THF solvated Sm derivative shows a "triangular"coordination geometry of samarium.

The reaction of (COT)YCp* with 1,2,3,4-tetramethyl-2-methyleneimidazoline results in the formation of $(COT)Cp^*Y(CH_2{=}CC_2N_2Me_4)$ (Schumann et al. 1995c) where the "end-on" coordinated olefin is characterized by a $Y{-}CH_2{-}C$ angle of 123.1°.

By reacting $LnCl_3$ with NaCp and K_2COT (Wen et al. 1991) the compounds CpLnCOT·*n*THF (Ln = Pr, Nd, $n = 2$; Ln = Gd, $n = 1$) are obtained, while in the reaction

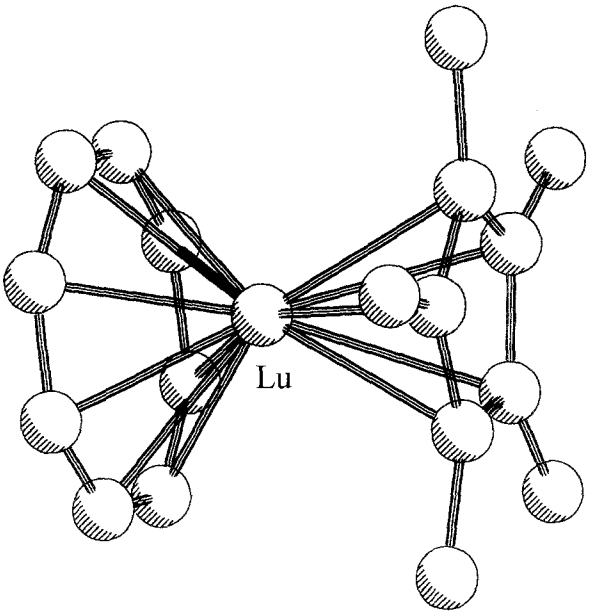

Fig. 42. Crystal structure of [(COT)-LuCp*] (Schumann et al. 1989b).

of $LnCl_3$, KC_9H_7 and K_2COT, the mixed indenyl derivatives are produced: (Ind)LnCOT·2THF (Ln = Pr, Nd). The X-ray structures of CpPrCOT·2THF and IndPrCOT·2THF have been determined in which compounds are characterized by non-parallel sandwich structures.

The synthesis and approximate X-ray structure of the Sm derivative (Ind)Sm(COT)-($N_2C_{10}H_8$) (Wrobleski et al. 1986b) have been reported. One benzylcyclopentadienyl (η^5), one (COT) (η^8) and two oxygen atoms of DME are coordinated to Gd(III) in the complex (COT)Gd($C_6H_5CH_2C_5H_4$)DME (Xia et al. 1996) with a formal coordination number 10. The (COT)Sm($C_5R_4PR'_2$) compounds (Visseaux et al. 1992) are useful precursors for bimetallic complexes. The reaction of the new ligand $HC_5R_4PMe_2$ (as its potassium salt) with [COTSmCl(THF)$_2$] produces the complexes (COT)Sm($C_5R_4PR'_2$) (R = H, Me; R′ = Me, Ph). They can react with $CpRh(CO)_2$ giving the heterobimetallic species (COT)Sm(μ-$C_5R_4PR'_2$)RhCp(CO), with phosphido-bridges between Sm^{III} and Rh^{I}, characterized by IR, ^1H and ^{31}P NMR spectra. The X-ray analysis of (COT)Sm($C_5H_4PPh_2$)(THF)$_2$ shows a pseudo-tetrahedral geometry around the metal ion with η^8-COT and η^5-$C_5H_4PPh_2$ coordination.

Ligand redistribution problems, with the production of stable M[COT_2Ln] species (M = alkalimetals), are often met in the preparation of COT σ-bonded derivatives, particularly when the chelating ligand *o*-$C_6H_4CH_2NMe_2$(L) has been used for the steric saturation of the complex. [(COT)Lu(*o*-$C_6H_4CH_2NMe_2$)]THF is formed from COTLuCl(THF) and LiL in THF (also the corresponding Er) (Wayda and Rogers 1985). On the contrary, the middle and early lanthanides give as the main byproduct [Li(THF)$_4$][$(COT)_2Ln$]. [(COT)LnCl(THF)$_2$] when reacted with $LiCH_2SiMe_3$ (1:4) gives

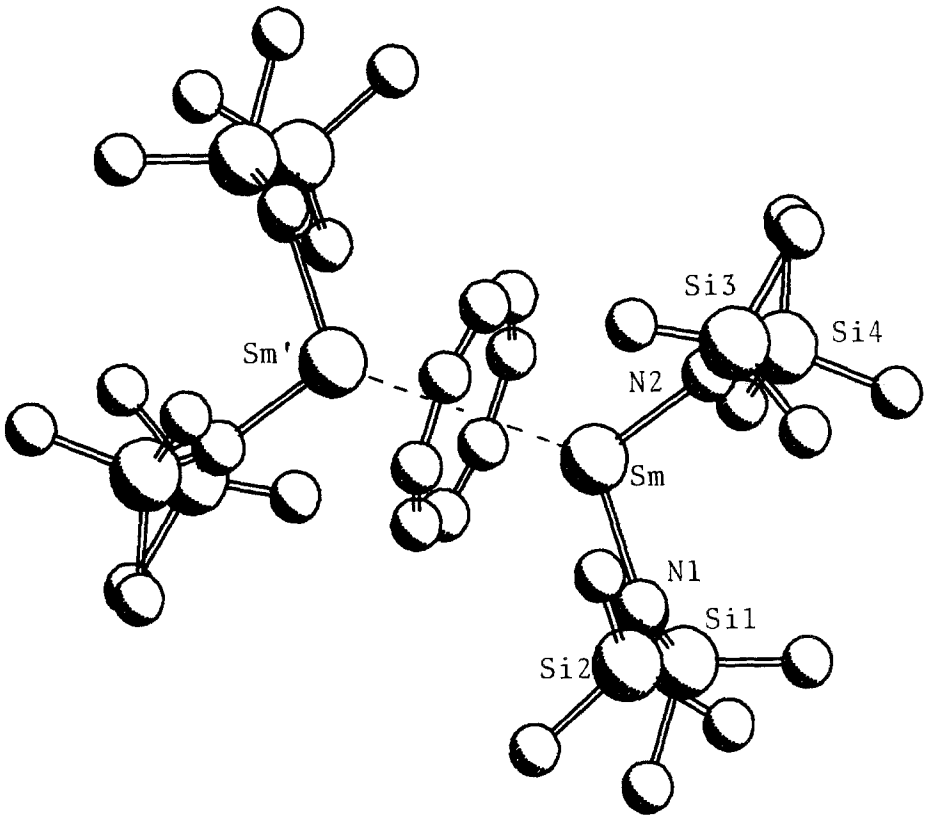

Fig. 43. Crystal structure of $\{Sm[N(SiMe_3)_2]_2\}_2(\mu\text{-COT})$ (Schumann et al. 1993b).

$[(COT)Ln(CH_2SiMe_3)_2][Li(THF)_2]$ (Ln = Y, Sm, Lu; Schumann et al. 1993c). The X-ray structure of the Sm derivative shows a triangular geometry around Sm and an unusual bonding of the Li cation to two carbon atoms of the COT ring besides the two THF oxygens. With bis-trimethylsilylamide $[N(SiMe_3)_2]^-$ the compounds $(COT)LnN(SiMe_3)_2 \cdot THF$ (Ln = Y, Gd, Er, Lu) and $\{Sm[N(SiMe_3)_2]_2\}_2(\mu\text{-COT})$ have been synthesized. The X-ray structure of the latter is an unusual "inverse sandwich" (Schumann et al. 1993b) where the two $Sm[N(SiMe_3)_2]_2$ units are symmetrically bridged by the COT ligand (fig. 43). Ln to nitrogen bonds in mono-COT species are present in the THF solvate pyrazol-1-yl, $[Ph_2P(NSiMe_3)_2]^-$ and $[4\text{–}XC_6H_4C(NSiMe_3)_2]^-$ (X = H, MeO and CF_3) derivatives COTLnL(THF) (Kilimann and Edelmann 1993, 1994, Schumann et al. 1995d). Monomeric aryloxy and siloxy complexes COTLnOR(THF) have been characterized by NMR and mass spectroscopy (Ln = Y, Lu; R = C^tBu_3, $SiPh_3$; Schumann et al. 1993a). $[(COT)Y(\mu\text{-OPh})(THF)_2]_2$ is dimeric like the triflate derivatives $\{COTLn[\mu,\eta^2\text{-}O_2S(O)CF_3](THF)_2\}_2$ (Ln = Ce, Pr, Nd, Sm, Y; Kilimann and Edelmann 1994, Kilimann et al. 1994a). The X-ray structure of the Nd derivative has been determined. From Sm metal, COT, diaryldisulfide or dienyl diselenide COT complexes

with Sm–S and Sm–Se can be obtained of the type $[(COT)Sm(\mu\text{-}ER)(THF)_n]_2$ (Mashima et al. 1993, Mashima et al. 1994a; $n=2$) (ER = SPh, $SC_6H_2Me_3$-2,4,6 and SePh, $n=1$, ER = SC_6H_2-^{i}Pr$_2$-2,4,6. The X-ray structure of $[(COT)Sm(\mu\text{-}SPh)(THF)_2]_2$ is analogous to that of the Nd triflate (Mashima et al. 1993) but with μ-SPh bridges.

Cerium forms stable COT complexes only when tetravalent. The first one synthesized, the dicyclooctatetraenyl $Ce(COT)_2$ was pyrophoric, but stable in water. Self-consistent field calculations established that the ground state in cerocene is almost entirely $4f^1$ corresponding to the formulation $Ce^{3+}(COT^{1.5-})_2$ rather than to $Ce^{4+}(COT^{-2})_2$ (Dolg et al. 1991). The methyl substituent in the COT ring stabilizes the structure of bis(methylCOT)cerium(IV) (Boussie et al. 1991) which presents an unusual non-linear Cg–Ce–Cg angle of 176° that "may arise from intramolecular electronic effects". The COT substituents are not fully staggered and the two COT are equidistant from the Ce.

More substituted COT ligands allow the syntheses of 1,1′,4,4′-tetrakis(trimethylsilyl)-cerocene (Fischer 1994) and of 1,1′,3,3′,6,6′-hexakis(trimethylsilyl)cerocene (Kilimann et al. 1994b) starting from Ce trichloride and Ce tristriflate, respectively. Their solubility and stability to oxidative decomposition and their ready availability make these compounds interesting candidates for novel one electron-transfer reactions. The X-ray structure of $Ce[1,3,6\text{-}(Me_3Si)_3C_8H_5]_2$ shows a Cg–Ce–Cg angle of 176.1°.

An unusual organolanthanide complex containing two different lanthanides is obtained in a redox reaction between the cerocene derivative with Yb powder in THF:

$$2Ce\left[1,3,6\text{-}\left((Me_3Si)_3\,C_8H_5\right)_2\right]_2 + Yb \xrightarrow{THF} \left[Yb\,(THF)_6\right]\left[Ce\left(1,3,6\text{-}(Me_3Si)_3\,C_8H_5\right)_2\right].$$

Upon heating in vacuo the "salt" is converted to the heterobimetallic tetradecker sandwich complex (COT′)Ce(μ-COT′)Yb(μ-COT′)Ce(COT′) (COT′ = 1,3,6-$(Me_3Si)_3C_8H_5$) according to the spectroscopic results (Edelmann 1995b).

2.3.2. *Actinides*

A milestone in the chemistry of 5f elements with COT was the synthesis of the uranocene $U(COT)_2$ (Streitwieser and Müller-Westerhoff 1968b).

$$UCl_4 + 2K_2(COT) \xrightarrow{THF} U(COT)_2 + 4KCl.$$

The same procedure was used for the analogous Th derivative (Streitwieser and Müller-Westerhoff 1968c). The molecular structure of the isostructural "uranocene" and "thorocene" has a D_{8h} molecular symmetry (Avdeef et al. 1972). In terms of orbital symmetry, uranocene is an interesting f-orbital homolog of ferrocene.

Electronic structure calculations on actinide $An(COT)_2$ compounds with the semi-empirical LCAO and the SCF-Xα scattered wave formalisms indicate the significance of some covalent interaction. However, the Xα-calculations show that metal $6d_{xz}6d_{yz}$-ligand e″g overlap may be important in addition to greater metal–ligand bond covalency for uranocene than for thorocene and a prediction of a $J_z = \pm 3$ ground state for uranocene. The crystal structure of (Kdiglyme)$(MeCOT)_2U^{III}$ (diglyme = diethyleneglycoldimethylether)

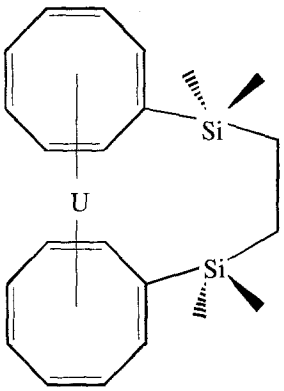

Scheme 20.

reveals an asymmetrical displacement of uranium between the two COT and a non-linear Cg–U–Cg angle (176°; Boussie et al. 1991).

The first bridged uranocene (Streitwieser et al. 1993) obtained by reacting in THF, UCl_4 with $K_2[1,2\text{-}C_8H_6(SiMe_2)_2]$ ethane has the monomeric structure shown in scheme 20 from mass and NMR spectral results.

A novel synthetic route for the preparation of "half-sandwich" COT, Th and U derivatives is presented for $(COT)U^{IV}(BH_4)_2$ derivative (Baudry et al. 1990a):

$$(COT)_2U + U(BH_4)_4 \rightarrow 2(COT)U(BH_4)_2 \leftarrow 2COT + 2U(BH_4)_4.$$

$(COT)U(BH_4)_2$ can be converted into Lewis base adducts $(COT)U(BH_4)_2L$ ($L = PPh_3$, THF, $OPPh_3$) and to the mixed ring derivative $COT(Cp)UBH_4L$ ($L = THF$, $OPPh_3$):

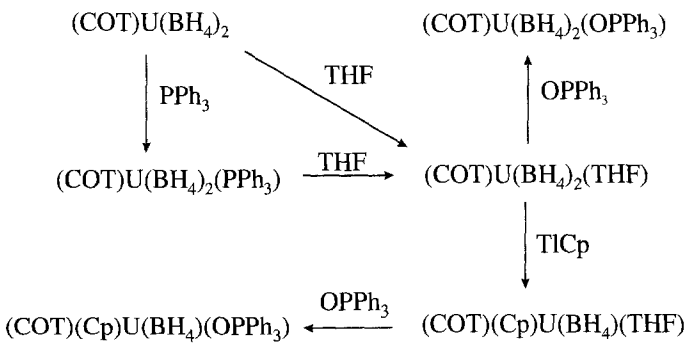

The interest in different ligand combinations on a metal center is due to the multiple reactive coordination sites offering multiple reactive positions at the neutral electrophilic metal center on a pseudo bent metallocene coordination sphere. The structure of the borohydride complex $(COT)U(BH_4)_2(OPPh_3)$ (Baudry et al. 1990a) consists of discrete molecules with a "piano stool" configuration, it is the first to be determined for a mono-COT U derivative. Mixed ligand Th derivatives can be obtained by the reaction

$$(COT)\,ThCl_2\,(THF)_2 + Cp^*MgCl \cdot THF \xrightarrow{\text{toluene}} (COT)ThCp^*Cl(THF)_x + MgCl_2.$$

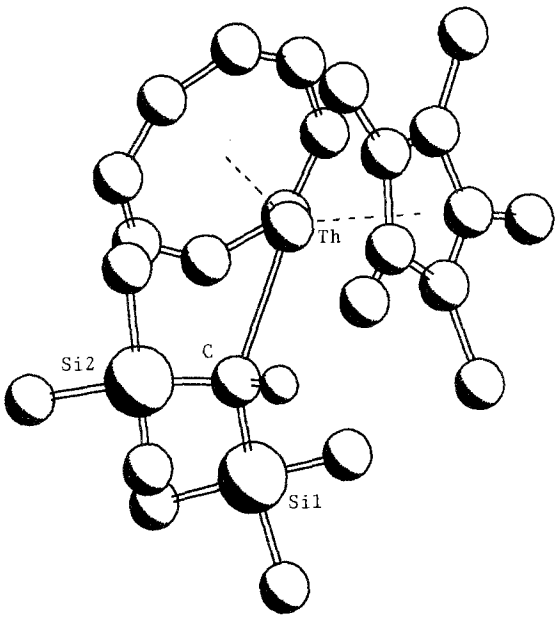

Fig. 44. Crystal structure of [Cp*(COT)-ThCH(SiMe$_3$)$_2$] (Gilbert et al. 1989).

Reaction of this compound with ^{t}BuCHMgCl affords (COT)ThCp*(μ-Cl)$_2$MgCH$_2^t$Bu-(THF) that can be considered as a "Grignard adduct" of (COT)Cp*ThCl (Gilbert et al. 1989). Its formation was rather surprising as many Cp$_3$ThR complexes are prepared from RMgX and Cp$_3$ThCl. The bonding mode shown in the crystal structure is typical of the Cp*Th(X)(Y) system. Significant dimensions are Th–Cg$_{(COT)}$, 2.02 Å; Th–Cg$^*_{(Cp)}$, 2.54 Å; Cg–Th–Cg, 138.0°; Th–Cl, 2.890(3) Å. (COT)Cp*ThCl(THF) desolvates at 100°C yielding the dimer [(COT)Cp*ThCl]$_2$ which reacts with LiCH(SiMe$_3$)$_2$ giving the monomeric alkyl (COT)Cp*Th[CH(SiMe$_3$)$_2$] derivative.

$$[(COT)Cp^*ThCl]_2 + 2LiCH(SiMe_3)_2 \xrightarrow{\text{toluene}} 2[(COT)Cp^*ThCH(SiMe_3)_2] + 2LiCl.$$

X-ray determination of the structure of the latter confirmed the monomeric formulation, the "bent sandwich" conformation and the presence of a σ-bonded alkyl group. The Th–C σ-bond distance is 2.54(1) Å. An agostic interaction Th–H of 2.71(9) Å is also present (fig. 44). The reaction of the alkyl complex with H_2 in alkane solvent produces an oligomeric hydride [COTCp*ThH]$_x$.

The first mixed-ring U^{III} complex [(COT)(Cp*)U(THF)] (Schake et al. 1993), obtained from Cp*UI$_2$(THF)$_3$ and K$_2$(COT) in THF, has been characterized by NMR and IR spectra. It reacts with Me$_2$bpy to give the adduct (COT)Cp*U(Me$_2$bpy) (Mebpy = 4,4′dimethyl-2,2′-bipyridine). The Cp*–U–(COT) angle of 138.2° is comparable to that of the Th derivative.

The mono cyclooctatetraenyl uranium dichloride pyridine adduct (COT)UCl$_2$(Py)$_2$ was obtained by heating the THF derivative with an excess of pyridine. Its crystal structure

is analogous to that of the non-isomorphous derivative $(COT)ThCl_2(THF)$ (Zalkin et al. 1980) and shows the usual distorted tetrahedral coordination around the metal ion.

The reaction of $(COT)UCl_2(THF)_2$ with Na(acac):

$$(COT)\,UCl_2(THF)_2 + 2Na\,(CH_3COCHCOCH_3) \xrightarrow[-20°C]{THF} (COT)U\,(CH_3COCHCOCH_3)_2\,,$$

produces the "acac" derivative. The $(COT)U(acac)_2$ structure (Boussie et al. 1990) shows an average U–C bond distance of 2.694 Å, longer than that found in the chloride derivative (2.644 Å) .

The reaction

$$(COT)UCl_2(THF)_2 + PMe_3 \rightarrow (COT)UCl_2PMe_3(THF)_x + (2-x)THF$$

has been investigated by variable ^1H NMR spectroscopy showing an exchange behavior for this process. Activation parameters have been also measured, as well as the reactivity of $(COT)UCl_2(THF)_2$ with mono, bidentate alkyl metal and alkoxy metal reagents.

$(COT)AnCl_2(THF)_2$ (An = Th, U) by metathetic reaction with $NaN(SiMe_3)_2$ produces the diamide complexes $COTAn[N(SiMe_3)_2]_2$ (Gilbert et al. 1988). The X-ray structure of the thorium derivative shows an unsaturated pseudo-seven coordinate compound where one carbon of each silyl amide ligand is in the direction of the thorium at a distance of 3.147(15) and 3.041(13) Å, respectively; this suggests a probable agostic interaction with the attached hydrogens. The solution NMR data indicate weak interactions. The analogous Ln anionic derivatives (Y, Gd, Er, Lu) are all THF solvated only with the isolobal $CH(SiMe_3)_2$. A quite similar coordination geometry around the metal ion is present in $(THF)_2Li(\mu\text{-}\eta^2\text{:}\eta^8\text{-}COT)Sm[CH(SiMe_3)_2]_2$ (Schumann et al. 1993c).

Mixed alkoxide-BH_4 and bis(alkoxide) compounds $[(COT)U(BH_4)(OR)]$ and $[(COT)U(OR)_2]$ (R = Et, ^{i}Pr or ^{t}Bu) can be obtained by alcoholysis of $[(COT)U(BH_4)_2]$ (Arliguie et al. 1992). Their structure and dynamic behavior in solution have been studied by NMR spectroscopy. The complexes $(COT)U(BH_4)(OR)$ are monomers in THF while $(COT)U(OR)_2$ are dimers in THF and monomers in pyridine. In the solid state structures of the two dimers $[(COT)U(BH_4)(\mu\text{-}OEt)]_2$ (fig. 45) and $[(COT)U(O^iPr)(\mu\text{-}O^iPr)]_2$ there are two bridging alkoxide groups, while the COT ligands are parallel and *trans* oriented in the BH_4 derivative and *cis* oriented in the (O^iPr) derivative, probably because of the greater steric hindrance of BH_4 than of the O^iPr ligand at the metal center.

When thiol or NaSR reagents (R = ^{n}Bu or ^{i}Pr) react with $(COT)U(BH_4)_2$ (Leverd et al. 1994) bis-thiolate complexes $[(COT)U(SR)_2]$ are produced. For R = ^{t}Bu a monomeric compound $(COT)U(S^tBu)_3$ has been isolated; its crystal structure shows a three-legged piano stool geometry, while the isopropane derivative $[(COT)U(\mu\text{-}S^iPr)_2]_2$ is a centrosymmetric dimer with four bridging S^iPr ligands. This different behavior seems to be due to electronic effects, the ligand $(COT)U(SR)_2$ being less electron rich than the corresponding $(COT)U(OR)_2$. COT complexes with U^{III} are rare. The $K(RC_8H_7)_2U$ (R = H, Me) complexes have been obtained by potassium reduction of the corresponding uranocenes (Billiau et al. 1981, Eisenberg et al. 1990).

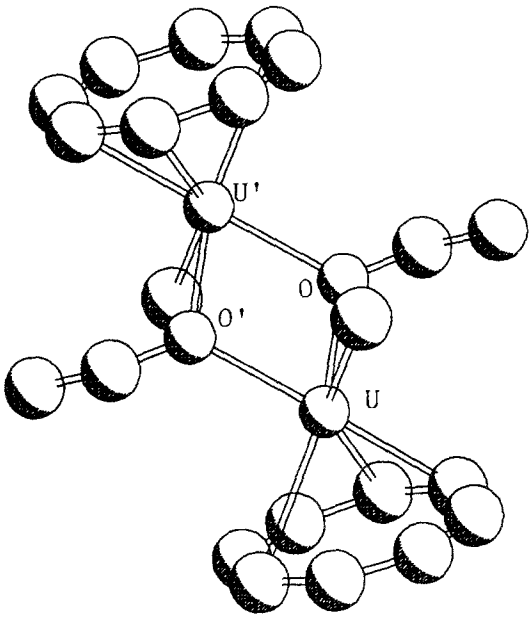

Fig. 45. Crystal structure of $[(COT)U(BH_4)(\mu\text{-}OEt)]_2$ (Arliguie et al. 1992).

2.4. *Cyclopentadienyl compounds with hydride ligands*

2.4.1. *Lanthanides*

The early 80's saw the beginning of the preparation and characterization of rare earth organo hydride compounds (Schumann and Genthe 1981, Evans et al. 1982b) by hydrogenolysis of Cp_2Y, Er and Lu alkyl derivatives at atmospheric or high pressure.

$$Cp_2Lu\text{–}R\,(THF) + H_2 \xrightarrow{\text{THF, 50 atm}} \frac{1}{n}\,[Cp_2Lu\text{–}H(THF)]_n + RH,$$

where R = ^{t}Bu, CH_2SiMe_3, CH_2CMe_3, CH_2Ph.

$$2(MeCp)_2Ln\text{–}{}^t\!Bu(THF) + 2H_2 \xrightarrow{\text{toluene}} [(MeCp)_2Ln\text{–}H(THF)]_2 + 2{}^t\!BuH,$$

where Ln = Y, Er, Lu.

$$[(MeCp)_2ErCH_2(SiMe_3)]_2 + 2H_2 \xrightarrow{\text{toluene 70–80°C}} [(MeCp)_2Er\text{–}H]_2 + 2SiMe_4.$$

The dimeric nature of these hydrides was established by cryoscopic molecular weight measurements in benzene (Marks and Ernst 1982) and confirmed by the X-ray analysis (Evans et al. 1982b) of $[(MeCp)_2Y(THF)(\mu\text{-}H)]_2$ and the Er analog.

Different lutetium hydride species can be obtained according to the following reactions (Schumann et al. 1986a).

$$Cp_2LuCl + NaH \xrightarrow{\text{THF}} [Na(THF)_6][(Cp_2LuH)_3H],$$

$$Cp_3Lu + NaH \xrightarrow{\text{THF}} [Na(THF)_6][(Cp_3Lu)_2H] \cdot 2THF.$$

The X-ray structure of $[Na(THF)_6][(Cp_3Lu)_2(\mu\text{-}H)]\cdot 2THF$ shows a centrosymmetric dimeric anion, with a single hydrogen bridge. The hydrogenolysis of the solvent free

derivative $Cp^*_2SmC(Ph)=C(Ph)SmCp^*$ in hexane solution produces the orange solvent-free $[Cp^*_2Sm(\mu\text{-}H)]_2$ (Evans et al. 1983c). The X-ray structure shows one of the Cp^*_2Sm units rotated with respect to the other by 87° such that the molecule shows approximate S_4 symmetry. A dimeric structure is present in the isomorphous pair $[Cp''_2Ln(\mu\text{-}H)]_2$ (Ln = Ce, Sm) (Gun'ko et al. 1992; $Cp'' = {}^tBu_2C_5H_3$) synthesized from the corresponding $[Cp''_2LnAlH_4\cdot L]_2$ with an excess of triethylaminoalane THF mixture. The Cp'' ligands are staggered and the Ce···Ce separation is 3.90(1) while Sm···Sm is 3.77(2) Å. The low value for the Cg–Sm–Cg angle 121.5° versus 133.5° for the cerium derivative could be related to a "distinct type of hybrid MO orbital orientation for the Cp''_2Sm moiety".

A new type of anionic complex is represented by the structure of the trinuclear polyhydride complex $[Cp_2ErH]_3Cl[Li(THF)_4]$ (Evans et al. 1987c). It is formed from cation–anion pairs. In the anion three Cp_2Er units are connected by hydrogen and chlorine bridges in a triangular array with one $(\mu^3\text{-}H)(Er\text{–}H_{av.}$ 2.18 Å), two $(\mu^2\text{-}H)(Er\text{–}H_{av.}$ 2.34 Å) and one (μ–Cl) bridges.

An analogous anion structural type is present in $[Li(THF)_3][(Cp_2LuH)_3H]$ (Evans et al. 1982a). Hydrogenolysis of $[(1,3\text{-}Me_2Cp)_2Y(\mu\text{-}Me)]_2$ in a THF/hexane (Evans et al. 1987c) produces different hydride complexes, depending on the crystallization conditions. The trimer $[(1,3\text{-}Me_2Cp)_2Y(\mu\text{–}H)]_3$ crystallizes from toluene and, when recrystallized from THF, produces the dimer $[(1,3Me_2Cp)_2Y(THF)(\mu\text{-}H)]_2$; in the presence of Li salts a third product can be obtained $[(1,3Me_2Cp)_2Y(\mu\text{–}H)]_3(\mu^3\text{-}H)[Li(THF)_4]$ where the anion has the same structure as the Er trimer. The dimethyl substituted Cp complexes are more soluble than their monosubstituted and unsubstituted Cp analogs. The dimer $[(1,3Me_2Cp)_2(THF)Y(\mu\text{-}H)]_2$ is characterized by a nearly square planar geometry, for the four cyclopentadienyl ring centroids (it was about tetrahedral in $[Cp^*_2Sm(\mu\text{-}H)]_2$ (Evans et al. 1983c). The X-ray crystal structure of $\{[Cp_2Y(\mu\text{-}OCH_3)]_3(\mu^3\text{-}H)\}_2[Li(THF)_3]_2$ (Evans et al. 1988f) shows $\{[Cp_2Y(\mu\text{-}OCH_3)]_3(\mu^3\text{-}H)\}^-$ to be a triangular arrangement of the three Cp_2Y units bridged by methoxide groups in the anion. The central hydride ligand was identified only by ^1H NMR spectroscopy. The cation $\{[(THF)_3Li]_2[Cp_2Y(\mu\text{-}OCH_3)]_3(\mu^3\text{-}H)\}^+$ has the same ligand arrangement as in the anion, except for two additional $Li(THF)_3$ moieties.

Compounds of the type $[(Me_3Si)_2C_5H_3]_2LnBH_4(THF)$ (Ln = La, Pr, Nd and Sm) have been prepared with BH_4 as tridentate ligand. With Y and Yb, and with the solvent free Sc complex BH_4 behaves as bidentate ligand. The X-ray analysis of the Sc derivative confirms the structure. The Sc–H bond length is 2.03(4) Å (Lappert et al. 1983b). The structure of $[(C_5H_3{}^tBu_2)_2Sm(\mu\text{-}BH_4)]_2$ (Gun'ko et al. 1992) is an example of $[(\mu^3\text{-}H)_2B(\mu^2\text{-}H)_2]$ bridging as is the isostructural Ce derivative $[(C_5H_3{}^tBu_2)_2Ce(\mu\text{-}BH_4)]_2$ (Lobkovskii et al. 1991).

The possible use of unsolvated lanthanidocene hydrides as catalysts in alkene C–H bond activation, hydrogenation of alkynes etc. gave rise to much research into the synthesis and characterization of a series of aluminohydride organolanthanidocene derivatives. The structures of these compounds generally contain a dimeric fragment (Cp_2MX) or substituted (Cp'_2MX) (M = Ln, Y) connected to AlH_3L fragments by bridging hydrogen

bonds. The aluminum hydride derivatives are generally more labile than simple hydride complexes and that should enhance their catalytic activity.

The synthesis is generally an easy process involving the addition of AlH_3 to the appropriate lanthanidocenes (or yttriocenes) in the form of the appropriate alkyl or halide derivative. X-ray structure determination is the best way of clarifying the somewhat complicated hydrogen bridging modes in these compounds. The structure of $[Cp_2YCl]_2[AlH_3OEt_2]$ (Lobkovskii et al. 1982) is polymeric: the $Cp_2Y(\mu\text{-}Cl)_2YCp_2$ dimeric units are connected to $AlH_3 \cdot OEt_2$ moieties via Y–H–Al bridges, forming infinite chains: dimer–AlH_3OEt_2–dimer.

Three hydride bridges per metal center were observed in: $[Cp_2Y(\mu^3\text{–}H)(\mu^2\text{-}H)AlH_2\text{-}(THF)]_2$ (Bel'skii et al. 1984a), $[Cp_2Y(\mu^3\text{–}H)(\mu^2\text{-}H)AlH_2(NEt_3)]_2$, $[Cp_2Y(\mu^3\text{-}H)(\mu^2\text{–}H)AlH_2(\mu\text{-}H)_2AlH(OEt_2)]_2$ (Bel'skii et al. 1984b). The interaction of Cp_2YCl with $LiAlH_4$ (2:1) produces both $[Cp_2YCl]_2AlH_3OEt_2$ and $[Cp_2Y]_2AlH_4Cl \cdot L \cdot C_6H_6$ ($L = NEt_3$, THF). The X-ray analysis carried out on the NEt derivative shows, a trimetallic structure, in a triangular array where in the center a hydrogen is μ^3-bonded to the three metal ions which are further connected on the periphery by hydrogen and chlorine bridges (Erofeev et al. 1987). The interaction of Cp_2LuCl with $LiAlH_4$ in the presence of Et_3N, produces the dimeric complex $[Cp_2LuAlH_4NEt_3]_2$ which is coordinatively and electronically saturated. In the presence of THF, the THF derivative is produced. (Both are isomorphous with the Y analog; see above.) The crystals of the dimer undergo dissociation under X-ray (MoKα) radiation exposure (about 2 h) producing the monomeric unsaturated $Cp_2Lu(\mu^2\text{-}H)AlH_3NEt_3$ compound with a monodentate AlH_4 group (Knyazhanskii et al. 1987). The changes in the solid state transformation are reflected in the breaking of all four Lu–H bridge bonds with a change in the Al coordination polyhedron from trigonal bipyramid to a distorted square pyramid with a bridge hydrogen atom as axial ligand. The unstable $Cp''_2LuAlH_4 \cdot Et_2O$ (Knyazhanskii et al. 1991) aluminohydride complex decomposes along three pathways: (i) desolvation, (ii) dissociation of solvated aluminium hydride, and (iii) destruction of the metallocene moiety to produce the polynuclear complex $[(^tBu_2C_5H_3)LuH]_4[AlH_4 \cdot Et_2O]_2[AlH_4]_2$. Its structure is characterized by the previously unknown tetrahedral metal core made of Lu atoms bound by bridging hydrogens and tri-(AlH_4) and tetra-dentate ($AlH_4 \cdot Et_2O$) groups.

The polynuclear compounds are important for understanding the "aging" and deactivation in the Ziegler–Natta catalytic systems which include Al alkyls or hydrides (Bel'skii et al. 1991a). In this context the octanuclear complex $Cp''_5Sm_4(AlH_4)_3H_3(Me_2NC_2H_4\text{-}NMe_2)_2(tmed)(Cp''C_5H'_3Bu_2)$ (Bel'skii et al. 1991b) is obtained by reacting Cp''_2Sm with AlH_3 in ether or Cp''_2SmTHF with AlH_3 in THF with excess of tmed and pentane. (The process involves the $Sm^{II} \rightarrow Sm^{III}$ oxidation). Its structure is characterized by a cyclic metal core of the shape of a "sitting frog". The connection between the different metal centers is made by μ^2 and μ^3 bridging hydrogens. The formation of this octanuclear compound is a further demonstration of the tendency of aluminohydride metallocene complexes, to form rather stable polynuclear species.

The $[Cp_2Sm(\mu^3\text{-}H)]_2[(\mu^2\text{-}H)_2AlHNEt_3]_2$ and $[Cp'_2Sm]_2(\mu^2\text{-}H)\mu\text{-}[(\mu^3\text{-}H)_2Al(\mu^2\text{-}H)_2 \cdot Me_2NC_2H_4NMe_2]$ ($Cp' = C_5H'_4Bu$) compounds (Bel'skii et al. 1991c) are characterized

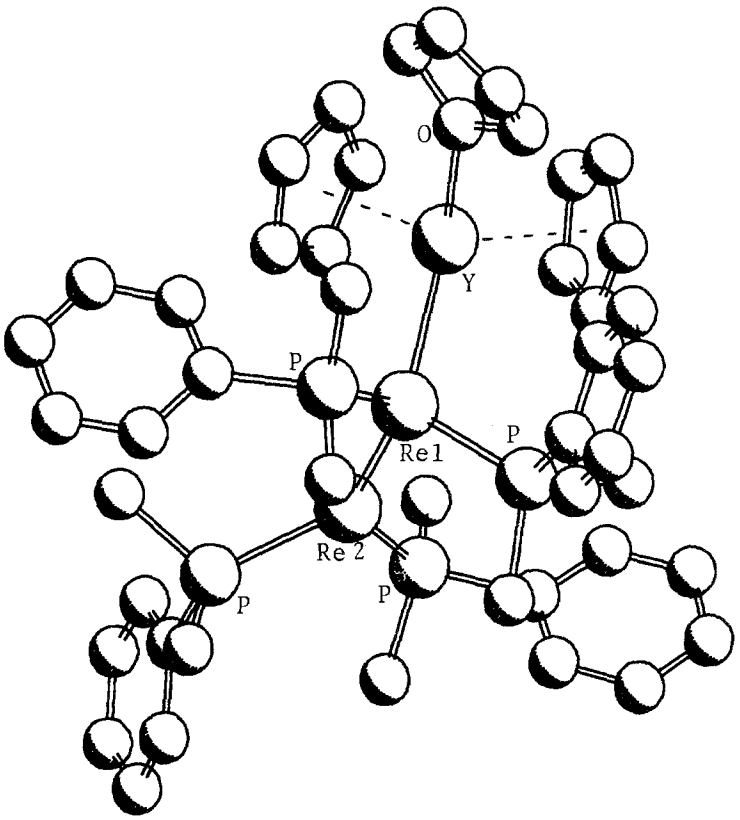

Fig. 46. Crystal structure of $[Cp_2Y(THF)Re_2H_7(PMe_2Ph)_4]$ (Alvarez et al. 1990).

by a formal 20 electron configuration. This coordinative oversaturation is considered important for the prediction of reactivity and catalytic activity of the transition metal complexes. In both complexes the Sm atom is coordinated by four hydrides. The separation Sm···Al is similar, however the introduction of the strong bidentate Lewis base tmed (=tetramethylethylendiamine) changes the type of binding of the AlH_4 moiety, having two μ^3 and two μ^2 bridging hydrogens to each samarium atom $[(\mu^3\text{-}H)_2Al(\mu^2\text{-}H)_2]$.

The Sm^{III} complex $\{[Cp'_2Sm(\mu^3\text{-}H)][(\mu^{2-}H)_2\cdot AlH\cdot THF]\}_2$ is, from X-ray data, a centrosymmetric dimer where the central planar $[Sm(\mu\text{-}H)]_2$ metallacycle is connected to Al by additional bridging hydrogens. The eight membered metallacycle SmHAlHSmHAlH is in a chair conformation (Gun'ko et al. 1990). Heterometallic hydride complexes of the type $Cp_2LnRe_2H_7(PMe_2Ph)_4$ have been obtained from $Cp_2LnMe(THF)$ (Ln=Y, Lu) and $Re_2H_8(PMe_2Ph)_4$ in THF (Alvarez et al. 1990), but the solid state structures of the respective Y and Lu derivatives are markedly different, because of the presence in the first of a THF molecule. $Cp_2Y(THF)Re_2H_7(PMe_2Ph)_4$ has an open triangular structure (fig. 46) with one Re(2)···Y separation of 4.186(2) Å and the other Re(1)···Y

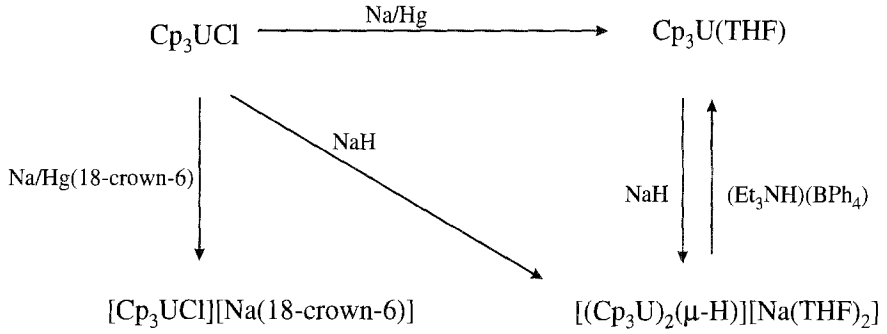

Scheme 21.

of 3.090(2) Å suggesting the presence of a hydride-bridge, for the latter. A similar hypothesis accounts for the short Re···Re distance (2.576(1) Å). The bridging hydride ligands were indicated by ^{1}H NMR spectrum ($J_{Y-H} = 7.2$ Hz). The THF free molecule of $Cp_2LuRe_2H_7(PMe_2Ph)_4$ adopts a closed triangular shape for the three metals. Also in this case hydride bridges are proposed, on the basis of the metallic distances and NMR spectra.

Monocyclopentadienyl hydride derivatives are potential catalysts for olefine oligomerization and polymerization. They can be stabilized by hindering Cp substituted derivatives such as $^tBu_2C_5H_3$, C_5Me_5 or chelating ones like $Me_4C_5SiMe_2N^tBu$; an example of a structurally characterized complex is the centrosymmetric dimer $\{Me_4C_5SiMe_2(\eta^1N^tBu)$-$Sc(PMe_3)(\mu\text{-}H)\}_2$ (Shapiro et al. 1990) which is a regiospecific catalyst for polymerization of α-olefins (Shapiro et al. 1994). The Sc coordination is trigonal bipyramidal.

The pentamethylated ligand (Cp*) in association with alkoxides was used by Schaverien (1992a, 1994a) to synthesize a series of hydride derivatives $[Cp^*(2,6\text{-}^tBu_2C_6H_3O)Y]_2(\mu$-$H)(\mu\text{-}R)$ R = Et, ^{n}Pr, ^{n}Bu, C_6H_{13}, C≡CSiMe$_3$ as useful models for the first insertion step in alkene polimerization processes. A stable Cp* dicarbollide derivative probably useful as an olefin polymerization catalyst, is $[Li(THF)]_2[Cp^*(C_2B_9H_{11})ScH]_2$ (Bazan et al. 1993) which as been characterized by X-ray analysis.

2.4.2. *Actinides*

The first organo 5f hydrides synthesized were $[Cp^*_2AnH_2]_2$ and $[Cp^*_2ThClH]_2$ and their dimeric structure was obtained by neutron diffraction studies (Broach et al. 1979; An = U, Th).

Hydrogenolysis of Cp^*_2Ubis(hydrocarbyls) in the presence of dmpe (Duttera et al. 1982) gave the novel U^{II} bis(phosphine) hydride derivative $Cp^*_2U(dmpe)H$. The usual "bent sandwich" configuration of the Cp* ligand is present in its crystal structure.

The reduction of U(IV) species Cp_3UCl to U(III) by sodium amalgam in THF, or in presence of 18-crown-6 ether gave the products indicated in scheme 21 (Le Maréchal et al. 1989b).

A bidentate bridging mode (Porchia et al. 1987b, Zanella et al. 1987) of a boron hydride ligand to a 5f actinide metal has been achieved, by alkyl substitution of two hydrogens

of the BH_4^- anion in the compound $Cp_3U(HBBN)$ [BBN = 9-borabicyclo(3.3.1)nonane] obtained according to:

$$Cp_3UCl + Na(HBBN) \xrightarrow[\text{room t.}]{THF} Cp_3U(HBBN) + NaCl.$$

The IR and NMR data were consistent with the bidentate bridging mode of the HBBN ligand as confirmed by X-ray analysis. The pseudotetrahedral arrangement of the ligands around U is characterized by the average Cg–U–Cg angle of 115(1)°. The $U–C_{(Cp)av;}$ is 2.76(1) Å, and the U–B distance 2.78(3) Å is typical for a bidentate bridge (the H were not located). The complex exhibits the characteristic properties of tetrahydroborate uranium complexes as molecularity, volatility, thermal stability and resistance to Lewis bases.

The borohydride, Cp_3UBH_4, can be obtained by reaction of several tricyclopentadienyl uranium derivatives, Cp3U–Z (Z = Me, Et, Ph, NEt_2, OMe, F, $CONEt_2$, CO^{n}Bu) with substituted borohydrides, $H_3B–Z'$ (Z' = THF, BH_3, SMe_2; Porchia et al. 1987a). The chemical and physical properties of $Cp_3U(BH_4)$, $(MeCp)_3U(BH_4)$, $Cp_3U(H_3BMe)$, $Cp_3U(H_3BEt)$ and $Cp_3U(H_3BPh)$ have been investigated together with a partial structure determination of $Cp_3U(BH_4)$ showing a trihapto coordination of the borohydride group to the uranium atom (U···B = 2.48 Å; Zanella et al. 1988). By reduction of Cp_3UBH_4 with Na/Hg the anionic U^{III} compound [Na(18-crown-6)][Cp_3UBH_4] has been obtained (Le Maréchal et al. 1988). As observed in almost all the covalent tetrahydroborates (Zanella et al. 1988) the room temperature ^1H NMR spectrum of Cp_3UBH_4 shows the bridging and terminal BH_4 hydrogens to be magnetically equivalent, probably due to a rapid intramolecular hydrogen interchange. In the case of $Cp_3U(H_3BPh)$ it has been possible to separate the ^1H NMR contact and dipolar (pseudocontact) contributions. This is the first contact shift data for a metal-bound hydride in a paramagnetic complex (Marks and Kolb 1977).

Reaction of $U(BH_4)_3 \cdot n$THF with $Cp^*_2Th(PPh_2)_2$ in THF/toluene in the presence of NaCl produced [$Na(THF)_6$][$Cp^*U(BH_3)_2$] (Ryan et al. 1989) with the unexpected migration of a Cp from thorium to the uranium center. The X-ray analysis shows the $Cp^*U(BH_4)_3$ moieties coordinated by three tridentate groups, according to the characteristic U–B distance of 2.61 Å(av.). The stoichiometry of the complex and the black color of the crystal (due to a facile $U^{III} \rightarrow U^{IV}$ charge transfer process) suggest a mixed valent compound of average uranium oxidation state of 3.5. Reactions of the cationic species [$(RC_5H_4)_3Th$]BPh_4 (R = Me_3Si, ^{t}Bu) with ^{t}BuLi yields the new thorium hydrides $(RC_5H_4)_3ThH$ characterized by NMR spectroscopy (Weydert et al. 1995).

2.5. *Heterometallic cyclopentadienyl compounds with transition metals*

2.5.1. *Lanthanides*

The coordinative unsaturation of some organo-lanthanide species can be overcome by the insertion of transition metal complexes containing donor atom ligands such as for example nitrosyl or carbonyl groups. The first studies on the subject deal with the

synthesis of compounds containing either metal–metal bonds or lanthanide–isocarbonyl or –isonitrosyl interactions. The reaction of Cp_3Ln or $(MeCp)_3Ln$ (Ln = Sm, Gd, Dy, Ho, Er, Yb) with $Co_2(CO)_8$, $MeCpMn(CO)_3$, $[CpFe(CO)_2]_2$, $CpCr(NO)_2Cl$, $CpM(CO)_2(NO)$ (M = Cr, Mo, W) yields compounds containing either isonitrosyl or isocarbonyl linkages to the lanthanide ions, as confirmed by IR spectroscopy (Tilley and Andersen 1982).

Isocarbonyl bridges are in general more frequent with W, Mo, Mn, Fe, Co metal ions. For the Cp_2Ln moieties an example of isocarbonyl bridges between the two metal centers is $(THF)Cp_2Yb(\mu\text{-}OC)Co(CO)_3$ derivative (Magomedov et al. 1989) but surprisingly in $(THF)Cp_2Lu\text{–}Ru(CO)_2Cp$ the two metal centers are directly connected by a Lu–Ru bond (2.955(2) Å; Magomedov et al. 1990). The analogous La complex (Beletskaya et al. 1993a) as well as $(THF)[(1,3\text{-}MeSi)_2C_5H_3]_2Lu\text{–}Ru(CO)_2Cp$ and $Cp^*_2Lu\text{–}Ru(CO)_2Cp$ have also been isolated.

An unusual 12-membered ring is found in $[Cp''_2Ce(\mu\text{-}OC)W(CO)Cp(\mu\text{-}CO)]_2$ (Cp'' = 1,3-$(SiMe_3)_2$-C_5H_3). The ring is formed by Ce–O = C–W groups with the O–C–W angle essentially linear at 178° while the Ce–O–C angle is 154°. This structure is not very stable, breaking up in acetonitrile solution to form $[Cp''_2Ce(NCMe)_x]^+$ ions (Hazin et al. 1988, 1990). The use of a diphenylphosphine substituted cyclopentadienide ligand has led to the synthesis of another heterobimetallic complex $[(C_5H_4PPh_2)_2Yb(THF)_2PtMe_2]\cdot THF$ (Deacon et al. 1989c). The X-ray crystal structure reveals a pseudotetrahedral environment around the Yb^{2+} ion, comprising two oxygen atoms from the THF ligands and two η^5-$C_5H_4PPh_2$ ligands.

The first pentamethylcyclopentadienyl lanthanide derivative containing transition metals in the same molecule to be synthesized was $Cp^*_2Yb(\mu\text{-}OC)Co(CO)_3\cdot THF$ (Evans et al. 1988f). The structural characterization of the compound (by X-rays) shows the two coordination tetrahedra around each metal ion (Yb or Co) connected via a CO bridge.

A wide range of Cp^*_2Ln transition metal complexes with Ln–OC–M bridges has been obtained because of the electron transfer properties of Cp^*_2Ln toward transition metal carbonyl derivatives. The easy crystallization of the Cp* species, compared with unsubstituted Cp, allowed the X-ray characterization of many compounds. The X-ray structure (Boncella and Andersen 1984a) of $Cp^*_2YbMn(CO)_5\cdot 0.25PhMe$ shows polymeric chains of $[Cp^*_2Yb(\mu\text{-}OC)_3Mn(CO)_2]$ units with dimeric moieties $[Cp^*_2Yb(\mu\text{-}OC)_3Mn(CO)_3]_2$ packed between the polymeric sheets. "Contact ion pair formation tends to localize electron density into the manganese–carbon bonds that are part of the Mn–CO–Yb interaction". The structure of $[(Cp^*_2Yb)_2(\mu^3\text{-}OC)_4Co_3(CpSiMe_3)_2]$ has been also reported (Boncella and Andersen 1984b). Carbonyl bridges are present in the tetranuclear complex $[Cp^*_2Sm(\mu\text{-}OC)_2FeCp^*]_2$ prepared according to the reaction (Recknagel et al. 1991d)

$$2Cp^*_2Sm(THF) + [Cp^*Fe(CO)_2]_2 \rightarrow [Cp^*_2Sm(\mu\text{-}OC)_2FeCp^*]_2.$$

(Its molecular structure is characterized by bridging OC units with Sm–O distance average of 2.34 Å.) A different type of linkage in the lower oxidation state products includes the attachment of η^2-alkene group to Yb in $Cp^*_2Yb(\mu\text{-}C_2H_4)Pt(PPh_3)_2$ (Burns and Andersen 1987c).

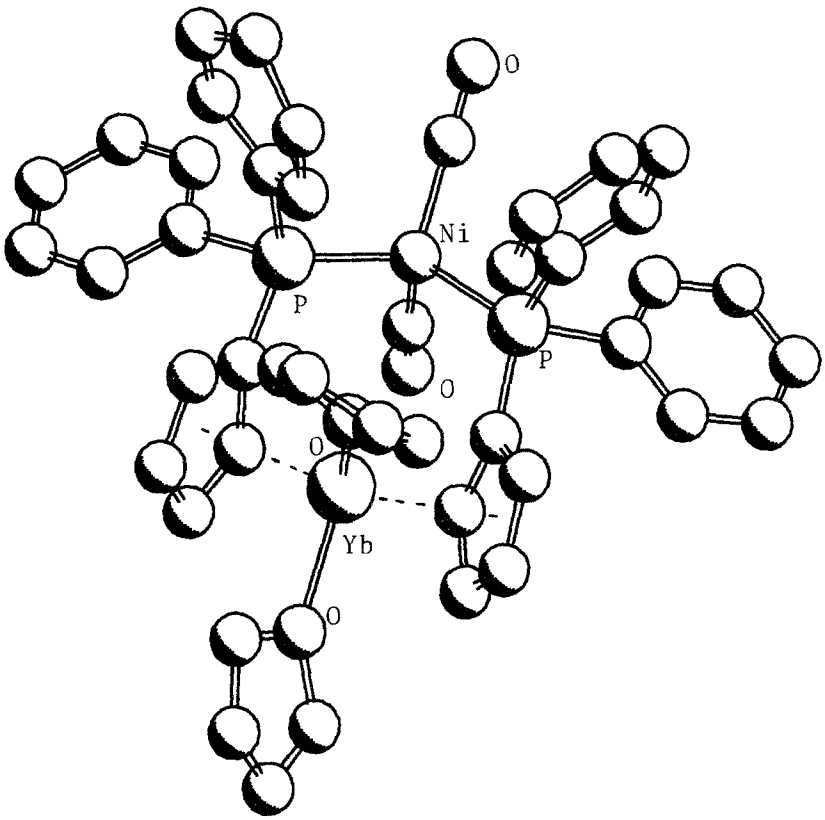

Fig. 47. Crystal structure of $[Yb(THF)_2(C_5H_4PPh_2)_2Ni(CO)_2]$ (Deacon et al. 1982).

The phosphinoytterbocene $[(C_5H_4PPh_2)Yb_2(THF)]$ which by reaction with $Ni(CO)_2(PPh_3)_2$, $Mo(CO)_4$(nbd) (nbd = norbornadiene) or $PtMe_2$(COD) (COD = cycloocta-1,5-diene) in toluene gives $[(C_5H_4PPh_2)_2Yb(THF)X]\cdot n$PhMe (X = $Ni(CO)_2$, $Mo(CO)_4$ or $PtMe_2$, $n = 2/3$ or 1) and $[(C_5H_4PPh_2)_2Yb(THF)_2X]\cdot$THF [X = $PtMe_2$, $Mo(CO)_4$ and $Ni(CO)_2$ (unsolvated)] has been synthesized (Deacon et al. 1982). The crystal structure of the latter shows that around ytterbium there is a pseudo-tetrahedral arrangement of two THF ligands and of the cyclopentadienyl ring centroids of two η^5-diphenylphosphinocyclopentadienide ligands which are also bonded via P atoms to the $Ni(CO)_2$ group (fig. 47).

Very recently tetrathiometallate anions like $[MoS_4]^{2-}$ and $[WS_4]^{2-}$ have been used for the synthesis of new mixed metal Mo–Sm and W–Sm complexes (Evans et al. 1995b). In the trimetallic Mo(V) complex $\{[Cp^*_2Sm]_2Mo(\mu\text{-}S)_4\}(PPh_4)$ (its solid state structure shows about identical $Cp^*_2Sm(\mu\text{-}S)_2$ units) reduction of the metal center of the tetrathiometallate unit occurs while in the bimetallic W(VI) complex $[Cp^*_2Sm(\mu\text{-}S)_2WS_2]PPh_4$ there is no reduction of the W(VI) metal ion; this is consistent with the different redox potentials of MoS_4^{2-} and WS_4^{2-}.

2.5.2. *Actinides*

Dicyclopentadienyl uranium bis(diethylamide) reacts with metal carbonyl hydrides to give isocarbonyl-bridged binuclear complexes (Marks and Ernst 1982) such as for example $Cp_2U[(\mu\text{-}OC)MoCp(CO)_2]_2$.

A heterometallic compound can be made by the reaction

$$K[L_2ReH_6] + Cp_3UCl \rightarrow L_2ReH_6UCp_3,$$

where L is a triarylphosphine. At 30°C all the hydride ligands are apparently equivalent in the ^1H NMR spectrum and as the temperature is reduced no variation is observed. Nevertheless, at least three bridging hydrides are considered to be present (Baudry and Ephritikhine 1986). Heterobinuclear products formed in the reactions

$$(RCp)_3AnCl + NaM(Cp)(CO)_2 \rightarrow (RCp)_3An\text{–}MCp(CO)_2,$$

where R = H; An = Th, U; M = Fe, Ru; R = Me; An = Th; exhibit hindered rotation around the metal–metal bonds and facile cleavage by alcohols and ketones. The free energies of activation for rotation vary from 50 to 60 kJ mol^{-1} (Sternal and Marks 1987). Bi- and triheteronuclear complexes of uranium and group VIB metals were also prepared (Dormond and Moise 1985) according to the reactions:

$$Cp_3UCl + Na[M(CO)_3Cp'] \rightarrow Cp_3U[OCM(CO)_2Cp'] + NaCl,$$

where M = Mo, W; Cp′ = C_5H_5 or C_5Me_5.

$$Cp_2U(NEt_2)_2 + 2H[Mo(CO)_3Cp] \rightarrow Cp_2U[OCMo(CO)_2Cp]_2 + 2HNEt_2.$$

The complexes show low CO stretching frequencies typical of isocarbonyl linkages between Mo or W and uranium.

Deprotonated metalla-β diphosphinites of the type $M[(PR_2O)_2]$ (R = alkyl, aryl or alkoxy) may act as bidentate ligands toward another metal ion. An unusual pentanuclear coordination complex $U\{Ni[P(O)(OMe)_2]_2Cp\}_4$ is obtained from $\{Ni[P(O)(OMe)_2]_2Cp\}NH_4$ and UCl_4 in THF (Paine et al. 1982). Its structure determined by X-ray diffraction, shows a central uranium surrounded by four $\{Ni[P(O)(OMe)_2]_2\}^-$ ligands η^2-bonded via phosphoryl oxygen atoms in a square antiprismatic arrangement without significant interactions between the metal ions. Polynuclear species such as $Cp_2U[(O_2C_2CHPMe_2R)Fe_2Cp_2(CO)_2]_2$ (R = Me, C_6H_5; Cramer et al. 1983) show the ability of the uranium–carbon multiple bond to react and reduce coordinated carbon monoxide indicating their possible use for the catalytic reduction of CO. A possible mechanism for compound formation involves the insertion of a terminal carbon of $[CpFe(CO)_2]_2$ into the uranium carbon bond of $Cp_3U{=}CHPR$. The insertion of a terminal carbonyl of the $CpMn(CO)_3$ moiety in the uranium–carbon bond in $Cp_3U{=}CHPMe_2Ph$ (Cramer et al. 1984c) is shown in the structure of $Cp(OC)_3MnC(OUCp_3){=}CHPMe_2Ph$.

The geometry around uranium is as usual, but the U–O bond distance is short 2.13(1) Å, with a large U–O–C angle 160(1)° in line with a multiple, U–O bond character. A further example of an insertion product of a $W(CO)_6$ molecule in $Cp_3U{=}CHPPh_2Me$ (Cramer et al. 1986) is the complex $(OC)_5WC(OUCp_3){=}CHPPh_2Me$ where the coordinated carbon monoxide is converted to the enolate of an aldehyde and involves cleavage of the original W–C bond:

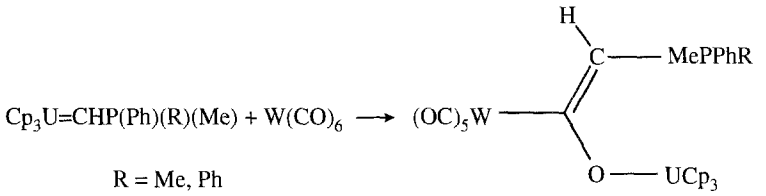

Its structural parameters are analogous to those reported for the Mn derivative. By heating the complex to 90°C in THF solution for 48 h a new product was produced, where an unusual metal migration is present, with a different type of carbonyl activation:

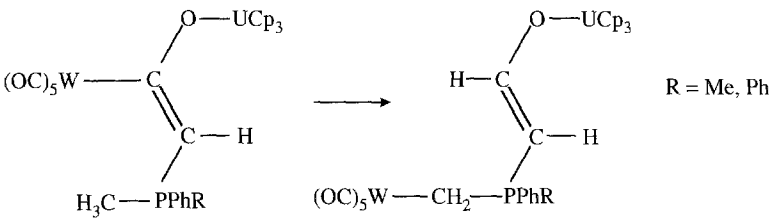

This reaction is characteristic only of the W derivative. The X-ray crystal structure of $Cp_3UOCH{=}CHPPh_2CH_2W(CO)_5$ confirms the scheme formulation.

The oxygen affinity of actinides is still used for the activation of small molecules (Cramer et al. 1990). The reaction of $CpCo(CO)_2$ with $Cp_3U{=}CHPMeRPh$ (R = Ph or Me) is the insertion of a terminal carbonyl in to the U=C bond. The cobalt derivative represents a further example of M–C cleavage and the first of C–P cleavage as demonstrated by the crystal structure of $Cp(OC)CoC(OUCp_3){=}CHPMe_2Ph$ (fig. 48).

The phosphido ligands provide stable bridge anchors for bimetallic units in the complex $Cp^*_2Th(\mu\text{-}PPh_2)_2Ni(CO)_2$ (Ritchey et al. 1985) in addition to bonding interaction between the thorium and nickel atoms as shown by the X-ray diffraction results. The Th–Ni distance of 3.206(2) Å is considered as a donor–acceptor bond from nickel(0) to the electron deficient Th^{IV} center. Replacement of the $Ni(CO)_2$ fragment with an electron-rich transition-metal donor is made with the preparation (Hay et al. 1986) of the red-brown, air sensitive $Cp^*_2Th(\mu\text{-}PPh_2)_2PtPMe_3$:

$$Cp^*_2Th(PPh_2)_2 + Pt(COD)_2 + PMe_3 \xrightarrow{toluene} Cp^*_2Th(\mu\text{-}PPh_2)_2PtPMe_3 + 2COD,$$

where COD = 1,5-cyclooctadiene.

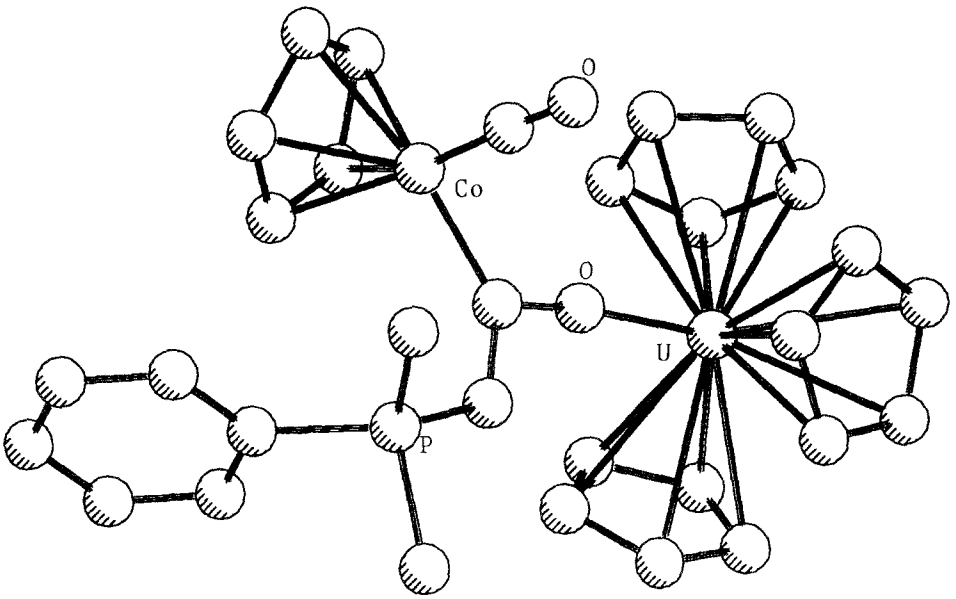

Fig. 48. Crystal structure of [Cp(OC)CoC(OUCp$_3$)=CHPMe$_2$Ph] (Cramer et al. 1990).

The ^{195}Pt–^{31}P coupling constants in the ^{31}P NMR spectrum 25°C toluene-d_8 of 2459 Hz (μ-PPh$_2$) and 2556 Hz (PMe$_3$) are taken as an indication of four coordinate platinum(0). The X-ray diffraction study gave the Th–Pt distance of 2.984(1) Å which was interpreted as a direct thorium platinum bond. Theoretical calculations suggest that Th–Pt bond can be regarded as a formal donor–acceptor or dative bond from the "filled" d^{10} shell of Pt into the "empty" d shell of Th.

The first complex with "direct, unsupported" actinide to transition metal bond is $Cp_2^*ThRu(Cp)(CO)_2$ (Sternal et al. 1985) obtained by reacting $Cp_2^*ThX_2$ (X=Cl, I) with $CpRu(CO)_2Na$:

$$Cp_2^*ThX_2 + CpRu(CO)_2Na \rightarrow Cp_2^*Th(X)RuCp(CO)_2 + NaX,$$

The X-ray structure determination of the iodine derivative shows a Th–Ru bond of 3.0277(6) Å comparable to the observed distances of 2.87–3.24 Å in Th–Ru intermetallics. Spectroscopic results indicate a similar structure for the chlorine derivative.

Molecular orbital calculations on the Th–Ni interaction in $Cp_2Th(\mu\text{-}Ph_2)_2Ni(CO)_2$ have been published (Ortiz 1986). The bonding in the closely related $Cp_2ITh\text{-}RuCp(CO)_2$ has been interpreted by molecular orbital calculations in terms of electron-pair donation from a Ru^0 fragment to a $d^0f^0Th^{IV}$ atom (Bursten and Novo-Gradac 1987).

New types of actinide–organotransition metal molecules with μ-methylene can be obtained (Smith et al. 1987) according to the equation

$Cp^*_2Th(CH_2CMe_2CH_2) + (1,2\text{-}R'_2C_5H_3)_2MMe_2 \xrightarrow{\text{Hexane}}$ + CMe_4

M = Zr, R' = H
M = Hf, R' = H
M = Zr, R' = Me

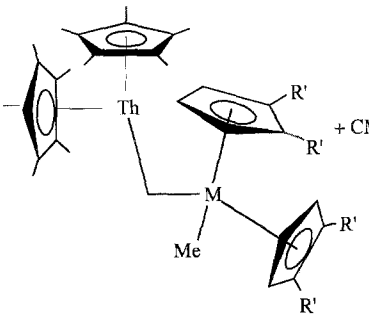

The structural formulation is supported by NMR spectroscopy, mass spectroscopy and X-ray diffraction analysis. The $Cp^*_2Th(\mu\text{-}CH_2)(\mu\text{-}1\text{-}\eta^1\text{:}\eta^5\text{-}3,4\text{-}Me_2C_5H_2)Zr(1,2\text{-}Me_2C_5H_3)$-Me molecule consists of two "bent metallocene" units connected *via* shared methylene and Cp ligands. The Th–Zr distance of 3.727 Å represents a non-bonding metal–metal interaction. The Th–C methylene distance of 2.377(8) Å has a multiple bond character. The NMR variable temperature spectra show an upfield displacement and a small $^1J_{C-H}$ (85–95Hz) of the second methylene resonance suggesting an "agostic interaction".

The first example of a U–Sn bond was found in the complex Cp_3USnPh_3 (Porchia et al. 1986) obtained according to the equation

$$Cp_3UNEt_2 + HSnPh_3 \rightarrow Cp_3USnPh_3 + HNEt_2.$$

The main feature is the U–Sn bond length of 3.166 Å.

A novel oxo-centered trimetal cluster of two uraniums and one magnesium: $\{Cp^*U[\mu\text{-}(CH_2)P(Ph)_2(CH_2)_2]\}_2Mg[CH_2PMePh_2]_2(\mu^3\text{-}O)(\mu^2\text{-}O)(\mu^2\text{-}Cl)_2$ has been grown in a NMR tube, containing Cp^*UCl_2 (synthesized with a Grignard reagent) and $Li(CH_2)(CH_2)Ph_2$ in THF. Its characterization has been made by X-ray diffraction analysis on the only single crystal obtained (Cramer et al. 1988c) (fig. 49). The molecule is chiral due to the orientation of the phosphoylide groups bound to Mg. The coordination around uranium is an irregular octahedron formed by Cp*, chloride, the μ^2-oxide, two $\text{-}CH_2PPh_2CH_2\text{-}$ ligands which bridge the two uranium atoms and the μ^3-oxide which centers the three metals. No metal–metal bonding interactions are present in the structure.

Polyoxoanion-supported organoactinides have been prepared and characterized by reaction of $MW_5O_{19}^{3-}$ (M = Nb, Ta) anions with Cp_3AnCl (An = Th, U). The X-ray crystal structure of the tetrabutyl ammonium salt $[(n\text{-}C_4H_9)_4N]_5[Cp_3U(NbW_5O_{19})_2]$ (Day et al. 1985b), shows for the anion a trigonal bipyramidal coordination geometry, the two axial ligands O-NbW_5O_{18} have U–$O_{av.}$ bond distance of 2.36 Å. The same coordination geometry around the An ions have been deduced for all four compounds from IR and ^{17}O-NMR) spectra.

The polyoxoanion $[ClTiW_5O_{18}]^{3-}$ reacts with Cp_3UCl affording the unexpected $\{[Cp_2U]_2(\mu\text{-}k^2O\text{-}TiW_5O_{19})_2\}^{4-}$ anion, isolated as the CH_3CN solvate of its $(n\text{-}C_4H_9)_4N^+$

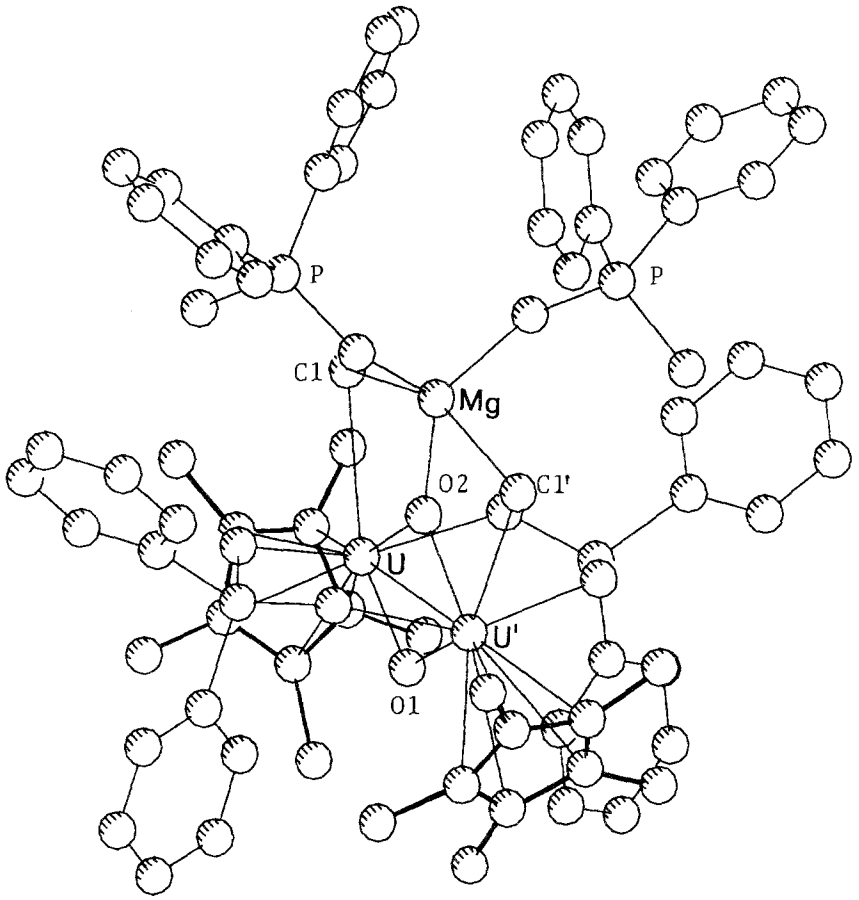

Fig. 49. Crystal structure of $\{Cp^*U[\mu\text{-}(CH_2)P(Ph)_2(CH_2)]\}_2Mg[CH_2PMePh_2]_2(\mu^3\text{-}O)(\mu^2\text{-}O)(\mu^2\text{-}Cl)_2$ (Cramer et al. 1988c).

salt (Day et al. 1985a). The dimeric structure shows two $[TiW_5O_{19}]^{4-}$ anions bridged by two "bent sandwich" $[Cp_2U]^{2+}$ units with a formal nine coordination to the uranium(IV). The stability of the complex has been related to the steric bulk of the polyoxoanion blocking the U^{IV} coordination sphere.

A heterobimetallic derivative $[(Me_4Fv)_2FeThCl_2]$, unique for actinide chemistry, has been recently synthesized (Scott and Hitchcock 1995) with the fulvalene (Fv) ligand (Me_4Fv = 1,2,3,4-tetramethylfulvalenediyl). In the X-ray structure (fig. 50) of the red crystals the two Me_4Fv ligands are bridging the Fe and $ThCl_2$ centers with an angle Cg–Th–Cg of 138.5° in the expected range, while the Th–C_{Cp} bond lengths (av. 2.79 Å) and Th–Cl of 2.63 Å are at the lower limit when compared with those of the $Cp^*_2ThX_2$ derivatives. The complex undergoes a quasi reversible one-electron oxidation at 0.15 V vs. to the ferrocenium/ferrocene couple.

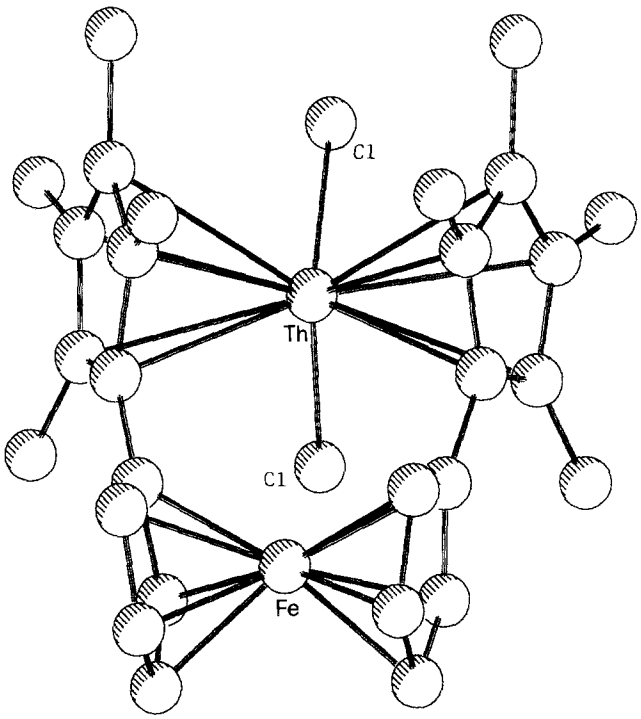

Fig. 50. Crystal structure of $[(Me_4Fv)_2FeThCl_2]$ (Scott and Hitchcock 1995).

2.6. *Other ligands*

2.6.1. *Arene complexes (lanthanides and actinides)*

The chemistry of the arene complexes of the f-block elements is relatively new and only a limited number of compounds have been reported. The first f-block–arene complex to be synthesized is the U^{III} complex $U(\eta^6\text{-}C_6H_6)(AlCl_4)_3$ (Cesari et al. 1971) which was obtained from UCl_4, $AlCl_3$ and Al powder in benzene. A somewhat similar synthesis was employed for the first arene–lanthanide complex $Sm(\eta^6\text{-}C_6Me_6)(AlCl_4)_3 \cdot 1.5$ toluene (Cotton and Schwotzer 1986, 1987) prepared from $SmCl_3$, $AlCl_3$ and hexamethylbenzene in refluxing toluene in the presence of Al foil. A variety of other lanthanide and actinide complexes was similarly obtained from the metal chloride, $AlCl_3$ and the appropriate aromatic hydrocarbon, which often acts also as the solvent. An interesting practical aspect of this type of arylation reaction is the solubilization of f metal halides in aromatic hydrocarbons. Metal vapor syntheses have been successfully used to obtain an interesting series of zero valent lanthanide complexes of $1,3,5\text{-}C_6H_5\text{-}^tBu_3$ as the sandwich compounds $[Ln(0)(\eta^6\text{-}^tBu_3C_6H_3)_2]$. This procedure was successful for Ln = Nd, Tb, Dy, Ho, Er and Lu; for Ln = Gd, La, Pr, Sm, thermally unstable complexes were obtained, while for Ln = Ce, Eu, Tm and Yb, no isolable compounds were obtained (Brennan et al. 1987b, Anderson et al. 1989). This pattern was rationalized in terms of

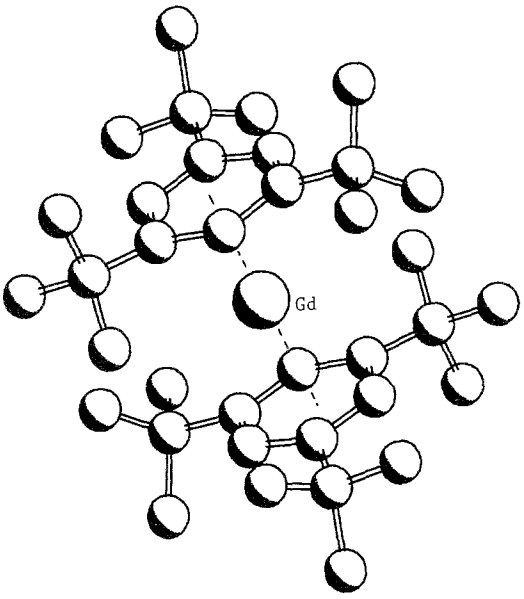

Fig. 51. Crystal structure of $[(\eta^6\text{-}C_6H_3{}^tBu_3)_2\text{-}Gd]$ (Brennan et al. 1987b).

a bonding model in which the promotion energy from $f^n s^2$ to $f^{n-1}d^1s^2$ is an important factor. Where this energy is large, stable complexes are not formed. The X-ray structure of $[Gd(\eta^6\text{-}{}^tBu_3C_6H_3)_2]$ (fig. 51) represents a unique example of an arene lanthanide complex with a sandwich structure (Gd–$C_{(\eta^6)}$ 2.630(4) Å; Brennan et al. 1987b). With scandium, in addition to the scandium(0) sandwich compound, a scandium(II) derivative is unexpectedly obtained $[Sc(\eta\text{-}{}^tBu_3C_6H_3)\{\eta^6,\eta^1\text{-}{}^tBu_2(CMe_2CH_2)C_6H_3\}H]$ (Cloke et al. 1991b). The low stability of compounds of early lanthanides, despite their favorable electronic properties, is attributed to the inability of the $^tBu_3C_6H_3$ ligand to sterically saturate these larger ions.

In all f-block arene complexes for which the X-ray structures are known, the aromatic rings behave in the usual manner as η^6 ligands. Following the convention of considering the center of the C6 ring as a single coordination site, the most of the arene–lanthanide(III) complexes are seven coordinate with pentagonal bipyramidal geometry. Lower coordination numbers are observed when the ligands are very bulky or the metal is in a lower oxidation state. The complexes of formula $Sm(\eta^6\text{-}C_6Me_6)(AlCl_4)_3\cdot 1.5$toluene, $Sm(\eta^6\text{-}m\text{-}Me_2C_6H_4)(AlCl_4)_3$ (Fan et al. 1989b).

$Ln(\eta^6\text{-}C_6H_6)(AlCl_4)_3\cdot$benzene (Ln = La, Nd, Sm; Fan et al. 1989a) all have an essentially pentagonal bipyramidal geometry as shown in scheme 22.

In the Eu^{II} tetramer $[Eu(C_6Me_6)(AlCl_4)_2]_4$ (Liang et al. 1991) the centrosymmetric structure is characterized by two bridging and one chelating $AlCl_4^-$ moiety around each Eu. The $(C_6Me_6)\eta^6$-bonded ligand completes the metal coordination sphere. The Eu–C bond distance averages 2.999(23) Å. For this complex a possible involvement of C_6Me_6 ligand in the Eu^{III}–Eu^{II} redox process was suggested on the basis of GSMS spectra results. The

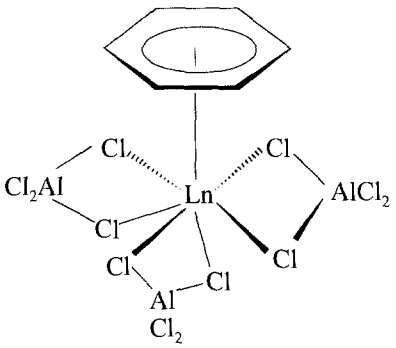

Scheme 22.

effect of bulky arene ligands is evident in Yb(*o*-2,6-$Ph_2C_6H_3)_3$ (Deacon et al. 1990) where there is an intramolecular Yb···π arene interaction of 2.978(6) Å from one of the phenyl substituents of the aryloxide in this low coordinate complex.

Recently, a fully characterized La naphthalene derivative (μ-η^4:η^4-$C_{10}H_8$)[$LaI_2(THF)_3$]$_2$ has been reported (Fedushkin et al. 1995) where the two $LaI_2(THF)_3$ moieties share the bridging naphthalene anion with a molecular geometry of the same type as (μ-η^4:η^4PhCH=CH–CH=CHPh)[$LaI_2(THF)_3$]$_2$ (Mashima et al. 1994b).

Arene actinide complexes, so far limited to uranium, show a greater variety of structures than the arene lanthanide species and are often di- or polynuclear. Examples of mononuclear species are (C_6H_6)U($AlCl_4$)$_3$ (Cesari et al. 1971) and the hexamethyl benzene analog. The compounds are isostructural. The uranium is bonded to a hexahapto benzene ligand and to three bidentate $AlCl_4$ moieties, resulting in a pentagonal bipyramidal coordination geometry. There is no evidence of a particularly strong π-bonding interaction. They are also isostructural with the Sm derivative previously mentioned (Cotton and Schwotzer 1986, 1987). The dimensions allowing for the difference between the ionic radii of uranium and samarium, are comparable, suggesting that the acceptor orbitals are comparable in the two series and that the f orbitals are not substantially involved in arene bonding.

(C_6Me_6)U(BH_4)$_3$ has been prepared according to (Baudry et al. 1989)

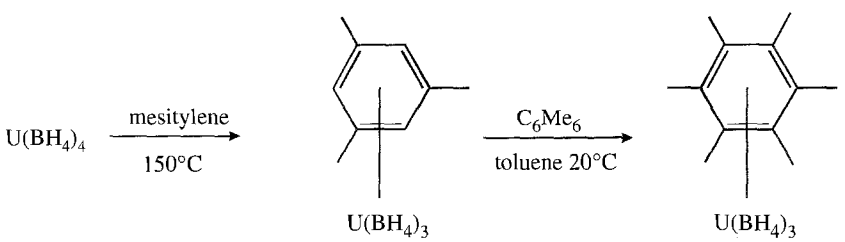

(I) (II) (III)

The ^{1}H NMR spectrum of (**II**) exhibits a large resonance at 150 ppm corresponding to the borohydride ligands. Its X-ray structure shows a distorted tetrahedral arrangement of the

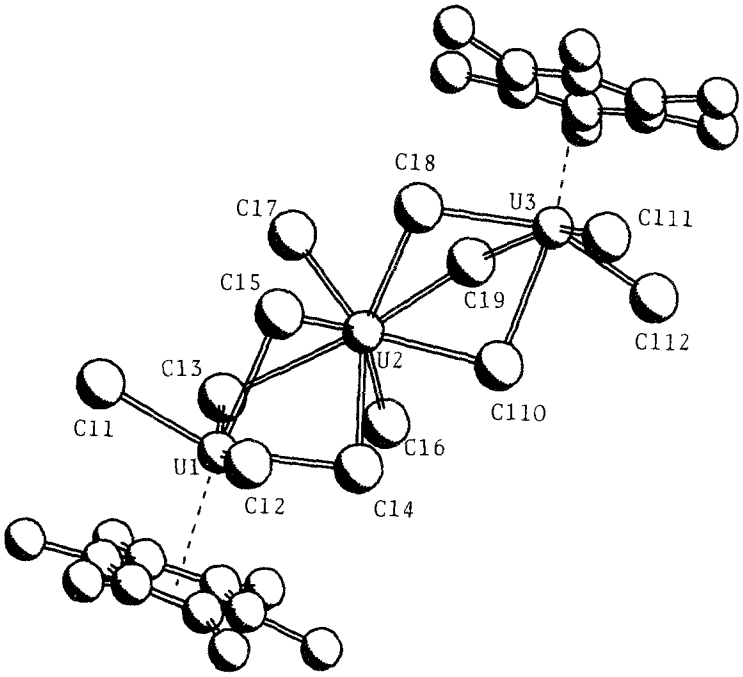

Fig. 52. Crystal structure of $\{[U(C_6Me_6)Cl_2(\mu\text{-}Cl)_3]_2UCl_2\}$ (Campbell et al. 1986).

ligands around uranium with the planar C_6Me_6 moiety parallel to the plane of the three boron atoms. U–B of 2.57(3) Å is characteristic for tridentate BH_4 ligands (U–C average 2.93 Å).

The dinuclear complex cation $[(C_6Me_6)UCl_2]_2(\mu\text{-}Cl)_3^+$ in $U_2Cl_7(C_6Me_6)AlCl_4$ (Cotton and Schwotzer 1985) consists of a face sharing bisoctahedron with the η^6-C_6Me_6 ligand occupying one octahedral coordination site. The tetrahedral $AlCl_4^-$ anion balances the positive charge. The trinuclear complex $\{[(C_6Me_6)UCl_2(\mu\text{-}Cl)_3]_2UCl_2\}$ (Campbell et al. 1986) can be derived from the dinuclear one by formal insertion of a UCl_5 sub unit into the $(\mu\text{-}Cl)_3$ bridge (fig. 52). The central uranium is at the center of a distorted square antiprism defined by the two terminal and the six bridging chlorine which connect, on opposite sides, the two octahedrally coordinated $(C_6Me_6)UCl_2$ moieties. This leads to a symmetrical bent chain of uranium atoms with an U(1)–U(2)–U(3) angle of 142.2° and a U···U distance of 4.033(3) Å. Its solid state ^{13}C NMR spectrum shows a temperature-dependent behavior.

The structure of another trimeric compound $[U_3(\mu^3\text{-}Cl)_2(\mu^2\text{-}Cl)_3(\mu^1,\eta^2\text{-}AlCl_4)_3(\eta^6\text{-}C_6Me_6)_3][AlCl_4]$ (Cotton et al. 1986) has been also determined. An unprecedented structure (Sluys et al. 1988) of an arene U^{III} complex is shown by $[U(O\text{-}2,6\text{-}{}^iPr_2C_6H_3)_3]_2$ having an unusual dimerization of the $[U(O\text{-}2,6\text{-}{}^iPr_2C_6H_3)_3]$ moiety via arene (fig. 53). Each uranium is bonded to two terminal phenoxide oxygens to one bridging phenoxide and to an arene ring, of a phenoxide coming from its centrosymmetric actinide partner in

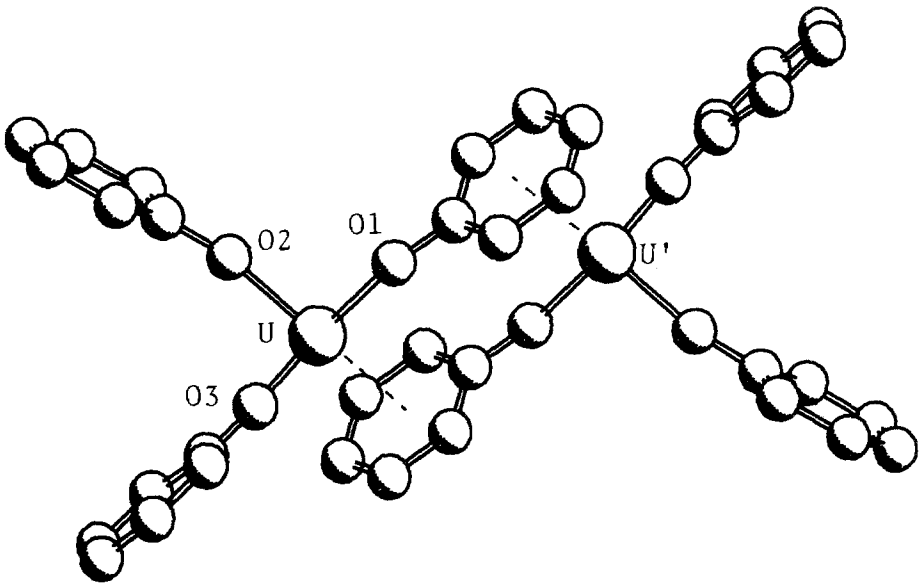

Fig. 53. Crystal structure of $[U(O\text{-}2,6^{i}Pr_2C_6H_3)_3]_2$ (Sluys et al. 1988) (isopropyls omitted for clarity).

the dimer with an U–U separation of 5.345 Å. The short U–O distances (2.13 and 2.21 Å) and the large U–O–C angles (157 and 166°) could be indicative of π-bonding to the metal ion.

2.6.2. *Miscellaneous*

2.6.2.1. *Lanthanides.* Reaction of $LuCl_3$ with (2,4-dimethylpentadienyl)potassium in THF yields as a major product $(\eta^5\text{-}Me_2C_5H_5)_2Lu(\eta^3\text{-}Me_2C_5H_5)$ (Schumann and Dietrich 1991). Its structure indicates that one of the ligands is bonded η^3 to Lu with Lu–$C_{av.}$ 2.59(1) Å, while the other two are η^5-bonded with Lu–$C_{av.}$ of 2.645 Å. The same reaction produces as a secondary product $(\eta^5\text{-}Me_2C_5H_5)Lu(\eta^5\text{:}\eta^3 MeC_5H_5CH_2CH_2\text{-}CHMeC_3H_3Me)$ (Zielinski et al. 1995). The X-ray structure shows the presence around the lutetium ion of one 2,4-Me_2-pentadienyl η^5-bonded and one η^5:η^3 chelate ligand resulting from the "end-to-end" fusion of two 2,4-Me_2-pentadienyl ligands (fig. 54) with the same trend of Lu to carbon bond distances as in the previously quoted derivative.

The introduction of a heteroatom in the five membered ring ligands like C_4Me_4E (E = P, As) allowed the synthesis of $(C_4Me_4E)_2Ln(THF)_2$ (Ln = Yb, Sm; Nief et al. 1993, Nief and Mathey 1991). The X-ray structure of $(2,5\text{-}Ph_2C_4H_2P)_2Yb(THF)_2$ (Nief et al. 1993) is typical of the corresponding Cp* metallocenes. An example of a η^5-bonded azacyclopentadienyl ligand is represented by $(2,5\text{-}^{t}Bu_2C_4H_2N)YbCl_2(THF)$ obtained by reaction between $YbCl_3(THF)$ and $Na(NC_4H^{t}_2Bu_2\text{-}2,5)$ (Schumann et al. 1995c).

The interest in organometallic carboranes is due to their close electronic similarity with the cyclopentadienide ligand as shown (Hawthorne et al. 1988) in a study of the frontier orbital of the nido-carborane $(C_2R_2B_9H_9)^{-2}$ (R = H or a cage carbon) and of the

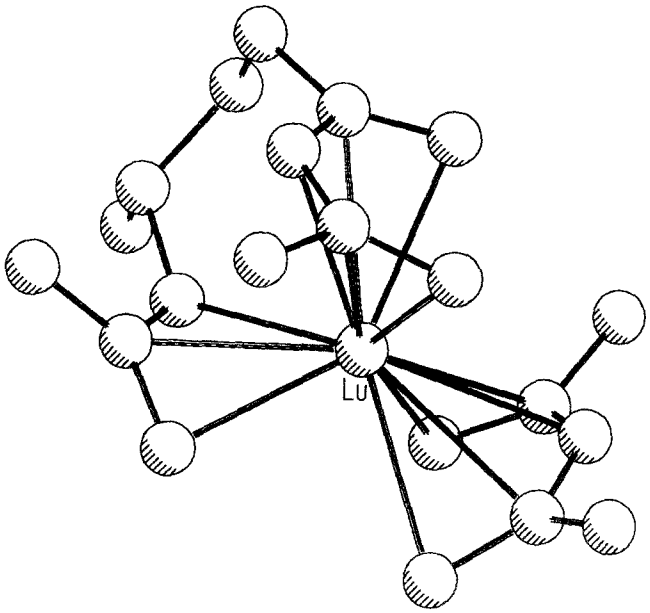

Fig. 54. Crystal structure of $(\eta^5\text{-}Me_2C_5H_5)Lu(\eta^5{:}\eta^3\text{-}MeC_5H_5(CH_2)_2CHMeC_3H_3Me)$ (Zielinski et al. 1995).

(C_5R_5) ion. There are a few reports of lanthanide complexes with carborane, sandwich and halfsandwich complexes of Sm, Eu, Gd, Yb (Zhang et al. 1995).

The first X-ray analysis of the SmTHF adduct (Manning et al. 1988) $[(Ph_3P)_2N]$-$[(\eta^5C_2B_9H_{11})_2Sm(THF)_2]$ is shown in fig. 55. Two other anions of the Gd derivatives $Na[(C_2B_9H_{11})_2Gd](THF)$ and $[Bu_4N][(C_2B_9H_{11})_2Gd](THF)$ have been characterized only by spectral data (Lebedev et al. 1988). The X-ray structures of two isostructural trinuclear carborane clusters (Ln = Gd, Oki et al. 1992; Tb, Zhang et al. 1995) consists of three closo-terbacarboranes, three cage bridged Li(THF) units and three Tb-bridged chlorolithiocarborane that form a tricapped trigonal prism with Tb atoms in the capping position $\{\mu^3\text{-}OMe\text{-}[\mu\text{-}1\text{-}Li\text{-}2,3(SiMe_3)_2\text{-}2,3\text{-}C_2B_4H_4]_3\}\{\mu^3\text{-}O\text{-}[\mu\text{-}1\text{-}Tb\text{-}2,3\text{-}(SiMe_3)_2\text{-}2,3\text{-}C_2B_4H_4]_3\}\text{-}[Li(THF)_3]\cdot C_6H_6$. New mixed $2,3\text{-}C_2B_4$ and $2,4\text{-}C_2B_4Er^{III}$ carborane bent-sandwich complexes have been recently synthesized (Hosmane et al. 1995) of the type shown in scheme 23.

With the $(C_2B_9H_{11})^{2-}$ ligand and bivalent lanthanides, half sandwich compounds have been obtained while bent sandwich structures are present in the trivalent lanthanides (Manning et al. 1988, 1991) similar to the uranacarborane. With the larger $C_2B_{10}H_{12}$ ligand, the type of the complex is related to the metal:carborane molar ratios used in the synthesis; (1:1) gives polymeric structures for Eu and Sm $[Ln(C_2B_{10}H_{12})(THF)_3]_8$ while the bent sandwich Eu derivative $[NEt_4]_2[1,1\text{-}(THF)_2\text{-}commo\text{-}1,1'\text{-}Eu(1,2,4\text{-}EuC_2B_{10}H_{12})_2]$ is obtained with excess ligand (Khattar et al. 1991, 1992).

With a ligand to $LnCl_3$ (2:1) ratio the paramagnetic isostructural sandwich species $\{[\eta^5\text{-}1\text{-}Ln\text{-}2,3\text{-}(SiMe_3)_2\text{-}2,3\text{-}C_2B_4H_4]_3[(\mu^2\text{-}1\text{-}Li\text{-}2,3\text{-}(SiMe_3)_2\text{-}2,3\text{-}C_2B_4H_4)_3(\mu^3\text{-}OMe)]\text{-}$

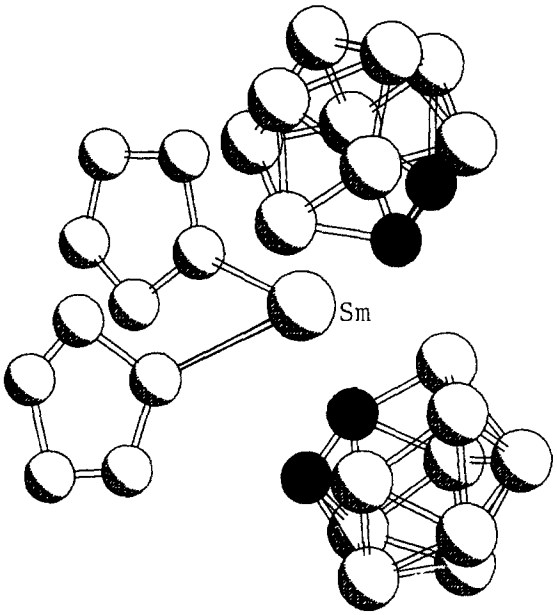

Fig. 55. Crystal structure of the anion of $[(Ph_3P)_2N][(C_2B_9H_{11})_2Sm(THF)_2]$ (Manning et al. 1988).

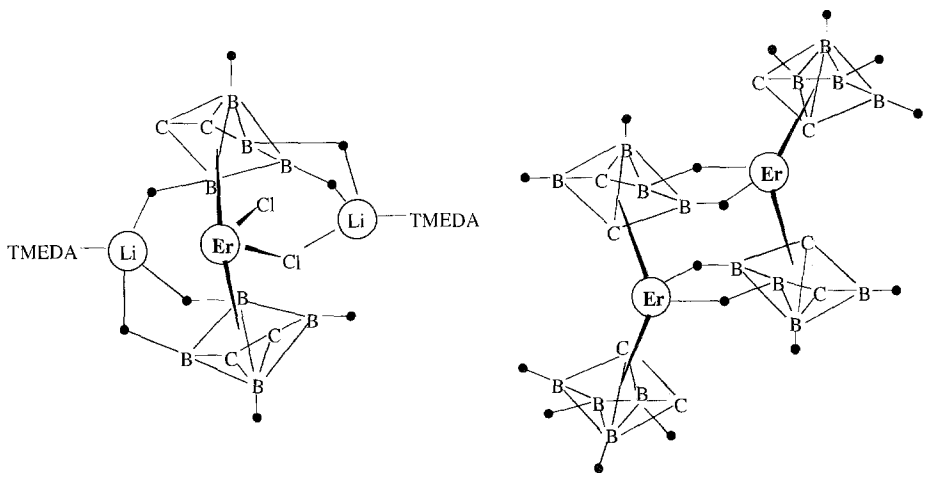

Scheme 23.

$[\mu^2\text{-Li(THF)}]_3(\mu^3\text{-O})\}$ (Ln = Sm, Gd, Tb, Dy and Ho; Hosmane et al. 1996) have been synthesized and were structurally characterized by X-ray analysis and the Sm also by NMR spectroscopy.

2.6.2.2. *Actinides.* Unique examples of cycloheptatrienyl complexes with f elements are reported (Arliguie et al. 1994b) with the anions $[(X_3U)_2(\mu\text{-}C_7H_7)]^-$ ($X = NEt_2$, BH_4), synthesized from UX_4 and $K[C_7H_9]$. An inverse sandwich structure has been

detected, by X-ray analysis, in the anion of the $[U(BH_4)(THF)_5][\{(BH_4)_3U\}_2(\mu\text{-}\eta^7\text{-}C_7H_7)]$ derivative. The cyclic ligand is planar and perpendicular to the U-(μ-$\eta^7C_7H_7$)-U axis with a U···U separation of 4.263(8) Å. This topology is reminiscent of the inverse sandwich structure of $[Sm\{M(SiMe_3)_2\}]_2(\mu\text{-COT})$ (Schumann et al. 1993b). The same authors (Arliguie et al. 1995) report for the cycloheptatrienyl ligand, an "uranocene-type" structure in the complex $[K(18\text{-crown-6})][U(\eta\text{-}C_7H_7)_2]$. The two rings are in a staggered conformation with U–C average distance of 2.53(2) Å, this is shorter than that in the bridged anion previously reported (2.69(2) Å) and is ascribed to an increased metal valency. The cycloheptatrienyl ligand is formally described as $C_7H_7^{3-}$ anion, consequently the formal U oxidation state is (V) (Green et al. 1994).

The use of the steric mimic ligand $\eta\text{-}C_4Me_4P(tmp)$ of the C_5Me_5 ligand has allowed (Gradoz et al. 1992a) the synthesis of $U(tmp)_3X$ (X = Cl, H, Me, O^{i}Pr) derivatives. The crystal structure of $U(tmp)_3Cl$ shows the three phospholyl ligands pentahapto bonded to the uranium with U–C_{ring} distances varying from 2.82(1) to 2.97(1) Å. The ring centroids and the uranium ion are almost coplanar, minimizing the ligand repulsions (U–P is 2.927(4) Å and U–Cl 2.67(1) Å). Other phospholyl uranium complexes (Baudry et al. 1990b, Gradoz et al. 1992b) have been synthesized according to scheme 24. The X-ray structure of the monomer (**4**) shows the phospholyl ligand pentahapto bonded to uranium (confirming the ^{31}P NMR data) with short U–B distance 2.55 Å typical of tridentate BH_4 ligation. The crystal structure of the dimer (**2**) (Gradoz et al. 1994) represents the only example of a U^{III} phospholyl complex. The two BH_4 ligands are in the *cis*-position with respect to the U–P–U–P ring and possibly this configuration is maintained in solution.

3. Perspectives

In the last few years the interest in application of organoactinides has experienced some decline as compared to the worldwide interest during the 1950–1960's despite their very interesting reactivity and their possible use (mainly of U and Th) in industry.

Organoactinides have been widely used in organic synthesis and catalysis because the $Cp^*_2AnR_2$ complexes (An = Th, U; R = alkyl, H) are powerful catalysts for alkene hydrogenation and polymerization. The introduction of bulky substituents on the cyclopentadienyl ligands has permitted the synthesis of U^{III} and Th^{III} base-free derivatives. Reactions with organoamido functional groups resulted in the formation of complexes with uranium in the rare U^V oxidation state. These compounds are of potential relevance in ceramic processes. The synthesis of heterometallic hydride complexes with f element and d transition metals, plus a variety of alumino compounds, offer new perspectives in structural and reactivity patterns due to the presence of different metal centers. This suggests the validity of the approach to newly designed organoactinide and organolanthanide complexes with specific steric and electronic requirements.

The most important industrial applications involving organolanthanides, are in Ziegler–Natta polymerization of olefins and as reagents in stoichiometric organic synthesis. The

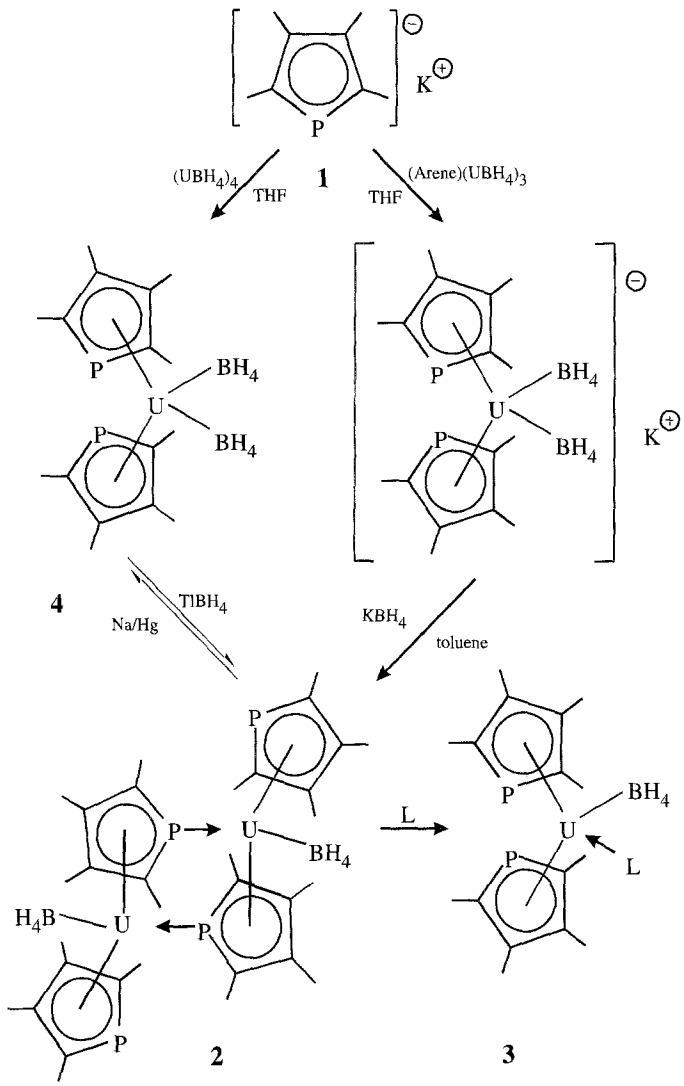

(L = THF, PPh_3O)

Scheme 24.

growing interest of organolanthanides as volatile precursors for MOCVD applications in the manufacture of semiconductors has its origin in the very interesting magnetic properties of the lanthanides, and suggest their use in many optoelectronic apparatus. A promising future could be foreseen for the enantiomerically pure organolanthanides in the enantioselective catalytic hydrogenation, alkylation and hydroamination of prochiral unsaturated systems.

Taking into account that the first commercial applications of lanthanide derivatives goes back to ca. 1980, and that to date there are over 80 well-defined industrial applications which reflect a continuously growing market, undoubtedly the future will see the chemistry of lanthanides and of organolanthanides as a center of interest both in academic and industrial research.

4. Acknowledgements

We are particularly grateful to Prof. M.R. Truter, Department of Chemistry, University College, London, UK, for helpful discussions and for editing the manuscript. We also thank Dr. F. Benetollo, ICTIMA-CNR, Padova, Italy, for valuable assistance.

References

Adam, M., E.T.K. Haupt and R.D. Fischer, 1990a, Bull. Magn. Reson. **12**, 101.

Adam, M., K. Yünlü and R.D. Fischer, 1990b, Organomet. Chem. **387**, C13.

Adam, M., G. Massarweh and R.D. Fischer, 1991, J. Organomet. Chem. **405**, C33.

Adam, M., C. Villiers, M. Ephritikhine, M. Lance, M. Nierlich and J. Vigner, 1993, J. Organomet. Chem. **445**, 99.

Ahmed, I., and K.W. Bagnall, 1984, J. Less-Common Met. **99**, 285.

Aitken, C., J.P. Barry, F. Gauvin, J.F. Harrod, A. Malek and D. Rousseau, 1989, Organometallics **8**, 1732.

Akhnoukh, T., J. Møller, K. Qiao, X.-Fu Li and R.D. Fischer, 1991, J. Organomet. Chem. **408**, 47.

Albrecht, I., E. Hahn, J. Pickardt and H. Schumann, 1985, Inorg. Chim. Acta **110**, 145.

Alcock, N.W., J.M. Brown and J.J. Pérez-Torrente, 1992, Tetrahedron Lett. **33**, 389.

Aleksanyam, V.T., G.K. Borisov, I.A. Garbuzova and G.G. Devyatykh, 1977, J. Organomet. Chem. **131**, 251.

Alvarez Jr, D., K.G. Caulton, W.J. Evans and J.W. Ziller, 1990, J. Am. Chem. Soc. **112**, 5674.

Amberger, H.D., and H. Schultze, 1987, Spectrochim. Acta **43A**, 1301.

Amberger, H.D., R.D. Fischer and K. Yünlü, 1986, Organomet. **5**, 2109.

Amberger, H.D., H. Reddmann, G. Shalimoff and N.M. Edelstein, 1987, Inorg. Chim. Acta **13**, 335.

Amberger, H.D., H. Reddmann and N. Edelstein, 1988, Inorg. Chim. Acta **141**, 313.

Amberger, H.D., H. Schultze, H. Reddmann, G.V. Shalimoff and N.M. Edelstein, 1989, J. Less-Common Met. **149**, 249.

Andersen, R.A., J.M. Boncella, C.J. Burns, R. Blom, A. Haaland and H.V. Volden, 1986, J. Organomet. Chem. **312**, C49.

Anderson, D.M., F.G.N. Cloke, P.A. Cox, N. Edelstein, J.C. Green, T. Pang, A.A. Sameh and G. Shalimoff, 1989, J. Chem. Soc. Chem. Commun., 53.

Arduini, A.L., J. Maliot, J. Takats, E. Ciliberto, I. Fragalà and P. Zanella, 1987, J. Organomet. Chem. **326**, 49.

Arliguie, T., D. Baudry, M. Ephritikhine, M. Nierlich, M. Lance and J. Vigner, 1992, J. Chem. Soc. Dalton Trans., 1019.

Arliguie, T., M. Ephritikhine, M. Lance, J. Vigner and M. Nierlich, 1994a, J. Organomet. Chem. **484**, 195.

Arliguie, T., M. Lance, M. Nierlich, J. Vigner and M. Ephritikhine, 1994b, J. Chem. Soc. Chem. Commun., 847.

Arliguie, T., M. Lance, M. Nierlich, J. Vigner and M. Ephritikhine, 1995, J. Chem. Soc. Chem. Commun., 183.

Arnaudet, L., P. Charpin, G. Folcher, M. Lance, M. Nierlich and D. Vigner, 1986, Organometallics **5**, 270.

Arney, D.S.J., and C.J. Burns, 1993, J. Am. Chem. Soc. **115**, 9840.

Arney, D.S.J., and C.J. Burns, 1995, J. Am. Chem. Soc. **117**, 9448.

Arney, D.S.J., C.J. Burns and D.C. Smith, 1992, J. Am. Chem. Soc. **114**, 10068.

Arnold, J., and C.G. Hoffman, 1990, J. Am. Chem. Soc. **112**, 8620.

Arnold, J., C.G. Hoffman, D.Y. Dawson and F. Hollander, 1993, Organometallics **12**, 3645.

Aslan, H., and R.D. Fischer, 1986, J. Organomet. Chem. **315**, C64.

Aslan, H., J. Forster, K. Yünlü and R.D. Fischer, 1988a, J. Organomet. Chem. **355**, 79.

Aslan, H., K. Yünlü, R.D. Fischer, G. Bombieri and F. Benetollo, 1988b, J. Organomet. Chem. **354**, 63.

Atwood, J.L., J.H. Burns and P.G. Laubereau, 1973, J. Am. Chem. Soc. **95**, 1830.

Atwood, J.L., W.E. Hunter, A.L. Wayda and W.J. Evans, 1981, Inorg. Chem. **20**, 4115.

Avdeef, A., K.N. Raymond, K.O. Hodgson and A. Zalkin, 1972, Inorg. Chem. **11**, 1083.

Bagnall, K.W., J. Edwards and A.C. Tempest, 1978, J. Chem. Soc. Dalton Trans., 295.

Bagnall, K.W., A. Beheshti, F. Heatley and A.C. Tempest, 1979, J. Less-Common Met. **64**, 267.

Bagnall, K.W., M.J. Plews, D. Brown, R.D. Fischer, E. Klahne, G.W. Langraf and G.R. Sienel, 1982, J. Chem. Soc. Dalton Trans., 1999.

Bagnall, K.W., M.J. Plews and D. Brown, 1983, J. Less-Common Met. **90**, 29.

Bagnall, K.W., F. Benetollo, G. Bombieri and G. De Paoli, 1984, J. Chem. Soc. Dalton Trans., 67.

Bagnall, K.W., G.F. Payne, N.W. Alcock, D.J. Flanders and D. Brown, 1986a, J. Chem. Soc. Dalton Trans., 783.

Bagnall, K.W., G.F. Payne and D. Brown, 1986b, J. Less-Common Met. **116**, 333.

Baker, E.C., K.N. Raymond, T.J. Marks and W.A. Wachter, 1974, J. Am. Chem. Soc. **96**, 7586.

Ballard, D.G.H., A. Courties, J. Holton, J. McMeeking and R. Pearce, 1978, J. Chem. Soc. Chem. Commun., 994.

Barnhart, D.M., R.J. Butcher, D.L. Clarck, J.C. Gordon, J.G. Watkin and B.D. Zwick, 1995, New J. Chem. **19**, 503.

Baudin, C., P. Charpin, M. Ephritikhine, M. Lance, M. Nierlich and J. Vigner, 1988, J. Organomet. Chem. **345**, 263.

Baudry, D., and M. Ephritikhine, 1986, J. Organomet. Chem. **311**, 189.

Baudry, D., and M. Ephritikhine, 1988, J. Organomet. Chem. **349**, 123.

Baudry, D., P. Dorion and M. Ephritikhine, 1988a, J. Organomet. Chem. **356**, 165.

Baudry, D., E. Bulot and M. Ephritikhine, 1988b, J. Chem. Soc. Chem. Commun., 1369.

Baudry, D., E. Bulot, P. Charpin, M. Ephritikhine, M. Lance, M. Nierlich and J. Vigner, 1989, J. Organomet. Chem. **371**, 155.

Baudry, D., E. Bulot, M. Ephritikhine, M. Nierlich, M. Lance and J. Vigner, 1990a, J. Organomet. Chem. **388**, 279.

Baudry, D., M. Ephritikhine, F. Nief, L. Ricard and F. Mathey, 1990b, Angew. Chem. Int. Ed. Engl. **29**, 1485.

Bazan, G.C., W.P. Schaefer and J.E. Bercaw, 1993, Organometallics **12**, 2126.

Beckman, W., and J. Goffard, 1988, J. Lanth. Act. Res. **2**, 187.

Beeckman, W., J. Goffart, J. Rebizant and M.R. Spirlet, 1986, J. Organomet. Chem. **307**, 23.

Beletskaya, I.P., A.Z. Voskoboynikov, E.B. Chuklanova, N.L. Kimillova, A.K. Shestakova, I.N. Pershina, A.I. Gusev and G.K.I. Magomedov, 1993a, J. Am. Chem. Soc. **115**, 3156.

Beletskaya, I.P., A.Z. Voskoboynikov, A.K. Shestakova, A.I. Yanovsky, G.K. Fukin, L.N. Zacharov, Y.T. Struchkov and H. Schumann, 1993b, J. Organomet. Chem. **468**, 121.

Beletskaya, I.P., A.Z. Voskoboynikov, A.K. Shestakova and H. Schumann, 1993c, J. Organomet. Chem. **463**, C1.

Bel'skii, V.K., B.H. Bulychev, A.B. Erofeev and G.L. Soloveichik, 1984a, J. Organomet. Chem. **268**, 107.

Bel'skii, V.K., A.B. Erofeev, B.M. Bulychev and G.L. Soloveichik, 1984b, J. Organomet. Chem. **365**, 123.

Bel'skii, V.K., Yu.K. Gun'ko, B.M. Bulychev, A.I. Sizov and G.L. Soloveichik, 1990, J. Organomet. Chem. **390**, 35.

Bel'skii, V.K., Yu.K. Gun'ko, E.B. Lobkovskii, B.M. Bulychev and G.L. Soloveichik, 1991a, Organomet. Chem. USSR **4**, 202.

Bel'skii, V.K., Yu.K. Gun'ko, B.M. Bulychev and G.L. Soloveichik, 1991b, J. Organomet. Chem. **420**, 43.

Bel'skii, V.K., Yu.K. Gun'ko, B.M. Bulychev and G.L. Soloveichik, 1991c, J. Organomet. Chem. **419**, 299.

Bel'skii, V.K., Yu.K. Gun'ko, G.D. Soloveichik and M.B. Bulychev, 1991d, Organomet. Chem. USSR **4**, 281.

Benetollo, F., G. Bombieri, C.B. Castellani, W. Jahn and R.D. Fischer, 1984, Inorg. Chim. Acta **95**, L7.

Berg, D.J., R.A. Andersen and A. Zalkin, 1988, Organometallics **7**, 1858.

Berg, D.J., C.J. Burns, R.A. Andersen and A. Zalkin, 1989, Organometallics **8**, 1865.

Berthet, J.C., M. Lance, M. Nierlich, J. Vigner and M. Ephritikhine, 1991a, J. Organomet. Chem. **420**, C9.

Berthet, J.C., J.F. Le Marchal, M. Nierlich, M. Lance, J. Vigner and M. Ephritikhine, 1991b, J. Organomet. Chem. **408**, 335.

Berthet, J.C., M. Ephritikhine, M. Nierlich, M. Lance and J. Vigner, 1993, J. Organomet. Chem. **460**, 47.

Berthet, J.C., J.F. Le Maréchal, M. Lance, M. Nierlich, J. Vigner and M. Ephritikhine, 1995, J. Chem. Soc. Dalton Trans., 3027.

Berton, A., M. Porchia, G. Rossetto and P. Zanella, 1986, J. Organomet. Chem. **302**, 351.

Beshouri, S.M., and A. Zalkin, 1989, Acta Crystallogr. C **45**, 1221.

Bettonville, S., J. Goffart and J. Fuger, 1989, J. Organomet. Chem. **377**, 59.

Billiau, F., G. Folcher, H. Marquet-Ellis, P. Rigny and E. Saito, 1981, J. Am. Chem. Soc. **103**, 5603.

Blake, P.C., H.F. Lappert, J.L. Atwood and H. Zhang, 1986a, J. Chem. Soc. Chem. Commun., 1148.

Blake, P.C., M.F. Lappert, R.G. Taylor, J.L. Atwood, W.E. Hunter and H. Zhang, 1986b, J. Chem. Soc. Chem. Commun., 1394.

Blake, P.C., M.F. Lappert, R.G. Taylor, J.L. Atwood and H. Zhang, 1987, Inorg. Chim. Acta **139**, 13.

Blake, P.C., E. Hey, M.F. Lappert, J.L. Atwood and H. Zhang, 1988a, J. Organomet. Chem. **353**, 307.

Blake, P.C., M.F. Lappert, J.L. Atwood and H. Zhang, 1988b, J. Chem. Soc. Chem. Commun., 1436.

Blake, P.C., M.F. Lappert, R.G. Taylor, J.L. Atwood, W.E. Hunter and H. Zhang, 1995, J. Chem. Soc. Dalton Trans., 3335.

Bochkarev, M.N., A.A. Trifonov, G.A. Razuvaev, M.A. Ilatovskaya, V.B. Shur and M.E. Vol'pin, 1987, Dokl. Akad. Nauk USSR **295**, 1381.

Bochkarev, M.N., G.S. Kalinina, L.N. Sacharov and S.Ya. Korshev, 1989, Organic Compounds of the Rare Earths (Nauka, Moscow) 230 p.

Bochkarev, M.N., V.V. Khramenkov, Y.F. Rad'Kov, L.N. Zakharov and Y.T. Struchkov, 1991, J. Organomet. Chem. **421**, 29.

Boisson, C., J.C. Berthet, M. Nierlich and M. Ephritikhine, 1996, J. Chem. Soc. Dalton Trans., 2129.

Bombieri, G., G. De Paoli, A. Del Pra and K.W. Bagnall, 1978, Inorg. Nucl. Chem. Lett. **14**, 359.

Bombieri, G., F. Benetollo, K.W. Bagnall, M.J. Plews and D.J. Brown, 1983a, J. Chem. Soc. Dalton Trans., 45.

Bombieri, G., F. Benetollo, E. Klahne and R.D. Fischer, 1983b, J. Chem. Soc. Dalton Trans., 1115.

Boncella, J.M., and R.A. Andersen, 1984a, Inorg. Chem. **23**, 432.

Boncella, J.M., and R.A. Andersen, 1984b, J. Chem. Soc. Chem. Commun., 809.

Booij, M., A. Meetsma and J.H. Teuben, 1991, Organometallics **10**, 3246.

Borisov, A.P., V.D. Hakhaev, A.B. Erofeev and G.N. Boiko, 1986, Vestn. Mosk. Univ. Ser. 2 Khim. **27**, 321.

Borisov, G.K., S.G. Krasnova and G.G. Devyatykh, 1973, Russ. J. Inorg. Chem. **18**, 346.

Borisov, G.K., S.G. Chuganova and G.G. Devyatykh, 1975, Russ. J. Inorg. Chem. **18**, 346.

Bottomley, F., D.E. Paez and P.S. White, 1985, J. Organomet. Chem. **191**, 35.

Boussie, T.R., R.M. Moore Jr, A. Streitwieser, A. Zalkin, J. Brennan and K.A. Smith, 1990, Organometallics **9**, 2010.

Boussie, T.R., D.C. Eisenberg, J. Rigsbee, A. Streitwieser and A. Zalkin, 1991, Organometallics **10**, 1922.

Brennan, J.G., and R.A. Andersen, 1985, J. Am. Chem. Soc. **107**, 514.

Brennan, J.G., and A. Zalkin, 1985, Acta Crystallogr. C **41**, 1038.

Brennan, J.G., R.A. Andersen and J.L. Robbins, 1986a, J. Am. Chem. Soc. **108**, 335.

Brennan, J.G., R.A. Andersen and A. Zalkin, 1986b, Inorg. Chem. **25**, 1756.

Brennan, J.G., R.A. Andersen and A. Zalkin, 1986c, Inorg. Chem. **25**, 1761.

Brennan, J.G., S.D. Stults, R.A. Andersen and A. Zalkin, 1987a, Inorg. Chim. Acta **139**, 201.

Brennan, J.G., F.G.N. Cloke, A.A. Sameh and A. Zalkin, 1987b, J. Chem. Soc. Chem. Commun., 1668.

Brennan, J.G., S.D. Stults, R.A. Andersen and A. Zalkin, 1988a, Organometallics **7**, 1329.

Brennan, J.G., R.A. Andersen and A. Zalkin, 1988b, J. Am. Chem. Soc. **110**, 4554.

Brianese, N., U. Casellato, F. Ossola, M. Porchia, G. Rossetto, P. Zanella and R. Graziani, 1989, J. Organomet. Chem. **365**, 223.

Broach, R.W., A.J. Schultz, J.M. Williams, G.M. Brown, J.M. Manriquez, P.J. Fagan and T.J. Marks, 1979, Science **203**, 172.

Bruno, G., E. Ciliberto, R.D. Fischer, I. Fragalà and A.W. Spiegl, 1982b, Organometallics **1**, 1060.
Bruno, J.W., D.G. Kalina, E.A. Mintz and T.J. Marks, 1982a, J. Am. Chem. Soc. **104**, 1860.
Bruno, J.W., T.J. Marks and V.W. Day, 1982c, J. Am. Chem. Soc. **104**, 7357.
Bruno, J.W., T.J. Marks and V.W. Day, 1983, J. Organomet. Chem. **250**, 237.
Bruno, J.W., M.R. Duttera, C.M. Fendrick, C.M. Smith and T.J. Marks, 1984, Inorg. Chim. Acta **94**, 271,
Bruno, J.W., G.M. Smith, T.J. Marks, C.K. Fair, A.J. Schultz and J.M. Williams, 1986, J. Am. Chem. Soc. **108**, 40.
Burns, C.J., and R.A. Andersen, 1987a, J. Am. Chem. Soc. **109**, 941.
Burns, C.J., and R.A. Andersen, 1987b, J. Am. Chem. Soc. **109**, 5853.
Burns, C.J., and R.A. Andersen, 1987c, J. Am. Chem. Soc. **109**, 915.
Burns, C.J., and R.A. Andersen, 1989, J. Chem. Soc. Chem. Commun., 136.
Burns, C.J., and B.E. Bursten, 1989, Comments Inorg. Chem. **9**, 61.
Burns, C.J., and D.G. Lauberau, 1971, Inorg. Chem. **10**, 2789.
Burns, C.J., W.H. Baldwin and F.H. Fink, 1974, Inorg. Chem. **13**, 1916.
Burns, C.J., B.J. Berg and R.A. Andersen, 1987, J. Chem. Soc. Chem. Commun., 272.
Burns, J.H., 1974, J. Organomet. Chem. **76**, 225.
Bursten, B.E., and K.J. Novo-Gradac, 1987, J. Am. Chem. Soc. **109**, 904.
Bursten, B.E., and R.J. Strittmatter, 1987, J. Am. Chem. Soc. **109**, 6606.
Bursten, B.E., L.F. Rhodes and R.J. Strittmatter, 1989, J. Am. Chem. Soc. **111**, 2758.
Burton, N.C., F.G.N. Cloke, P.B. Hitchcock, H.C. Lemos and A.A. Sameh, 1989, J. Chem. Soc. Chem. Commun., 1462.
Butcher, J.R., D.L. Clark, S.K. Grumbine and J.G. Watkin, 1995, Organometallics **14**, 2799.
Calderazzo, F., R. Pappalardo and S. Losi, 1966, J. Inorg. Nucl. Chem. **28**, 987.
Campbell, G.C., F.A. Cotton, J.F. Haw and W. Schwotzer, 1986, Organometallics **5**, 274.
Campion, B.K., R.H. Heyn and D.T. Tilley, 1990a, Inorg. Chem. **29**, 4356.
Campion, B.K., R.H. Heyn and D.T. Tilley, 1990b, J. Am. Chem. Soc. **112**, 2011.
Campion, B.K., R.H. Heyn and D.T. Tilley, 1993, Organometallics **12**, 2584.
Carnall, W.T., 1979, in: Organometallics of the f-Elements, eds T.J. Marks and R.D. Fischer (Reidel, Dordrecht) ch. 9.
Cesari, M., U. Pedretti, A. Zazzetta, G. Lugli and W. Marconi, 1971, Inorg. Chim. Acta **5**, 439.
Chang, C.C., and N.K. Sung-Yu, 1986, Inorg. Chim. Acta **119**, 107.
Chang, C.C., N.K. Sung-Yu, C.W. Kang and C.T. Chang, 1987, Inorg. Chim. Acta **129**, 119.
Chauvin, Y., S. Heyworth, H. Olivier, F. Robert and L. Saussine, 1993, J. Organomet. Chem. **455**, 89.
Chen, J., G. Wu, P.J. Zheng, D.L. Deng, J. Hu and C.T. Qian, 1993, Jiegon Xuaxue (Chinese J. Struct. Chem.) **12**, 254.
Chen, M., G. Wu, W. Wu, S. Zhuang and Z. Huang, 1988, Organometallics **7**, 802.
Chen, W., G. Yu, S. Xiao, Y. Huang and X. Gao, 1983, Kexue Tongbao **28**, 1043.
Clair, M.St., W.P. Schaefer and J.E. Bercaw, 1991, Organometallics, 525.
Cloke, F.G.N., 1995, in: Comprehensive Organometallics Chemistry II, Vol. 4, eds E.W. Abel, F. Gordon, A. Stone and J. Wilkinson (Pergamon Press, Oxford) ch. 1.
Cloke, F.G.N., I.C. Dalby, P.B. Hitchcock, H. Karamallakis and G.A. Lawless, 1991a, J. Chem. Soc. Chem. Commun., 779.
Cloke, F.G.N., K. Khan and R.N. Perutz, 1991b, J. Chem. Soc. Chem. Commun., 1372.
Cloke, F.G.N., S.A. Hawkes, P.B. Hitchcock and P. Scott, 1994, Organometallics **13**, 2895.
Collin, J., J.L. Namy, C. Beid and H.B. Kagan, 1987, Inorg. Chim. Acta **140**, 29.
Conticello, V.P., L. Brard, M.A. Giardello, Y. Tsuji, M. Sabat, C.L. Stern and T.J. Marks, 1992, J. Am. Chem. Soc. **114**, 2761.
Cotton, F.A., and W. Schwotzer, 1985, Organometallics **4**, 942.
Cotton, F.A., and W. Schwotzer, 1986, J. Am. Chem. Soc. **108**, 4657.
Cotton, F.A., and W. Schwotzer, 1987, Organometallics **6**, 1275.
Cotton, F.A., W. Schwotzer and C.Q. Simpson, 1986, Angew. Chem. **25**, 637.
Cramer, R.E., R.B. Maynard and J.W. Gilje, 1978, J. Am. Chem. Soc. **100**, 5562.
Cramer, R.E., R.B. Maynard and J.W. Gilje, 1980, Inorg. Chem. **19**, 2564.
Cramer, R.E., R.B. Maynard and J.W. Gilje, 1981, Inorg. Chem. **20**, 2466.

Cramer, R.E., R.B. Maynard, J.C. Paw and J.W. Gilje, 1982, Organometallics **1**, 869.
Cramer, R.E., K.T. Higa, S.L. Pruskin and J.W. Gilje, 1983, J. Am. Chem. Soc. **105**, 6749.
Cramer, R.E., K. Panchanatheswaran and J.W. Gilje, 1984a, J. Am. Chem. Soc. **106**, 1853.
Cramer, R.E., A.L. Mori, R.B. Maynard, J.W. Gilje, K. Tatsumi and A. Nakamura, 1984b, J. Am. Chem. Soc. **106**, 5920.
Cramer, R.E., K.T. Higa and J.W. Gilje, 1984c, J. Am. Chem. Soc. **106**, 7245.
Cramer, R.E., K. Panchanatheswaran and J.W. Gilje, 1984d, Angew. Chem. Int. Ed. Engl. **23**, 912.
Cramer, R.E., J.H. Jeong and J.W. Gilje, 1986, Organometallics **5**, 2555.
Cramer, R.E., U. Engelhardt, K.T. Higa and J.W. Gilje, 1987a, Organometallics **6**, 41.
Cramer, R.E., J.H. Jeong and J.W. Gilje, 1987b, Organometallics **6**, 2010.
Cramer, R.E., M.A. Bruck, F. Edelmann, O. Afzal, J.W. Gilje and H. Schmidbaur, 1988a, Chem. Ber. **121**, 417.
Cramer, R.E., F. Edelman, A.L. Mori, S. Roth, J.W. Gilje, K. Tatsumi and A. Nakamura, 1988b, Organometallics **7**, 841.
Cramer, R.E., M.A. Bruck and J.W. Gilje, 1988c, Organometallics **7**, 1465.
Cramer, R.E., S. Roth, P. Edelmann, M.A. Bruck, K.C. Cohn and J.W. Gilje, 1989a, Organometallics **8**, 1192.
Cramer, R.E., S. Roth and J.W. Gilje, 1989b, Organometallics **8**, 2327.
Cramer, R.E., J.H. Jeong, P.N. Richmann and J.W. Gilje, 1990, Organometallics **9**, 1141.
Cramer, R.E., J. Hitt, T. Chung and J.W. Gilje, 1995a, New J. Chem. **19**, 509.
Cramer, R.E., K.A.N.S. Ariyaratne and J.W. Gilje, 1995b, Z. Anorg. Allg. Chem. **621**, 1856.
Cymbaluk, T.H., J.Z. Liu and R.D. Ernst, 1983, J. Organomet. Chem. **255**, 311.
Day, C.S., V.W. Day, R.D. Ernst and S.H. Vollmer, 1982, Organometallics **1**, 998.
Day, V.W., C.W. Earley, W.G. Klemperer and D.J. Maltbie, 1985a, J. Am. Chem. Soc. **107**, 8261.
Day, V.W., W.C. Klemperer and D.J. Maltbie, 1985b, Organometallics **4**, 104.
Deacon, G.B., and Q. Shen, 1996, J. Organomet. Chem. **511**, 1–17.
Deacon, G.B., and T.D. Tuong, 1988, Polyhedron **7**, 249.
Deacon, G.B., and D.L. Wilkinson, 1988, Inorg. Chim. Acta **142**, 155.
Deacon, G.B., and D.L. Wilkinson, 1989, Aust. J. Chem. **42**, 845.
Deacon, G.B., A.J. Koplick and T.D. Tuong, 1982, Polyhedron **1**, 423.
Deacon, G.B., T.D. Tuong and D.G. Vince, 1983, Polyhedron **2**, 969.
Deacon, G.B., A.J. Koplick and T.D. Tuong, 1984a, Aust. J. Chem. **37**, 517.
Deacon, G.B., G.D. Fallon, P.I. HacKinnon, R.H. Newnhan, G.N. Pain, T.D. Tuong and D.L. Wilkinson, 1984b, J. Organomet. Chem. **277**, C21.
Deacon, G.B., G.N. Pain and T.D. Tuong, 1985a, Polyhedron **4**, 17.
Deacon, G.B., C.D. Fallon and D.L. Wilkinson, 1985b, J. Organomet. Chem. **293**, 45.
Deacon, G.B., C.M. Forsyth, R.H. Newnham and T.D. Tuong, 1987a, Aust. J. Chem. **40**, 895.
Deacon, G.B., B.M. Gatehouse, S.N. Platts and D.L. Wilkinson, 1987b, Aust. J. Chem. **40**, 907.
Deacon, G.B., G.N. Pain and T.D. Tuong, 1989a, Inorg. Synth. **26**, 1149.
Deacon, G.B., B.M. Gatehouse and P.A. White, 1989b, Polyhedron **8**, 1983.
Deacon, G.B., A. Dietrich, C.M. Forsyth and H. Schumann, 1989c, Angew. Chem. **101**, 1374.
Deacon, G.B., S. Nickel, P. MacKinnon and E.R.T. Tiekink, 1990, Aust. J. Chem. **43**, 1245.
Deelman, B.J., S.L. Gonzales and J.W. Ziller, 1994, J. Am. Chem. Soc. **116**, 2600.
Delapalme, A., P. Schweiss, M.R. Spirlet, J. Rebizant and B. Kanellakopulos, 1988, Mater. Sci. Forum., 27.
Delapalme, A., P. Raison, G.H. Lander, J. Rebizant, P. Schweiss and B. Kanellakopulos, 1994, Z. Kristallogr. **209**, 727.
Deng, D., C. Qian, G. Wu and P. Zheng, 1990a, J. Chem. Soc. Chem. Commun., 880.
Deng, D., B. Li and C. Qian, 1990b, Polyhedron **9**, 1453.
Deng, D., C. Qian, F. Song, Z. Wang, G. Wu, P. Zheng, S. Jin and Y. Lin, 1993, J. Organomet. Chem. **458**, 83.
Deng, D., C. Qian, F. Song and Z. Wang, 1994, Sci. Sin. Sez. B **24**, 120.
Depaoli, G., P. Zanonato and G. Valle, 1990, Inorg. Chim. Acta **170**, 109.
Devyatykh, G.G., G.K. Borisov and S.G. Krasnova, 1972, Proc. Akad. Sci. USSR **203**, 204.

Devyatykh, G.G., N.V. Larin, P.E. Gaivoronkii, G.K. Borisov, S.G. Krasnova and L.F. Zyuzina, 1973, Proc. Akad. Sci. USSR, **208**, 111.

Devyatykh, G.G., I.B. Rabinovich, V.I. Telnoi, G.K. Borisov and L.F. Zyuzina, 1974, Proc. Acad. Sci. USSR **217**, 673.

Di Bella, S., G. Lanza, I.L. Fragalà and T.J. Marks, 1996, Organometallics **15**, 205.

Dolg, M., P. Fulde, W. Küchle, C.S. Neumann and H.J. Stoll, 1991, J. Chem. Phys. **94**, 3011.

Dormond, A., 1983, J. Organomet. Chem. **256**, 47.

Dormond, A., and C. Moise, 1985, Polyhedron **4**, 595.

Dormond, A., A.A. El Bouadili and C. Moise, 1984, J. Chem. Soc. Chem. Commun., 749.

Duncan, J.F., and F.G. Thomas, 1964, J. Chem. Soc., 360.

Duttera, M.R., P.J. Fagan, T.J. Marks and V.W. Day, 1982, J. Am. Chem. Soc. **104**, 865.

Duttera, M.R., V.W. Day and T.J. Marks, 1984, J. Am. Chem. Soc. **106**, 2907.

Edelmann, F.T., 1995a, Angew. Chem. Int. Ed. Engl. **34**, 2466.

Edelmann, F.T., 1995b, New J. Chem. **19**, 535.

Edelmann, M.A., M.F. Lappert, J.L. Atwood and H. Zhang, 1987, Inorg. Chim. Acta **139**, 185.

Edelmann, M.A., P.B. Hitchcock, J. Hu and M.F. Lappert, 1995, New J. Chem. **19**, 481.

Eggers, S.H., J. Kopf and R.D. Fischer, 1986a, J. Organomet. **5**, 383.

Eggers, S.H., W. Hinrichs, J. Kopf, W. Jahn and R.D. Fischer, 1986b, J. Organomet. Chem. **311**, 313.

Eggers, S.H., H. Schultze, J. Kopf and R.D. Fischer, 1986c, Angew. Chem. Int. Ed. Engl. **2**, 656.

Eggers, S.H., J. Kopf and R.D. Fischer, 1987, Acta Crystallogr. C **43**, 2288.

Eigenbrot Jr, C.W., and K.N. Raymond, 1982, Inorg. Chem. **21**, 2653.

Eisenberg, D.C., A. Streitwieser and W.K. Kot, 1990, Inorg. Chem. **29**, 10.

England, A.F., C.J. Burns and S.L. Buchwald, 1994, Organometallics **13**, 3491.

Ephritikhine, M., 1992, New J. Chem. **16**, 451.

Ernst, R.D., W.J. Kennelly, C.S. Day, V.W. Day and T.J. Marks, 1979, J. Am. Chem. Soc. **101**, 2656.

Erofeev, A.B., B.M. Bulychev, V.K. Bel'skii and G.L. Soloveichik, 1987, J. Organomet. Chem. **335**, 89.

Esser, L., 1991, Doctoral Thesis (TU Berlin).

Evans, W.J., 1985, Adv. Organomet. Chem. **24**, 131.

Evans, W.J., and D.K. Drummond, 1986, J. Am. Chem. Soc. **108**, 7440.

Evans, W.J., and D.K. Drummond, 1988a, Organometallics 7, 797.

Evans, W.J., and D.K. Drummond, 1988b, J. Am. Chem. Soc. **110**, 2772.

Evans, W.J., and D.K. Drummond, 1989, J. Am. Chem. Soc. **111**, 3329.

Evans, W.J., and M.A. Hosborn, 1987, J. Organomet. Chem. **326**, 299.

Evans, W.J., and M.S. Sollberger, 1986, J. Am. Chem. Soc. **108**, 6095.

Evans, W.J., and T.A. Ulibarri, 1987a, J. Am. Chem. Soc. **109**, 272.

Evans, W.J., and T.A. Ulibarri, 1987b, J. Am. Chem. Soc. **109**, 4292.

Evans, W.J., and T.A. Ulibarri, 1989, Polyhedron **8**, 1007.

Evans, W.J., and A.L. Wayda, 1980, J. Organomet. Chem. **202**, C6.

Evans, W.J., A.L. Wayda, W.E. Hunter and J.L. Atwood, 1981a, J. Chem. Soc. Chem. Commun., 292.

Evans, W.J., K.M. Coleson and S.C. Engerer, 1981b, Inorg. Chem. **20**, 4320.

Evans, W.J., A.L. Wayda, W.E. Hunter and J.L. Atwood, 1981c, J. Chem. Soc. Chem. Commun., 706.

Evans, W.J., J.H. Meadows, A.L. Wayda, W.E. Hunter and J.L. Atwood, 1982a, J. Am. Chem. Soc. **104**, 2015.

Evans, W.J., J.H. Meadows, A.L. Wayda, W.E. Hunter and J.L. Atwood, 1982b, J. Am. Chem. Soc. **104**, 2008.

Evans, W.J., J.H. Meadows, W.E. Hunter and J.L. Atwood, 1983a, Organometallics **2**, 1252.

Evans, W.J., I. Bloom, W.E. Hunter and J.L. Atwood, 1983b, Organometallics **2**, 709.

Evans, W.J., I. Bloom, W.E. Hunter and J.L. Atwood, 1983c, J. Am. Chem. Soc. **105**, 1401.

Evans, W.J., J.H. Meadows, W.E. Hunter and J.L. Atwood, 1984a, J. Am. Chem. Soc. **106**, 1291.

Evans, W.J., L.A. Hughes and T.P. Hanusa, 1984b, J. Am. Chem. Soc. **106**, 4270.

Evans, W.J., R. Dominguez, K.R. Levan and R.J. Doedens, 1985a, Organometallics **4**, 1836.

Evans, W.J., J.W. Grate, H.W. Choi, I. Bloom, W.E. Hunter and J.L. Atwood, 1985b, J. Am. Chem. Soc. **107**, 941.

Evans, W.J., T.T. Peterson, M.D. Rausch, W.E. Hunter, H. Zhang and J.L. Atwood, 1985c, Organometallics **3**, 554.

Evans, W.J., I. Bloom, W.E. Hunter and J.L. Atwood, 1985d, Organometallics **4**, 112.

Evans, W.J., J.W. Grate, I. Bloom, W.E. Hunter and J.L. Atwood, 1985e, J. Am. Chem. Soc. **107**, 405.

Evans, W.J., T.P. Hanusa and K.R. Levan, 1985f, Inorg. Chim. Acta **110**, 191.

Evans, W.J., J.W. Grate, L.A. Hughes, H. Zhang and J.L. Atwood, 1985g, J. Am. Chem. Soc. **107**, 3728.

Evans, W.J., J.W. Grate and R.J. Doedens, 1985h, J. Am. Chem. Soc. **107**, 1671.

Evans, W.J., R. Dominguez and T.P. Hanusa, 1986a, Organometallics **5**, 263.

Evans, W.J., R. Dominguez and T.P. Hanusa, 1986b, Organometallics **5**, 1291.

Evans, W.J., L.A. Hughes and T.P. Hanusa, 1986c, J. Organometal. **5**, 1285.

Evans, W.J., J.W. Grate, K.R. Levan, I. Bloom, T.T. Peterson, R.J. Doedens, H. Zhang and J.L. Atwood, 1986d, Inorg. Chem. **25**, 3614.

Evans, W.J., T.P. Hanusa, J.H. Meadows, W.E. Hunter and J.L. Atwood, 1987a, Organometallics **6**, 295.

Evans, W.J., D.K. Drummond, J.W. Grate, H. Zhang and J.L. Atwood, 1987b, J. Am. Chem. Soc. **109**, 3928.

Evans, W.J., D.K. Drummond, T.P. Hanusa and R.J. Doedens, 1987c, Organometallics **6**, 2279.

Evans, W.J., M.A. Hozbor, S.G. Bott, G.H. Robinson and J.L. Atwood, 1988a, Inorg. Chem. **27**, 1990.

Evans, W.J., D.K. Drummond, L.R. Chamberlain, R.J. Doedens, S.G. Bott, H. Zang and J.L. Atwood, 1988b, J. Am. Chem. Soc. **110**, 4983.

Evans, W.J., L.R. Chamberlain, T.A. Ulibarri and J.W. Ziller, 1988c, J. Am. Chem. Soc. **110**, 6423.

Evans, W.J., D.K. Drummond, L.A. Hughes, H. Zhand and J.L. Atwood, 1988d, Polyhedron **7**, 1693.

Evans, W.J., T.A. Ulibarri and H. Zhang, 1988e, J. Am. Chem. Soc. **110**, 6877.

Evans, W.J., M.S. Sollberger, S.I. Khan and R. Bau, 1988f, J. Am. Chem. Soc **110**, 439.

Evans, W.J., T.J. Deming and J.W. Ziller, 1989a, Organometallics **8**, 1581.

Evans, W.J., D.K. Drummond, T.P. Hanusa and J.M. Olofson, 1989b, J. Organomet. Chem. **376**, 311.

Evans, W.J., R.A. Keyer and J.W. Ziller, 1990a, J. Organomet. Chem. **394**, 87.

Evans, W.J., R.A. Keyer and J.W. Ziller, 1990b, Organometallics **9**, 2628.

Evans, W.J., T.A. Ulibarri and J.W. Ziller, 1990c, J. Am. Chem. Soc. **112**, 219.

Evans, W.J., T.A. Ulibarri and J.W. Ziller, 1990d, J. Am. Chem. Soc. **112**, 2314.

Evans, W.J., T.A. Ulibarri, L.R. Chamberlain, J.W. Ziller and D. Alvarez Jr, 1990e, Organometallics **9**, 2124.

Evans, W.J., S.L. Gonzales and J.W. Ziller, 1991a, J. Am. Chem. Soc. **113**, 7423.

Evans, W.J., T.A. Ulibarri and J.W. Ziller, 1991b, Organometallics **10**, 134.

Evans, W.J., S.L. Gonzales and J.W. Ziller, 1991c, J. Am. Chem. Soc. **113**, 9880.

Evans, W.J., M.S. Sollberger, J.L. Shreeve, J.M. Olofson, J.H. Rein and W.J. Ziller, 1992a, Inorg. Chem. **31**, 2492.

Evans, W.J., T.J. Boyle and J.W. Ziller, 1992b, Inorg. Chem. **31**, 1120.

Evans, W.J., G. Kociok-Köhn and J.W. Ziller, 1992c, Angew. Chem. **104**, 1114.

Evans, W.J., S.L. Gonzales and J.W. Ziller, 1992d, J. Chem. Soc. Chem. Commun., 1138.

Evans, W.J., T.J. Boyle and J.W. Ziller, 1993a, Organometallics **12**, 3998.

Evans, W.J., T.J. Boyle and J.W. Ziller, 1993b, J. Organomet. Chem. **462**, 141.

Evans, W.J., S.L. Gonzales and J.W. Ziller, 1994a, J. Am. Chem. Soc. **116**, 2600.

Evans, W.J., G.W. Rabe, J.W. Ziller and R.J. Doedens, 1994b, Inorg. Chem. **33**, 2719.

Evans, W.J., J.L. Shreeve and J.W. Ziller, 1994c, Organometallics **13**, 731.

Evans, W.J., G.W. Rabe, M.A. Ansari and J.W. Ziller, 1994d, Angew. Chem. **106**, 2200.

Evans, W.J., T.S. Gummersheimer, T.J. Boyle and J.W. Ziller, 1994e, Organometallics **13**, 1281.

Evans, W.J., T.S. Gummersheimer and J.W. Ziller, 1995a, Appl. Organomet. Chem. **9**, 437.

Evans, W.J., M.A. Ansari, J.W. Ziller and S.I. Khan, 1995b, Organometallics **14**, 3.

Evans, W.J., K.J. Forrestal, J. Leman and Y.W. Ziller, 1996, Organometallics **15**, 527.

Fagan, P.J., J.M. Manriquez, E.A. Maatta, A.M. Seyam and T.J. Marks, 1981a, J. Am. Chem. Soc. **103**, 6650.

Fagan, P.J., J.M. Manriquez, S.H. Vollmer, C.S. Day, V.W. Day and T.J. Marks, 1981b, J. Am. Chem. Soc. **103**, 2206.

Fagan, P.J., J.M. Manriquez, T.J. Marks, C.S. Day, S.H. Vollmer and V.W. Day, 1982, Organometallics **1**, 170.

Fan, B., Q. Shen and Y. Lin, 1989a, J. Organomet. Chem. **377**, 51.

Fan, B., Q. Shen and Y. Lin, 1989b, J. Organomet. Chem. **376**, 61.

Fan, Y., P. Lu, Z. Jin and W. Chen, 1984, Sci. Sin. Ser. B. **27**, 993.

Fedushkin, L.I., M.N. Bochkarev, H. Schumann, L. Esser and G. Kociok-Köhn, 1995, J. Organomet. Chem. **489**, 145.

Fendrick, C.M., L.D. Schertz, V.W. Day and T.J. Marks, 1988, Organometallics **7**, 1828.

Finke, R.G., G. Gaughan and R. Voegeli, 1982, J. Organomet. Chem. **229**, 179.

Finke, R.G., S.R. Keenan, D.A. Schiraldi and P.L. Watson, 1986, Organometallics **5**, 598.

Finke, R.G., S.R. Keenan and P.L. Watson, 1989, Organometallics **8**, 263.

Fischer, E.O., and Y. Hristidu, 1962, Z. Naturforsch. B **17**, 275.

Fischer, E.O., and A. Tribner, 1962, Z. Naturforsch. B **17**, 276.

Fischer, R.D., 1994, Angew. Chem. **106**, 2253.

Foyentin, M., G. Folcher and M. Ephritikhine, 1987a, J. Chem. Soc. Chem. Commun., 494.

Foyentin, M., G. Folcher and M. Ephritikhine, 1987b, J. Organomet. Chem. **335**, 201.

Fu, G., Y. Xu, Z. Xie and C. Qian, 1989, Acta Chim. Sin. 431.

Fuxing, G., W. Gecheng, J. Zhongsheng and C. Wenqi, 1992, J. Organomet. Chem. **438**, 289.

Gagné, M.R., C.L. Stern and T.J. Marks, 1992, J. Am. Chem. Soc. **114**, 275.

Gao, H., Q. Shen, J. Hu, S. Jin and Y. Lin, 1989, Chin. Sci. Bull. **34**, 614.

Gao, H., Q. Shen, J. Hu, S. Jin and Y. Lin, 1992, J. Organomet. Chem. **427**, 141.

Gilbert, T.M., R.R. Ryan and A.P. Sattelberger, 1988, Organometallics **7**, 2514.

Gilbert, T.M., R.R. Ryan and A.P. Sattelberger, 1989, Organometallics **8**, 857.

Gilje, J.W., and R.E. Cramer, 1987, Inorg. Chim. Acta. **139**, 177.

Girardello, M.A., V.P. Conticello, L. Brard, M. Sabat, A.L. Rheingold, C.L. Stern and T.J. Marks, 1994a, J. Am. Chem. Soc. **116**, 10212.

Girardello, M.A., V.P. Conticello, L. Brard, M.R. Gagné and T.J. Marks, 1994b, J. Am. Chem. Soc. **116**, 10241.

Gradeff, P.S., K. Yünlü, T.J. Deming, J.M. Olofson, J.W. Ziller and W.J. Evans, 1989, Inorg. Chem. **28**, 2600.

Gradoz, P., C. Boisson, D. Baudry, M. Lance, M. Nierlich, J. Vigner and M. Ephritikhine, 1992a, J. Chem. Soc. Chem. Commun., 1720.

Gradoz, P., D. Baudry, M. Ephritikhine, F. Nief and F. Mathey, 1992b, J. Chem. Soc. Dalton Trans., 3047.

Gradoz, P., M. Ephritikhine, M. Lance, J. Vigner and M. Nierlich, 1994, J. Organomet. Chem. **481**, 69.

Graper, J., and R.D. Fischer, 1994, J. Organomet. Chem. **471**, 87.

Green, J.C., 1989, Struct. Bonding **43**, 37.

Green, J.C., D. Hohl and N. Röesch, 1987, Organometallics **6**, 712.

Green, J.C., N. Kaltsoyannis, K. Nsize and N. Mc-Donald, 1994, J. Am. Chem. Soc. **116**, 1994.

Guan, J., Q. Shen, J. Hu and Y. Lin, 1990, Jiegou Huaxue **9**, 184.

Guan, J., S. Jin, Y. Lin and Q. Shen, 1992, Organometallics **11**, 2483.

Gulino, A., M. Casarin, V.P. Conticello, J.G. Gaudiello, H. Mauermann, I. Fragalà and T.J. Marks, 1988, Organometallics **7**, 2360.

Gulino, A., E. Ciliberto, S. Di Bella, I. Fragalà, A.M. Seyam and T.J. Marks, 1992, Organometallics **11**, 3248.

Gun'ko, Yu.K., B.M. Bulychev, A.I. Sizov, V.K. Bel'skii and G.L. Soloveichik, 1990, J. Organomet. Chem. **390**, 153.

Gun'ko, Yu.K., B.M. Bulychev, G.L. Soloveichik and V.K. Bel'skii, 1992, J. Organomet. Chem. **424**, 289.

Haan, K.H., J.L. De Boer, J.H. Teuben, A.L. Spek, B. Kojic-Prodic, G.R. Hays and R. Huis, 1986, Organometallics **5**, 1726.

Haan, K.H., G.A. Luinstra, A. Meetsma and J.H. Teuben, 1987, Organometallics **6**, 1509.

Hajela, S., W.P. Schaefer and J.E. Bercaw, 1992, Acta Crystallogr. C **48**, 1771.

Hall, S.W., J.C. Huffman, M.M. Miller, L.R. Avens, C.J. Burns, D.S.J. Arney, A.F. England and A.P. Sattelberger, 1993, Organometallics **12**, 752.

Hammel, A., and J. Weidlein, 1990, J. Organomet. Chem. **388**, 75.

Hammel, A., W. Schwarz and J. Weidlein, 1989, J. Organomet. Chem. **363**, C29.

Haug, H.O., 1971, J. Organomet. Chem. **30**, 53.

Hawthorne, M.F., D.C. Yong, T.D. Andrews, D.V. Howe, R.L. Pilling, A.D. Pitts, M. Reintjer, L.F. Waren Jr and P.A.J. Wegner, 1988, J. Am. Chem. Soc. **90**, 879.

Hay, P.J., R.R. Ryan, K.V. Salazar, D.A. Wrobleski and A.P. Sattelberger, 1986, J. Am. Chem. Soc. **108**, 313.

Hayes, R.G., and J.L. Thomas, 1969, J. Am. Chem. Soc. **91**, 6876.

Hazin, P.N., J.C. Huffman and J.W. Bruno, 1988, J. Chem. Soc. Chem. Commun., 1473.

Hazin, P.N., J.W. Bruno and G.K. Schultz, 1990, Organometallics **9**, 416.

Heeres, H.J., J. Renkema, M. Booji, A. Meetsma and J.H. Teuben, 1988, Organometallics **7**, 2495.

Heeres, H.J., J.H. Teuben and R.D. Rogers, 1989a, J. Organomet. Chem. **364**, 87.

Heeres, H.J., A. Meetsma, J.H. Teuben and R.D. Rogers, 1989b, Organometallics **8**, 2637.

Heeres, H.J., A. Meetsma and J.H. Teuben, 1991, J. Organomet. Chem. **414**, 351.

Heeres, H.J., M. Maters, J.H. Teuben, G. Helgesson and S. Jagner, 1992, Organometallics **11**, 350.

Herrmann, W.A., R. Anwander, M. Kleine, K. Ofele, J. Riede and W. Scherer, 1992, Chem. Ber. **125**, 2391.

Herrmann, W.A., R. Anwander, P. Munck and W. Scherer, 1993, Chem. Ber. **126**, 331.

Hinrichs, W., D. Melzer, M. Rehwoldt, V. Jahn and R.D. Fischer, 1983, J. Organomet. Chem. **251**, 299.

Hitchcock, P.B., M.F. Lappert and R.G. Taylor, 1984, J. Chem. Soc. Chem. Commun., 1082.

Hitchcock, P.B., M.F. Lappert and S. Prashar, 1991, J. Organomet. Chem. **413**, 79.

Hitchcock, P.B., J.A.K. Howard, M.F. Lappert and S. Prashar, 1992, J. Organomet. Chem. **437**, 177.

Höck, N., W. Oroschin, G. Paolucci and R.D. Fischer, 1986, Angew. Chem. Int. Ed. Engl. **25**, 738.

Hodgson, K.O., and K.N. Raymond, 1973, Inorg. Chem. **12**, 458.

Hoffmann, P., P. Stauffert, K. Tatsumi, A. Nakamura and R. Hoffmann, 1985, Organometallics **4**, 404.

Holton, J., M.F. Lappert, D.G.H. Ballard, R. Pearce, J.L. Atwood and W.E. Hunter, 1979, J. Chem. Soc. Dalton Trans., 54.

Hosmane, N.S., Y. Wang, H. Zhang, A.R. Oki, J.A. Maguire, E. Waldhör, W. Kaim, H. Binder and R.K. Kremer, 1995, Organometallics **14**, 1101.

Hosmane, N.S., Y. Wang, A.R. Oki, H. Zhang and J.A. Maguire, 1996, Organometallics **15**, 626.

Jacob, K., M. Glanz, K. Tittes and K.-H. Thiele, 1988, Z. Anorg. Allg. Chem. **556**, 170.

Jacob, K., J. Glanz, K. Tittes, K.-H. Thiele, I. Pavlik and A. Lycka, 1989, Z. Anorg. Allg. Chem. **577**, 145.

Jacob, K., W. Kretschmer, K.H. Thiele, H. Gornitzka, F.T. Edelmann, I. Pavilik, A. Lyska and J. Holerek, 1992, J. Organomet. Chem. **436**, 231.

Jacob, K., I. Pavlik and F.T. Edelmann, 1993, Anorg. Allg. Chem. **619**, 1957.

Jahn, W., K. Yünlü, W. Oroschin, H.D. Amberger and R.D. Fischer, 1984, Inorg. Chim. Act. **95**, 85.

Jemine, X., J. Goffart, J.-C. Berthet and M. Ephritikhine, 1992, J. Chem. Soc. Dalton Trans., 2439.

Jeske, G., H. Lauke, H. Mauermann, P.N. Swepston, H. Schumann and T.J. Marks, 1985a, J. Am. Chem. Soc. **107**, 8091.

Jeske, G., L.E. Schock, P.N. Swepston, H. Schumann and T.J. Marks, 1985b, J. Am. Chem. Soc. **107**, 8103.

Jia, L., X. Yang, C. Stern and T.J. Marks, 1994, Organometallics **13**, 3755.

Jin, J., S. Jin, Z. Jin and W. Chen, 1992, Polyhedron **11**, 2873.

Jin, J., X. Zhuang, Z. Jin and W. Chen, 1995, J. Organomet. Chem. **490**, C8.

Jin, Z., Y. Liu and W. Chen, 1988a, Sci. Sin. Ser. B **30**, 1136.

Jin, Z., N. Hu, Y. Yi, X. Xu and G. Liu, 1988b, Inorg. Chim. Acta **142**, 333.

Jin, Z., J. Guan, G. Wei, J. Hu and Q. Shen, 1990, Jiegou Huaxue **9**, 140.

John, J., and M. Tsutsui, 1980, J. Coord. Chem. **10**, 177.

Jusong, X., W. Gecheng, J. Zhongsheng and C. Wenqui, 1992, Zhongguo Xitu Xuebao **3**, 203.

Kaesz, H.D., 1989, Inorganic Synthesis (John Wiley, New York) 29.

Kalsotra, B.L., S.P. Anand, R.K. Multani and B.D. Jain, 1971, J. Organomet. Chem. **28**, 87.

Kanellakopulos, B., and K.W. Bagnall, 1971, International Review of Science, Inorganic Chemistry, Serie One, in: MTP, Vol. 7, eds H.J. Emeleus and K.W. Bagnall (University Park, Baltimore) p. 229.

Karova, S.A., V.K. Vasil'ev and V.N. Sokolov, 1985, Radiokhimika **27**, 723.

Kaupp, M., P. Schleyer, M. Dolg and H. Stoll, 1992a, J. Am. Chem. Soc. **114**, 8202.

Kaupp, M., O.P. Charkin and P. Schleyer, 1992b, Orgamometallics **11**, 2765.

Kepert, D.L., 1977, Prog. Inorg. Chem. **23**, 1.

Khattar, R., M.J. Manning, C.B. Knobler, S.E. Johnson and M.F. Hawthorne, 1991, Inorg. Chem. **30**, 1970.

Khattar, R., C.B. Knobler, S.E. Johnson and M.F. Hawthorne, 1992, Inorg. Chem. **31**, 268.

Kilimann, K., and F.T. Edelmann, 1993, J. Organomet. Chem. **444**, C15.

Kilimann, K., and F.T. Edelmann, 1994, J. Organomet. Chem. **469**, C5.

Kilimann, K., M. Schäfer, R. Herbst-Irmer and F.T. Edelmann, 1994a, J. Organomet. Chem. **469**, C10.

Kilimann, K., R. Herbst-Irmer, D. Stalke and F.T. Edelmann, 1994b, Angew. Chem. **106**, 1684.

Kinsley, S.A., A. Streitwieser Jr and A. Zalkin, 1985, Organometallics **4**, 52.

Kinsley, S.A., A. Streitwieser Jr and A. Zalkin, 1986, Acta Crystallogr. C **42**, 1092.

Knösel, F., H.W. Roesky and F. Edelmann, 1987, Inorg. Chim. Acta **139**, 187.

Knyazhanskii, S.Ya., B.M. Bulychev, V.K. Bel'skii and G.L. Soloveichik, 1987, J. Organomet. Chem. **327**, 173.

Knyazhanskii, S.Ya., E.B. Lobkovskii, B.M. Bulychev, V.K. Bel'skii and G.L. Soloveichik, 1991, J. Organomet. Chem. **419**, 311.

Kot, W.K., G.V. Shalimoff and N.M. Edelstein, 1988, J. Am. Chem. Soc. **110**, 986.

Lamberts, W., and H. Lueken, 1987, Inorg. Chim. Acta **132**, 119.

Lamberts, W., H. Lueken and U. Elsenhans, 1986, Inorg. Chim. Acta **121**, 81.

Lamberts, W., H. Lueken and B. Hessner, 1987a, Inorg. Chim. Acta **134**, 155.

Lamberts, W., B. Hessner and H. Lueken, 1987b, Inorg. Chim. Acta **139**, 215.

Lappert, M.F., A. Singh, J.L. Atwood and W.E. Hunter, 1981a, J. Chem. Soc. Chem. Commun., 1190.

Lappert, M.F., A. Singh, J.L. Atwood and W.E. Hunter, 1981b, J. Chem. Soc. Chem. Commun., 1191.

Lappert, M.F., A. Singh, J.L. Atwood, W.E. Hunter and H.M. Zhang, 1983a, J. Chem. Soc. Chem. Commun., 69.

Lappert, M.F., A. Singh, J.L. Atwood and W.E. Hunter, 1983b, J. Chem. Soc. Chem. Commun., 206.

Le Maréchal, J.F., M. Ephritikhine and G. Folcher, 1986, J. Organomet. Chem. **299**, 85.

Le Maréchal, J.-F., E. Bulot, D. Baudry, M. Ephritikhine, D. Hauchard and R. Godard, 1988, J. Organomet. Chem. **354**, C17.

Le Maréchal, J.F., C. Villiers, P. Charpin, M. Nierlich, M. Lance, J. Vigner and M. Ephritikhine, 1989a, J. Organomet. Chem. **279**, 259.

Le Maréchal, J.F., C. Villiers, P. Charpin, M. Lance, M. Nierlich, J. Vigner and M. Ephritikhine, 1989b, J. Chem. Soc. Chem. Commun., 308.

Lebedev, V.N., N.F. Shemyakin, S.P. Solodovnikov and L.I. Zakharkin, 1988, Metal. Khim. **1**, 718.

Leonov, M.R., G.V. Soloveva and S.V. Patrikeev, 1990, Metal. Khim. **3**, 343.

Leverd, P.C., T. Arliguie, M. Lance, M. Nierlich, J. Vigner and M. Ephritikhine, 1994, J. Chem. Soc. Dalton Trans., 501.

Leverd, P.C., M. Ephritikhine, M. Lance, J. Vigner and M. Nierlich, 1996, J. Organomet. Chem. **507**, 229.

Li, X., X. Feng, Y. Zu, H. Wang, J. Shi, L. Liu and P.N. Sun, 1986, Inorg. Chim. Acta **116**, 85.

Li, X., X. Feng, Y. Xu, H. Wang, P. Sun and J. Shi, 1987, Kexue Tongbao **32**, 1259.

Li, X.F., S. Eggers, J. Kopf, W. Jahn, R.D. Fischer, C. Apostolidis, B. Kanellakopulos, F. Benetollo, A. Polo and G. Bombieri, 1985, Inorg. Chim. Acta **100**, 183.

Li, Z., W. Chen, G. Xu and J. Ren, 1987, Wuji Huaxue **3**, 111.

Liang, Z., A.G. Marshal, J. Marçalo, N. Marques, A. Pires de Matos, I. Santos and D.A. Weil, 1991, Organometallics **10**, 2794.

Lin, Z., and T.J. Marks, 1987, J. Am. Chem. Soc. **109**, 7979.

Lin, Z., C.P. Brock and T.J. Marks, 1988, Inorg. Chim. Acta **141**, 145.

Lin, Z., Z. Jin and W. Chen, 1992, J. Struct. Chem. **11**, 30.

Lobkovskii, E.B., G.L. Soloveichik, A.B. Erofeev, B.M. Bulychev and V.K. Bel'skii, 1982, J. Organomet. Chem. **235**, 151.

Lobkovskii, E.B., G.L. Soloveichik, B.M. Bulychev, A.B. Erofeev, A.I. Gusev and N.I. Kirillova, 1983, J. Organomet. Chem. **254**, 167.

Lobkovskii, E.B., Y.K. Gun'ko, B.M. Bulychev, G.L. Soloveichik and M.Y. Antipin, 1991, J. Organomet. Chem. **406**, 343.

Lueken, H., J. Schmitz, W. Lamberts, P. Hannibal and K. Handrick, 1989, Inorg. Chim. Acta **156**, 119.

Magin, R.E., S. Manastyrskyj and M. Dubeck, 1963, J. Am. Chem. Soc. **85**, 672.

Magomedov, G.K., A.Z. Voskoboinikov and I.P. Beletskaya, 1989, Metal. Khim. **2**, 823.

Magomedov, G.K., A.Z. Voskoboinikov, E.B. Chuklanova, A.I. Gusev and I.P. Beletskaya, 1990, Metal. Khim. **3**, 706.

Maier, R., B. Kanellakopulos, C. Apostolidis and B. Nuber, 1992a, J. Organomet. Chem. **435**, 275.

Maier, R., B. Kanellakopulos and C. Apostolidis, 1992b, J. Organomet. Chem. **427**, 33.

Makhaev, V.D., Yu.B. Zvedov, N.G. Chernorukov and V.I. Berestenko, 1990, Vysokchist. Veshchestva, 210.

Manning, M.J., C.B. Knobler and M.F. Hawthorne, 1988, J. Am. Chem. Soc. **110**, 4458.

Manning, M.J., C.B. Knobler, R. Khattar and M.F. Hawthorne, 1991, Inorg. Chem. **30**, 2009.

Marçalo, J., N. Marques, A.P. De Matos and K.W. Bagnall, 1986, J. Less-Common Met. **122**, 219.

Mares, F., K.O. Hodgson and A. Streitwieser Jr, 1971, J. Organomet. Chem. **28**, C24.

Marks, T.J., and R.D. Ernst, 1982, in: Comprehensive Organometallic Chemistry, Vol. 3, eds F.G.A. Stone, G. Wilkinson and E.W. Abel (Pergamon Press, Oxford) ch. 21, pp 173–270.

Marks, T.J., and I.L. Fragalà, 1985, Fundamental and Technological Aspects of Organo-f-element Chemistry (Reidel, Dordrecht) p. 414.

Marks, T.J., and G.W. Grynkewich, 1976, Inorg. Chem. **15**, 1302.

Marks, T.J., and J.R. Kolb, 1977, Chem. Rev. **77**, 263.

Marks, T.J., and A. Streitwieser Jr, 1986, in: The Chemistry of the Actinide Elements, eds J.J. Katz, G.T. Seaborg and L.R. Morss, Vol. 2 (Chapman & Hall, London, New York) Ch. 22.

Marks, T.J., M.R. Gagne, S.P. Nolan, L.E. Shock, A.M. Seyam and D. Stern, 1989, Pure Appl. Chem. **61**, 1665.

Marsh, R.E., W.P. Schaefer, G.C. Bazan and J.E. Bercaw, 1992, Acta Crystallogr. C **48**, 1416.

Mashima, K., and H. Takaya, 1989, Tetrahedron Lett. **30**, 3697.

Mashima, K., Y. Nakayama, N. Kaneshima, Y. Kai and A. Nakamura, 1993, J. Chem. Soc. Chem. Commun., 1847.

Mashima, K., Y. Nakayama, A. Nakamura, N. Kaneshima, Y. Kai and H. Takaya, 1994a, J. Organomet. Chem. **473**, 85.

Mashima, K., H. Sugiyama and A. Nakamura, 1994b, J. Chem. Soc. Chem. Commun., 1581.

Masserwech, G., and R.D. Fischer, 1993, J. Organomet. Chem. **444**, 67.

Mauermann, H., P.N. Swepston and T.J. Marks, 1985, Organometallics **4**, 200.

Mayer, D., and J. Rebizant, 1993, J. Alloys & Compounds **190**, 269.

McGarvey, B.R., and S. Nagy, 1987, Inorg. Chem. **26**, 4198.

Meunier-Piret, J., and M. van Meerssche, 1984, Bull. Soc. Chim. Belg. **93**, 299.

Meunier-Piret, J., J.P. Declerq, G. Germain and M. van Meersche, 1980a, Bull. Soc. Chim. Belg. **89**, 121.

Meunier-Piret, J., G. Germain, J.P. Declercq and M. van Meerssche, 1980b, Bull. Chem. Soc. Belg. **89**, 241.

Mintz, E.A., K.G. Moloy, T.J. Marks and V.W. Day, 1982, J. Am. Chem. Soc. **104**, 4692.

Molander, G.A., H. Schumann, E.C.E. Rosenthal and J. Demtschuk, 1996, Organometallics **15**, 3817.

Moloy, K.G., T.J. Marks and V.W. Day, 1983, J. Am. Chem. Soc. **105**, 5696.

Moloy, K.G., P.J. Fagan, J.M. Henriquez and T.J. Marks, 1986, J. Am. Chem. Soc. **108**, 56.

Murad, E., and D.L. Hildenbrand, 1980, J. Chem. Phys. **73**, 4005.

Namy, J.L., J. Collin, J. Zhang and H.B. Kagan, 1987, J. Organomet. Chem. **328**, 81.

Ni, C., D. Deng and C. Qian, 1985, Inorg. Chim. Acta **110**, L7.

Ni, C., Z. Zhang, D. Deng and C. Qian, 1986, J. Organomet. Chem. **306**, 209.

Nief, F., and F. Mathey, 1991, Synlett., 745.

Nief, F., L. Ricard and F. Mathey, 1993, Polyhedron **12**, 19.

Oki, A.R., H. Zhang and N.S. Hosmane, 1992, Angew. Chem. Int. Ed. Engl. **31**, 432.

Ortiz, J.V., 1986, J. Am. Chem. Soc. **108**, 550.

Ossola, F., N. Brianese, M. Porchia, G. Rossetto and P. Zanella, 1986a, J. Organomet. Chem. **310**, C1.

Ossola, F., C. Rossetto, P. Zanella, C. Paolucci and R.D. Fischer, 1986b, J. Organomet. Chem. **309**, 55.

Ossola, F., N. Brianese, M. Porchia, G. Rossetto and P. Zanella, 1990, J. Chem. Soc. Dalton Trans., 877.

Paine, R.T., E.N. Duesler and D.C. Moody, 1982, Organometallics **1**, 1097.

Palenik, G.J., 1983, in: Systematics and the Properties of the Lanthanides, ed. S.P. Sinha (Reidel, Dordrecht) p. 153.

Paolucci, G., G. Rossetto, P. Zanella, K. Yünlü and R.D. Fischer, 1984, J. Organomet. Chem. **272**, 363.

Paolucci, G., G. Rossetto, P. Zanella and R.D. Fischer, 1985a, J. Organomet. Chem. **284**, 213.

Paolucci, G., P. Zanella and A. Berton, 1985b, J. Organomet. Chem. **295**, 317.

Paolucci, G., S. Daolio and P. Traldi, 1986, J. Organomet. Chem. **309**, 283.

Paolucci, G., R.D. Fischer, H. Breitbach, B. Pelli and P. Traldi, 1988, Organometallics **7**, 1918.

Paolucci, G., R.D. Fischer, F. Benetollo, R. Seraglia and G. Bombieri, 1991, J. Organomet. Chem. **412**, 327.

Paolucci, G., R. D'Ippolito, C. Ye, C. Qian, J. Graper and R.D. Fischer, 1994, J. Organomet. Chem. **471**, 97.

Parry, J., E. Carmona, S. Coles and M. Hursthouse, 1995, J. Am. Chem. Soc. **117**, 2649.

Pearson, R.G., 1963, J. Am. Chem. Soc. **85**, 3533.

Piers, W.E., P.J. Shapiro, E.E. Bunel and J.E. Bercaw, 1990, Synlett., 74.

Piers, W.E., E.E. Bunel and J.E. Bercaw, 1991, J. Organomet. Chem. **407**, 51.

Piers, W.E., D.J. Parks, L.R. MacGillivray and M.J. Zaworotro, 1994, Organometallics **13**, 4547.

Porchia, M., U. Casellato, F. Ossola, C. Rossetto, P. Zanella and R. Graziani, 1986, J. Chem. Soc. Chem. Commun., 1034.

Porchia, M., N. Brianese, F. Ossola, G. Rossetto and P. Zanella, 1987a, J. Chem. Soc. Dalton Trans., 691.

Porchia, M., F. Ossola, G. Rossetto, P. Zanella and N. Brianese, 1987b, J. Chem. Soc. Chem. Commun., 550.

Porchia, M., N. Brianese, U. Casellato, F. Ossola, G. Rossetto, P. Zanella and R. Graziani, 1989, J. Chem. Soc. Dalton Trans., 677.

Poremba, P., M. Noltemeyer, H.G. Schmidt and F.T. Edelmann, 1995, J. Organomet. Chem. **501**, 315.

Protchenko, A.V., L.N. Zakharov, M.N. Bochkarev and J.Y. Struchkov, 1993, J. Organomet. Chem. **447**, 209.

Qian, C., and Y. Ge, 1986, J. Organomet. Chem. **299**, 97.

Qian, C., and D. Zhu, 1993, J. Organomet. Chem. **445**, 79.

Qian, C., and D. Zhu, 1994, J. Chem. Soc. Dalton Trans., 1599.

Qian, C., G. Ye, H. Lu, Y. Li, J. Zhou and Y. Ge, 1983, J. Organomet. Chem. **247**, 161.

Qian, C., C. Ye, H. Lu, Y. Li and Y. Huang, 1984, J. Organomet. Chem. **263**, 333.

Qian, C., C. Ye and Y. Li, 1986, J. Organomet. Chem. **302**, 171.

Qian, C., Y. Ge, D. Deng and Y. Gu, 1987, Huaxue Xuebao **45**, 210.

Qian, C., Z. Xie and Y. Huang, 1990, J. Organomet. Chem. **398**, 251.

Qian, C., D. Zhu and Y. Gu, 1991, J. Organomet. Chem. **401**, 23.

Qian, C., B. Wang, D. Deng, G. Wu and P. Zheng, 1992, J. Organomet. Chem. **427**, C29.

Qian, C., X.-F. Zheng, B. Wang, D. Deng and J. Sun, 1994, J. Organomet. Chem. **466**, 101.

Qian, C., C. Zhu, Y. Lin and Y. Xing, 1996, J. Organomet. Chem. **507**, 41.

Qiao, K., R.D. Fischer, G. Paolucci, P. Traldi and E. Celon, 1990, Organometallics **9**, 1361.

Qiao, K., R.D. Fischer and G. Paolucci, 1993, J. Organomet. Chem. **456**, 185.

Raymond, K.H., and C.W. Eigenbrot, 1980, Acc. Chem. Res. **13**, 276.

Rebizant, J., M.R. Spirlet and J. Goffart, 1983, Acta Crystallogr. C **39**, 1041.

Rebizant, J., M.R. Spirlet and J. Goffart, 1985, Acta Crystallogr. C **41**, 334.

Rebizant, J., M.R. Spirlet, B. Kanellakopulos and E. Dornberger, 1986, J. Less-Common Met. **122**, 211.

Rebizant, J., C. Apostolidis, M.R. Spirlet and B. Kanellakopulos, 1987, Inorg. Chim. Acta **139**, 209.

Rebizant, J., C. Apostolidis, M.R. Spirlet and B. Kanellakopulos, 1988, Acta Crystallogr. C **44**, 614.

Rebizant, J., M.R. Spirlet, S. Bettonville and J. Goffart, 1989, Acta Crystallogr. C **45**, 1509.

Rebizant, J., M.R. Spirlet, C. Apostolidis and B. Kanellakopulos, 1990, Acta Crystallogr. C **46**, 2076.

Rebizant, J., M.R. Spirlet, C. Apostolidis and B. Kanellakopulos, 1992a, Acta Crystallogr. C **48**, 854.

Rebizant, J., M.R. Spirlet, C. Apostolidis and B. Kanellakopulos, 1992b, Acta Crystallogr. C **48**, 452.

Recknagel, A., F. Knösel, H. Gornitzka, M. Noltemeyer, F.T. Edelmann and U. Behrens, 1991a, J. Organomet. Chem. **417**, 363.

Recknagel, A., M. Noltemeyer, D. Stalke, U. Pieper, H.G. Schmidt and F.T. Edelmann, 1991b, J. Organomet. Chem. **411**, 347.

Recknagel, A., M. Noltemeyer and F.T. Edelmann, 1991c, J. Organomet. Chem. **410**, 53.

Recknagel, A., A. Steiner, S. Brooker, D. Stalke and F.T. Edelmann, 1991d, Chem. Ber. **124**, 1373.

Reddmann, H., H. Schulz and H.D. Amberger, 1991, J. Organomet. Chem. **411**, 331.

Reid, A.F., and P.C. Wailes, 1966, Inorg. Chem. **5**, 1213.

Reynolds, L.T., and G. Wilkinson, 1956, J. Inorg. Nucl. Chem. **2**, 246.

Richter, J., and F.T. Edelmann, 1996, Coord. Chem. Rev. **147**, 373.

Ritchey, J.M., A.J. Zozulin, D.A. Wrobleski, R.R. Ryan, H.J. Wasserman, D.C. Moody and R.T. Paine, 1985, J. Am. Chem. Soc. **107**, 501.

Rogers, R.D., R. Bynum and J.L. Atwood, 1980, J. Organomet. Chem. **192**, 65.

Rogers, R.D., J.L. Atwood, A. Eman, D.J. Sikora and M.D. Rausch, 1981, J. Organomet. Chem. **216**, 383.

Roitershtein, D.M., L.F. Rybakova, E.S. Petrov, A.M. Ellern, M. Antipin and T. Struchov, 1993, J. Organomet. Chem. **460**, 39.

Rosen, R.K., and A. Zalkin, 1989, Acta Crystallogr. C **45**, 1139.

Rosen, R.K., R.A. Andersen and N.M. Edelstein, 1990, J. Am. Chem. Soc. **112**, 4588.

Rossetto, G., N. Brianese, F. Ossola, M. Porchia, P. Zanella and S. Sostero, 1987, Chim. Acta **132**, 275.

Ryan, R.R., R.A. Pennemann and B. Kanellakopulos, 1975, J. Am. Chem. Soc. **97**, 4258.

Ryan, R.R., K.V. Salazar, N.N. Sauer and J.M. Ritchey, 1989, Inorg. Chim. Acta **162**, 221.

Schake, A.R., L.R. Avens, C.J. Burns, D.L. Clark, A.P. Sattelberger and W.H. Smith, 1993, Organometallics **12**, 1497.

Schaverien, C.J., 1992a, J. Chem. Soc. Chem. Commun., 11.

Schaverien, C.J., 1992b, Organometallics **11**, 3476.

Schaverien, C.J., 1994a, Adv. Organomet. Chem. **36**, 283.

Schaverien, C.J., 1994b, Organometallics **13**, 69.

Schaverien, C.J., H. Heijden and A.G. Orpen, 1989, Polyhedron **8**, 1850.

Scherer, O.J., B. Werner, G. Heckmann and G. Wolmershäuser, 1991, Angew. Chem. Int. Ed. Engl. **30**, 553.

Scherer, O.J., J. Schulze and G. Wolmershäuser, 1994, J. Organomet. Chem. **484**, C5.

Schlesener, G.J., and A.B. Ellis, 1983, Organometallics **2**, 529.

Schock, L.E., A.M. Seyam, M. Sabat and T.J. Marks, 1988, Polyhedron **7**, 1517.

Scholz, A., A. Smola, J. Scholz, J. Loebe, H. Schumann and K.-H. Thiele, 1991, Angew. Chem. Int. Ed. Engl. **30**, 435.

Scholz, J., A. Scholtz, R. Weimann, C. Janiak and H. Schumann, 1994, Angew. Chem. Int. Ed. Engl. **33**, 1171.

Schulz, H., H. Reddmann and H.D. Amberger, 1992a, J. Organomet. Chem. **440**, 317.

Schulz, H., H. Schultze, H. Reddmann, M. Link and H.D. Amberger, 1992b, J. Organomet. Chem. **424**, 139.

Schumann, H., and A. Dietrich, 1991, J. Organomet. Chem. **401**, C33.

Schumann, H., and W. Genthe, 1981, J. Organometal. Chem. **213**, C7.

Schumann, H., and F.W. Reier, 1984, Inorg. Chim. Acta **95**, 43.

Schumann, H., W. Genthe and N. Bruncks, 1981, Angew. Chem. Intl. Ed. Engl. **20**, 119.

Schumann, H., W. Genthe, N. Bruncks and J. Pickardt, 1982, Organometallics **1**, 1194.

Schumann, H., I. Albrecht, J. Pickardt and E. Hahn, 1984, J. Organomet. Chem. **276**, C5.

Schumann, H., H. Lauke, E. Hahn, M.J. Heeg and D. van der Helm, 1985a, Organometallics **4**, 321.

Schumann, H., F.W. Reier and E. Palamidis, 1985b, J. Organomet. Chem. **297**, C30.

Schumann, H., I. Albrecht and E. Hahn, 1985c, Angew. Chem. Int. Ed. Engl. **24**, 985.

Schumann, H., U. Genthe, E. Hahn, M.B. Hossain and D. Helm, 1986a, J. Organomet. Chem. **299**, 67.

Schumann, H., E. Palamidis, G. Schmid and R. Boese, 1986b, Angew. Chem. Int. Ed. Engl. **25**, 718.

Schumann, H., S. Nickel, J. Loebel and J. Pickardt, 1988a, Organometallics **7**, 2004.

Schumann, H., C. Janiak and J. Pickardt, 1988b, J. Organomet. Chem. **349**, 117.

Schumann, H., I. Albrecht, M. Gallagher, E. Hahn, C. Muchmore and J. Pickardt, 1988c, J. Organomet. Chem. **349**, 103.

Schumann, H., E. Palamidis, J. Loebel and J. Pickardt, 1988d, Organometallics **7**, 1008.

Schumann, H., I. Albrecht, M. Gallagher, E. Hahn, C. Janiak, C. Kolax, J. Loebel, S. Nickel and E. Palamidis, 1988e, Polyhedron **7**, 2307.

Schumann, H., J.A. Meese-Marktscheffel and A. Dietrich, 1989a, J. Organomet. Chem. **377**, C5.

Schumann, H., R.D. Koehn, F.W. Reier, A. Dietrich and J. Pickardt, 1989b, Organometallics **8**, 1388.

Schumann, H., E. Palamidis and J. Loebel, 1990a, J. Organomet. Chem. **384**, C49.

Schumann, H., P.R. Lee and A. Dietrich, 1990b, Chem. Ber. **123**, 1331.

Schumann, H., E. Palamidis and J. Loebel, 1990c, J. Organomet. Chem. **390**, 45.

Schumann, H., L. Esser, J. Loebel, A. Dietrich, D. Helm and X. Ji, 1991a, Organometallics **10**, 2585.

Schumann, H., J. Loebel, J. Pickardt, C. Qian and Z. Xie, 1991b, Organometallics **10**, 215.

Schumann, H., J.A. Meese-Marktscheffel, B. Gorella and F.H. Görlitz, 1992a, J. Organomet. Chem. **428**, C27.

Schumann, H., J.A. Meese-Marktscheffel, A. Dietrich and F.H. Görlitz, 1992b, J. Organomet. Chem. **430**, 299.

Schumann, H., J.A. Meese-Marktscheffel, A. Dietrich and J. Pickardt, 1992c, J. Organomet. Chem. **433**, 241.

Schumann, H., J. Winterfeld, R.D. Köhn, L. Esser, J. Sun and A. Dietrich, 1993a, Chem. Ber. **126**, 907.

Schumann, H., J. Winterfeld, L. Esser and G. Kociok-Köhn, 1993b, Angew. Chem. Int. Ed. Engl. **32**, 1208.

Schumann, H., J. Winterfeld, F.H. Gorlitz and J. Pickardt, 1993c, J. Chem. Soc. Chem. Commun., 623.

Schumann, H., M. Glanz and H. Hemling, 1993d, J. Organomet. Chem. **445**, C1.

Schumann, H., J.A. Meese-Marktscheffel and L. Esser, 1995a, Chem. Rev. **95**, 865–986.

Schumann, H., M. Glanz and H. Hemiling, 1995b, New J. Chem. **19**, 491.

Schumann, H., M. Glanz, J. Winterfeld, H. Hemiling, N. Kuhn, H. Bohnen, D. Blöser and R.J. Boese, 1995c, J. Organomet. Chem. **493**, C14.

Schumann, H., J. Winterfeld, H. Hemiling, F.E. Hahn, P. Reich, K.W. Brzezinka, F.T. Edelmann, U. Kilimann, M. Schäfer and R. Herbst-Irmer, 1995d, Chem. Ber. **128**, 395.

Schumann, H., E.C.E. Rosenthal, G. Kociok-Köhn, G.A. Molander and J. Winterfeld, 1995e, J. Organomet. Chem. **496**, 233.

Schumann, H., E.C.E. Rosenthal, J. Winterfeld, R. Weimann and J. Demtschuk, 1996, J. Organomet. Chem. **507**, 287.

Scott, P., and P.B. Hitchcock, 1995, J. Organomet. Chem. **497**, C1.

Secaur, C.A., V.W. Day, R.D. Ernst, W.J. Kennelly and T.J. Marks, 1976, J. Am. Chem. Soc. **98**, 3713.

Shannon, R.D., 1976, Acta Crystallogr. A **32**, 751.

Shapiro, P.J., E. Bunel, W.P. Schaefer and J.E. Bercaw, 1990, Organometallics **9**, 867.

Shapiro, P.J., W.D. Cotter, W.P. Schaefer, J.A. Labinger and J.E. Bercaw, 1994, J. Am. Chem. Soc. **116**, 4623.

Shen, Q., D. Zheng, L. Lin and Y. Lin, 1990a, J. Organomet. Chem. **391**, 307.

Shen, Q., D. Zheng, L. Lin and Y. Lin, 1990b, J. Organomet. Chem. **391**, 321.

Shen, Q., M. Qi and Y. Lin, 1990c, J. Organomet. Chem. **399**, 247.

Shen, Q., M. Qi, J. Guan and Y. Lin, 1991, J. Organomet. Chem. **406**, 353.

Sluys, W.G., C.J. Burns, J.C. Huffman and A.P. Sattelberger, 1988, J. Am. Chem. Soc. **110**, 5924.

Smith, G.M., H. Suzuki, D.C. Sonnenberger, V.W. Day and T.J. Marks, 1986, Organometallics **5**, 549.

Smith, G.M., M. Sabat and T.J. Marks, 1987, J. Am. Chem. Soc. **109**, 1854.

Sofield, C.D., and R.A. Andersen, 1995, J. Organomet. Chem. **501**, 271.

Sonnenberger, D.C., and J.G. Gaudiello, 1988, Inorg. Chem. **27**, 2747.

Sonnenberger, D.C., E.A. Mintz and T.J. Marks, 1984, J. Am. Chem. Soc. **106**, 3484.

Spirlet, M.R., and J. Goffart, 1995, J. Organomet. Chem. **493**, 149.

Spirlet, M.R., J. Rebizant and J. Goffart, 1982, Acta Crystallogr. B **38**, 2400.

Spirlet, M.R., J. Rebizant and J. Goffart, 1986, Lanth. Act. Res. **1**, 273.

Spirlet, M.R., J. Rebizant, C. Apostolidis and B. Kanellakopulos, 1987a, Inorg. Chim. Acta **139**, 211.

Spirlet, M.R., J. Rebizant, C. Apostolidis and B. Kanellakopulos, 1987b, Acta Crystallogr. C **43**, 2322.

Spirlet, M.R., J. Rebizant and J. Goffart, 1987c, Acta Crystallogr. C **43**, 354.

Spirlet, M.R., J. Rebizant, C. Apostolidis, G.D. Andreetti and B. Kanellakopulos, 1989, Acta Crystallogr. C **45**, 739.

Spirlet, M.R., J. Rebizant, C. Apostolidis, C. Bossche and B. Kanellakopulos, 1990a, Acta Crystallogr. C **46** 2318.

Spirlet, M.R., J. Rebizant, S. Bettonville and J. Goffart, 1990b, Acta Crystallogr. C **46**, 1234.

Spirlet, M.R., J. Rebizant, C. Apostolidis and B. Kanellakopulos, 1992a, Acta Crystallogr. C **48**, 2135.

Spirlet, M.R., J. Rebizant, S. Bettonville and J. Goffart, 1992b, Acta Crystallogr. C **48**, 1221.

Spirlet, M.R., J. Rebizant, C. Apostolidis and B. Kanellakopulos, 1993a, Acta Crystallogr. C **49**, 929.

Spirlet, M.R., J. Rebizant, S. Bettonville and J. Goffart, 1993b, J. Organomet. Chem. **460**, 177.

Stehr, J., and R.D. Fischer, 1992, J. Organomet. Chem. **430**, C1.

Stern, D., M. Sabat and T.J. Marks, 1990, J. Am. Chem. Soc. **112**, 9558.

Sternal, R.S., and T.J. Marks, 1987, Organometallics **6**, 2621.

Sternal, R.S., C.P. Brock and T.J. Marks, 1985, J. Am. Chem. Soc. **107**, 8270.

Sternal, R.S., M. Sabat and T.J. Marks, 1987, J. Am. Chem. Soc. **109**, 7920.

Stevens, R.C., R. Bau, R.E. Cramer, D. Afzal, J.W. Gilje and T.F. Koetzle, 1990, Organometallics **9**, 694.

Straub, T., W. Frank, G.J. Reiss and M.S. Eisen, 1996, J. Chem. Soc. Dalton Trans., 2541.

Streitwieser Jr, A., and U. Müller-Westerhoff, 1968a, J. Am. Chem. Soc. **90**, 7364.

Streitwieser Jr, A., and U. Müller-Westerhoff, 1968b, J. Am. Chem. Soc. **90**, 7368.

Streitwieser Jr, A., and U. Müller-Westerhoff, 1968c, J. Am. Chem. Soc. **91**, 7528.

Streitwieser Jr, A., H.T. Barros, H.K. Wang and T.R. Boussie, 1993, Organometallics **12**, 5023.

Strittmatter, R.J., and E.B. Bursten, 1991, J. Am. Chem. Soc. **113**, 552.

Stuedel, A., J. Stehr, E. Siebel and R.D. Fischer, 1996, J. Organomet. Chem. **510**, 197.

Stults, S.D., and A. Zalkin, 1987, Acta Crystallogr. C **43**, 430.

Stults, S.D., R.A. Andersen and A. Zalkin, 1989, J. Am. Chem. Soc. **111**, 4507.

Stults, S.D., R.A. Andersen and A. Zalkin, 1990a, Organometallics **9**, 115.

Stults, S.D., R.A. Andersen and A. Zalkin, 1990b, Organometallics **9**, 1623.

Stults, S.D., R.A. Andersen and A. Zalkin, 1993, J. Organomet. Chem. **462**, 175.

Suleimanov, G.Z., V.I. Bregadze, N.A. Koval'chuk and I.P. Beletskaya, 1982, J. Organometal. Chem. **235**, C17.

Sun, P., X. Feng, Y. Xu, A. Guo and X. Li, 1986, Zhongguo Kexue Jishu Daxue Xuebao **16**, 455.

Sun, Y., Q. Shen, S. Jin and Y. Lin, 1991, Yingyong Huaxue **8**, 23.

Swamy, S.J., J. Loebel, J. Pickardt and H. Schumann, 1988, J. Organomet. Chem. **353**, 27.

Swamy, S.J., J. Loebel and H. Schumann, 1989, J. Organomet. Chem. **379**, 51.

Tatsumi, K., and R. Hoffmann, 1984, Inorg. Chem. **23**, 1633.

Tatsumi, K., and A. Nakamura, 1984, J. Organomet. Chem. **272**, 141.

Tatsumi, K., and A. Nakamura, 1987a, Organometallics **6**, 427.

Tatsumi, K., and A. Nakamura, 1987b, J. Am. Chem. Soc. **109**, 3195.

Tatsumi, K., A. Nakamura, P. Hoffmann, P. Stauffert and R. Hoffmann, 1985, J. Am. Chem. Soc. **107**, 4440.

Tel'noi, V.I., I.B. Rabinovich, V.N. Larina, R.M. Leonov and G.V. Solov'eva, 1989, Radiokhim. **31**, 38.

Thomas, A.C., and A.B. Ellis, 1985, Organometallics **4**, 2223.

Thompson, M.E., and J.E. Bercaw, 1984, Pure Appl. Chem. **56**, 1.

Thompson, M.E., S.M. Baxter, A.R. Bulls, B.J. Burger, M.C. Nolan, B.D. Santarsiero, W.P. Shaefer and J.E. Bercaw, 1987, J. Am. Chem. Soc. **109**, 203.

Tilley, T.D., and R.A. Andersen, 1981, Inorg. Chem. **20**, 3267.

Tilley, T.D., and R.A. Andersen, 1982, J. Am. Chem. Soc. **104**, 1772.

Tilley, T.D., R.A. Andersen, B. Spencer, H. Ruben, A. Zalkin and D.H. Templeton, 1980, Inorg. Chem. **19**, 2999.

Tilley, T.D., R.A. Andersen, B. Spencer and A. Zalkin, 1982, Inorg. Chem. **21**, 2647.

Tilley, T.D., R.A. Andersen and A. Zalkin, 1983, Inorg. Chem. **22**, 856.

Trifonov, A.A., L.N. Zakharov, M.N. Bochkarev and Yu.T. Struchkov, 1994, Russ. Chem. Bull. **43**, 145.

Tsutsui, M., and H.J. Gysling, 1968, J. Am. Chem. Soc. **91**, 3175.

Tsutsui, M., and H.J. Gysling, 1969, J. Am. Chem. Soc. **90**, 6880.

Tsutsui, M., T. Takino and D. Lorenz, 1966, Z. Naturforsch. B **21**, 1.

Tsutsui, M., L.-B. Chen, D.E. Bergbriter and T.K. Miyamoto, 1982, J. Am. Chem. Soc. **104**, 855.

Villiers, C., and M. Ephritikhine, 1990, J. Organomet. Chem. **393**, 339.

Villiers, C., R. Adam and M. Ephritikhine, 1992, J. Chem. Soc. Chem. Commun., 1555.

Vinogradov, S.A., A.E. Mistrukov and I.P. Beletskaya, 1995, J. Chem. Soc. Dalton Trans., 2679.

Visseaux, M., A. Dormond, M.M. Kubicki, C. Moïse, D. Baudry and M. Ephritikhine, 1992, J. Organomet. Chem. **433**, 95.

Von Ammon, R., R.D. Fischer and B. Kanellakopulos, 1971, Chem. Ber. **104**, 1072.

Wang, B., D. Deng and C. Qian, 1995, New J. Chem. **19**, 515.

Wang, K.-G., E.D. Stevens and S.P. Nolan, 1992, Organometallics **11**, 1011.

Wang, X., and Z. Ye, 1985, Youji Huoxue, 389.

Wang, X., X. Zhou, R. Ren, J. Zhang, Y. Xia, R. Liu and S. Wang, 1986, Huaxue Xuebao **44**, 1155.

Wasserman, H.J., A.J. Zozulin, D.C. Moody, R.R. Ryan and K.V. Salazar, 1983, J. Organomet. Chem. **254**, 305.

Watson, P.L., 1980, J. Chem. Soc. Chem. Commun., 652.

Watson, P.L., 1982, J. Am. Chem. Soc. **104**, 337.

Watson, P.L., and G.W. Parshall, 1985, Acc. Chem. Res. **18**, 51.

Watson, P.L., and D.C. Roe, 1982, J. Am. Chem. Soc. **104**, 6471.

Watson, P.L., J.F. Whitney and R.L. Harlow, 1981, Inorg. Chem. **20**, 3271.

Watson, P.L., T.H. Tulip and I. Williams, 1990, Organometallics **9**, 1999.

Wayda, A.L., 1989, J. Organomet. Chem. **361**, 73.

Wayda, A.L., and R.D. Rogers, 1985, Organometallics **4**, 1440.

Wayda, A.L., J.L. Dye and R.D. Rogers, 1984, Organometallics **3**, 1605.

Wayda, A.L., I. Mukerji, J.L. Dye and R.D. Rogers, 1987, Organometallics **6**, 1328.

Weber, A., H. Suhr, H. Schumann and R.D. Koehn, 1990, Appl. Phys. A **51**, 520.

Weber, J., A. Molassioti, M.. Moser, A. Stapor, F. Scholz, G. Horcher, A. Forchel, A. Hammel, G. Laube and J. Weidlein, 1988, Appl. Phys. Lett **53**, 2525.

Weber, J., M. Moser, A. Stapor, P. Scholz, G. Bohnert, A. Hangleiter, A. Hammel, D. Wiedmann and J. Weldlein, 1990, J. Cryst. Growth **104**, 815.

Wedler, M., A. Recknagel and P.T. Edelmann, 1990, J. Organomet. Chem. **395**, C26.

Wen, K., Z. Yin and W. Chen, 1991, J. Chem. Soc. Chem. Commun., 680.

Weydert, M., and R. Andersen, 1993, J. Am. Chem. Soc. **115**, 8837.

Weydert, M., J.G. Brennan, R.A. Andersen and R.G. Bergmann, 1995, Organometallics **14**, 3924.

Wilkinson, G., and J.M. Birmingham, 1954, J. Am. Chem. Soc. **76**, 6210.

Wo, T.K., L. Fan and T. Ziegler, 1994, Organometallics **13**, 432.

Wong, C.H., T.M. Jen and T. Lee, 1965, Acta Crystallogr. **18**, 340.

Wrobleski, D.A., R.R. Ryan, H.J. Wasserman, K.V. Salazar, R.T. Paine and D.C. Moody, 1986a, Organometallics **5**, 90.

Wrobleski, D.A., D.T. Cromer, J.V. Ortiz, T.B. Rauschfuss, R.R. Ryan and A.P. Sattelberger, 1986b, J. Am. Chem. Soc. **108**, 174.

Wu, Z., Z. Ye and Z. Zhou, 1989, Polyhedron **8**, 2109.

Wu, Z., Z. Xu, X. You, X. Zhou, X. Huang and J. Chen, 1994a, Polyhedron **13**, 379.

Wu, Z., Z. Xu, X. You, X. Zhou, X. Huang and J. Chen, 1994b, J. Organomet. Chem. **483**, 107.

Wu, Z., Z. Huang, R. Cai, Z. Xu, X. You and X. Huang, 1996a, Polyhedron **15**, 13.

Wu, Z., D. Pan, Z. Huang and R. Cai, 1996b, Polyhedron **15**, 127.

Wu, Z., Z. Huang, R. Cai, X. Zhou, X. You and X. Huang, 1996c, J. Organomet. Chem. **506**, 25.

Wu, Z., W. Ma, Z. Huang and R. Cai, 1996d, Polyhedron **15**, 3427.

Xia, J., Z. Jin and W. Chen, 1991a, J. Chem. Soc. Chem. Commun., 1214.

Xia, J., Z. Jin, G. Lin and W. Chen, 1991b, J. Organomet. Chem. **408**, 173.

Xia, J., S. Yin and W. Chen, 1996, Polyhedron **15**, 809.

Xie, Z., F.E. Hahn and C. Qian, 1991a, J. Organomet. Chem. **414**, C12.

Xie, Z., C. Qian and Y. Huang, 1991b, J. Organomet. Chem. **412**, 61.

Yan, P., N. Hu, Z. Jin and W. Chen, 1990, J. Organomet. Chem. **391**, 313.

Yang, L., L. Dai, H. Ma and Z. Ye, 1989, Organometallics **8**, 1129.

Yang, L., C. Stern and T.J. Marks, 1991, Organometallics **10**, 840.

Yasuda, H., H. Yamamoto, K. Yokota, S. Miyake and A. Nakamura, 1992, J. Am. Chem. Soc. **114**, 4908.

Ye, Z., Z. Zhou, S. Yuan and Z. Luo, 1984, Youji Huaxue, 119.

Ye, Z., H. Ma and Y.J. Yu, 1986a, J. Less-Common Met. **126**, 405.

Ye, Z., Z. Zhou, Z. Lou, X. Wang and F. Shen, 1986b, Huaxue Xuebao **44**, 707.

Ye, Z., S. Wang, Y. Yu and L. Shi, 1990, Inorg. Chim. Acta **177**, 97.

Yu, Y., S. Wang, Z. Ye and H. Ma, 1991, Polyhedron **10**, 1599.

Zalkin, A., and D.J. Berg, 1988, Acta Crystallogr. C **44**, 1488.

Zalkin, A., and D.J. Berg, 1989, Acta Crystallogr. C **45**, 1630.

Zalkin, A., and S.M. Beshouri, 1988, Acta Crystallogr. C **44**, 1826.

Zalkin, A., and S.M. Beshouri, 1989a, Acta Crystallogr. C **45**, 1080.

Zalkin, A., and S.M. Beshouri, 1989b, Acta Crystallogr. C **45**, 1219.

Zalkin, A., and J.G. Brennan, 1985, Acta Crystallogr. C **41**, 1295.

Zalkin, A., and J.G. Brennan, 1987, Acta Crystallogr. C **43**, 1919.

Zalkin, A., D.H. Templeton, C. LeVanda and A. Streitwieser Jr, 1980, Inorg. Chem. **19**, 2560.

Zalkin, A., D.H. Templeton, W.D. Luke and A. Streitwieser Jr, 1982, Organometallics **1**, 618.

Zalkin, A., D.H. Templeton, R. Kluttz and A. Streitwieser Jr, 1985, Acta Crystallogr. C **41**, 1038.

Zalkin, A., J.G. Brennan and R.A. Andersen, 1987a, Acta Crystallogr. C **43**, 1706.

Zalkin, A., J.G. Brennan and R.A. Andersen, 1987b, Acta Crystallogr. C **43**, 418.

Zalkin, A., J.G. Brennan and R.A. Andersen, 1987c, Acta Crystallogr. C **43**, 421.

Zalkin, A., T.J. Henly and R.A. Andersen, 1987d, Acta Crystallogr. C **43**, 233.

Zalkin, A., J.G. Brennan and R.A. Andersen, 1988a, Acta Crystallogr. C **44**, 2104.

Zalkin, A., A.L. Stuart and R.A. Andersen, 1988b, Acta Crystallogr. C **44**, 2106.

Zanella, P., G. Rossetto and G. Paolucci, 1984a, Inorg. Chim. Acta **82**, 227.

Zanella, P., G. Rossetto, A. Berton and G. Paolucci, 1984b, Inorg. Chim. Acta **95**, 263.

Zanella, P., G. Paolucci, G. Rossetto, F. Benetollo, A. Polo, R.D. Fischer and G. Bombieri, 1985, J. Chem. Soc. Chem. Commun., 96.

Zanella, P., N. Brianese, U. Casellato, F. Ossola, M. Porchia, G. Rossetto and R. Graziani, 1987, J. Chem. Soc. Dalton Trans., 2039.

Zanella, P., N. Brianese, U. Casellato, F. Ossola, G. Rossetto and R. Graziani, 1988, Inorg. Chim. Acta **144**, 129.

Zazzetta, A., and A. Greco, 1979, Acta Crystallogr. B **35**, 457.

Zhang, H., A.R. Oki, Y. Wang, J.A. Maguire and N.S. Hosmane, 1995, Acta Crystallogr. C **51**, 635.

Zhennan, Z., W. Zhongzhik, D. Baohu and Y. Zhonwen, 1989, Polyhedron **8**, 17.

Zhongwen, Y., M. Huaizhu and Y. Yonghfei, 1986, J. Less-Common Met. **126**, 405.

Zhou, J., Y. Ge and C. Qian, 1984, Synth. React. Inorg. Met. Org. Chem. **14**, 651.

Zhou, J., H. Ma, Z. Wu, X. You, Z. Xu and X. Huang, 1995, J. Organomet. Chem. **503**, 11.

Zielinski, M., D.K. Drummond, P.S. Iyer, J.T. Leman and W.J. Evans, 1995, Organometallics **14**, 724.

AUTHOR INDEX

SUBJECT INDEX